SLAC-R-978

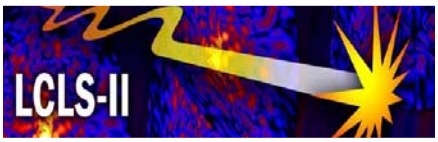

Linac Coherent Light Source II (LCLS-II)

Conceptual Design Report

SLAC-I-060-003-000-00

Work supported in part by US Department of Energy contract DE-AC02-76SF00515.

SLAC National Accelerator Laboratory, Menlo Park, CA 94025

Linac Coherent Light Source II Conceptual Design Report

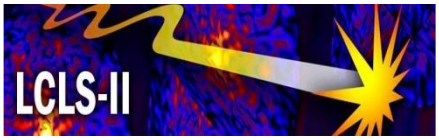

Index of Chapters

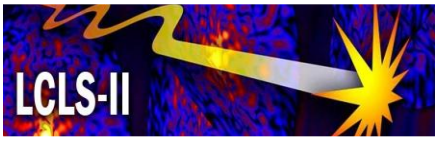

1 Executive Summary

Technical Synopsis

The mission, scope, schedule and cost of the LCLS-II Project are summarized.

1.1 Mission Need

The LCLS-II Project is designed to support the DOE Office of Science mission, as described in the 22 April 2010 Mission Need Statement. The scope of the Project was chosen to provide an increase in capabilities and capacity for the facility both at project completion in 2017 and in the subsequent decade.

The Project is designed to address all points of the Mission Need Statement (MNS):

1. Expanded spectral reach.
2. Capability to provide x-ray beams with controllable polarization.
3. Capability to provide "pump" pulses over a vastly extended range of photon energies to a sample, synchronized to LCLS-II x-ray probe pulses with controllable inter-pulse time delay.
4. Increase of user access through parallel rather than serial x-ray beam use within the constraint of a $300M-$400M Total Project Cost (TPC) range.

1.2 Scope of Conceptual Design

The LCLS-II Project will construct:

- A hard x-ray undulator source (2-13 keV).
- A soft x-ray undulator source (250-2,000 eV).
- A dedicated, independent electron source for these new undulators, using sectors 10-20 of the SLAC linac.
- Modifications to existing SLAC facilities for the injector and new shielded enclosures for the undulator sources, beam dumps and x-ray front ends.
- A new experiment hall capable of accommodating four experiment stations.
- Relocation of the two soft x-ray instruments in the existing Near Experiment Hall (NEH) to the new experiment hall (Experiment Hall-II).

1.3 Key Performance Parameters

Table 1.1. Key Performance Parameters for the LCLS-II Project.

Performance Measure	Threshold Key Performance Parameters	Key Performance Parameters – Objectives
Electron Beam Energy	13.5 GeV	13.5 GeV
Photon Beam Tuning Range	800-8,000 eV	250-13,000 eV
X-ray Pulse Energy, single shot	$>10^6$ photons/(mm*0.1% BW)	$>10^{12}$ photons/(mm^2*0.1% BW)
Electron Pulse Duration	<100 fs	<3 to 500 fs
Linac Repetition Rate	120 Hz	120 Hz
Undulator Source Repetition Rate	60 Hz	60 Hz
Additional Space for Instruments	4 Experiment Stations	4 Experiment Stations
Facilities Gross Square Feet	>30,000 GSF	59,685 GSF

1.4 Estimated Cost

The Total Project Cost range is $300M-$400M. A detailed cost estimate has been performed. A detailed cost estimate has been completed which confirms that the project scope described in this report can be accomplished within the TPC range.

1.5 Schedule

The Project can be completed by the end of FY2017. In order to allocate sufficient "float" time between the early finish data and the Critical Decision 4 milestone, it is appropriate to place the latter in 4QFY2018. The Project schedule will require at least one long (6 month) shutdown of operations for construction of the Beam Transport Hall extension and for tunneling. Every effort will be made to minimize impact on facility operation, by taking advantage of the expected annual shutdowns for LCLS-II installations.

Revision Record

Revision	Date Revised	Description of Change
R001	April 14, 2011	KPPs and budget updated.
R000	April 8, 2011	Original release.

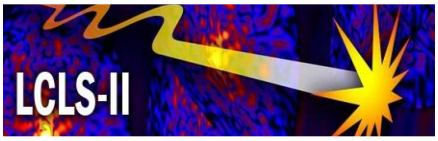

2 Overview

Technical Synopsis

A key objective of LCLS-II is to maintain near-term international leadership in the study of matter on the fundamental atomic length scale and the associated ultrafast time scales of atomic motion and electronic transformation. Clearly, such studies promise scientific breakthroughs in key areas of societal needs like energy, environment, health and technology, and they are uniquely enabled by forefront X-ray Free Electron Laser (X-FEL) facilities. While the implementation of LCLS-II extends to about 2017, it is important to realize that LCLS-II only constitutes a stepping stone to what we believe is needed over a longer time scale. At present, a practical time horizon for planning is about 15 years into the future, matching that of worldwide planning activities for competitive X-FEL facilities in Europe and Asia. We therefore envision LCLS-II as an important stage in development to what is required by about 2025, tentatively called LCLS-2025, for continued US leadership even as new facilities around the world are being completed. We envision LCLS primarily as a hard x-ray FEL facility with some soft x-ray capabilities. A survey of planned X-FEL facilities around the world suggests that US planning to 2025 needs to include an internationally competitive soft x-ray FEL facility which complements the LCLS plans outlined in this document.

The Linac Coherent Light Source II (LCLS-II) Project will construct the following additions to the Linac Coherent Light Source facility:

- *A new hard x-ray undulator source (2-13 keV).*
- *A new soft x-ray undulator source (250-2,000 eV).*
- *A dedicated, independent electron source, using sectors 10-20 of the SLAC linac.*
- *A new experiment hall accommodating four experiment stations.*
- *Relocation of existing soft x-ray instruments to the new experiment hall.*

The new undulator sources will produce coherent plane-polarized x-rays by self-amplified spontaneous emission (SASE). They will be designed for straightforward extension of their capabilities to include full temporal coherence and polarization control.

The LCLS-II Project will position SLAC to retain its status as the world's preeminent Free-Electron Laser (FEL) research center, even as other FEL facilities begin operation around the world. The total project cost range is estimated to be $300M-$400M. The proposed completion date is September 2017.

2.1 Introduction: Roadmap to LCLS 2025

The competitive international environment in terms of X-FELs is illustrated in Figure 2.1. Here we have plotted the growth in the number of hard x-ray stations at X-FEL facilities in Europe and Asia and compared them to two scenarios for the development of LCLS.

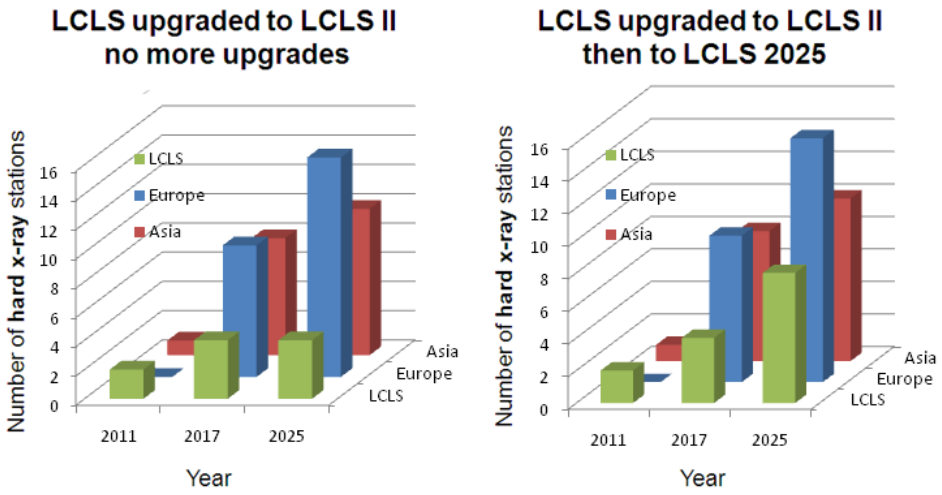

Figure 2.1. Projected growth of the number of simultaneously operating hard x-ray stations at X-FEL facilities in Europe (Germany and Switzerland) and Asia (Japan and Korea)[1], in comparison with two LCLS upgrade scenarios.

On the left, we have assumed that the LCLS-II upgrade, which increases the simultaneously operating hard x-ray stations from one to four, provides the total US capacity until 2025. Simultaneous operation of x-ray instruments will be provided by the three undulators and by thin crystal offset monochromators, which split the x-ray beam into a Bragg diffracted and a transmitted beam. On the right we illustrate the need for further upgrades to remain competitive for the next 15 years. The scientific objectives for LCLS-II in this document provide the capacity shown on the left but are optimized within the "LCLS-2025" scenario shown on the right. Note that we envision LCLS-2025 to have eight hard (shown) plus two soft x-ray (not shown) stations in total.

In this report we therefore present a technical design of LCLS-II that not only provides for additional capacity when completed but best supports the overall growth plan toward LCLS-2025. The overall scope of LCLS-2025 is shown in Figure 2.2. It includes three independent injectors and linac sections, feeding electron beams interchangeably into two separate undulator halls, each filled with two independent undulator sources. Each undulator source is envisioned to consist of a self-seeding arrangement of two undulators separated by a monochromator, and polarization control of two of the four sources. The existing Near Experimental Hall (NEH) and Far Experimental Hall (FEH) will house six hard x-ray stations while the new experimental hall (EH2) will contain two hard and 2 soft x-ray stations. This concept supports the capacity increase by a factor of ten suggested by the projected growth of the LCLS users in that it allows simultaneous operation of all 10 experimental stations (eight hard x-ray and two soft x-ray).

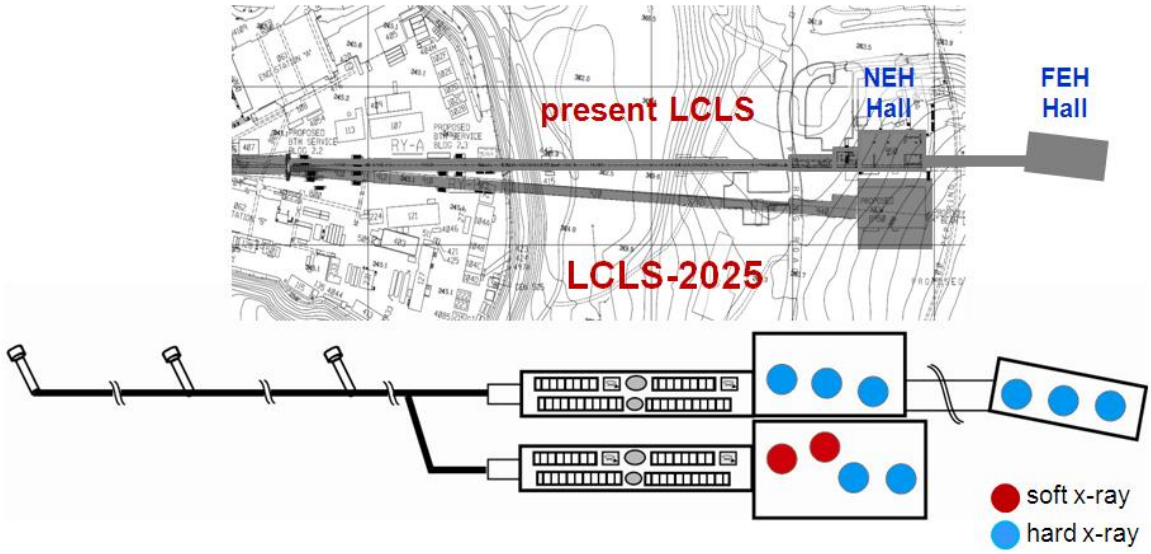

Figure 2.2. Envisioned scope of LCLS-2025 as discussed in the text.

Figure 2.3 compares two LCLS-II scenarios, each taking a different path to the same overall LCLS-2025 concept. The “one-tunnel” scenario, presented in the original LCLS-II proposal, involves no major conventional construction and utilizes the existing LCLS tunnel for LCLS-II capacity increase. It provides a second undulator in the existing tunnel for separate delivery of soft and hard x-rays to the existing AMO and SXR soft x-ray stations and the XPP, XCS, CXI and MEC hard x-ray stations. As indicated by the blue curve, in the longer run, this scenario would require construction of the second undulator tunnel and additional experimental hall shown in Figure 2.2 in the 2017-2025 time period with scientific use of the new facilities delayed until around 2023. The LCLS-II “two tunnel” scenario presented in this report includes construction of the second undulator tunnel and additional experimental hall by 2017. It offers a comparable capability extension as the first scenario with simultaneous operation of up to five instruments by 2017. However, the existence of the conventional infrastructure allows continuous expansion of the capacity in the 2017-2025 period as indicated by the red curve. After 2017 the staircase shape of the red curve represents the possible installation of new x-ray instruments every two years, which will require additional funding after the completion of the LCLSII project.

Figure 2.3 shows that by 2017 both the baseline and two-tunnel options provide similar capacity, namely operation of up to five stations simultaneously. However it is inevitable that, as a wider range of specialized and sophisticated capabilities are added to the LCLS x-ray sources, it will become ever more difficult to schedule experiments for which the split x-ray beam can be concurrently optimized. Without increased capacity, access to new LCLS capabilities will be severely limited.

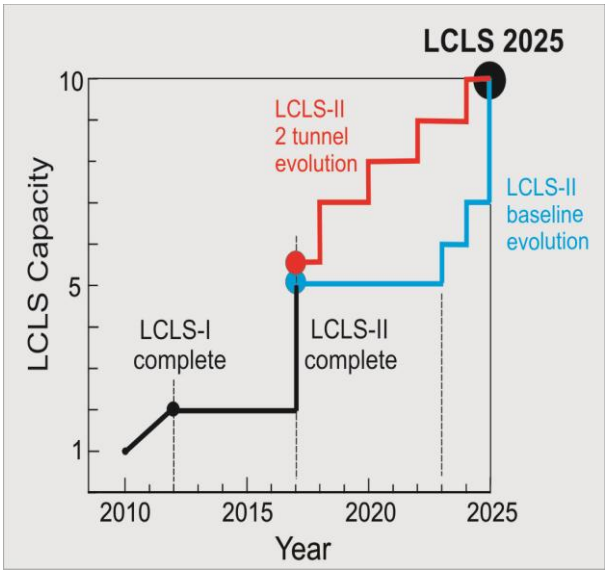

Figure 2.3. Conceptual diagram for the LCLS capacity growth under two scenarios as discussed in the text.

2.2 LCLS-II Project Scope

Today and, perhaps, for a few years to come, the LCLS is the world's preeminent x-ray free-electron laser user facility. Its 14 GeV electron source and single fixed-gap undulator can provide intense x-ray pulses to one of four experiment stations in operation today[2]. By 2012, all six stations will be operational. While there is room in the existing undulator hall to add another x-ray source, there is no room for new instruments. In order to remain at the forefront of ultrafast x-ray science, the LCLS facility must be expanded to accommodate more x-ray sources and instruments.

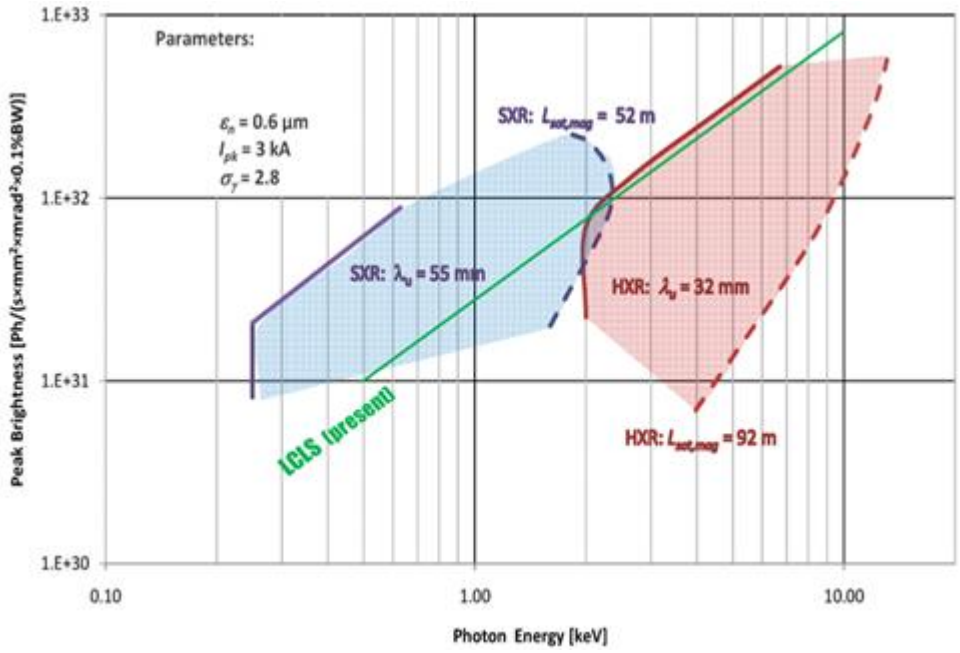

Figure 2.4. Brightness at saturation and tuning range of LCLS-II undulator sources. The range of the hard x-ray source(HXR) is shown in red, while the soft x-ray source(SXR) is shown in blue.

The LCLS-II Project concept has been developed to provide the new facilities and capacity for expansion required to firmly position SLAC as the world's preeminent free-electron laser research center. With two new, independently controllable x-ray sources in a new undulator hall, it will be possible to simultaneously provide tunable soft and hard x-ray beams, one optimized for 250-2,000 eV photons and the other optimized for 2,000-13,000 eV. Figure 2.4 shows the photon energy ranges of the HXR and SXR undulators. With a dedicated injector, these two new sources will operate completely independent of the existing LCLS x-ray source, so that existing and new sources may be optimized to meet the specific needs of each experiment. This is a major step beyond present capabilities of LCLS, which can only provide a single x-ray beam optimized for one experiment at a time. At the completion of this project, the LCLS facility will be positioned to implement further upgrades necessary to keep its place at the forefront of the field it has pioneered: ultrafast x-ray research.

The LCLS-II Project will create room for expansion to keep pace with the explosive growth of research opportunities and user demand that has already begun even before existing LCLS facilities reach full capacity in 2012. SLAC will be positioned to continue its leadership as the world's most powerful and capable x-ray laser facility into the next two decades. The LCLS-II Project will add two new undulator sources and space for four new instruments to the existing facility. At the completion of the LCLS-II project, the expanded LCLS facility will accommodate a total of four undulator sources and ten experiment stations.

This expansion of the LCLS facility will build upon the proven performance characteristics of the LCLS, enabling groundbreaking research in a wide range of scientific disciplines. LCLS-II will create unbounded opportunity for research into atomic-level dynamics of processes that are fundamentally important to materials science, chemistry and the life sciences. The LCLS-II conceptual design provides greatly enhanced capacity and capability for the LCLS facility.

The Linac Coherent Light Source II (LCLS-II) Project conceptual design will provide the following facility enhancements:

- A hard x-ray undulator source (2-13 keV).
- A soft x-ray undulator source (250-2,000 eV).
- A dedicated, independent electron source for these new undulators, using sectors 10-20 of the SLAC linac.
- Modifications to existing SLAC facilities for the injector and a new shielded enclosure for the two new undulator sources, beam dumps and x-ray front ends.
- A new experiment hall capable of accommodating four experiment stations.
- Relocation of the two soft x-ray instruments in the existing Near Experiment Hall to the new experiment hall (Experiment Hall-II).

The undulator sources will produce spatially coherent plane-polarized x-rays by self-amplified spontaneous emission (SASE). They will be designed to be compatible with future upgrades to include full temporal coherence and polarization control.

Much of the new technical systems and facilities will be virtually identical to those constructed in the original LCLS Project (LCLS-I). The LCLS-II Project will build on experience and lessons learned during LCLS-I construction, commissioning and operation so as to reduce cost, schedule and technical risk.

The LCLS-II Project will enable expansion of LCLS to keep pace with the explosive growth of research opportunities and user demand which will saturate the existing facility by 2012. SLAC will be positioned to continue its preeminence as the world's most powerful and capable x-ray laser facility into the next two decades.

2.3 Key Performance Parameters

The key performance parameters (KPP) for LCLS have been selected to guarantee that the project has provided functioning facilities and systems required to ultimately meet the Mission Need. The KPP must be achieved and verified before the Department of Energy approves Critical Decision 4, the official acknowledgement that the project has been completed. DOE recognizes that scientific research facilities with technical performance goals at or beyond the state of the art can be difficult to bring to optimum performance, especially on a schedule set in place 5-7 years in advance of project completion. In order to permit prudent management of project technical and schedule risks, DOE sets the KPP at levels less challenging than the design goals for the new facility. In this way, the commissioning time required for optimization of performance are shifted outside the project schedule to the post-project phase. As the Project progresses from conceptual design approval (Critical Decision 1) to approval of the Project Baseline (Critical Decision 2), the KPP will be reexamined and revised as necessary to reflect the approved project scope and hence the requirements for Critical Decision 4.

Table 2.1. Key Performance Parameters for the LCLS-II Project.

Performance Measure	Threshold Key Performance Parameters	Key Performance Parameters – Objectives
Electron Beam Energy	13.5 GeV	13.5 GeV
Photon Beam Tuning Range	800-8,000 eV	250-13,000 eV
X-ray Pulse Energy, single shot	$>10^6$ photons/(mm*0.1% BW)	$>10^{12}$ photons/(mm^2*0.1% BW)
Electron Pulse Duration	<100 fs	<3 to 500 fs
Linac Repetition Rate	120 Hz	120 Hz
Undulator Source Repetition Rate	60 Hz	60 Hz
Additional Space for Instruments	4 Experiment Stations	4 Experiment Stations
Facilities Gross Square Feet	>30,000 GSF	59,685 GSF

This Conceptual Design Report describes a facility with capabilities far beyond the requirements of the KPP. The CDR predictions are based on comprehensive understanding of the performance capabilities of the LCLS facility, which have been thoroughly studied since lasing was first achieved in April 2009.

2.4 Cost Range

The Total Project Cost (TPC) cost range for LCLS-II is $300M-$400M. The DOE prescribes a cost range for a proposed project at the time of Critcal Decision 0 in order to define a framework for the conceptual design. The cost range also determines the levels of DOE management who must approve the Critical Decisions. It is understood that more detailed planning and engineering design will be required to ensure that the three essential definitions of a project baseline (technical scope, cost and schedule) are actually consistent. At this point, the necessary adjustments are made to create a consistent project baseline, and the DOE approval process begins. When Critical Decision 2 (CD-2) is approved, the TPC becomes rigidly defined and is generally not changed except by act of Congress.

The project is expected to handle any cost overruns and delays without exceeding the TPC. It is standard practice for Office of Science projects to define a technical scope and associated cost estimate that is significantly less than the TPC. The difference between the estimated cost at completion (EAC) and the requested budget (TPC) is generally termed "contingency" or "management reserve" for Office of Science projects (this terminology is not uniform across DOE). A proposed project with insufficient contingency in its baseline will not receive CD-2 approval. The sufficiency of contingency is assessed prior to CD-2 by DOE through a well-developed project baseline review process. The Office of Science has accumulated data on a wide variety of projects it has authorized and managed.[3]

In order that the LCLS-II conceptual design meet DOE expectations for mission need, scope, cost, schedule and risk management, this conceptual design report has not explicitly included self-seeding and polarization control in the project scope. In terms of cost, these items do not appear to constitute a large fraction of the cost estimate. However, for reasons described in this chapter and in Chapter 3, the LCLS-II concept has given highest priority to building the conventional facilities necessary to ensure the long-range future of LCLS. Unhappy experience has repeatedly demonstrated that cost risks of civil construction, and especially tunneling, are frequently the dominant risks in an Office of Science Project.

At this stage of planning, LCLS-II must address the cost risks by allocating approximately 30% contingency within the Total Project Cost. After assigning appropriate contingency to technical systems, SLAC cannot responsibly propose the inclusion of seeding and polarization control in the project baseline without undue risk of exceeding the maximum of the TPC range. As cost estimates are improved, it may be possible to add high-priority items such as hard x-ray seeding and soft x-ray polarization control to the project baseline.

2.5 Schedule

Assuming that long-lead procurement budget authority is provided in FY2012 and civil construction can begin well before the end of 2013, the LCLS-II project can be completed in FY2017.

Table 2.2. Proposed dates for Project Milestones.

Milestone Event	Target Date
CD-0 Approve Mission Need	4/22/10 actual
CD-1 Approve Alternative Selection and Cost Range	August 2011
CD-3A Approve Long-lead Procurement Performance Baseline and Start of Construction	Q1FY2012 (12/31/11)
CD-2 Approve Performance Baseline (Level 1)	Q3FY2012 (6/30/12)
CD-3B Approve Start of Construction (Level 1)	Q2FY2013 (3/31/13)
CD-4 Approve Start of Operation (Level 1)	Q4FY2018 (9/30/18)

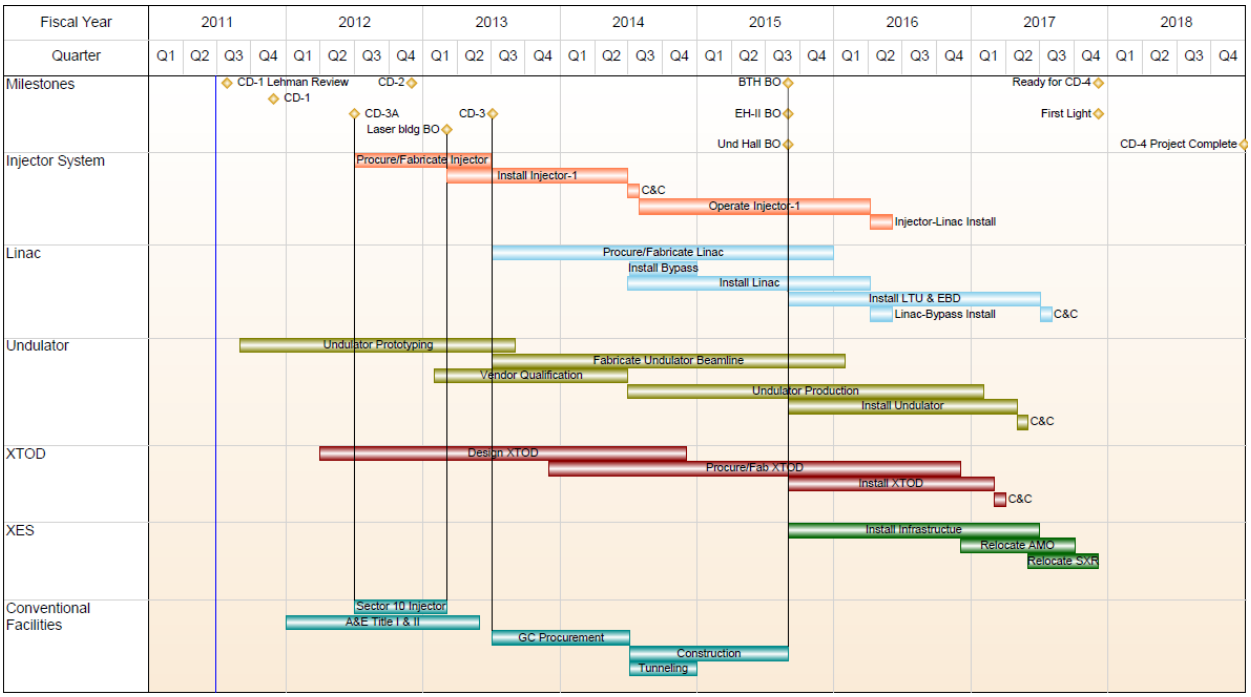

Figure 2.5. LCLS-II construction schedule.

2.6 LCLS-II Mission Need

The Mission Need Statement (MNS) for LCLS-II, approved on April 22, 2010, identifies “a need for BES to build a new, or upgrade an existing x-ray free-electron laser (X-FEL) facility that provides an unprecedented temporal resolution and unmatched coherence and brightness. In this context, the only practical and cost efficient alternative to achieve this mission is to upgrade the Linac Coherent Light Source at the SLAC National Accelerator Laboratory (SLAC).” The LCLS-II Project addresses this mission need in a way that is both cost-effective and scientifically ambitious. The scope of the project has been determined after consideration of the full array of alternatives.

2.6.1 Scientific Objectives and Opportunities

The MNS acknowledges the cost-effectiveness of expanding/upgrading the LCLS. It identifies several key capabilities to be addressed by LCLS-II, subject to the constraint of the preliminary baseline range of $300M-$400M.

The LCLS-II project scope is defined to squarely address the principal performance gaps identified in the MNS: spectral range and parallel operation. Furthermore, when the project is completed at the end of 2017, it will be possible to conduct operations in one undulator hall and associated experiment hall while maintenance and upgrades are carried out in the other. This will dramatically increase the scientific productivity and scientific reach of LCLS over the next 20 years.LCLS-II systems will be designed to permit straightforward implementation of polarization control and extended pump capability. As reported in Appendix D, the requirements for implementation of these capabilities are well-understood. Some of these capabilities (hard x-ray seeding and possibly soft x-ray polarization control) will be implemented in the present LCLS undulator source before LCLS-II is completed.

2.7 Alternatives Analysis

Alternatives for fulfilling the Mission Need at LCLS were thoroughly evaluated in arriving at the present conceptual design. In requesting approval of CD-1 it is appropriate to consider all reasonable alternatives. The leading options are:

- Construct the expansion of LCLS as described in this conceptual design report.
- Construct a soft x-ray source in the existing LCLS tunnel.
- Construct a new FEL facility at a "green field" site.

One important basis of comparison for these options is capacity to support experiments. LCLS is preparing to implement thin crystal offset monochromators to split the beam between the "hard" x-ray (HXR) instruments, with the goal of providing x-rays concurrently to all four HXR stations. Beam splitting will multiply the capacity of LCLS by a significant factor. However the capacity increase from beam splitting will depend on matching the properties of the split beams to experiments so as to optimize concurrent operation. Soft x-ray experiments at LCLS frequently request specific wavelengths, e.g. to ionize oxygen or neon. A single experiment is also likely to request changes in photon energy once or twice a day, along with changes in pulse duration as well. For LCLS as it is presently configured, it appears reasonable to assume that the two soft x-ray instruments will not be operable concurrently since the x-ray beam parameters must be tailored to a given experiment on a shift-by-shift basis. It must be kept in mind, however, that because it is a new facility with only four of its six instruments in operation, LCLS has yet to build a comprehensive database of operating modes matched to the needs of its entire user community. Estimates of the total number of experiments per year are dependent on the efficiency of concurrent running modes. However with the same assumptions applied to all scenarios, comparisons are still meaningful.

It is assumed that

- LCLS will schedule user experiments during 4,000 hours per year of operation
- Each experiment will receive an allocation of 60 hours of x-ray beam time
- The "status quo", or baseline for comparison of options, is LCLS as a single undulator source; we assume LCLS would run 2,000 hours at soft x-ray wavelengths supporting one experiment at a time and 2,000 hours at hard x-ray wavelengths, supporting four experiments concurrently. In the status quo scenario, 166 experiments are performed at LCLS every year.
- After LCLS-II is complete, both electron sources will support 4,000 hours of experiments annually
- In all scenarios, all available experiment stations are assumed to be operable; ten stations for scenario 1 and six stations for scenario 2.
- LCLS will operate two soft x-ray stations; all other stations are assumed to require "hard" x-ray beams
- A soft x-ray experiment requires a dedicated undulator, and no significant increase in capacity can be expected by splitting the soft x-ray beam for concurrent use in two experiments
- After technical and scheduling problems are solved, all "hard" x-ray stations operate concurrently (this is clearly an optimistic scenario, for the sake of comparison).

- If a self-seeded soft x-ray source is constructed in the existing tunnel (scenario 2), it will operate as a self-seeded source for one experiment 50% of the time, and it will run as two independent SASE sources the rest of the time

We consider the first alternative, construction of the LCLS as described in this conceptual design. In this scenario, the facility will ultimately operate two soft x-ray experiments and eight hard x-ray experiments. This scenario will support 67 soft x-ray experiments per year and 8 x 67=536 hard x-ray experiments per year. The total for this scenario is 603 experiments per year.

Using the status quo 166 experiments per year as a baseline, the ultimate capacity of the facility is increased 360% compared to the status quo in scenario 1, and 164% compared to option 2. Soft x-ray tuning range is extended down to the vitally important carbon K edge at the completion of the project. Since this alternative also includes a new hard x-ray SASE source optimized to produce 2,000-13,000 eV x-rays, the existing LCLS undulator can be modified to produce harder x-rays (~20 keV) while preserving the overall performance of the facility in its present operating range. This can be accomplished simply by exchanging shims in the undulator to increase the magnet gap and hence reduce K. In this way the first alternative is responsive to the first key capability cited in the mission need statement. This option also makes it possible to apply lessons learned from LCLS research to the construction of new instruments in the additional space provided for instruments. With the added capacity provided by LCLS-II, new instrumentation and capabilities can be added without interrupting research with the existing instruments, an important advantage of this option. Polarization control can be added in the future to the new soft x-ray source by installing a small number of APPLE-II undulators. This can be done with no impact to the operation schedule and a cost impact of less than $10M.

Soft x-ray self-seeding is a more expensive enhancement, requiring the addition of over 30 meters of undulator and x-ray optics. New instruments can be added in MIE projects, with minimal disruption to ongoing operation.

In the second alternative, electrons would be provided by a new injector linac, and accelerated in Sectors 10-20 of the SLAC linac; this is identical to the first, preferred alternative. These electron bunches would be transported through the BTH to pass through two variable-gap undulators arranged in series. In self-seeding mode, the two undulators would constitute a single source of temporally coherent x-ray pulses. Alternatively, the undulators could be operated as two SASE sources with somewhat limited independent tuning capability, each providing an x-ray beam to a different instrument. Each undulator would have polarization control capability. Since this option does not entail construction of a second undulator tunnel and experiment hall, it has been termed the “one tunnel” option. If the soft x-ray source is run in seeded mode 50% of the available beam time, it will provide beam to 2 x (33) + 1 x (34)= 100 experiments per year. Meanwhile the hard x-ray source will provide beam to four stations, for 4 x 67=268 experiments per year. The total in this scenario is 368 experiments per year.

The “one tunnel” option would permit simultaneous independent operation of the original linac and fixed-gap undulator, which would most likely be dedicated to production of hard x-rays. It would increase throughput by perhaps as much as 220% compared to the status quo, by providing a second x-ray beam delivered to the existing experiment halls. However it would not provide space for more instruments, seriously hindering the implementation of new instruments in the future. As the operation of the LCLS and new x-ray FEL facilities continue the science case for completely new instruments will emerge. Because this option does not provide a new hard x-ray source, there would be less flexibility in providing hard x-ray beams with different characteristics to the individual hard x-ray instruments. In all

cases but more seriously for the “one tunnel” option, there will be a challenge to satisfy the needs of the different hard x-ray experiments which operate concurrently.

There is little to be learned from comparing capacities of the first two alternatives with a “green field” alternative, for which the number of undulators is not defined. It is reasonable to assume that a soft- or hard x-ray undulator in a “green field” facility will support the same number of experiments supported by a soft- or hard x-ray sources in the first two alternatives. The primary consideration in this scenario is the initial cost. The third option, construction of a “green field” FEL user facility, would require (at minimum) construction of a new linear accelerator and associated facilities at a cost approaching $1B, duplication of the LCLS-I project scope (>$400M) as well as the six scientific instruments in place today or under construction (>$80M). A “green field” facility with two complete injector linacs and future potential for 28 GeV operation would cost an additional $2B or more. Despite the obvious advantages of higher electron energy the cost of the accelerator has deterred many new FEL projects from building accelerators matching LCLS capabilities; the SLAC linac, operable as three independent 14 GeV accelerators, is an asset that no competing facility can afford to duplicate . The SLAC linac gives LCLS fundamental scientific and operational advantages that will be unique worldwide in the foreseeable future.

Expansion of the LCLS facility is, without doubt, the best alternative for fulfillment of the Office of Science mission need in 2017 and beyond. LCLS-II will be built on a firm foundation of experience with the LCLS facility, providing the advantages of low technical risk combined with unparalleled technical capabilities to support world-leading ultrafast x-ray research.

2.8 Acquisition Strategy

The Department of Energy can best fulfill the Mission Need by selecting Stanford University, Managing and Operating (M&O) contractor for SLAC National Accelerator Laboratory, to execute the LCLS-II Project.

The design, fabrication, assembly, installation and testing, for the LCLS-II project will be largely performed by the SLAC/LCLS-II scientific and technical staff. The LCLS-II will subcontract the undulator system to the Lawrence Berkeley National Laboratory. The remaining subcontracted work to be performed for LCLS-II consists of hardware fabrication and conventional facilities construction.

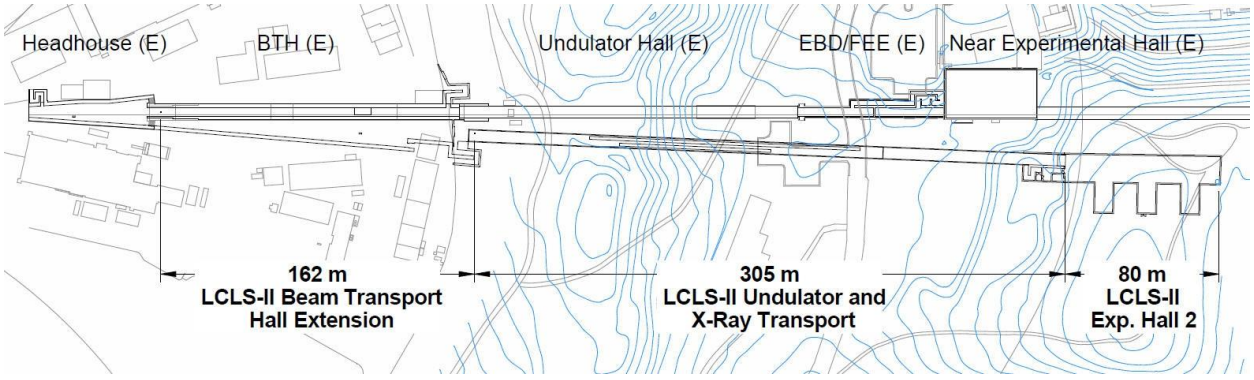

Figure 2.6. Layout of LCLS-I and LCLS-II. Items labeled with (E) are existing LCLS facilities.

1. Figure 2.1 makes the following assumptions for the future capacity of the x-ray FEL facilities. In 2011 there are no hard x-ray instruments at European FEL facilities, 1 at SCSS and 2 at LCLS. In 2017, there will be 6 hard x-ray instruments at the EUXFEL, 3 at SwissFEL, 4 at SCSS, 4 at the Korean FEL and 4 at LCLS. In 2025, there will be 9 hard x-ray instruments at the EUXFEL, 6 at SwissFEL, 6 at SCSS, 4 at the Korean FEL and either 4 or 8 at LCLS.
2. A more complete description of the present-day LCLS facility may be found in Appendix C. Here, the reader will find a description of present performance, planned near-term enhancements and the two options for expansion built into the existing facility.
3. Data on contingency management for Office of Science Projects can be found at http://www.science.doe.gov/opa/13costcontingency.html

Revision Record

Revision	Date Revised	Description of Change
R003	May 5, 2011	Figure 2.6 modified.
R002	April 14, 2011	Table 2.2 (milestones) updated.
R001	April 14, 2011	KPPs and budget updated.
R000	April 8, 2011	Original release.

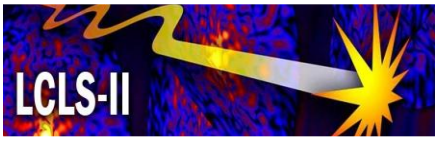

3 Scientific Objectives of LCLS-II

Technical Synopsis

This chapter outlines the scientific objectives of LCLS-II, building on the original Linac Coherent Light Source II (LCLS-II) Proposal (SLAC-I-060-001-000-00) *which highlighted the needs for this facility from a scientific use point of view. Here we focus our discussion on specific scientific objectives which have driven the technical scope and design of LCLS-II presented in the other chapters of this document.*

The scientific objective for LCLS-II is to provide increased user capacity and enhanced scientific capabilities upon its completion around 2017 while at the same time optimizing the path to LCLS-2025. Leveraging the pioneering design and success of LCLS-I, the upgrades in capacity and capability envisioned for LCLS-II will enable scientific discovery not achievable with LCLS-I. The expanded LCLS facility will support a wide range of scientific disciplines and the improved x-ray capabilities will not just benefit a single special field but serve the entire range of science from advanced materials to life sciences.

LCLS-II addresses the looming reality of insufficient capacity of LCLS-I to accommodate the fast growing number of users excited by its early success. LCLS-II will increase user access through parallel rather than serial x-ray beam use, allowing simultaneous operation of up to 5 instruments instead of a single instrument at LCLS-I. Key to the capacity increase is the use of two independent linacs, a total of three undulators and three experimental halls, facilitating separate hard and soft x-ray experiments. The existing four hard x-ray instruments will be served with radiation produced by the present injector, linac section and undulator, modified to extend the maximum photon energy, and will remain in the existing near and far experimental halls of LCLS-I. The two soft x-ray instruments will be relocated into the new experimental hall and will be served by the new injector, linac section and a new undulator. A variable-gap hard x-ray source, optimized for photon energies 2,000-13,000 eV, will also deliver x-rays to the new hall. LCLS-II will construct space for two new instruments, to be served by this source. This scheme not only supports increased capacity by the availability of separate hard and soft x-ray beams, but because of the two separate electron beams and variable gap undulators, the x-ray beams may have different photon energy and pulse length. Therefore the properties of the hard and soft x-ray pulses are completely decoupled and the capability is improved as well.

From a scientific perspective LCLS-II will deliver key extensions in capability by extending the spectral range. It will increase the present 10 keV limit up to 20 keV for the study of thick 3D materials with increased x-ray penetration and spatial resolution, and extend the soft x-ray spectral range down to the carbon K absorption edge for the study of chemical transformations of key carbon based molecular complexes.

Over the next few years we are also targeting specific areas for Research & Development (R&D) and these capabilities will be implemented at LCLS as soon as they are proven. Depending on cost we envision implementing some of these capabilities with operations funds or adding them after completion of LCLS-II with separate funds. R&D areas are:

- *x-ray self-seeding, especially in the hard x-ray region, for optimum intensity per bandwidth and pulse length;*
- *polarization control in the soft x-ray region for the separation of charge and spin effects in materials;*

3.1 Introduction: Optimizing Near and Long Term LCLS Scientific Objectives

In this chapter we review the scientific objectives which drive the technical design choices made for LCLS-II. An important consideration in planning for LCLS-II is the anticipated increase in the number of LCLS users shown in Figure 3.1. The plotted increase in users, requiring an increase in experimental capacity, is based on the extrapolated growth in users during the first year of LCLS operation, the scientific vision and beam time demand expressed by the LCLS user community at several workshops, and input from international experts. Over the next fifteen years we anticipate a 10x increase in user demand. LCLS-II will support this overall objective.

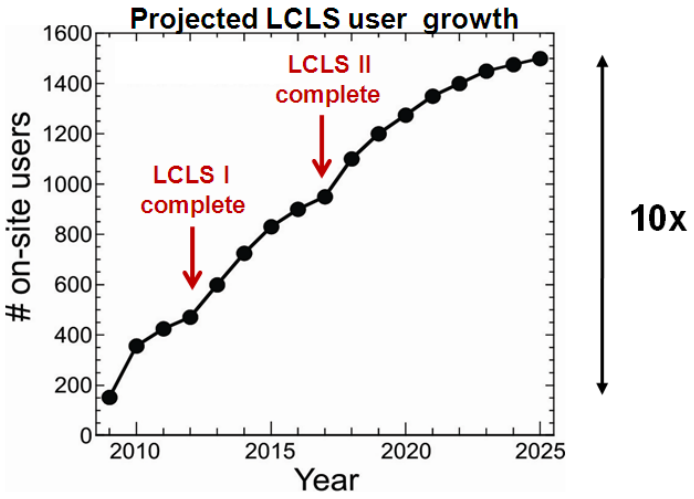

Figure 3.1. Anticipated growth in the number of on-site LCLS users.

We have indicated two key steps in LCLS development by red arrows, the completion of all six LCLS-I instruments by 2012, and the capacity increase enabled by LCLS-II due to additional facilities and simultaneous use of experimental stations. Within our total planning horizon of 2025 we envision a 10x capacity increase which involves another step in the 2017-2025 period as shown.

The LCLS-II conceptual design was chosen as the optimum balance of immediate (2017) and longer term (2017-2025) LCLS science objectives. LCLS-II Project deliverables are based on a global view of the future of LCLS, including planned development activities at the LCLS facility that will be pursued in parallel as part of LCLS operations.

The optimum expansion strategy for LCLS must include facilities to support new instruments along with new undulator sources. Although the LCLS and its users are following a meteoric learning curve, consensus is already forming as to what will be the most important extensions of capability. In the following text we will describe these likely extensions and their accommodation within the expanded LCLS facility.

Based on input from the user community, we can identify the following desired future scientific capabilities of LCLS:

1. Extension to harder x-rays >10 keV for the study of thick 3D materials with increased x-ray penetration and spatial resolution.
2. Extended soft x-ray spectral range to below the carbon absorption edge at 280eV for the study of chemical transformations of key carbon based molecular complexes.

3. Creation of transform-limited x-ray pulses, i.e. optimum intensity per bandwidth and pulse length through seeding for improved signal to noise.
4. Availability of linear and circular polaration for the separation of charge and spin effects in materials.

Of the desired capabilities listed above, items 1 and 2 are met by the LCLS-II conceptual design. These are arguably the most important capabilities since they provide LCLS users with extended soft and hard x-ray capabilities.

Considerable effort has been invested in theoretical investigations leading to Item 3, the creation of transform-limited pulses. Based on accelerator research at SLAC and elsewhere in the world, it is clear that the lowest-risk strategy for implementation at all wavelengths to be spanned by LCLS is "self-seeding", in which a "seed" pulse of x-rays is produced from monochromatized Free Electron Laser (FEL) radiation from an LCLS undulator. This pulse is then superimposed on an electron bunch in another undulator for amplification. The result is an amplified replica of the input pulse, rather than amplified shot noise typical of Self Amplified Spontaneous Emission (SASE) radiation. As described in Appendix D, space requirements for self-seeding the LCLS-II hard and soft x-ray sources have been carefully studied, and the results are integrated in the LCLS-II design. An alternative for soft x-ray seeding with significant advantages but more technical risk, "echo-enhanced harmonic generation" (EEHG), is also the subject of active theoretical and experimental investigations at SLAC. A recently proposed technique for hard x-ray self-seeding may reduce the cost of hard x-ray seeding low enough to consider adding this to the LCLS-II scope (see Appendices C and D).

The beam physics issues and radiation properties relevant to item 4, x-ray polarization control, have also been thoroughly studied for soft x-ray photon energies. Appendix D describes alternative approaches that could be implemented in the LCLS-II soft x-ray source. Inclusion of soft x-ray polarization control in LCLS-II would leave insufficient contingency for this stage of planning the project. However the estimated cost is low enough to consider adding this to the LCLS-II scope at a later date. Hard x-ray polarization control may be implemented in a simple manner by crystals and consequently could be provided by LCLS-I operations.

The hard x-ray undulator in the new tunnel, producing x-rays up to 13 keV, provides beam to an experimental area in the new hall. LCLS-II will construct the necessary beam diagnostics and optical transport so that this new hard x-ray beam can be readily used by new experimental stations. As was the case for LCLS-I, concepts for new instruments will be solicited in an open call, and selected by peer review. These instruments will be designed in anticipation of the new capabilities envisioned for LCLS x-ray sources, at the completion of LCLS-II and beyond. This process will unfold over the next few years, and will surely be informed and influenced by new results and discoveries at the hard x-ray instruments just beginning to operate at LCLS. An example of a likely candidate for a new proposal might be a structural biology instrument for imaging of proteins with atomic resolution, employing Multiple Anomalous Diffraction (MAD) phasing at the Se K edge (12.6 keV), and non-resonant imaging of cells and viruses with nanometer resolution. The funding of this instrument could follow the models of the Soft X-ray (SXR) and Matter in Extreme Condition (MEC) instruments, either through a user consortium or direct third party [e.g., National Institutes of Health (NIH) or Biological and Environmental Research (BER)] funding.

3.2 Early Science at LCLS-I

Starting with the first user assisted commissioning experiments in the fall of 2009, the demand for LCLS beam time has outnumbered the available time by more than four to one. The excitement in the scientific community is being fueled by the early results that have already led to several high impact publications (see references) with an additional number in progress. The LCLS performance has significantly exceeded the baseline parameters (pulse length, energy range), a fact that has already proved to be critical for many experiments. Early results also show that many of the suggested concepts are successful. In particular, we have learned that:

- Multi-photon and non-linear processes within atoms and molecules in the short wavelength regime have been observed for the first time as reported in the first published experimental results from the LCLS. Capitalizing on the uniquely intense LCLS pulse focused to a spot of about a micron in diameter, sequential multiple ionization (with each electron ionized by one photon) and even non-sequential ionization (where two photons are required to ionize a single electron) of atoms and molecules have been studied. The intense LCLS pulse also produced a significant fraction of the target atoms and molecules with both K shell electrons ionized, a state referred to as a double core-hole state. Recent, and as yet unpublished, results capitalized on the exceptional chemical sensitivity of double core hole states to identify atoms in different chemical environments within a molecule that cannot be distinguished in typical electron spectroscopy (refs: Young, Berrah, Hoener, Doumy, Fang).

- Pump-probe experiments using an optical laser synchronized with the LCLS x-ray pulse have demonstrated that atomic and molecular targets can be prepared in non-equilibrium or temporally evolving states and can be studied using the x-ray experimental techniques developed at synchrotrons. In recently published results, molecular nitrogen was shown to be impulsively aligned with a short pulse optical laser by measuring ion time-of-flight spectra of the molecules ionized by the subsequent x-ray pulse. The subsequent study used this alignment technique to measure Auger electron spectra of the aligned nitrogen molecules. This technique proves valuable in distinguishing the rich molecular Auger spectral features (to be published) and is immune to the approximations underlying similar synchrotron based coincidence techniques. The short LCLS x-ray pulse is critical for such experiments where a short optical pulse is used to control the molecule under study (refs: Cryan, Glownia).

- A recent, as yet unpublished, x-ray pump-x-ray probe experiment has shown that the double slotted emittance spoiler technique can produce two pulses of few femtoseconds each. They were then used to probe x-ray induced bleaching of core-level resonant absorption in oxygen. This experiment pioneers the use of multiple x-ray pulses separated by less than ~ 200 fs. It has led to another recent experiment that promises to both measure LCLS pulse profile directly in the time domain and to measure the strong x-ray field induced carrier dynamics in thin film materials.

- The concept of `probe-before-destroy' has proven successful, which opens the door for imaging of nanocrystals and nanostructures. Initial hard x-ray protein nanocrystallography experiments, where micron-sized and smaller crystals of photosystem I are suspended in a buffer solution and streamed into the region of interaction with the focused LCLS x-ray beam, have yielded single-shot diffraction patterns that are comparable to the best results obtained with larger crystals at storage ring user facilities. The flexibility in x-ray pulse duration provided by the LCLS provides valuable insight in the quest to maximize signal while minimizing dose (ref: Chapman).

- The concept of single shot imaging of individual viruses and cells has also been realized for the mimivirus (ref: Seibert). In the future, high resolution and three dimensional reconstructions of non-reproducible objects promise significant potential impact on biology
- Soft x-ray single shot spectroscopy and imaging of solids and surfaces is possible. Despite large cross sections, ultra-short pulses can beat electronic "damage", i.e. changes in valence configurations and electron densities. This allows element specific soft x-ray probes to be carried out on ultrafast timescales. Using photoelectron and x-ray emission spectroscopy the ability to characterize temporal evolution of chemical bonds between molecules on surfaces has been demonstrated. This is the first step toward watching surface catalysis in real time on the intrinsic time scale.
- Taking advantage of the transverse coherence of the LCLS single shot holography has been demonstrated. This can be used to image magnetic nanostructures.
- Diffraction from correlated electron systems has been used to study the long-range electronic order from which phenomena such as superconductivity and magnetoresistance originate. The ultrafast temporal development of such electronic order provides nanoscale insight into the emergent properties of these materials.
- Hard x-ray single shot coherent diffraction has been observed on both disordered and crystalline systems.

As a consequence of this early success there is an increasing demand for beam time. Other facilities around the world have taken notice of the early scientific results at LCLS and are accelerating their XFEL projects. To keep up with the increasing demand and stay ahead of the worldwide competition, it is critical to strategically enhance the capacity of the LCLS.

3.3 Scientific Value of Different Capabilities and their Scope within LCLS-II

In this section we shall consider in turn the scientific significance of the four enhanced capabilities listed above. At the end of each section we outline how we plan to implement the capabilities.

3.3.1 Extended Hard X-Ray Capabilities to >10 keV

The extended photon energy range of LCLS-II benefits both x-ray absorption and x-ray scattering experiments. Many elements have prominent inner shell transitions above 8 keV which may be utilized for elemental and chemical specificity in both absorption and resonant or anomalous scattering experiments. Such experiments in the range > 10 keV are commonly carried out at conventional synchrotron facilities.

For many scattering experiments it is not necessary to continuously vary the x-ray energy or fine-tune to a core shell resonance. Generally, however, it is desirable to have a large photon energy exceeding 10 keV. This optimizes probing condensed matter systems on the atomic length scale by minimizing deleterious absorption while preserving scattering cross sections and increasing the available momentum transfer (spatial resolution). LCLS-II, with its intrinsic lateral coherence is envisioned to be especially powerful for the study of disordered solids and liquids with hard x-rays, using techniques like Coherent X-ray Imaging and X-ray Photon Correlation Spectroscopy.

Because of increased x-ray penetration, the energy range above 8 keV will open up access to ultrafast diffraction studies of shock wave induced dynamics, leading, for example, to the understanding of real-time fracture of materials on the nano scale. LCLS-II will enable diffraction studies that elucidate the

symmetries of liquids and disordered materials at the interfaces that control reactivity and stability. These systems will be accessible in their 'natural state' using coherent high energy x-rays from LCLS-II. Such studies will contribute to our understanding of the stability of chemical contaminants in the environment and the structure of reactants at catalytic surfaces. LCLS-II will allow us to go beyond early investigations of photosynthetic water splitting at LCLS. It will teach us how nature efficiently channels energy flow into the reaction center on the femtosecond time scale, pointing the way toward the creation of a viable artificial photosynthetic system.

In our LCLS-II proposal we outlined specific areas of science that would benefit from harder x-rays and we briefly review them here.

3.3.1.1 Understanding Disordered Systems and Their Dynamics

In the last century, x-rays and neutrons have successfully unraveled the structure and dynamics of perfect crystals that are in or close to equilibrium by means of elastic and inelastic scattering studies. The determination of bulk crystalline structure is now routine, and based on concepts like the Brillouin zone and the associated electron, phonon and magnon energy dispersions; a robust understanding of the electronic and magnetic structure and their dynamics has been established.

A challenge of the 21st century is to go beyond periodic systems and equilibrium structure; this is where X-ray Free Electron Lasers (X-FELs) shine. In contrast to crystalline materials, it remains a challenge to properly understand and describe non-periodic or disordered systems such as liquids, glasses, amorphous systems and mesoporous assemblies. The description of the complexity and unique properties of disordered systems requires the determination of the degree of disorder and associated correlation lengths. Typically, conventional diffraction can be used for correlation lengths larger than 3 nm, as is the case for polycrystals, but the determination of local short range order below 3 nm has been notoriously difficult and elusive owing to the weakness of coherent diffraction signals.

Glasses and amorphous systems can exhibit local order and symmetries on nanometer scales while appearing disordered over longer distances. They do not present any translational symmetry but can accommodate different local symmetries within the same system. For example, icosahedral local order is a forbidden motif in periodic structures. The dynamics and lifetimes of these mysterious localized configurations within disordered systems have fascinated scientist for decades. They are predicted to be at the origin of some of the fundamental metastable states of matter such as the undercooled and glassy liquid state which, together with amorphous solids, are of great interest because such materials may display novel smart functions of use in advanced technologies.

Liquids comprise another class of disordered matter with important short-range ordering. Arguably the most important one of all, water, it is also the one presenting the most peculiar properties such as increased density upon melting, increased viscosity under pressure, density maximum at 4°C, high surface tension and many more. One of the most basic unsolved questions remains the microscopic structure of water, which may in fact be fluctuating on the ultrafast time scale. The ultra-short pulse duration of the LCLS may be capable of providing a single structural snapshot in liquid water, on time scales much faster than the dynamical rearrangement of the hydrogen bonding network.

Because of the possibility of increased momentum transfer, hard x-rays are particularly valuable for the study of the short range structure. LCLS-II ensures that the pulses have diffraction capabilities at atomic resolution while allowing snap shots of dynamics on a time scale that is only limited by the pulse length.

3.3.1.2 Understanding Photosynthetic Water Splitting

The light-induced oxidation of water to dioxygen during photosynthesis by green plants and cyanobacteria is a process that occurs throughout the biosphere and is essential to life on Earth. Coupled to the reduction of carbon dioxide, biological photosynthesis contributes foodstuffs for nutrition while recycling CO_2 from the atmosphere and replacing it with O_2. By utilizing sunlight to power these energy-requiring reactions, photosynthesis serves as a model for addressing societal energy needs as we enter an era of climate change and diminishing fossil hydrocarbon resources.

Central to this problem is the question: What is the molecular and electronic structure of the Oxygen-Evolving Complex (OEC), containing a Mn_4CaO_X complex, of Photosystem II (PS II) in its ground state and throughout the catalytic cycle? Results based on x-ray crystallography have produced maps of moderate resolution (2.9-3.8 Å). While there is essential agreement among the crystallographic models about the location of the Mn_4Ca cluster within the PS II complex, there is no agreement about the proposed arrangement of metal atoms within the cluster.

Synchrotron-based crystallography is fundamentally limited by the problem of radiation damage. X-ray diffraction from PS II crystals using coherent ultra-short pulses can possibly overcome this limitation. In order to solve the structure of the intact Mn_4Ca cluster at atomic resolution, the x-ray photon energy must be at least 12 keV, and the largest possible flux must be provided.

3.3.1.3 Understanding Materials in Extreme States

Hard x-rays are particularly important for probing samples in-situ at high pressure. The threshold of one absorption length for a pair of 2.5 mm-thick diamonds with which most x-ray diffraction experiments have been conducted is 15 keV. Extending the tunability of the photon energy of the existing LCLS undulator up to 20 keV makes possible such experiments in the ultra fast domain enabling high-pressure Diamond Anvil Cell (DAC) studies such as anomalous x-ray diffraction for element specific crystal structure, and x-ray absorption, x-ray Raman scattering and x-ray emission spectroscopies [X-ray Absorption Scattering (XAS), X-ray Raman Scattering (XRS), X-ray Emission Spectroscopy (XES)] for precise atomic and electronic structure determinations. Combining these techniques with temporal resolution on the femtosecond time scale is particularly powerful for the study of disordered systems under extreme pressures and temperatures.

The behavior of materials under thermomechanical extremes of high pressure and temperature is at the heart of many energy problems and scientific investigations. Major breakthroughs and discoveries have been made by compressing samples to megabar pressures in a DAC, heating to thousands of degrees with a focused infrared laser through the optically transparent diamond windows, and probing with synchrotron radiation. Laser-heating, however, is associated with a set of intrinsic problems that restrict the temperature stability, uniformity, temporal structure, maximum temperature limit, and coordination with the x-ray beam from a storage ring source. These problems could be resolved by using the intense pulsed x-rays from LCLS-II to heat *and* probe the DAC samples.

X-ray heating in a DAC offers exciting opportunities, enabling materials studies in many disciplines. It could open the whole suite of static high-pressure probes for warm condensed matter ($> 10^4$ K) research, which is currently only accessible by dynamic studies with very limited probes. It could advance studies of planetary interiors, enabling study of the Earth's inner core pressure-temperature conditions (330–360 GPa, 5000-6000 K) for the first time, and open the outer core conditions for routine, reproducible investigations. The element-specific characteristics of x-ray heating can be used for precise high pressure-temperature studies of a large range of materials. Heating with pulsed x-rays, will also enable a variety of chemical kinetics, calorimetric, and transport properties measurements.

3.3.1.4 LCLS-II Strategy to produce Hard X-Rays > 10keV

LCLS-II extends the photon energy range to high energies in two ways. The LCLS-II hard x-ray undulator is designed to reach a maximum photon energy of 13 keV, beyond the 9 keV maximum where the LCLS-I can presently operate. The 13 keV maximum photon energy provides access to the Se K edge, which has been important for protein crystallography experiments. In addition, the move of the Atomic, Molecular and Optical Science (AMO) and SXR instruments to the LCLS-II soft x-ray undulator allows the modification of the LCLS-I undulator. In this undulator the magnetic gap will be increased by exchanging shims in the support structures. This modification will decrease the K parameter allowing the LCLS-I undulator to reach 20 keV. Extending the maximum photon energy to a higher value reduces the pulse energy; for example, the modification of the LCLS-I undulator raises the maximum photon energy from 10 to 20 keV but lowers the pulse energy by a factor of two at 10 keV. Consequently, it has been deemed optimal to provide a maximum photon energy of 13 keV at the LCLS-II HXR undulator and 20 keV at the modified LCLS-I undulator.

3.3.2 Extended Soft X-ray Capabilities down to 250eV

The extension of the lower design limit of the LCLS spectral range from 800 eV to 250 eV, and the ability to fine tune the x-ray energy, creates significant new scientific opportunities. The LCLS facility after the LCLS-II upgrade will reach the K absorption edges of the important elements C (280 eV) and N (400 eV), which are presently outside the spectral range of LCLS, in addition to O (530 eV), which has recently been reached at LCLS. The chemistry of carbon, nitrogen and oxygen underlies some of the most important processes in our world. Life in its present form would not exist without photosynthesis involving the sunlight initiated catalytic conversion of water and CO_2 into oxygen and hydrocarbons. This process generates both molecular oxygen and basic hydrocarbon food and thus constitutes the basic of life as we know it. Catalytic processes involving various carbon complexes underlie some of the largest industries worldwide, the chemical and oil industries with world-wide revenues of nearly five trillion dollars. They provide the world with many of the basic products underlying everyday life such as pharmaceuticals, plastics, fertilizers, petrochemicals and gasoline. LCLS-II will play a significant role in understanding the temporal evolution of chemical processes and bonding associated with the key elements C, N and O.

3.3.2.1 Real Time Observation of Surface Reactions in Catalysis

Nearly all chemical reactions of importance to mankind occur at surfaces and interfaces. As such, catalytic processes on solid surfaces form the backbone of the chemical industry and are involved in most chemical transformations related to renewable energy. One of the great challenges in surface chemistry is to capture and ultimately control the transition states active in surface reactions. Probing reaction dynamics on the femtosecond time scale and monitoring the electronic and geometric structural changes along the reaction path of elementary processes will enable us to obtain a full picture of surface mediated chemical reactions which are at the very core of catalysis.

Following real-time surface chemical transformations has always been a major goal and challenge in surface dynamics. In most ultrafast dynamics studies the reaction is triggered by an optical laser pulse and the response of the reactants is monitored by a molecule-specific probe such as vibrational-resonant sum-frequency generation. However, most of these studies have been related to vibrational dynamics, desorption, and diffusion processes, and have not directly followed a reaction in which a species is fully transformed. Due to the low concentration of reactants, large substrate absorption, and extremely short electronic excited state lifetimes, the tools of ultra-fast spectroscopy developed for studies in bulk media have not been generally applicable to metal surfaces.

Both X-ray Emission Spectroscopy (XES) and X-ray Photoelectron Spectroscopy (XPS) have the unique ability to provide an atom-specific probe of the electronic structure and application of these techniques to ultra-fast spectroscopy would open entirely new windows into the realm of atomic motion and electronic structure rearrangements, and thereby chemical dynamics. Since most of the molecular species of importance to the essential catalytic processes contain C, N and O atoms we need a soft x-ray source that covers the energy region starting somewhat below the carbon K edge at 280 eV to the oxygen K edge at 530 eV.

3.3.2.2 Understanding Correlated Materials

Many fascinating phenomena exhibited by correlated materials are known as “emergence” in which electrons form a variety of exotic quantum phases bearing little resemblance to expectations derived from the constituents of the compounds alone. These exotic phases, including unconventional high temperature superconductivity, charge/spin ordering, fractional quantum Hall effects, etc., are derived from strongly intertwined spin, charge and lattice degrees of freedom. The delicate interplay between these degrees of freedom also causes these exotic phases to be extremely sensitive to the external perturbations, generally yielding rich phase diagrams as functions of chemical compositions and external (magnetic) fields of correlated materials. The proximity of various phases, especially near a quantum critical point, can partition a material into electronically distinct domains which experience temporal and spatial fluctuations over many time and length scales.

The spectral range of 250-800 eV covers many important absorption edges of a wide range of interesting correlated materials. Especially for the important transition metal oxides, tuning to different absorption edges such as the oxygen K-edge (~ 530 eV) and the L-edges of manganese (~640 eV), iron (~710 eV), cobalt (~780 eV), and nickel (~850 eV) provides important complementary information on the hybridized metal-3d and ligand oxygen-2p orbitals which determine the ground state properties and the low energy excitations. With the unique time structure of x-ray produced by the LCLS-II, dynamics of these electronic states can be studied with a temporal resolution of 10 fs. In addition, this spectral range also covers the K-edges of carbon (~ 280 eV), allowing the study of carbon-based materials, such as C60 and diamondoids, which is also a focus of band-gap engineering at the quantum level in small molecules.

3.3.2.3 LCLS-II Strategy to produce Soft X-Rays > 250eV

The LCLS-II extends the photon energy range to lower energies through the design of the soft x-ray undulator. The LCLS-II soft x-ray undulator, described in Chapter 7, has a variable magnetic gap and can access photon energies as low as 250 eV. This new soft x-ray source will also provide a considerable increase in brightness compared with present LCLS performance.

3.3.3 Creation of Transform-limited X-Ray Pulses through Self-Seeding

Two important measures of the quality of a photon source are its “transverse” and “longitudinal” coherence. Conventional SASE X-FELs like LCLS-I provide transversely coherent beams but only limited longitudinal coherence. The x-rays are in phase for tens of micrometers across a plane perpendicular to the beam direction and produce a well defined interference or scattering pattern but they are only in phase across a slice of tens of nanometers along the beam direction. When the sample is thinner than the longitudinal coherence length, SASE beams are sufficient for coherent imaging, and even such imperfect beams can therefore be used for coherent imaging of non-periodic objects such a macromolecules or materials in the form of thin films.

More sophisticated experiments, however, require both transverse and longitudinal coherence. Longitudinal or temporal coherence is defined by the spectral or band width of the x-rays and the

longitudinal coherence length is given by $\xi = \lambda(\lambda/\Delta\lambda)$ where λ is the wavelength. For SASE X-FEL pulses one typically has $\lambda/\Delta\lambda \sim 200$, indicating the limited value of ξ, especially at short wavelengths. In principle, one can create a longitudinally coherent source by use of a monochromator with $\lambda/\Delta\lambda$ values of a few thousand, but this is often undesirable because of loss of intensity. Also for pulsed sources like X-FELs, monochromatization may lengthen the pulse because the product of pulse length Δt and energy band width ΔE must exceed a minimum value defined by the energy-time uncertainty relation $\Delta E\ \Delta t \geq \nabla$. In practice, one uses the classical Fourier transform method to define the minimum correlation value which depends on the pulse shape. An important goal for advanced X-FEL sources like LCLS-II is the creation of x-ray pulses which for a given pulse length have the minimum allowed energy width. Such pulses are called "transform-limited".

Transform-limited pulses are important for several reasons. First they naturally provide the maximum intensity within the minimum energy window for a given pulse length and therefore no monochromator is needed. Second, time dependent measurements with transform-limited pulses may be Fourier transformed into the frequency domain yielding complementary information to experiments that measure energy spectra. Third, for coherent imaging of 3D (thick) samples the longitudinal coherence properties of a SASE beam may be insufficient because the x-rays need to be in phase over the entire sample thickness. Fourth, transform-limited pulses maximize the number of photons in the coherence volume (degeneracy parameter) and therefore are desirable for studies of all non-linear processes.

Finally, for LCLS-II, transform-limited pulses are particularly valuable since they naturally support efficient beam splitting of hard x-ray beams by Bragg diffraction. In contrast to the broad SASE bandwidth $\Delta\lambda/\lambda \sim 10^{-3}$ - 10^{-2}, transform-limited x-ray bandwidths are of order 10^{-4}, for < 10 fs x-ray pulse durations, and match the Bragg width of crystal monochromators. Thus by use of thin crystals one may obtain two split beams, a transmitted as well as a Bragg reflected beam, with minimum intensity loss.

3.3.3.1 LCLS-II Strategy to produce Transform-limited Pulses

We have an ongoing R&D program to produce transform-limited pulses by self-seeding. In this scheme one superimposes a photon pulse created by monochromatizing the SASE radiation from a first undulator on the electron bunch as it traverses a second undulator. One no longer relies on the formation of self-nucleating regions as in SASE but imprints or "seeds" longer-range order in the electron beam by the superimposed well defined photon field. The FEL amplification process will proceed; however the seeding field ensures that the proper phases are imprinted on the electron bunch throughout its length. This process is aided by the fact that the imprinting photon field advances exactly by one wavelength λ relative to the electron bunch per undulator period, since the electrons move slightly slower than the speed of light c. The properties of the amplified x-ray pulse are determined by the imprinted order of the seed. The brightness is enhanced over the SASE case by a factor of about 100. This enhancement is the result of reducing the bandwidth of the FEL radiation by about a factor of 100 while keeping the number of photons constant.

Over the next few years we will be exploring how to create transform-limited pulses by means of seeding, with emphasis on hard x-rays. We are emphasizing hard x-rays because the payoff is expected to be highest. The seeding schemes are described in detail in Appendix D. The seeding is included in the Conceptual Design Report (CDR) future work and falls outside the scope of LCLS-II because of needed R&D, in particular, to experimentally demonstrate hard x-ray seeding. If the novel concept for hard x-ray seeding is proven, its estimated cost is low enough to consider adding to the LCLS-II scope.

3.3.4 Variable X-Ray Polarization

The dominant interaction of photons with the charge and the spin of the sample arises from the action of the electric field vector. Linearly polarized light preferentially accelerates the charge in the direction of the *E*-field and can therefore probe anisotropies of the charge distribution in a sample. Circularly polarized light possesses an angular momentum which can couple (through the spin-orbit interaction) to the spins or magnetic moments in the sample. The ability to study and differentiate charge and spin phenomena in materials through polarization dependent x-ray absorption and scattering measurements has been extensively and successfully used for the last 20 years.

The largest impacts of polarization dependent x-ray studies have been in surface science (linear polarization) and magnetic materials (circular polarization), because of the intrinsic anisotropy of such systems. While surfaces themselves are anisotropic, structural and bonding anisotropies are even stronger in chemisorbed molecules. Over the years, linearly polarized soft x-rays have been extensively used to determine orientational anisotropy and reactivity effects for molecules bonded to surfaces.

The second major field of impact of polarized x-rays has been in the field of nano magnetism. Here circularly polarized light has been used to determine the size of magnetic moments and their anisotropies in thin films and multilayers and to image magnetic order on the nanoscale. For modern nanoscale magnetic materials consisting of a small number of atoms, x-rays have emerged as the technique of choice, overcoming the limitation in spatial resolution of optical lasers and the small cross sections of neutrons. X-Rays have proven particularly powerful when their nanoscale spatial resolution is combined with femtosecond temporal resolution. In this area the capabilities of x-rays are truly unique.

More generally, polarization dependent studies provide the means of distinguishing charge and spin effects in materials, and variable polarization beam lines have become important assets of all synchrotron radiation facilities. LCLS-I does not offer the ability of polarization control and the beams are simply linearly polarized.

Polarization control is most important yet most difficult in the soft x-ray region. While x-ray transmission through Bragg phase shifters can be used to change the polarization at hard x-ray energies, in the soft x-ray region the polarization needs to be controlled by means of changes in the electron beam trajectory in the undulator source.

The scientific importance of soft x-rays arises from the large cross sections and large size (up to about 30%) of polarization dependent effects at absorption edges and the fact that the key absorption edges lie in the soft x-ray region. For example, the soft x-ray region contains the K edges of key chemical elements C, N and O and through $1s \rightarrow 2p$ dipole transitions information is obtained of the bonding contributions of the *p* valence orbitals. Also in the soft x-ray region are the L edges of the 3*d* transition metal elements which through $2p \rightarrow 3d$ dipole transitions give information on the *d* valence orbitals responsible for magnetism and the role of the *d*-orbitals in correlated oxide materials. The elementary ferromagnets Fe, Co and Ni, for example, form the basis for information storage in the form of nanoscale magnetic bits, while novel and fascinating phenomena associated with transition metal oxides such as high temperature superconductivity and colossal magnetoresistance not only challenge the existing concepts of condensed matter physics, but these materials may become the basis for a post-silicon technology era.

3.3.4.1 Femtosecond Control of Spins on the Nanoscale

As an example we mention the technological demand for the ever-increasing speed of information storage and processing. This has triggered an intense search for ways to control the magnetization by

means other than magnetic fields which in practice are always created by current flow in wires. Because of the induction laws such current pulses have limited the processing times per bit to tens of picoseconds or tens of GHz. A promising approach to overcome the present speed limit is the control of the magnetization by light pulses, the shortest man-made triggers. Many groups are presently exploring the question whether polarized laser light can manipulate or even switch the magnetization. This could revolutionize the speed of data storage and manipulation.

In order to follow the evolution of the magnetization triggered by a laser pulse, it is important to have circularly polarized x-rays. However, they are presently not available at LCLS.

3.3.4.2 LCLS Strategy to produce Variable Polarization

For the reasons given above, our plans for polarization control at LCLS-II mostly concentrate on soft x-rays. At LCLS-I, elliptical polarization has been generated by a transmission multilayer; however this method has a quite low efficiency of 10^{-2} - 10^{-3}. A description of several schemes which produce variable polarization directly from the undulator source are presented in Appendix D. Determining which of these schemes is most effective is an area of ongoing investigation at the LCLS. All schemes involve adding an APPLE-type undulator at the end of the LCLS-II soft x-ray undulator. Space is reserved in the LCLS-II design for this APPLE-type undulator. Variable polarization is included in the CDR future work and falls outside the scope of LCLS-II. Inclusion of soft x-ray polarization control in LCLS-II would leave insufficient contingency for this stage of planning the project. However the estimated cost is low enough to consider adding this to the LCLS-II scope at a later date.

3.4 References

Berrah, et al, *Non-linear processes in the interaction of atoms and molecules with intense EUV and X-ray fields from SASE free electron lasers (FELs),* Journal of Modern Optics **57**, 1015 (2010) doi: 10.1080/09500340.2010.487946

Chapman, et al, *Femtosecond X-ray Protein Nanocrystallography,* Nature 470, 73–77 (03 February 2011) doi:10.1038/nature09750

Cryan, et al, *Auger Electron Angular Distribution of Double Core-Hole States in the Molecular Reference Frame,* Phys. Rev. Lett. **105**, 083004 (2010) doi: 10.1103/PhysRevLett.105.083004

Doumy, et al, *Nonlinear Atomic Response to Intense Ultrashort X Rays,* Physical Review Letters 106, 083002 (24 February 2011) doi/10.1103/PhysRevLett.106.083002

Fang, et al, *Double Core-Hole Production in N2: Beating the Auger Clock,* Phys. Rev. Lett. **105**, 083005 (2010) doi: 10.1103/PhysRevLett.105.083005

Glownia, et al, *Time-resolved pump-probe experiments at the LCLS*,Optics Express **18**, 017620, (2010) doi:10.1364/OE.18.017620

Hoener, et al, *Ultraintense X-Ray Induced Ionization, Dissociation, and Frustrated Absorption in Molecular Nitrogen,* Phys. Rev. Lett. **104**, 253002 (2010) doi: 10.1103/PhysRevLett.104.253002

Seibert et al *Single Mimivirus Particles Intercepted and Imaged with an X-ray Laser,* Nature **470**, 78–81 (03 February 2011) doi:10.1038/nature09748

Young, et al, *Femtosecond electronic response of atoms to ultra-intense X-rays*, Nature **466**, 56 (2010) doi:10.1038/nature09177

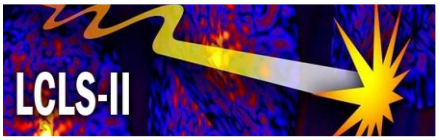

4 FEL Physics

Technical Synopsis

This chapter presents an introduction to the Free Electron Laser (FEL) physics and the general requirements on the electron beam parameters in order to support FEL lasing and saturation for output photon energies in the 250 eV to 13-keV range. It also describes the FEL transverse and temporal properties in the Self Amplified Spontaneous Emission (SASE) mode, which is the baseline for the LCLS-II.

4.1 Introduction and Overview

An FEL is a tunable source of coherent radiation that uses a bunch of relativistic electrons to resonantly amplify an electromagnetic wave through an undulator. The initial electromagnetic wave can be an external source that co-propagates with the electron bunch or the spontaneous emission generated by random electron microbunching (i.e., shot noise) in the undulator. Resonant interaction between the wave, the undulator field, and the electron bunch creates coherent electron density modulations on the scale of the resonant wavelength, which then lead to the exponential growth of the radiation power at this wavelength in a long undulator. The exponential growth in radiation power ceases when the FEL-induced energy spread on the electron bunch stops and then begins to decrease the FEL microbunching.

The first lasing and operation of the LCLS-I [1] has produced results in very good agreement with standard FEL theory and numerical simulations, indicating that FEL physics in the x-ray wavelength range is well understood. The LCLS-II FEL design is closely based on the very successful LCLS-I FEL design. The main differences are the use of variable-gap undulators instead of fixed-gap undulators, as well as the arrangement of two undulator lines in parallel. The baseline LCLS-II will operate in SASE mode for both the hard and soft x-ray FELs. Future expansion options for the LCLS-II include polarization control and seeding for both FELs.

The basic electron beam requirements are discussed in Section 4.2 and the expected x-ray FEL characteristics are discussed in Section 4.3.

4.2 Electron Beam Requirements

A relativistic electron beam entering the undulator will generate spontaneous undulator radiation. If the beam energy is γmc^2, the undulator period is λ_u, and the undulator parameter is K, the wavelength of the undulator radiation in the forward direction is

$$\lambda = \frac{\lambda_u}{2\gamma^2}\left(1+\frac{K^2}{2}\right). \tag{1}$$

The undulator parameter K is defined as

$$K = \frac{eB_0\lambda_u}{2\pi mc} = 0.934 B_0[Tesla]\lambda_u[cm], \tag{2}$$

where B_0 is the peak magnetic field for a planar undulator. For a variable-gap undulator (see Chapter 7), the magnetic field can be changed by adjusting the undulator gap, and the typical field strength can be varied from a few kG to slightly above 1 Tesla. For a permanent magnet undulator that has a few cm-long period, the undulator parameter K varies between 1 and 10. For the LCLS-II hard x-ray FEL, undulator parameters have been chosen such that a 13 GeV beam is necessary to generate 1 Angstrom wavelength radiation.

The spontaneous radiation can be amplified by the FEL instability if the electron beam quality is sufficiently high; this process has been called self-amplified spontaneous emission (SASE) [2,3]. High gain FELs are often characterized by the FEL Pierce parameter ρ [3]

$$\rho = \left(\frac{1}{16}\frac{I_{pk}}{I_A}\frac{K^2[JJ]^2\lambda_u^2}{4\pi^2\gamma^3\sigma_x^2}\right)^{1/3} = \left(\frac{1}{4}\frac{I_{pk}}{I_A}\frac{K^2[JJ]^2\gamma\lambda^2}{(1+K^2/2)^2 4\pi^2\sigma_x^2}\right)^{1/3}. \tag{3}$$

Here I_{pk} is the electron peak current, I_A=17 kA, [JJ] is the Bessel function coupling factor associated with a planar undulator, γ is the electron beam Lorentz factor, and σ_x is the rms electron beam size in the undulator. The SASE process is largely determined by the FEL Pierce parameter, which ranges from 3×10^{-3} for soft x-ray FELs to 5×10^{-4} for hard x-ray FELs. For example, the power gain length is

$$L_G = (1+\eta)L_{G0} \text{ with } L_{G0} = \frac{\lambda_u}{4\pi\sqrt{3}\rho}, \tag{4}$$

where η is a gain degradation parameter due to radiation diffraction, beam emittance and energy spread [4]. The FEL saturation power is roughly ρP_{beam}, where P_{beam} is the electron beam power. Beginning from shot noise, it typically takes a SASE FEL about 18 to 20 L_G to reach saturation.

The electron beam quality has to be extremely high in order to obtain a relatively short FEL gain length (i.e., η in Equation (4) should be smaller than unity). For a typical x-ray FEL, this requires

$$I_e \sim \text{a few kA}, \quad \varepsilon_{x,y} \sim \lambda/(4\pi), \qquad \sigma_\delta << \rho. \tag{5}$$

Here all beam parameters refer to their "slice" values (i.e., those corresponding to temporal slice whose length is that of a typical SASE spike as described in Section 4.3. The high peak current electron bunch can be obtained by magnetic bunch compression upstream in the linac. The unnormalized emittance in Equation (5) is determined by the final beam energy, the injector performance, and control of any emittance degradation that can occur in the bunch compressors and other dipole optics , or might arise from wakefields associated with the linac cavities. The relative energy spread is determined by the final beam energy, intentional growth via a laser heater (to control the longitudinal microbunching instability) just downstream from the injector, and by conservation of longitudinal emittance in the bunch compression process. The FEL design parameters and simulation studies will be given in Chapter 5. The chosen accelerator design to achieve the required electron beam beam brightness will be presented in Chapter 6.

4.3 FEL X-Ray Properties

The SASE FEL radiation from a planar undulator is linearly polarized in the plane of the electron's wiggle motion. The resonant interaction between the relativistic electrons, the undulator and radiation will amplify spontaneous emission that lies near the fundamental undulator radiation frequency. The typical SASE bandwidth at FEL saturation is [5]

$$\frac{\sigma_\omega}{\omega} \approx \rho \sim 3\times10^{-3} \text{ to } 5\times10^{-4}. \tag{6}$$

Although many transverse modes can be excited at the beginning of the undulator, by the end of the exponential growth regime a fundamental mode with the highest growth rate (generally the TEM00 mode) will dominate. As a result, a SASE FEL has excellent transverse coherence at saturation and can usually be approximated by a fundamental Gaussian mode. In the x-ray wavelength range, the rms radiation mode size in the exponential growth regime can be estimated by [6]

$$\sigma_r = \sqrt{\sigma_x \sigma_D}, \text{ with } \sigma_D = \sqrt{\frac{\lambda L_{G0}}{4\pi}}. \tag{7}$$

The rms divergence is then

$$\sigma_{r'} = \frac{\lambda/(4\pi)}{\sigma_r} = \frac{\left(\lambda/(4\pi)\right)^{3/4}}{L_{G0}^{1/4}\sigma_x^{1/2}} . \quad (8)$$

After FEL saturation, the radiation divergence stays more or less constant, while the rms mode size starts to increase due to diffraction. Therefore, Equation (8) can be regarded as a lower limit of the FEL divergence angle.

Due to its startup from shot noise, the temporal behavior and fluctuations of a SASE FEL are those of chaotic, polarized light. The SASE light consists of random temporal spikes whose characteristic duration is the coherence time [7]. Close to FEL saturation, the coherence time is given by

$$\tau_c = \frac{\sqrt{\pi}}{\sigma_\omega} \approx \frac{\lambda/c}{2\sqrt{\pi}\rho} . \quad (9)$$

If the radiation pulse duration T is much longer than τ_c, the radiation will consist of $M > 1$ independent modes. The shot-to-shot statistical fluctuation of the SASE pulse energy W in the exponential growth regime is then given by

$$\frac{\sigma_W}{<W>} = \frac{1}{\sqrt{M}} \text{ , where } M = \frac{T}{\tau_c} . \quad (10)$$

In the frequency domain, the SASE spectrum also exhibits spiky behavior, with M independent modes falling within the full normalized spectral bandwidth ~2ρ. For the nominal LCLS-II 250 pC bunch charge and 80 fs bunch duration, M can be on the order 100. The statistical fluctuation before saturation can thus be on the level of 10%. Saturation effects reduce the statistical fluctuation to a much smaller level.

In addition to statistical fluctuations, the output SASE pulse energy will fluctuate when the machine parameters change from shot to shot. For baseline design parameters with M~100, we expect that that shot-to-shot machine variations typically will be the dominant source of fluctuations.

In a high-gain FEL near saturation, strong microbunching at the fundamental wavelength can drive substantial levels of harmonic microbunching. For a planar undulator, this harmonic microbunching can lead to significant radiation at the odd harmonics being generated in the forward direction, with the third harmonic power reaching the 1%-level relative to the fundamental power at saturation [6]. The relative spectral bandwidth of the harmonic radiation is similar to that of the fundamental. Since even harmonics can only be emitted off-axis for aligned electron beams, the coherent radiation from even harmonic microbunching is largely suppressed. For example, the 2nd harmonic content is expected to be on the order of 10^{-4} as compared to the fundamental power level.

The baseline LCLS-II project will construct two SASE-based undulator lines. To reduce the output radiation bandwidth and to suppress the spiky temporal structure arising from the SASE process, possible future LCLS-II upgrades include self-seeding and external seeding options. Polarization control units could be added after the main planar undulator to provide flexible x-ray polarization. These future upgrade options are discussed in Appendix D.

4.4 References

1. P. Emma et al., *First lasing and operation of an ångstrom-wavelength free-electron laser*, Nature Photonics **4**, 641 (2010).

2. K. Kondratenko and E. Saldin, *Generating of coherent radiation by a relativistic electron beam in an ondulator*, Part. Accel. **10**, 207 (1980).

3. R. Bonifacio, C. Pellegrini, and L. Narducci, *Collective instabilities and high-gain regime in a free electron laser*, Opt. Commun. **50**, 373 (1984).

4. L.-H. Yu, S. Krinsky, R. Gluckstern, *Calculation of universal scaling function for free-electron-laser gain*, Phys. Rev. Lett. **64**, 3011 (1990);

   M. Xie, *Design Optimization for an x-Ray free electron laser driven by SLAC linac*, in Proceedings of the 1995 Particle Accelerator Conference (IEEE, Piscataway, NJ, 1995), p. 183.

5. K.-J. Kim, *Three-dimensional analysis of coherent amplification and self-amplified spontaneous emission in free-electron lasers*, Phys. Rev. Lett. **57**, 1871 (1986);

   J.-M. Wang and L.-H. Yu, *A transient analysis of a bunched beam free electron laser*, Nucl. Instrum. Methods A **250**, 484 (1986).

6. Z. Huang and K.-J. Kim, *Review of x-ray free-electron laser theory*, Phys. Rev. ST Accel. Beams **10**, 034801 (2007).

7. E. Saldin, E. Schneidmiller, and M. Yurkov, *Statistical properties of radiation from VUV and X-ray free electron laser*, Opt. Commun. **148**, 383 (1998).

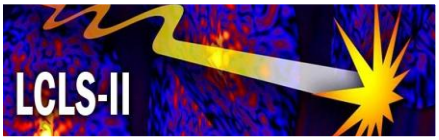

5 FEL Parameters and Performance

Technical Synopsis

The Free Electron Laser (FEL) parameter optimization and performance characterizations that are described in this chapter are based upon three-dimensional theory and computer models. The investigations led to a selection of the best parameters while also examining performance sensitivity to changes in beam characteristics, accelerator components and to unavoidable imperfections in the settings of the beam characteristics, magnetic and mechanical components and electron beam monitoring. The focusing of the electron beam plays an important role in the production of the FEL radiation. The LCLS-II undulator optics design has been optimized in terms of its focusing lattice and strength. The electron optics consists of 8.8-m long Focusing-Drift-Defocussing-Drift (FODO) cell. Focusing is provided by placing electromagnetic quadrupoles in the breaks between the undulator sections, while electron orbit correction is obtained by small lateral displacements of the quadrupoles. Simulations indicate that the HXR FEL radiation saturates at a length of ~92 m and the SXR FEL radiation at a length of ~55 m. The proposed LCLS-II undulator system has a total magnetic length of about 108.8 m for HXR and 61.2 m for SXR, since it is a requirement that the FEL operate in the saturation regime. This choice not only gives the maximum output power, but also reduces the pulse-to-pulse fluctuations of the radiation.

Complete simulations of the LCLS-II, starting from the photocathode, and continuing through injector, linac, and undulator have been carried out to gain an understanding of each system's impact on LCLS-II operation. The simulations, reported in this chapter, include thermal, Radio Frequency (RF), and space charge effects in the injector system, and wakefields and Coherent Synchrotron Radiation (CSR) in the linac-compressor system. The results of the simulations, presented for 0.25 nC bunch charge, show that, under idealized conditions, the vertical and horizontal beam slice emittances are small, about 0.6 mm mrad (normalized) and well preserved through linac and bunch compressors. Even with this small beam emittance, wakefield effects in the linac and compressors reduce the LCLS-II output power and produce a transverse displacement and energy tails along the bunch

The possibility of changing (i.e., lowering) the output radiation power was investigated. This may be desirable if the peak power on the sample is excessive and/or if required for other experimental purposes. The reduction in power, by either reducing the electron current or by increasing the beam emittance, is accompanied by an increase in fluctuations of the output power due to fluctuations in the beam characteristics from pulse-to-pulse, since the FEL no longer operates in the saturation regime. Power can also be controlled through a slotted spoiler, which spoils the emittance for most of the bunch except for a small slice. This control couples power with bunch length, which is often undesirable. Such coupling also exists when using bunch charge to control power. The latter also changes linac wakefield and effects stability. For this reason, a better way to reduce output power is by placing an FEL absorption cell in the path of the radiation, as discussed in Chapter 8.

During LCLS-II commissioning both the electron beam and the x-ray radiation will be intensively studied and compared to the predictions of these simulations.

5.1 Introduction and Overview

The FEL SASE process will produce pulses of coherent x-ray radiation in the LCLS-II undulator with a harmonic spectrum that is wavelength-adjustable over a large range. The operational wavelength can be controlled by changing the energy of the electrons as described in Chapter 4 or by changing the undulator gap. The LCLS-II linac is designed to accelerate electrons to a final energy that is adjustable within the operational nominal range between 4.2 GeV and 13.5 GeV. The FEL photon energy is proportional to the square of the electron energy and dependent on the gap height of the variable gap undulators. The supported fundamental FEL photon energy range is 0.25 keV – 2 keV for the Soft X-Ray (SXR) undulator and 2 keV – 13 keV for the Hard X-Ray (HXR) undulator. There will also be coherent 3rd harmonic radiation emission at about 1% of the fundamental intensity. In addition to the coherent harmonic emission, there will be a continuous spectrum of ordinary, incoherent undulator radiation; this component will be much more intense than that found from ordinary insertion devices due to the high energy of the electron beam and the great length of the undulator.

There will be two undulators, aligned in parallel, one for each spectral range (HXR and SXR). Each undulator consists of individual undulator segments (32 for HXR and 18 for SXR) that are separated from one another by 1-m-long breaks that provide space for focusing, steering, vacuum components and longitudinal phase shifters. The latter consist of extremely weak chicanes and are required by the variable gap design.

For the proposed LCLS-II baseline parameter set, FEL theory [1] predicts that the SASE process will saturate at or before 92 m for the HXR undulator and at or before 52 m for that of the SXR. These lengths include the breaks between undulator segments. The tolerance budget for the undulator and the electron beam parameters has been set to limit the increase in saturation length to no more than 2 (power) gain lengths, or about 10 m, leading to a total magnetic length of the LCLS-II undulators of 108.8 m (HXR) and 61.2 m (SXR).

5.2 Layout, Nominal Parameters and Operating Range

5.2.1 Layout of the HXR and SXR Undulators

The LCLS-II undulator system will be comprised of two separate undulators, one for producing hard x-ray (HXR) radiation the other for soft x-ray (SXR) radiation. Both undulators will be mounted in parallel and will need to cover different photon energy ranges for the same electron beam energy. A conceptual layout is shown in Figure 5.1. Each of the two undulators will be comprised of individual undulator segments, each 3.4 m in length. These segments will be separated by 1-m-long break sections that will house a quadrupole, an RF cavity Beam Position Monitor (BPM), and a longitudinal phase shifter. A listing of the main dimensions is given in Table 5.1.

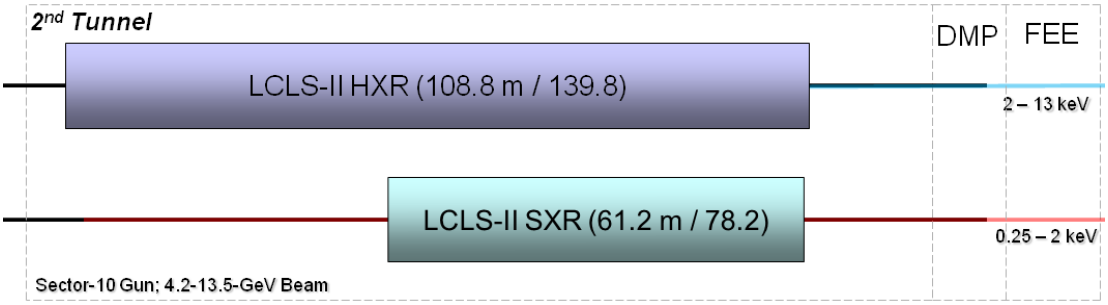

Figure 5.1. Layout of the two LCLS-II undulators in the new tunnel.

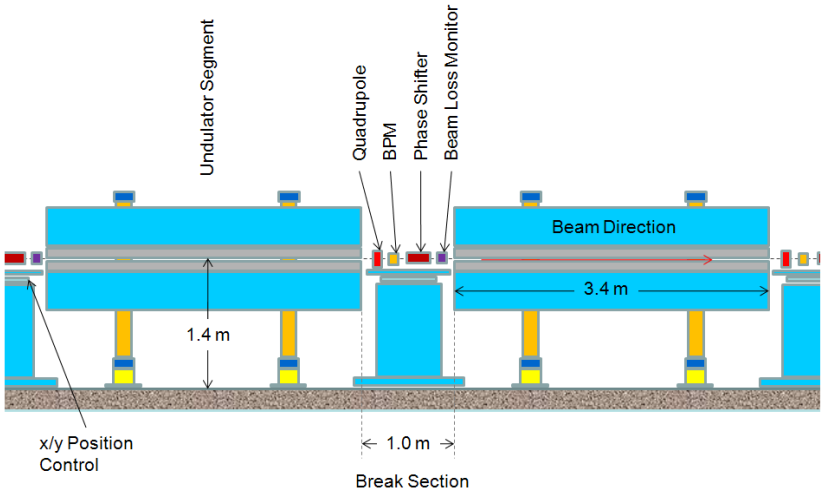

Figure 5.2. Layout of a cell in each of the two undulators. The board supporting the break section components will be equipped with remote x/y position adjusters in support of beam base alignment.

Table 5.1. Basic nominal LCLS-II undulator dimensions.

Parameter	Symbol	Unit	HXR	SXR
Undulator gap	g	mm	7.2 – 20.1	7.2 – 35.5
Undulator period length	λ_u	mm	32	55
Number of periods per segment			106	61
Individual segment length	L_{seg}	m	3.400	3.400
Number of installed segments			32	18
Total length of all installed segments	$L_{u,mag}$	m	108.800	61.200
Break section length	L_{Break}	m	1.000	1.000
Total undulator length	L_u	m	139.800	78.200

5.2.2 Nominal X-Ray Parameters and Operating Range

Table 5.2. Nominal LCLS-II undulator parameters.

Parameter	Symbol	Unit	HXR	SXR
K range	K		0.83 – 3.76	1.34 – 9.90
Photon energy range		keV	2 – 13	0.25 – 2
Photon energy range at 4.2 GeV		keV	2 – 4	0.25 – 1.6
Photon energy range at 8.5 GeV*		keV	2.7 – 9.7	0.25 – 2
Photon energy range at 13.5 GeV		keV	6.7 – 13	0.63 – 1.7

*largest gap based tuning range

Figure 5.7 to Figure 5.11 show performance estimates for the LCLS-II undulators.

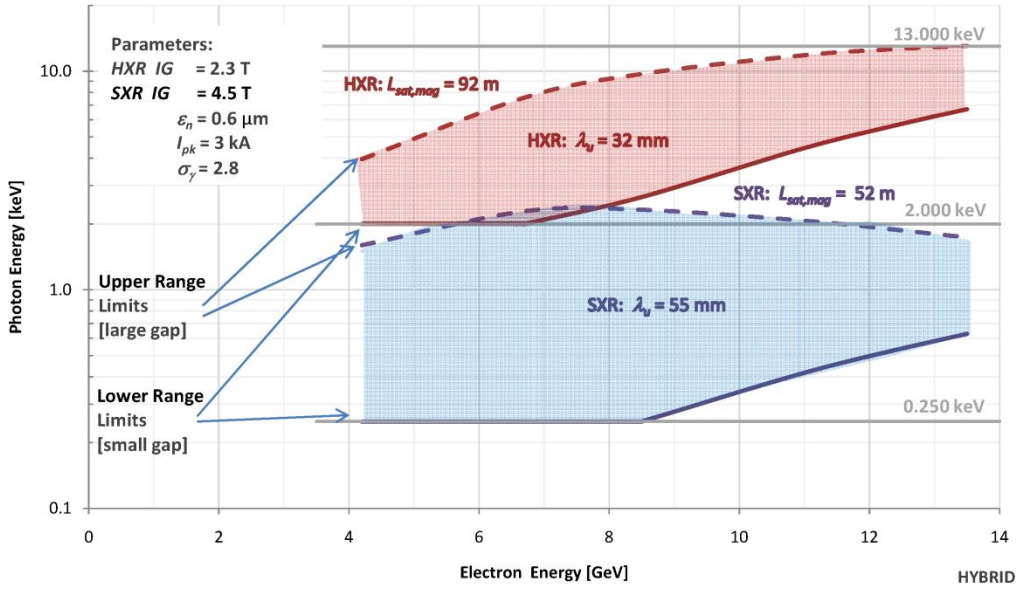

Figure 5.3. Ranges of available photon energy for the two parallel undulators (HXR, red lines; SXR, blue lines) using the same electron beam parameters.

The dashed lines indicate the large-gap-end of the range while the solid lines refer to the small-gap end (see Figure 5.4 for corresponding gap heights). The lowest SXR energy range of 250 eV will be available for electron beam energies below 8.5 GeV. The highest HXR energy (13 keV) requires operating at the highest projected electron beam energy of 13.5 GeV.

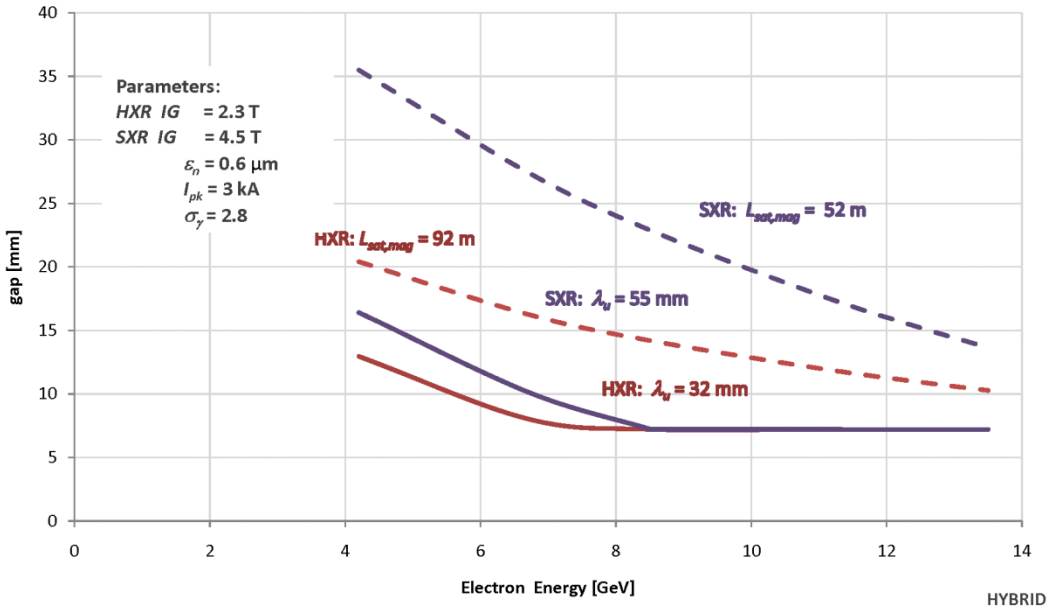

Figure 5.4. Undulator gap height ranges for the two parallel undulators (HXR, SXR) needed to provide the photon energy ranges shown in Figure 5.3.

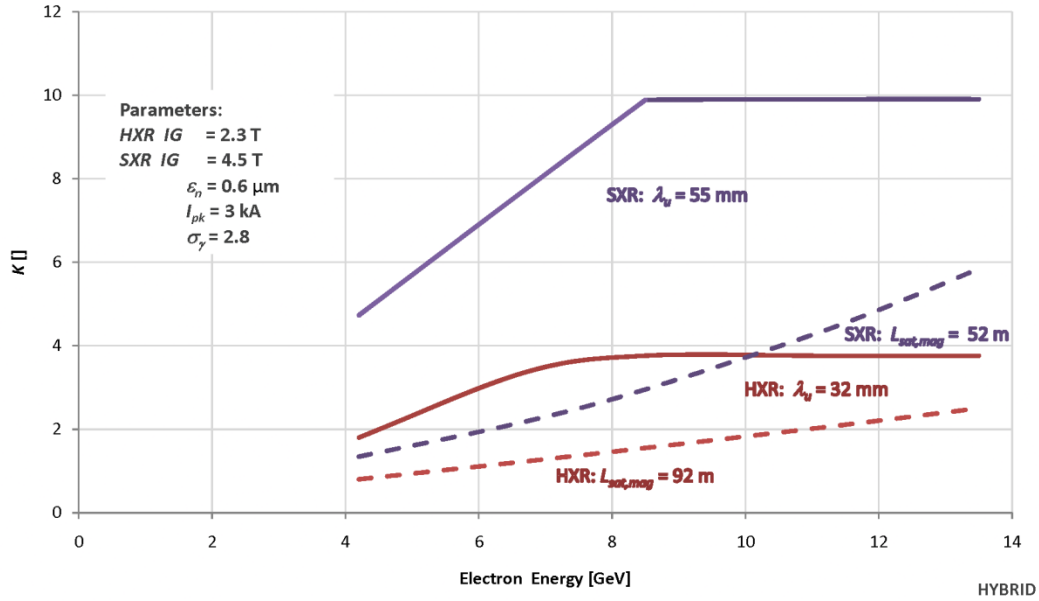

Figure 5.5. Ranges of undulator K parameters for the two undulators (HXR, red lines; SXR, blue lines).

The dashed lines indicate the large-gap-end of the range while the solid lines refer to the small-gap-end (see Figure 5.4 for corresponding gap heights).

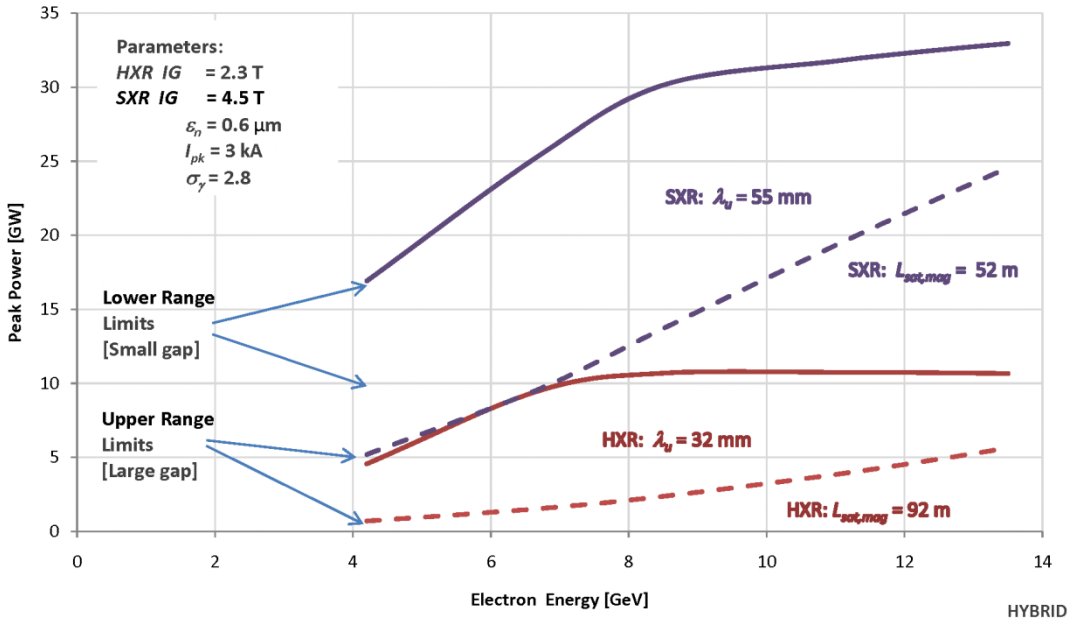

Figure 5.6. Ranges of peak x-ray power at saturation for the two undulators (HXR, red lines; SXR; blue lines)when operated at a given electron beam energy.

The dashed lines indicate the large-gap end of the range while the solid lines refer to the small-gap end (see Figure 5.4 for corresponding gap heights). Significantly more radiation power might be produced by post-saturation undulator strength tapering, although at slightly reduced beam quality, *i.e.* larger divergence and bandwidth.

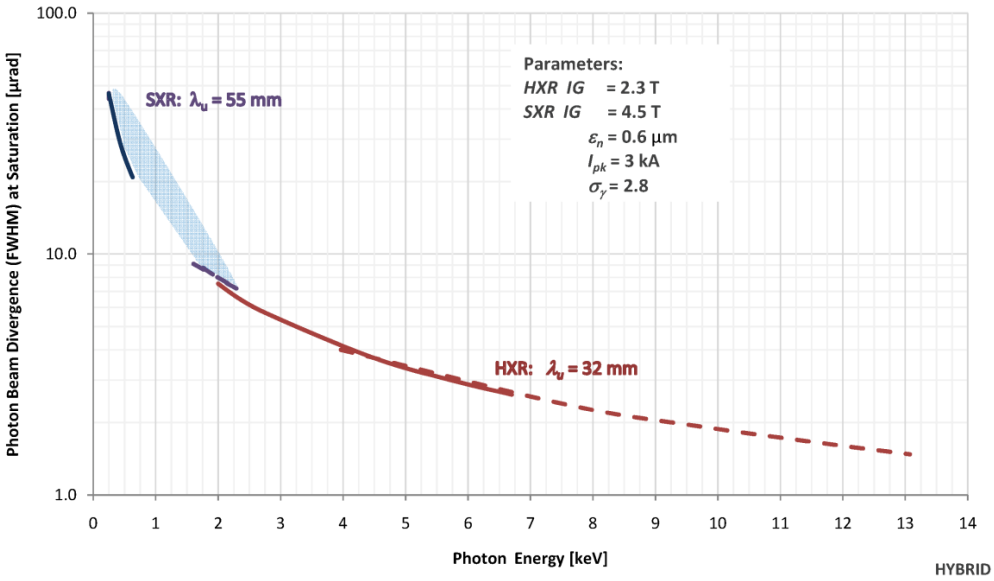

Figure 5.7. Nominal far-field divergence angles at saturation for the two undulators (HXR, red lines; SXR; blue lines) using the same electron beam parameters.

The dashed lines indicate the large-gap end of the range while solid lines refer to the small-gap end (see Figure 5.4 for corresponding gap heights). The divergence angle depends predominantly on photon energy.

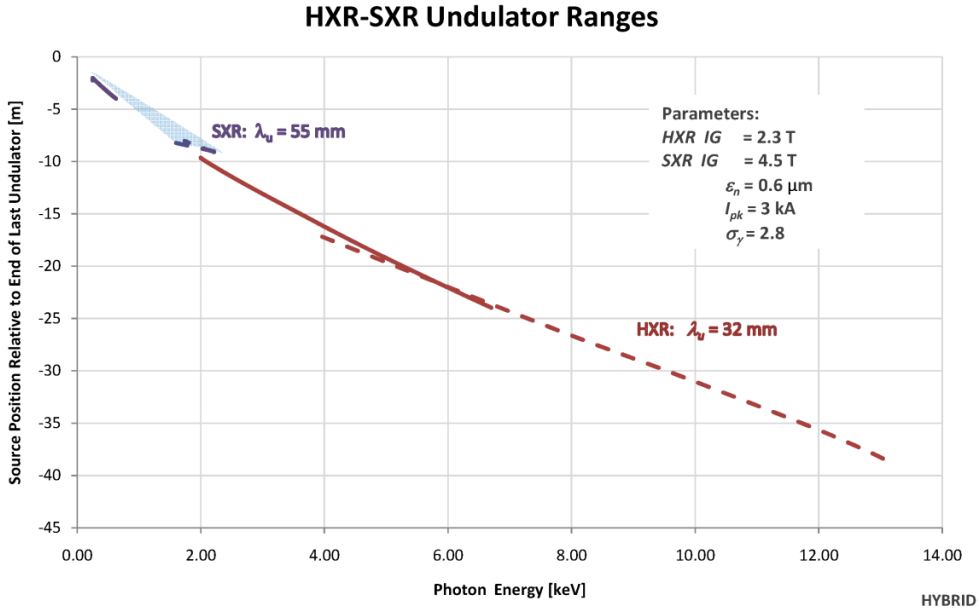

Figure 5.8. Nominal radiation source point location after the last undulator at saturation for the two undulators (HXR, red lines; SXR, blue lines) using the same electron beam parameters.

Note: the calculation assumes that saturation occurs in the last undulator. The dashed lines indicate the large-gap-end of the range while the solid lines refer to the small-gap end (see Figure 5.4 for corresponding gap heights). The source point location depends predominantly on photon energy.

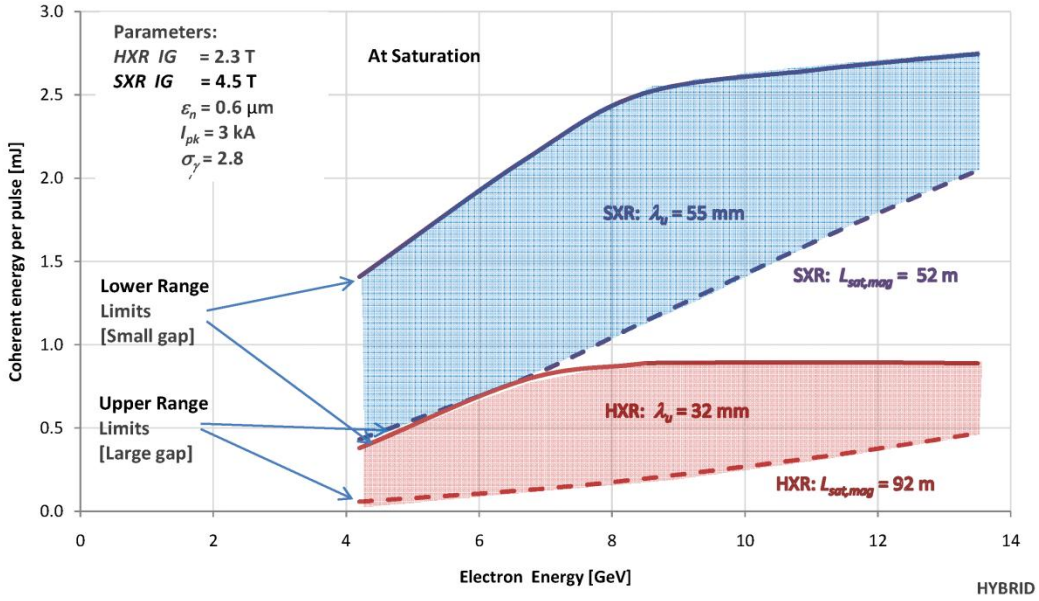

Figure 5.9. Ranges of coherent photon energy per for the two undulators (HXR; red lines, SXR; blue lines) at the saturation point. Intensities are calculated for 83 fs (fwhm) pulse width.

The dashed lines indicate the large-gap-end of the range while the solid lines refer to the small-gap-end (see Figure 5.4 for corresponding gap heights).

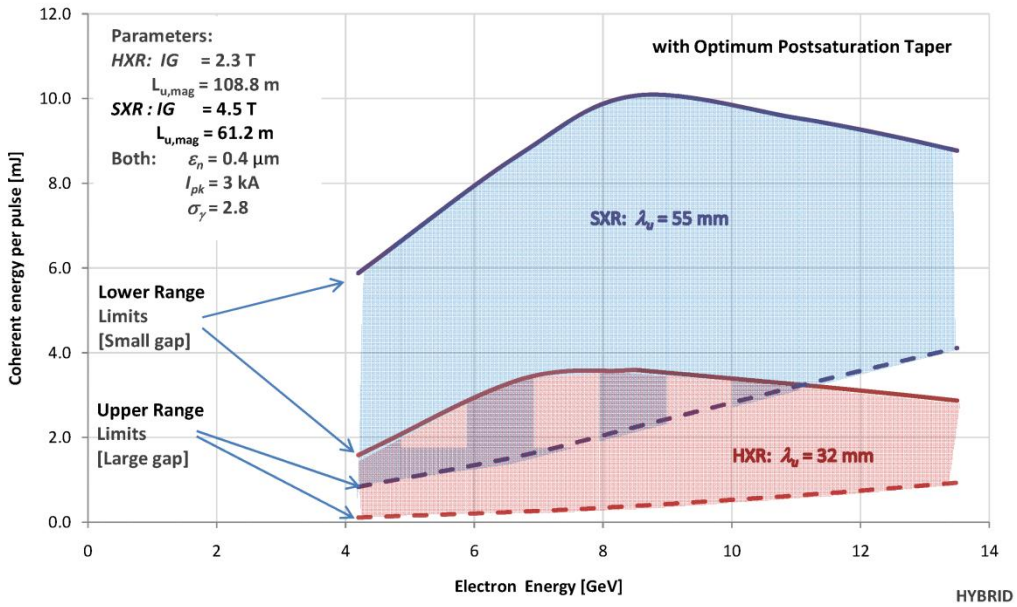

Figure 5.10. Ranges of per-pulse photon intensity for the two undulators (HXR; red lines, SXR; blue lines) when applying optimum post-saturation taper. Intensities are calculated for 83 fs (fwhm) pulse width.

The dashed lines indicate the large-gap-end of the range while the solid lines refer to the small-gap-end (see Figure 5.4 for corresponding gap heights).

For the focusing lattice for the two undulators is based on a FODO lattice, which provides the best performance for x-ray FELS and was also successfully used in LCLS-I. The focusing strength for the HXR and SXR undulators is different to optimize performance. In both cases, the quadrupole gradient will not be changed with electron energy. The resulting change in beta function with energy (see Figure 5.17) keeps the FEL close to optimum performance. The energy independent gradient improves the convergence of beam based alignment.

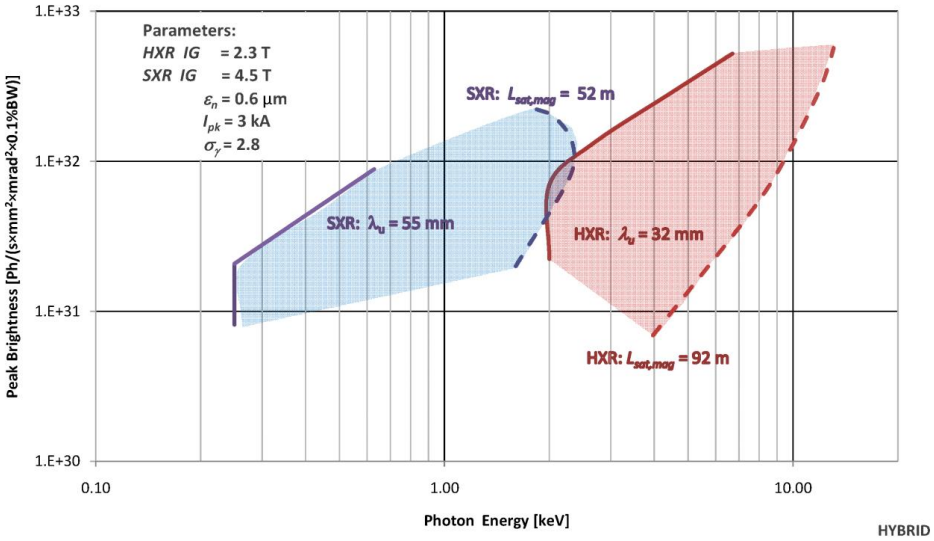

Figure 5.11. Nominal peak brightness ranges for the two undulators (HXR; red lines, SXR; blue lines) at saturation.

The dashed lines indicate the large-gap end of the range while the solid lines refer to the small-gap end (see Figure 5.4 for corresponding gap heights).

5.3 Stability and Control Requirements

5.3.1 Electron Beam Arrival Time

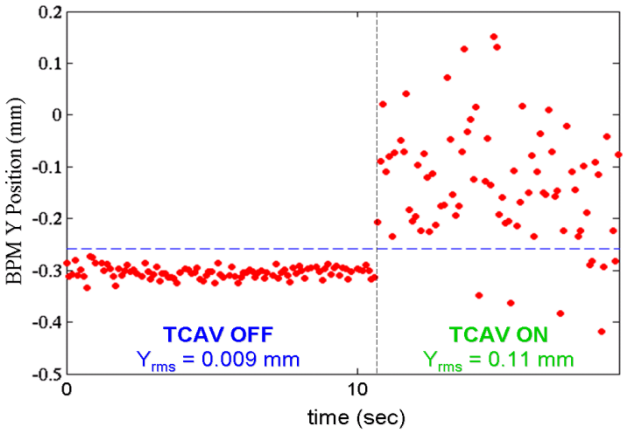

Figure 5.12. BPM y-position jitter measured with TCAV3 OFF (left side) and ON (right side). The increased y-jitter represents the bunch timing jitter of 46 fs rms with respect to RF.

The rms arrival time of the electron beam at the end of the accelerator is expected to be about 50 fs, similar to the measured LCLS-I level. In the LCLS-I, the bunch timing jitter after BC2, with respect to the RF, is measured with a BPM after the transverse RF deflector (Figure 5.12) effectively converts the arrival time into a transverse "*y*" position. This BPM y-position jitter is measured with the deflector set at a zero-crossing phase. A calibration is made scanning the deflector phase and recording the BPM y-position and, shows a very linear response: 2.34 mm/deg (970 fs/deg). Consequently, the 0.11-mm rms y-jitter in Figure 5.12 represents at bunch timing jitter of 46 fs rms, measured with a resolution of 4 fs (0.009 mm).

5.3.2 Pulse Duration

The required peak current for lasing within the designed undulator length is 3 kA for both the HXR and the SXR undulators: hence the maximum allowable electron pulse duration is directly proportional to the charge. For example, for bunch charges of 250 pC, we expect the electron Full Width at Half Maximum (FWHM) pulse length to be about 80 fs or less. At 20 pC, we expect the electron FWHM pulse length to be about 7 fs. Shorter x-ray pulse lengths can be obtained with lower charge (~10 pC) and more aggressive compression: alternatively, they may be obtained with the slotted spoiler method. Thus, the expected photon pulse length range is from 100-1 fs.

5.3.3 Wavelength

The FEL wavelength range is given in Figure 5.3. The expected electron energy jitter at the entrance of the undulator is about 0.03-0.09% (see Figure 5.13), depending on the electron beam energy. The resulting photon wavelength jitter should be twice as much, *i.e*, 0.06-0.18 %.

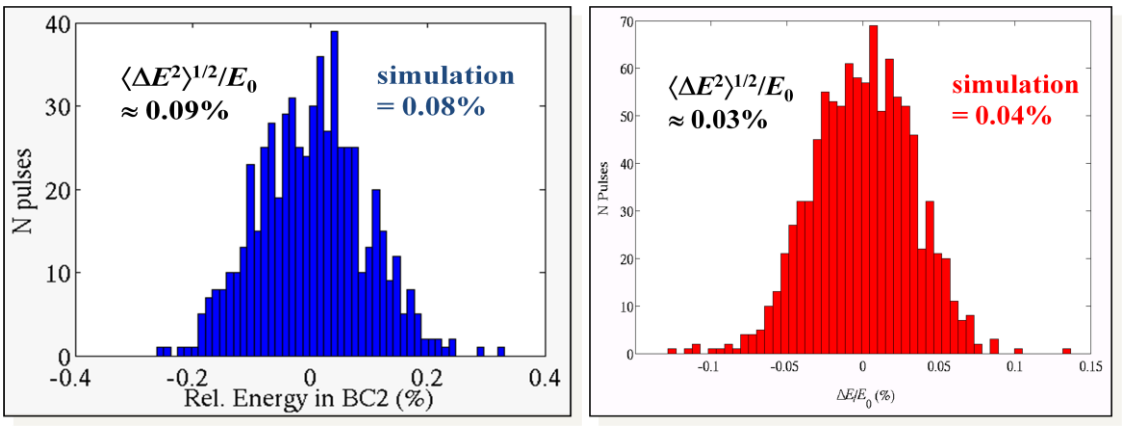

Figure 5.13. Measured LCLS-I electron energy jitter in BC2 (at 4.3 GeV, blue) and at the linac end (13.6 GeV, red).

5.3.4 Bandwidth

The expected FWHM FEL bandwidth is about 0.2% to 0.3% for hard x-rays (~10 keV) and 1% to 1.5% for soft x-rays (1-2 keV). If the bunch is over-compressed in Bunch Compressor 2 (BC2), linac wakefields will add to the rf chirp and produce an energy-chirped electron bunch at the entrance of the undulator. The chirped FEL bandwidth can be as large as 1% for hard x-rays and a few percent for soft x-rays. Figure 5.14 shows the measured LCLS-I hard x-ray spectra under various compression conditions.

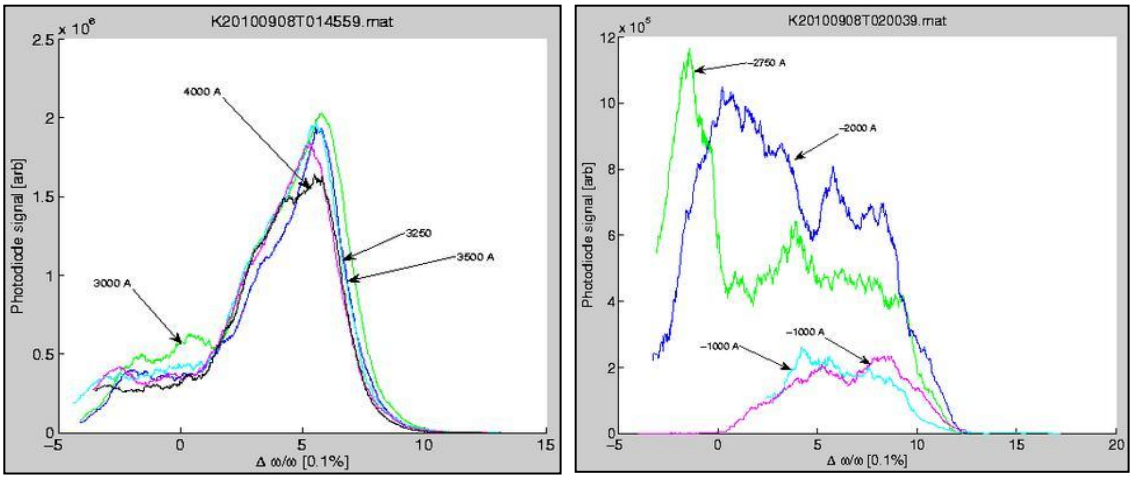

Figure 5.14. Measured LCLS-I FEL spectrum at 8.3 keV using a scanning monochromator.

The left plot shows the FEL spectra when the electron beam is under-compressed in BC2 for several peak current values. The right plot shows the FEL spectra when the electron beam is over-compressed in BC2 (indicated by negative peak current values).

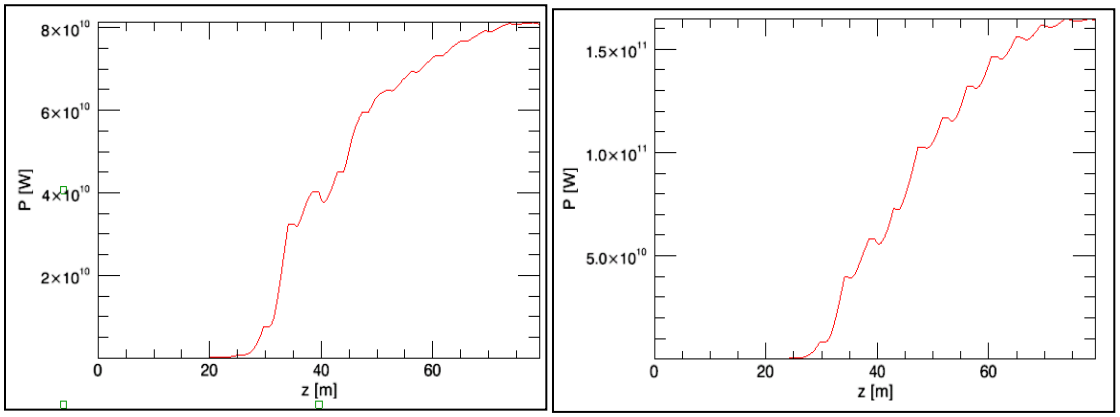

Figure 5.15. SXR power (at photon energy 250 eV) driven by 8.5 GeV electron beam without (left) and with (right) undulator taper. The normalized emittance of the electron beam is assumed to be 0.4 μm, and the peak current is 3 kA.

5.3.5 Pulse Energy

For the HXR, the FEL pulse energy is expected to be at about 2 mJ for 250 pC charge and about 0.2 mJ for 20 pC charge. The expected rms pulse energy fluctuation is about 3 -10 %. For the SXR, at relatively long wavelengths and relatively high electron energies, the FEL power can approach or exceed 100 GW. As shown in Figure 5.15, if the normalized slice emittance is 0.4 μm instead of the baseline parameter of 0.6 μm (achieved by the LCLS-I performance), a SXR FEL at the photon energy 250 eV driven by the 8.5-GeV electron beam can generate 80 GW radiation power over the entire undulator length. With a 2% quadratic taper over the last half of the undulator length, the power can double to 160 GW. For a 250-pC charge compressed to 3 kA, the electron bunch duration is 80 fs (FWHM). Thus, the SXR can produce a maximum pulse energy of 13 mJ!

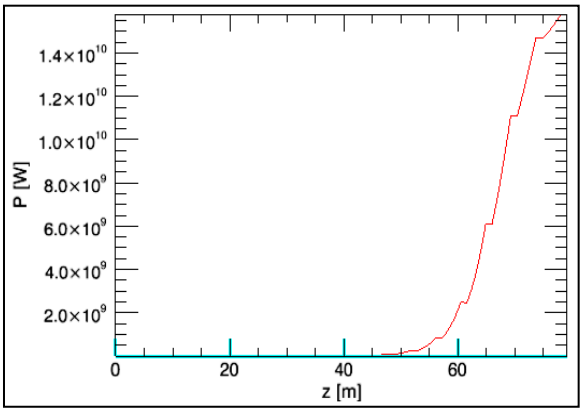

Figure 5.16. SXR power (at photon energy 250 eV) driven by 8.5 GeV electron beam. The normalized emittance of the electron beam is spoiled to about 5 μm in order to reduce the FEL power, and the peak current remains the same at 3 kA.

To avoid excessive power on the sample, we investigate methods to control (lower) the output power. One effective method is to spoil the beam emittance by a thin metallic foil in the SXR bypass line. In order to preserve beam optics matching, it is necessary to insert a pair of foils separated by 90 degrees of betatron phase advance. Assuming the normalized emittance is increased to 5 µm, the saturated soft x-ray FEL power is reduced to 15 GW, with the photon pulse energy on the order of 1 mJ (see Figure 5.16).

5.3.6 Coherence

The FEL is expected to have very good transverse coherence, approaching 80-90% at the FEL saturation. The expected temporal coherence length will range from a few hundred attoseconds to a few femtoseconds, depending on the FEL wavelength.

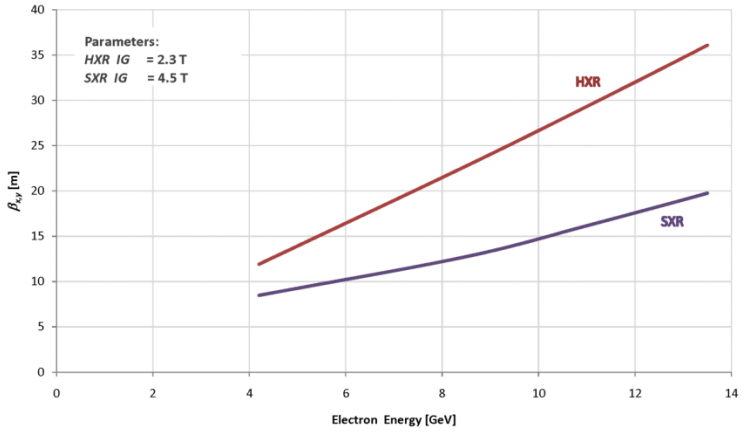

Figure 5.17. Average beta-functions over the operational energy range for the two undulators (HXR, red lines; SXR, blue lines).

The integrated quadrupole gradients (IG) are different for each undulator but will be constant with energy in support of Beam Based Alignment (BBA) (see Chapter 8). The integrated quadrupole gradient for the SXR undulator was chosen as low as possible, i.e., to keep the phase advance per FODO cell just below 90° at the lowest energy.

5.4 FODO Lattice Optimization

Both LCLS-II Undulators (HXR and SXR) use a FODO lattice to focus the electron beam and keep the average beta function constant along the undulator. Both FODO lattices have the same cell length of 4.4 m but different focal lengths. The average beta function required for optimum FEL gain is roughly proportional to electron energy for a given gap and undulator period. At a constant (but small) strength of focusing quadrupole magnets, the beta function will be proportional to energy. Also, the beam-based-alignment algorithm favors a constant quadrupole gradient. Therefore, at LCLS-II, like LCLS-I, the FODO lattice will operate at a constant gradient. The gradients used for HXR will be weaker (larger beta function) than for SXR to optimize performance (see below). Figure 5.17 shows the beta function and quadrupole gradients used for the two LCLS-II undulators.

Figure 5.18 to Figure 5.29 show the impact of the FODO lattice on the FEL performance LCLS-II undulators. The tiny red circle in the upper middle indicates the proposed operating point.

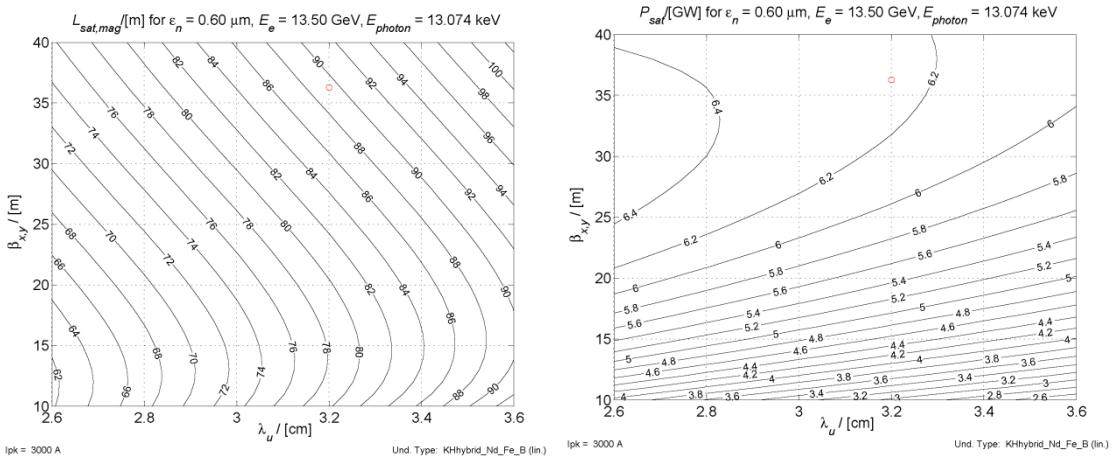

Figure 5.18. HXR saturation length (left) and saturation power (right) at the highest electron energy of 13.5 GeV and at largest operational gap. *Note: The tiny red circle in the upper middle indicates the proposed operating point.*

This choice sets the beta function of the HXR undulator for maximum output power (brightness) at the high electron energy limit (see right plot).

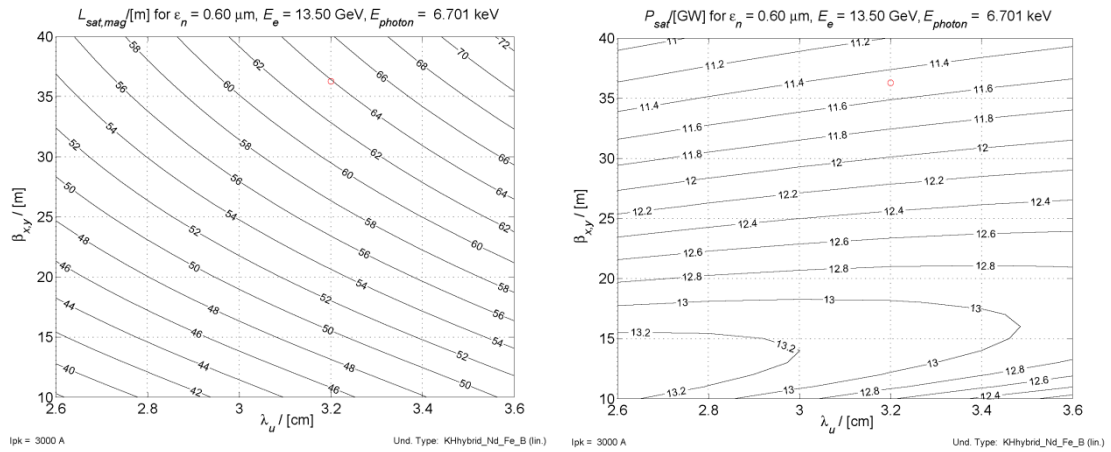

Figure 5.19. HXR saturation length (left) and saturation power (right) at the highest electron energy of 13.5 GeV and at the smallest operational gap. *Note: The tiny red circle in the upper middle indicates the proposed operating point.*

Note: The operating point is not at the optimum for this closed gap configuration output power reduction from about 13 GW to 11.5 GW is about 12 %. The chosen operating point keeps the phase advance per cell below 90°, which reduces electron beam cross section oscillations as it travels along the undulator.

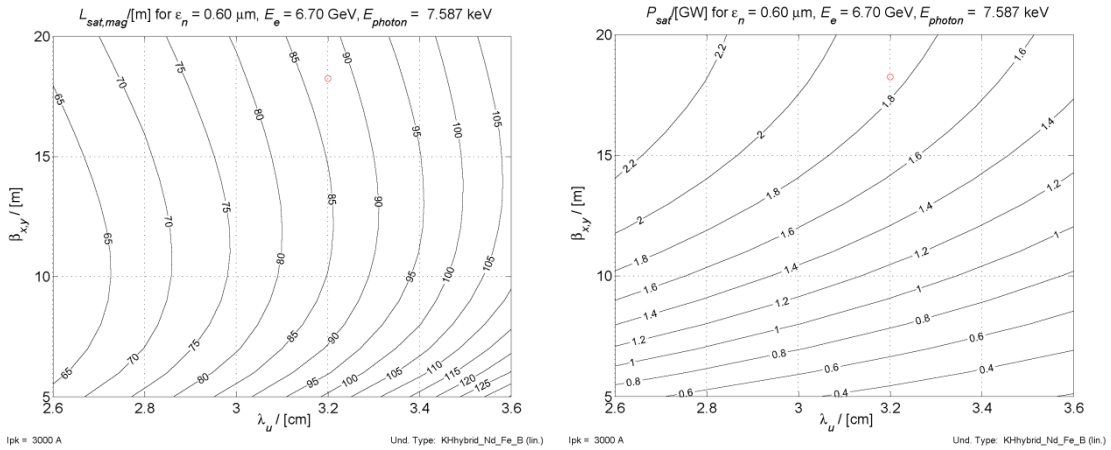

Figure 5.20. HXR saturation length at 6.7 GeV at largest operational gap. *Note: The tiny red circle in the upper middle indicates the proposed operating point.*

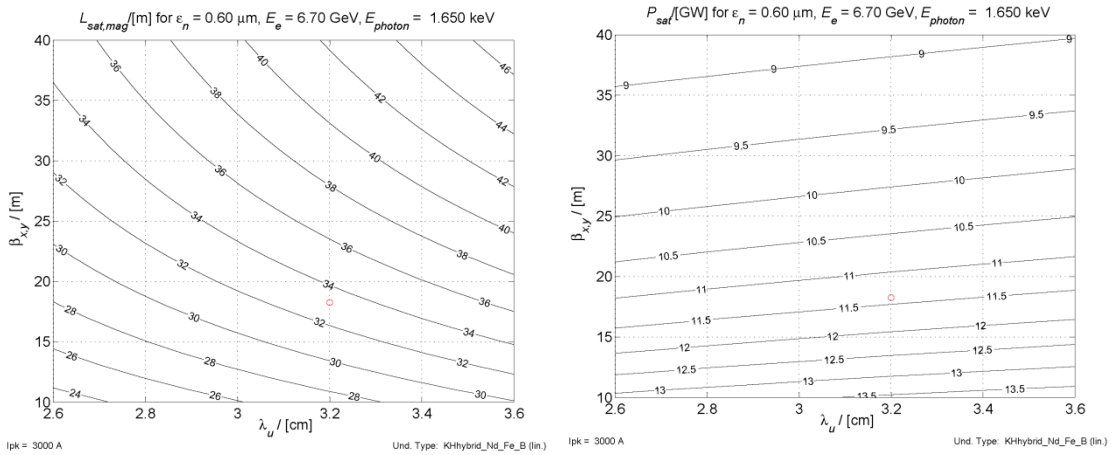

Figure 5.21. HXR saturation length and saturation power at 6.7 GeV at smallest operational gap. *Note: The tiny red circle in the upper middle indicates the proposed operating point.*

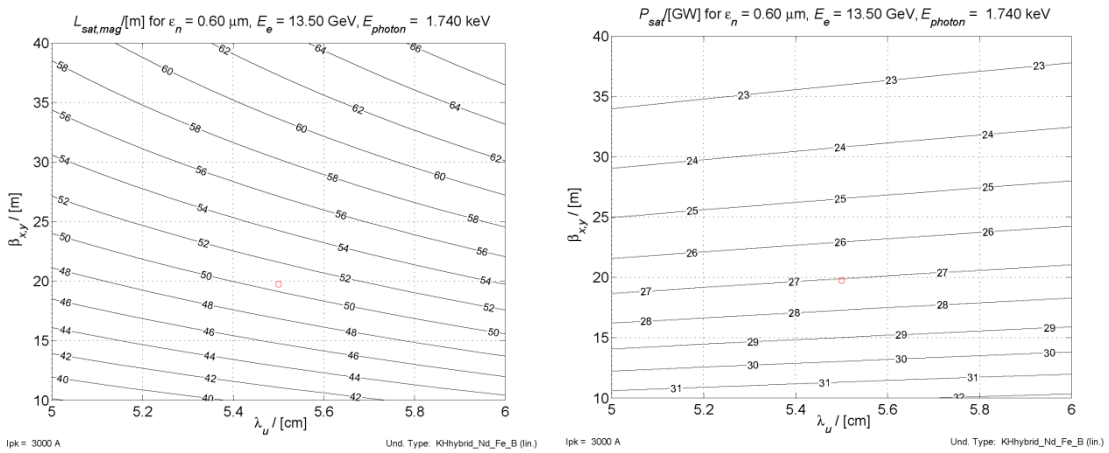

Figure 5.22. SXR saturation length and saturation power at 13.5 GeV at largest operational gap. *Note: The tiny red circle in the upper middle indicates the proposed operating point.*

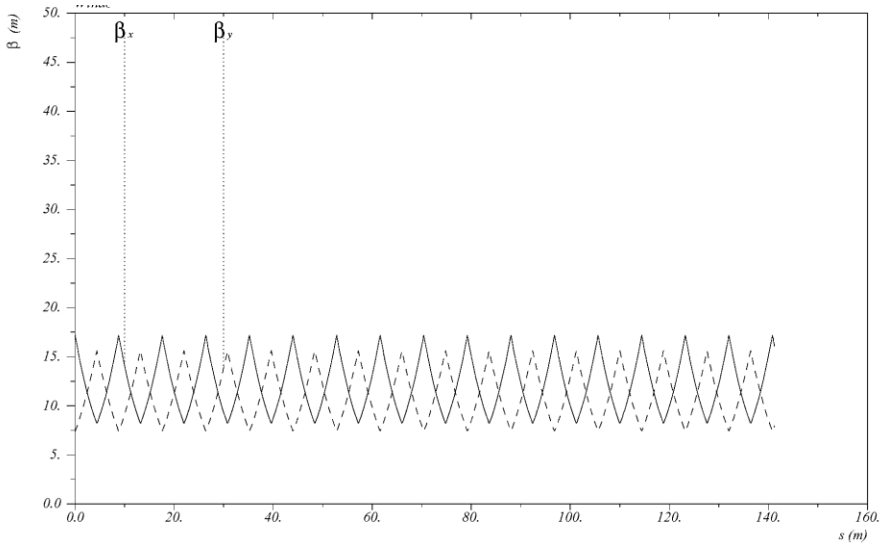

Figure 5.23. HXR beta functions at E=4.2 GeV; integrated QF gradient=2.3 T; K=3.5.

The Quadrupole Defocusing (QD) strength was reduced by 4 % to compensate some of the vertical undulator focusing.

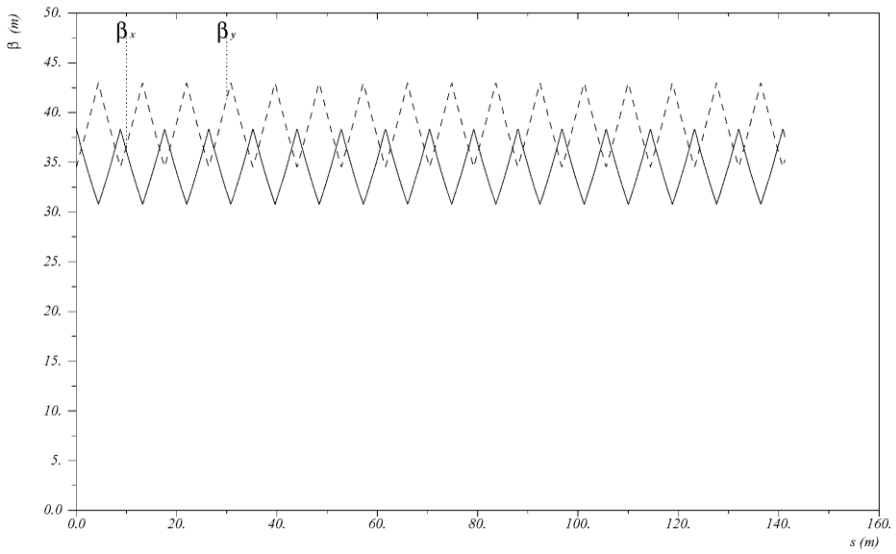

Figure 5.24. HXR beta functions at E=13.5 GeV; integrated QF gradient=2.3 T; K=3.5.

The QD strength was reduced by 4 % to compensate some of the vertical undulator focusing.

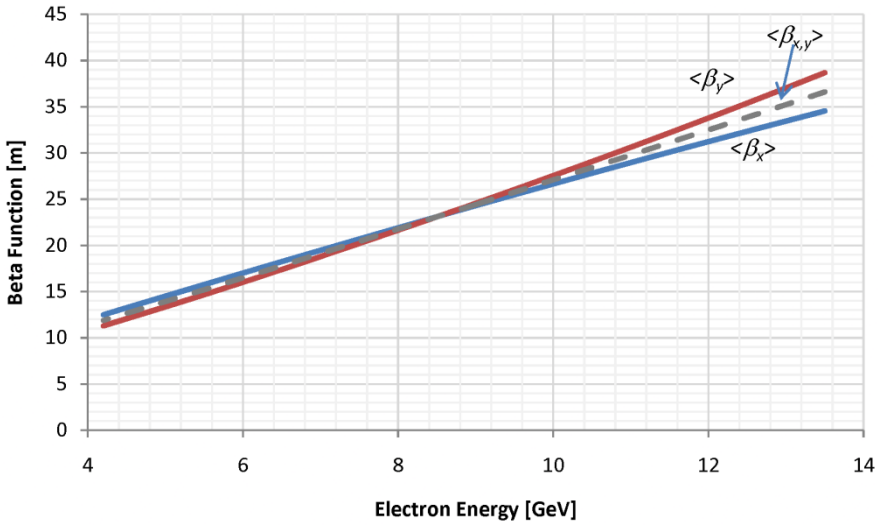

Figure 5.25. HXR average beta functions vs electron energy; integrated QF gradient=2.3 T; K=3.5.

The QD strength was reduced by 4 % to compensate some of the vertical undulator focusing. The average beta functions change linearly with energy over the entire range. The increased slope for the vertical beta function as well as difference between the two is due to the vertical undulator focusing. The calculation uses a K value close to the highest expected. At lower K values, the vertical beta function will change towards the horizontal beta function.

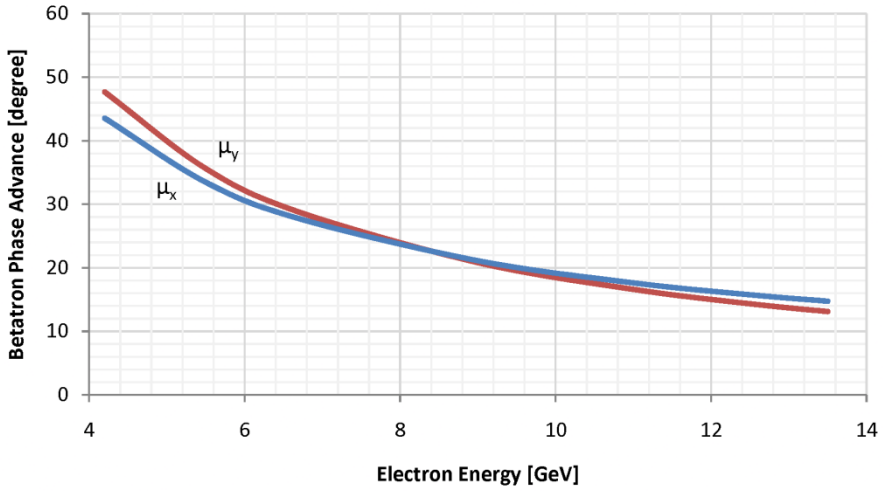

Figure 5.26. HXR betatron phase advance per FODO cell vs electron energy. integrated QF gradient = 2.3 T; K=3.5.

The QD strength was reduced by 4% to compensate some of the vertical undulator focusing. The phase advance per cell is well below 90°. This is desirable to reduce beam cross section oscillations as the electron beam travels along the undulator.

For the SXR undulator, stronger focusing (lower beta function) will give better performance (see Figure 5.22). The beta-function chosen was determined by the FODO cell length and the constant quadrupole gradient over the operational electron energy range. The quadrupole strength was chosen to provide about 90° betatron phase advance at the lowest electron energy of 4.2 GeV.

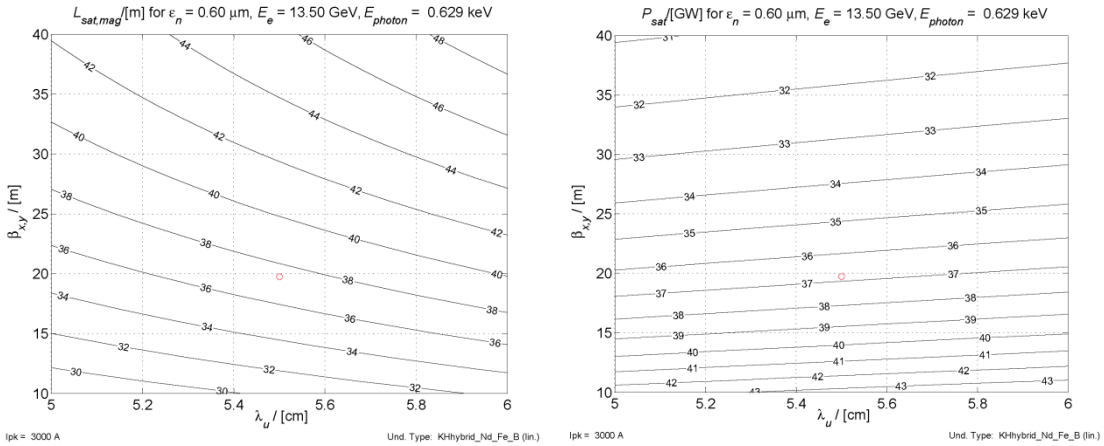

Figure 5.27. SXR saturation power at 13.5 GeV at smallest operational gap. *Note: The tiny red circle, close to the center, indicates the proposed operating point.*

The optimum average beta function, which is significantly lower, can not be achieved due to the limit set by the FODO cell length.

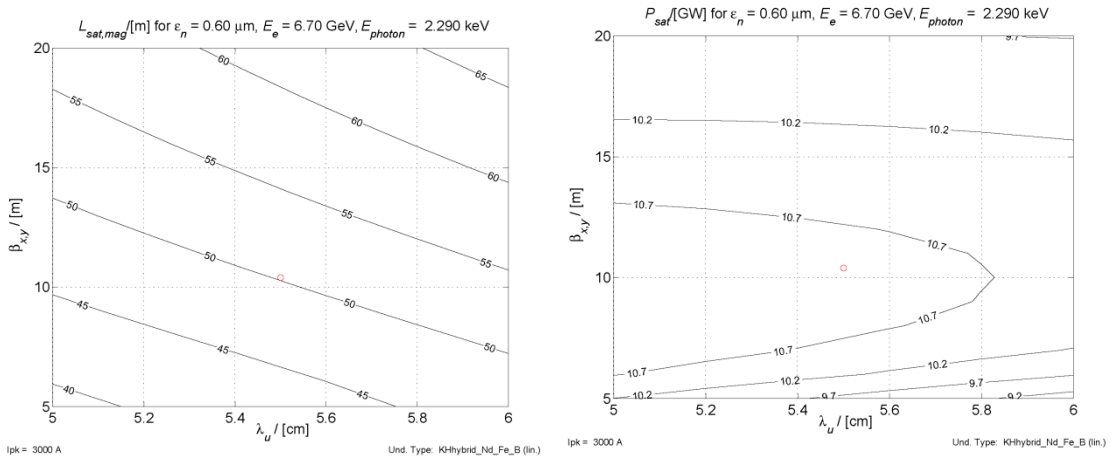

Figure 5.28. SXR saturation length and saturation power at 6.7 GeV at largest operational gap. *Note: The tiny red circle, close to the center, indicates the proposed operating point*.

At this point, the beta function is at its optimum value.

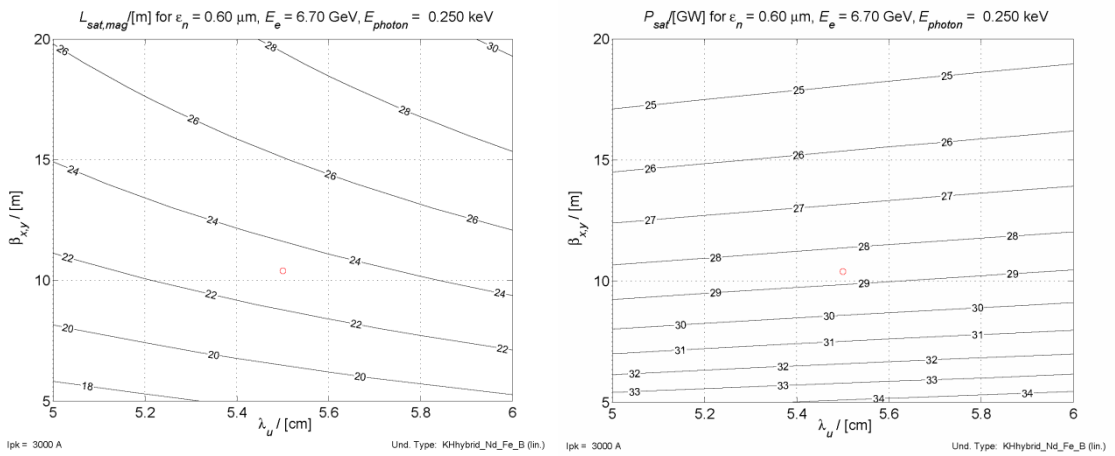

Figure 5.29. SXR saturation length and saturation power at 6.7 GeV at smallest operational gap. *Note: The tiny red circle, close to the center, indicates the proposed operating point.*

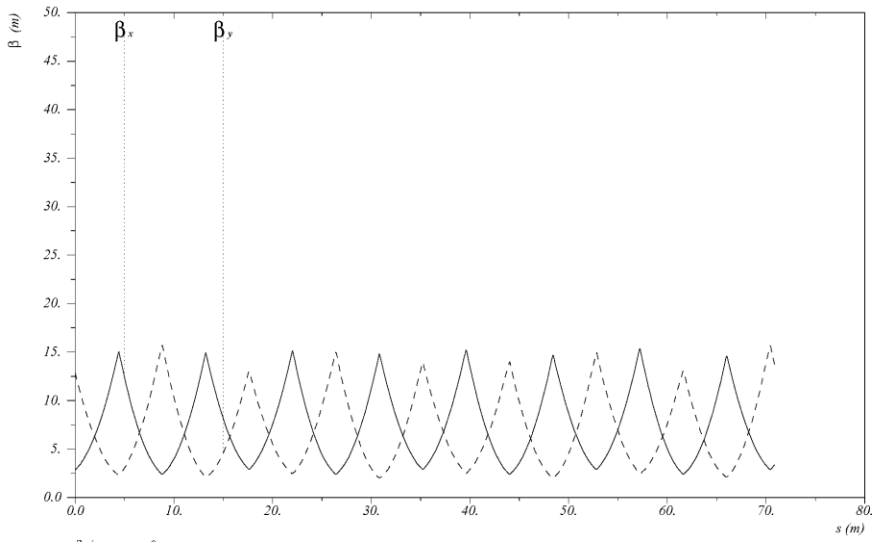

Figure 5.30. SXR beta functions at E=4.2 GeV; integrated quad gradient=4.5 T; K=9.9.

The relative effect of vertical undulator focusing on the beta function is smaller compared to the HXR undulator because of the stronger quadrupole gradient even though the undulator K is larger.

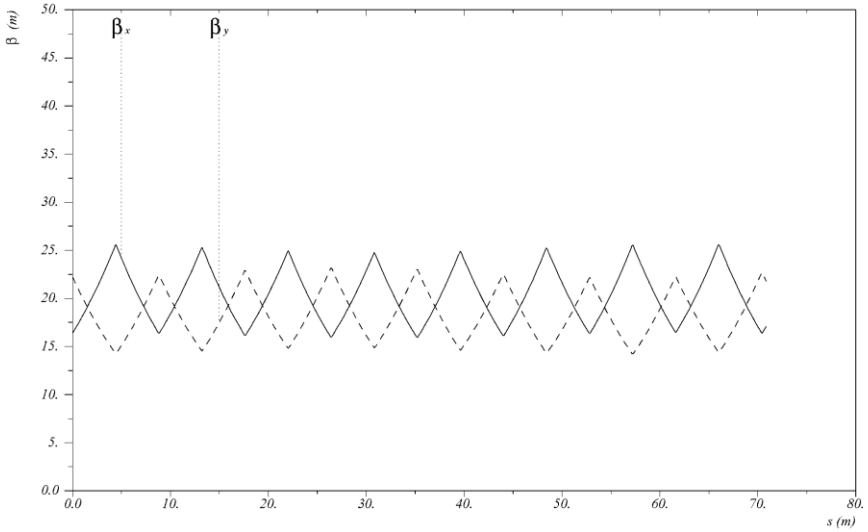

Figure 5.31. SXR beta functions at E=13.5 GeV; integrated quad gradient=4.5 T; K=9.9.

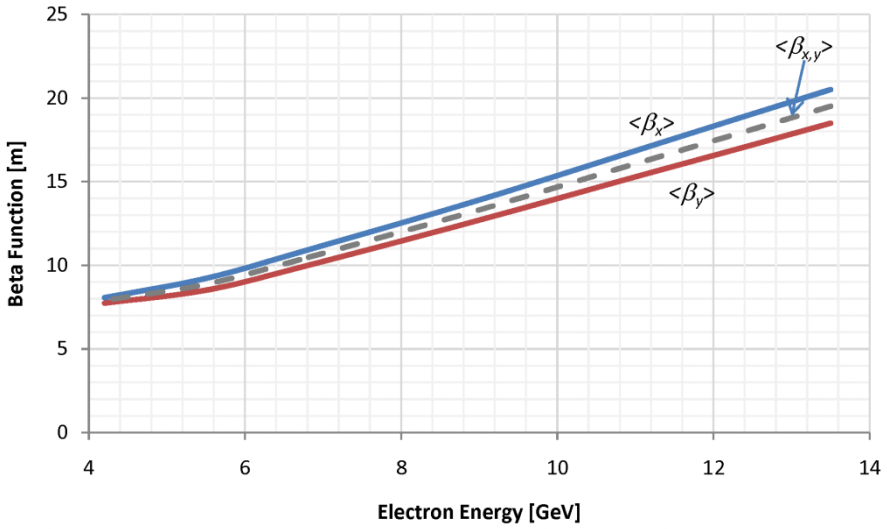

Figure 5.32. SXR average beta functions vs electron energy. integrated quad gradient=4.5 T; K=9.9.

The beta functions change linearly with energy for high electron energies but approches it minimum value (close to the FODO cell length) at low electron energies as the phase advance per cell approaches 90°. The difference between the two is due to the vertical undulator focusing. The calculation uses the highest expected K value. At lower K values, the vertical beta function will change towards the horizontal beta function.

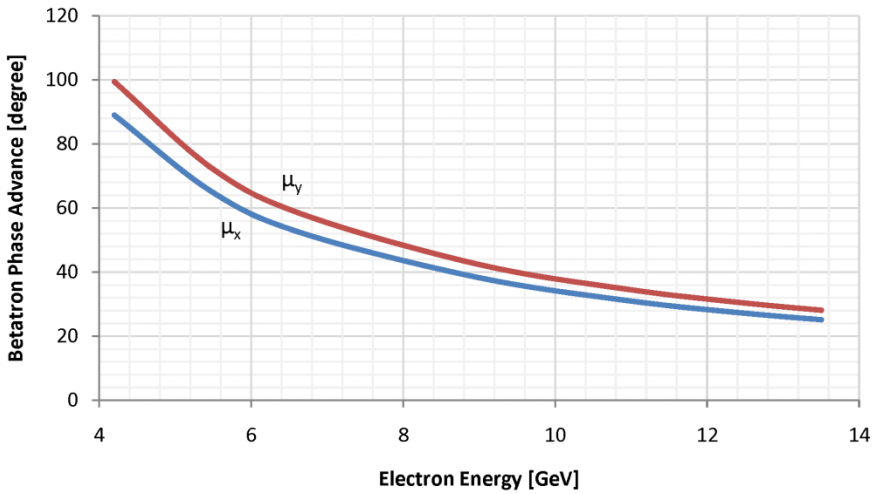

Figure 5.33. SXR betatron phase advance per FODO cell vs electron energy. integrated quad gradient=4.5 T; K=9.9.

The phase advance per cell in the horizontal plane just reaches 90°. It exceeds 90° in the vertical plane, because of the additional undulator focusing. Focusing has been increased in the SXR undulator compared to the HXR undulator to improve performance in the mid-electron-energy range.

5.5 Electron Beam Parameters

Particle tracking studies (start-to-end simulations, S2E) have been performed throughout the injector, accelerator, and FEL by stringing together results from *Parmela* (injector) and *Elegant* [2] (linac). Included in the tracking are longitudinal wakefields, coherent synchrotron radiation (CSR), incoherent synchrotron radiation (ISR), and 2nd-order optics (*e.g.*, chromatic effects). Space charge forces are only included in the *Parmela* run up to 64 MeV, with output particles transferred to *Elegant*. All components are error free here (e.g., perfect alignment). These simulations are described in detail in Chapter 6. Figure 5.34 and Figure 5.35 show the transverse and longitudinal beam profiles at the entrance to the undulator as a result of these simulations. The horizontal tail in the transverse beam profile comes predominantly from coherent synchrotron radiation in the linac and the bunch compressors. Larger emittances associated with this tail distribution reduces its contribution to the lasing process. The energy tails in the longitudinal phase space distribution come from wakefields and bunch compression. The larger energy spread reduces their contribution to the lasing process, as well. Table 5.3 summarizes the most important properties of the electron beam at the undulator entrances.

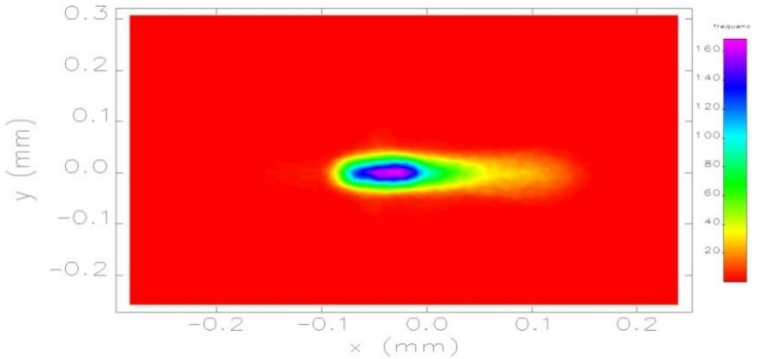

Figure 5.34. Expected transverse electron beam profile at the entrance to the undulator as predicted by start-to-end simulations.

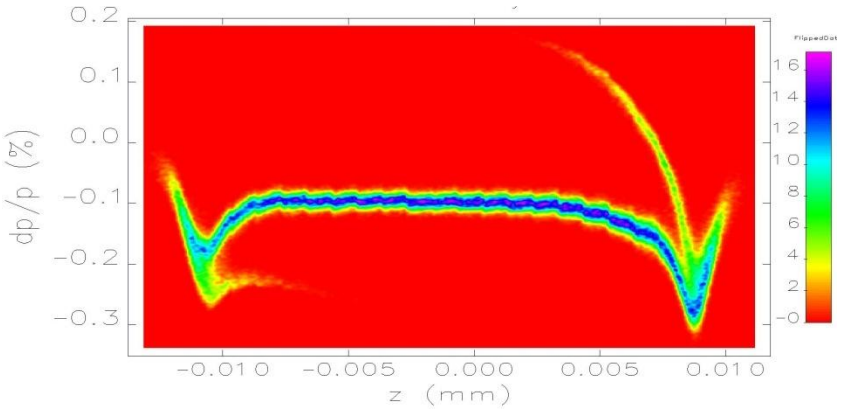

Figure 5.35. Expected longitudinal electron beam phase space distribution at the entrance to the undulator as predicted by start-to-end simulations.

The figure shows that the energy chirp in the core of the electron bunch can be removed but the energy tails at the beginning and end of the bunch are unavoidable.

Table 5.3. Electron Beam parameters at the entrance to HXR and SXR undulators.

Parameter	Symbol	Unit	Low e⁻ Energy	High e⁻ Energy
Electron Energy	E	GeV	4.2	13.5
Norm proj emittance (x/y)	ε_n	µm	1.5/0.6	1.5/0.6
Total energy spread	$\Delta p/p$	%	0.09	0.03
Slice energy spread		%	0.03	0.01
Bunch length (rms)	σ_z	mm	0.0072	0.0072
Peak current	I_{pk}	A	3000	3000

5.6 FEL Simulations and Performance Projections

Start-to-end simulations are carried out for the LCLS-II FELs, using the accelerator configuration discussed in Chapter 6 and the undulator parameters list in Table 5.1. Two-hundred thousand macroparticles modeling the 250-pC electron bunch are tracked in the injector and the accelerator till the entrance of the undulator. These particles are converted into FEL simulation code Genesis 1.3 [3] to model the SASE process, taking into account the undulator vacuum chamber wakefield and spontaneous undulator emission. Simulations are carried out for both SXR and HXR lines.

For SXR, a 4.2-GeV electron beam is used to generate soft x-rays around 1 keV photon energy. The peak current and the wakefield energy loss along the bunch coordinate are calculated as shown in Figure 5.36. The FEL power evolution along the undulator as well as the output spectrum are illustrated in Figure 5.37. Snapshots of FEL temporal profiles at different undulator locations are shown in Figure 5.38. The double-horn current spikes (at the head and tail) do not contribute strongly to the lasing because of their much increased energy spread.

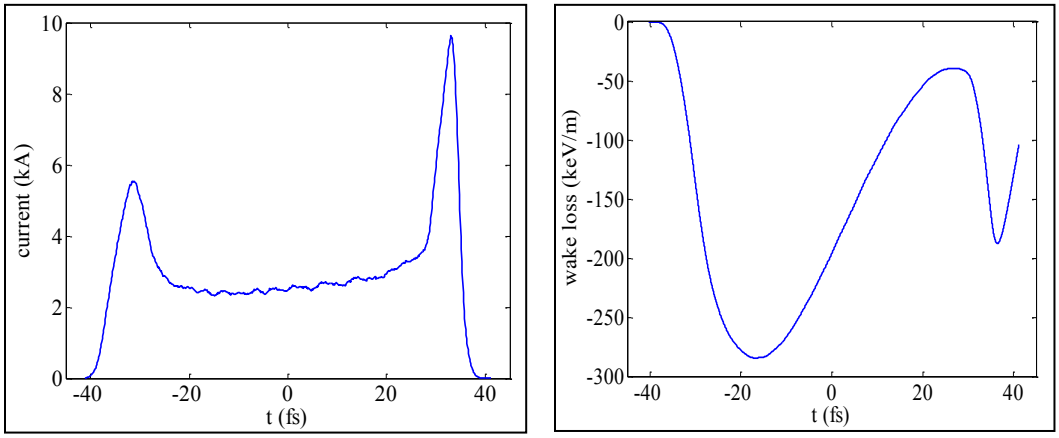

Figure 5.36. Electron bunch current profile at 4.2 GeV and the wake loss along the bunch in the undulator (bunch head to the left).

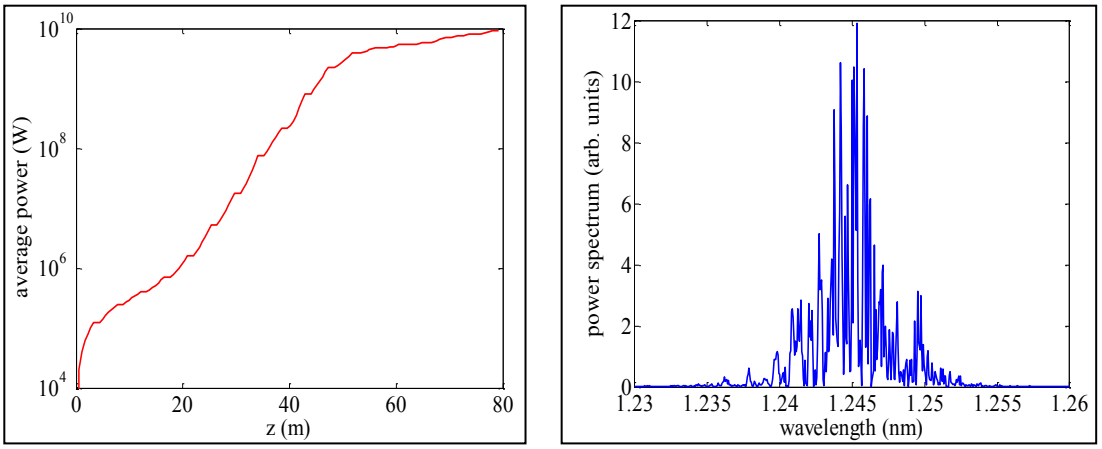

Figure 5.37. (Left) 1 keV soft x-ray average power vs. undulator beamline distance. (Right) Output power spectrum as a function of photon wavelength.

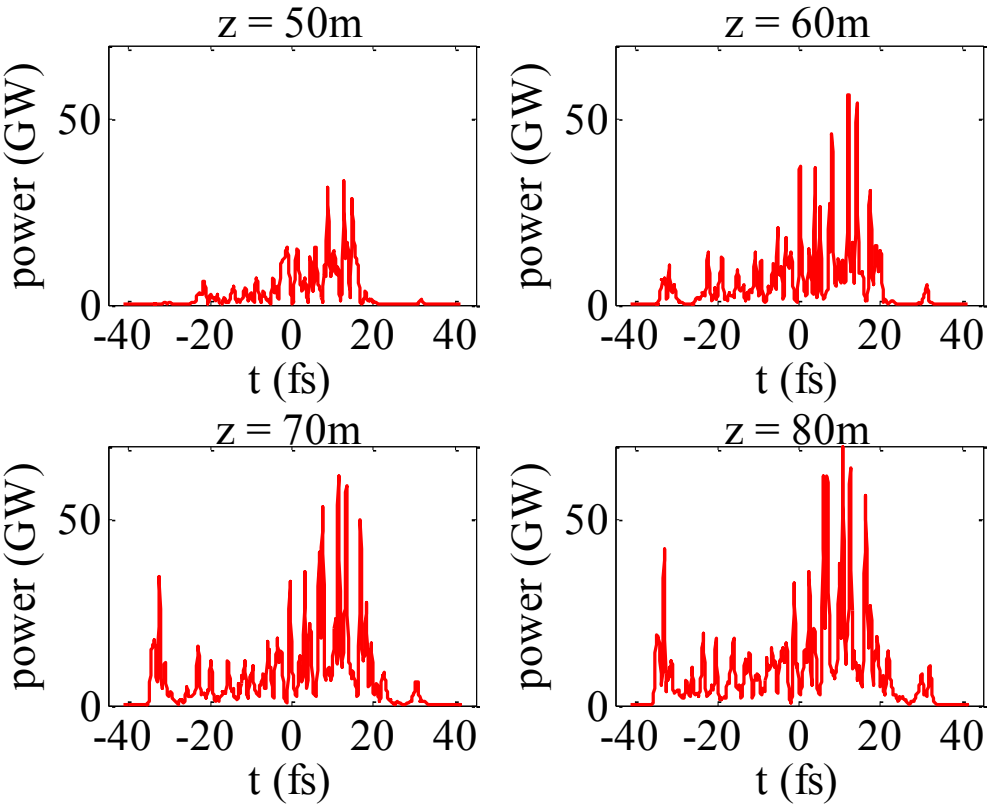

Figure 5.38. 1 keV FEL temporal profiles at four different undulator beamline distances.

For HXR, a 13.5-GeV electron beam is used to generate hard x-rays around 13 keV photon energy. The peak current and the wakefield energy loss along the bunch coordinate are calculated as shown in Figure 5.39. The FEL power evolution along the undulator as well as the output spectrum are illustrated in Figure 5.40. Snapshots of FEL temporal profiles at different undulator locations are shown in Figure 5.41. The double-horn current spikes contribute significantly to the lasing process.

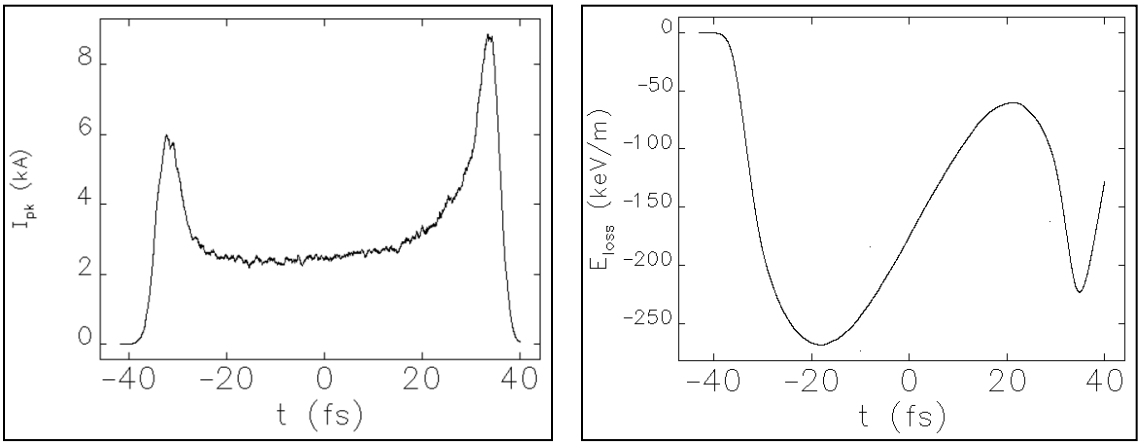

Figure 5.39. (Left) Electron bunch current profile at 13.5 GeV and (Right) the wake loss along the bunch in the undulator (bunch head to the left hand side in each figure).

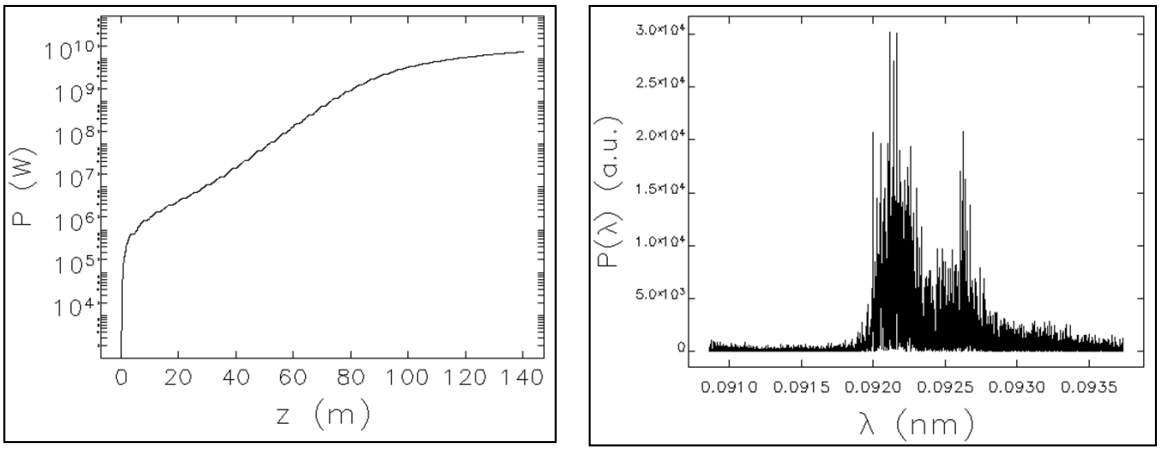

Figure 5.40. (Left) 13 keV hard x-ray average power along the undulator beamline. (Right) Output power spectrum as a function of photon wavelength.

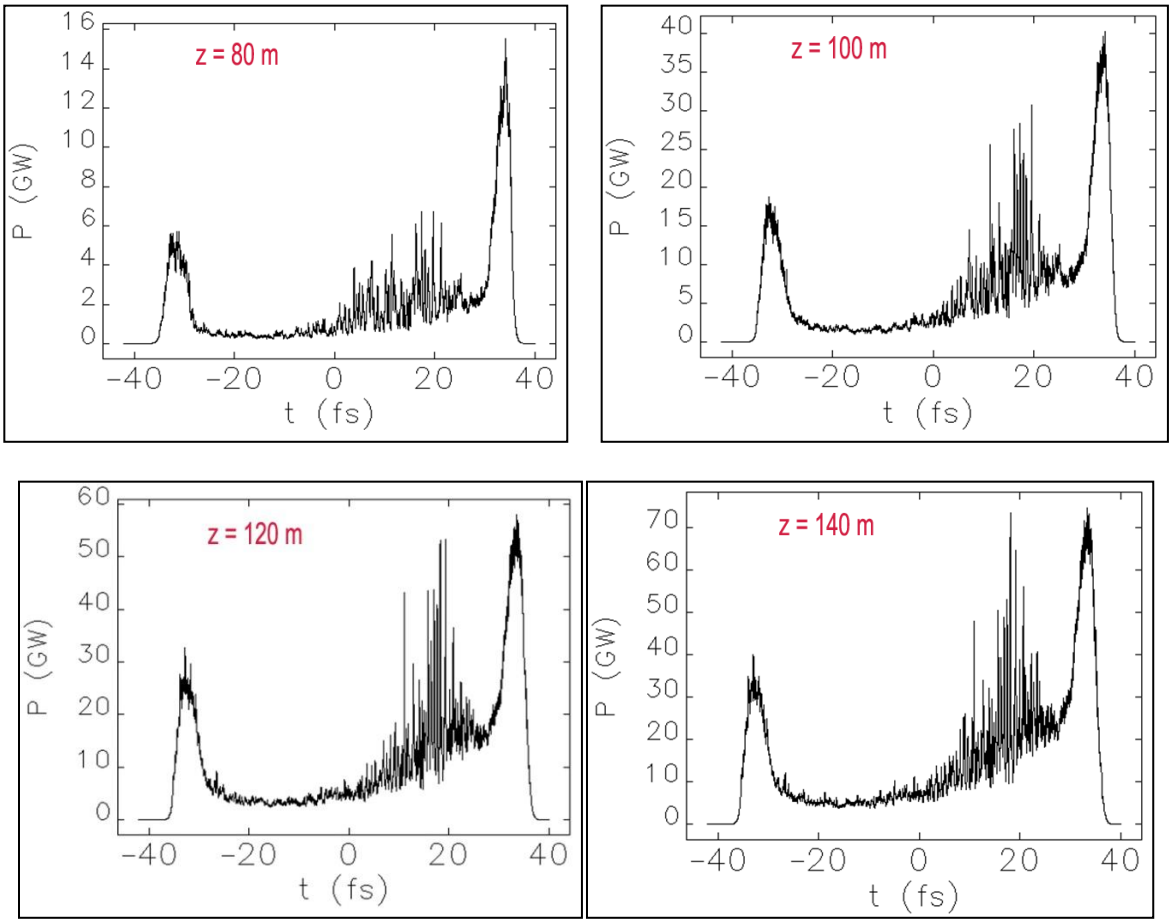

Figure 5.41. 13 keV FEL temporal profiles at four different undulator beamline distances.

5.7 References

1. M. Xie, *Design Optimization for an X-Ray Free Electron Laser Driven by SLAC Linac*, in Proceedings of the 1995 Particle Accelerator Conference (IEEE, Piscataway, NJ, 1995), p. 183.
2. M. Borland, Report No. ANL/APS LS-287, 2000.
3. S. Reiche, Nucl. Instrum. Methods A 429, 243 (1999).

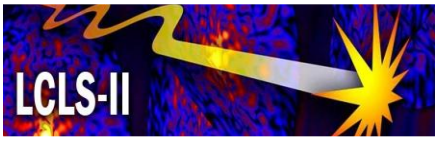

6 Accelerator

Technical Synopsis

In order for the Self Amplified Spontaneous Emission (SASE) Free Electron Laser (FEL) to operate in saturation, a high electron peak current with small transverse and longitudinal emittance is required. The LCLS-II will operate within a range of photon energies from 13 to 0.25 keV using two parallel FEL undulators. The most challenging parameters coincide with the 13-keV configuration with maximum peak current of 3.0 kA, transverse normalized 'slice' emittance of 0.6 μm, and top energy of 14 GeV. Since the RF photocathode gun produces 0.25 nC in a bunch length of 3 ps, corresponding to a peak current of 35 A, the bunch must be compressed by a factor of 85 before entering the undulator. The acceleration and compression is done in the 2nd kilometer of the slightly modified SLAC linac.

The bunch compressors consist of a series of magnetic chicanes arranged and located such that non-linearities in the compression and acceleration process (longitudinal wakefields, RF curvature, and second order momentum compaction) are approximately compensated. A short section of X-band deceleration (19 MeV, 11.424 GHz) is also used prior to the first compressor in order to linearize the compression. An optimal choice of linac design parameters both cancels the correlated energy spread after the final compression, and desensitizes the system to phase and charge variations. The electron energy at the first compressor is 250 MeV. This choice avoids space charge effects, while compressing the bunch early enough in the linac to ease the effects of transverse wakefields. In the first compressor, the bunch length is reduced from ~0.6 mm to 0.13 mm rms. The second compressor produces a 7-μm bunch. The energy of the second compressor, 4.2 GeV, is chosen as a balance between the conflicting requirements of longitudinal emittance dilution due to synchrotron radiation, and the need to cancel the final correlated energy spread. The design of the compressors is dominated by the need to reduce Coherent Synchrotron Radiation (CSR) effects, which are most pronounced for short bunches. The most significant effect of CSR is to generate a correlated energy gradient along the bunch. By using a weak chicane and a large initial correlated energy spread, the effect of CSR on the transverse emittance can be controlled.

Simulations have been made which calculate emittance dilution in the linac due to transverse wakefields and anomalous momentum dispersion, each of which arises with component misalignments. These simulations include realistic correction techniques and successfully demonstrate the level of transverse emittance preservation required. Diagnostics, correction techniques, and feedback systems have also been incorporated into the design. Finally, the acceleration and compression systems are flexible enough to allow a high degree of operational variation in beam parameter choices, such as bunch charge, final beam energy, and an optional electron beam energy chirp.

6.1 Accelerator - Introduction and Overview

The LCLS-II accelerator design is closely based on the very successful LCLS-I design [1, 2], but moved one kilometer (1016 m) upstream to occupy linac sectors 11-20 (the second kilometer of the SLAC linac), rather than the LCLS-I location, which uses sectors 21-30 (the third kilometer of the SLAC linac). As in LCLS-I, a new LCLS-type injector will be built at Sector 10 in the existing off-axis bunker and two new bunch compressor chicanes will be added. An electron bypass line will be used to transport the beam around LCLS-I using the existing, but modified PEP-II high-energy transport line suspended from the linac tunnel ceiling. This allows LCLS-II electron beam parameters which are completely independent of LCLS-I. The new LCLS-II beam will feed two new FELs in a new tunnel targeting both hard and soft x-rays with a pair of new side-by-side (parallel) undulators. The accelerator requirements are described below.

6.1.1 Differences with Respect to LCLS-I

The LCLS-II design is very closely based on the LCLS-I design, but there are some *required* differences (based on existing linac layout or new user needs) and some *desired* differences (based on LCLS-I experience). These differences are worth listing here for those who are already quite familiar with the LCLS-I.

- A long (1200 m) bypass line is needed to deliver the electron beam around the existing LCLS-I linac and into the existing beam-transfer hall (BTH). [*required*]
- A new horizontal bend system (2.4°) is needed in the BTH to divert the electron beam into a new undulator hall just south of the existing LCLS-I undulator hall. [*required*]
- After this 2.4° bend, the new linac-to-undulator (LTU) electron transport line splits into two segments, using a pulsed bend magnet, in order to feed two new parallel undulators which are 2.5 meters apart. [*required*]
- Two separate electron beam dumps are required. [*required*]
- With four fewer klystrons avaible than in LCLS-I (~0.9 GeV) the final beam energy in LCLS-II will be <0.5 GeV lower than LCLS-I [Radio Frequency (RF) phasing was optimized to minimize this loss]. [*required*]
- The electron dump will include a soft-bend magnet to redirect the coherent edge radiation off of the x-ray Ytterium-Aluminum-Garnet (YAG) screens downstream of the dump. [*desired*]
- There are many smaller differences, such as fewer Optical Transition Radiation (OTR) screens (which do not work well with the high-brightness LCLS beam), but such detail is beyond the scope of this description. [*desired*]

6.1.2 Accelerator Requirements and Parameters

To drive two new parallel hard and soft x-ray FEL undulators [Hard X-ray (HXR) and Soft X-ray (SXR)] into SASE saturation, the electron beam must meet a specific set of requirements (already well met in LCLS-I). The electron emittance, peak current, energy, energy spread, and stability has been chosen to meet the FEL requirements for both the HXR and SXR FELs within their required photon energy ranges (2-13 keV for the HXR FEL and 0.25-2 keV for the SXR FEL). These electron parameters are listed below in Table 6.1. A schematic layout of the accelerator is also shown in Figure 6.1 with beam parameters listed at various points along the accelerator. The electron beam optics from cathode to the start of the HXR undulator is also plotted in Figure 6.2.

Table 6.1. Nominal electron beam parameters in the undulator and their operational ranges. The terms "slice" and "projected" in the table refer to time-sliced (about 1-10 fs) and bunch-length-integrated beam parameters, respectively.

Parameter	Symbol	Unit	Nominal	Range
Final electron energy	E_f	GeV	13.5	4.2 - 15
Electron bunch charge	Q_0	nC	0.25	0.01 - 1.0
Pulse repetition rate	f_{rep}	Hz	120	1 - 120
Number of electron bunches per RF pulse	N_b	-	1	1 - 2
Electron transverse, rms, normalized, *slice* emittance	$\gamma\varepsilon_{x,y\text{-}s}$	μm	0.6	0.1 - 1.2
Electron transverse, rms, normalized, *projected* emittance	$\gamma\varepsilon_{x,y\text{-}p}$	μm	1.0	0.1 - 1.6
Final electron peak current	I_{pk}	kA	3.0	0.5 - 5.0
Final electron bunch length (rms)	σ_z	μm	7	1 - 50
Electron rms *slice* energy spread	$\sigma_{E\text{-}s}$	MeV	1.4	0.1 - 1.5
Electron rms *projected* energy spread	$\sigma_{E\text{-}p}$	MeV	2	0.7 - 70
Max. avg. e^- beam power (15 GeV, 1 nC, 1 bunch/pulse)	P_b	kW	1.8	0.04 - 1.8
Dump design for avg. e^- beam power (large safety factor)	P_D	kW	5	-

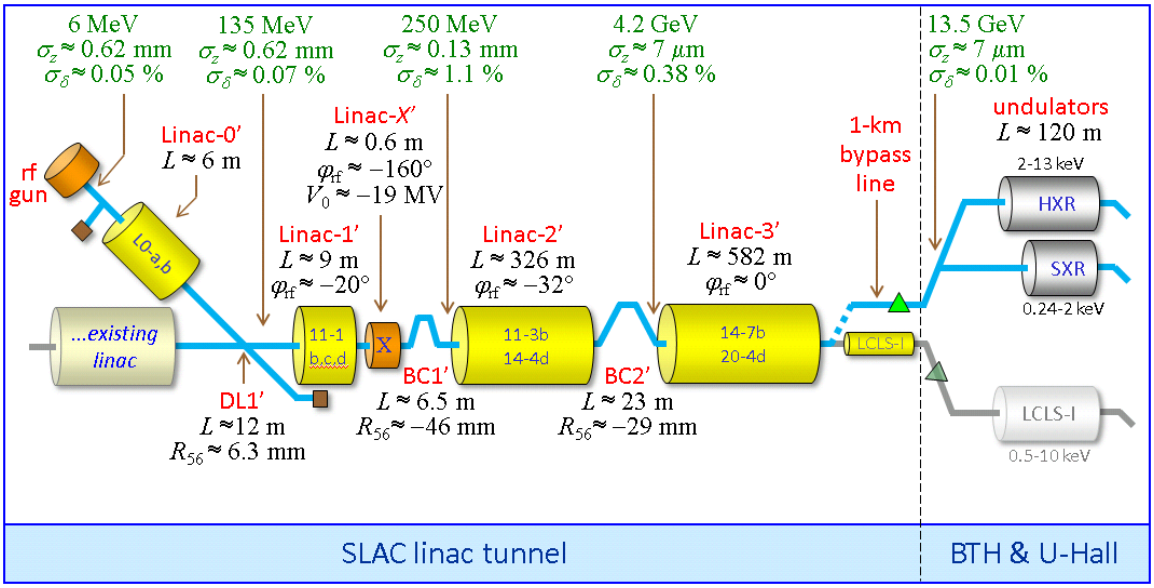

Figure 6.1. Schematic layout of LCLS-II injector, linac, bunch compressors, and undulators, with main parameters listed for 120-Hz operation with one 250-pC electron bunch at 13.5 GeV.

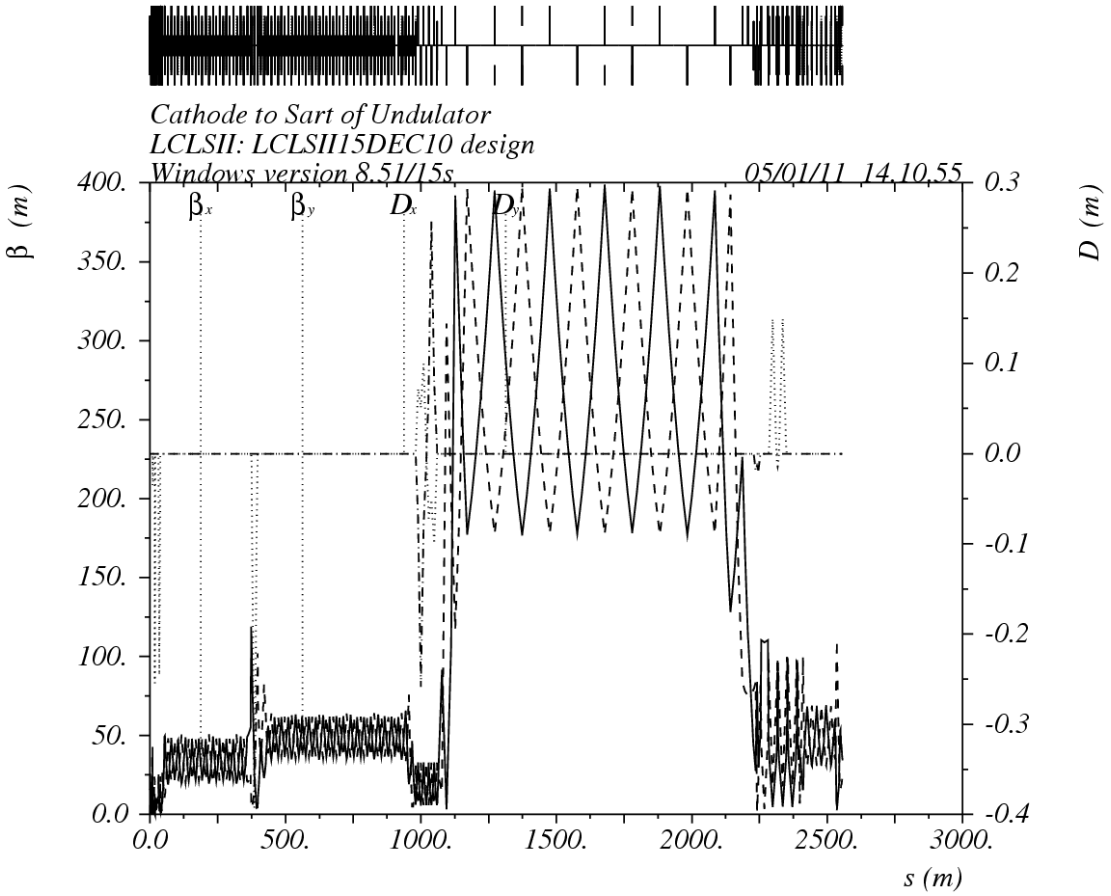

Figure 6.2. Linac optics (using MAD 8.51) from cathode (s = 0) to the start of the HXR undulator (s ≈ 2550 m). BC1 is at s ≈ 20 m, BC2 is at s ≈ 380 m, and the large beta function section is due to the 101.6-m quadrupole magnet spacing in the bypass line.

6.1.3 Accelerator Layout

The LCLS-II accelerator layout will occupy the second kilometer of the SLAC S-band linac (2.856 GHz), from sector 11 through 20, in order to generate up to a 14 GeV electron beam at 120 Hz. The electron beam must then bypass around the existing LCLS-I accelerator in sectors 21-30 and connect up in a new undulator hall just south of the existing hall. To accomplish this, the beam will be deflected in the middle of Sector 20, up and over (with rolled DC dipole magnets), to the existing PEP-II 9-GeV bypass line which is suspended from the ceiling in the linac tunnel. This existing bypass line is 25.570 inches above and 25.610 inches to the south of the main linac axis and includes focusing magnets, beam position monitors, and steering coils in each sector (101.6 m per sector). Most of this bypass FODO line will be used “as is”, except for a new optics design for the bends in Sector 20 and the beam matching into and out of the bypass FODO cells. In addition, the bypass line will be extended in a straight path all the way through the Beam Switch Yard (BSY), through the 17-m thick iron “muon plug wall”, and into the existing Beam Transport Hall (BTH), where it will emerge 25.570 inches above and 25.610 inches south of the existing LCLS-I beamline there. New DC horizontal bending magnets will then direct the beam into the new undulator hall just to the south of the LCLS-I undulator hall and at an angle of 2.4 degrees. The new undulators will remain about 25 inches higher in elevation than the LCLS-I, but the floor in the new hall can be built such that the floor-to-beamline height is optimal for the new undulator layout (e.g., 1.4 meters as in LCLS-I). Note that a small vertical upward bend (4.6 mrad) is included in the BTH, as exists in

LCLS-I [3], so that the intrinsic downward pitch angle of the SLAC linac is removed and the undulators are level with their local gravity vector. In addition, a separate SXR branch line takes every other electron bunch to the Soft X-ray (SXR) undulator which is parallel to the Hard X-ray (HXR) undulator and separated horizontally by 2.5 meters. The electrons to the HXR undulator are not deflected, but continue straight into the HXR undulator (see Figure 6.3).

6.1.4 Brief Description of the Accelerator

A single bunch of electrons is generated at a 120-Hz repetition rate in an S-band (2.856 GHz) RF photocathode gun (see "RF gun" in Figure 6.1) by exciting a copper cathode with Ultra-Violet (UV) laser light from a high-power drive laser system located in the linac gallery above the existing Sector 10 off-axis injector vault. The electrons are then accelerated to 6 MeV in the gun where the transverse emittance is formed by choosing an appropriate UV laser spot size on the cathode (~1.2 mm diameter for 250 pC) and using a strong focusing solenoid magnet immediately after the gun.

Further acceleration in the injector vault (see "Linac-0‴ in Figure 6.1) takes the beam energy up to 135 MeV where it is horizontally deflected by 35 degrees into the main SLAC linac at the start of Sector 11 (see "DL1‴ in Figure 6.1). The beam is then accelerated about 20° off of the RF crest where a nearly linear electron energy chirp (time-energy correlation) is generated (see "Linac-1‴ in Figure 6.1). The energy chirp is linearized using an X-band (11.424 GHz = 4×2.856 GHz) RF accelerating section (see "Linac-X‴ in Figure 6.1) to slightly decelerate the beam ($\Delta E \approx -19$ MeV). A 6-m long, four-dipole magnetic chicane at 250 MeV (see "BC1" in Figure 6.1) compresses the bunch length from 600 μm to about 120 μm rms. More off-crest acceleration follows (see "Linac-2‴ in Figure 6.1) to 4.2 GeV where a second chicane (see "BC2" in Figure 6.1) compresses the bunch length to its final 7-μm rms length, generating 3 kA of peak current with a 250-pC nominal bunch charge. The last accelerator section (see "Linac-3‴ in Figure 6.1) accelerates at the RF crest phase up to 13.5 GeV (variable down to 4.2 GeV).

The beam is extracted from the linac in the middle of Sector 20 and transported along the linac ceiling in the existing but modified PEP-II bypass line (see "1-km bypass line" in Figure 6.1), where some beam halo collimators and emittance measurement instruments are located. The beam is then carried into the BTH and deflected horizontally by 2.4 degrees toward the south.

Finally, the electron beam is then divided and switched at 60 Hz with a pulsed horizontal bending magnet between a Hard X-ray (HXR) and a Soft X-ray (SXR) undulator. The undulators are adjacent and parallel with a 2.5-m horizontal separation in a new undulator tunnel (see Figure 6.3). The electrons which are bound for the HXR undulator are not kicked by the pulsed magnet, but continue straight into the HXR undulator. This is done because the beam brightness and stability requirements for the HXR FEL are much more demanding than for the SXR FEL. The electrons which are bound for the SXR undulator are kicked by the pulsed magnet by 0.6° and then bent into the SXR undulator using DC dipole magnets.

The two separated electron beams are then each directed into their own separate dump lines, diagnosed, and discarded. The FEL x-rays are transported into two separate x-ray front end diagnostics section (FEES and FEEH) and delivered to the experimental stations in a new LCLS-II experimental hall.

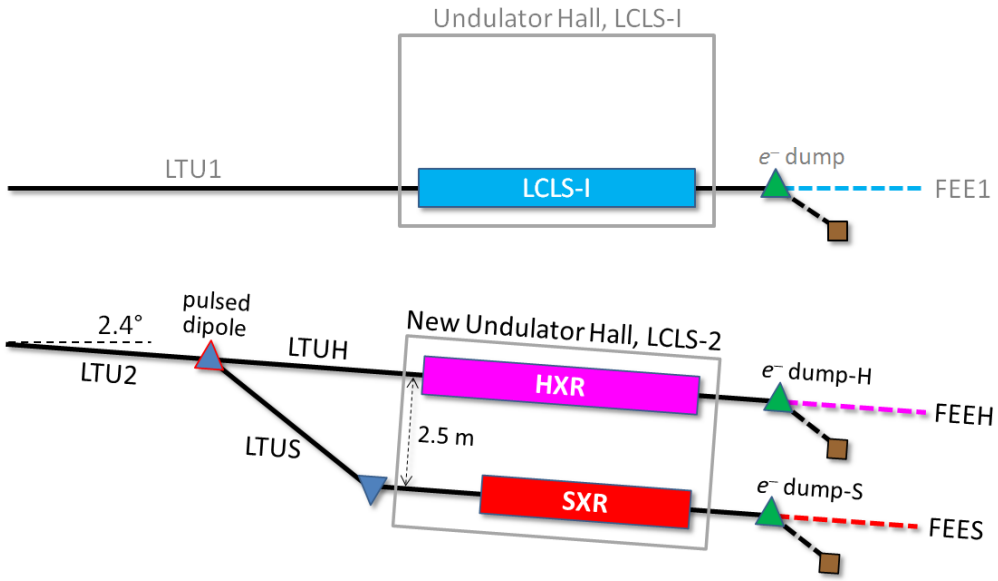

Figure 6.3. The new set of parallel hard (HXR) and soft (SXR) undulators within their new tunnel at a common 2.4-deg angle (bottom) with respect to LCLS-I (top).

The electron beam is distributed to each FEL at 60 Hz (or 120 Hz with 2-bunch operation) using a pulsed dipole magnet into the SXR branchline Linac-To-Undulator Soft X-ray (LTUS). All bends are horizontal here, except the e^- dump bends.

6.2 Drive Laser

The injector drive laser serves two purposes in the LCLS-II injector: The UV output is used to illuminate the copper cathode producing the electrons for acceleration and the Infra-Red (IR) output is used in the laser heater (Sections 6.2.2 and 6.3.3.5). A copper cathode has been demonstrated to produce very good thermal emittance levels, long lifetimes (>2 years in LCLS-I), and does not require extreme vacuum pressure control (~10^{-9} Torr), but it also has a fairly low quantum efficiency (QE) of about 3×10^{-5} (for UV light at 253 nm). The low *QE* requires an ultra-violet (UV) laser pulse energy of 20-40 μJ on the cathode for a 250-pC electron bunch, as has been demonstrated at LCLS-I for several years [4]. In LCLS-I the entire system has been very reliable with up-time >98%. The drive laser system is composed of the following components:

- The laser, which produces the UV beam for electron generation and the IR beam for the heater.
- The gun transport system, which conditions the UV beam to meet the required spatial and temporal parameters, and projects the beam onto the cathode at near normal incidence.
- The heater transport, which conditions the IR beam to meet the required spatial and temporal parameters and launches the beam through the heater undulator.
- Diagnostics that allow all relevant beam parameters to be measured at the appropriate places in the system, integrated with feedback loops for pointing stability.
- The laser hall that provides the environmental conditions required by the laser, which serves to limit the exposure to laser hazards and includes a laser safety system that meets SLAC, DOE, OSHA, and ANSI laser safety standards.

6.2.1 Drive Laser Specifications

As is the case in LCLS-I, the drive laser itself will be based on chirped pulse amplification (CPA) in Ti:sapphire followed by harmonic conversion to the required UV wavelength. In this case we begin with a mode-locked Ti:sapphire oscillator that generates a 68-MHz train of nano-Joule level pulses in the 750-780 nm wavelength range. The 68-MHz repetition rate is important because it is commensurate with the RF timing systems of the SLAC linac, allowing the laser oscillator to be synchronized to the linac. Because these pulses are roughly 30 fs in duration the time-bandwidth limited spectral width is roughly 30 nm. In CPA systems, this large spectral width is exploited to stretch the pulse to a width of >150 ps by passing the pulses though a device with significant group velocity dispersion. This stretcher expands the pulses temporally so that they can be amplified to higher energy without the risk of damaging the amplifier components. After the pulses are amplified to the desired energy, they can be compressed back to the 30-fs level in a device with group velocity dispersion that cancels that of the stretcher. In the case of LCLS, we spectrally filter the pulse from 30 nm down to 1 nm and adjust the compression process to adjust the pulse width between 2 and 10 ps FWHM.

The laser consists of commercially available laser hardware with minor modifications to meet our specific needs. In the case of the laser oscillator, there are at least two companies that can provide an oscillator (Figure 6.4) that meets the LCLS-II requirements. Between the LCLS-I injector and the NEH experimental laser systems, we are currently operating several of these oscillators from both companies and have worked with both companies to make the required modifications.

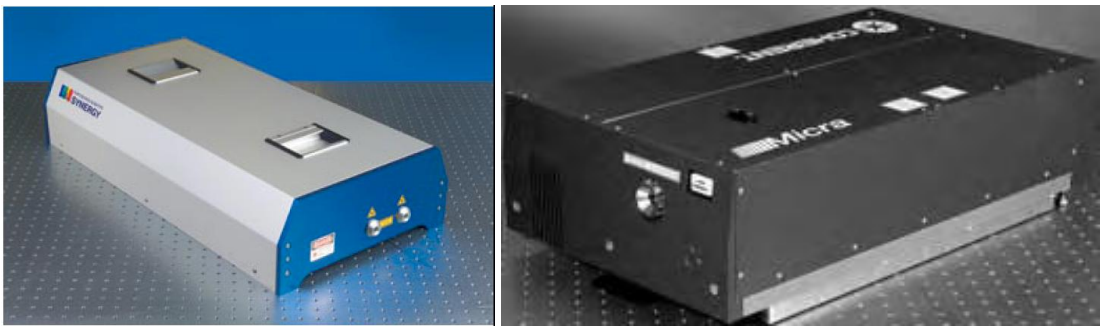

Figure 6.4. Commercially available mode-locked oscillators that meet LCLS-II requirements.

The stretcher, amplifiers, and compressor used in LCLS-I are also commercially available devices with minor modifications. In all cases, the first stage of amplification is performed in a regenerative amplifier (regen) based on Ti:sapphire pumped by frequency doubled Nd:YAG or Nd:YLF and running at 120 Hz repetition rate. The regenerative amplifier provides very high gain in a compact space, raising the pulse energy from nJ to mJ. We are currently using regens from two different companies (Figure 6.5) with SLAC modifications to force the amplifier to operate at the desired wavelength. Following the regen, one or more multi-pass Ti:sapphire amplifiers can be used to increase the pulse energy to the required level. We currently operate multi-pass amplifiers from commercial companies as well as SLAC designed units.

Figure 6.5. An example of a commercial regenerative amplifier (regen).

After amplification to the desired energy and compression to the desired pulse width, the 760-nm pulse is frequency doubled and then tripled to 253 nm. The final output parameters required are shown in Table 6.2.

Table 6.2. Parameters of the UV drive laser system ("nominal" 250-pC bunch charge).

Parameter	Symbol	Unit	Nominal	Range
Operating wavelength (for Cu cathode)	λ_{UV}	nm	253	250-260
Pulse repetition rate	f_{rep}	Hz	120	1-120
Number of laser pulses per RF pulse	N_b	-	1	1-2
Nominal pulse energy on cathode	U	μJ	20-40	0-250
Maximum pulse energy on cathode	u_{max}	μJ	250	-
Laser spot diameter on cathode	d	mm	1.2	0.5-2.0
Pulse length (FWHM)	Δt	ps	5	2-10
Longitudinal pulse shape	-	-	Gaussian	-
Transverse pulse shape	-	-	uniform	-
Spatial homogeneity on cathode (peak-to-peak)	-	%	<15	-
Longitudinal homogeneity on cathode (peak-to-peak)	-	%	<10	-
Optical energy jitter (in UV, rms)	-	%	<2	-
Laser-to-RF phase jitter (rms)	-	ps	<0.2	-
Laser rms position jitter on cathode / rms spot size	-	%	<3	-

Once laser pulses are produced with these parameters, they leave the laser and move into the transport system. The transport system consists of three primary parts: The upstairs beam conditioning and transport, the transport tube down to the injector vault (evacuated for most of the distance), and the gun laser transport in the vault. Drawings of the optical components upstairs and in the vault are shown in Figure 6.6 and Figure 6.7.

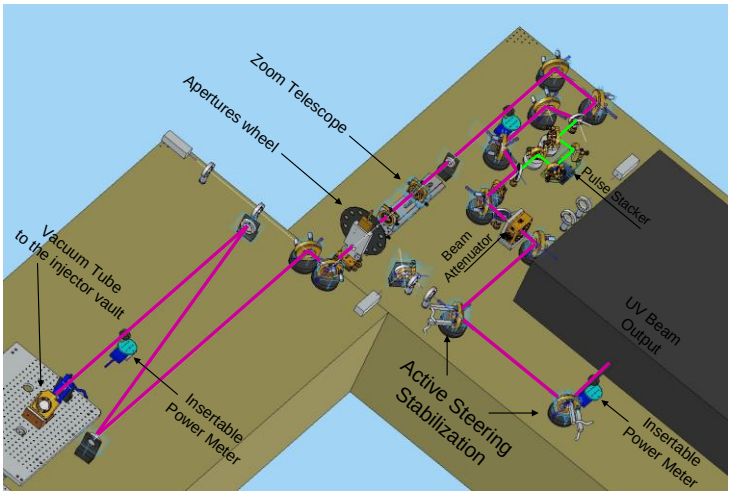

Figure 6.6. Upstairs laser beam conditioning and transport.

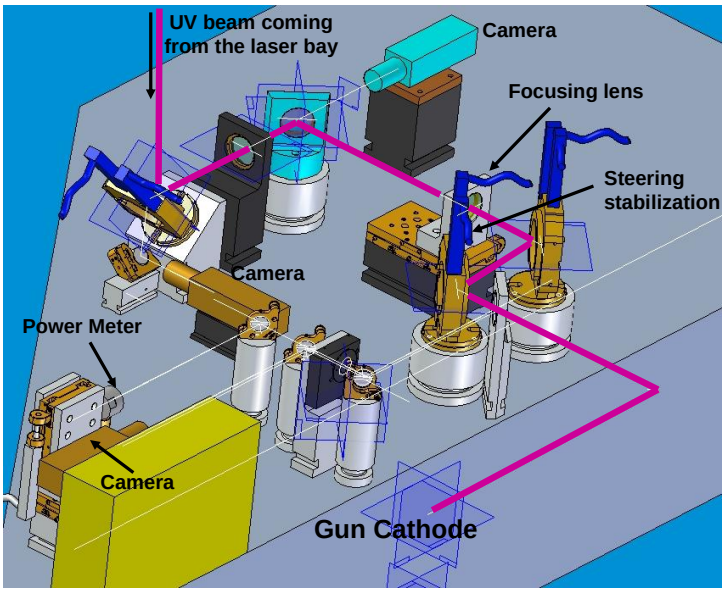

Figure 6.7. Laser transport system in the vault.

Upstairs, the beam is first propagated through a beam pointing stabilization system consisting of two cameras and two motorized mirrors. After that the beam passes through a waveplate and polarizer that allows the laser pulse energy to be controlled in a feedback loop that measures the charge produced from the gun. The pulses can then be sent into a pulse stacker that allows for more temporal control or multi-bunch production. The beam diameter is then adjusted in a zoom telescope before being spatially clipped on one of twelve apertures that allow production of a more uniform, flat-top spatial distribution. This aperture is then relay imaged through the transport pipes, to the vault transport optics where the image is reformed on the photocathode. Before reaching the cathode a fraction of the pulse is sampled for another pointing stabilization system, an energy measurement, and an equivalent plane imaging system that allows the spatial profile on the cathode to be monitored on the Virtual Cathode Camera (VCC). The spatial profile for LCLS-I as seen on the VCC is shown in Figure 6.8.

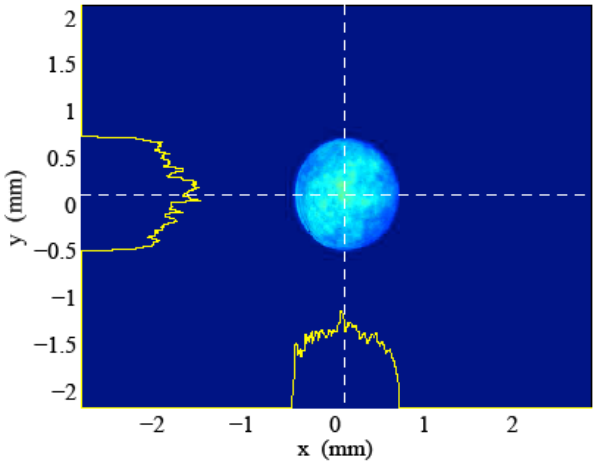

Figure 6.8. Spatial profile on cathode as recorded by Virtual Cathode Camera in LCLS-I. Yellow curves are "line-out" traces showing the instantaneous distribution along that line.

6.2.2 Laser Heater

The laser heater [4] has been performing well in LCLS-I for at least 2 years now [5]. The IR beam used for the heater (Section 6.3.3.5) is extracted from the drive laser as the spent beam which is left over after the frequency tripler crystal; therefore it is well synchronized to the electron beam. The requirements for the laser in the heater system are listed in Table 6.3.

Table 6.3. IR laser parameters of the laser-heater system.

Parameter	Symbol	Unit	Nominal	Range
Maximum IR pulse energy in the undulator	u	μJ	10	0-200
IR wavelength	λ_{IR}	nm	758	750-780
Max. IR pulse rate	f_{rep}	Hz	120	1-120
IR beam size at center of the undulator (rms)	$\sigma_{x,y}$	μm	200	100-300
IR pulse length in undulator (FWHM)	$\Delta\tau_{FWHM}$	ps	12	10-20
Laser beam Rayleigh range	L_R	cm	50	42-1600
Laser pulse energy in the undulator	P_E	μJ	6	0-200
Laser power in undulator	P_L	MW	0.5	0-17
Laser rms beam size in undulator	$\sigma_{L\text{-}x,y}$	mm	0.2	0.16-0.3
Position stability of IR beam in und. (rms)	$\Delta x/\sigma_x$	%	<20	-
Timing stability of IR beam in und. (rms)	$\Delta t/\Delta\tau_{FWHM}$	%	<30	-

Figure 6.9. (Left) Optical bench attached to the ceiling of the vault and relay imaging lens and tube that transports the beam to the heater. (Right) Laser heater optical table with diagnostics and controls.

IR light for the laser heater is taken from the residual IR that comes out of the tripler. Because the tripler efficiency is roughly 10%, we have roughly 10 times the UV energy (>10 mJ) left in the IR which is more than the required amount shown in Table 6.3. The IR is sent through a parallel grating pulse stretcher to produce the required temporal width and is then relay imaged first to an optical bench that is attached to the ceiling (see Figure 6.9) in the vault and then to the heater interaction region. There are pointing stability lock loops and diagnostics included as part of this optical transport system.

6.2.3 Laser Room

The laser room serves several purposes. It provides a stable clean environment for the laser. It also serves to limit access to the laser hazard zone and provides the infrastructure for the Laser Safety System (LSS). The laser room is at ground level above the injector vault and the UV and IR beams are transported through 10-meter long vacuum pipes that will be installed in a penetration to the injector tunnel (see Figure 6.10).

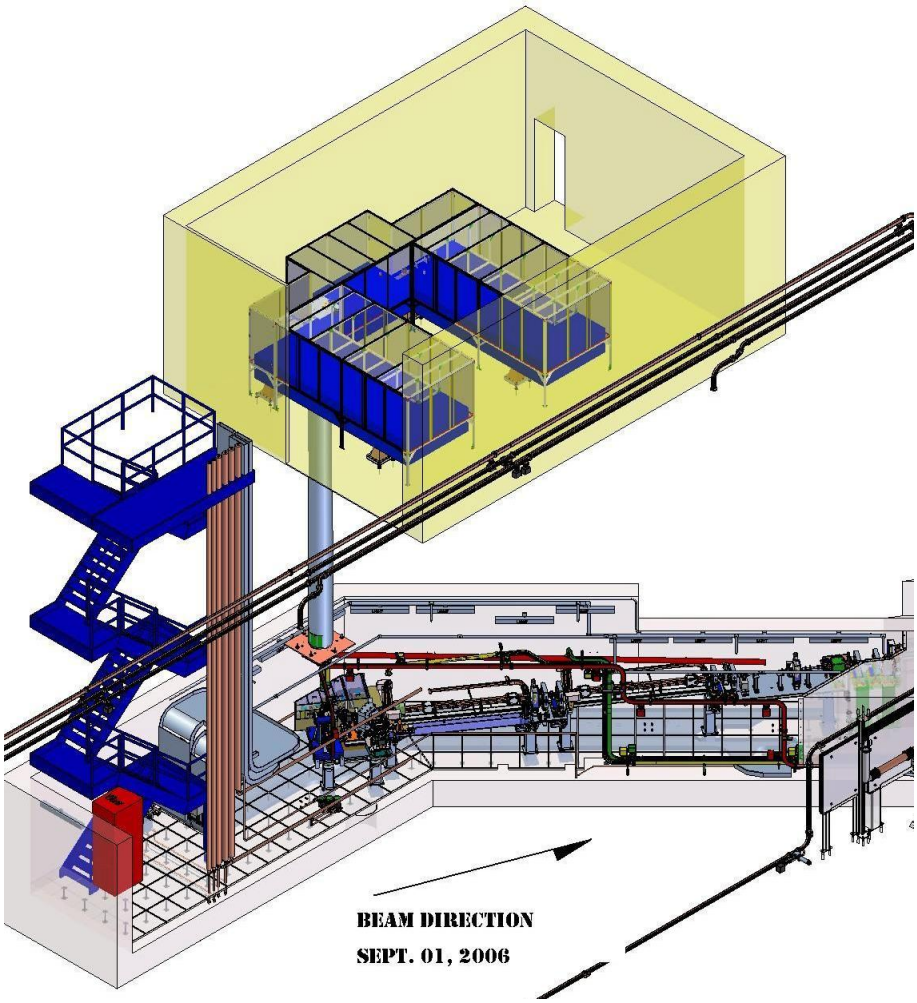

Figure 6.10. Laser room above the injector vault. Silver pipe is UV transport to laser bench attached to ceiling. Red pipe is IR transport to heater.

The laser room is designed to provide a temperature stability of better than ±1°F at a humidity of 50% ± 10%. The conditioned air is filtered by High Efficiency Particulate Air (HEPA) filters, providing a clean environment for the laser system. The LSS controls the operational state as well as entry and exit to and from the room. If there are interlock faults, the LSS will insert the required shutters or turn off lasers as described in the facility Standard Operating Procedure (SOP).

6.3 Electron Gun and Injector

The LCLS-II FEL performance relies critically on the electron gun and injector beam quality. The six-dimensional electron beam brightness must be high enough and the beam stability must be good enough or the FEL performance, especially at short wavelengths (~1 Å), may be significantly compromised. The electron beam requirements from the gun and injector are listed in Table 6.4 with the time-sliced transverse emittance as the most critical parameters. The performance of the LCLS-I gun and injector is described in Ref. [6].

Table 6.4. Electron beam requirements from the electron gun and injector (before L1-linac).

Parameter	Symbol	Unit	Nominal	Range
Electron bunch charge	Q_0	nC	0.25	0.01 - 1.0
Pulse repetition rate	f_{rep}	Hz	120	1 - 120
Electron energy after injector (before L1-linac)	E_0	MeV	135	120 - 150
Number of electron bunches per RF pulse	N_b	-	1	1 - 2
Electron transverse, rms, normalized, *slice* emittance	$\gamma\varepsilon_{x,y\text{-}s}$	μm	0.5	0.1 - 1.0
Electron transverse, rms, normalized, *projected* emittance	$\gamma\varepsilon_{x,y\text{-}p}$	μm	0.6	0.2 - 1.2
Electron longitudinal, rms, normalized emittance (heated)	$\gamma\varepsilon_z$	μm	20	<0.4 - 40
Electron peak current (before BC1)	I_{pk}	A	35	5 - 100
Electron rms bunch length ((before BC1)	σ_z	mm	0.6	0.2 - 1.0
Electron rms *slice* energy spread (heater at nom.)	$\sigma_{E\text{-}s}$	keV	17	<1 - 20
Electron rms *projected* energy spread	$\sigma_{E\text{-}p}$	keV	70	10 - 150
RMS transverse stability (norm. to rms spot size)	x_{rms}/σ_x	%	<4	-
RMS energy stability (norm. to rms spot size)	E_{rms}/E_0	%	<0.1	-
RMS relative bunch charge stability	$\Delta Q_{rms}/Q_0$	%	<2	-
RMS bunch arrival time stability (before BC1)	Δt_{rms}	ps	<0.3	-

6.3.1 Electron Gun Design and Performance

The performance of the existing gun in LCLS-I has been outstanding owing to a careful design [7]. The LCLS-II injector will use the same gun design, which has been proven to meet all requirements for the LCLS-II injector (Figure 6.11).

The gun is a 1.6-cell normal conducting copper structure at S-band RF frequency (2.856 GHz) with dual feed RF input and copper cathode supported on the back-plane of the half cell. The gun fields are fully rotationally symmetric by incorporating dual feed (to eliminate dipole fields) and a racetrack geometry (to cancel quadrupole fields induced by the dual feed) for the full cell into which the RF is coupled. The RF gun parameters are listed in Table 6.5.

The entire Gun-To-Linac (GTL) beamline from the gun exit to the entrance of the first linac section has been designed to mitigate wakefields. This includes tapering of the beam tube through the gun solenoid,

the vacuum valve after the gun solenoid, all bellows, diagnostics, and the vacuum chamber for the gun-spectrometer magnet. The beamline is pumped through longitudinal slots to minimize the wakes.

The LCLS-I gun has produced exceptional transverse normalized emittance levels of 0.4 μm at a 250-pC bunch charge with a reasonably uniform spatial UV (253 nm) laser transverse distribution (1.2-mm diameter) on the photocathode and a Gaussian temporal laser pulse with 3-4-ps FWHM at up to 120 Hz (~35 A peak current). The RF field on the cathode is set at 115 MV/m producing a 6.0-MeV electron beam at the gun exit. The cathode quantum efficiency has been variable at 2-6$\times 10^{-5}$ with a 30-deg laser phase w.r.t. the gun RF zero-crossing.

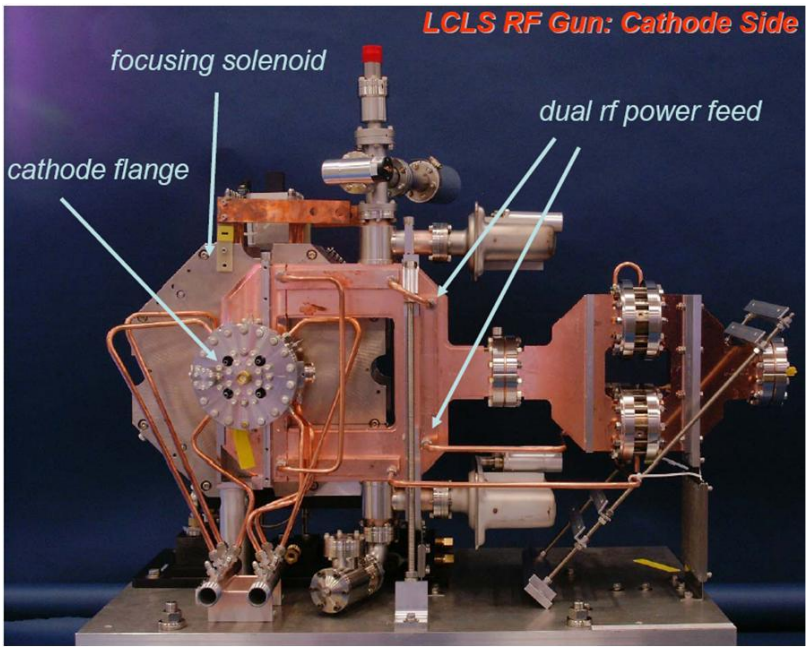

Figure 6.11. The LCLS-I RF photocathode gun seen from the cathode side.

Table 6.5. RF photocathode electron gun parameters.

Parameter	Symbol	Unit	Nominal	Range
Cathode material	-	-	Cu	-
Minimum useable diameter of cathode	d_u	mm	12	-
Expected cathode quantum efficiency (at 253 nm UV)	QE	10^{-5}	4	1 - 10
Peak RF field (2856 MHz)	E_{pk}	MV/m	120	100 - 130
Electron energy after gun	E_0	MeV	6.0	5.5 - 6.2
Electron energy spread, rms (before heater)	σ_E	keV	~1	0.1 - 5
RF repetition rate	f_{rep}	Hz	120	10 - 120
RF pulse duration (one bunch per RF pulse)	Δt_{RF}	μs	1.3	1 - 3
Peak RF power	P_{RF}	MW	10	7 - 12
Number of cells	N_c	-	1.6	-
Length of gun	L_{gun}	m	0.17	-

To minimize the possibility of cathode surface contamination, expedite possible cathode changes, and reduce the overall risk of a cathode change, the LCLS-II RF gun may be equipped with a load-lock system. The load-lock will contain at least one spare cathode and will facilitate a cathode change procedure without breaking the gun vacuum.

6.3.2 Photocathode

The main area of gun improvement is the copper photocathode. The cathode has only been changed once in period of more than 3 years and the present cathode has been operating reasonably well for the 28 months of July 2008 to Nov. 2010, and continuing. Operation of the LCLS-I gun shows a slow degradation of the quantum efficiency due to surface contamination caused by reduction of hydrocarbons on the surface of the cathode. This phenomenon occurs primarily in the area of laser exposure (see Figure 6.12). It is possible (and common) to move the drive laser spot by 1 to 2 beam diameters but a 10 to 20 percent increase of the transverse emittance takes place. To remedy this problem, we plan to use one of the oblique gun ports to attach a surface cleaning device such as a hydrogen plasma source (Figure 6.13). An R&D program to develop this process is currently underway. In-situ laser cleaning has not been successful at LCLS.

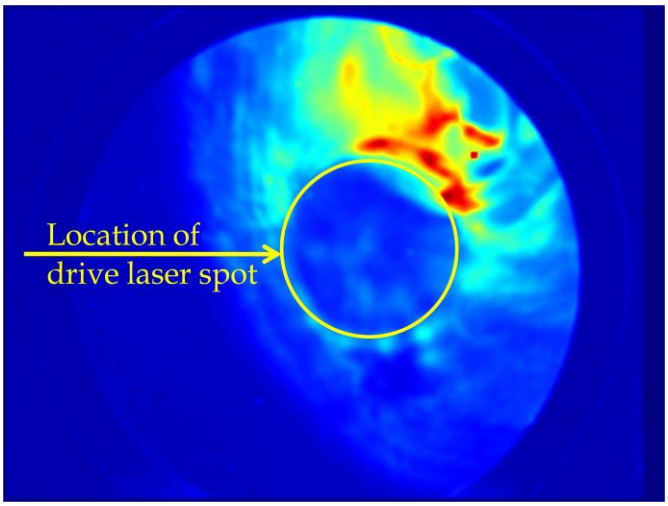

Figure 6.12. Degradation of cathode quantum efficiency due to surface contamination.

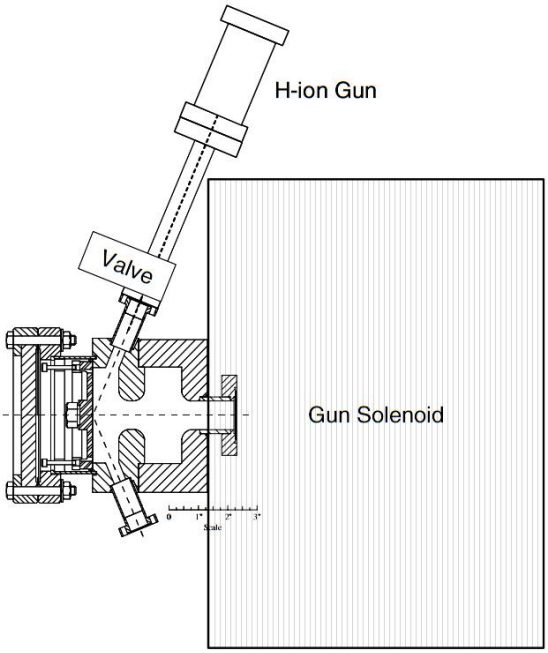

Figure 6.13. Integration of Hydrogen Plasma source into gun for in-situ cathode surface cleaning.

6.3.3 Electron Injector

The electron injector optics, from cathode through the Dog Leg (DL1) system, is shown in Figure 6.14 with the laser heater undulator gap and chicane at their nominal setting (strong vertical focusing from each of these components). A layout of the LCLS-I injector vault is also shown in Figure 6.15, with the LCLS-II layout almost identical.

The LCLS-I injector has performed quite well, as described in [6], and consists of the drive laser, the RF photocathode gun, two 3-m long S-band RF accelerating structures, the laser heater system, a transverse RF deflecting cavity, and a 35-deg bend system (DL1) to bring the beam into the main SLAC linac. In addition, a gun spectrometer is located immediately after the gun and can be switched on when

needed, and a 135-MeV spectrometer is located adjacent to the DL1 bend system, which can also be switched on easily. These allow high resolution energy and energy spread measurements at these key locations. The gun accelerates the electrons to 6 MeV, while the two S-band structures accelerate to 63 MeV (first section, L0a, 19 MV/m) and then to 135 MeV (second section, L0b, 24 MV/m). Several YAG and OTR screens, and optional wire-scanners, are available, in conjunction with the transverse RF deflector, to measure projected emittance, slice emittance (horizontally only), absolute bunch length, projected and slice energy spread, and final energy chirp. The system has performed quite well and will be a nearly identical copy for LCLS-II. Beam diagnostics for the LCLS-II injector, and beyond, are described in Section 6.11.

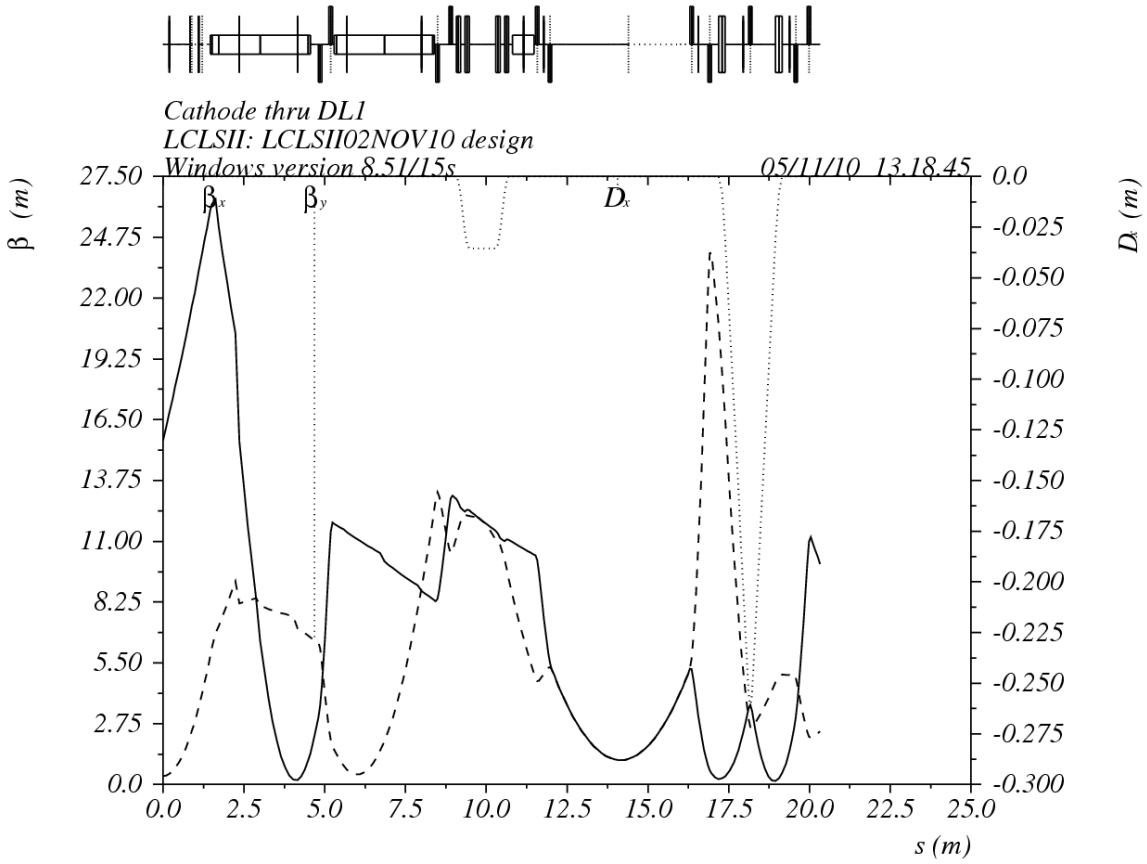

Figure 6.14. The electron injector optics and layout from cathode through the DL1 dog-leg system (with heater chicane ON and laser-heater undulator at its nominal gap of 34 mm).

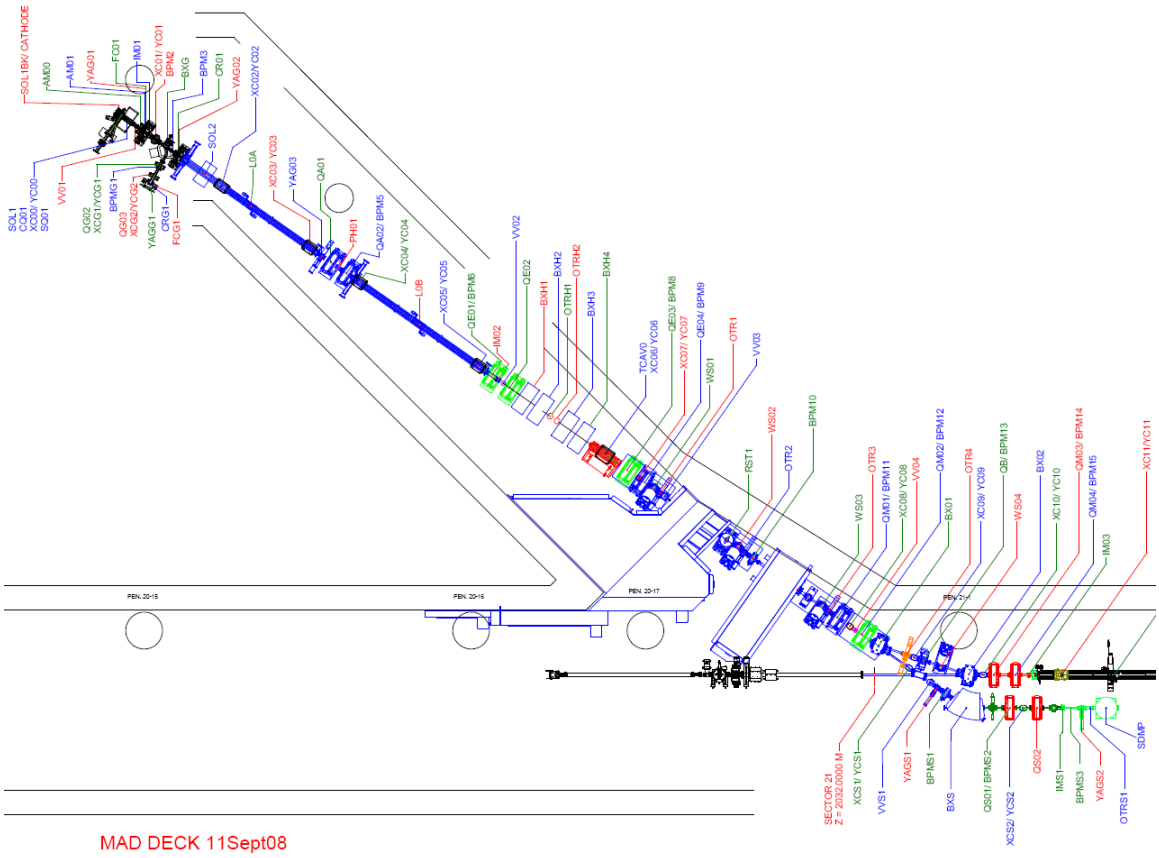

Figure 6.15. Layout of the LCLS-I injector vault, which is nearly identical to the LCLS-II layout.

6.3.3.1 Transverse Projected Emittance Measurements

The projected emittance of the LCLS beam depends strongly on the spatial and somewhat on the temporal beam profile from the UV laser. Extensive beam dynamics simulations for LCLS-I were carried out and the performance of the injector was found to be optimal for a flat spatial distribution of the drive laser beam with a Gaussian temporal profile of ~5 ps FWHM.

A simulation, using *Impact-T* [8], of the evolution of the transverse injector emittance and beam sizes of a 250-pC beam up to an electron energy of 135 MeV is given in Figure 6.16 and the electron energy along the injector is shown in Figure 6.17. A measurement of the transverse projected injector emittance as measured for the LCLS-I injector is given in Figure 6.18. Simulations indicate further improvement is possible by carefully shaping the spatial distribution of the drive laser transverse and temporal profile, but the improvements are only at the 10% level.

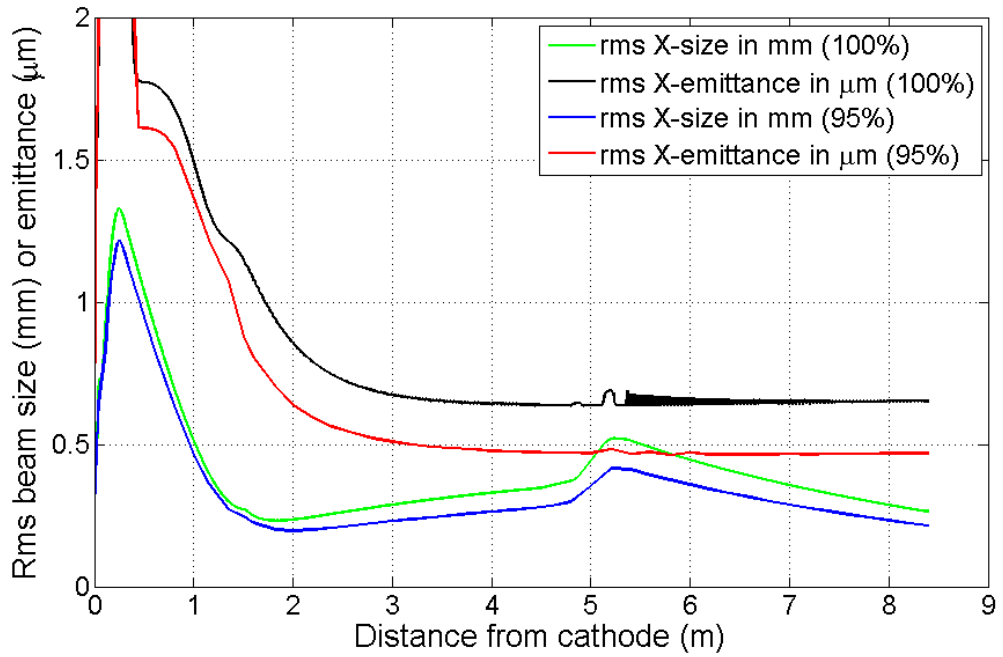

Figure 6.16. Simulation of the emittance and beam size evolution through the injector, from cathode up to exit of L0b RF structure at 135 MeV (250 pC).

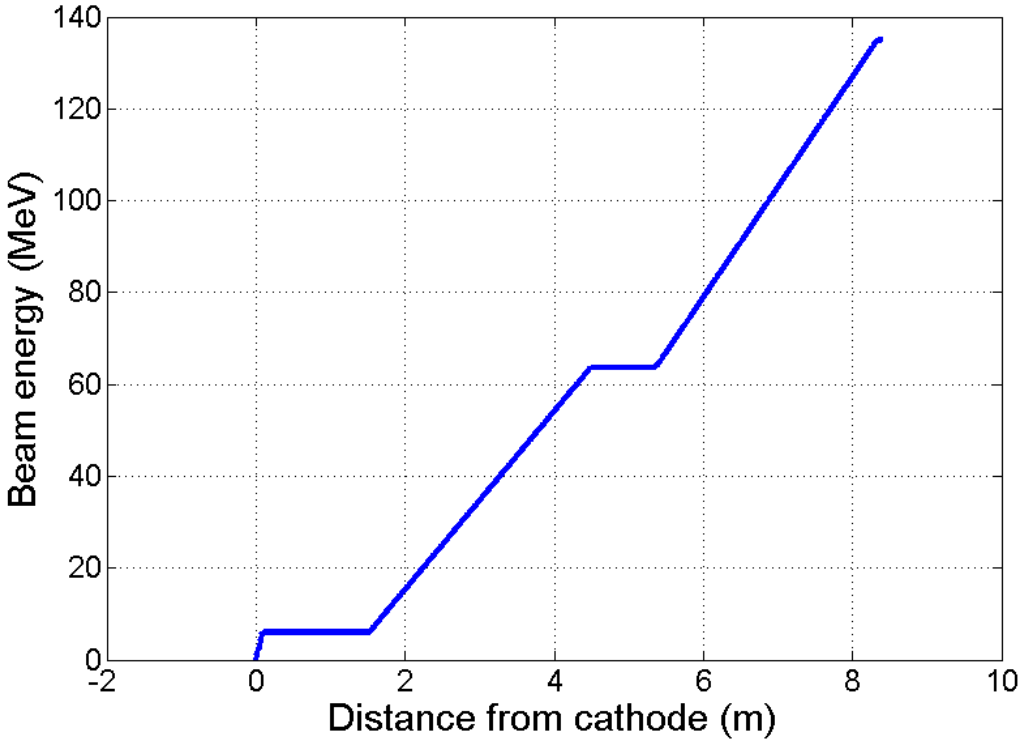

Figure 6.17. Electron energy from cathode to end of L0b accelerator section at 135 MeV.

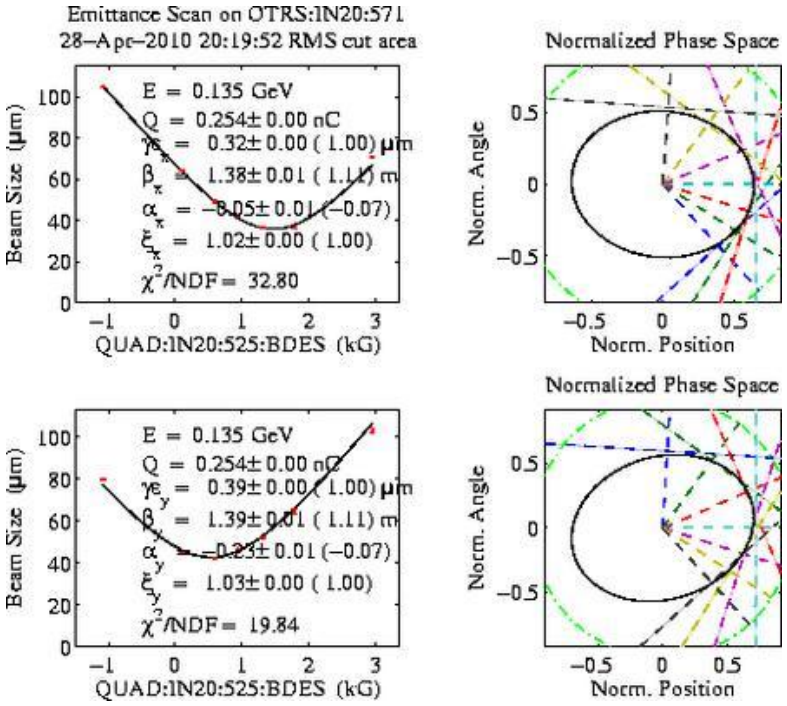

Figure 6.18. Measured projected emittance at OTR2 (s = 14 m in Figure 6.14 at 135 MeV and 250 pC). This case represents one of the smaller observed emittance values. Results actually vary between 0.35 μm and 0.55 μm at 250 pC.

6.3.3.2 Slice Emittance Measurements

An example of a slice emittance measurement for nominal operating conditions at 250 pC bunch charge is given in Figure 6.19 and Figure 6.20, indicating that the LCLS-I results are well within the range needed for LCLS-II. Tracking simulations show good agreement with LCLS-I measurements (Figure 6.21), while phase space simulations are shown in Figure 6.22. Descriptions for 95% of the particles are included, where 5% of the particles with the largest action (position and angle normalized with β and α and summed as squares) are cut away in order to better examine the core of the beam. The parameters for these simulations are listed in Table 6.6.

Table 6.6. Parameters for the injector tracking simulations below.

Parameter	Symbol	Unit	Value
Thermal transverse emittance per rms laser spot size	$\gamma\varepsilon_{x,y}/\sigma_{x,y}$	0.9	μm/mm-rms
Bunch charge	Q	250	pC
Laser FWHM pulse duration (Gaussian)	Δt	5	ps
Laser diameter on the cathode	d	1.2	mm
Electron energy from the gun	E_0	6	MeV
Final rms bunch length at 135 MeV	σ_z	0.59	mm
Slice rms energy spread in core at 135 MeV	σ_E	0.6	keV
Relative projected rms energy spread at 135 MeV	σ_δ	0.073	%

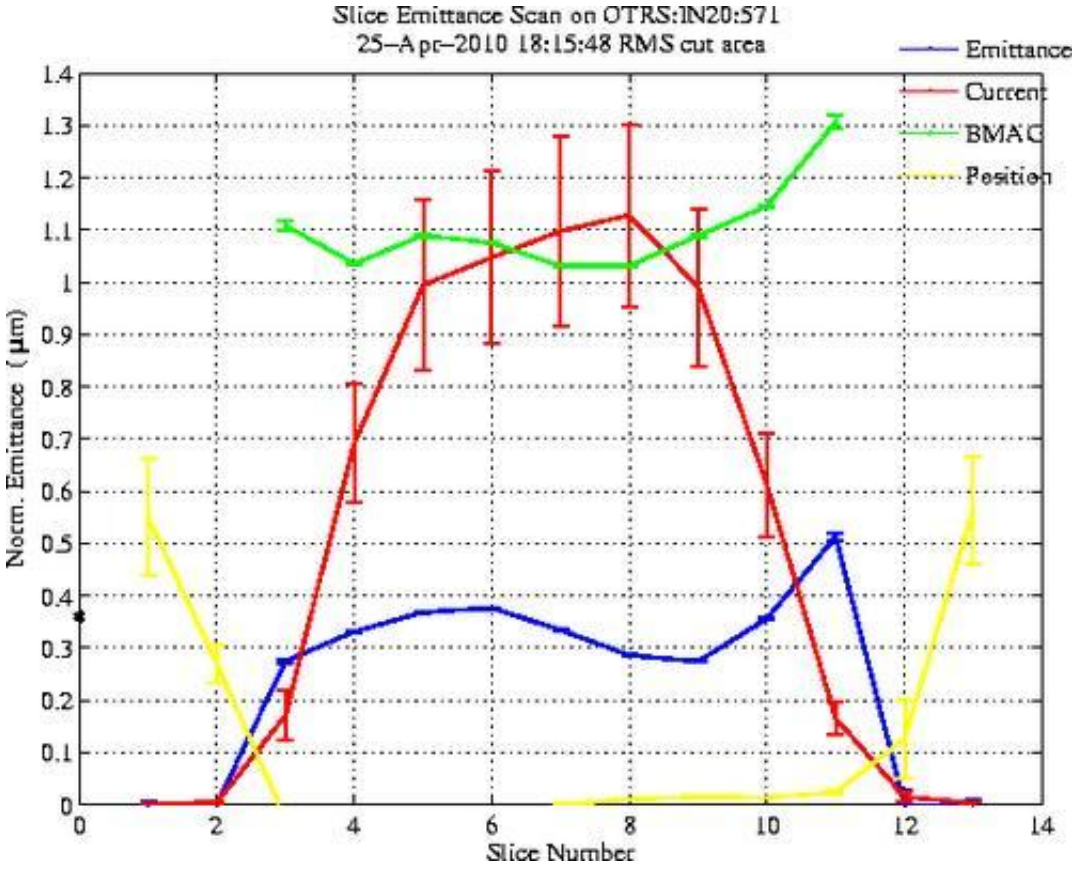

Figure 6.19. Horizontal emittance (blue) measurement (LCLS-I) on OTR2 at 135 MeV ($\gamma\varepsilon_x$ < 0.4 μm at s = 14 m in Figure 6.14) as a function of slice number, where each slice is about 1 ps long (250 pC).

The red curve is the temporal beam profile (arb. units) and the green curve is the beta-mismatch amplitude factor where 1.0 is the ideal matching condition.

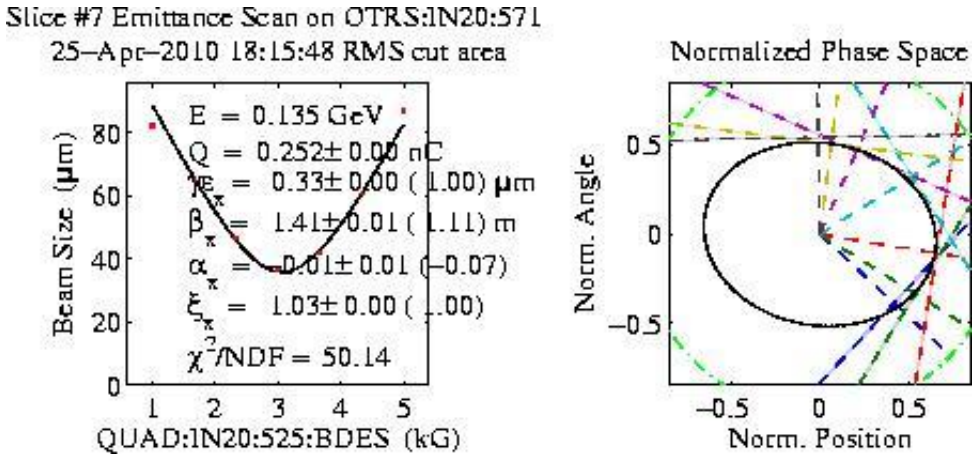

Figure 6.20. LCLS-I slice emittance measurement ($\gamma\varepsilon_x$ = 0.33 μm at OTR2, 135 MeV, 250 pC), central slice.

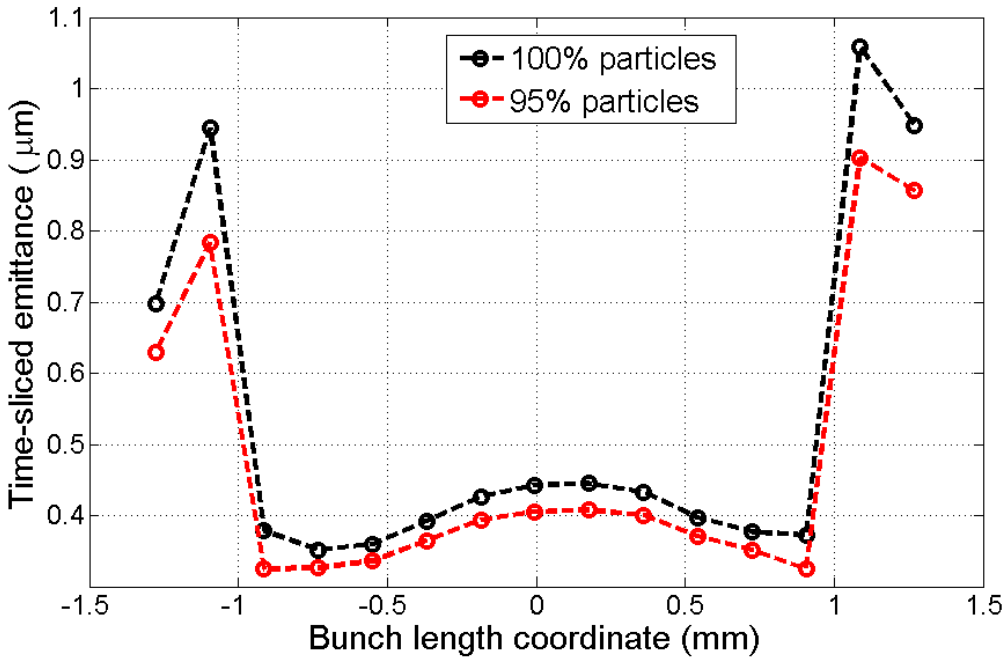

Figure 6.21. Simulated slice emittance (250 pC, 135 MeV). The lower curve (red) is shown for 95% of the electrons in order to cut large tails which have little role in the FEL gain.

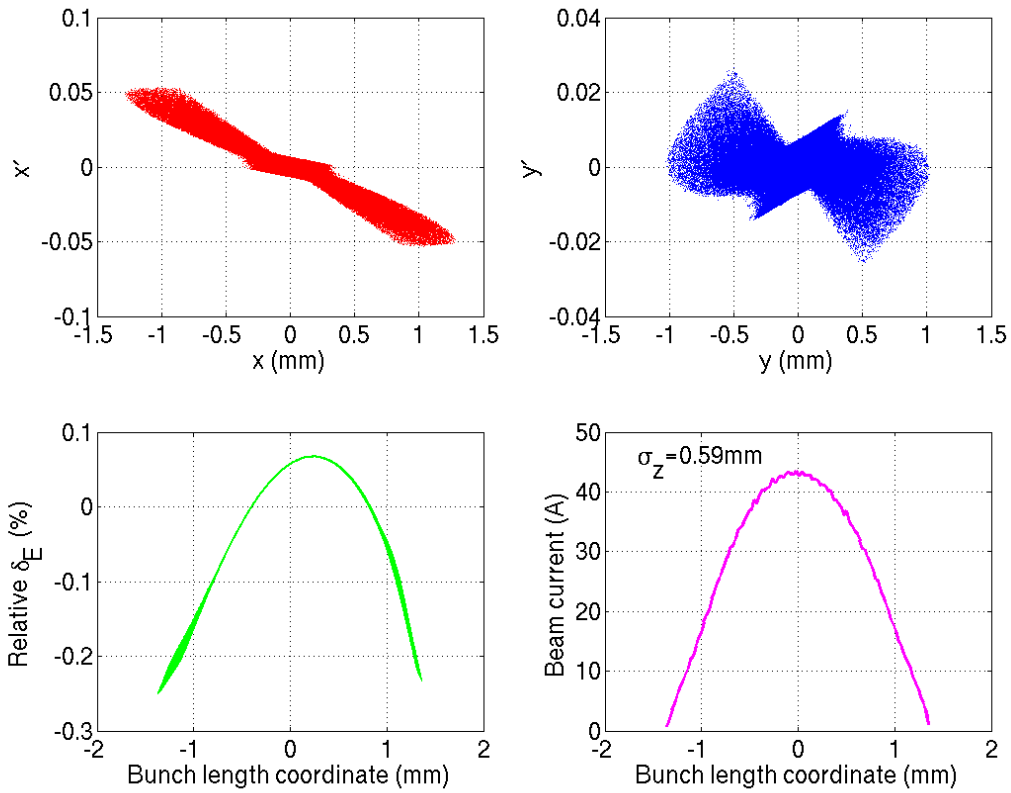

Figure 6.22. Simulated 6D phase space of electron bunch at 250 pC and 135 MeV showing the very small slice energy spread (0.6 keV rms, lower left) and the parabolic temporal distribution (0.59 mm rms, lower right). The projected emittance (95%) is 0.47 mm.

6.3.3.3 6-MeV Spectrometer

A dipole magnet is located just downstream of the RF gun and can be switched on in order to measure the absolute energy and energy spread from the gun using a YAG screen. The energy measurement is used to calibrate the gun RF amplitude read-back in units of MV. The magnetic fields of the spectrometer bend (85°) are precisely measured prior to installation and the magnet includes a small trim coil so that its field can be reliably zeroed for normal operations (spectrometer off). A YAG screen and Faraday cup are located at the end of this short spectrometer (see Figure 6.23).

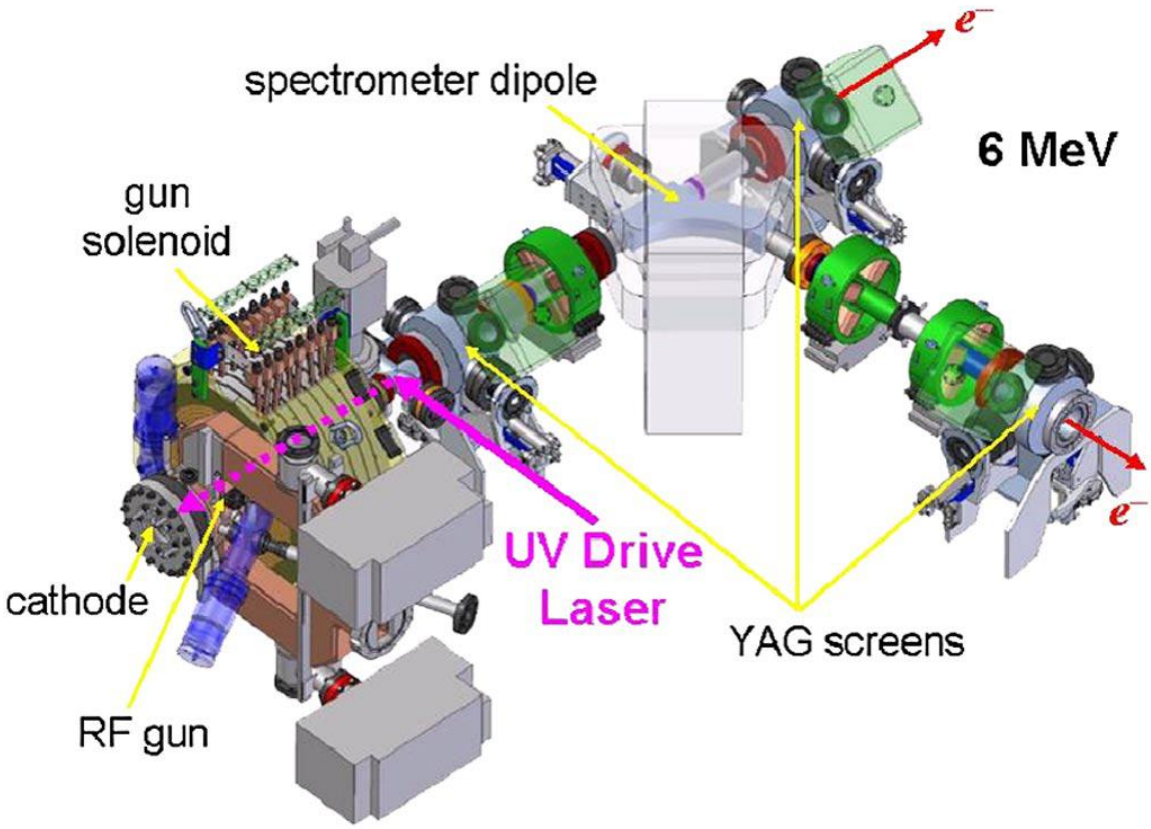

Figure 6.23. The gun and gun-to-linac (GTL) transport, including spectrometer, YAG screens, and solenoid. The drive laser actually enters on the opposite side. None of the green quadrupole magnets will be installed since they are unnecessary.

6.3.3.4 135-MeV Spectrometer

At the end of the injector the two bend magnets (net 35°) to the main linac can be switched off and the electron beam can be taken to a special high-resolution spectrometer system at 135 MeV (see lower right side of Figure 6.15). A 35-deg bend magnet is located here with a short spectrometer beamline, two quadrupole magnets, and a YAG screen. The horizontal dispersion at the final YAG screen is almost 700 mm while the beta function is <1 meter, which allows precision energy and energy spread measurements. In addition, the transverse RF deflector in the injector can be switched on to reveal the electron population in longitudinal phase space, where the vertical coordinate on the YAG screen becomes the bunch length coordinate (due to the deflector) and the horizontal axis on the YAG screen is the energy coordinate due to the 35-deg spectrometer bend (see Figure 6.24). In this way, the slice energy spread can be measured down to a resolution of about 6 keV rms (4×10^{-5}) and the energy-time correlation can be clearly seen (*e.g.*, beam at crest phase).

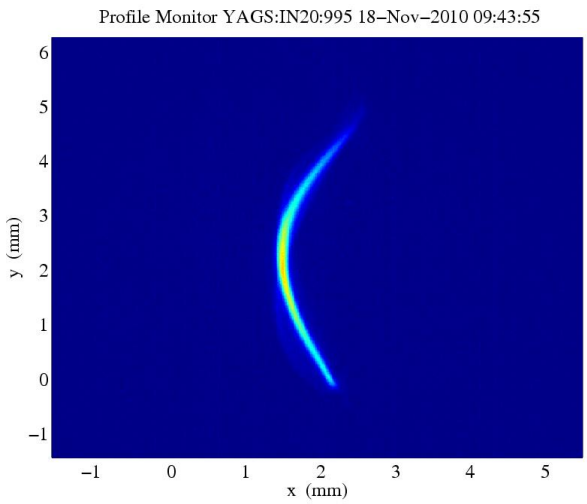

Figure 6.24. Measured beam image on YAG screen after the 135-MeV spectrometer bend with RF deflector switched on reveals longitudinal phase space directly on the screen. Here the vertical axis represents time (1 mm is approx. 2 ps) and the horizontal axis is energy (1 mm is approx. 0.2%).

The lack of a linear *x-y* correlation here indicates proper RF phasing in the injector, with no energy chirp on the beam.

6.3.3.5 Laser Heater System

The injector system will incorporate a laser/electron beam heater system (an inverse free electron laser) in order to generate an increased intrinsic energy spread in the electron beam [2]. This produces Laudau damping in the bunch compressor chicanes which suppresses the micro-bunching instabilities driven by Coherent Synchrotron Radiation (CSR) in the bunch compressors, and Longitudinal Space Charge (LSC) forces in the linac. The heater system is located just downbeam of the L0b accelerator section at 135 MeV in the off-axis LCLS injector housing (see Figure 6.25).

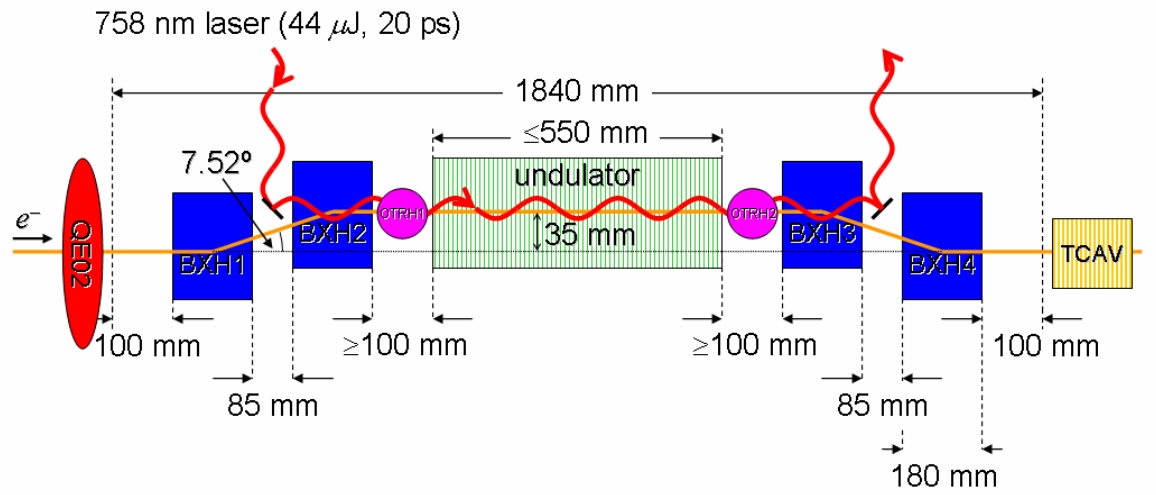

Figure 6.25. The laser-heater system in a weak chicane with co-propagating laser beam. The blue squares represent chicane magnets and the green rectangle represents the 9-period undulator.

Two OTR screens with photo-diodes are included to aid in achieving spatial and temporal overlap of the co-propagating laser and electron beams. Dimensions and laser power are approximate.

The electron beam (~5 ps long) propagates collinearly with the Ti:sapphire laser pulse (~10 ps long, 758 nm wavelength) through a 55-cm long, 9-period, adjustable gap, planar, permanent magnet undulator located within a magnetic chicane. The laser-electron interaction modulates the electron energy along its bunch length with a period equal to that of the laser (758 nm). The chicane provides convenient injection of the laser beam and, more importantly, an effective time-smearing of the energy-modulation due to the path length dependence (through the last two chicane bends) on each electron's horizontal angle in the undulator (finite transverse emittance). This smearing erases all time-structure on the bunch and produces an effective 'thermal' local energy spread [2]. A 0.5-MW laser power (6 μJ in 12 ps), and system parameters given in Table 6.7, will produce a 17-keV rms local energy spread, rather than the very small level (<1 keV rms at 250 pC) expected from the RF gun. The 1-keV level is too small to be of any advantage in the nominal configuration of the 1.5-Å x-ray FEL, and is also too small to generate any Landau damping in the bunch compressors. The heated energy spread of 17 keV becomes a 1×10^{-4} rms relative energy spread in the x-ray FEL (at 13.5 GeV and with a bunch compression factor of ~85), which is small enough to have a negligible impact on 13-keV x-ray FEL production, but large enough to effectively Landau damp the beam instabilities in the accelerator. Modeling studies show the local (uncorrelated) energy spread can be increased up to 100 keV rms in the laser heater chicane (17 MW or 200 μJ in 12 ps) and not affect the transverse emittance significantly. The heater's system parameters are listed in Table 6.7, while its laser parameters are above in Table 6.3. The laser heater electron optics functions are shown in Figure 6.26.

Table 6.7. Laser-heater electron beam, chicane, and undulator parameters.

Parameter	Symbol	Unit	Nominal	Range
Electron energy	E	MeV	135	120-180
Electron bunch length (FWHM)	Δt	ps	5	1-10
Electron transverse beam size (rms)	$\sigma_{x,y}$	mm	0.2	0.16-0.25
Undulator period	λ_u	cm	5.4	-
Undulator parameter	K	-	1.385	1.047-2.229
Undulator minimum gap	g	mm	34	25-100
Number of undulator periods	N_u	-	9	-
Chicane magnet eff. length	L_B	m	0.18	-
Bend angle of each chicane magnet	θ	deg	7.52	0-7.52
Beam offset in chicane center	$\lvert\eta_x\rvert$	mm	35	0-35
Required spatial overlap of laser and *e*-beam	$\lvert\Delta x\rvert = \lvert\Delta y\rvert$	mm	<0.2	-
Total rms energy spread induced	σ_E	keV	17	0-100

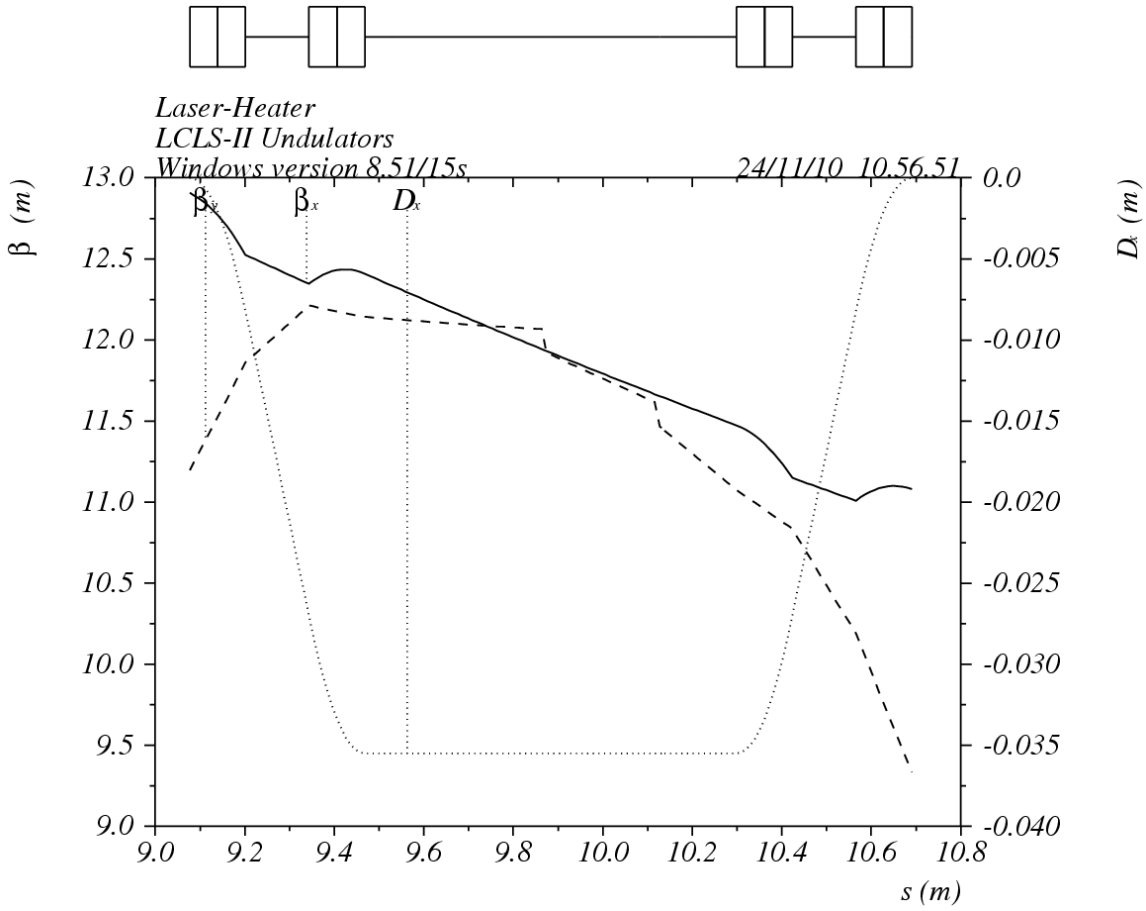

Figure 6.26. The laser heater electron optics in the LCLS-II injector at 135 MeV.

6.3.3.6 Linac Injector Horizontal Bend System (DL1)

The function of the low-energy 'Dog-Leg' (DL1) is to transport 135-MeV electrons from the new injector into the existing SLAC linac. While it is possible to design the dog-leg as a first bunch compression stage, this necessitates a large incoming correlated energy spread of 1-2%. In this case, the chromaticity of the quadrupole magnet within the dog-leg, required for a linear achromat, will generate large second order dispersion which needs sextupole compensation. Due to this, and also the need for easy R_{56} tuning (not natural in a dog-leg), DL1 is designed as a simple transport line. Its design requirements are:

- Provide a horizontal beamline deflection of 35° over a short distance,
- Should not alter the bunch length (*i.e.*, should be nearly isochronous),
- Should introduce no significant transverse emittance dilution,
- Should provide a dispersive section for energy and energy spread measurement.

A simple system that satisfies these conditions is composed of two dipole magnets of equal strength with a field lens located between them to produce a linear achromat. The dipoles are rectangular bends. A profile monitor based on Optical Transition Radiation (OTR) and a BPM at the high dispersion point will provide energy and energy spread measurements.

Table 6.8. Parameters of the linac injector horizontal bend system (DL1).

Parameter	Symbol	Unit	Value
Beam energy	E_{DL1}	MeV	135
Total horizontal deflection (sum of 2 bends)	θ	deg	35
RMS bunch length	σ_z	mm	0.6
RMS energy spread throughout beamline (at 135 MeV)	σ_δ	%	0.07
Momentum compaction	R_{56}	mm	6.3
Second order momentum compaction	T_{566}	mm	140
Length of each of two dipole magnets	L_B	m	0.20
Bend angle of each dipole	$\lvert\theta_B\rvert$	deg	17.5
Magnetic field of each dipole	$\lvert B\rvert$	kG	6.9
Maximum horizontal dispersion	$\lvert\eta\rvert_{max}$	m	263
Projected emittance dilution due to CSR (at $\gamma\varepsilon_0$ = 0.6 μm)	$\Delta\varepsilon_{CSR}/\varepsilon_0$	%	<1

The momentum compaction, R_{56}, of such a system for ultra-relativistic electrons and small angles is

$$R_{56} \approx \frac{1}{3}\theta_B^2 L_B\,, \tag{1}$$

where θ_B and L_B are the bend angle and length of each dipole, respectively. A 1.3-meter long beamline with two 17.5° bends provides the required deflection and the 20-cm long dipoles produce an R_{56} of 6.3 mm (opposite sign of a chicane). Therefore, an extreme electron which is off energy by 1% will move axially by only 60 μm, which is small compared to the 0.6-mm rms bunch length. The effect of the second order momentum compaction, T_{566}, is even less. Note, the nominal incoming relative rms energy spread from L0 is actually 0.07% rms. The system is therefore, for all practical purposes, isochronous. Nevertheless, the non-zero R_{56} value and the second order term of T_{566} ≈ 0.14 m has been taken into account throughout the design and stability optimization, and in the 2D and 6D particle tracking.

6.3.3.7 Injector Vacuum Systems

The pressure requirements for the LCLS-II gun/injector vacuum systems are listed in Table 6.9. To maintain a differential pumping regime with a vacuum gradient that is lowest away from the gun, an additional ion pump (with respect to LCLS-I) will be located immediately downstream of the RF gun at the location that was occupied by a YAG screen, which is not often used in LCLS-I. The RGA originally installed on the gun in LCLS-I will be installed at this location. A fast DAQ system will be implemented to allow detailed tracking of vacuum events. The LCLS-I injector was upgraded with such a system in 2010.

Table 6.9. Injector vacuum system pressure requirements.

LCLS-1 equivalent	Unit	Value
Waveguides	Torr	$<1\times10^{-8}$
Gun	Torr	$<5\times10^{-10}$
GTL	Torr	$<5\times10^{-9}$
L0A/B	Torr	$<5\times10^{-9}$

6.4 Main LCLS-II Linac

The main linac of the LCLS-II (sectors 11-20) may accelerate the electron beam as high as 15 GeV using about 850 meters of S-band (2.856 GHz) radio frequency (RF) traveling-wave accelerating structures, most of which are already installed in the SLAC linac. Some modifications of the linac sectors 10-20 are needed, which are similar but not identical to what was done in LCLS-I in sectors 20-30. Some of these modifications are costly and may eliminate future linac functionality (such as positron production at Sector 19), so it is worth examining the FEL performance tradeoffs with respect to electron energy. Figure 6.27 shows a plot of the estimated FEL saturation length and peak power at a 13-keV photon energy versus the final linac electron energy (other supporting parameters are listed in the plot title). The undulator length will need to be increased by only 3 meters if the electron energy were reduced from 13.5 GeV to 12.5 GeV, but the FEL peak power drops by about 18%. Therefore, the design is to accelerate the electron beam to 13.5 GeV.

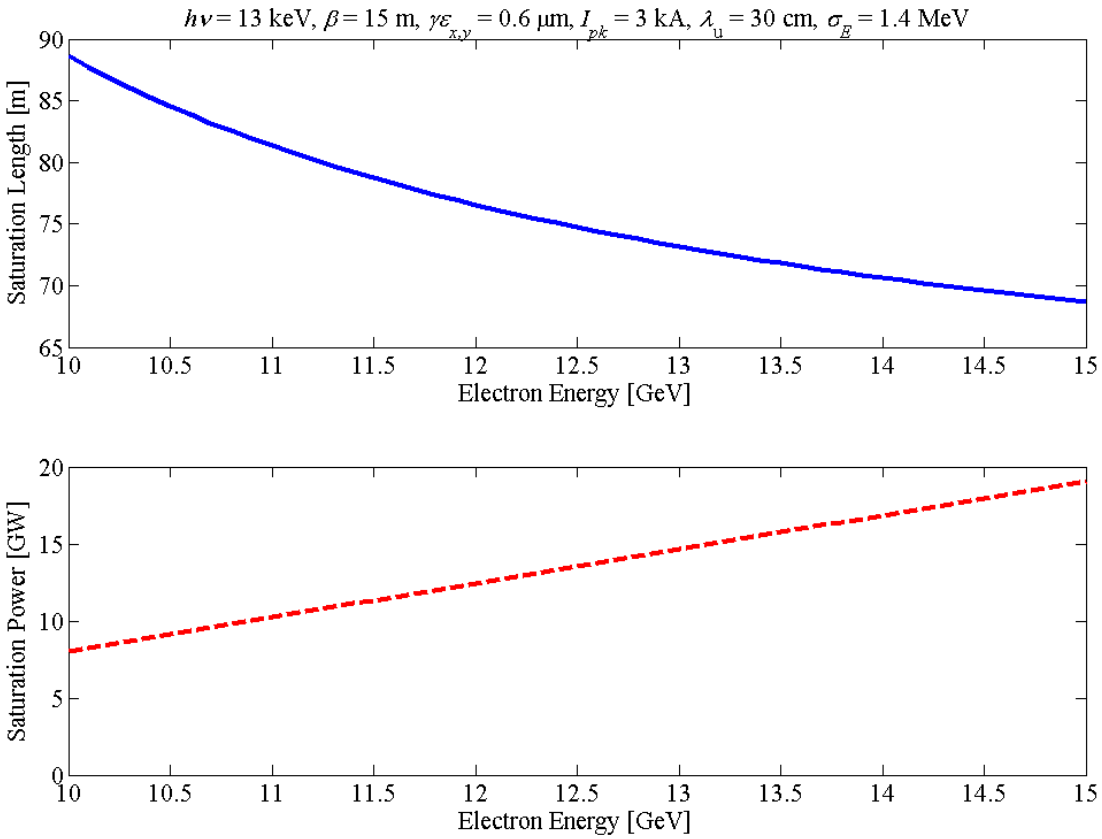

Figure 6.27. Estimated FEL saturation length and power [9], at a 13-keV constant photon energy, as a function of electron energy with parameters listed in the title. The undulator length must increase by 3 meters by dropping from 13.5 GeV to 12.5 GeV.

The main linac for LCLS-II (as in LCLS-I) is segmented into 4 separate sections, as shown in Figure 6.1. The first section is called the L0-linac (or L0) and is composed of the two 3-m long S-band accelerating structure after the gun, L0a and L0b. These take the electron beam to 135 MeV. The second section is the L1-linac (L1) composed of three 3-m long S-band accelerating structure and one X-band 4th harmonic accelerating structure just prior to the Bunch Compressor 1 (BC1) chicane. Here the bunch is accelerating off the RF crest (20 degS) up to 250 MeV and then compressed partially in the BC1 chicane. The X-band RF section is used to linearize the energy chirp prior to BC1 so that the bunch compression transformation is much more linear, leaving no sharp spikes on the bunch current profile. The L2-linac (~326 m) follows the BC1 chicane and also accelerates off crest (~32 degS) up to 4.2 GeV where the Bunch Compressor 2 (BC2) chicane executes the final bunch length compression. Beyond the BC2 is the L3-linac (582 m) which accelerates on crest to any energy from 4.2 to ~14 GeV (by switching on and off various klystrons). The strong longitudinal wakefield of these 582-m of RF structures, with the very short bunch length (~7 μm rms), very effectively cancels the remnant energy chirp on the electron bunch which exists immediately after the BC2 compressor (see Figure 6.33). The final total energy spread after L3 is then extremely small at about 0.03% rms, with the time-sliced spread at the 0.01% level (with laser heater set at nominal).

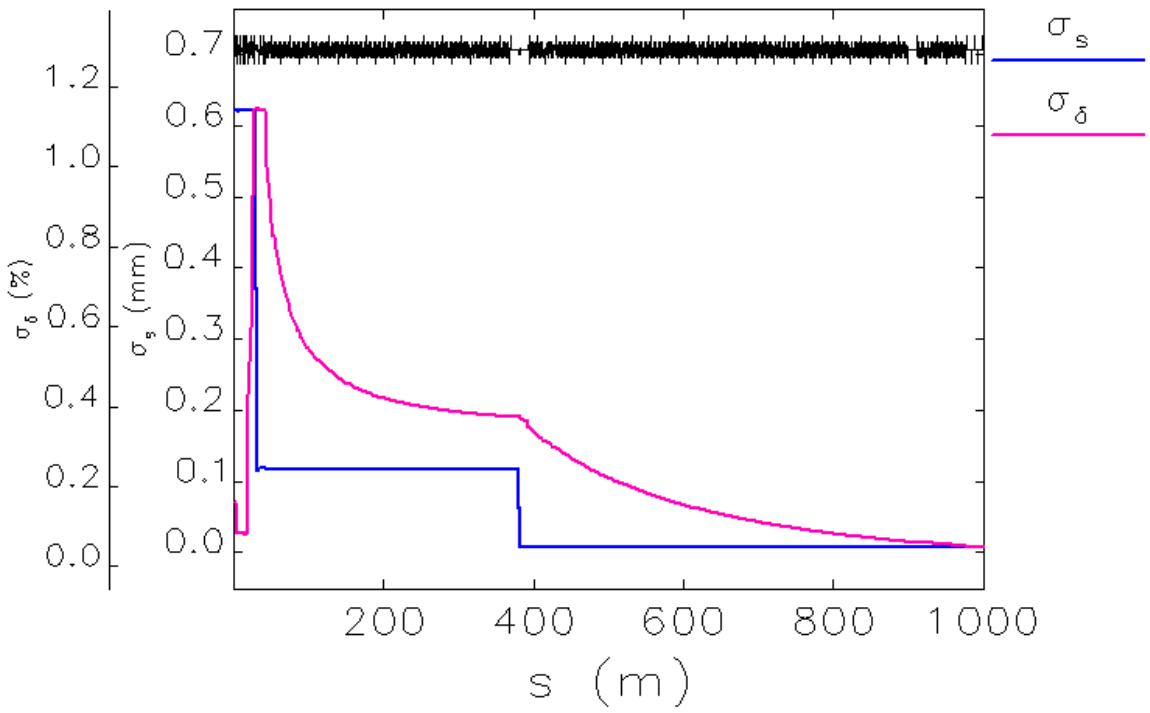

Figure 6.28. The rms bunch length, σ_s, and the rms relative energy spread, σ_δ, plotted all along the main LCLS-II linac from cathode to start of the 1-km long bypass line (250 pC).

Various RF and compression configurations are possible for different bunch charge levels, different bunch length settings, or even to establish chirped beams, which are sometimes requested by users.

The transverse optics in the various linac sections are designed to minimize transverse wakefield effects and also to loosen magnet alignment tolerances. Each section, with its different bunch length and energy spread values (see Figure 6.28), must be optimized separately.

6.4.1 Linac Energy Management

With two bunch compressor chicanes to be located within these 850 meters of linac, and the RF phase of the first long section of linac (L2) to be set significantly off crest (–30° to –40°), it is worth optimizing the layout and establishing a reasonable number of spare klystrons in each long linac section, L2 and L3. Starting with the LCLS-I design, with BC1 at 250 MeV and the BC2 location at 4.3 GeV, we note that 4 klystrons in Sector 20 (20-5,6,7, 8) will not be available, since the beam must be kicked at 20-5 upward into the bypass line on the linac tunnel ceiling and straightened out after the new Sector 20 wall ("FACET wall"). This means that the LCLS-II accelerator will have 4 fewer klystrons than LCLS-I and therefore slightly lower maximum electron energy. To estimate a comfortable nominal and maximum final energy we start by repeating the BC1 location at 250 MeV, displacing the 11-2a,b,c,d and 11-3a RF structures (~15 m, including emittance diagnostics after BC1). We also note that the L2 linac may need to run with up to a 40° off-crest RF phase to allow significant 'over-compression' (an optional energy chirp for the users).In addition, there should be at least 2 spare klystrons in L2 in this 40-deg worst case, and we need 2 klystrons reserved for BC2 energy feedback control (one of the 2 spares should be a special spare energy-feedback station). With the BC1 energy as E_1, we can calculate the BC2 energy, E_2, and the final linac energy, E_3, as

$$E_2 = E_1 + N_{k2}\Delta E_k \cos\varphi_2 + N_{f2}\Delta E_k \cos\varphi_{2f} \quad (2)$$

$$E_3 = E_2 + N_{k3}\Delta E_k \cos\varphi_3 + N_{f3}\Delta E_k \cos\varphi_{3f} \quad (3)$$

where ΔE_k is the average energy gain of each klystron (taken as 225 MeV or 18.5 MV/m average gradient), N_{k2} as the number of powered klystrons in L2 at an RF phase of φ_2, N_{f2} as the number of powered energy-feedback klystrons in L2 at a phase of φ_{2f}, N_{k3} as the number of powered klystrons in L3 at an RF phase of φ_3, and N_{f3} as the number of powered energy-feedback klystrons in L3 at a phase of φ_{3f}. Choosing E_1 = 0.25 GeV, $E_2 \approx$ 4.2 GeV (not much lower than LCLS-I in order to control CSR emittance growth in BC2), E_3 = 13.5 GeV (conservative limit with reasonable spares), and also choosing N_{f2} = 2, $\varphi_{2f} \approx$ 60°, and φ_3 = 0 (all typical in LCLS-I), and N_{f3} = 6 and $\varphi_{3f} \approx$ 30° (with 6 feedback tubes here rather than 16 in LCLS-I), we find that N_{k2} = 22 and N_{k3} = 36. Since we require 2 feedback stations and 2 spares in L2 (one of these is a special feedback spare), plus 6 feedback stations and 3 spares in L3, then the total number of available tubes in L2 is 26, and 45 in L3. With these klystrons, and by locating BC1 at its mirror location with respect to LCLS-I (*i.e.*, exactly 1016 m upstream), we find that BC2 should be located at 14-5 and 14-6, displacing the 24 meters of RF sections there.

The linac layout is shown in Figure 6.29. Note that the nominal phase of L2 is about −32° giving more commonly 4 spare klystrons in L2. With all spares powered and at an L2 phase of −32°, and with $\varphi_{2f} \approx$ 20°, the BC2 can run at up to 4.9 GeV. With this BC2 energy and all L3 spares powered, and with $\varphi_{3f} \approx$ 25°, the final energy can be as high as 14.8 GeV, but not sustainable for long periods.

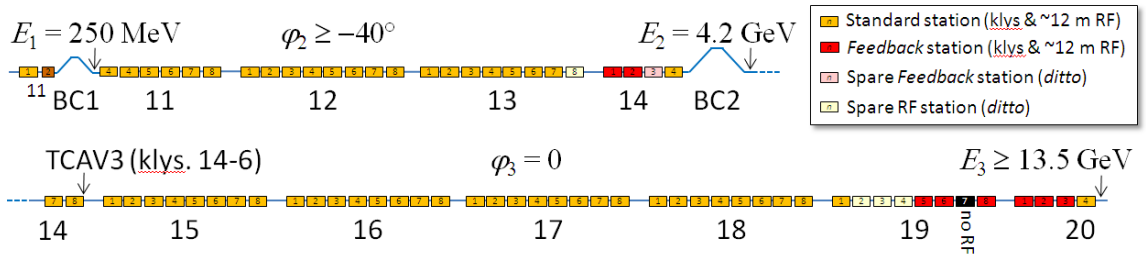

Figure 6.29. Linac klystron distribution showing sectors 11-20 where each box represents one klystron (typically 12 meters of accelerator with 225 MeV energy gain on crest).

The yellow boxes are typical stations usually with four 3-m RF sections, the red boxes are energy-feedback stations, the white boxes are spare stations reserved when failures arise, the pink station at 14-3 is a special spare energy-feedback station in L2, and the brown station at 11-2 is the X-band RF station, LX.

Table 6.10 lists, for each LCLS-II linac section, the total number of klystrons potentially available, N_{Klys}, the number of klystrons held in reserve, N_{res}, the largest off-crest RF phase, φ_i, the on-crest average energy gain per klystron, ΔE_k, the beam loading energy loss at Q = 0.25 nC, ΔE_B, the nominal final energy, E_{nom}, of that section, and the maximum energy, E_{max}.

Table 6.10. Energy management parameters for the four main linac sections. The average energy gain is based on 19.3 MV/m and all LCLS-modified linac structure lengths.

Linac	N_{klys}	N_{res}	φ_i [deg]	ΔE_k [GeV]	ΔE_B [MeV]	E_i [GeV]	E_{nom} [GeV]	E_{max} [GeV]
L0	2	0	–1.0	0.075	<1	0.006	0.135	0.150
L1	1	0	–20.0	0.190	<1	0.135	0.268	0.300
LX	1	0	–160	−0.019	<1	0.268	0.250	0.300
L2	25	2	–40	0.225	8	0.25	4.20	5.00
L3	47	3	0	0.225	15	4.20	13.5	15.0

6.4.2 Linac Optics

The electron optics in the various linac sections are designed to minimize transverse wakefield effects and also to loosen magnet and RF structure alignment tolerances. Each section, with its different bunch length and energy spread values (see Figure 6.28), must be optimized separately. The optics functions of the L1, L2, and L3 linac sections are plotted in Figure 6.30, Figure 6.31 and Figure 6.32, respectively.

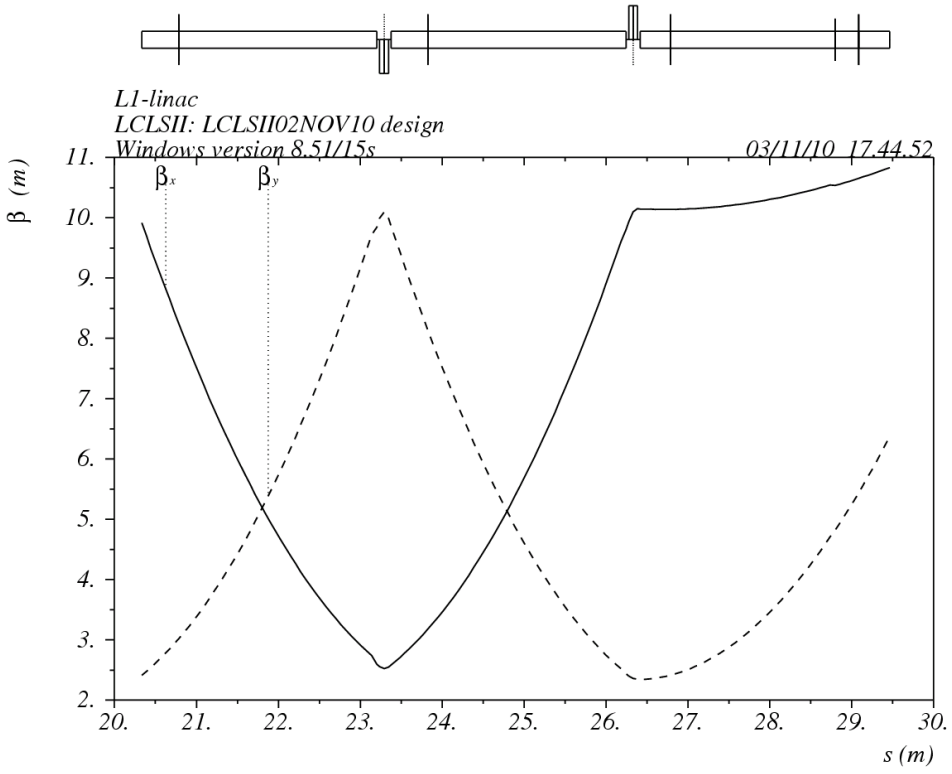

Figure 6.30. The optics functions of the L1-linac.

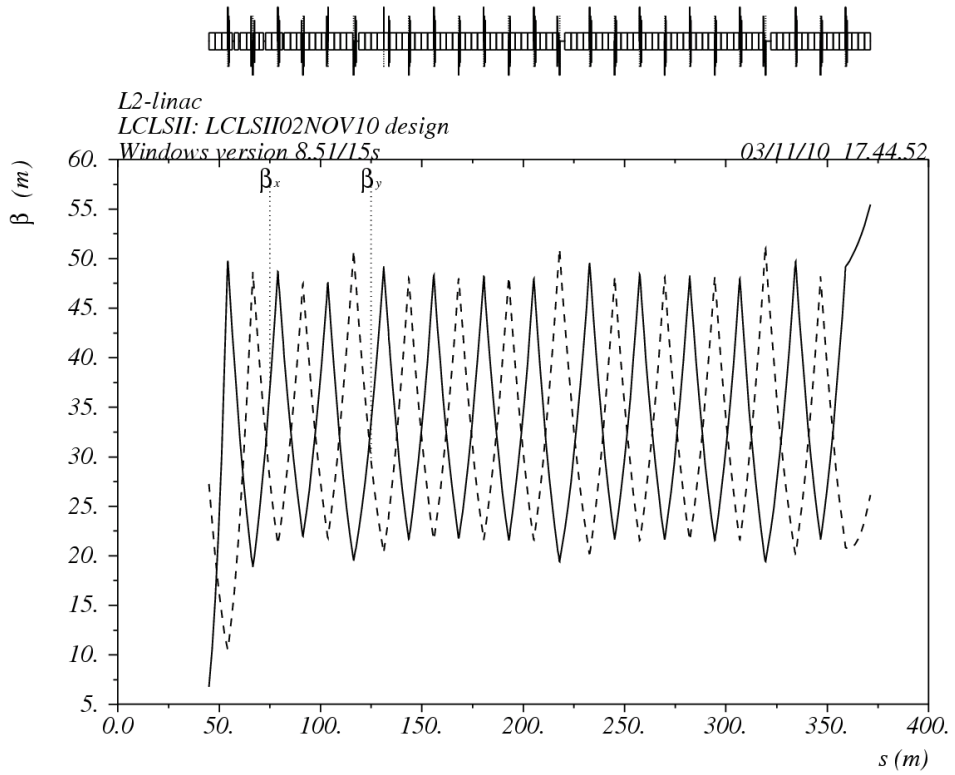

Figure 6.31. The optics functions of the L2-linac.

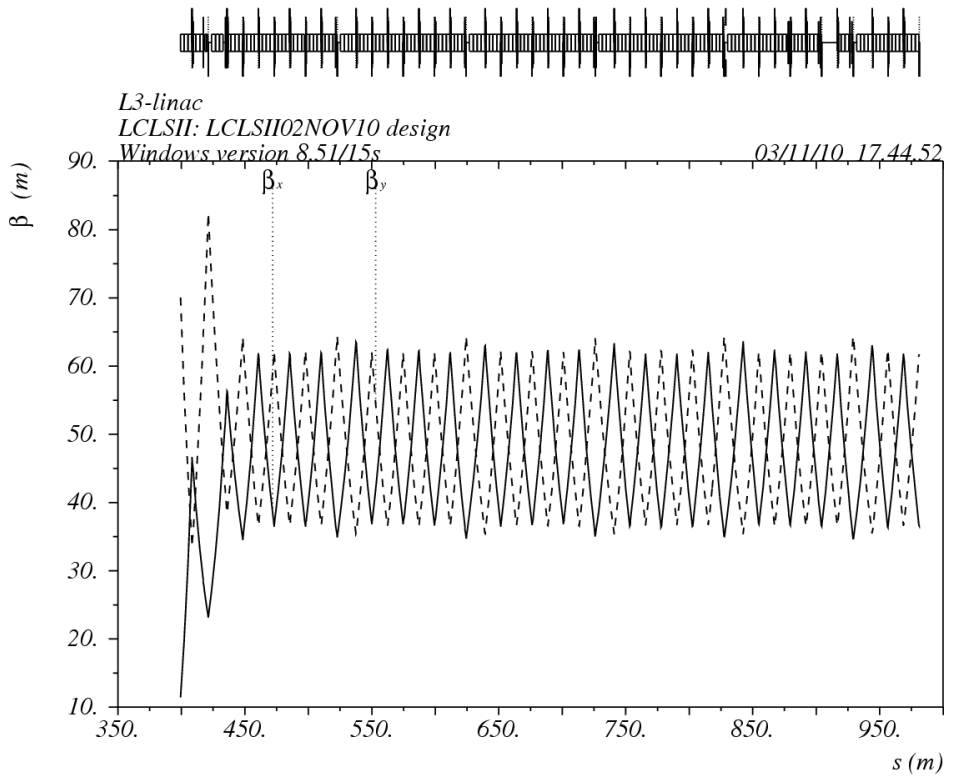

Figure 6.32. The optics functions of the L3-linac.

6.4.3 Linac Modifications and Installation Issues

The SLAC linac between sectors 11 through 20 must be modified to install the main components of the LCLS-II, especially considering the new bunch compressor chicanes. A list of the linac beamline modifications follows:

- The 11-1b and 11-1c RF sections must be cut down from 10-foot sections to 9.4 feet in order to insert a quadrupole magnet after each in the L1-linac (there has never been an 11-1a RF section in the linac and this will continue). The three sections (b, c, d) should then be powered with a 50%, 25%, 25%, power split, respectively.
- All four of the 11-2a, b, c, and d 10-foot RF sections need to be removed to install the new BC1 compressor chicane.
- The 11-2 RF modulator will be modified and used to power the new X-band RF section (L1X) using a new X-band klystron.
- The 11-3a 10-foot RF section is not presently (2010) installed and will remain uninstalled in order to make room for the post-BC1 diagnostic section.
- The 11-3b and c sections are presently installed but were optimized in location and design for positron production in the 1970's. These old sections will be removed and replaced with new, standard 10-foot sections at the standard 11-3b and c locations.
- The 11-3d 10-foot section is not presently (2010) installed but will be reinstalled. The RF power split will then be 50%, 25%, 25% for 11-3b, c, d, respectively.
- The four 10-foot RF sections at 13-5d, 13-7d, 14-1d, and 14-3d will each be replaced by a 9.4-foot section in order to install four new wire scanners.
- All eight of the 14-5a, b, c, d and 14-6a, b, c, d 10-foot RF sections will be removed to install the new BC2 compressor chicane.
- The 14-5 klystron and modulator will not be used in LCLS-II and the 14-6 klystron and modulator will be used to power the transverse RF deflector (TCAV3b) at 14-8d.
- The 14-7a 10-foot RF section will be removed in order to make room for the post-BC2 matching quadrupoles and the RF power split will be 50%, 25%, 25% for the 14-7b, c, d sections, respectively.
- The 14-8d 10-foot RF section will be removed in order to make room for the TCAV3b transverse RF deflector and the RF power split will be 25%, 25%, 50% for the 14-8a, b, c sections, respectively.
- The 15-1d 10-foot RF section will be removed in order to make room for the BXKIKb pulsed kicker and the RF power split will be 25%, 25%, 50% for the 15-1a, b, c sections, respectively.
- The 15-6d 10-foot RF section will be replaced by one 7-foot RF section in order to make room for the OTR_TCAV3 screen.
- The entire 12-m long 19-7 section is not installed at present (*SLC* e^+ source from the 1980's). These sections will likely not be re-installed.

- None of the sections in 20-1, 20-2, 20-3, 20-4 (four 40-foot DLWG sections) are presently installed (*FACET* modifications in 2010). These sections will all be re-installed. (Note that the four 20-1 sections were not present even prior to *FACET*.)

6.5 Bunch Compression

In order to drive the FELs to SASE saturation, the final electron bunch must be compressed in length to several thousand amperes of peak current. The bunch compression system must meet several basic requirements as follows:

- To improve stability and to avoid significant space charge forces, two separate and independently adjustable stages of bunch compression should be included.
- Each compressor stage should be based on a simple four-dipole magnetic chicane, which is simple, easily adjustable, and achromatic to all orders.
- The first compressor should be located as far upstream as possible, but at high enough energy to avoid space charge effects after compression.
- The second compressor should be located as far upstream as possible, but at high enough energy to avoid space charge effects, and also located so that the remnant energy chirp after compression is fully cancelled by the longitudinal wakefield of the post-BC2 linac.
- Each chicane should be remotely adjustable with a motor-controlled translation stage so that a reasonable sized aperture BPM and OTR screen can be included.

Bunch compression in the LCLS-II is closely based on the successful design of LCLS-I. The compression is accomplished by the standard method where a linear energy chirp (energy correlation along the bunch) is generated by accelerating at an RF phase, φ, which is a few tens of degrees away from the RF crest. With the correct sign of correlation (*i.e.*, $\varphi < 0$), the head of the bunch (low energy particles) will travel a longer distance within the four-dipole magnetic chicane (bunch compressor), while the tail of the bunch (high energy particles) will travel a shorter path, effectively compressing the bunch length. Since this process leaves a remnant energy chirp which needs to be removed (assuming 'under-compression', where compression is finished before reaching the minimum bunch length), it is best to complete this compression well before the end of the linac, so that the strong longitudinal wakefields of the S-band accelerating structures can be used to cancel this remnant chirp. Interestingly, if the bunch is set to 'over-compression', where compression proceeds beyond the minimum bunch length, the wakefield-induced energy chirp can be made to *add* to the remnant chirp, rather than cancelling it, and a large energy chirp can be formed over the bunch, and therefore also over the x-rays, for use in the experimental situations when a chirped x-ray beam is requested.

The compression factor for a 4-dipole chicane is encompassed in its R_{56} value, where each electron is delayed or advanced by its energy deviation with respect to the reference particle (design energy). If the relative energy deviation is expressed as $\delta (= \Delta E/E_0)$, then the electron delay (or advance) is written as

$$\Delta z = R_{56}\delta \,. \qquad (4)$$

The R_{56} coefficient is related to the chicane strength through the following formula

$$R_{56} \approx -2\theta^2\left(\Delta L + \frac{2}{3}L_B\right), \tag{5}$$

where θ (<< 1) is the bend angle of each dipole magnet, ΔL is the drift distance between 1st and 2nd (and 3rd and 4th) dipoles, and L_B is the magnetic length of each magnet.

A 2D (energy and *z*) particle tracking simulation of the LCLS-II compression process (using *LiTrack* [10]) is shown in Figure 6.33 (see Section 6.10 for 6D tracking) with the center column showing the particle populations in longitudinal phase space, the left column showing the relative energy profile, and the right column showing the temporal profile (the *z*-coordinate). Longitudinal wakefields of the SLAC S-band accelerating structures are included, along with resistive-wall wakefields of the 1240-m long, 2-inch-diameter stainless steel bypass line, and the 330-m long, 1.625-inch-diameter copper plated LTU beam pipes are included (see Section 6.10).

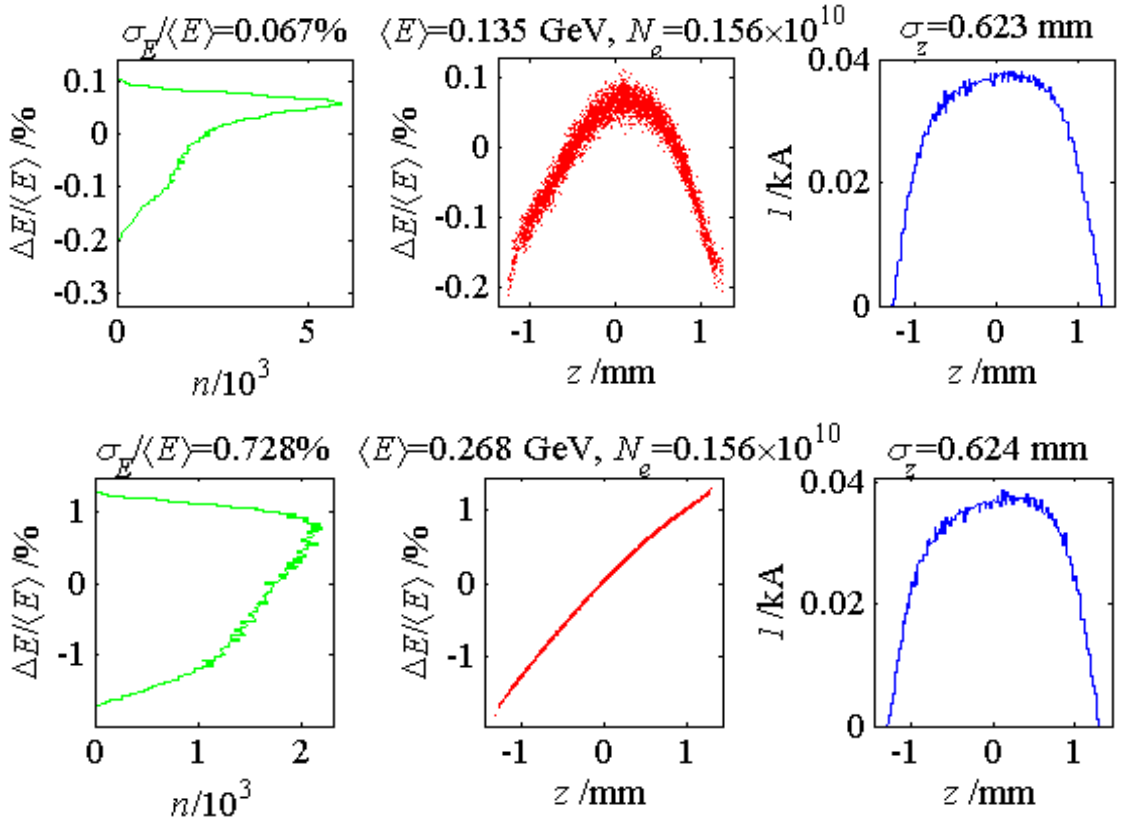

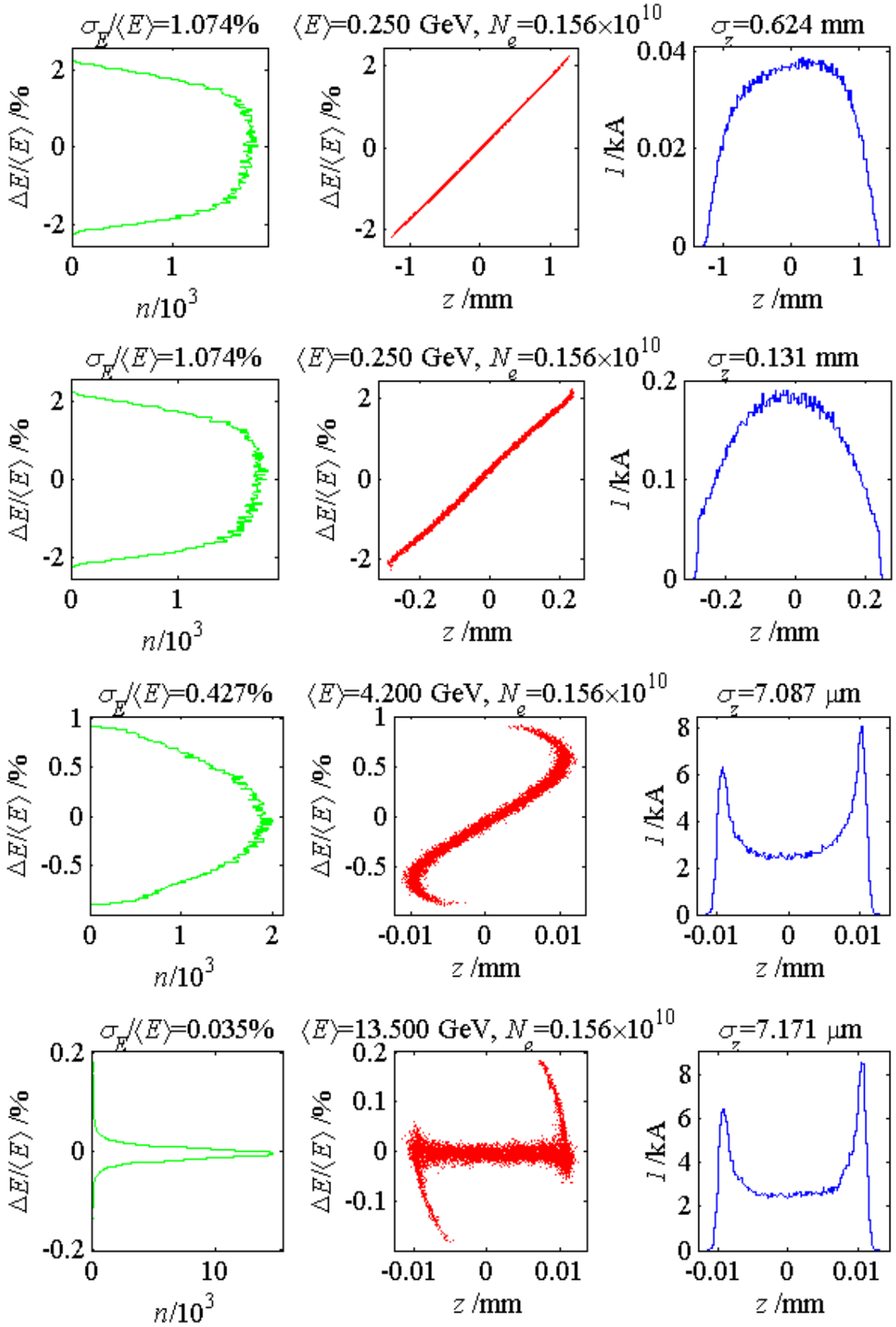

Figure 6.33. 2D tracking simulation of the bunch compression process.

Details pertaining to Figure 6.33: starting at the end of the L0b section at 135 MeV (top row), before the X_band RF at 268 MeV (2nd row), after the X-band RF linearizer at 250 MeV (3rd row), after BC1 at 250 MeV (4th row), after BC2 at 4.2 GeV (5th row), and at the start of the undulator at 13.5 GeV (bottom row).

For better stability and also to minimize space-charge forces at low energy, two stages of bunch compression are included in the LCLS-II design, as shown in Figure 6.1. These two separate stages, a short compressor at 250 MeV and a second longer chicane at 4.2 GeV, are described below individually and practically identical to the LCLS-I designs.

6.5.1 Stability Requirements and System Tolerances

The final level of bunch compression is quite sensitive to RF phase and amplitude variations in the different sections of linac. In addition, the final electron energy (and therefore photon energy), plus the bunch arrival time can also be quite sensitive to the RF, as well as variations of the bunch charge, drive-laser timing, and bunch compressor settings. These three final quantities (peak current, energy, and arrival time) have been studied using particle tracking (with *LiTrack*) while varying many of the system parameters. Table 6.11 lists the various parameters (mostly phase and amplitude of each major linac section), plus the bunch charge, drive-laser timing, and bunch compressor settings. Each of the first three numerical columns in the table [*i.e.*, $(\Delta I_{pk}/I_{pk})_{\rm rms}$, $(\Delta E/E)_{\rm rms}$, and $(\Delta t)_{\rm rms}$] lists that parameter's sensitivity. For example, the "L0 RF phase error" entry, under the heading "**$(\Delta E/E)_{\rm rms}$ < 0.1%**", means that a variation of 1.75 degS of the L0-linac RF phase (L0a and L0b together) causes a 0.1% final electron energy change. These three columns of sensitivities are then used to generate a total stability budget, which appears in **bold** under the "**tolerance**" heading. If these tolerances are met (similar levels as LCLS-I), all three final parameters ($\Delta I_{pk}/I_{pk}$, $\Delta E/E$, and Δt) will simultaneously be held below the levels indicated in the table header (*i.e.*, $(\Delta I_{pk}/I_{pk})_{\rm rms}$ < 12%, $(\Delta E/E)_{\rm rms}$ < 0.1%, and $(\Delta t)_{\rm rms}$ < 100 fs).

Table 6.11. Jitter sensitivities and final tolerances (in bold) at 250 pC (see text for table description).

Parameter	Symbol	$(\Delta I_{pk}/I_{pk})_{\rm rms}$ < 12%	$(\Delta E/E)_{\rm rms}$ < 0.1%	$(\Delta t)_{\rm rms}$ < 100 fs	tolerance	unit
Relative bunch charge	$\Delta Q/Q$	3.89	68.0	55.3	**1.00**	%
Drive-laser timing error	$\Delta\tau$	2.80	4.40	2.50	**0.20**	psec
L0 RF phase error	$\Delta\varphi_0$	0.50	1.75	7.35	**0.10**	degS
L1 RF phase error	$\Delta\varphi_1$	0.18	0.58	2.81	**0.07**	degS
LX RF phase error	$\Delta\varphi_x$	3.12	4.18	28.0	**0.50**	degX
L2 RF phase error	$\Delta\varphi_2$	0.11	0.29	0.10	**0.05**	degS
L3 RF phase error	$\Delta\varphi_3$	6.25	2.59	41.6	**0.30**	degS
L0 RF rel. amplitude error	$\Delta V/V_0$	0.14	0.40	2.06	**0.07**	%
L1 RF rel. amplitude error	$\Delta V/V_1$	0.13	0.36	1.85	**0.06**	%
LX RF rel. amplitude error	$\Delta V/V_x$	0.89	2.74	14.9	**0.25**	%
L2 RF rel. amplitude error	$\Delta V/V_2$	0.40	0.34	0.11	**0.07**	%
L3 RF rel. amplitude error	$\Delta V/V_3$	6.20	0.15	3.39	**0.10**	%
BC1 rel. field error	$\Delta B/B_1$	0.14	0.37	1.85	**0.02**	%
BC2 rel. field error	$\Delta B/B_2$	0.71	4.42	0.21	**0.10**	%

Each "sensitivity" is calculated by finding (using *LiTrack* [10]) the change necessary to generate a ±12% peak current change, a ±0.1% relative electron energy change, and a ±100 fs bunch arrival time change. We then assume that the different errors (*e.g.*, charge and L2 RF phase) are independent and therefore add in quadrature. We then divide down the sensitivities (choosing by hand how much to push on each one based on what has been accomplished in the past) until all three of the jitter issues meet our tolerances. The peak current tolerance is the most demanding, and the chosen tolerances listed just meet the <12% rms peak current jitter need. In fact the other two sums (energy and timing) actually come out smaller than the jitter goals by about 15% each, although this is not shown in the table.

It is also worth noting that some of the linac sections (primarily the L0, L2, and L3 linacs) are composed of many klystrons (2, 25, and 47, respectively – see Table 6.10) whereas the tolerances Table 6.11 correspond to the total linac section, rather than individual klystrons. If the phase and amplitude jitter is uncorrelated from klystron to klystron (likely not fully the case) then the individual klystron tolerances will be $\sqrt{N_k}$ larger (*e.g.*, 5-times larger, or 0.25 degS for L2 phase).

6.5.2 The First Bunch Compressor (BC1)

The BC1 is the first bunch compressor stage and is a 4-dipole magnetic chicane with path length dependence on particle energy (R_{56}). The dipole magnets are rectangular bends and energy and energy spread diagnostics are included at the center of this chicane. The parameters of BC1 are listed in Table 6.12 and the electron optics are shown in Figure 6.34.

Table 6.12. Parameters and operational range of 1st bunch compressor chicane, BC1.

Parameter	Symbol	Unit	Nominal	Range
Beam energy	E	GeV	0.250	0.2 - 0.3
Initial rms bunch length	σ_{z_i}	mm	0.6	0.2 - 1.0
Final rms bunch length	σ_{z_f}	mm	0.13	0.01- 1.0
RMS total incoming relative energy spread (at 250 MeV)	σ_δ	%	1.1	0 - 1.6
RMS uncorrelated relative energy spread before BC1 (at 250 MeV)	σ_{δ_u}	10^{-5}	7	0.4 - 10
Momentum compaction	R_{56}	mm	−46	−65 - 0
Second order momentum compaction	T_{566}	mm	+69	0 - 98
Total chicane length (1st bend to last)	L_{total}	m	6.5	-
Floor length of each of four dipole magnets	L_B	m	0.20	-
Floor length of drift between first two and last two dipoles	ΔL	m	2.43	-
Floor length of drift between center two dipoles	ΔL_c	m	0.83	-
Bend angle of each dipole	$\lvert\theta_B\rvert$	deg	5.39	0 - 6.4
Magnetic field of each dipole	$\lvert B\rvert$	kG	3.9	0 - 4.6
Maximum dispersion in chicane center (≈ beamline excursion)	$\lvert\eta_{\max}\rvert$	m	0.244	0 - 0.296
Projected CSR emittance dilution ($\gamma\varepsilon_0$ = 0.6 μm)	$\Delta\varepsilon_{\text{CSR}}/\varepsilon_0$	%	5	-

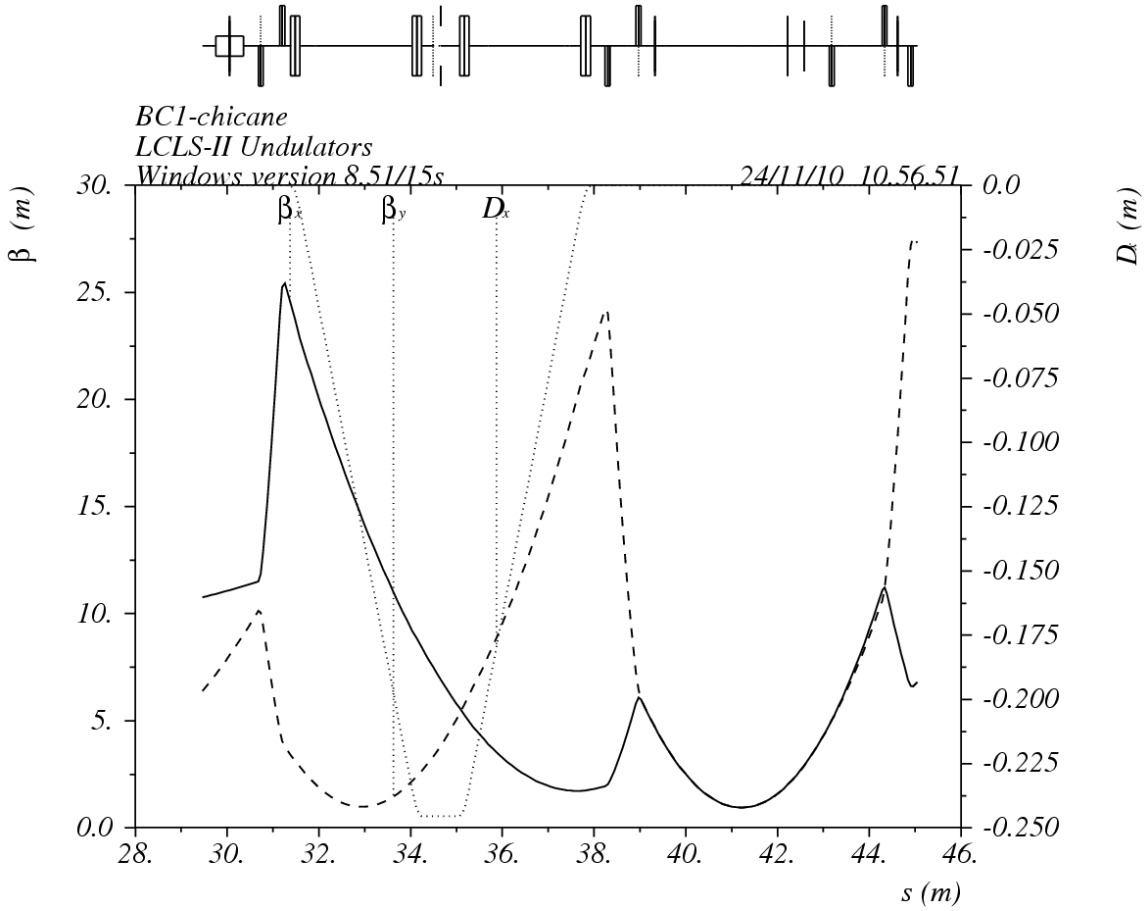

Figure 6.34. The BC1 electron optics functions starting just before the X-band RF section and ending just before the beginning of the L2-linac.

6.5.3 The Second Bunch Compressor (BC2)

BC2 is the second bunch compressor stage, and like BC1, is a 4-dipole magnetic chicane which is almost 3-times longer than BC1. It also introduces path length dependence on particle energy (R_{56}) in order to compress an energy-chirped electron bunch. The dipole magnets are rectangular bends and energy and energy spread diagnostics are included at the center of this chicane. The BC2 parameters are listed in Table 6.13 and the electron optics are shown in Figure 6.35.

Table 6.13. Parameters and operational range of 2nd bunch compressor chicane, BC2.

Parameter	Symbol	Unit	Nominal	Range
Beam energy	E	GeV	4.20	4.0 - 4.8
Initial rms bunch length	σ_{zi}	μm	130	600 - 10
Final rms bunch length	σ_{zf}	μm	7	<1 - 600
RMS incoming relative energy spread (at 4.2 GeV)	σ_δ	%	0.43	0 - 1
RMS uncorrelated relative energy spread (at 4.2 GeV, with heater)	σ_{δ_u}	10^{-5}	3	0.02 - 10
Net momentum compaction	R_{56}	m	−29.0	−50 - 0
Net second order momentum compaction	T_{566}	m	+43.5	0 - 75
Total system length (1st bend to last)	L_{total}	m	23.0	-
Floor length of each of four dipole magnets	L_B	m	0.54	-
Floor length of drift between first two and last two dipoles	ΔL	m	9.86	-
Floor length of drift between center two dipoles	ΔL_c	m	0.83	-
Bend angle for each of four dipoles	$\lvert\theta_B\rvert$	deg	2.2	0 - 2.8
Magnetic field for each of four dipoles	$\lvert B\rvert$	kG	11	0 - 14
Maximum dispersion in chicane center (≈ beamline excursion)	$\lvert\eta_{\max}\rvert$	m	0.392	0.515
Slice emittance dilution due to ISR of chicane only (at $\gamma\varepsilon_0$ = 0.6 μm)	$\Delta\varepsilon_{\text{ISR}}/\varepsilon_0$	%	1.07	0 - 4
Projected emittance dilution due to CSR (includes all particles)	$\varepsilon_{x\text{-CSR}}/\varepsilon_{x0}$		2.3	0 - 3
rms ISR relative energy spread of chicane only (at 4.2 GeV)	$\sigma_{\delta\text{ISR}}$	10^{-6}	6	0 - 13

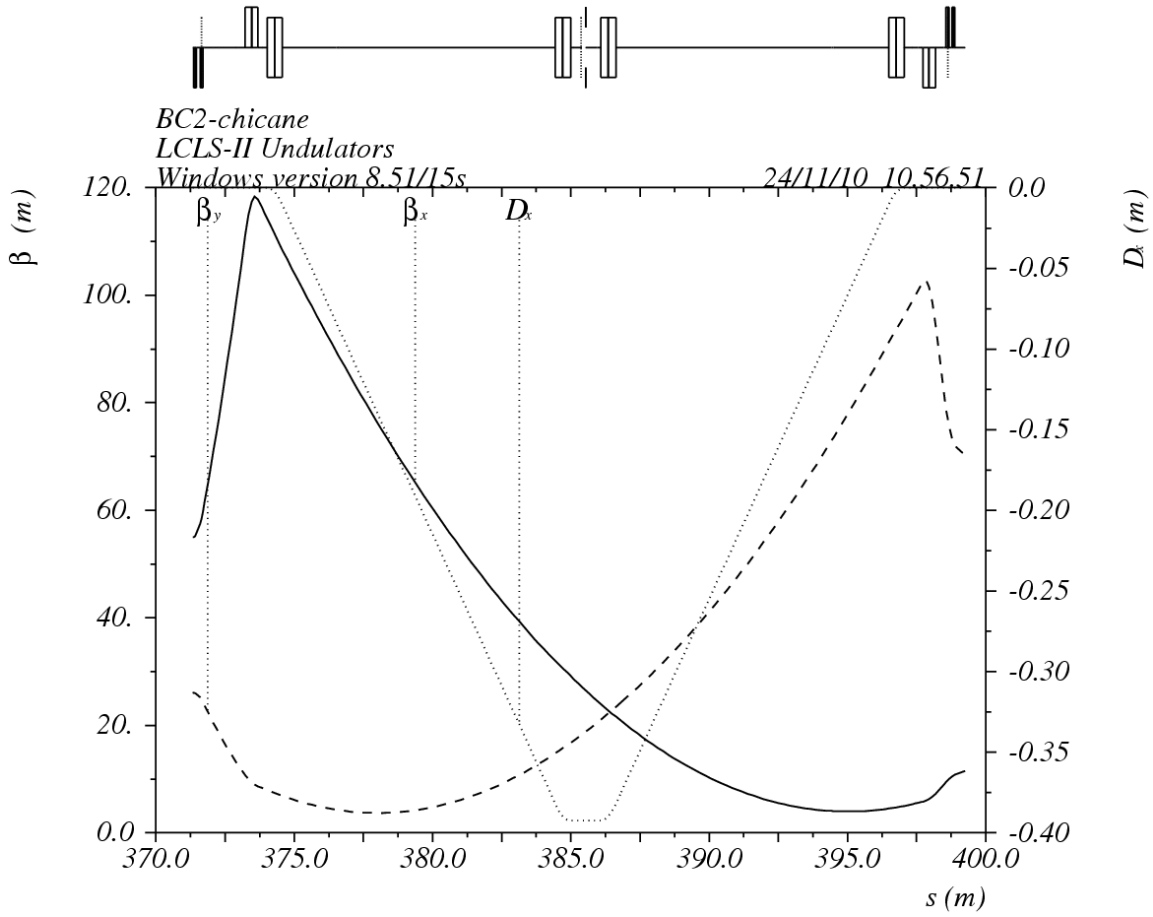

Figure 6.35. The BC2 electron optics functions starting a few meters before the first dipole magnet and ending just before the beginning of the L3-linac.

The design of BC2 must be carefully optimized to minimize the effects of coherent synchrotron radiation (CSR) in the last bends where the bunch reaches its shortest length and begins to radiate like a point charge (see Figure 6.36). The long system length (23 m) and the weak bends (~2°) are based on the successful design of the LCLS-I 2nd compressor which shows tolerable, although significant emittance growth [11]. The simulated time-sliced emittance before and after BC2 is shown in Figure 6.37.

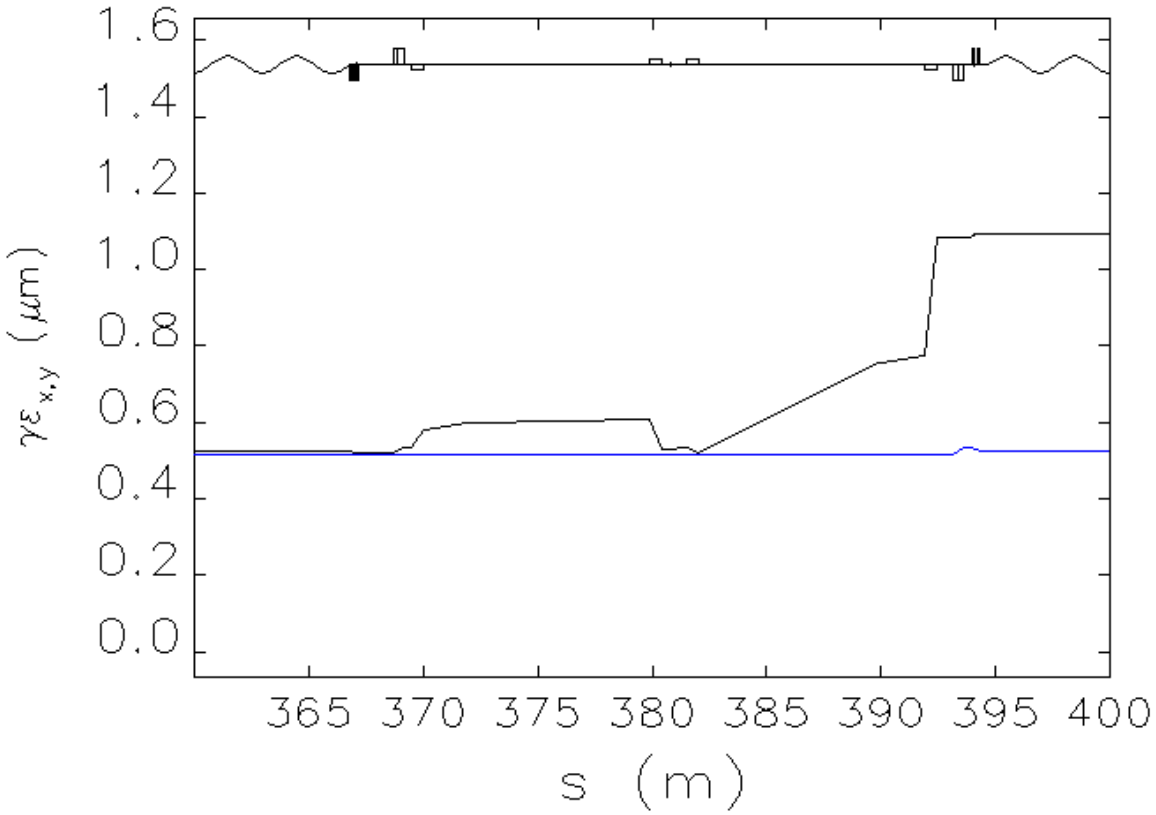

Figure 6.36. Horizontal emittance growth (black) across the BC2 chicane with the double-horned temporal distribution (7.2 μm rms bunch length after BC2).

The calculation removes the linear correlations in x and x' with energy in order to reveal only the irrecoverable CSR effect. The projected emittance after the BC2 without removing these linear correlation is 1.32 μm. The blue line is the vertical emittance, which is not affected by the horizontal bend magnets.

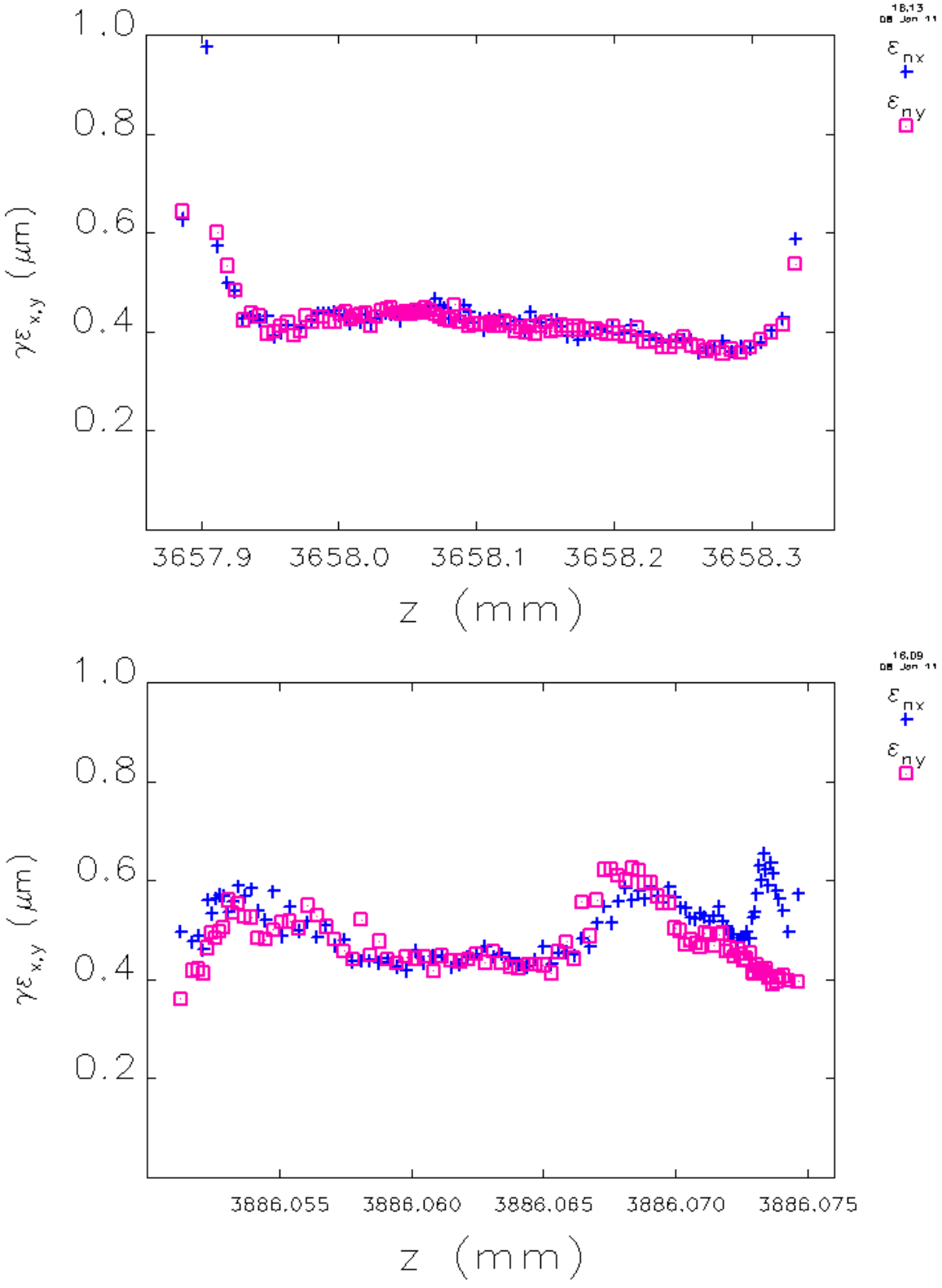

Figure 6.37. time-sliced emittance ("+"=horizontal and "□"=vertical) before the BC2 chicane (top) and after (bottom) with the double-horned temporal distribution (7.2 μm rms bunch length after BC2).

With reference to Figure 6.37, the slice emittance in the bunch core is not much affected by CSR. The "z" axis on both plots spans a duration of 83 fs.

6.6 LCLS-II Bypass Line

The LCLS-II accelerator is based on the existing second kilometer of the SLAC linac at sectors 11-20. In order to deliver the electron beam from this accelerator to the new undulators a bypass line must be included around the existing LCLS-I accelerator at sectors 21-30. This is accomplished by using the existing PEP-II high-energy bypass line which is presently suspended from the ceiling of the linac tunnel.

6.6.1 Bypass Line Design

After acceleration to anywhere between 4.2 and 13.5 GeV, the LCLS-II electron bunch is deflected, using a two-bend dog-leg, upward (25.570") and to the south (25.610") at the 20-5 location (just after Q20501) into the existing PEP-II High Energy Ring (HER) bypass line, which is presently installed on the ceiling of the SLAC linac tunnel. The deflection (11.7 mrad) is accomplished with one rolled (44.96 deg) bend magnet just after the 20-5 quadrupole magnet and the beam is straightened again using a second rolled dipole of opposite but equal strength on the linac ceiling. This means that the dog-leg beam pipe must pass through the existing FACET wall in Sector 20 at an 11.7-mrad angle. The effects of CSR are not large but are included in the particle tracking of section 6.10. The dog-leg optics are shown in Figure 6.38.

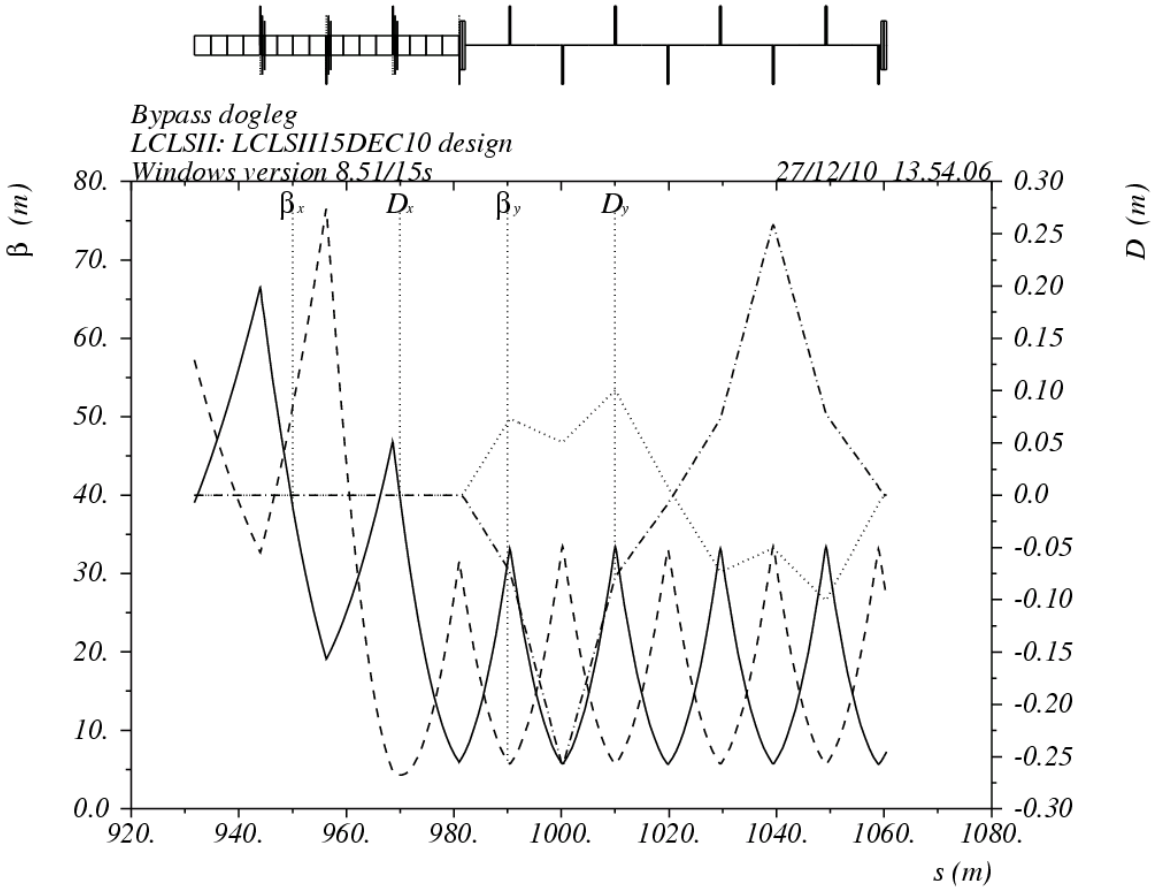

Figure 6.38. Bypass line dog-leg from the start of Sector 20 to the last dog-leg bend on the linac ceiling in Sector 21. The existing FACET wall is at s ≈ 1025 m.

The bypass line will be used to divert the LCLS-II electron beam around the existing LCLS-I accelerator located in sectors 21-30. The existing bypass line will be modified in Sector 30 to extend along its present direction in a straight line through the 17-m thick muon-plug wall (a new 3" hole must be created) and into the existing BTHW enclosure, about 25" above and 25" to the south of the existing LCLS-I electron transport beamline, where dipole magnets will bend the LCLS-II beam about 2.4 degrees toward the south and into a new undulator tunnel.

The existing bypass line (previously used for a 9-GeV electron beam in PEP-II from about 1998 to 2008) is a 2-inch diameter pipe suspended from the linac tunnel ceiling with one quadrupole focusing magnet located in every sector (101.6-m quadrupole magnet spacing), a BPM, and an *x* and *y* steering corrector located near the quadrupole. (The beam pipe is already wrapped with mu-metal for magnetic shielding along its full length.) These quadrupole magnets, BPMs, and steering correctors will remain in their present positions through sectors 21-30, although a few will be relocated in order to match the LCLS-II beam into the long Focussing-Drift-Defocusing-Drift (FODO) cells. The phase advance per cell in the FODO section of the bypass line will be 45°/cell, which provides uniform phase space sampling for transverse emittance measurements (see below) and also transverse halo collimation (see below). The optics functions of the entire bypass line, from the '20-5' take-off point to the start of the 17-m thick muon-plug wall, are shown in Figure 6.39 and parameters are in Table 6.14. The bypass line magnets are quite weak, and their alignment, vibration, and field quality tolerances are not particularly demanding, even with the larger beta functions here (and very small energy spread).

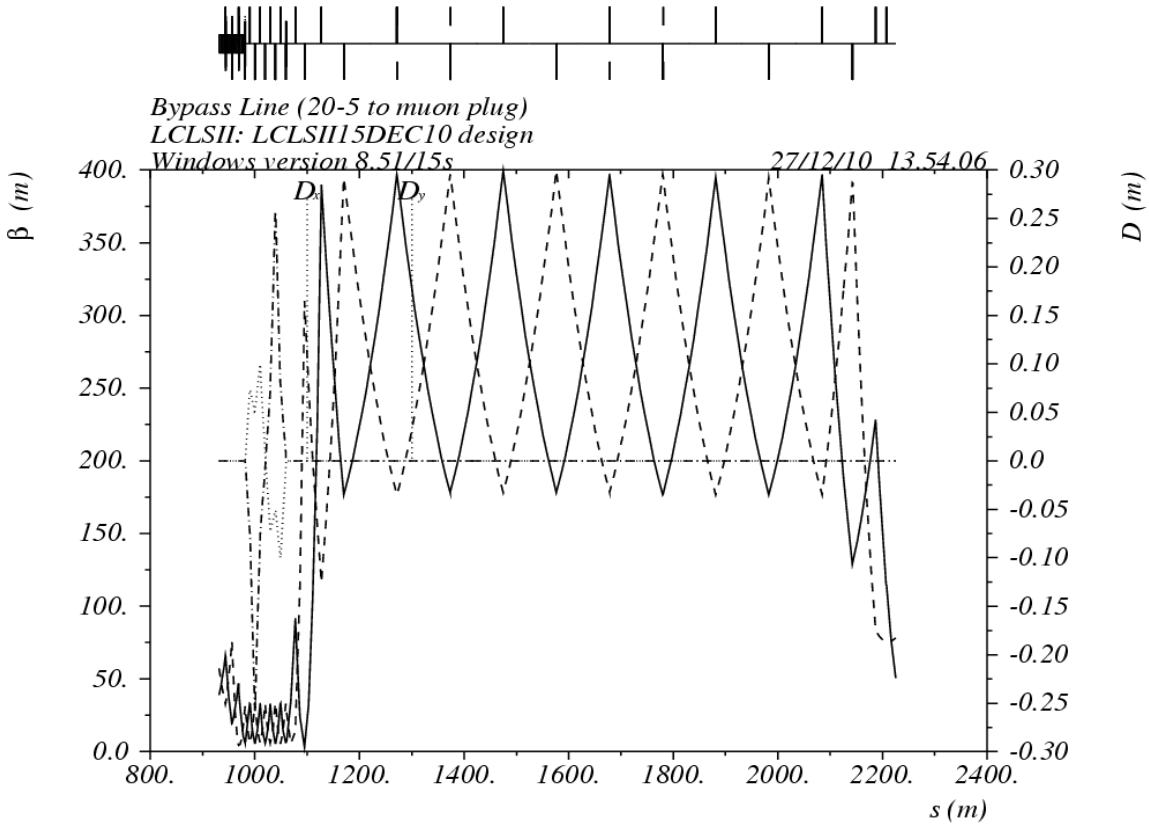

Figure 6.39. The LCLS-II electron bypass line from 20-5 in the linac (Q20501) to the muon-plug wall entrance. The large beta functions in the bypass line are due to the existing 101.6-m long quadrupole magnet spacing from the old PEP-II HER bypass line design.

Table 6.14. Nominal parameters of the bypass dog-leg (250 pC).

Parameter	Symbol	Unit	Nominal	Range
Nominal high-end beam energy	E	GeV	13.5	4.2 - 15
Nominal rms bunch length throughout dog-leg	σ_z	μm	7	-
Net momentum compaction	R_{56}	mm	0.046	-
Net second order mom. compaction	T_{566}	mm	29.5	-
Length of each of 2 rolled dipole magnets	L_r	m	1.0	-
Bend angle of each of 2 rolled dipoles	$\lvert\theta_r\rvert$	deg	0.67	-
Roll angle of each of 2 dipoles	$\lvert\varphi_r\rvert$	deg	44.96	-
Magnetic field of each rolled dipole (at 13.5 GeV)	$\lvert B_r\rvert$	kG	5.27	1.64 - 5.85
Slice x-emittance dilution due to ISR ($\gamma\varepsilon_0$ = 0.6 μm)	$\Delta\varepsilon_{x\text{-ISR}}/\varepsilon_0$	%	0.07	-
Slice y-emittance dilution due to ISR ($\gamma\varepsilon_0$ = 0.6 μm)	$\Delta\varepsilon_{y\text{-ISR}}/\varepsilon_0$	%	0.23	-
Projected x-emittance dilution due to CSR ($\gamma\varepsilon_0$ = 0.6 μm)	$\Delta\varepsilon_{x\text{-CSR}}/\varepsilon_0$	%	3	-
Projected y-emittance dilution due to CSR ($\gamma\varepsilon_0$ = 0.6 μm)	$\Delta\varepsilon_{y\text{-CSR}}/\varepsilon_0$	%	19	-
RMS ISR relative energy spread (at 13.5 GeV)	$\sigma_{\delta\text{ISR}}$	10^{-6}	7.7	0.4 - 10

6.6.2 Bypass Line Diagnostics

The bypass line will include four separate wire-scanners, each separated by one 45° FODO cell (2 quadrupole magnets/cell) in order to provide transverse emittance measurements after the linac. One wire-scanner will be placed in the bypass line in sectors 24, 26, 28, and 30 (*i.e.*, in Figure 6.39 these are at: s = 1424 m, s = 1627 m, s = 1831 m, and s = 2034 m, respectively, where the x and y beam sizes are nominally equal at 78 μm rms for a 13.5-GeV beam). The phase advance per cell of 45° allows the optimal measurement of emittance using 4 wire-scanners. In addition, a 5th wire scanner (vertical beam size) will be included just after the first dog-leg bend magnet in Sector 20, in order to allow energy spread measurements there ($\eta_y \approx 251$ mm, $\beta_y \approx 32$ m).

6.6.3 Bypass Line Collimation

The bypass line will also include 4-8 adjustable transverse collimators (half this many in each plane - final count to be determined with detailed tracking). Each collimator has two independently adjustable jaws which are typically set at 30-40 times the rms beam size at that location (70 to 130 μm rms, depending on beam energy – see Figure 6.40).This is similar to the collimation system used in LCLS-I in sectors 29-30. LCLS-II will need new collimators and the bypass line is an ideal location for these, with its uniform phase advance, large beta functions (~275 m), and lack of RF sections. To determine the jaw settings and exact number of collimators, this system will be studied using particle tracking, as was done in LCLS-I [12].

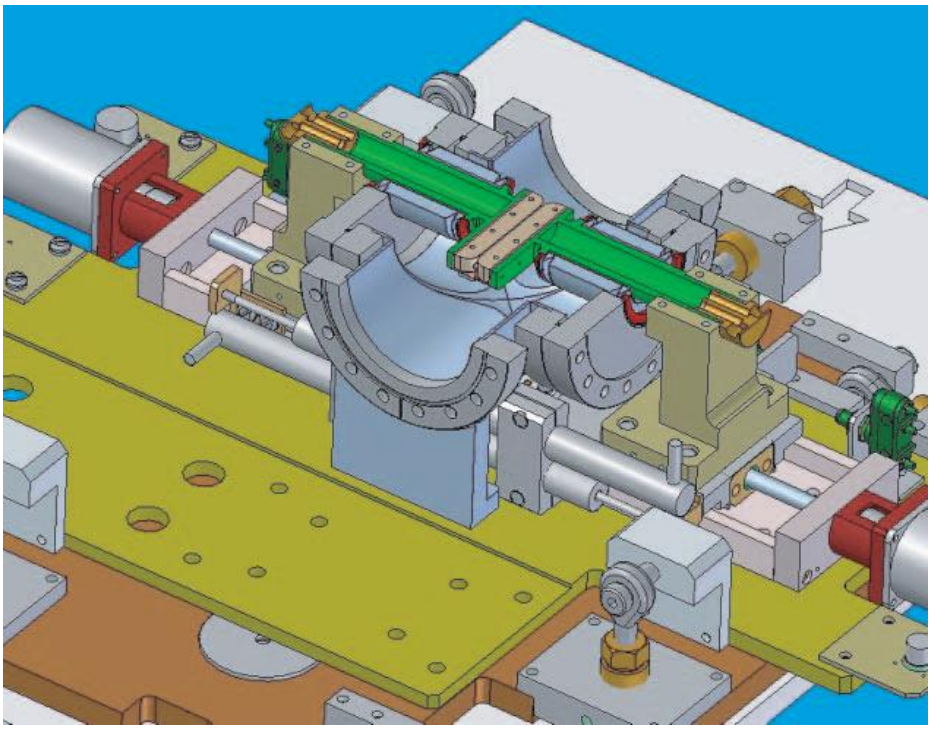

Figure 6.40. Section view of a typical adjustable collimator with jaws fully inserted here (beam travels from upper right to lower left here).

6.6.4 Resistive-Wall Wakefields in the Bypass Line Beam Pipe

The 1200-m long bypass line (from Sector 20 to muon plug wall exit) is composed entirely of 2-inch-diameter cylindrical stainless steel beam pipe. The pipe will generate a longitudinal resistive point-charge wakefield according to

$$\frac{\Delta E}{E_0}(s) = \frac{4qcZ_0L}{\pi r^2 E_0}\left(\frac{1}{3}e^{-s/s_0}\cos\frac{\sqrt{3}s}{s_0} - \frac{\sqrt{2}}{\pi}\int_0^\infty \frac{dx\, x^2 e^{-x^2 s/s_0}}{x^6+8}\right), \qquad (6)$$

where q is the bunch charge (0.25 nC), c is the speed of light, Z_0 is the free-space impedance, L is the length of the beam pipe (1200 m), r is the beam pipe radius (25.4 mm), and E_0 is the electron energy (13.5 GeV). Here s is the bunch length coordinate and s_0 is the characteristic wakefield length given by

$$s_0 \equiv \left(\frac{2r^2}{Z_0\sigma}\right)^{1/3}, \qquad (7)$$

where σ is the conductivity of the inner surface of stainless steel pipe (1.4×10^6 /Ω/m). The formula in Equation (6) is accurate when the rms bunch length (7.2 μm) is less than s_0 (≈ 135 μm), which is the case here. For the parameters in parenthesis, the induced rms relative energy spread for a uniform temporal bunch distribution (3 kA) is approximately 0.032% (see Figure 6.41). This effect is included in the tracking studies of Section 6.10 and is also shown below in Figure 6.42 with the "real" longitudinal phase space at 13.5 GeV just before (top) and just after the wakefield is applied to the LCLS-II temporal distribution (at

right in both plots). This resistive-wall wakefield is dominantly a linear chirp affect, which has been compensated in the design.

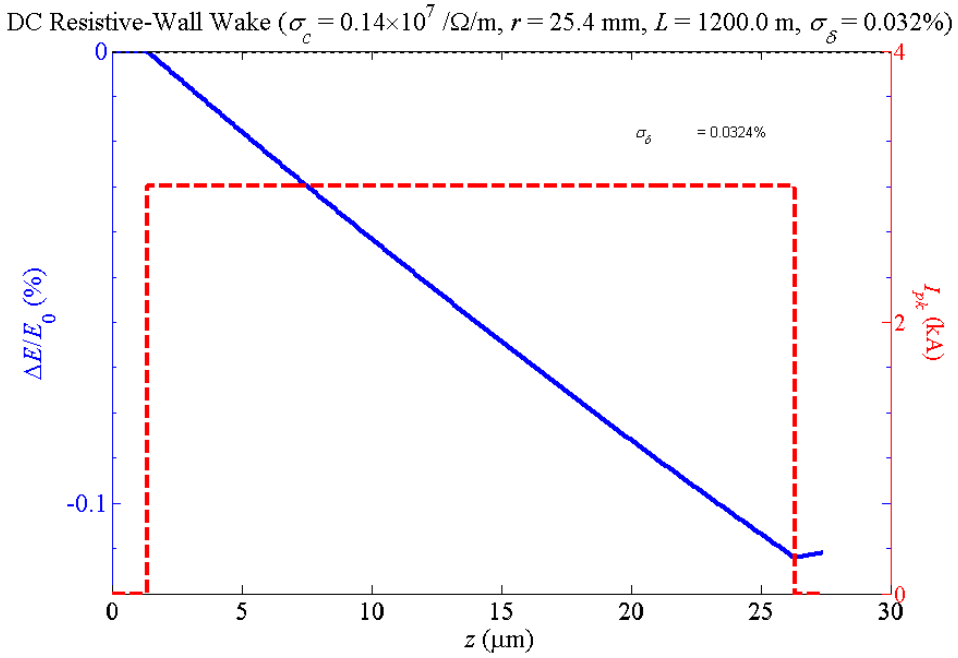

Figure 6.41. Resistive wall wakefield (blue) for a uniform temporal distribution (red) with parameters listed in Table 6.14.

The red-dashed curve is the uniform temporal distribution (3 kA) and the blue-solid curve is the resistive-wall wake-induced relative energy chirp over the 1200 meter beamline (almost perfectly linear here). The rms energy spread is 0.0324%.

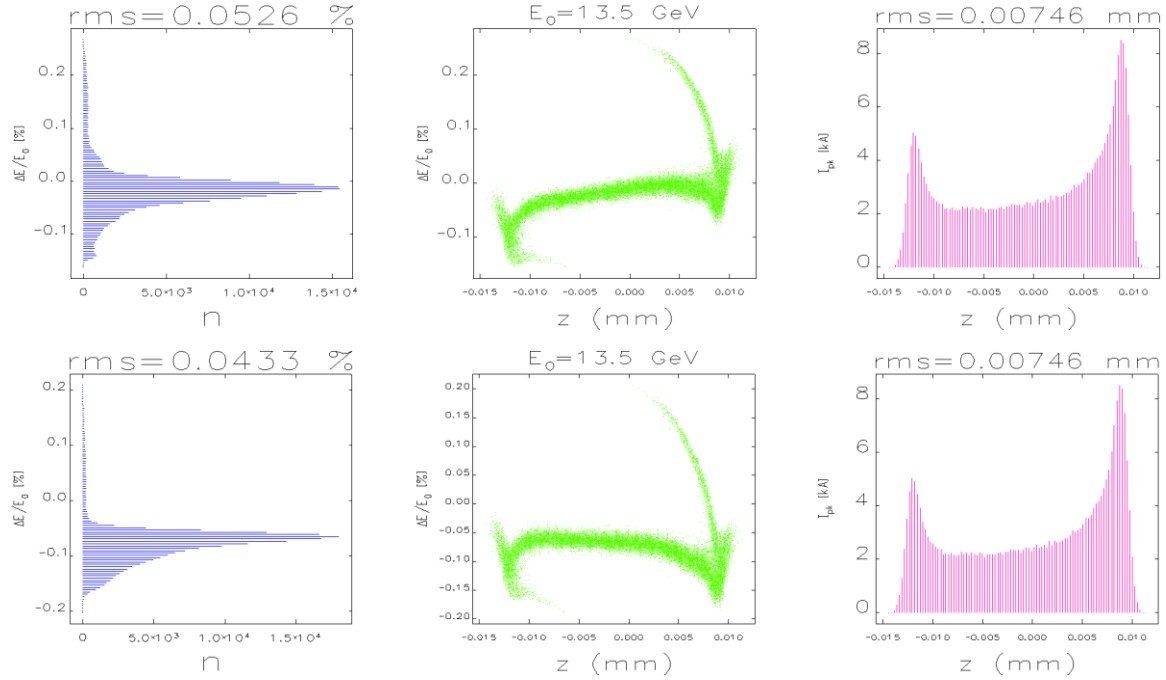

Figure 6.42. The effects of the longitudinal resistive-wall wakefield.

Figure 6.42 shows the effects of the longitudinal resistive-wall wakefield of the 1200-m long, stainless steel bypass line showing longitudinal phase space at 13.5 GeV just before (top) and just after the wakefield is applied to the LCLS-II temporal distribution (at right in both plots). It is also worth noting that the monopole resistive wakefield described above does not depend on radial offset and the transverse resistive wakefield, with reasonable alignment, is quite small due to the short bunch.

6.6.5 Installation Issues

The bypass line will use as many of the existing and installed magnets, BPMs, and vacuum pipes as possible, requiring some modifications in the area upstream of Sector 23 and again in and downstream of Sector 30, with three new quads/BPMs/corrector sets added upstream of Sector 23 and five more added downstream of Sector 30 for proper matching into and out of the bypass line. The existing quadrupole magnets in the PEP-II bypass line are capable of reaching the required field gradients for the LCLS-II bypass line, so most of its components will be reused, although some new power supplies will be needed. In addition, the LCLS-II bypass line must pass through the existing Sector 20 (FACET) wall about 14 inches above and 14 inches south of the present beamline axis, requiring a 3-inch hole be bored through this 2-ft thick wall.

Finally, as discussed above, the existing bypass line will be extended in Sector 30 (existing bend magnets will be removed there) along its present line through the 17-m thick muon plug wall and into the existing BTHW (see Section 6.7) where beam will be transported through the new LTU2 transport line and into the undulator hall.

6.7 Linac-to-Undulator Transport (LTU2)

The requirements for beam transport from the end of the bypass line to the LCLS-II undulators are fairly simple. The new Linac-to-Undulator (LTU2) transport line must:

- Include 2.4° of horizontal bends Dog Leg 2 (DL2) to follow the existing BTH enclosure, direct the beam into the new undulator hall, and also to introduce precise energy and energy spread measurement capability, all without generating significant CSR or other emittance dilution effects,
- Include precise transverse emittance and matching diagnostics and correction magnets for final verification/tuning prior to each undulator,
- Include adjustable and fixed collimators to protect the undulators from radiation damage,
- Provide adjustable undulator-input beta-matching for each undulator and for the various beam energies desired (*i.e.*, various radiation wavelengths),
- Not alter the bunch length (must be nearly isochronous),
- Share the BTH-West tunnel with the existing LCLS-I LTU line,
- Adjust the vertical beamline angle to remove the 0.3˚ downward linac angle (as in LCLS-I) so experimental areas do not need to be located too far below ground level.

In addition to these features, the final section of the LTU2 will have a branch line where one electron bunch can be split off at up to 60 Hz (or 120 Hz with future 2-bunch operation) into a parallel soft x-ray undulator adjacent to the main hard x-ray undulator. The beamline parameters are listed in Table 6.15 with the LTU2 optics shown in Figure 6.43 from muon plug wall to the start of the HXR undulator. The separate SXR branch line is discussed in Section 6.7.3.

Table 6.15. Nominal parameters of the new Linac-to-Undulator (LTU2) beamline (250 pC).

Parameter	Symbol	Unit	Nominal	Range
Nominal high-end beam energy	E	GeV	13.5	4.2 - 15
Total horizontal beamline bend angle	$\Delta\theta_x$	deg	2.4	-
Total vertical beamline angle change (levels the undulators)	$\Delta\theta_y$	deg	0.26	-
Nominal rms bunch length throughout dog-leg	σ_z	μm	7	-
RMS *projected* relative energy spread	σ_δ	%	<0.1	0.01 – 1.0
RMS *slice* energy spread	σ_{δ_u}	%	0.010	0.002 - 0.030
Net momentum compaction (not including bypass line)	R_{56}	mm	0	-
Net second order mom. compaction (not incl. bypass line)	T_{566}	mm	9.7	-
Length of each of four horizontal dipole magnets	L_H	m	2.62	2.62
Length of each of two vertical dipole magnets	L_V	m	1.025	-
Bend angle of each of 4 horizontal dipoles	$\lvert\theta_H\rvert$	deg	0.6	-
Bend angle of each of 2 vertical dipoles	$\lvert\theta_V\rvert$	deg	0.13	-
Magnetic field of each horizontal dipole	$\lvert B_H\rvert$	kG	1.80	0.56 - 2.00
Magnetic field of each vertical dipole	$\lvert B_V\rvert$	kG	1.03	0.32 – 1.14
Maximum horizontal dispersion	$\lvert\eta_{\max}\rvert$	m	0.150	-
x-emittance dilution due to ISR (at $\gamma\varepsilon_0$ = 0.6 μm)	$\Delta\varepsilon_{x\text{-ISR}}/\varepsilon_0$	%	0.18	-
Projected emittance dilution due to CSR (at $\gamma\varepsilon_0$ = 0.6 μm)	$\Delta\varepsilon_{\text{CSR}}/\varepsilon_0$	%	~5	-
RMS ISR relative energy spread	$\sigma_{\delta\text{ISR}}$	10^{-6}	3.5	1.9 – 4.6

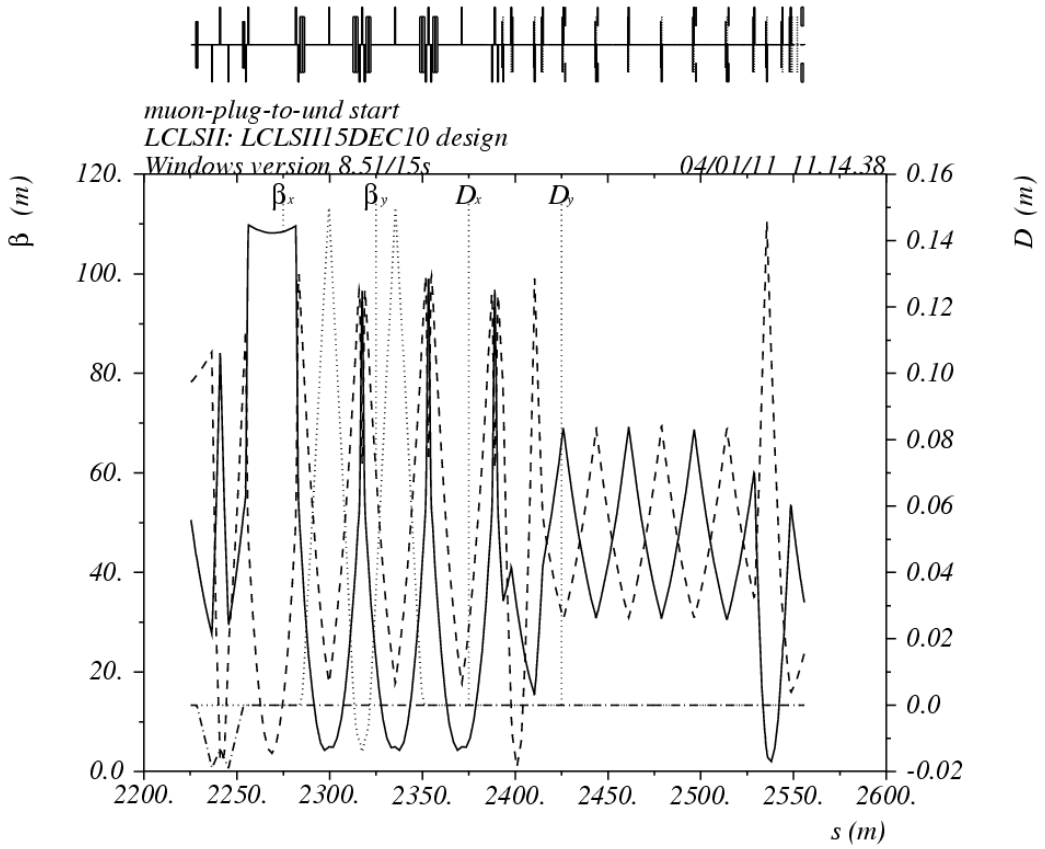

Figure 6.43. Optics functions of the LCLS-II Linac-To-Undulator (LTU2) beamline.

Figure 6.43 (above) shows optics functions of the LCLS-II Linac-To-Undulator (LTU2) beamline from muon plug wall to start of HXR undulator, including the 0.3-deg vertical bend system (*s* = 2225 to 2260 m), the 2.4-deg horizontal bend system (*s* = 2280 to 2350 m), the emittance diagnostic and collimation section (*s* = 2420 to 2525 m), and the HXR undulator matching section (*s* = 2525 to 2560 m). The 5th bend magnet (at *s* = 2360 m) is the pulsed dipole (off here) which feeds the SXR branch line (see Section 6.7.3).

6.7.1 LTU Diagnostics

The LTU2 beamline will include four separate wire-scanners, each separated by one 45° FODO cell (2 quadrupole magnets/cell) after the DL2 bends, in order to provide transverse emittance measurements just prior to the HXR undulator (see emittance diagnostic and collimation section in Figure 6.43). Each wire-scanner will be placed where the *x* and *y* beam sizes are nominally equal (32 μm rms at 13.5 GeV). The phase advance per cell of 45° allows the optimal measurement of emittance and beta function using 4 wire-scanners. In addition, a 5th wire scanner will be included between the 1st and 2nd DL2 bend magnets in order to allow energy spread measurements there (at *s* ≈ 2300 m in Figure 6.43).

6.7.2 LTU Collimation

The LTU beamline will also include 4 adjustable transverse collimators (2 in *x* and 2 in *y*). Each collimator has two independently adjustable jaws which are typically set at 40-50 times the rms beam size at that location (about a 3-mm collimator gap - see emittance diagnostic and collimation section in Figure 6.43). This 'clean-up' collimation pass (after the bypass line primary collimation in Section 6.6.3) is similar to

the collimation system used in LCLS-I. To determine the jaw settings this system will be studied using particle tracking, as was done in LCLS-I [13]. In addition, two energy collimators will be included in the LTU2 DL2 bend system (one at $s \approx 2300$ m and another at $s \approx 2330$ m in Figure 6.43), especially designed to truncate any off-energy dark current which is transported this far [12]. A final fixed protection collimator just in front of each undulator will fully shadow the undulator apertures and protect from extreme trajectories which may enter off axis at the undulator entrance.

6.7.3 SXR Branch Line

The LTU2 beamline also has a separate branch line where one electron bunch can be split off at up to 60 Hz (or 120 Hz with future 2-bunch operation) into the parallel soft x-ray (SXR) undulator adjacent to the main hard x-ray (HXR) undulator (see Figure 6.3). The SXR branch line starts just after the 2.4-deg LTU2 bend (see Figure 6.44), where a pulsed (<8-ms rise and fall times) dipole magnet is located in order to bend one electron bunch off to the south by 0.6 degrees (the HXR electrons are not deflected at all, but continue along the main LTU2 and into the HXR undulator). A second 0.6-deg bend (same as the four LTU bends) just 30 meters downstream forms a linear achromat. This second bend might be another pulsed magnet, powered in series with the first one, so that common mode kick errors are locally cancelled and kicker regulation will be eased (~0.05% rms). This double achromat bend is followed by an 80-m long drift section and one more double bend achromat (see Figure 6.45) in order to generate the 2.5-m HXR-to-SXR horizontal, but parallel beamline separation. The effects of CSR on the bend-plane SXR emittance is well controlled at the level of ~5% projected growth (see Figure 6.46, which includes the double-horned temporal distribution of the LCLS bunch). Parameters of the LTUS dog-leg are listed in Table 6.16.

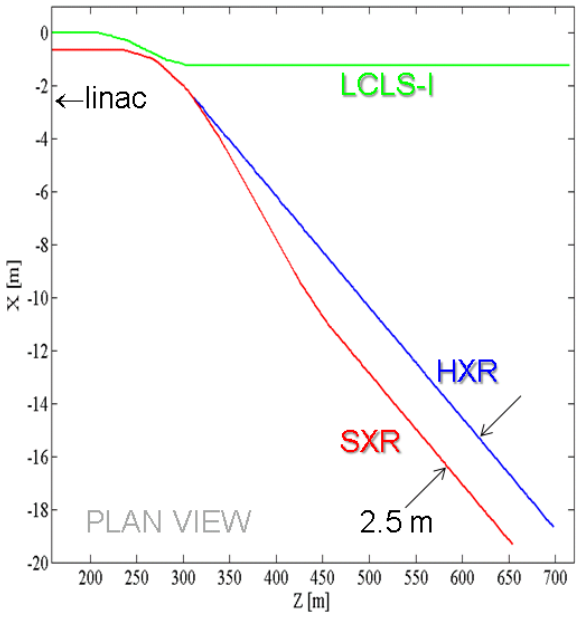

Figure 6.44. Plan view of the LCLS-I (green) and LCLS-II (blue and red) electron beam lines leading to the entrances of their respective undulators. The red line is the SXR branch line with kicker at the red-blue line convergence point. Tunnel walls are not shown and a 2-ft height difference (not shown) exists between the LCLS-I and the new LCLS-II transport lines.

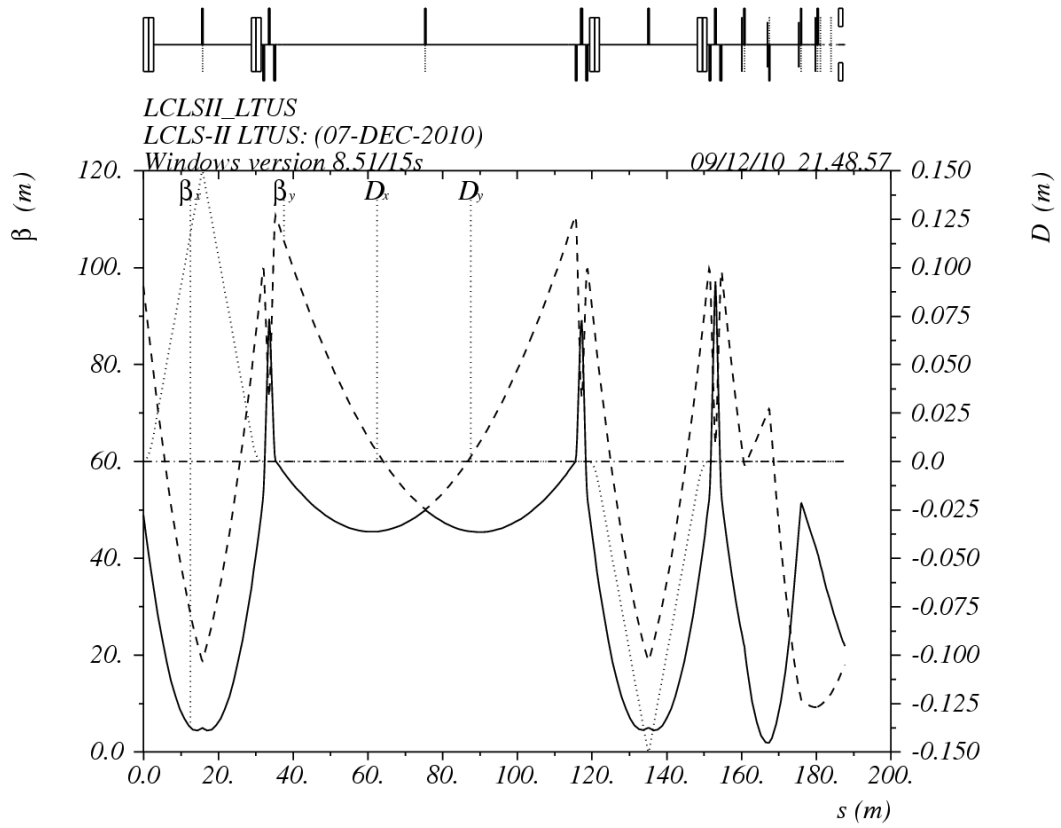

Figure 6.45. Electron beam optics functions in the SXR branch line, after the 2.4-deg LTU bend, which generates the HXR/SXR horizontal separation of 2.5 m. The plot starts at the first bend magnet, which will be a kicker/septum system for 60-Hz separation.

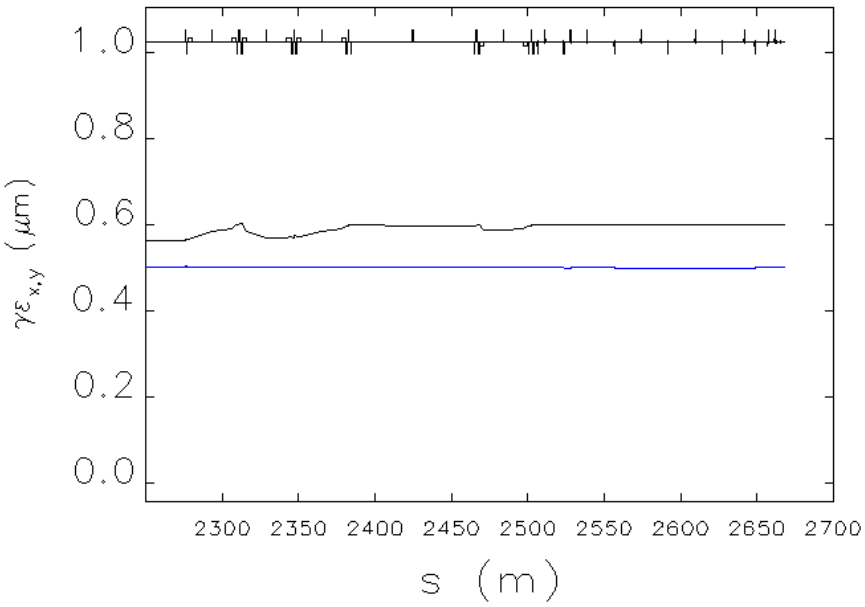

Figure 6.46. Emittance across LTU2 bend system (horizontal in black and vertical in blue), including the 2.4-deg LTU bends and the SXR branch line optics (8 dipoles total).

With reference to Figure 6.46, the horizontal emittance is almost unchanged by CSR through this bend system. The SXR undulator starts somewhere after *s* = 2650 m.

Table 6.16. Nominal parameters of the LTUS dog-leg (250 pC).

Parameter	Symbol	Unit	Nominal	Range
Nominal high-end beam energy	E	GeV	13.5	4.2 - 15
Nominal rms bunch length throughout dog-leg	σ_z	μm	7	-
Net momentum compaction	R_{56}	mm	0.191	-
Net second order mom. compaction	T_{566}	mm	9.12	-
Length of each of 4 dipole magnets	L_r	m	2.62	-
Bend angle of each of 4 dipoles	$\lvert\theta_H\rvert$	deg	0.6	-
Magnetic field of each dipole (at 13.5 GeV)	$\lvert B_r\rvert$	kG	1.80	0.56 – 2.00
Emittance dilution due to ISR (at $\gamma\varepsilon_0$ = 0.6 μm)	$\Delta\varepsilon_{ISR}/\varepsilon_0$	%	<1	-
Projected emittance dilution due to CSR (at $\gamma\varepsilon_0$ = 0.6 μm)	$\Delta\varepsilon_{CSR}/\varepsilon_0$	%	<3	-
RMS ISR relative energy spread (at 13.5 GeV)	$\sigma_{\delta ISR}$	10^{-6}	3.5	1.9 – 4.6

6.7.4 Future Two-Bunch Operation at 120-Hz per FEL

The baseline LCLS-II design supports the acceleration of only one electron bunch per RF pulse, although it is clearly possible to run with two or more bunches, as has already been demonstrated briefly at LCLS-I [14]. Two-bunch operation at an RF rate of 120 Hz allows one bunch to be sent to HXR and the other to SXR all within one 120-Hz cycle, allowing 120-Hz operation of both LCLS-II FELs simultaneously. This is a much more efficient use of the 120-Hz RF power used by the linac. Such two-bunch operation will likely be of great interest soon after the baseline FEL-II commissioning is fully complete. Since this important upgrade must be consistent with the LTU2 optics described above, we present one possible solution here.

Typically the two bunches within one RF pulse will be separated in time by 50-100 ns (60 ns in the SLC era of the 1990's and 8.4 ns in the 2010 tests at LCLS-I). This close time-separation requires replacing the simple pulsed magnet scheme with a fast kicker with rise or fall time of <50 ns. The kicker would likely be located in the LTU2 line (at *s* ≈ 2325 m in Figure 6.43), about 30 meters upbeam of the pulsed dipole magnet described above, and would kick one bunch downward by about 0.13 mrad. This vertical kick angle becomes a vertical offset of −7 mm at the face of the pulsed magnet (see Figure 6.47), which will (by then) be replaced by a horizontal-bending Lambertson magnet. The Lambertson magnet has a field-free region at nominal beam height (kicker off), and a vertical field-region which is 7 mm below this (see Figure 6.48). The vertical field in the Lambertson magnet then deflects this electron bunch horizontally into the SXR branch line by an initial angle of 0.6 deg. As shown in Figure 6.45, there are also three more 0.6-deg horizontal DC bend magnets after this Lambertson magnet, which transport the electrons into the SXR undulator. Note that two weak DC vertical dipoles will also be installed in the LTUS line after the Lambertson magnet in order to remove the vertical offset and angle. The small resulting vertical dispersion will also need to be appropriately suppressed.

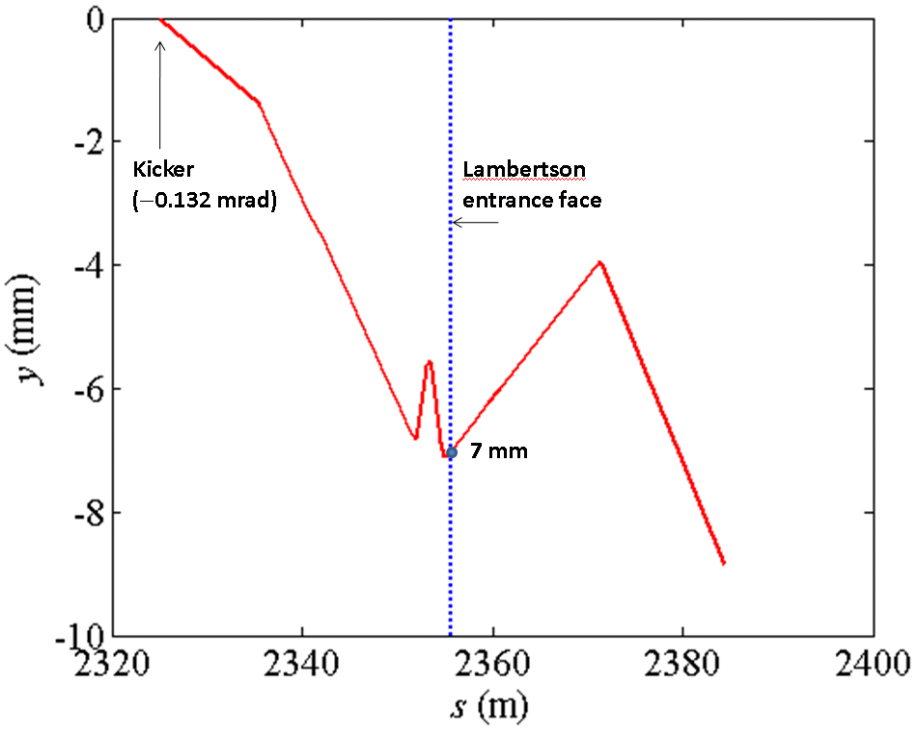

Figure 6.47. Vertical e^- trajectory after fast vertical kicker in LTU2 at s = 2325 m.

The kick becomes a vertical offset of −7 mm at the Lambertson magnet. Small vertical DC dipoles (not shown) will be added after the Lambertson to restore the vertical trajectory to zero.

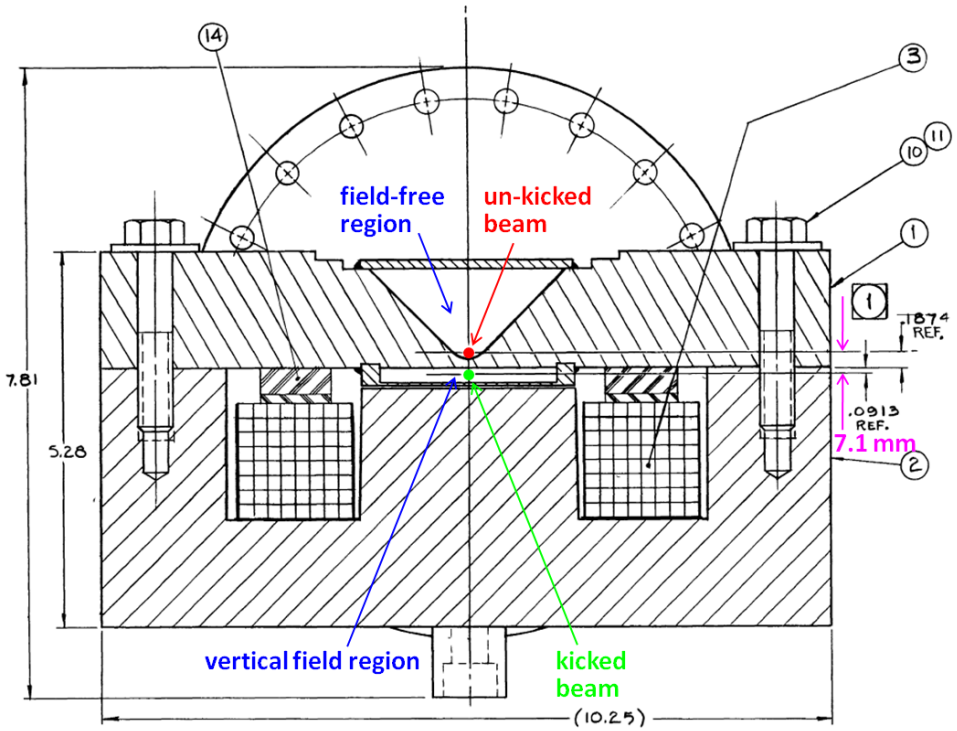

Figure 6.48. Cross-section of a horizontal deflecting Lambertson septum magnet used in the SLC at SLAC with 7-mm field-transition vertical spacing and a horizontal field integral similar to that needed at LCLS-II for future two-bunch operation at 120 Hz in each FEL.

6.7.5 Resistive-Wall Wakefields in the LTU Beam Pipe

The 330-m long LTU2 beamline (from muon plug wall exit to HXR or SXR undulator entrance) is composed mostly of 1.625-inch-diameter cylindrical stainless steel beam pipe with a few micron thick copper plating on the inside to increase the conductivity. The pipe will generate a longitudinal resistive wakefield which generates an rms relative energy spread as described in Section 6.6.4.

Here the conductivity of the inner surface of the copper-plated pipe is 5.8×10^7 /Ω/m. For the parameters listed here, the induced rms relative energy spread for a uniform temporal bunch distribution (3 kA) is approximately 0.0086% (see Figure 6.49). This effect is included in the tracking studies of Section 6.10 and is also shown below in Figure 6.50 with the "real" longitudinal phase space at 13.5 GeV just before (top) and just after the wakefield is applied to the LCLS-II temporal distribution (at right in both plots). This resistive-wall wakefield is very small here and mostly a linear chirp affect. This resistive-wall wakefield of the LTU2 is almost insignificant due to the copper plating.

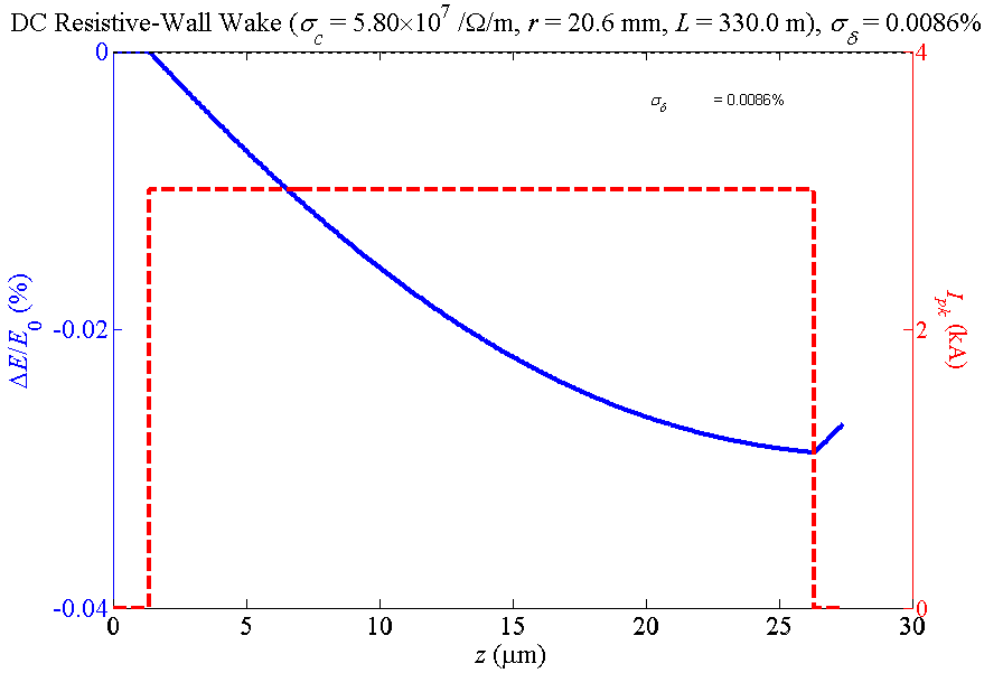

Figure 6.49. Resistive wall wakefield (blue) for a uniform temporal distribution (red) with parameters listed above.

The red-dashed curve is the uniform temporal distribution and the blue-solid curve is the resistive-wall wake-induced relative energy chirp over the 330 meter beamline (mostly linear here).

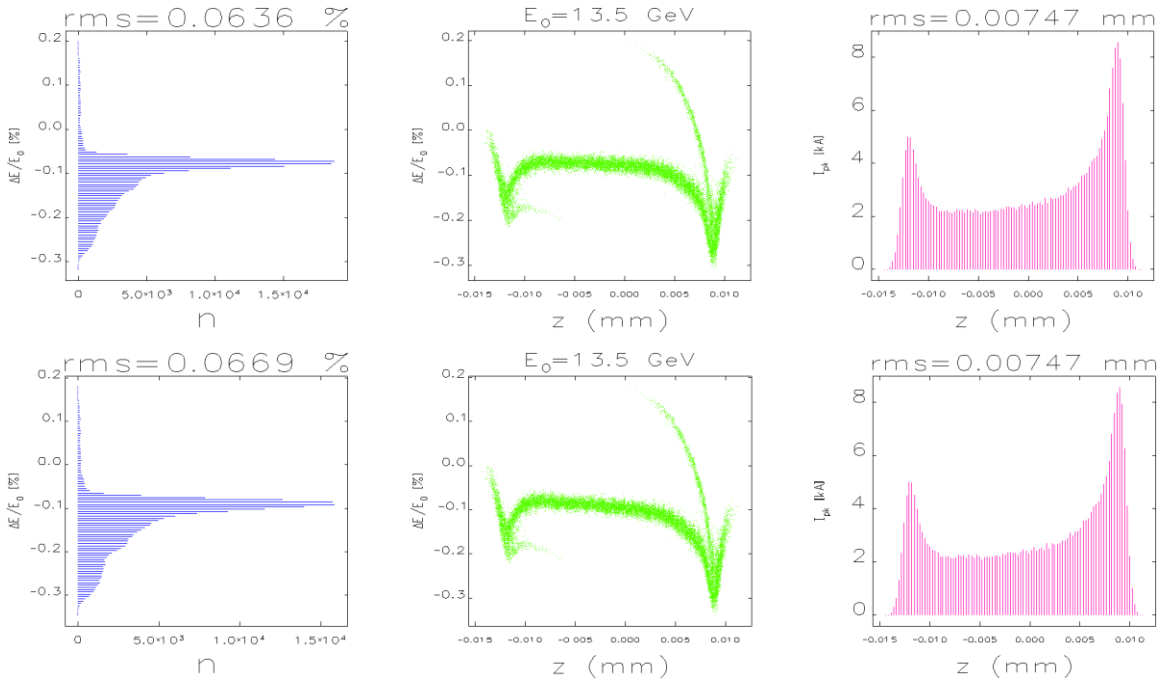

Figure 6.50. The effects of the longitudinal resistive-wall wakefield

Figure 6.50 shows the effects of the longitudinal resistive-wall wakefield of the 330-m long LTU2 copper-plated pipe showing the longitudinal phase space at 13.5 GeV just before (top) and just after the wakefield is applied to the LCLS-II temporal distribution (at right in both plots).

6.8 Electron Dump Lines

The requirements for the two LCLS-II dump lines (HXR and SXR) follow:

- There will exist two separate but adjacent dump lines with each one dedicated to the hard or soft x-ray undulator beam,
- Must bend the spent electron beam downward at about 5° into a 5-kW beam dump with appropriate shielding and cooling,
- Must include relative energy and energy spread diagnostics to measure the effects of FEL and undulator wakefields on the electron beam,
- Must include high-resolution BPMs after the dump bends to routinely measure the energy loss due to the FEL interaction,
- Must provide a safety dump with horizontal permanent magnets to protect the experimental hall from electrons in case the main dump magnets trip off,
- As a redundant safety measure, the dump magnets should also be powered in series with the upstream horizontal DL2 bends in the BTH so that beam can never arrive at the dump bends if the main power supply is off.

The dump lines simply discard the spent electron beam safely and include a few diagnostics to measure the energy and energy spread after passage through the long undulators. Powered vertical bend magnets (net 5° per dump) bend the electron beam down, about 40 meters after each undulator, to a shielded, water-cooled copper dump which absorbs the full beam power (designed for a maximum of 5 kW). In addition, a set of horizontally deflecting permanent magnets are situated on the x-ray beamline. If the powered vertical dipoles lose their field, the permanent magnets will sweep the electrons (4 - 15 GeV) safely away from the x-ray line downstream. In addition, as a redundant safety measure, the vertical bends will be powered in series with the upstream DL2 horizontal LTU bends (net 2.4°) so that the electron beam can never be transported to the dump line when the vertical dump magnet power supply is off. Table 6.17 lists the dumpline parameters and Figure 6.51 shows the optics along the dumpline. The LCLS-I design is shown here since the LCLS-II design has not yet been detailed, but will be very similar to LCLS-I.

Table 6.17. Nominal parameters of the electron beam dump and its transport line (250 pC).

Parameter	Symbol	Unit	Value
Total vertical bend angle of dumpline	θ_y	deg	5
Maximum rms total relative energy spread (at 4.2 GeV)	σ_E/E	%	1.0
Length of each of 3 vertical dipole magnets	L_V	m	1.4
Bend angle of each of 3 vertical dipole magnets	$\lvert\theta_V\rvert$	deg	1.67
Max. magnetic field of each vertical dipole (at 14 GeV)	$\lvert B_V\rvert$	kG	13.6
Nominal electron beam average power in dump (14 GeV)	P_e	W	420
Max. electron beam average power in dump	$P_{e\text{-}max}$	kW	5

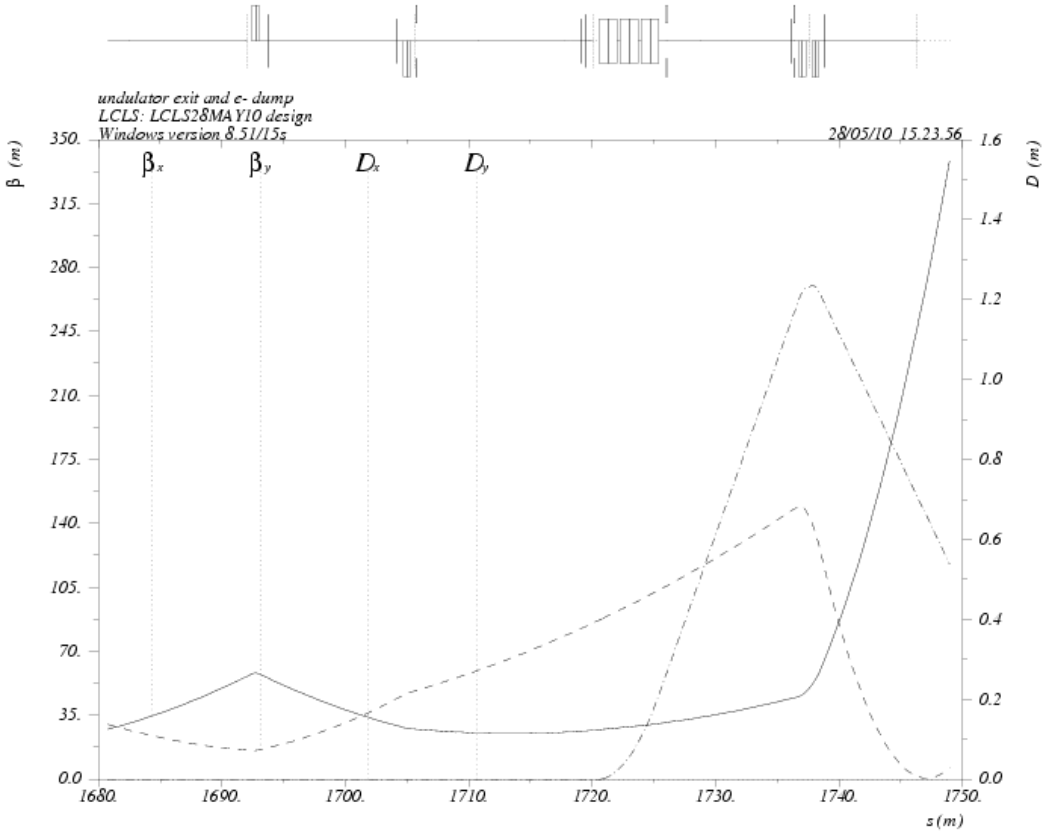

Figure 6.51. Optics of the electron dumpline (for LCLS-I) starting at the end of the undulator and finishing at the dump face. The 3 vertical dipoles are at s = 1720 to 1730 m but the permanent magnets are not shown here, since they are on the x-ray line.

6.9 Radio Frequency (RF) Systems

The RF system for LCLS-II has several performance requirements as follows:

- The high-power RF system must make use of the existing linac RF stations in an efficient and convenient configuration.
- The RF system needs to provide adjustable phase and amplitude for each main linac section (*i.e.*, Gun, L0a, L0b, TCAV0, L1, LX, TCAV1, L2, TCAV3, L3, TCAV4).
- The phase and amplitude stability must meet the stringent requirements described in this section.
- The timing (phasing) of the LCLS-II should be locked to the timing of the LCLS-I accelerator, but with an adjustable relative phase over at least $\pm\pi$.
- Several transverse RF deflectors must be included in order to measure the electron bunch length at various locations.

The LCLS-I has been successfully delivering beam to users since October 2009 with the stability and availability of the RF systems meeting all requirements. With this clear success, the RF systems for LCLS-II will be modeled after the design of LCLS-I.

The installed complement of S-band (2.856 GHz) klystrons in the SLAC linac, from Sector 10 through Sector 20, is capable of accelerating the LCLS-II beam to at least the required energy of 13.5 GeV (with the first four Sector 20 RF systems restored). In addition to setting the electron beam energy, and hence the optical wavelength of the LCLS-II FEL, precise control of RF phase and amplitude is required to manipulate the longitudinal phase space of the beam to produce the desired short bunch at the end of the linac. Specifically, the linac RF is used to introduce an energy-time correlation along the bunch for compression and to compensate for longitudinal wakefields generated by the accelerating structures. This process is supplemented with an additional, higher-harmonic X-band (11.424 GHz) accelerating structure installed just upstream of the first bunch compressor. The success of the bunch compression and wakefield compensation schemes require very tight tolerances for phase and amplitude control of the linac. Methods used in LCLS-I to achieve this will be duplicated for LCLS-II.

6.9.1 The RF systems stability tolerances

The RF system stability tolerances specify the pulse-to-pulse rms variations that are acceptable in linac phase and amplitude, while still maintaining the desired peak current and energy at the entrance to the undulator. These pulse-to-pulse random variations cannot be corrected by feedback and therefore place upper limits on the phase and amplitude noise level of individual components, such as klystrons. Longer-term drift, ranging from several seconds to several days, will be corrected by feedback systems. Beam-based diagnostics of relative bunch length and relative energy will be used to provide feedback for the RF phase and amplitude to control variations slower than ~0.5 Hz.

As for LCLS-I, the LCLS-II will require some modifications and improvements to the SLAC linac RF system to meet these tight tolerances. The changes must remain compatible with the other SLAC linac functions and allow synchronization between LCLS-I and LCLS-II.

Although beam-based feedback will be the final mechanism to stabilize RF phase and amplitude, there are several reasons for keeping the low level RF distribution system as stable as possible. Some development work on feedback tuning algorithms is to be expected before subsystems can be cascaded together. Any extension in the duration over which the beam remains stable and within tolerance makes the task of tuning easier, both during the period of commissioning the accelerator and subsequent operation.

6.9.2 Radio Frequency (RF) Distribution in the SLAC Main Linac

The RF is generated by a stress compensated cut quartz crystal located at Sector 0, which is 1 km up stream of the LCLS-II injector. The RF from the crystal oscillator is multiplied up to 476 MHz and distributed along the 3-km linac on an air dielectric rigid coax referred to as the Main Drive Line (MDL). The timing system fiducial, which is locked to 8.5-MHz damping ring turn frequency, and the 360-Hz harmonic of the power lines is also distributed down the MDL. A coupler will be added in Sector 11 to pick off some of the 476-MHz and generate the RF frequencies required for LCLS-II. By using the same oscillator as the RF source for both LCLS-I and LCLS-II, the two machines will be inherently locked together. Since the RF is distributed along the 2 miles with a rigid coax with a speed of 0.98*c*, the beams, to a very large degree, stay synchronized with the RF. This limits the bandwidth of noise which will cause errors between the two beams of LCLS-I and LCLS-II. The RF reference system will be distributed to the near hall with a fiber based stabilized link. The RF distribution points are shown Figure 6.52.

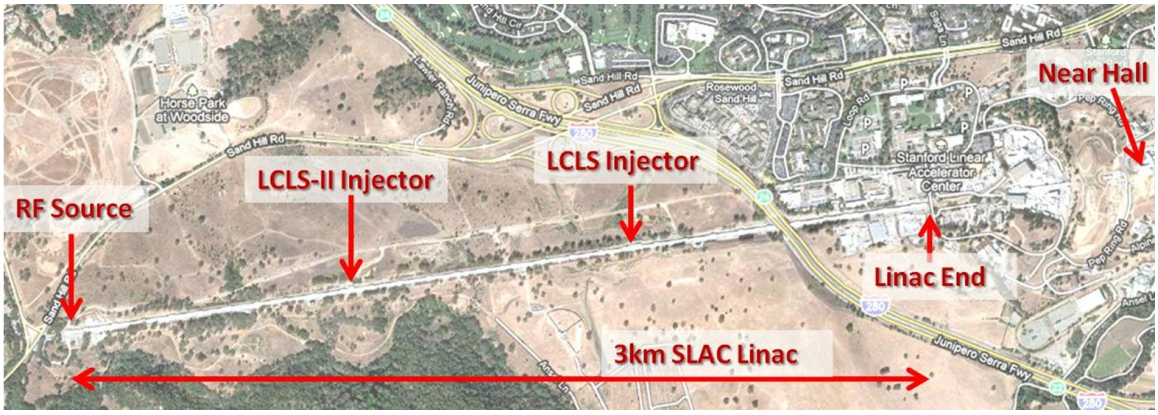

Figure 6.52. Three kilometer SLAC Linac with RF distribution points indicated.

The SLAC linac is divided into 30 sectors, of which the LCLS-II will utilize sectors 10 through 20. The RF distribution for two adjacent, nominal sectors is shown in Figure 6.53, showing how the RF power is derived for each sector and distributed to each of the eight klystrons (typical) in the sector.

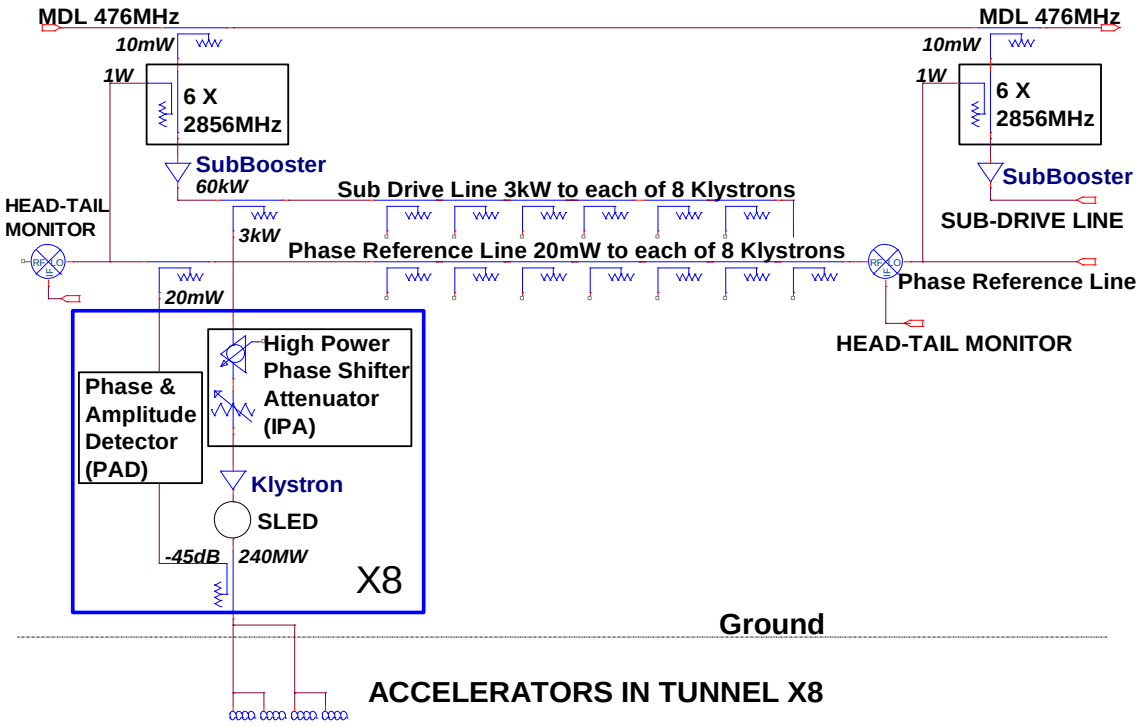

Figure 6.53. Schematic of two adjacent, nominal linac sectors showing distribution of RF power to the 8 klystrons per sector.

At each sector boundary a ×6-multiplier is coupled to the MDL and provides 2856-MHz power for the sector phase reference line and the sub-booster klystron. The sub-booster klystron produces 60 kW of pulsed RF power to drive the Sub-Drive Line (SDL). The SDL and the Phase Reference Line (PRL) run the length of one sector (101.6 m) and are temperature stabilized over most of their length. The SDL provides 3 kW of RF power to each klystron and the PRL provides 20 mW of RF power to the Phase and Amplitude Detector (PAD).

The injector consists of a mode-locked laser, RF gun, two S-band accelerating structures, and one S-band transverse deflector. Once the beam enters the linac it passes through an S-band (2.856 GHz) accelerator and then an X-band (11.424 GHz) accelerator. The RF stability and phase relationship between these sections is critical to stable operation of LCLS-II. Since these stations are centrally located, as with their counterparts in LCLS-I, a temperature stabilized enclosure will be built in the linac gallery at the end of Sector 20 to route temperature sensitive RF cables from the tunnel which measure phase and amplitude of the RF devices. This enclosure is referred to as the "RF Hut" for LCLS-I. The routing of sensitive measurement cables and the area layout is shown in Figure 6.54.

RF cables will be run in the tunnel to Sector 14, where an RF phasing cavity, a second transverse deflector, and the L2 energy feedback klystrons will be located. Another cable will route the RF reference from Sector 14 to Sector 19 and 20, where another phasing cavity and L3 feedback klystrons will be located.

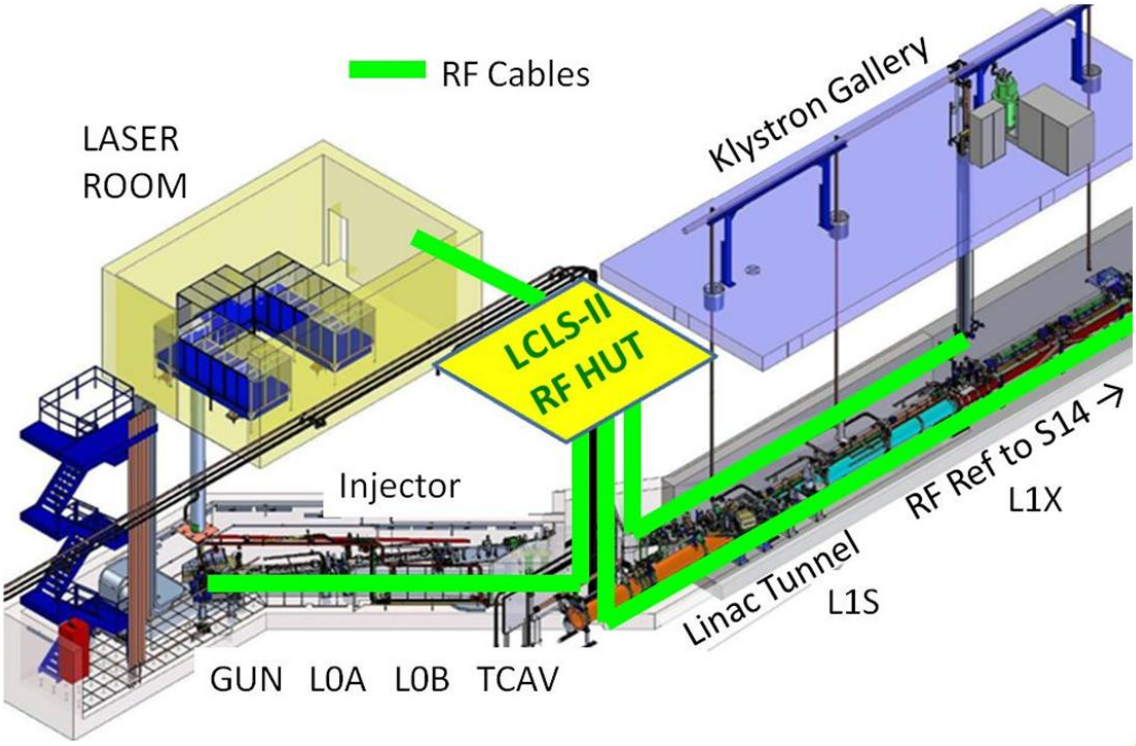

Figure 6.54. Layout of the injector area with the new temperature stabilized LCLS-II "RF Hut" at the end of Sector 20, the laser room, and the routing of temperature sensitive RF cables.

There will be a phase reference cable continued on to the LCLS-I RF Hut to provide phasing information between LCLS-I and LCLS-II. A phase detector will be added to the LCLS-I RF Hut to measure the difference in timing between the two machines.

6.9.3 Improvements to the RF Control System

A low noise RF control system is required to meet LCLS-II specifications for jitter and drift. The RF control system will be modeled after LCLS-I, in that it will go on top of the existing linac system. This will add a tighter control of phase and amplitude for individual klystrons in the injector and for feedback klystrons in L2 and L3. The majority of the klystrons in L2 and L3 will use existing linac controls and not require any changes.

6.9.3.1 L2 and L3 RF Distribution and Control

In LCLS-I, a separate phase reference line is used to control the phases of the klystrons in L2. This phase reference line went to four sectors and has a Phase and Amplitude Controller (PAC) which is used to adjust the overall L2 phase based on beam-based measurements. In LCLS-II the L2 phase reference line will need to control klystrons in four sectors, as in LCLS-I. Sectors 11, 12, 13, and a portion of the klystrons in Sector 14 will need to be controlled by the L2 phase reference line (see Figure 6.29). Three amplitude feedback klystrons will be used in Sector 14. These feedback klystrons will require solid-state sub-boosters (SSSBs), PADs and PACs. The two remaining klystrons at the end of Sector 14 will be outfitted with SSSBs and tied into the RF of the L3-linac.

The L3-linac in LCLS-II will need to have separate control from the MDL, since the MDL also drives L3 in LCLS-I. To achieve this control, PACs will be placed at the drops from the MDL for Sectors 15 to 20. PACs and SSSBs will be installed in Sectors 19 and 20 for each klystron so individual klystrons in these sectors can be used for the final energy feedback.

6.9.3.2 Sub-Boosters

The present linac uses one klystron sub-booster per sector to provide 60 kW of drive power divided into 8 klystrons. Low power phase control is therefore only done at the input side to the sub-booster klystron and hence changes the phase of all 8 klystrons. The high power mechanical phase shifters on the individual klystrons are only capable of coarser, 0.125° steps. Also they were not designed for pulse-to-pulse operation, typically making only a few tens of phase corrections per day in the present linac operation.

The three klystrons in the injector, the L1-linac klystron, the three feedback control klystrons in L2 and the twelve feedback control klystrons in L3, as well as the special X-band and RF deflector klystrons, will require individual sub-boosters. This allows PACs to be used at each individual klystron, on the input side to its sub-booster, to enable the necessary pulse-to-pulse phase control with fine resolution. LCLS-II will then require a total of 21 solid state sub-boosters.

6.9.3.3 Phase and Amplitude Detectors and Control Units

The Phase and Amplitude Detectors (PADs) designed and built for LCLS-I are capable of measuring phase variations down to <30 fs (<0.03 degS) as shown in the plot for phase jitter on the LCLS-I Gun in Figure 6.55.

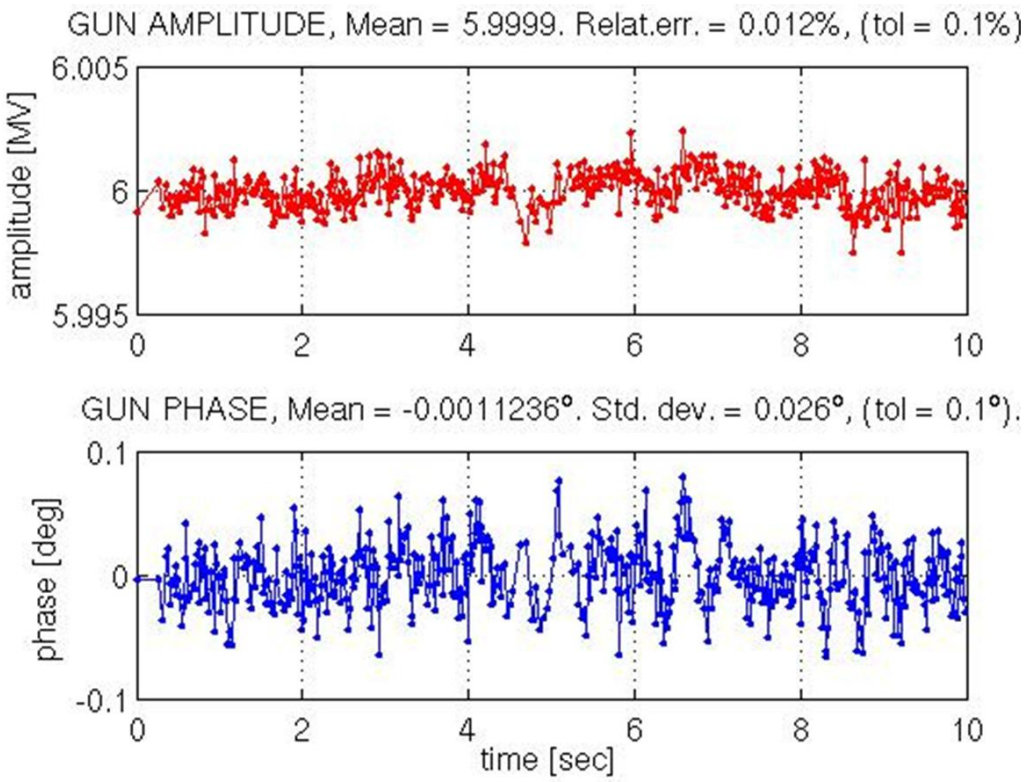

Figure 6.55. LCLS-I gun RF phase and amplitude jitter measurements over 10 seconds at 60 Hz.

The PADs use low noise RF and Local Oscillator signals to down-mix the RF to 25.5 MHz. The RF is then digitized at a 102-MHz sample rate and digitally down-mixed to baseband. The signals are integrated over the portion of the RF pulse of interest and made available as EPICS Process Variables (PVs) on TCPIP Ethernet. A second Ethernet, User Datagram Protocol (UDP), port sends out data at beam rate for feedback and Beam Synchronous Acquisition (BSA). Matlab programs will be (are) used to read and analyze the PVs. There will be 35 total RF PADs used for LCLS-II.

The LCLS Phase and Amplitude Controllers (PACs) use high speed Diamond Anvil Cells (DACs) to put out a waveform that is up-converted to the RF frequency. LCLS-II will use similar type electronics to control the phase and amplitude of the RF system. Both the drive laser at the gun and the spare drive laser will have their own PACs. There will be 33 PACs at all klystrons, sectors, and lasers that require control.

6.9.3.4 Timing System

The present linac timing system is based on 360-Hz fiducials superimposed on the 476-MHz RF that is distributed along the 2-mile linac. LCLS-I uses an Event Generator (EVG) which reads beam code information over a serial link and superimposes the beam code information and a 119-MHz clock on a 2.38-GHz high speed serial link. This high speed serial link is then distributed to Event Receivers (EVRs). This EVR based timing system will be used to supply LCLS-II with triggers that are locked to the linac RF.

6.9.3.5 Synchronization Pulses for Experiments

A new 2856-MHz phase reference line is planned to provide the LCLS-II scientific experiments with RF for synchronization. It will take advantage of fiber optic technology to avoid attenuation over the longer distance. A distribution system for the synchronization pulses is planned in the experimental halls.

6.9.3.6 Beam Diagnostics

Pulse-to-pulse measurements of relative bunch length after each bunch compressor will be available for feedback control of the RF phase. These will be (are) based on CSR detectors (pyro-electron thermal detectors). The bunch length monitors will be calibrated against the absolute bunch length measurement using the RF deflecting cavities (see Section 6.11).

Direct measurement of the beam phase with respect to the linac RF is desirable from the point of view of feedback control. However, the thermal sources of phase drift that need to be compensated in the RF distribution systems are equally likely to disturb the phase measurement at the 0.1º S-band level required here. A technique of measuring the phase of the beam-induced signal in the accelerating structures relative to the RF drive has been studied. One accelerating structure per klystron in a typical linac station is equipped with an output coupler on its load, where such measurements can be made. This may be a suitable technique for long-term phase control at the sub 1-degS level in the L2 and L3-linacs. This measurement requires a dynamic range of over 120 dB and has been done using the configuration shown in Figure 6.56. By using two channels of Analog to Digital Converter (ADC), one channel with a 60-dB attenuator to measure the RF and the other channel with a limiter to protect the ADC that will handle 1 kW of RF input power from the klystron, to measure the 0.5 mW of beam induced RF, we achieved 120 dB of dynamic range. The 1-kW RF and 0.5-mW beam signal from the output of the accelerator structure is split into two paths. One path has a 60-dB attenuator and the other path has a limiter. The 60-dB attenuator gives 1 mW of power from the RF. The limiter limits the RF to 13 mW to protect the circuits and allows 0.25 mW of beam power to pass. This has been tested on LCLS-I with very good results.

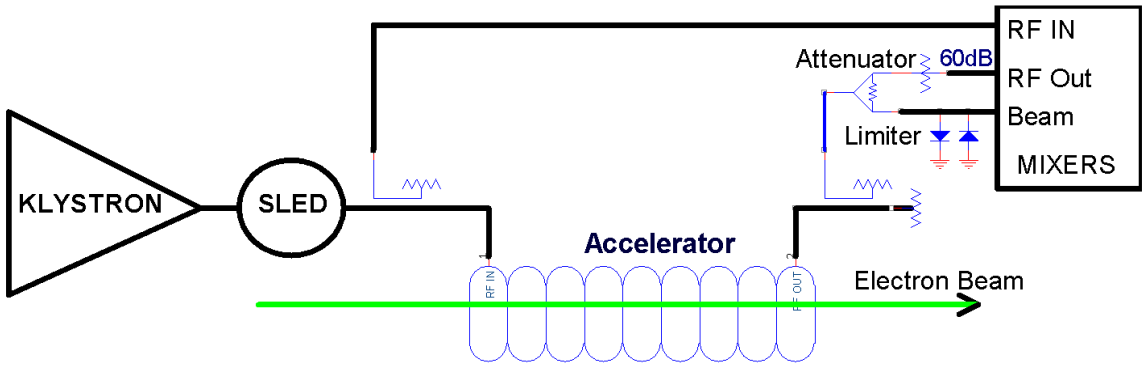

Figure 6.56. Beam and RF phase measurement from output of accelerator structure.

6.9.4 Layout and Performance of the Present SLAC Linac RF

LCLS-II will use klystrons 10-5 to 20-4 in the linac. The injector area, RF Gun, L0a, L0b, TCAV0, L1S and L1X, will be done similar to LCLS-I using klystron stations 10-5 to 11-2. The L2-linac will consist of 26 klystrons from 11-3 to 14-4 and the L3-linac will consist of 45 klystrons from 14-7 to 20-4 (see Figure 6.29).

The LCLS-II gun will be driven from klystron 10-6. The SLED cavity will be removed and enough waveguide, more than 600 ns, will be installed to provide isolation in time for the klystron from the reflected power of the standing wave gun. This method provides better isolation than a circulator and requires no sulfur hexafluoride gas.

L0a will be driven from klystron 10-7 and L0b will be driven from klystron 10-8. Both of these stations will have the SLED cavities removed and waveguide will be routed to the structures in the off axis injector bunker. These two 3-m long structures will be SLAC type structures modified with dual feed inputs, but single outputs (as in LCLS-I). Inputs and outputs of the structures will have Bethe hole couplers and new high power loads with vacuum ion pumps directly on each load.

The TCAV0 transverse deflector in the injector will be driven with klystron 10-5 using a high power 10 dB coupler to drop the power level to 0.5 MW. The SLED cavity will be removed from this station. Both input and output of the structure will have Bethe hole couplers and the output will have a new high power load.

Two of the three L1S structures (11-1b and 11-1c) will be shortened to 9.4 feet so quads can be placed between them. The L1S station will have the SLED cavity remain as is. Bethe hole couplers will be added to the input of the 11-1b section and to the outputs of all the sections. New high power loads will be installed at the outputs of the three structures with vacuum ion pumps directly on each load.

The X-Band station will be placed at klystron station 11-2. The station will be a copy of the 21-2 LCLS-I X-Band station with about 20 MV of peak RF. All high power S-Band components at 11-2, including the four 3-m long structures will be removed to make room for BC1.

Table 6.18 gives the no-load energy gain (in MeV) of the klystrons in the L2 and L3-linacs. Klystrons 11-3, 20-1, 20-2, 20-3, and 20-4 were set to 225 MeV since data was not available. The total energy gain available for L2 is 5.7 GeV at crest RF phase. The total energy gain in L3 is 9.7 GeV. Nominal LCLS-II operational energy is 13.5 GeV.

Table 6.18. Unloaded energy gain (MeV) of each klystron in L2 and L3.

	Sector	1	2	3	4	5	6	7	8
L2	11			225	178	224	233	160	201
	12	213	217	221	226	220	204	198	199
	13	258	242	234	240	187	220	239	232
	14	213	212	235	234			238	229
L3	15	235	212	230	218	235	214	205	235
	16	214	169	213	220	228	148	244	151
	17	235	219	214	188	179	216	247	224
	18	197	216	227	197	229	161	193	238
	19	235	247	220	218	206	206		249
	20	225	225	225	225				

Station 11-3 does not presently exist in the linac and will need to be installed and configured differently since the typical penetration does not exist there. The modifications to the linac for L3 will consist of reinstalling stations 20-2, 20-3, and 20-4. Station 20-1 will be built and installed, since it has not existed prior to this project. This will require a significant amount of work since this station does not have any existing components at present. The second transverse RF deflector, TCAV3, will be located at 14-8d, but powered from klystron 14-6. Its klystron SLED cavity will be removed and waveguide routed to TCAV3 at 14-8d.

6.10 Particle Tracking Results

Particle tracking studies have been performed throughout the injector, accelerator, and FEL by stringing together results from *Parmela* (injector) and *Elegant* [15] (linac). Included in the tracking are longitudinal wakefields, Coherent Synchrotron Radiation (CSR), Incoherent Synchrotron Radiation (ISR), and 2nd-order optics (*e.g.*, chromatic effects). Space charge forces are only included in the *Parmela* run up to 64 MeV, with output particles transferred to *Elegant*. All components are error free here (*e.g.*, perfect alignment). The results are summarized here.

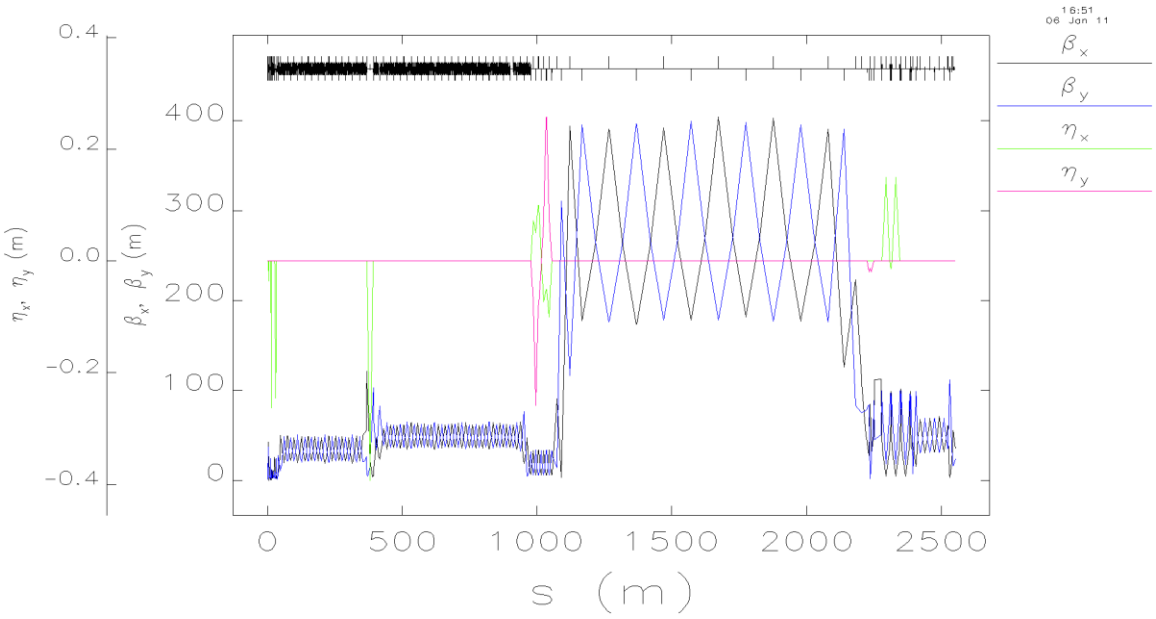

Figure 6.57. Optics across entire LCLS-II (using Elegant 23.1.2), from exit of L0a (at 64 MeV) to the start of the HXR undulator. The pulsed magnet to the SXR branch line (at s ≈ 2350 m) is switched off here.

The following list describes the various effects which are included in the particle tracking.

- 2E5 macro particles representing a 250-pC electron bunch was tracked through *Parmela*, which includes space charge forces, up to the exit of the L0a accelerator section at 63.5 MeV. The initial temporal profile, with a 0.62-mm rms duration, is shown in Figure 6.58.
- First and second-order optics of dipole, quadrupole, and solenoid magnets (there are no sextupoles or skew quadrupoles in the LCLS-II), and sinusoidal RF fields.
- Longitudinal wakefields of the SLAC S-band RF accelerating structures with 326.3 meters of structures between BC1 and BC2, and 581.7 meters after BC2.
- Resistive-wall wakefields of the 1240 meters of 2-inch diameter stainless steel beam pipe (from Sector 20-5 to the exit of the muon-plug wall).
- Resistive-wall wakefields of the 330 meters of 1.625-inch diameter copper plated beam pipe (from the exit of the muon-plug wall up to the HXR or SXR undulator entrance).
- CSR applied to all bends using the 1D line-charge model in *Elegant*, which includes transient fields but ignores the transverse beam dimensions (typically not of major impact).

- ISR applied to all bends, which impacts the slice energy spread and slice emittance, although by insignificant levels.
- An increased slice energy spread (17 keV rms) at 135 MeV such as what is produced by the nominal laser heater system.
- All components are error-free, including perfect alignment. The steering effects of the CSR-induced energy loss in all bends is removed here as well.

Figure 6.57 shows the optics functions across the entire LCLS-II from the exit of the L0a RF structure (at 64 MeV) to the start of the HXR undulator, using *Elegant 23.1.2* (compare with MAD results in Figure 6.2). The pulsed magnet which directs beam into the parallel SXR branch line (at $s \approx 2350$ m) is switched off here.

Figure 6.59 shows the projected horizontal and vertical emittance values across the LCLS-II accelerator from L0a exit (64 MeV) to HXR undulator entrance (13.5 GeV). This is the nominal configuration with 250 pC and 3 kA peak current in the HXR undulator.

Finally, the final longitudinal phase space at 13.5 GeV, at the entrance to the HXR undulator, is shown in Figure 6.60, and the time-sliced horizontal and vertical emittance levels along the electron bunch length (90-fs full scale in this plot) are shown in Figure 6.61, showing almost no increase of the core slice emittance.

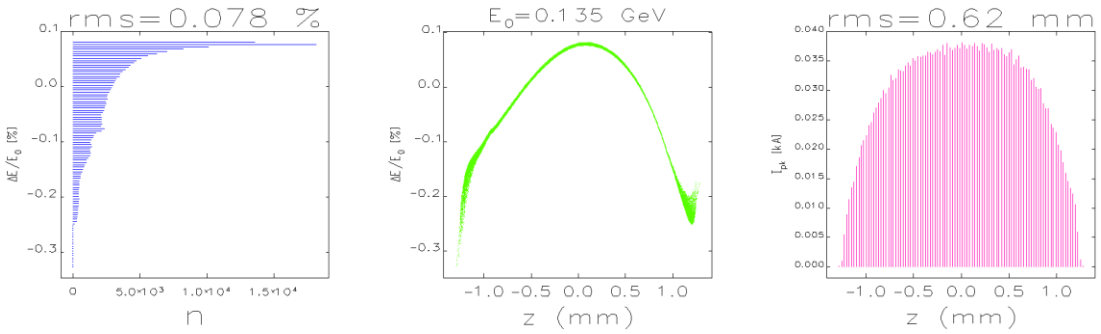

Figure 6.58. Initial longitudinal phase space at 135 MeV after the L0b RF section, which is phased at -2.7° off the RF crest in order to remove a linear chirp from the gun (250 pC).

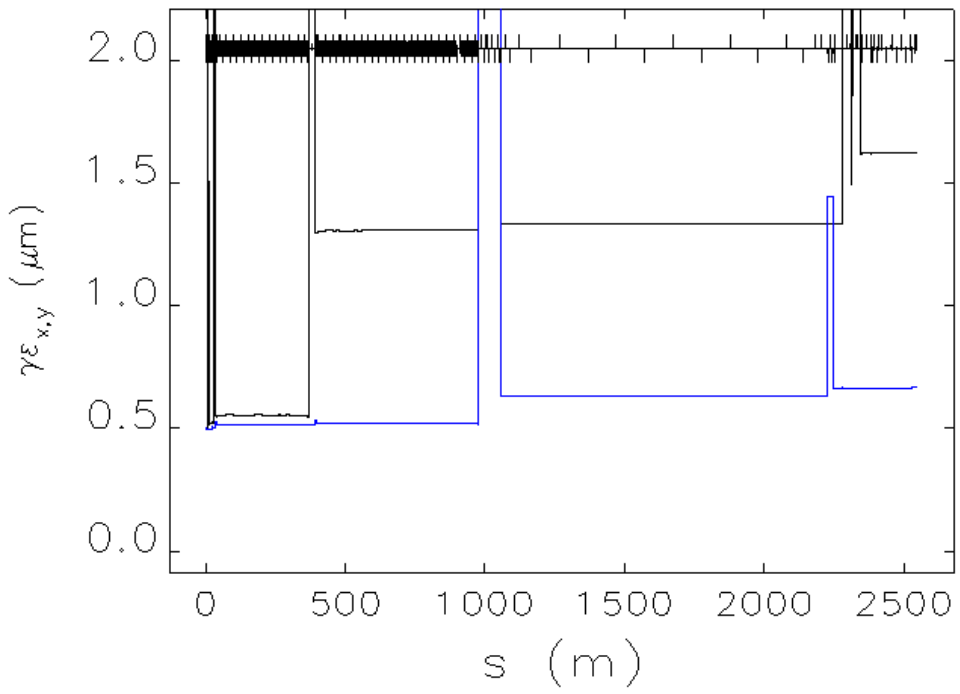

Figure 6.59. Projected emittance (black is horizontal and blue is vertical) along the LCLS-II accelerator from L0a exit (64 MeV) to HXR undulator entrance (large emittance excursions are due to local dispersion).

Referencing Figure 6.59, this is the nominal configuration with 250 pC and 3 kA peak current in the HXR undulator. The BC2 is at *s* ≈ 380 m, the bypass dog-leg is at *s* ≈ 1000 m, and the 2.4-deg DL2 bends are at *s* ≈ 2300 m.

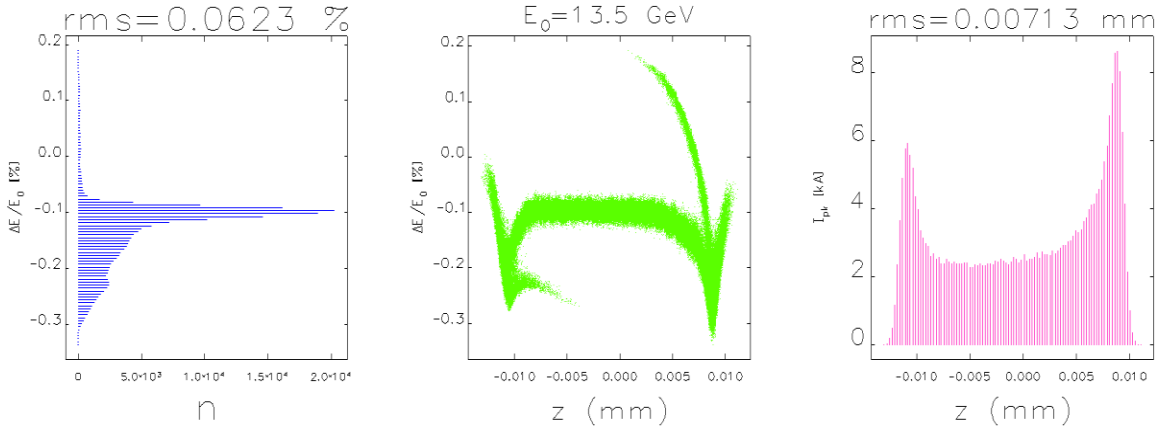

Figure 6.60. Final longitudinal phase space at 13.5 GeV at the entrance to the HXR undulator with 3-kA mean peak current and 250 pC, including CSR in all bends (L2 RF phase = -31.8°).

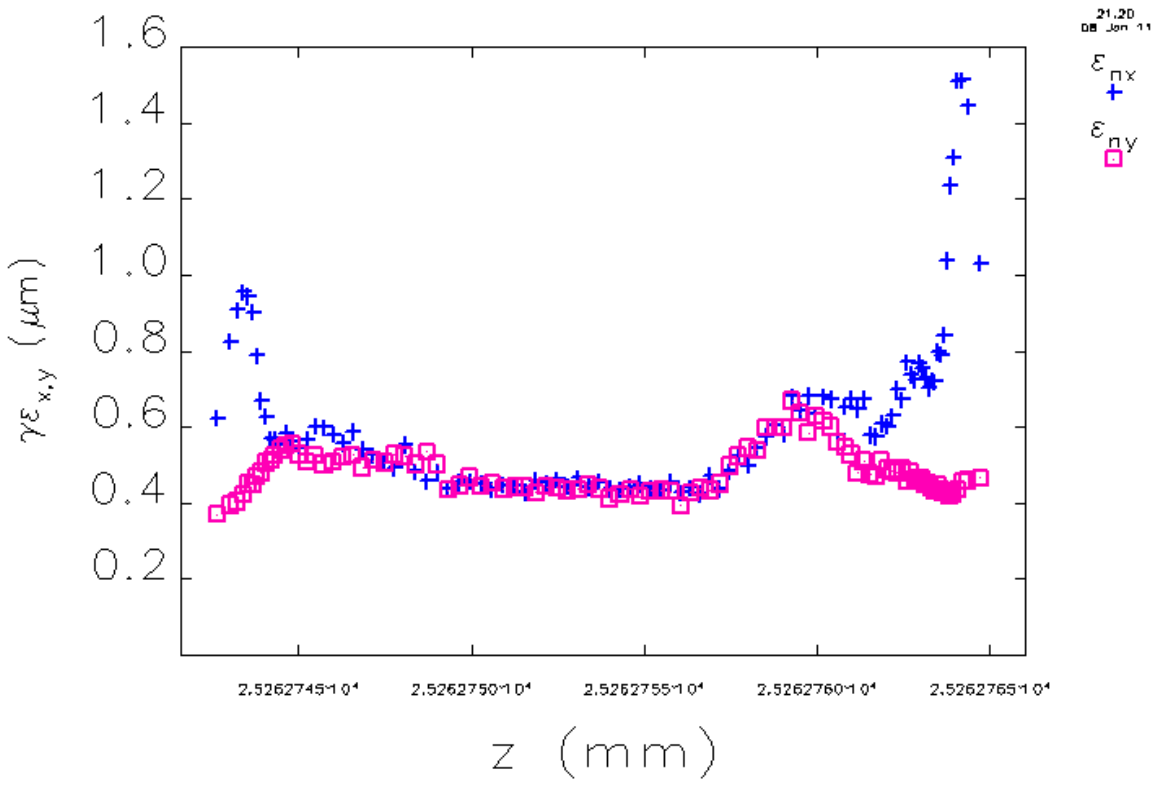

Figure 6.61. The time-sliced horizontal (blue "+") and vertical (magenta squares) emittance values along the electron bunch length. The "z" axis here spans a duration of 90 fs.

6.11 Instrumentation, Diagnostics, Feedback, and Collimation

Critical to the preservation of the transverse emittance and the generation of a low-energy spread electron bunch are the precise measurement techniques and correction schemes used to initially commission and maintain the machine. The LCLS-II accelerator, as in the LCLS-I, has many phase space diagnostics and correction schemes built into the design. The relevant beamlines and optics are specifically designed to enhance the performance of these critical diagnostics. In addition, the permanent magnet undulators are fairly sensitive to beam loss and integrated radiation dose levels. For this reason adjustable collimation is included in both the bypass line (Section 6.6.3) and the LTU (Section 6.7).

6.11.1 Beam Position Monitors (BPMs)

Beam position monitors (BPMs) are distributed over all electron beamlines with one in or near each quadrupole focusing magnet, or tight group of focusing magnets (*e.g.*, triplets in the LTU). The undulator BPMs are special cavity type monitors with sub-micron position resolution while all other BPMs are stripline type with 5-10 micron resolution. A few large aperture BPMs are used in locations where the beam size is very large (center of BC1, center of BC2, and the electron dumpline). There are ~140 stripline BPMs and 36 cavity-BPMs in LCLS-I, with a similar number used in LCLS-II.

6.11.2 Electron Beam Profile Monitors (Screens and Wire Scanners)

Several intercepting electron beam screens and wire-scanners are used throughout the accelerator to measure the transverse beam size. The screens are mostly Yttrium Aluminum Garnet (YAG) and Optical

Transition Radiation (OTR), with one or two older phosphorescent screens still in use. The OTR screens have been problematic, generating significant Coherent OTR (COTR) as well, which does not replicate the rms beam size well. For this reason many of the downstream OTR screens (beyond BC1) have not been very useful in LCLS-I and many will not be installed in LCLS-II. Beam size measurements are mostly made using wire-scanners, except for the OTR2 screen at 135 MeV which is located prior to compression and COTR is minimal. This screen is the 'work-horse' for injector measurements using the standard quadrupole-scan method.

6.11.3 Transverse Emittance Diagnostics

There are five different transverse emittance diagnostic stations distributed along the LCLS-II accelerator. In three of these cases the emittance measurement is accomplished with four consecutive profile monitors placed along the beamline with appropriate phase advance between monitors to optimize resolution. (Only three monitors are necessary, with four used to improve resolution and provide redundancy.) The two low-energy stations use three consecutive profile monitors over a drift section. These allow non-invasive emittance measurements to be made during normal machine operation, or can also be made using a 'quadrupole-scan' technique, taking advantage of the nominal beam waist on the center profile monitor. The emittance measurement stations and their parameters are summarized below in Table 6.19.

Table 6.19. Transverse emittance measurement stations along the LCLS-II ($\gamma\varepsilon_{x,y}$ = 0.6 μm). The L2-ED diagnostic section at the end of the linac serves as the post-BC2 emittance measurement section so that more RF does not have to be removed to locate a new diagnostic section after BC2.

Location	Station Name	Energy (GeV)	σ_x (μm)	σ_y (μm)	No. of Prof. Monitors	Existing
Following L0	ED0	0.135	50-95	50-95	3	No
Following BC1	ED1	0.250	46-68	36-68	3	No
At the end of Linac-2	L2-ED	3.1-4.0	70-60	40-47	4	No
Bypass line	BP-ED	4.2-13.5	140-78	78-140	4	No
Prior to HXR undulator	ED2	4.2-13.5	58-32	32-58	4	No

6.11.4 Bunch Length Diagnostics

The peak current delivered to the undulator is a critical parameter. It is determined by both the charge and the final bunch length. To setup the compression, the bunch length needs to be measured before and after BC1, and after BC2. In addition, once the bunch compressors are set up, a bunch length feedback system will be required for stabilization of the compression. Such a feedback system has been fully tested at LCLS-I with good success over the range of 0.5-Hz and below.

The bunch lengths of interest range from 1000 μm rms to <1μm rms (10 psec to <10 fs FWHM). Transverse RF deflectors have been used at LCLS-I to measure down to about 3 μm rms, but no simple way has yet been devised to measure below 3 μm, although new ideas are being pursued [16]. Relative bunch length monitors have been designed to use coherent synchrotron radiation (CSR) and have demonstrated fast, non-invasive measurements in LCLS-I. They, however, provide only a relative bunch length measurement and need external calibration.

6.11.4.1 Transverse RF Deflectors

A very simple technique to measure the very short electron bunch is to use a transverse RF deflecting cavity. This idea has been used in the past [17], [18] and has been quite successful at the LCLS-I. The high frequency time variation of the deflecting field is used to 'pitch' the electron bunch, while the resulting transverse beam width is measured on a simple profile monitor. This is a reliable, single-shot measure of the absolute bunch length. The technique is completely analogous to a streak camera, but with much better potential resolution down to about 10 fs rms, depending on the energy and vertical emittance. Detailed studies have been made of this technique [19], including wakefield and chromatic effects, and beam measurements have also been made [20]. A design for a 2.44-meter long S-band RF deflecting structure is available at SLAC, was fabricated and tested in the early 1960s [21], and is now used in LCLS-I. A cut-away view of the S-band traveling-wave rf-deflector is shown in Figure 6.62. A new deflecting structure will need to be fabricated.

The bunch length, σ_z, can be calculated from knowledge of the deflecting voltage, V_0, the RF wavelength, λ_{rf}, and the beam energy at the screen, E_s.

$$\sigma_z \approx \frac{\lambda_{rf}}{2\pi} \frac{E_s}{|eV_0 \sin \Delta\psi \cos \varphi|} \sqrt{\frac{\sigma_y^2 - \sigma_{y0}^2}{\beta_d \beta_s}} \tag{8}$$

Included here is the product of $(\beta_d \beta_s)^{1/2} \sin(\Delta\psi)$, which is the (measurable) vertical transfer matrix element from angle-to-position and deflector-to-screen. Finally, φ is the RF phase of the deflector ($\varphi = 0$ at zero-crossing) and σ_y and σ_{y0} are the measured vertical beam sizes with RF on and off, respectively. The voltage of the deflector is easily calibrated using simple BPM measurements as a function of RF phase. The RF deflecting structure will be placed downstream of the BC2 chicane at 4.6 GeV at the 14-8d location where an existing 3-meter accelerating structure will need to be removed. The screen will be located at the 15-902 location where space is available. In addition, a second RF deflector (55 cm long) will be located in the injector at 135 MeV, as in the LCLS-I, providing <0.1 ps resolution of the 5-ps long bunch there (see Figure 6.63). And if the budget allows, a third deflector will be located after BC1 and a fourth, X-band (11.424 GHz) deflector after the undulator to allow continual bunch length measurements during LCLS-II operations.

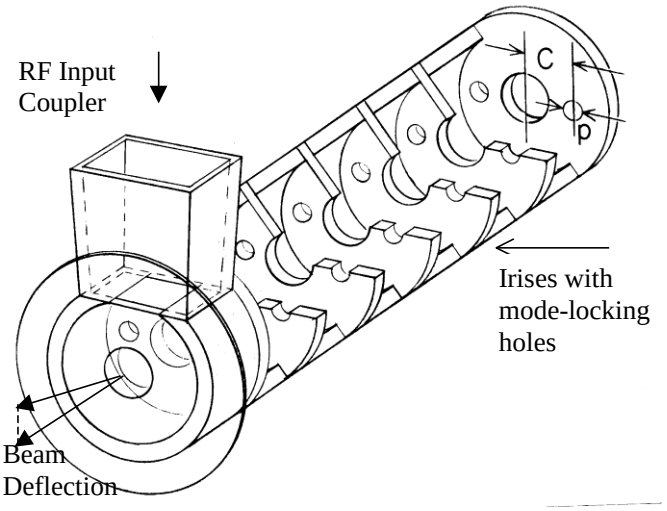

Figure 6.62. Schematic of a SLAC S-band transverse deflecting structure. The kick is vertical here.

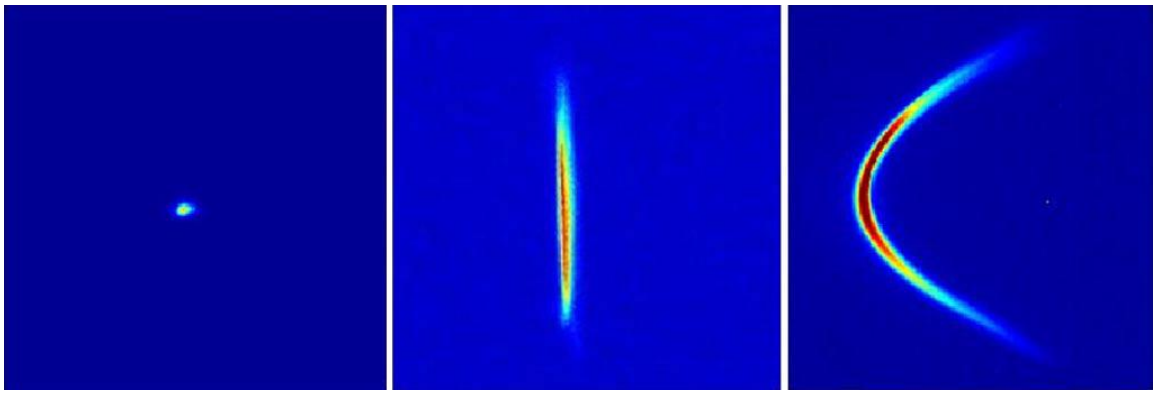

Figure 6.63. OTR image with RF deflector ''OFF'' (left) and ''ON'' (middle), to measure slice emittance. YAG screen after a bend (right) with deflector ON, reveals longitudinal phase space directly on the screen. The horizontal axis (±4 mm) is the horizontal beam coordinate in the left two plots, but it becomes relative energy in the right plot (±0.8%). The vertical axis (±4 mm) is the vertical beam coordinate in the far left plot, but it becomes time in the two right plots (±8 ps).

6.11.5 Beam Energy Spread Diagnostics

The electron energy spread is typically measured using a profile monitor at a location with large momentum dispersion and small beta function. Several locations have been designed into the LCLS-II optics in order to enable this measurement. The key locations are after the fun at 6 MeV where a spectrometer magnet can be switched on; in the DL1 dog-leg system at 135 MeV (35 deg bend from injector into the linac); the 135-MeV spectrometer which is an off-axis diagnostic with high resolution; the BC1 first bunch compressor, the BC2 second bunch compressor, the bypass line just after the end of the linac, the DL2 dog-leg just prior to the undulators, and the two electron dump lines after the undulators. Each of these locations will be equipped to allow adequate energy spread measurements along the LCLS-II accelerator as described below.

6.11.5.1 DL1 Energy Spread Diagnostics

The energy spread measurement in DL1 is made with one of two possible profile monitors (a retractable OTR screen and a wire-scanner) located between the two dipoles of DL1 at the point where the horizontal dispersion function reaches a value of $|\eta_x| \approx 154$ mm with a horizontal beta function of $\beta_x \approx 1.5$ m. For the nominal emittance and nominal energy spread of $\sigma_\delta \approx 0.07\%$ at 135 MeV, the betatron beam size is 58 μm, but the dispersive size is 77 μm. This produces a systematic energy spread measurement error of 25%. The statistical error depends on the profile monitor and should be 5–10%. A more accurate measurement of this same energy spread is available in the 135-MeV spectrometer, which can be switched on or off at any time (see below).

6.11.5.2 135-MeV Spectrometer

The energy spread measurement in the 135-MeV spectrometer is made with a profile monitors (a retractable YAG screen) located after the 35-deg BXS bend magnet where the horizontal dispersion function reaches a value of $|\eta_x| \approx 887$ mm with a horizontal beta function of $\beta_x \approx 0.13$ m. For the nominal emittance and nominal energy spread of $\sigma_\delta \approx 0.07\%$ at 135 MeV, the betatron beam size is 17 μm, but the dispersive size is 444 μm. This produces no significant systematic energy spread measurement error. The statistical error depends on the profile monitor and should be 5–10%.

6.11.5.3 BC1 Energy Spread Diagnostics

The energy-spread after the first compressor, BC1, is made with a profile monitor (a retractable OTR screen which is not greatly compromised by COTR) located in the center of the chicane at a point where the horizontal dispersion function is $\eta_x \approx 245$ mm and the horizontal beta function converges towards a minimum of $\beta_x \approx 6.3$ m. For the nominal emittance and nominal energy spread of $\sigma_\delta \approx 1.1\%$ at 250 MeV, the betatron beam size is 88 μm, but the dispersive size is 2.7 mm. This produces no systematic error in the energy-spread measurement. The collimator jaws in BC1, upstream of the profile monitor, can be used to select energy bands for diagnostic purposes.

6.11.5.4 BC2 Energy Spread Diagnostics

The energy-spread after the second compressor, BC2, is also made with a single profile monitor (a retractable OTR screen which is also not greatly compromised by COTR) located in the center of the second chicane at a point where the horizontal dispersion function is $\eta_x \approx 392$ mm and the beta function converges towards a minimum of $\beta_x \approx 26$ m. For the nominal emittance and nominal energy spread of $\sigma_\delta \approx 0.43\%$ at 4.2 GeV, the betatron beam size is 44 μm, but the dispersive size is 1.5 mm. As in the case of BC1, this produces no systematic error in the energy-spread measurement. As in BC1, the collimator jaws in BC2, upstream of the profile monitor, can also be used for diagnostic purposes.

6.11.5.5 Bypass Line Energy Spread Diagnostics

The energy spread at the end of the linac in the first bends of the bypass line is made with a wire-scanner located where the vertical dispersion function is $\eta_y \approx 251$ mm and the beta function is $\beta_y \approx 32$ m. For the nominal emittance and a total rms energy spread of $\sigma_\delta \approx 0.03\%$ at 13.5 GeV, the betatron beam size is 27 μm, but the dispersive size is 75 μm. The total beam size is then 80 μm, and a vertical profile produces an energy spread measurement accuracy of 6% at 13.5 GeV. The time-sliced energy spread is actually only 0.01% rms, so this measurement is only barely able to resolve this level. Of course, the betatron beam size can always be subtracted in quadrature if the emittance and beta function are known.

6.11.5.6 DL2 Energy Spread Diagnostics

The energy spread measurement just before the undulator in DL2 is made with a profile monitor (a retractable YAG screen) located where the dispersion function is $\eta_x \approx 140$ mm and the beta function converges towards a minimum of $\beta_x \approx 5.0$ m. For the nominal emittance and a total rms energy spread of $\sigma_\delta \approx 0.03\%$, the betatron beam size is 11 μm, but the dispersive size is 42 μm. The total beam size is then 43 μm, and a horizontal profile monitor produces an energy spread measurement accuracy of 3% at 13.5 GeV. Similarly the time-sliced energy spread is actually only 0.01% rms, which is possible but difficult to resolve. Of course, the betatron beam size can always be subtracted in quadrature if the emittance and beta function are known.

6.11.5.7 Dump Line Energy Spread Diagnostics

The energy spread measurement after the undulator in the dump line is made with a profile monitor (a retractable YAG screen) located where the vertical dispersion function is $\eta_y \approx 698$ mm and the beta function converges towards a minimum of $\beta_x \approx 1.3$ m. For the nominal emittance and a total rms energy spread of $\sigma_\delta \approx 0.03\%$, the betatron beam size is 5 μm, but the dispersive size is 210 μm, which produces

no systematic error in the energy-spread measurement. At this location, however, the energy spread will likely be dominated by FEL and wakefield effects in the undulator.

6.11.6 Trajectory Feedback Systems

Trajectory feedback systems will be placed at the exit of the gun, in the injector, at the entrance of the L2-linac, the L3-linac and at the undulator entrance. As at the SLC [22], these systems will each be composed of approximately ten BPMs which record both *x* and *y* positions, preceded by a set of two horizontal and two vertical fast dipole corrector magnets controlled by a microprocessor based feedback system.

In order to control transverse orbit variations to better than $1/10^{th}$ of the beam size, the individual one-pulse BPM resolution for the various 10-BPM feedback systems described above needs to be <10 μm rms. Trajectory variations which occur at frequencies below ~5 Hz will be stabilized. Faster variations cannot be damped significantly and will need to be identified at the source. In addition, a bunch charge feedback loop will maintain the bunch charge by reading a toroid and controlling the UV laser energy per pulse with a waveplate.

Transverse vibrations of quadrupole magnets will generate orbit variations, which if fast enough will not be damped by feedback systems. Tolerance calculations indicate that uncorrelated random vibrations of all LCLS-II quadrupoles must be at the level of <100 nm rms, to hold the rms beam stability at <10% of the rms beam size there. Measurements in the SLC indicate that existing linac magnet vibrations are <250 nm [23] with the highest frequency content at 59 Hz and 10 Hz driven by cooling water. These observed vibrations will need to be improved about a factor of two to achieve stability goals. At lower energies most of the new quadrupole magnets are air-cooled and have looser vibration tolerances.

6.11.7 Energy and Bunch Length Feedback Systems

Energy feedback systems will be placed in each bending region (DL1, BC1, BC2, and DL2). A single BPM or group of BPMs placed at a high dispersion point will be used to determine energy variations, and upstream RF will be used to stabilize the energy. A group of klystron phases will be used to control the energy while maintaining the correlated energy spread such that bunch compression in each system is also held constant. At the same time the bunch length will be controlled after BC1 and after BC2 defining a 6×6 feedback loops system that has already been fully tested and now operational at LCLS-I.

6.11.8 Collimation Systems

Several adjustable collimator jaw sets will be distributed along the machine in order to protect the permanent magnet undulators. The primary transverse collimation will take place in the bypass line (see Section 6.6.3) and the final transverse 'clean-up' collimation pass will be done in the LTU beamline (see Section 6.7.2), about 100 meters upstream of the undulators. In addition, two energy collimators will be included in the LTU bend system (DL2), especially designed to truncate any dark current which is transported this far [12]. A final fixed protection collimator just in front of each undulator will fully shadow the undulator apertures and protect from extreme trajectories which may enter off axis at the undulator entrance.

6.12 Future Options

Several other operating modes are possible in the long term if the x-ray science generates an appropriate motivation to develop these.

6.12.1 Multi-Bunch Operation

The LCLS-II may provide diagnostics and software capable of operating 2 electron bunches within one RF pulse with ~50-ns spacing at 120 Hz. However, a much faster kicker system, at least, would be needed in order to operate both the HXR and the SXR undulators each at 120 Hz.

6.12.2 28-GeV Operation

The possibility to connect the two LCLS machines at Sector 20 is open if this becomes an attractive option in the long term. This would allow an FEL operating at up to 28 GeV which might produce hundreds of GW of peak x-ray power at sub-Angstrom levels. This is not a trivial alteration, requiring many new magnets and power supplies capable of operating at twice the LCLS energy. In addition, a new undulator system would be required to take advantage of the high energy beam and to target the appropriate x-ray wavelengths and peak power levels. In any case, this option is still possible but would require a detailed design effort to properly execute.

6.13 References

1. J. Arthur et al., SLAC-R-593, 2002.
2. P. Emma, et al., *Nature Photonics*, **4**, 641-647 (2010).
3. http://www.slac.stanford.edu/cgi-wrap/getdoc/slac-tn-05-021.pdf.
4. Z. Huang *et al.*, Phys. Rev. ST Accel. Beams **7**, 074401 (2004).
5. Z. Huang *et al.*, Phys. Rev ST – Accel. Beams **13**, 020703 (2010).
6. R. Akre *et al.*, Phys. Rev ST – Accel. Beams **11**, 030703 (2008).
7. D. H. Dowell *et al.*, *The Development of the Linac Coherent Light Source RF Gun*, http://www-bd.fnal.gov/icfabd/Newsletter46.pdf.
8. J. Qiang et al., Phys. Rev. ST Accel. Beams **9**, 044204 (2006).
9. M. Xie, Proc. of the 1995 Part. Accel. Conf., Dallas, TX, May 1-5, 1995.
10. K. Bane, P. Emma, Proc. of the 2005 Part. Accel. Conf., Knoxville, TN, May 16-20, 2005.
11. K.L.F. Bane *et al.*, Phys. Rev. ST Accel. Beams **12**, 030704 (2009).
12. P. Emma, *et al.*, *Linac Coherent Light Source Electron Beam Collimation*, Proc. of EPAC-2006, Edinburgh, Scotland, June 26-30, 2006.
13. P. Emma, *et al.*, *Linac Coherent Light Source Electron Beam Collimation*, Proc. of EPAC-2006, Edinburgh, Scotland, June 26-30, 2006.
14. F.-J. Decker *et al.*, Proc. of the 2010 FEL Conf., Malmo, Sweden, Aug. 23-27, 2010.
15. M. Borland, Report No. ANL/APS LS-287, 2000.
16. Z. Huang et al., Phys. Rev. ST Accel. Beams 13, 092801 (2010).
17. G. A. Loew, O. H. Altenmueller, *Design and Applications of R.F. Deflecting Structures at SLAC*, PUB-135, Aug. 1965.
18. R.H. Miller, R.F. Koontz, D.D. Tsang, *The SLAC Injector*, *IEEE Trans. Nucl. Sci.*, June 1965, p. 804-8.
19. P. Emma, J. Frisch, and P. Krejcik, *A Transverse RF Deflecting Structure for Bunch Length and Phase Space Diagnostics*, LCLS-TN-00-12, August 2000.

20. P. Emma, et al., Bunch *Length Measurements Using a Transverse RF Deflecting Structure in the SLAC Linac,* Proceedings of the 2002 European Particle Accelerator Conference, Paris, France, June 3-7, 2002.

21. O. H. Altenmueller, R. R. Larsen, and G. A. Loew, *Investigations of Traveling-Wave Separators for the Stanford Two-Mile Linear Accelerator*, The Review of Scientific Instruments, Vol. 35, Number 4, April 1964.

22. T. Himel et al., *Adaptive Cascaded Beam-Based Feedback at the SLC*, Proceedings of the 1993 Part. Accel. Conf., Washington, DC, 1993.

23. J. L. Turner *et al.*, *Vibration Studies of the Stanford Linear Accelerator*, Proceedings of the 1995 Part. Accel. Conf., Dallas, TX, 1995.

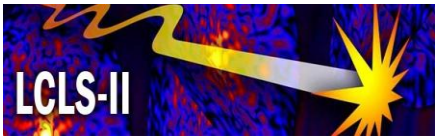

7 Undulators

Technical Synopsis

The LCLS-II project includes 2 new undulators: one for generating hard x-rays (2,000 – 13,000 eV) (HXR) and the other one for generating soft x-rays (250 – 2,000 eV) (SXR). Each undulator is comprised of individual undulator segments separated by 1-m-long break sections. Each undulator segment will be a variable gap permanent-magnet planar hybrid device with a nominal minimum gap height of 7.2 mm and a total segment length of 3.40 m. The HXR Undulator is made up of 32 individual undulator segments, each with 106 32- mm-long periods. The SXR Undulator is made up of 18 individual undulator segments, each with 61 55- mm-long periods. The poles will be made of vanadium permendur and the magnet blocks of a grade of NdFeB with a high intrinsic coercivity for better resistance to radiation-induced demagnetization. The electron beam will be focused by two separated function Focussing-Drift-Defocusing-Drift (FODO) lattices, using electromagnetic quadrupoles placed between the undulator segments. These focusing or defocusing lenses will share the drift spaces (break sections) between the undulator segments with electron beam position monitors, and phase shifters. The break sections will be 1 m long. The electron beam trajectory must be straight to within a few microns over a distance of ~10 m to limit phase errors between electron and photon beams. It is shown that this specification can be achieved with beam-based techniques.

Provision will be made for magnetic tuning of the undulator segments. Tolerances have been developed that will set the magnetic tuning requirements for the individual undulator segments.

The smoothness requirement for the inside surface of the vacuum chamber is analyzed, and found to be achievable. Diagnostics for the electron beam will include Beam Position Monitors and Beam Loss Monitors after each undulator segment, at the ends of the undulator line.

7.1 Introduction and Overview

The LCLS-II undulators will operate as a single pass Free Electron Laser (FEL) in the Self-Amplified Spontaneous Emission (SASE) regime. Exponential gain of the coherent radiation intensity and saturation after about twenty power gain lengths are predicted by theory (see Chapter 4). An FEL operating at saturation will have a more stable radiation output. Therefore, a goal in the design of the undulator line is to allow saturation to be reached while minimizing the required undulator length. Minimizing the undulator length helped guide many of the parameter choices for the undulator line and was also used in allocating error tolerances.

7.2 Undulator Layout

7.2.1 Introduction

The LCLS-II undulator system will be comprised of two separate undulators, one for producing hard x-ray (HXR) radiation the other for soft x-ray (SXR) radiation. Both undulators will be mounted in parallel and will cover different photon energy ranges for the same electron beam energy. A conceptual layout is shown in Figure 7.1. Each of the two undulators will be comprised of individual undulator segments, each 3.4 m in length. These segments will be separated by 1-m-long break sections that will house a quadrupole, an RF cavity Beam Position Monitor (RFBPM), and a phase shifter. A listing of the main dimensions is given in The minimum undulator gap is limited to 7.2 mm to allow installation of a vacuum chamber with 6 mm outer height with sufficient clearance to safely stop the undulator jaws before they damage the chamber. With this minimum gap the undulator periods were chosen to provide levels of FEL brightness comparable to the LCLS-I brightness (see Figure 7.3) but still keeping the overall undulator length short to control the overall cost.

Table 7.1.

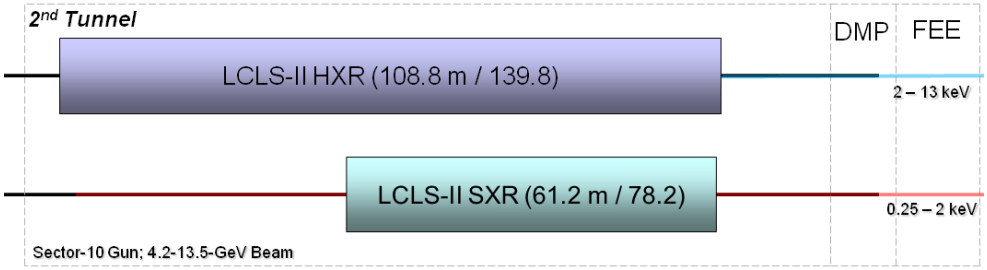

Figure 7.1. Schematic layout of the two undulators in the new Undulator Hall ("2nd Tunnel").

The magnetic and total lengths are listed on each undulator. Each undulator is comprised of individual segments (HXR: 32; SXR: 18). The segments are separated from one another by 1-m long diagnostics and beam control sections. The dimensions in the following figure are not to scale. For detailed layout of the HXR and SXR undulator see Figure 7.2 below.

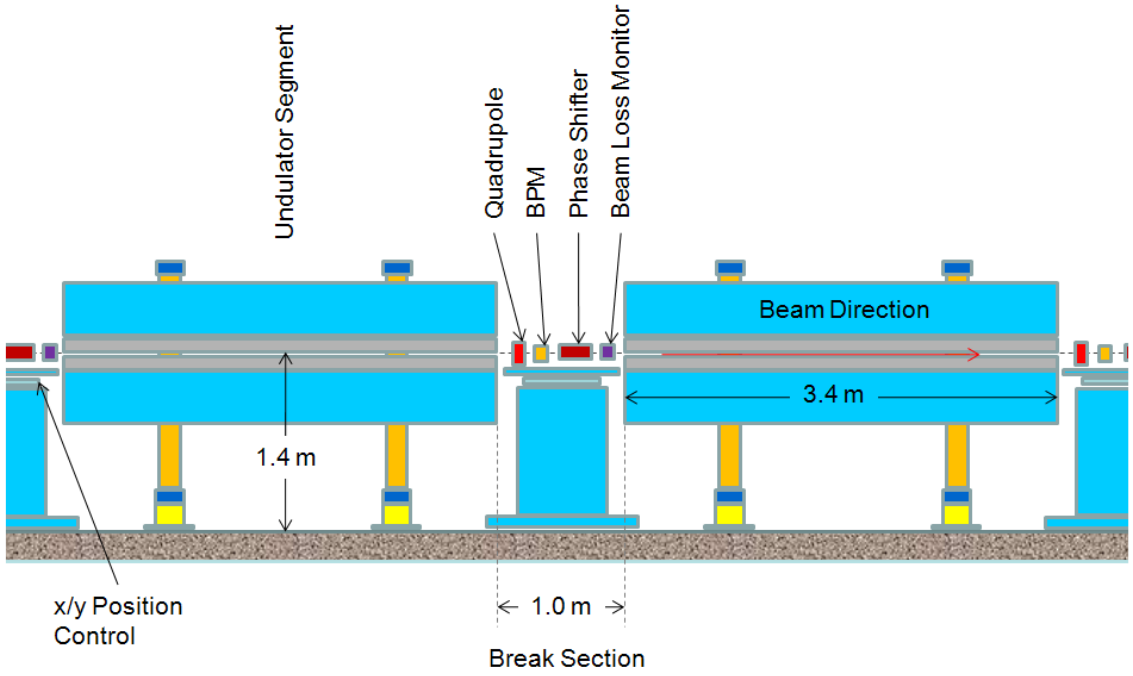

Figure 7.2. Schematic layout of two individual undulator segments and intermediate break sections for the HXR and SXR undulators.

All break sections have the same 1-m length. Both undulators use the same dimensions. Shown is 1/16 of the HXR undulator or 1/9 of the SXR undulator.

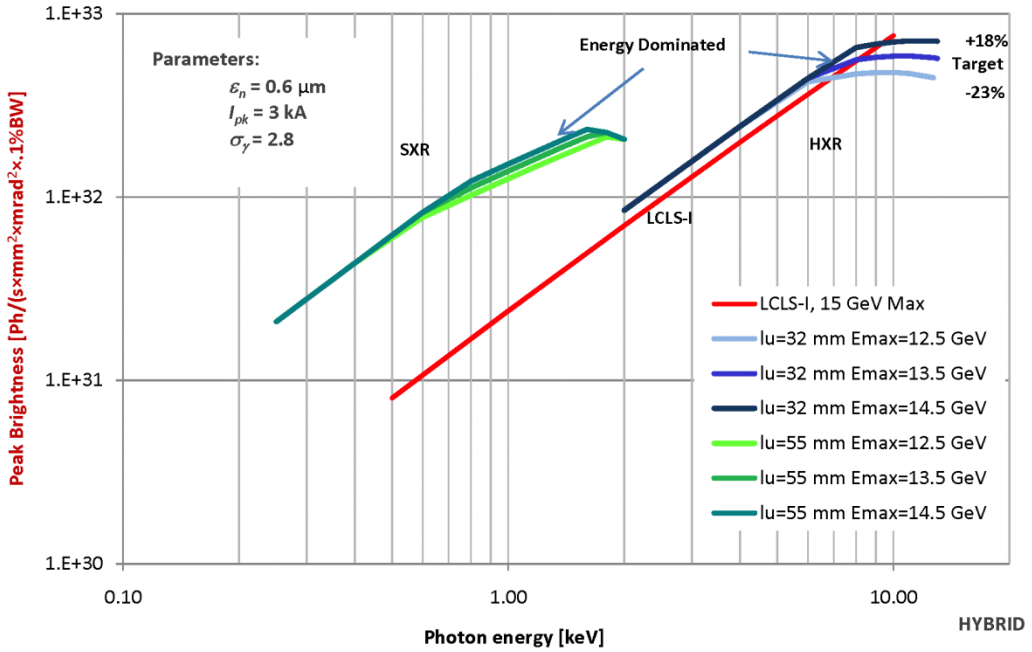

Figure 7.3. Comparison of HXR, SXR, and LCLS-I brightnesses for different undulator periods and electron beam energies. Note: For all cases, the "conservative" parameters, shown in the graph, were used, for the purpose of comparision. Actually achieved LCLS-I brightness levels exceed the ones shown. The LCLS-II graphs are shown for three different maximum electron energy to demonstrate the influence that parameter on maximum brightness.

The minimum undulator gap is limited to 7.2 mm to allow installation of a vacuum chamber with 6 mm outer height with sufficient clearance to safely stop the undulator jaws before they damage the chamber. With this minimum gap the undulator periods were chosen to provide levels of FEL brightness comparable to the LCLS-I brightness (see Figure 7.3) but still keeping the overall undulator length short to control the overall cost.

Table 7.1. Basic nominal LCLS-II undulator dimensions.

Parameter	Symbol	Unit	HXR	SXR
Undulator gap	g	mm	7.2 – 20.1	7.2 – 35.5
K range	K	mm	0.83 – 3.76	1.34 – 9.90
Undulator period length	λ_u	mm	32	55
Number of periods per segment			106	61
Individual segment length	L_{seg}	m	3.400	3.400
Number of installed segments			32	18
Total undulator length	L_u	m	139.800	78.200
Total length of all installed segments	$L_{u,mag}$	m	108.800	61.200
Break section length	L_{Break}	m	1.000	1.000
Total undulator length	Lu	m	139.800	78.200

7.2.2 Description

The undulator segments for both the HXR and SXR undulators will use a common variable gap design, similar in concept to the one used by the European X-ray Free Electron Laser (XFEL) project (see Figure 7.4). The difference between the HXR and SXR will be in the period length of the magnet structure.

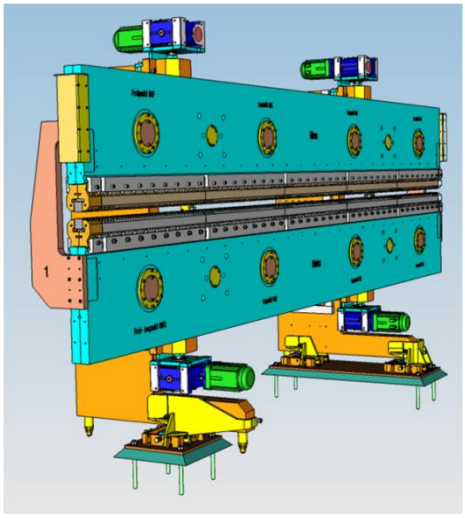

Figure 7.4. Undulator segment design for the European XFEL project [1].

7.3 Focusing Scheme

7.3.1 Introduction

The FEL process depends on transverse beam size, which will be controlled by a FODO lattice based on individual focusing and defocusing quadrupole magnets located in the break sections between undulator segments. The optimum average beta-functions for the two undulators are different. The SXR line requires a smaller average beta function (stronger focusing) than the HXR line. The proposed beta functions are shown in Figure 7.5. Performance estimates for the proposed beta functions are shown in Chapter 5. The focusing parameters are listed in Table 7.2.

Table 7.2. Nominal LCLS-II undulator focusing parameters.

Parameter	Symbol	Unit	HXR	SXR
Focusing lattice			FODO	FODO
Integrated quadrupole gradient	$\int Gdz$	T	2.3	4.5
Spacing between quadrupole magnets		m	4.4	4.4
Number of undulator line quadrupole magnets			32	18
Number of matching quadrupoles			4	4
Average beta function range	$\beta_{x,y}$	m	33 – 12	18 – 8

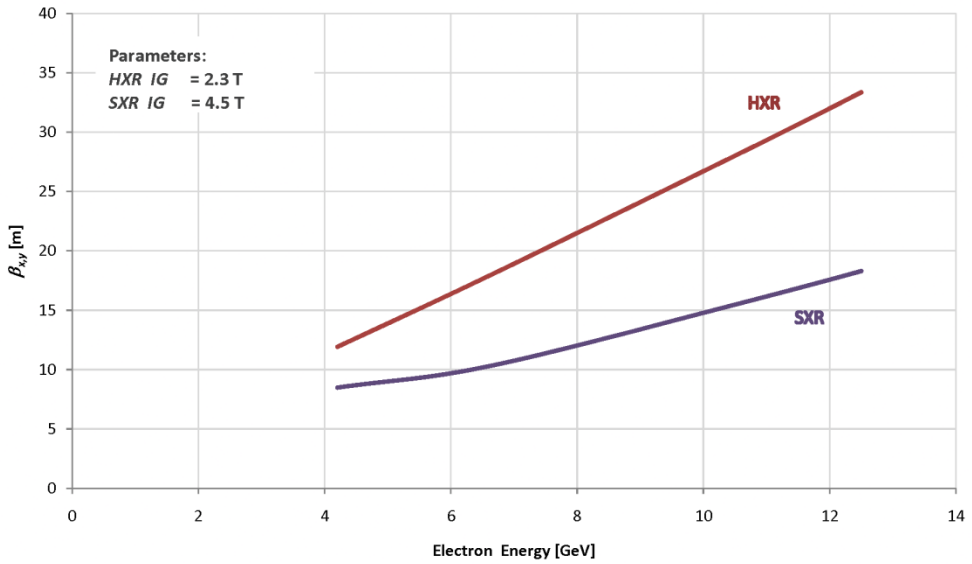

Figure 7.5. Average beta functions in both planes along the undulator for integrated quadrupole gradients of 2.3 T (HXR) and 4.5 T (SXR).

7.4 Cell Components

7.4.1 Introduction

Both LCLS-II undulator lines will be comprised of individual cells, containing a variable gap hybrid permanent magnet undulator segment, an electromagnetic quadrupole with horizontal and vertical correctors incorporated, an RF cavity beam position monitor (RFBPM), a phase shifter and various vacuum components. There will be a 1-m-long space between undulator segments ("break section") after each undulator segment to house the additional components. Technical details to the cell components are given in this chapter.

7.4.2 Undulator Segments

The basic characteristics of the undulator segments are listed in Table 7.3.

Table 7.3. Nominal undulator parameters.

Parameter	Symbol	Unit	HXR	SXR
Undulator gap	g	mm	7.2 – 20.1	7.2 – 35.5
K range	K		0.83 – 3.76	1.34 – 9.90
Undulator period length	λ_u	mm	32	55
Number of periods per segment			106	61
Individual segment length	L_{seg}	m	3.400	3.400
Number of installed segments			32	18

7.4.3 Quadrupoles

Table 7.4. Nominal LCLS-II undulator focusing parameters.

Parameter	Symbol	Unit	nominal	Range
Integrated QF gradient (HXR)	$IG_{QF,HXR}$	T	2.3	±5.0
Integrated QD gradient (HXR)	$IG_{QD,HXR}$	T	-2.3	±5.0
Integrated QF gradient (SXR)	$IG_{QF,SXR}$	T	4.5	±5.0
Integrated QD gradient (SXR)	$IG_{QD,SXR}$	T	-4.5	±5.0
Magnetic length		m	0.1	
Integrated horizontal and vertical HXR corrector field		Tm	0	$\pm 10^{-3}$
Integrated horizontal and vertical SXR corrector field		Tm	0	$\pm 10^{-3}$
Total number of installed undulator quadrupoles			50	

The basic characteristics of the undulator quadrupoles are listed in Table 7.4. They will be similar to the LCLS-I quadrupoles, i.e., bi-polar electromagnetic devices with laminated core. Bi-polar dipole correction coils for both vertical and horizontal corrections will be integrated in the design. The four matching quadrupoles needed for each undulator line are described in Chapter 6.

7.4.4 Beam Position Monitors

The radio frequency beam position monitors (RFBPMs) will be similar to those used for LCLS-I. The basic characteristics are listed in Table 7.5. There will be one RFBPM installed after each undulator quadrupole following an undulator segment. There will be one extra RFBPM in front of each of the two undulators and two extra RFBPMs in each of the two Linac-To-Undulator (LTU) beamlines [Linac-To-Undulator Hard X-ray (LTUH) and Linac-To-Undulator Soft X-ray (LTUS)], see chapter 6) leading to the two undulators.

Table 7.5. Nominal LCLS-II undulator focusing parameters.

Parameter	Symbol	Unit	nominal	Range
Horizontal and vertical resolution	$\sigma_{x,y}$	nm	250	
Total length		m	~0.1	
Total number of installed undulator quadrupoles			56	

7.4.5 Phase Shifter

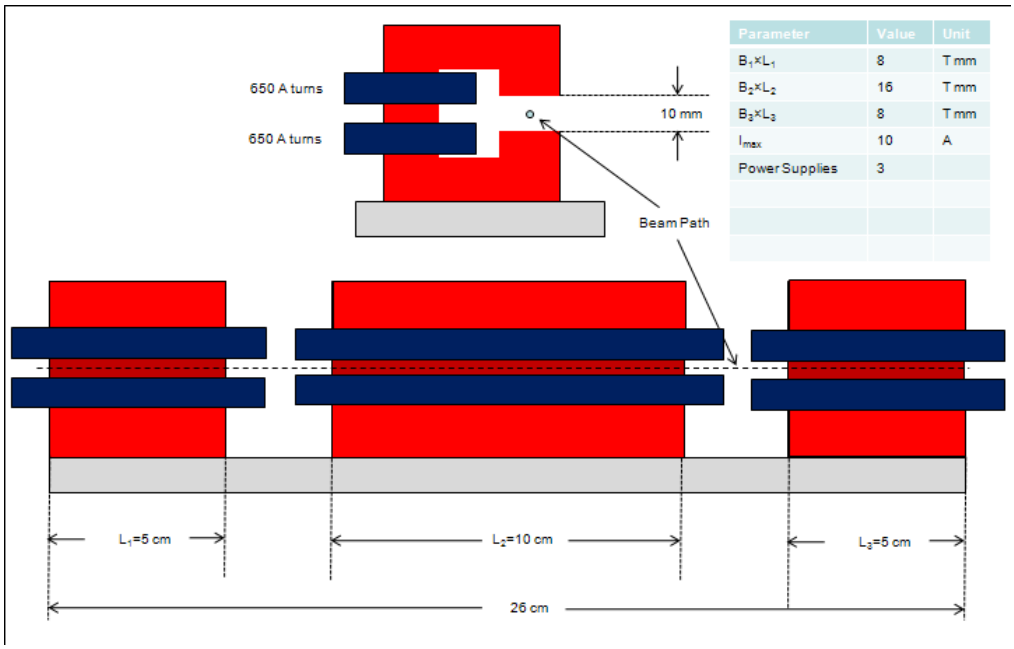

Figure 7.6. Schematic sketch of an electromagnetic phase shifter that would fit in the allotted space in the break sections between undulator segments.

Travelling in the undulator segment, the electrons' oscillatory motion is matched to the phase of the FEL radiation. In the break section this phase relation is changed due to the change in forward velocity of the electrons. The correct phase relation must be restored in the next undulator segment in order to

continue the SASE process. The break-section phase slippage is a function of the undulator strength. Since this strength can change in the LCLS-II undulator segments, phase shifter magnets are needed to keep the total break length slippage equal to a multiple of 360° for all values of K in the undulator. This phase slippage correction can only be done by adding length to the electron path in LCLS-II this will be done with a three-magnet chicane. The chicane needs to be strongest at the highest electron energies and at the longest photon wavelengths (or lowest photon energies). The highest strength is required at a photon energy of 250 eV and an electron energy at 13.5 GeV. The chicane should provide a phase shift exceeding ±180°. One phase shifter is needed in every break section. The same phase shifter design will be used for both HXR and SXR. A schematic sketch is shown in Figure 7.6; a list of the basic phase shifter parameters is given in Table 7.6.

Table 7.6. Nominal LCLS-II phase shifter parameters for ±180° phase shift between 250 eV photons and 13.5 GeV electrons.

Parameter	Symbol	Unit	nominal	Range
Phase shifter type			3-magnet chicane	
Length of chicane magnets 1 and 3		m	0.05	
Length of chicane magnet 2		m	0.10	
Spacing between chicane magnets		m	0.03	
Total length		m	0.26	
Total number of installed phase shifters			48	
Dipole type			C-shape Fe core	
Dipole gap		m	0.01	
Maximum dipole field		T	0.159	± 0.16 T
Maximum integrated dipole field of magnets 1 and 3		μTm	7930	±8030
Maximum integrated dipole field of the magnet 2		μTm	15860	±15900
Maximum excitation current		A-turns	1262	

7.4.6 Beam Loss Monitors

Beam Loss Monitors (BLMs) are being used at LCLS-I in front of every undulator segments to inhibit beam operation when radiation doses exceed thresholds. These monitors collect radiation information based on the Cerenkov effects in a Quartz fork. The specific fork design used is less than optimum [2] and will be improved for LCLS-II.

7.4.7 Vacuum Chamber

The vacuum chamber for the LCLS-II undulator segments will be similar to the one used for LCLS-I. It will have elliptical cross section with 5 mm inner height, 11.5 mm inner width and 0.5 mm wall thickness. It will be made from extruded aluminum with polished inner surface to reduce roughness to the required tolerance (see below).

7.5 Undulator Tolerances

7.5.1 Introduction

The sensitivity of the FEL process to several undulator parameters has been determined with GENESIS simulations as part of a tolerance analysis. For each parameter, the simulation established how it affects FEL performance. The dependence could be fitted with a Gaussian function resulting in the fit parameter (σ_i).

$$e^{-\frac{1}{2}\sum f_i^2} = P/P_0 \quad (1)$$

Table 7.7. LCLS-II undulator tolerance budget.

Parameter	Symbol	Unit	σ_t	f_i	σf_i
Optics Mismatch [1]			0.71	0.452	0.32
Launch Error		μm	30	0.186	3.7
$\Delta K/K$		%	0.06	0.4	0.024
Segment vertical position error		μm	268	0.77	80
Quadrupole gradient		%	8.8	0.029	0.25
Quadrupole transverse position		μm	4.71	0.214	1.0

Fractions (f_i) of the fit parameter (σ_i) were selected such that $e^{-\frac{1}{2}\sum f_i^2} = P/P_0$ = 0.75. P and P_0 are the FEL power levels for parameters at full tolerance level and for the error-free case, respectively. Some of these tolerances, i.e., horizontal segment placement, x_{Und}, undulator parameter, K_{eff}, and quadrupole gradient, k_{QUAD}, have been verified using the LCLS-I beam. In both situations, i.e., in simulation as well as with the actual electron beam, tolerances have been obtained based on random parameter distributions. For instance to determine the sensitivity of the FEL output to a given rms tolerance value, $\Delta\langle K\rangle_{rms}$, of the undulator parameter, ΔK_i (33 numbers), were randomly selected to form a flat-top distribution in the range $K_{eff} \pm \sqrt{3}\langle\Delta K\rangle_{rms}$. The horizontal position of each undulator was then changed to detune by ΔK_i and the FEL intensity was measured. The FEL intensity was determined either at the end of the undulator (i.e., after saturation) or at the saturation point of the undisturbed device.

[1] Defined via Twiss parameters as $\sqrt{(\beta\gamma_0 - 2\alpha\alpha_0 + \gamma\beta_0)/2 - 1}$

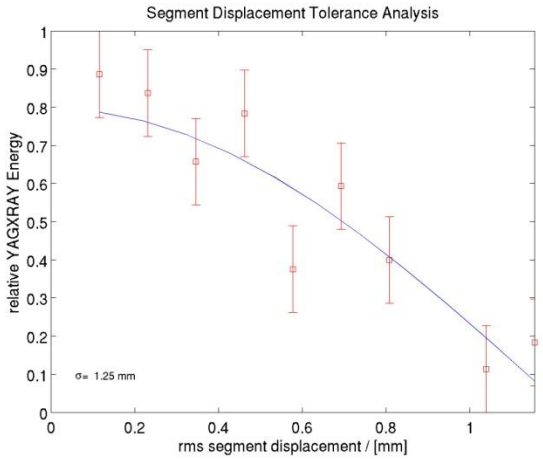

Figure 7.7. Relative FEL intensity after the last undulator segment extracted from the Ce:YAG screen as a function of random horizontal undulator segment positioning errors.

The data were collected in 2009 during LCLS-I machine studies.

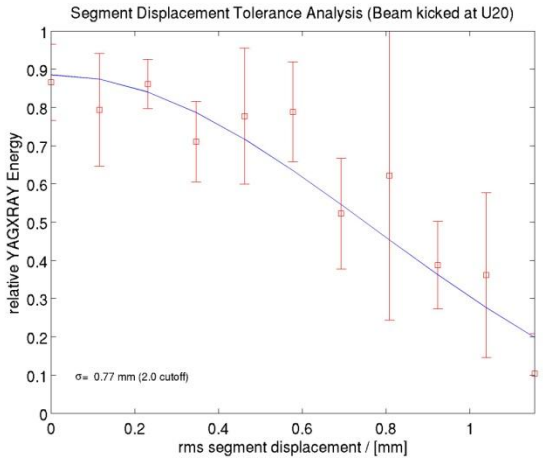

Figure 7.8. Measurements of relative LCLS-I FEL intensity at the 80-m location extracted from the Ce:YAG screen as a function of random horizontal undulator segment positioning errors.

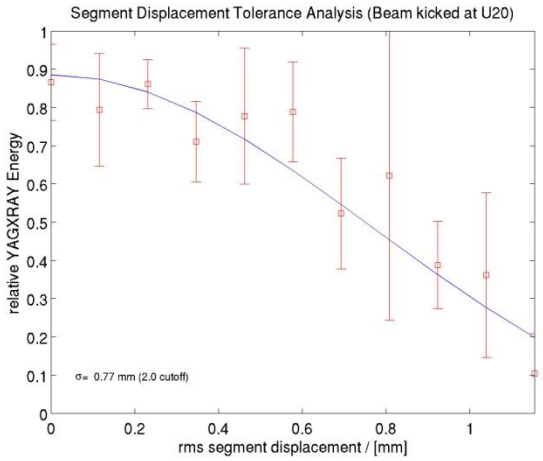

Figure 7.9. Data from LCLS machine studies relative FEL intensity after the last undulator segment extracted from average FEL electron energy loss as a function of random quadrupole gradient errors.

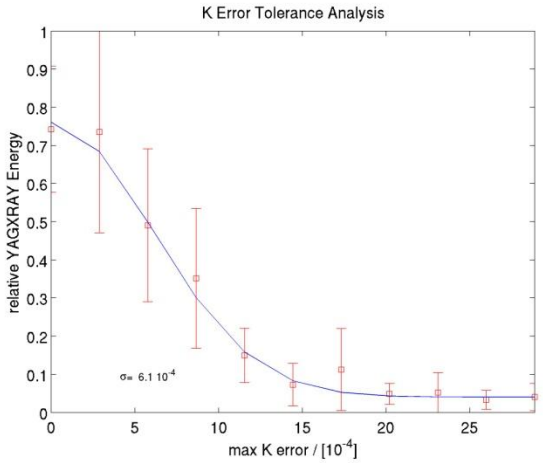

Figure 7.10. Data from LCLS machine studies. Relative FEL intensity after the last undulator segment extracted from the Ce:YAG screen as a function of random K errors.

In the data collected in LCLS-I machine studies, several distributions for the same rms parameter value were generated to study the dependence on the random seed value. Figures 7.7 to 7.10 show some of the results. The error bars are the rms values of the distributions of the results for different random seeds. The vertical axes are in arbitrary units. The solid lines in the figures show the result of Gaussian fits to the data.

7.6 Undulator Magnetic Measurements and Tuning

Most of the magnetic measurement and tuning techniques that were used for LCLS-I can be applied to LCLS-II. Measurements and corrections of variable-gap segments, however, bring new challenges. These include the Earth's magnetic field, fiducializing large undulators, and Magnetic Measurement Facility (MMF) limitations. A summary of the current status and potential challenges follows.

7.6.1 Undulator Tuning

The undulator tuning for LCLS-II will be similar to LCLS-I, but the variable strength of the undulators will require a much more extensive set of measurements. There will also be small differences in the shimming techniques used. The lack of a magnetic shield on the undulators will require measurement and correction of the background magnetic fields.

The principles and methods of undulator tuning have been documented in a technical note [3]. The note shows how most quantities of interest are calculated and which adjustments to the undulator magnetic field are required to change these quantities. The principles outlined are the same for LCLS-II as they are for LCLS-I.

The implementation of the shims for LCLS-II will be different than for LCLS-I. In LCLS-I, the gap was fixed and the poles were fixed. All correction fields were made by adding permeable material which altered the undulator field. Having movable poles in LCLS-II will allow us to do field corrections by changing pole heights and angles. The general procedure for doing the corrections will remain the same. The effect of pole motions will be measured and parameterized. These parameterizations will be used in a computer program or by a tuning expert to determine the necessary pole motions to correct the trajectories, phase, etc. The computer algorithm to determine the shim strengths is given in [4].

For adjustable gap undulators, the shimming to correct trajectories, phase, field integrals, etc. is all done at minimum gap. In this way, the undulator field errors are corrected when the effect of the field errors

is the largest. As the gap is increased, the effect of both the field errors and the correction fields is reduced. If the field errors and corrections don't track each other as the gap is opened, then additional corrections must be made which change with the gap setting. This will be done with powered correction coils. Coils will also be required to compensate external fields as the gap is changed. Extra shims can be added to do corrections at large gaps, but their effect must be carefully checked at minimum gap.

7.6.2 Magnetic Measurement Systems

A number of different systems are used to measure undulators in the Magnetic Measurement Facility (MMF) [5] [6]. A brief list follows. Hall probes carried by a precision bench are used to determine trajectories, phase errors, K value, etc. [7]. The average trajectories are checked using one period long coils. This check ensures that errors like the planar Hall effect are small. Hall probes are unsuitable for accurate determination of the overall field integrals. A long coil system gives the first and second field integrals [8] [9]. The undulators are aligned relative to the bench using a capacitive sensor system and cam mover system[10]. A temperature measurement system accurately gives the undulator temperature [11] [12]. Fiducialization is done using a combination of Hall probe measurements in special high gradient magnets attached to the undulator, and Coordinate Measuring Machine (CMM) measurements to locate relevant tooling balls [13] [14]. The CMM is also used to do extensive mechanical measurements on the undulator and also on the girder which holds the undulator [15].

The MMF has some capability to repair damaged undulators and build undulator prototypes. A permanent magnet block magnetizer is used to repair radiation damage, and also to demagnetize undulator end blocks. Measurement systems must check the blocks before/after magnetization. A Helmholtz coil system is used to measure the magnetic moment of the blocks. A hall probe mapping system is used to localize radiation damage in magnet blocks.

The MMF also has a system to accurately fiducialize quadrupoles, as is required for the quadrupoles between undulator segments. The fiducialization is done by a vibrating wire system built onto a coordinate measuring machine [16][17][18][19].

The MMF has several calibration systems. A large electromagnet is used to calibrate Hall probes. Both conventional and flowing water Nuclear Magnetic Resonances (NMRs) are used. A chiller keeps the probe at room temperature in the magnet. The temperature of the undulators is measured with thermistors. The thermistors are calibrated in a water bath using a reference thermometer [20]. The reference thermometer can be inserted in any thermistor mount to check the measurement in place. The magnets used to fiducialize the undulators need to be calibrated to determine a point with given magnetic field relative to tooling balls [21]. A special fixture allowing magnet flips is used for this.

The MMF employs a number of secondary measurement systems to constantly check for errors. The undulator benches have reference magnets in which an NMR can be inserted to constantly monitor Hall probe accuracy. Survey crews use alignment scopes to check for significant fiducialization errors, which could occur if a fiducialization magnet was bumped on the way to the CMM, for instance [22]. Handheld reference thermometers verify temperature. Most importantly, reference magnets (undulator or quadrupole) are used to continuously monitor the whole measurement process.

The reference undulator was measured many times during the tuning of the LCLS-I undulators. These data sets give estimates of the random errors in the tuned undulators [23]. The measured trajectories in the reference undulator are reproducible to within and envelope of ±1.5 μm. Changes in the phase errors are less than ±2 deg between data sets. The phase advance in the cell varies by less than ±2 deg between data sets. The rms variation between data sets of the first integral of B_x is 9.98 μTm, and the rms variation of the second integral of B_x is 17.4 μTm². The rms variation of the first integral of B_y is 6.65 μTm, and the rms variation of the second integral of B_y is 12.3 μTm². The rms variation of the x-

position of the fiducialized beam axis in the reference undulator is 35 µm during the production run. This corresponds to an rms uncertainty in the K value of $\Delta K/K=2.7\times10^{-5}$. The rms variation of the y-position of the fiducialized beam axis for repeated measurements of the reference undulator is 4 µm during the production run.

7.6.3 Magnetic Measurement Facility

The Magnetic Measurement Facility (MMF), a laboratory whose temperature is controlled to 0.1 ºC, presently has all equipment necessary to measure and tune LCLS-I undulators, including two undulator measurement benches. A high precision 7-meter bench from Kugler Corp. is used to do all final measurements. Since LCLS-I radiation damage checks and other LCLS-I measurements must be performed in an ongoing manner, this bench must not be altered for LCLS-II measurements. The second bench is 5 meters long and is less precise. It was manufactured by Dover Corp. The Dover bench was loaned to SLAC by ANL for rough tuning of LCLS-I undulators, and it performed adequately for this purpose. This bench has never been used at SLAC for final tuning of an undulator. The Dover bench must be replaced for LCLS-II measurements. It could still be used for rough tuning, however.

A limitation of the MMF is the material handling infrastructure. The crane in the tuning laboratory can only lift 2 tons. If LCLS-II undulators weigh less than this, both bench locations could conceivably be used for LCLS-II fine tuning, providing the LCLS-I setup is not changed. If LCLS-II undulators weigh more than 2 tons, they must be wheeled into place at the present Dover bench location. At present, they can only be brought to the door side of the bench, which determines their orientation in the Earth's magnetic field. This may potentially be different than the orientation in the tunnel, causing significant field errors. This must not happen. Either a major modification to the MMF to allow access to the other side of the measurement bench will be required, or a new location for the measurements must be found.

7.6.4 Compensating for Background Fields

The LCLS-I undulators were measured in the same orientation as they have in the tunnel [24][25][26]. This was done to minimize background field errors. In addition, the LCLS-I undulators had a magnetic shield to reduce the effect of the difference of the background field in the tunnel compared to the MMF.

LCLS-II undulators will likely not have magnetic shields, especially if they have variable gap. This makes background fields a much larger problem. The undulators will continue to be measured in the same orientation as they will have in the tunnel. This will minimize the effect of the external horizontal field, especially as the gap is opened.

Without a magnetic shield on the undulators, further effort to deal with external fields is required. Trim coils will be placed on each undulator. A large Helmholtz coil will be built to apply external fields to one undulator in order to characterize the resulting field in the gap, and the necessary current in the trim windings to correct it. A map of the magnetic field in the tunnel will be made. The difference between the tunnel field and the field in the MMF, along with the characterization from the test undulator in the large Helmholtz coil, will determine how to set the current in the trim windings for each undulator position in the tunnel. A portable system to measure field integrals will be used in the tunnel to check the final field integrals. A portable vibrating wire system for making these measurements in the tunnel is under development [27].Moving coil measurements as done in the MMF could alternately be performed.

7.6.5 Fiducializing Large Undulators

The LCLS-I undulators were fiducialized in a three step process [28][29]. First, the Hall probe was positioned to move along the desired beam axis. The distance the Hall probe was required to move from the beam axis to a zero field point in fiducialization magnets at each end of the undulator was recorded. Second, the distance from the zero field point to tooling balls on the fiducialization magnet was determined using a special calibration fixture. Third, the distance from the tooling balls on the fiducialization magnets to tooling balls on the undulator was determined with a CMM.

If the LCLS-II undulators are large, the final step of measuring tooling ball positions will not be possible with a CMM. Other measuring instruments are only accurate to approximately 25 μm. A detailed look at the error budget for this measurement will be made, and an alternative strategy will be developed.

The throughput of the MMF for LCLS-I undulators was approximately one undulator every two weeks. This included time to come to thermal equilibrium, mechanical measurements on the CMM, mechanical straightening of the gap centerline with checks on the CMM, rough tuning on the Dover bench, fine tuning on the Kugler bench, making a final data set on the Kugler bench, fiducialization on the Kugler bench, fiducialization on the CMM, and final mechanical measurements on the CMM, All this work was done in parallel at the CMM, Dover bench, Kugler bench, and a separate stand for mechanical work such as applying shims and gap straightening.

LCLS-II undulators will require all the steps mentioned above. Depending on their size, CMM measurements may need to be replaced with another device, but the measurements are still required. In addition, LCLS-II undulators will have an adjustable feature, i.e. an adjustable gap or adjustable row phase. This will require a larger tuning effort and a more extensive final data set. Field integral corrections as a function of gap must be determined. We estimate that the throughput of the MMF for adjustable gap undulators will be one undulator every three weeks.

It will likely be required to increase the MMF throughput. A determination will be made of what facilities will be necessary to meet all measurement requirements so that to best ensures the throughput needed by LCLS-II.

7.7 Wakefield Effects in the Undulator

7.7.1 Overview

When the electron beam moves through the undulator it will excite longitudinal and transverse wakefields due to the resistance, roughness and the discontinuities in the beam tube wall. Let us assume that the wall geometry is cylindrically symmetric. Then the longitudinal (monopole) wakefield will generate an energy loss and an increase in energy spread independent of the beam orbit, and the transverse (dipole) wakefield will generate an emittance growth that does depend on the orbit. It is, however, important to recognize that the forces due to the wakefields are correlated with longitudinal position. Assuming the bunch is composed of many slices at different longitudinal positions, the wakefields affect only the centroid values of the slices — i.e., the average energy and the average position of the slices in, respectively, the longitudinal and the transverse case. The distributions of the slices about their centroid are not affected.

The critical issues concerning the electron beam with respect to wakefield effects in the undulator are:

- The absolute value of the maximum relative energy deviation of a bunch “slice” (slippage length: ~0.5 μm) with respect to the mean of the whole bunch generated over the length of the

undulator at 13.5 GeV should be less than ~0.1%. This tolerance is derived from GINGER simulations.

- The dilution of the "projected" emittance (emittance projected over the entire bunch) should not exceed ~10%.
- The mean energy loss over the undulator, including radiation losses, will determine the necessary taper of the magnetic fields of the undulator dipoles.

Because very similar vacuum chamber geometries, the undulator wakefields in the LCLS-II undulator will be very similar to those in the LCLS-I undulator, which are well understood [30]. Detailed wakefield budgets have been established for LCLS-I and used to derive tolerances for vacuum chamber roughness, geometry and alignment. An equivalent wakefield budget analysis will be carried out for the LCLS-II undulator system, as well.

7.8 Radiation Damage Estimates

7.8.1 Introduction

The undulators used for LCLS-I and LCLS-II are based on rare earth permanent magnet material (NdFeB), which can be demagnetized by ionizing radiation. Radiation damage studies have been carried out at LCLS-I and at other facilities around the world. The most recent publication shows that high-energy electrons lost from third- or fourth-generation light source beams can lead to the generation of star events, which are strongly correlated with the demagnetization of undulator magnets [31].

To protect the LCLS-I undulators from excessive radiation, one Beam Loss Monitor (BLM), i.e., a Cerenkov-Radiator and Photomultiplier Tube is installed right in front of each of the 33 undulator segments. The photomultiplier signals are integrated over 1 s and compared with a threshold level by the Machine Protection System (MPS), which trips the electron beam in case of a violation. The threshold level is set such that the radiation from the beam hitting a 40 µm diameter carbon fiber Beam Finder Wire (BFW) is just acceptable. With MARS simulations, it was determined that this threshold should correspond to a maximum neutron fluence in the magnet blocks of 8.4×104 neutrons/cm2/nC. The BLM signal for such an event is well above background. A full BFW-Scan (66 wires, about 7 interception points per scan and wire, about 100 hits per interception point) is performed a few times per year, at the most. The MPS does not allow operation with more than one BFW inserted at a time. The BLM signal is very close to the background when no BFW is inserted. Initially, mostly PEP-II-type BLMs were used, which were located more than about 10 cm away from the beam pipe. They did not show a signal above threshold during normal beam operation. At the time this Conceptual Design Report (CDR) was written (early 2011), the ANL type BLMs that were designed and build as part of the LCLS-I project are installed in front of each undulator segment. Their radiator part has a fork design that encloses the beam pipe on three sides. They are therefore more sensitive than the PEP-II style monitors and generate a signal that is (barely) above threshold during normal beam operation.

These BLMs constitute one of several radiation protection layers.

Those layers are

1. A system of beam collimators in the LTU, that limit the 6 dimensional phase space such that, according to simulations, halo electrons will not be able to reach the undulator vacuum chamber if the steerers, downstream of the last collimator, are set correctly.
2. Each of the 33 undulator RFBPMs is monitored by the MPS to keep the beam inside a 1 mm radius envelope relative to the beam pipe center. The girder design together with BBA ensures

that a zero reading of the RFBPMs implies that the beam is close to the center of the vacuum chamber to better than 100 µm. The 1 mm radius is sufficient to keep the electron beam that has a diameter of less than 100 µm away from the ±2.5 mm vertical vacuum chamber extension.

3. The BLMs are the third layer of defense to trip the beam if actual radiation levels are detected. Once the trip level has been exceeded, not more than one electron bunch will enter the undulator hall.

4. Two toroids in comparator-configuration mounted before the first and after the last segment to detect larger charge losses along the undulators.

The main protection comes from layer 1. Layer 2 trips the beam occasionally. Layer 3 does not trip the beam in normal operation. Layer 4 never tripped the beam after it was properly calibrated.

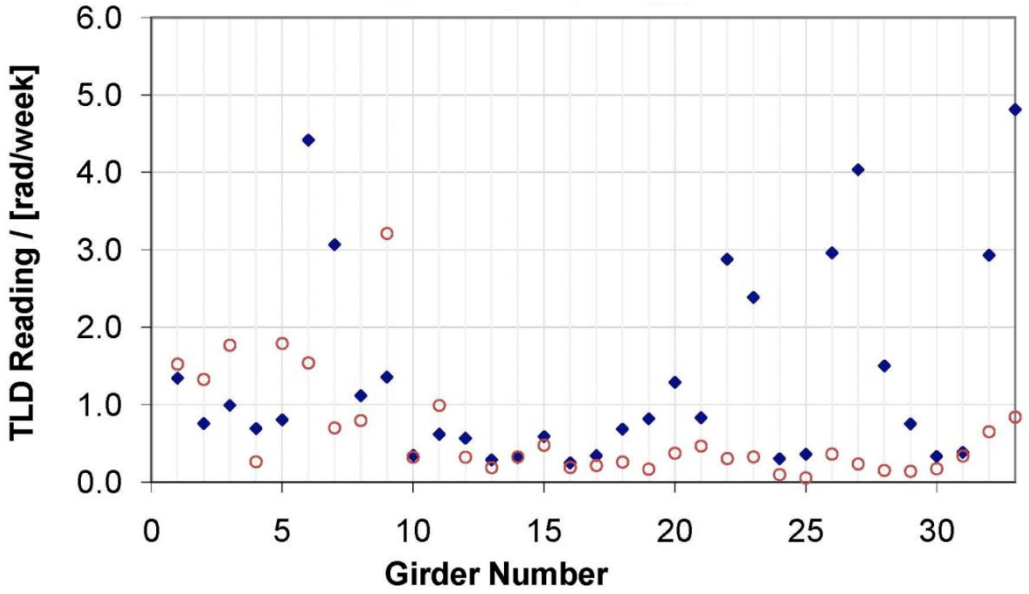

Figure 7.11. Typical high energy (> ~.5 MeV) dose rates (rad/week) measured at LCLS-I over the span of about 6 months, 3/16/2010 – 5/26/2010 (circles) and 5/26/2010 – 9/24/2010 (diamonds) , show the very low levels achieved.

At SLAC, the degree of demagnetization of spare LCLS-I undulator magnet blocks was measured using high doses of radiation generated by a 13.6 GeV electron beam hitting a copper cylinder. The measured demagnetization levels were correlated to photon doses and neutron fluencies as calculated from a FLUKA model. The experiment (T-493) was carried out in 2007 at End Station A (ESA). Its publication is still pending. Measured magnet damage spanned a range between 0.34 % and 9.7% and showed a linear correlation with both the estimated photon dose and the neutron fluence in the magnet. The extrapolated neutron fluence required for a demagnetization degree of 0.01% is 6.4×1010 n/cm2. This is more than 6 orders of magnitude above the BLM threshold. In addition, one thermo-luminescent dosimeter (TLD) is installed right in front of each undulator segment. They are mounted in a 1.6-mm-thick lead housing and are read in 2 - 4 months intervals. The lead shielding sets a threshold of a few keV and attenuates the non-damaging synchrotron radiation component, which can produce a 400 times stronger signal at the last undulator in unshielded TLDs, thus hiding the reading of the damaging component. The readout results are pretty steady (see Figure 7.11) and show about 100 mGy/week at 60 Hz beam operation with at 250 pC bunch charge.

At these levels, no measurable radiation damage is expected during the operational lifetime of the project. Nevertheless an undulator segment is removed from the undulator tunnel roughly every two months and measured in the MMF.

After more than a year of beam operation, no significant changes of the K parameter or the field integrals are detected. The relative changes measured for the K parameters are in the range $\pm 2\times10^{-5}$.

The same level of radiation protection used for LCLS-I will be implemented for the LCLS-II undulators.

7.9 Temperature Stabilization

7.9.1 Introduction

The temperature stability in the undulator hall is critical for stable FEL operation. The LCLS-I tunnel temperature control system provides the required stability (see Figure 7.12) and will be the base for the LCLS-II system.

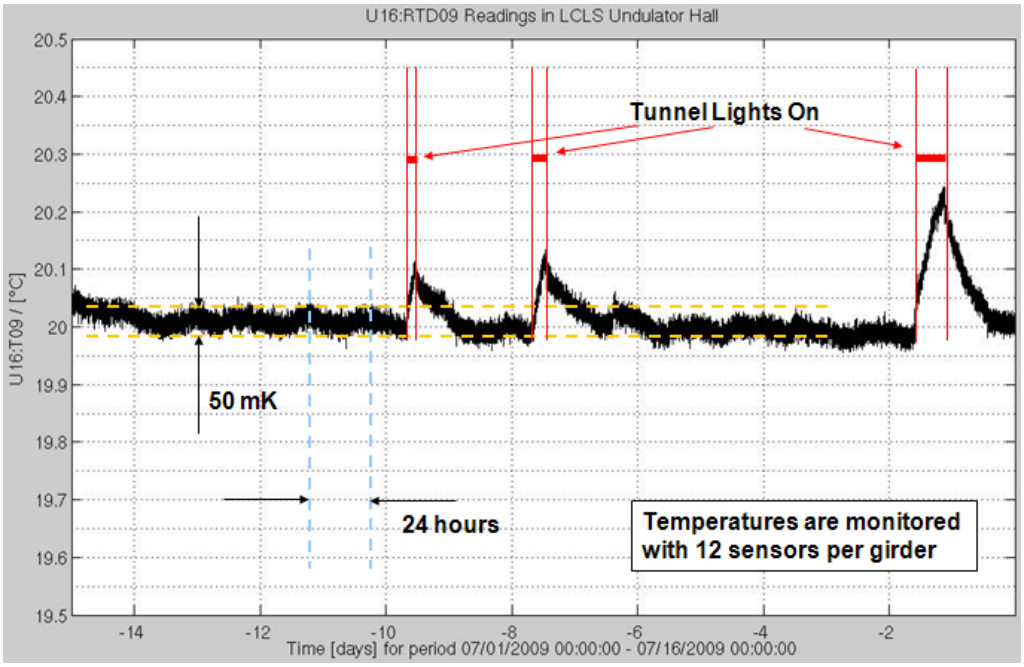

Figure 7.12. Temperature profile for one of the LCLS-I undulators (U16).

Shown is the temperature of the Ti-strongback. During regular operation, the diurnal temperature variation is within a range of 0.05° C. During tunnel access, the tunnel lights are turned on. The extra energy that is released by the fluorescent lights results in the observed increase in the temperature of the undulator strongback.

7.9.2 Undulator Hall Power Budget

The heat balance of the LCLS-I Undulator Hall has been well established and serves as a basis for the LCLS-II Heating, Ventilation and Air Conditioning (HVAC) design. Contributions to the power balance from effects such as the cooling of the tunnel walls and floor, the presence of insulated hot water and chilled water lines, and lighting, should be the nearly the same for LCLS-I and LCLS-II. However the heat load from the LCLS-II undulator systems is of order five times higher for two reasons: there are two undulator lines instead of one, and to control the undulator gaps the undulators use large motors that are not present in LCLS-I.

7.9.3 Temperature Control

The LCLS-I air conditioning system releases a constant flow of temperature controlled air into the undulator tunnel right at the upstream thermal barrier wall, keeping the temperature at this point constant. As the air moves down the beam line, it picks up the extra energy released by the undulator system, which causes a slow increase in air temperature along the tunnel. For LCLS-I this increase is less than 1.0º C by the time the air is removed from the tunnel at the downstream thermal barrier.

The LCLS-I Undulator systems generate slightly more than the 50 W/m heat budget for which they were designed. For the same temperature tolerance, higher heat loads cannot be tolerated without proportionally increasing the volumetric air flow. To implement this system for LCLS-II would be expensive, require large ducting and register areas in the tunnel, and the high air velocity could induce vibration in the sensitive undulator components. There are two approaches to mitigate this problem: re-cooling the air at one or more stations distributed along the tunnel, and using a precision tempered-water cooling system to absorb the heat from the equipment before it is transferred to the air. LCLS-II will use the latter, precision tempered-water cooling system to remove as much heat as possible from the components before it is transferred to the air. Provision for fan-coil units to be placed at regular intervals along the tunnel is made by providing space for the units and valves to the hot water and chilled water lines, just as was done for LCLS-I. This design feature allows the possibility of accepting more power load in future upgrades without rebuilding the entire cooling system. It could also provide a relatively easy fix if the precision tempered-water system is unable to extract sufficient heat from the components

7.9.4 Temperature Monitoring

The temperature of the most important undulator system component will be monitored continuously during operation. There will be at least three temperature sensors attached to the magnet structure of each undulator segment. Also, the bodies of the electromagnetic quadrupole and phase shifter magnets as well as the undulator and quadrupole support structures will be equipped with temperature sensors. The temperature measurements of the undulator magnet structure will be used in the calculation of the effective undulator strength for each device.

7.10 Undulator Alignment Strategies

The LCLS-I alignment strategy [32] has been very successful in producing a straight electron beam trajectory, sufficient for high FEL gain, using a BBA procedure based on variable electron energies. LCLS-II will use a quite similar strategy even though there are system differences, such as variable gap and large undulator size, that require special considerations. The alignment concept for both, the SXR and the HXR undulator lines will be similar. The core feature of the alignment concept is the same electron beam based alignment as is done for LCLS-I, which measures the trajectory for 3 or 4 different electron energies. For LCLS-II, these electron energies will span the entire operating range between 4.2 GeV and 13.5 GeV. None of the undulator fields (i.e., quadrupole gradients, corrector strength, undulator gaps) will be varied during the measurements. The measurements can be done in parallel for the SXR and HXR lines, i.e., for a given setting of the accelerator energy, both trajectories can be measured as the electron beam is switched between the two lines. As a result of these 3 - 4 sets of trajectory measurements, the BPM offset errors and quadrupole position errors are calculated and independently corrected for each line. The correction of the BPM offsets will be done by changing the values of process variables in the control system.

The quadrupole position errors will be corrected by remotely adjusting their position. In order to make these adjustments possible, each quadrupole, together with all the other break section components, i.e., BPM, phase shifter etc. will be mounted on a common support structure which can be remotely positioned with cam movers, similar to how the LCLS-I girder positions are controlled. This procedure will align the quadrupoles such that the electron beam is straight and that it passes the quadrupoles very close to their magnetic axes.

A small offset on the order of 20 μm (rms) will remain, just enough so that the small fields related to those offsets compensate any additional remnant field integrals that exist outside of the quadrupoles, i.e., coming from the remnant field integrals of the undulators and phase shifters and from the earth magnetic field. The tolerance for field integrals between quadrupoles are 40 μTm^2 for the first and 50 μTm^2 for the second field integrals. The field integrals from the earth magnetic field will exceed these tolerances and need to be corrected with long dipole coils (vertical field) along the undulator.

During the BBA procedure, the undulator segments will be at a fixed gap of 10 mm as measured with linear encoders. It is expected that undulator field integrals will significantly vary as the gap is changed. This will change electron beam steering, which will be corrected with the dipole correctors that are incorporated into the quadrupole magnets.

The required corrections will first be measured in the magnet measurement lab and later fine tuned based on BPM readings using the beam position monitors. This is similar to what is currently done at LCLS-I, where field integrals change and quadrupoles move (due to girder twist) as undulator segments are moved in and out.

During initial installation of the components, the quadrupole magnets will be aligned to a straight line within a local error of 100 μm (rms) and a walk-off amplitude of less than 250 μm. Both, the quadrupoles and the undulator jaws will be equipped with tooling balls that will have been fiducialized to the magnetic axis of the devices. For the undulator this fiducialization will be done at a 10 mm gap.

The undulators, which will be installed independently of the quadrupole magnets, will than be aligned in the tunnel such that their magnetic axes are centered between the magnetic axes of the neigbouring quadrupoles. This procedure has been successfully applied several times for the LCLS-I undulator segments since operations began. Using laser trackers, a precision of about 50 μm (rms) can be achieved. This alignment technique will be repeated after the first beam based alignment procedure has been applied and used to set the quadrupoles to the correct positions to allow FEL operation.

The vacuum chamber, which needs to be centered around the electron beam to a tolerance of 200 μm in the verical and 300 μm in the horizontal will mounted to the floor and aligned relative to the quadrupole and undulator segment centers during the initial alignment procedure and corrected as additional alignment corrections are applied to the components. It is expected that the initial BBA procedure will move the quadrupole positions by less that 500 μm. There will be sufficient clearance between the qudadrupoles and the vacuum chamber to allow for this movement. Once, lasing has been achieved, BBA moves the quarupoles by less than ± 60 μm based on LCLS-I experience.
In LCLS-I, there are indication that the BBA procedure does not put the electron beam onto a straight line over the entire undulator line but can leave bows in the trajectory with sagitta amplitudes in the order of 20 μm, which can cause the x-ray beam to wander at the experimental stations after BBA procedures as well as when changing the number of active undulators. This is currently under investigation at LCLS-I. It is expected that the additions of extra constrains in the BBA algorithm will reduce the problem, significantly.

7.11 References

1. J. Pflueger, European XFEL. *Undulator Systems for the European XFEL*, Talk presented at the EFST Workshop on Advanced Undulator Physics and Technology for Light Sources, Shanghai, December 3-4, 2009.
2. J.C. Dooling, W. Berg, B.X. Yang, M.S. Leitner, A.S. Fisher, H.-D. Nuhn*, Modeling the Optical Coupling Efficiency of the Linac Coherent Light Source Beam Loss Monitor Radiator*, Proceedings of BIW10, Santa Fe, New Mexico, US.
3. Z. Wolf, *Introduction To LCLS Undulator* Tuning, LCLS-TN-04-7, June, 2004.
4. Z. Wolf, *Algorithms To Automate LCLS Undulator Tuning*, LCLS-TN-06-8, April, 2006.
5. Z. Wolf, et al., *LCLS Undulator System Tuning and Magnetic Measurements*, Proceedings. Part. Accel. Conf. 2009, Vancouver.
6. Z. Wolf, Y. Levashov, H-D. Nuhn, I. Vasserman., *LCLS Undulator Test Plan*, LCLS-TN-06-17, December, 2006.
7. Z. Wolf, *Requirements For The LCLS Undulator Magnetic Measurement Bench*, LCLS-TN-04-8, August, 2004.
8. Z. Wolf, *Undulator Field Integral Measurements*, LCLS-TN-05-22, August, 2005.
9. Z. Wolf, Y. Levashov, *Undulator Long Coil Measurement System Tests*, LCLS-TN-07-3, April, 2007.
10. G. Bowden, *Roller Cam Positioners*, LCLS-TN-05-28, October, 2005.
11. Z. Wolf, S. Kaplounenko, *Temperature Measurements In The Magnetic Measurement Facility*, LCLS-TN-05-9, April, 2005.
12. Z. Wolf, Y. Levashov, *Undulator K Value Temperature Dependence*, LCLS-TN-09-4, October, 2009.
13. Z. Wolf, et al.., *LCLS Undulator Fiducialization Plan*, LCLS-TN-07-2, April, 2007.
14. Y. Levashov, Z. Wolf, *Tests Of Coordinate Transfer From Magnetic To Mechanical Reference For LCLS Undulator Fiducialization*, LCLS-TN-05-10, April, 2005.
15. Z. Wolf, et al., *Girder Alignment Plan*, LCLS-TN-08-3, March, 2008.
16. Z. Wolf, A *Vibrating Wire System For Quadrupole Fiducialization*, LCLS-TN-05-11, May, 2005.
17. Z. Wolf, *LCLS Undulator Quadrupole Fiducialization Plan*, LCLS-TN-07-7, August, 2007.
18. M. Levashov, Z. Wolf, *Commissioning A Vibrating Wire System For Quadrupole Fiducialization*, LCLS-TN-07-8, September, 2007.
19. S. Anderson, et al., *Magnetic Measurement Results Of The LCLS Undulator Quadrupoles*, LCLS-TN-09-1, January, 2010.
20. Z . Wolf, S. Kaplounenko, *Temperature Measurements In The Magnetic Measurement Facility*, LCLS-TN-05-9, April, 2005.
21. Y. Levashov, Z. Wolf, *Tests Of Coordinate Transfer From Magnetic To Mechanical Reference For LCLS Undulator Fiducialization*, LCLS-TN-05-10, April, 2005.
22. Z. Wolf, *Introduction To LCLS Undulator Tuning*, LCLS-TN-04-7, June, 2004.
23. Z. Wolf and Y. Levashov, *Reference Undulator Measurement Results*, LCLS-TN-09-3, August, 2009.
24. A. Fisher, H-D. Nuhn, J. Welch, *Magnetic Measurements Of The Background Field In The Undulator Hall With Ductwork And Cable Trays*, LCLS-TN-08-4, March, 2008.
25. A. Fisher, H-D. Nuhn, J. Welch, *Magnetic Measurements Of The Background Field In The Undulator Hall*, LCLS-TN-08-2, February, 2008.

26. K. Hacker, Z. Wolf, *Earth's Magnetic Field Measurements For The LCLS Undulators*, LCLS-TN-05-4, February, 2005.

27. A. Temnykh, Y. Levashov, Z. Wolf, *A Study of Undulator Magnets Characterization Using the Vibrating Wire Technique*, Nucl. Instr. And Meth. A 622 (2010) 650.

28. Z. Wolf, et al.., *LCLS Undulator Fiducialization Plan*, LCLS-TN-07-2, April, 2007.

29. Y. Levashov, Z. Wolf, *Tests Of Coordinate Transfer From Magnetic To Mechanical Reference For LCLS Undulator Fiducialization*, LCLS-TN-05-10, April, 2005.

30. Linac Coherent Light Source (LCLS) Conceptual Design Report, SLAC-R-593. Apr 2002. 543 pp.

31. Y. Asano, T. Bizen, and X. Marechal, J. Synchrotron Rad. **16** (2009), 317-324.

32 H.-D. Nuhn , P.J. Emma, G.L. Gassner, C.M. LeCocq, F. Peters and R.E. Ruland, *Electron Beam Alignment Strategy in the LCLS Undulators*, FEL2006 Proceeding, 2006, Berlin, Germany.

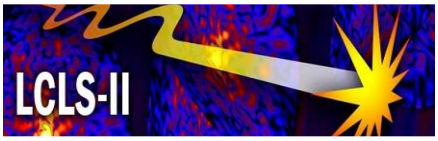

8 X-ray Beam Transport and Diagnostics

Technical Synopsis

The role of the X-Ray Beam Transport, Optics and Diagnostics (XTOD) System is to prepare, characterize, and transport Free Electron Laser (FEL) beams from electron beam dump to experimental stations. Mirrors control the paths of the x-ray beams, while x-ray diagnostics both measure and control beam characteristics. Bremsstrahlung and very hard spontaneous synchrotron radiation are generated by the electron beam and accompany the x-rays beams produced in the undulators. The XTOD system is designed to collimate and absorb this radiation down to levels that can safely be handled by the local shielding in the experimental areas.

There are two principle challenges that are overcome in the design of the XTOD components: delivering extremely high peak power and preserving transverse coherence. Both of these challenges were met by the LCLS-I system, but over a smaller wavelength range than is required for LCLS-II. At the long wavelength end of the operating range the challenge is most acute because of small x-ray attenuation lengths, which increase the sensitivity to high peak power, and large x-ray angular divergence, which leads to large FEL beam sizes. To avoid damage from high peak power the distance of the XTOD components from the effective source point is made just long enough to reduce the peak fluence to tolerable levels, but not so long as to create excessively large beam size from the diverging beams. To accommodate large beam sizes, mirrors lengths are set to the maximum length of what can be achieved given the requirements of extremely low figure errors. LCLS-II will build on the knowledge and proven designs of the LCLS. The expanded spectral range and particularly the increase in pulse energy at long wavelengths will require development of larger optics with new coatings and changes in the diagnostic systems.

8.1 Introduction

In LCLS-II the x-ray beams are produced from two parallel undulators by an electron beam that can be directed into hard x-ray or the soft x-ray undulator on a pulse-by-pulse basis. The resulting x-ray beams are directed to the four possible experimental stations using combinations of insertable and fixed mirrors. The raw x-ray beams generated in the undulators co-propagate with high energy bremsstrahlung and the higher harmonics of spontaneous synchrotron radiation. The mirror system, collimators, and adjustable apertures are used to filter out these undesirable radiations before they reach the experiments. X-ray diagnostics measure the pulse energy, beam sizes and spectrum. Gas and solid attenuators are used to provide lower pulse energies when needed by the experiments.

8.1.1 Scope

The X-Ray Beam Transport and Diagnostics System (XTOD) encompasses the beamlines, mirrors, diagnostics, supports, and other x-ray instruments needed to transport x-ray beams from the point where they are separated from the electron beam to where the beams enter the experimental hall. Each beamline starts with the vacuum chamber where the electron beam and x-ray beams are separated into different vacuum channels. In both the Hard X-ray (HXR) and Soft X-Ray (SXR) transport lines the primary beam may be directed into one or the other of the two branching beamlines by a combination of fixed and insertable mirrors. The scope of the XTOD portion of the beamlines ends at vacuum valves downstream of the main shield wall just after the beams enter the new experimental hall.

Downstream of the aforementioned vacuum valves is the scope of the Experimental Systems described in Chapter 9. The AMO and SXR instruments will be moved to the two soft x-ray branch lines in the experimental hall. Two hard x-ray experimental stations are envisioned as part of the long range plan, but are not part of the LCLS-II project.

8.1.2 Objectives

The X-Ray Beam Transport, Optics and Diagnostics System (XTOD) serve several functions. The diagnostics characterize the FEL x-ray beams in terms of their spatial distribution and their intensity. There is a capability to attenuate the x-rays as well as for aperturing. There will be capability to measure the spontaneous spectrum from individual undulators. Mirrors deflect the x-rays from the bremsstrahlung radiation and provide horizontal separation for the different x-ray instruments in the experimental hall. Finally, radiation shielding and collimation are provided.

The x-ray optics and diagnostics are largely based on the experience from LCLS-I, but there are three areas development is needed due the extensions in capabilities of the LCLS in general and for the LCLS-II in particular. First is damage from high FEL beam fluence at long wavelengths. Second is obtaining and holding the long, high figure quality optics required for operating at the lowest energies. The third is pulse energy monitoring. Development is required to extend gas energy monitors to the sort energy end of the LCLS-II spectral range. Improvements are also need in absolute energy calibration of these systems. How these issues will be dealt with is discussed in their respective sections below. The issue of timing and pulse length measurement is discussed with experimental systems in chapter 9.

8.2 General Considerations

The overall design of the XTOD is guided by the combination of a wide operating range of wavelengths and the limitations of materials with respect to high x-ray fluence per pulse. The operating range is derived from the needs of the experimental program and is summarized in Table 8.1. High fluence

damage issues are especially important in determining the distance from the end of the undulators of stoppers, collimators, and mirrors. These issues are discussed in general in Section 8.2.2 as well as in detail in each of the sections describing these components.

8.2.1 X-Ray Beam Operating Parameters

Key parameters describing the operating range for the output of XTOD system are given in Table 8.1. The range of values given for the parameters should be obtainable for users during normal operation. Except for the repetition rate, the values of parameters are not independent of each other. For example, the maximum available pulse energy listed will not be obtainable at the shortest pulse length. To a smaller degree there is coupling between the SXR and HXR beams. Since both x-ray beams are derived from one electron beam, the pulse length and pulse energy will be coupled. Variable gap undulators allow for a wide range independent photon energy operations on the two primary beamlines. See section 5.2.2 for discussion of simultaneous operating range of the two undulator systems.

Table 8.1. Overall XTOD operating parameters.

	SXR Beamline	HXR Beamline	Symbol	Unit
Photon energy	0.25 – 2.0	2.0-13.0	u_r	keV
Repetition rate	One-shot to 120	One-shot to 120		Hz
Pulse energy (max)	4.5-12	4.5-8	E_{FEL}	mJ
Attenuation factor available	1-10^{-6}	1-10^{-6}		
Pulse duration (rms)	1-200	1-200		fs
Divergence, rms (max)	7.3-35	1.7-15	σ_δ	μrad
Maximum operating power per pulse	12-4	8-4		mJ

The range of available maximum pulse energies refers to pulse energies that can be obtained at different photon energies assuming a standard pulse length. Gas and solid attenuators are capable of attenuating by a factor between 1 and 10-6 for all photon beam energies. Beam divergence varies inversely with photon energy with a maximum divergence angle for minimum photon energy, but is not generally tunable. The divergence angles quoted in the table include a factor of two over the calculated beam divergences at saturation. At LCLS-I measured beam divergences during operation range from one to two times the calculated values with two times being most common.

8.2.2 Damage Issues

While the average power of LCLS-II is modest, the peak power of these short, intense, x-ray pulses can be enormous and at long wavelengths could result in fluence levels that could exceed the damage threshold of all materials not at grazing incidence. This is particularly important issue in the design and location of the stoppers and mirrors of the SXR beamlines.

There are three simple techniques to reduce the effect of the high peak power beam on the stoppers and mirrors: providing adequate distance from the end of the undulator, choosing low-Z refractory materials to absorb the beam, and reducing the angle of incidence on optical components. In the range of interest for stopper or mirror placement, the distance to the FEL source is much larger than the Rayleigh length, and the peak fluence decreases as the inverse square of the distance to the end of the

undulator. On the other hand, the beam size increases with distance and can become too large for the mirrors system to accommodate. In the LCLS-II design the first SXR mirror is placed 100 m from the end of the undulator. At this distance the beam stay-clear for 250 to 400 eV photons is slightly larger than the projected mirror size based on 1000 mm long mirrors at a grazing angle that reflects 2000eV radiation. Some diffraction effects will by noticeable for such photons, though there will be relatively little energy loss. Beams with photon energies from 400 to 2000 eV will not have significant diffraction from the mirror aperturing.

At LCLS-I bulk boron carbide (B_4C), with its low absorption coefficient and high melting temperature, has proven to be a suitable material for absorbing high peak fluence beams, and each stopper and collimator features this material at its leading surface. For mirror surfaces both B_4C and SiC have been used as the optical coating. This experience has given us sufficient information about the damage fluence to design LCLS-II components to a safe working dose.

The single shot damage threshold of B_4C was determined at LCLS-I in a focused beam to be 0.8eV/atom, which agrees well with the melt threshold for this material [1]. Although this threshold is quite high and probably only attainable in the unfocussed beam at the lowest photon energies and close to the source, there is concern about possible multi-shot damage mechanisms proposed to occur at significantly lower thresholds. So far it has been demonstrated that B_4C survives multi-shot exposure at a dose of at least 0.1eV/atom and may be used to this dose as a passive absorber in safety systems.

The maximum safe working dose pulse can be converted in to a Pulse Energy Limit for mirrors and stoppers, assuming divergence calculated from FEL theory. This was done for the SXR line, and the results are shown in Figure 8.1 as a function of photon energy. It assumes the mirror grazing angle is 14.4 mrad, and that both the stopper and mirror coating are made of B_4C. The distance from the end of the undulator to the mirror is 100 m, and to the stopper is 121 m. See Table 8.2 for a full list of parameters used in the calculation. Also plotted is the operational maximum pulse energy, a pulse energy obtainable with favorable tuning, calculated from FEL theory. The maximum pulse energy calculation technique was validated within 20% against pulse energies measured for 2 keV photons at LCLS-I.

Figure 8.1 shows that the pulse energy limit for the SXR mirror is larger than the maximum operational pulse energy for all photon energies. Calculations indicate the stopper (which absorbs the beam at normal incidence) could experience an excessive dose for photon energies less than about 500 eV at the maximum expected operating parameters. Moving the stopper further from the undulator is not practical as the beam could not be refocused by practical length fixed angle of incidence mirrors

To resolve the issue of potentially damaging doses at Personnel Protection System (PPS) absorbers, either material that can absorb the high fluences safely must be proven, or separate active Machine Protection System (MPS) absorbers will be used to shield them. Further materials damage tests are planned for the near future. The goal is to see if higher multi-shot threshold can be validate and to check that the thresholds are valid down to 250eV. As B_4C or other materials have not yet been proven as safe passive absorbers at highest projected dose, LCLS-II assumes active systems will be required to ensure beam containment at the lowest energies. MPS shutters are currently used on LCLS in front of the first PPS stopper so that the stopper is never exposed to the FEL pulse energy unless the MPS failed. Engineering active MPS systems should be a relatively straight forward extension from existing active systems.

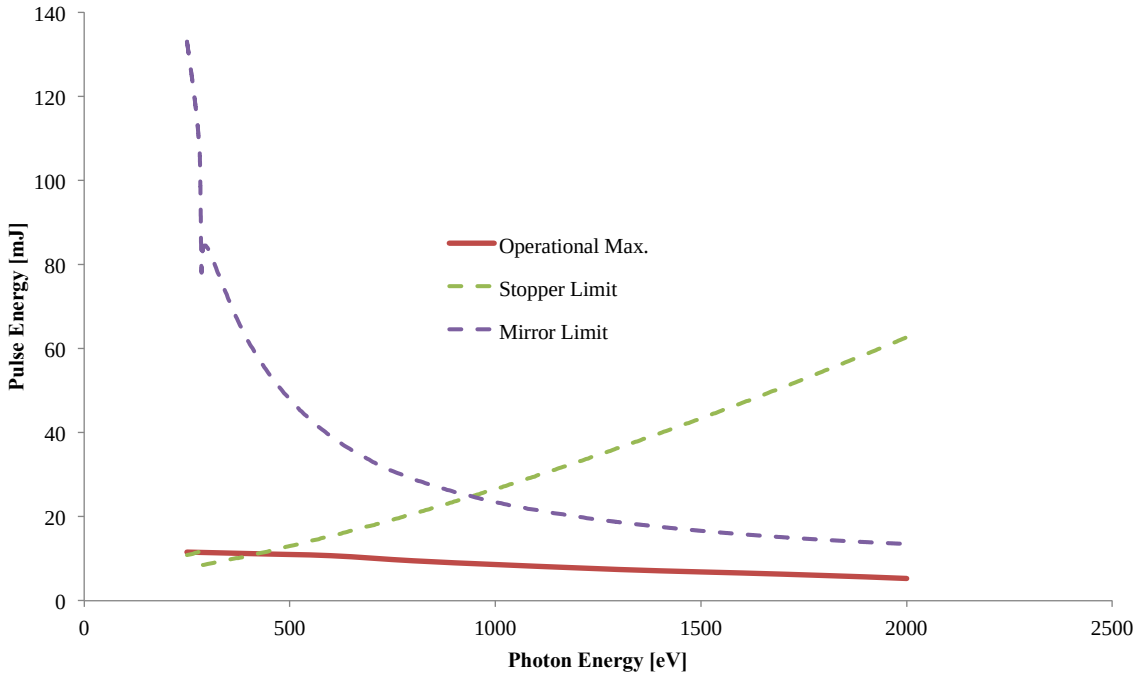

Figure 8.1. The dashed curves represent the maximum pulse energy for which the stopper of mirror has a dose of less than 0.1 eV. The solid red curve is the calculated operational maximum pulse energy.

Table 8.2. Parameters used to calculate a pulse energy limit for mirrors and stoppers on the SXR beamline.

Parameter	Symbol	Unit	Value
Photon energy	u_r	keV	0.25-2.0
Source location (upstream from end of undulator)	*D0*	m	0
Divergence, rms	σ_δ	μrad	3.9-22.6
Mirror distance from end of undulator		m	100
Mirror grazing angle		mrad	14.4
Stopper distance from end of undulator		m	121
Safe working dose per pulse for B_4C		eV/atom	0.1

The mirrors and stoppers of the HXR beamline have much less potential for high-fluence damage compared with those of the SXR beamlines because of the higher photon energy range and lower grazing angle of the mirrors. Nevertheless we estimate that the first mirror should be spaced at least 15 m from the end of the HXR undulator. At the planned distance of 50 m, to the first B_4C coated HXR mirror, the calculated pulse energy damage threshold is much larger than what can be generated by the FEL.

8.2.3 Shielding and Radiation Protection

The bulk of the shielding needed to stop undesirable radiation from reaching the experimental areas is composed of a thick concrete and steel wall on the west end of the experimental hall. This wall fills the tunnel cross section and is made nearly 4 meters thick to match the thickness of the combined Wall 1 and Wall 2 of the LCLS-I. In combination with collimators, it effectively stops bremsstrahlung, scattered spontaneous radiation, and thermal neutrons from reaching the interior of the experimental hall. Local shielding is be used to reduce the radiation levels when practical. Above the accelerator enclosure, at least 15 feet of earth provides adequate shielding needed for generally accessible areas.

The location of the shielding wall presents a somewhat different concept than that used for LCLS-I where the bulk of the XTOD components were located in a separate housing, the “Front End Enclosure”. In the LCLS-II concept there is more flexibility available for the placement of XTOD components, one instead of two shielding walls, and one instead of two access mazes required to get between the accelerator housing and the experimental area. The components of the XTOD system are essentially contained in the same personnel protection zone that also contains the undulator and electron beam dump, and is terminated by a shield wall adjacent to the experimental hall. The Personnel Protection System (PPS) (not part of the XTOD) insures that it is not possible to enter this area while the electron beam is in operation. The XTOD system provides shielding, collimation, and stoppers to prevent significant radiation from escaping this area during operation. In the experimental hall, the radiation levels are kept very low and the building is accessible during normal operation.

The main component of radiation is bremsstrahlung primarily caused by an electron beam going through some material such a wire from a wire-scanner. Radiation issues including required shielding and safety systems are presented in detail in Chapter 14 on radiological considerations. The bremsstrahlung that strikes the first mirror will generally scatter, rather than reflect. Local shielding prevents this scattered radiation from reaching Experimental Hall. The second mirror in the x-ray beamlines is shielded from primary bremsstrahlung but will be hit by some of the scattered bremsstrahlung from the first mirror and scatter it again. However, with appropriately designed collimators, this twice-scattered radiation is at low enough level that after further shielding it can be allowed to reach the experimental hall.

The effectiveness of the shielding is evaluated using methods described in Chapter 14, radiological considerations.

8.2.4 CSR Filtering

The LCLS electron beam produces visible light from diffraction, synchrotron and magnet edge radiation. This light propagates collinearly with the x-ray beam and can interfere with diagnostics and experiments. In LCLS-I the principal source of this background is coherent edge radiation formed at the start of the start of the electron beam dump magnets. LCLS-II employs a "soft" first bend magnet to reduce the amount of radiated light.

8.2.5 Harmonic Filtering

From FEL simulations and measurements at LCLS, the FEL radiation may contain a 2^{nd} harmonic with intensity as high as 0.05 % of the fundamental and a 3^{rd} harmonic with intensity as high as 1 % of the fundamental. The x-ray beam transport mirrors will provide a photon energy cut-off according to the mirror incidence angle. For the soft x-ray mirrors, the maximum photon energy efficiently reflected is

~2200 eV. For the hard x-ray mirrors, the photon energy cut-off is at ~ 14 keV. If additional harmonic suppression is required, it must be provided by the x-ray instruments.

8.2.6 X-ray Stay-clear

The x-ray stay-clear envelope represents a surface in space that during normal operation should be free of physical objects (except mirrors) that would otherwise distort or attenuate the x-ray beams. The stay-clear envelope definition allows for the beam size variation as a function of longitudinal coordinate and is just sufficient to accommodate all the expected operating conditions and photon energies. Beam size is calculated from estimates of source location and divergence angle. At any give longitudinal position the size of the stay-clear envelope is proportional to the beam size according to the stay-clear criteria discussed below.

8.2.7 Maximum beam divergence

While beam divergence and source location depend on many parameters, for the purpose of defining the stay-clear envelope we use the set of operating parameters which give the maximum beam divergence angle. Generally the maximum divergence occurs at the longest operating wavelength for both the HXR and SXR undulators. Different combinations of electron beam energy and K can generate the same FEL wavelength, but the beam divergence is only weakly dependent on these parameters. The measured divergence on LCLS varies between that calculated for the ideal Self Amplified Spontaneous Emission (SASE) FEL at saturation to roughly 2 times that at saturation. This depends in an as yet undetermined way on the operating parameters and fine details of the alignment of the undulators. Understanding the causes of the larger divergence and mitigating their effect is an ongoing area of development. At this time the conservative maximum divergence for defining apertures and the length of mirrors is 2 times that at saturation.

8.2.8 Stay-clear criteria

The ratio of the stay-clear envelope size to the maximal beam size is the “stay-clear criteria”. The stay-clear criteria chosen for the LCLS-II x-ray beam is expressed as a stay-clear diameter, and is two times the full-width (FW), half-maximum of the maximally divergent beam size. For a Gaussian x-ray beam it is equivalent to a requiring a clear diameter equal to 4.7 times the beam σ. If the x-ray beam passes through a circular aperture with opening diameter equal to 2 times the FW of the beam, the modulation of the beam profile caused by diffraction would be roughly comparable to the effect of mirror imperfections. No additional size is included to account for mechanical tolerances or alignment errors. Such errors are relatively small but should be taken into account in the design of the components.

An example of the maximally divergent SXR beam profile calculated based on FEL theory in [2] is shown in Figure 8.2. An arbitrary factor of two in beam divergence is applied to the theory to take into account that measured beam sizes are up to a factor of two larger than those calculated by this method. In the left plot is the profile that would be obtained if there are no apertures present.

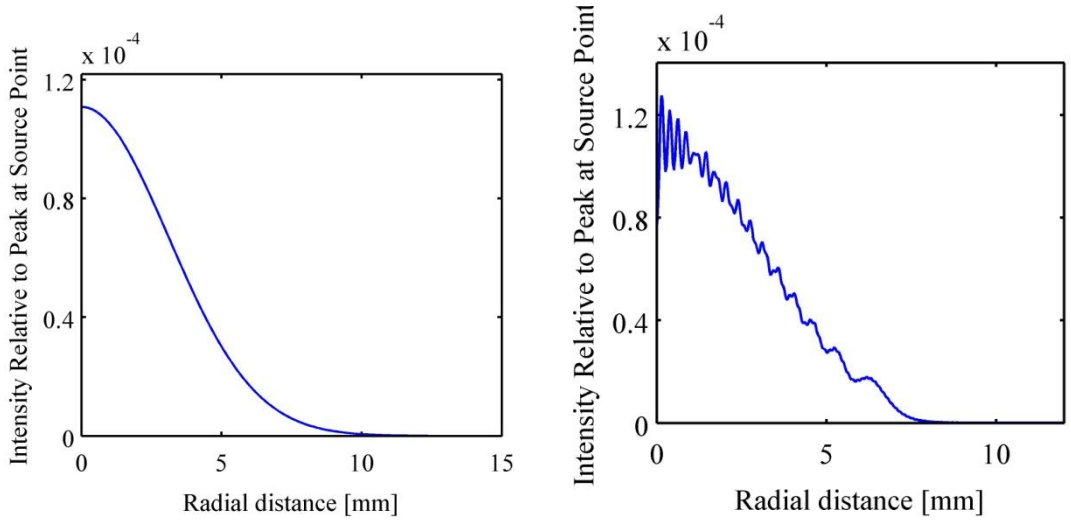

Figure 8.2. Calculated radial profiles of FEL intensity, with no aperture (left graph) and with a aperture at two times the beam diameter (right graph), 75 meters from the end of the SXR undulator.

The plot on the right shows diffraction effects 75 m downstream of a circular aperture with an opening diameter of two times the FWHM of the undistorted distribution. As expected there is significant distortion due to diffraction of the circular aperture. If the aperture diameter was 3 times the beam Full Width (FW), there would be little diffraction observed. However, such a generous stay-clear criteria puts a severe constraint on the mirrors and is of little benefit since there will be distortion of the beam profile due to mirror imperfections that are expected to be comparable to those shown in this example.

Table 8.3. Parameters used to define the SXR and HXR x-ray stay-clear envelopes.

Parameter	SXR	HXR	Symbol	Unit
Photon energy	2	.25	u_r	keV
Source location (LCLS coordinates)	678	692	$Z0$	m
Source location (upstream from end of undulator)	6	20	$D0$	m
Divergence, rms	45	7.4	$\sigma\delta$	μrad
Stay-clear criteria (diameter clear/FWHM of beam)	2	2	S	
Stay-clear criteria (diameter clear / σ of beam)	4.7	4.7	S_σ	

8.3 Beamline Overview

A schematic overview of the undulators and x-ray beamlines is shown in Figure 8.3. With this layout the transverse separation between experimental stations and the adjacent beamlines is considerably larger than in LCLS-I. There are 2.5 m separating the hard and soft x-ray lines and the separation between the soft x-ray lines is 1.6 m. The hard x-ray lines have tightest arrangement with only 0.9 m separation at the upstream HXR station. All beamlines, x-ray and electron, have at least one side with access space adequate for installation, maintenance, and fire egress. The overall length of the undulator and optical transport tunnel is determined by the required space SXR beamline systems. It includes space for post-LCLS-II upgrades of soft-x-ray seeding and polarized soft x-ray generation, and sufficient distance to avoid high fluence damage to the mirrors and stoppers.

In the upper half of Figure 8.3, the medium blue rectangle labeled HXR represents the hard x-ray undulator and the solid blue lines represent the hard x-rays beamlines. The light blue rectangle at the upstream end of the HXR undulator represents extra undulators reserved for extending the taper for the post-LCLS-II self-seeding upgrade. The layout is drawn to-scale, but the beamlines, undulators, and experimental stations (colored circles) are drawn schematically. The primary hard x-ray beam is deflected horizontally through an angle of 4.6 mrad by the first mirror, M1H, located about 50 m from the end of the undulator. The mirror M2H is inserted to bring the x-ray beam back parallel to the input beam or retracted to direct the beam on to M3H after which the beam is at 9.2 mrad form the primary incoming beam (See Figure 8.4). The beamlines then pass through the collimation system (not shown) and main shielding wall at the end of the tunnel to reach the hard x-ray experimental stations.

The SXR undulator is depicted as a solid purple rectangle in Figure 8.3. The light purple rectangle just upstream of the SXR undulator represents the space reserved for micro-bunching undulators and self-seeding optics. The downstream light purple rectangle represents the space required for polarization. The primary soft x-ray lines, shown as a solid orange lines in the lower half of Figure 8.3 , reach the first mirror, M1S (see Figure 8.4), about 100 meters after the end of the SXR undulator. The 100 m spacing was chosen to prevent damage to the mirror, particularly from high energy pulses of 1.5 to 2.0 keV x-rays. The second soft x-ray mirror, M2S, and the third, M3S have the same, but mirrored, configuration as the HXR mirrors with the M2S being inserted or retracted. The SXR mirrors deflect the beam through 28 mrad at each mirror, so one branch line is parallel to the incoming beam and the other is at 56 mrad (see Figure 8.4).

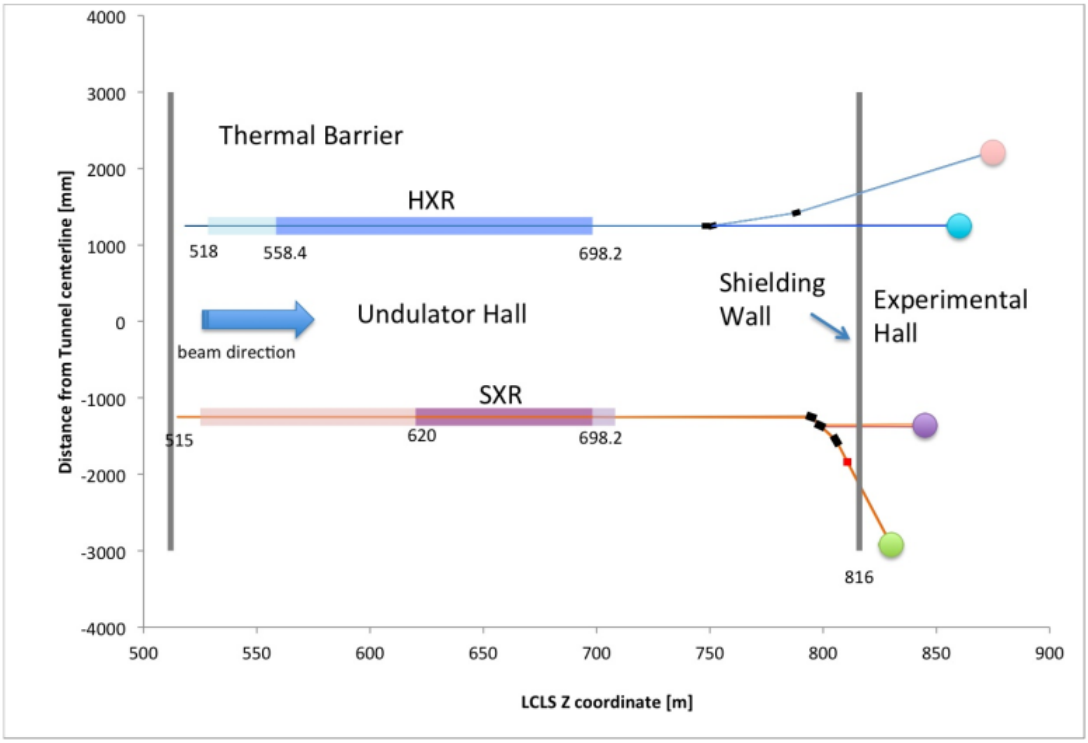

Figure 8.3. Schematic layout of the undulators and both the hard and soft x-ray beamlines.

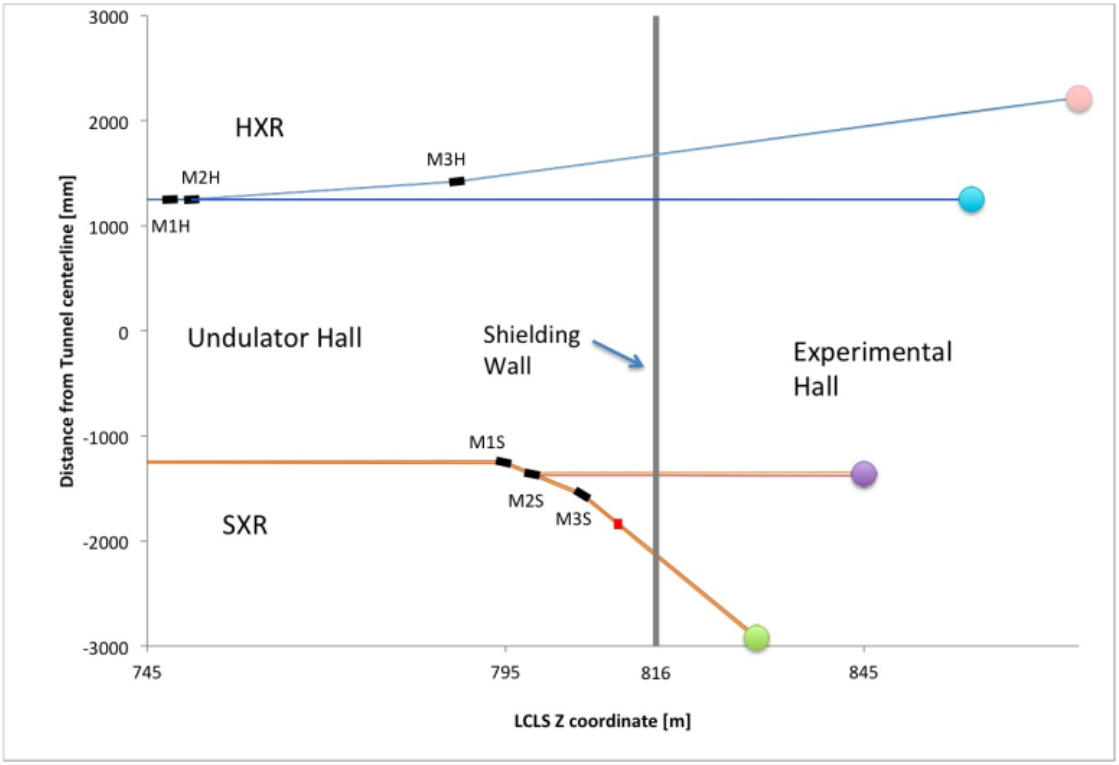

Figure 8.4. Close up of the SXR and HXR mirror systems. M2H and M2X can be inserted or retracted to send beam to one or another their respective experimental stations.

8.3.1 Beam Distribution and Instrument Layout

The hard and soft x-ray undulators are separated by 2.5m. The beam line front ends will be in the downstream end of the tunnel and separated from the experimental hall (EH2) by a shield wall. As shown in Figure 8.5, the two adjacent HXR and SXR beamlines are parallel and separated by slightly over 2.5m. The outer HXR line is at 9.2 mrad and the outer SXR line is at 56 mrad from the straight ahead lines. The upstream SXR experimental station is ~1.6 m and the upstream HXR one is ~0.9 m laterally their respective downstream lines.

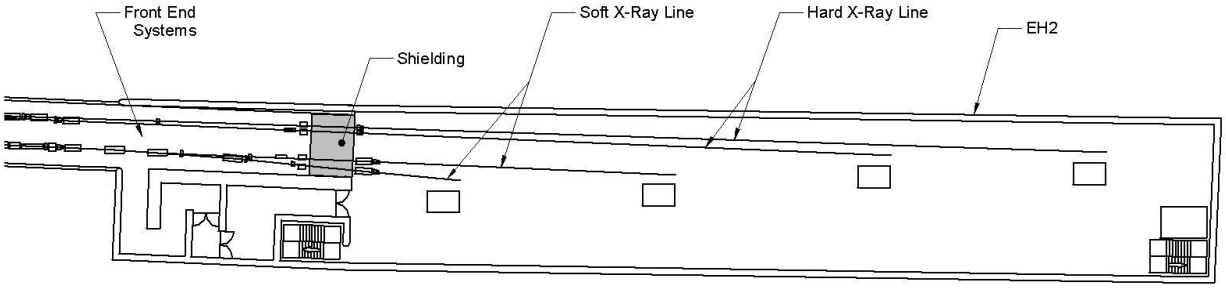

Figure 8.5. Layout of the downstream end of the tunnel and experimental hall showing how the beams will be delivered to the experimental stations. The AMO and SXR instruments will go in the open experimental hall and the future hard x-ray instruments will be housed in hutches. The HXR hutches, control and setup alcoves are not shown.

The soft x-ray experiments (AMO and SXR) are to in an open hall which has space reserved for future hutches to be designed around hard x-ray instruments. There is additional space on the experimental floor level of the building for setup of experiments and control rooms. See Figure 8.5.

The basic configuration for the front ends are:

- A multi-purpose diagnostic system for characterizing the FEL beam when the before and variable apertures, attenuators or stoppers. This type of flexible system has been found to be very useful on LCLS-I.
- Collimator for Bremsstrahlung radiation.
- Adjustable aperture to define the FEL beam and minimize spontaneous radiation.
- First energy monitor for pulse-by-pulse energy measurement.
- Attenuator: solid for the HXR line, gas for the SXR line.
- Second energy monitor for pulse-by-pulse energy measurement after the attenuator.
- Calorimeter for absolute time averaged energy measurement and for calibrating the pulse-by-pulse energy monitors.
- A second multi-purpose diagnostic system. This will be of the same flexible design as the first.
- High resolution beam imager.
- Spectrometer (hard x-ray front end only).
- Collimator for Bremsstrahlung radiation.

- Second adjustable aperture for defining the acceptance into the optical systems.
- On the HXR line the spectrometer. On the SXR line the spectrometer is part of one of the instruments that is located in the experimental hall.
- Front end optics, collimators and stoppers.
- A safety beam dump in the direct line of the undulators upstream of the shield wall.

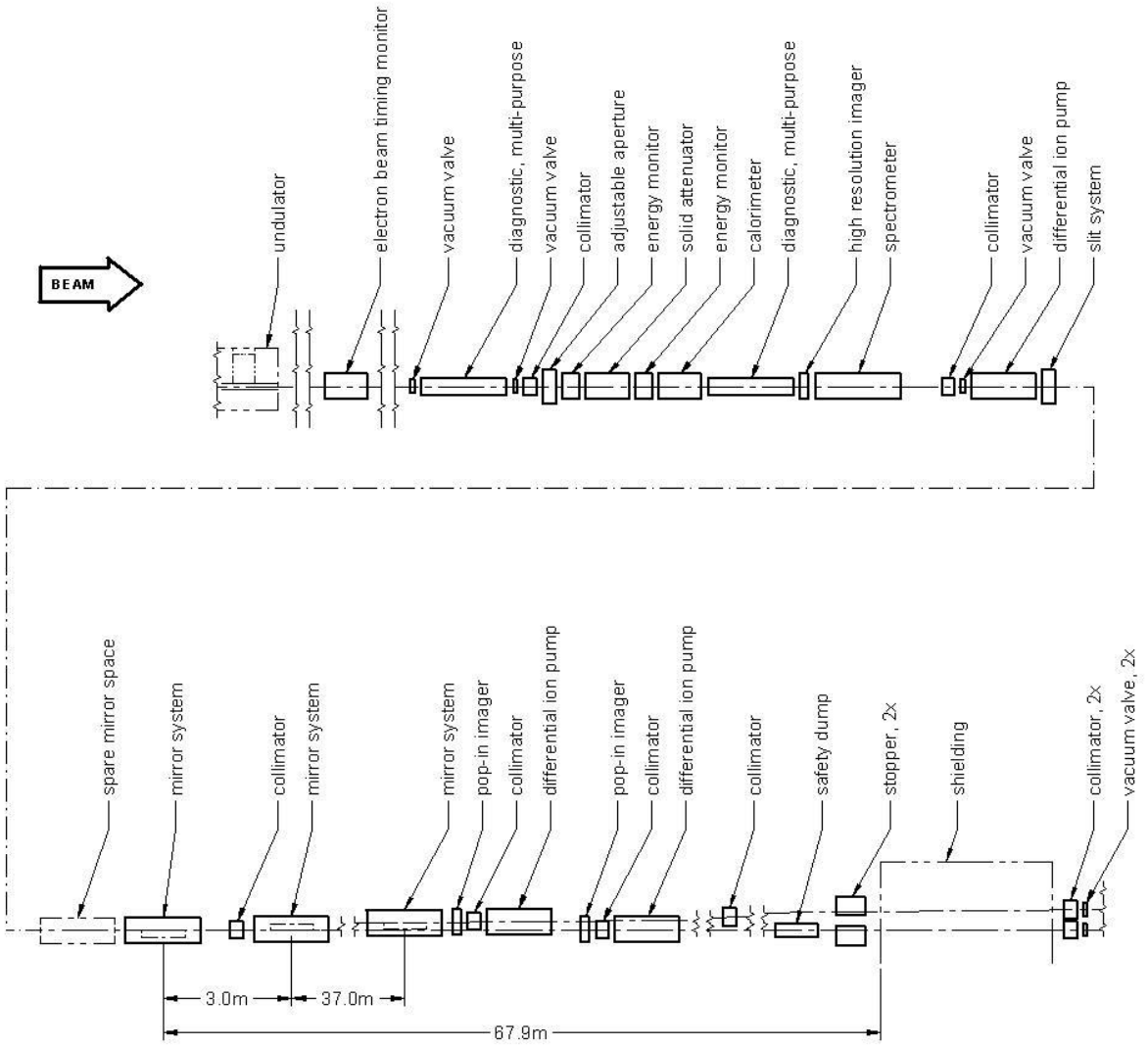

Figure 8.6. HXR front end component layout from the final electron beam timing monitor through the shield wall separating the tunnel from the experimental hall.

Figure 8.6 and Figure 8.7 show the layouts of the HXR and SXR front ends, respectively. The non-intercepting electron beam timing monitors, which are part of the electron beam systems, are referenced in sections 8.4.3 as the phase cavities. Upstream of their optical systems the main differences between HXR and SXR front ends are the attenuators, solid on the HXR and gas on the SXR, and the HXR system has a high resolution x-ray spectrometer. The SXR system will use the monochromator/spectrometer to be moved over with the existing SXR instrument.

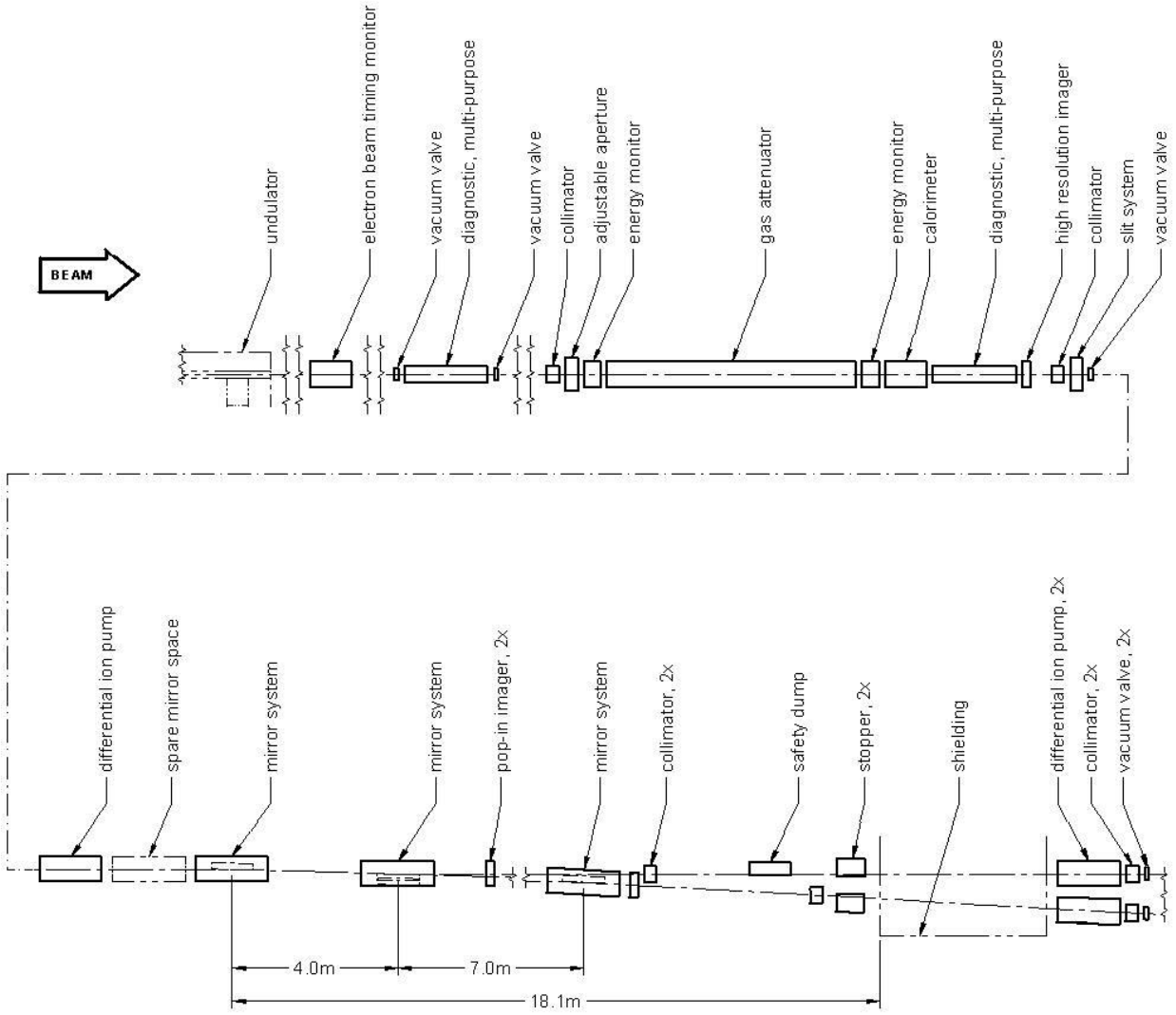

Figure 8.7. SXR front end component layout from the final electron beam timing monitor through the shield wall separating the tunnel from the experimental hall.

Downstream of the second adjustable slits are the optical systems for the respective beamlines. Two mirrors are required in the optical path upstream of the shield wall for all beamlines. Two mirrors are shown in the HXR front end, Figure 8.6, but space is reserved for a third. This third mirror could be configured in a similar, though mirrored, configuration to that shown for the SXR mirror in Figure 8.4. Further collimators and stoppers are required on each branch line to define and stop the FEL beams, and Bremsstrahlung radiation. The HXR and SXR mirror system vacuum environments are separated from adjacent parts of the beamline by up beam and down beam positioned differential pumping systems.

8.3.2 Optics

Mirrors deflect and hence separate the x-rays from the bremsstrahlung radiation and provide horizontal separation for the different x-ray instruments in the experimental hall. The mirrors must accept the x-ray divergence at the minimum photon energy. Damage criteria need to be satisfied. Finally, mirror specifications should be developed in order to preserve the x-ray wavefront properties for the focusing in the x-ray instruments.

8.3.3 Operational Modes

Hard and soft x-ray beams are provided simultaneously by the individual undulators. Two sets of diagnostics characterize the hard and soft x-ray beams. An insertable mirror is used in both the HXR and SXR lines to alternatively deliver beam to one of two respective instruments. The soft x-ray instruments consist of the Atomic, Molecular and Optical (AMO) instrument and the Soft X-ray materials Research (SXR) instrument that will be moved from the LCLS Near Experimental Hall (NEH) to the LCLS-II Experimental Hall (EH2). Instruments for the new hard x-ray beamlines are not in the scope of the LCLS-II project but are anticipated soon after the completion of the construction of LCLS-II.

8.4 Components

In this section concepts are described in some detail for each of the components that are part of the XTOD. In addition there is a description of the supporting mechanical and vacuum systems.

8.4.1 General Mechanical and Vacuum

The beam transport mechanical and vacuum system contains approximately 350 meters of vacuum beam pipe and x-ray instrumentation that is maintained at a nominal base pressure of 10^{-7} Torr by approximately 50 ion pumps. In order to leverage existing infrastructure, the basic design of the beam transport section is based on the existing LCLS-I system. Shown in these sections are repeated through the tunnel and experiment hall, filling the space between the undulators and dedicated instrumentation.

The basic beam transport system has stainless steel pipes connected with metal seal gaskets and welded Conflat flanges. The pumping section consists of a stainless-steel cross that accommodates the ion pump, vacuum gauge(s), and roughing/vent valve where appropriate. Each ion pump has its own power supply. The section terminates with a bellows for alignment and an all metal isolation valve where needed. Each assembly is supported by a box tube welded stand and adjustable aluminum brackets.

Some LCLS-II components (e.g., the gas attenuator and offset mirror system) require base pressures above or below the nominal 10^{-7} Torr. These instruments will be isolated by commercially supplied differential pumping sections. In the case of the gas attenuator, a series of fixed and adjustable apertures are combined with large capacity turbo pumps to separate high and low pressure sections.

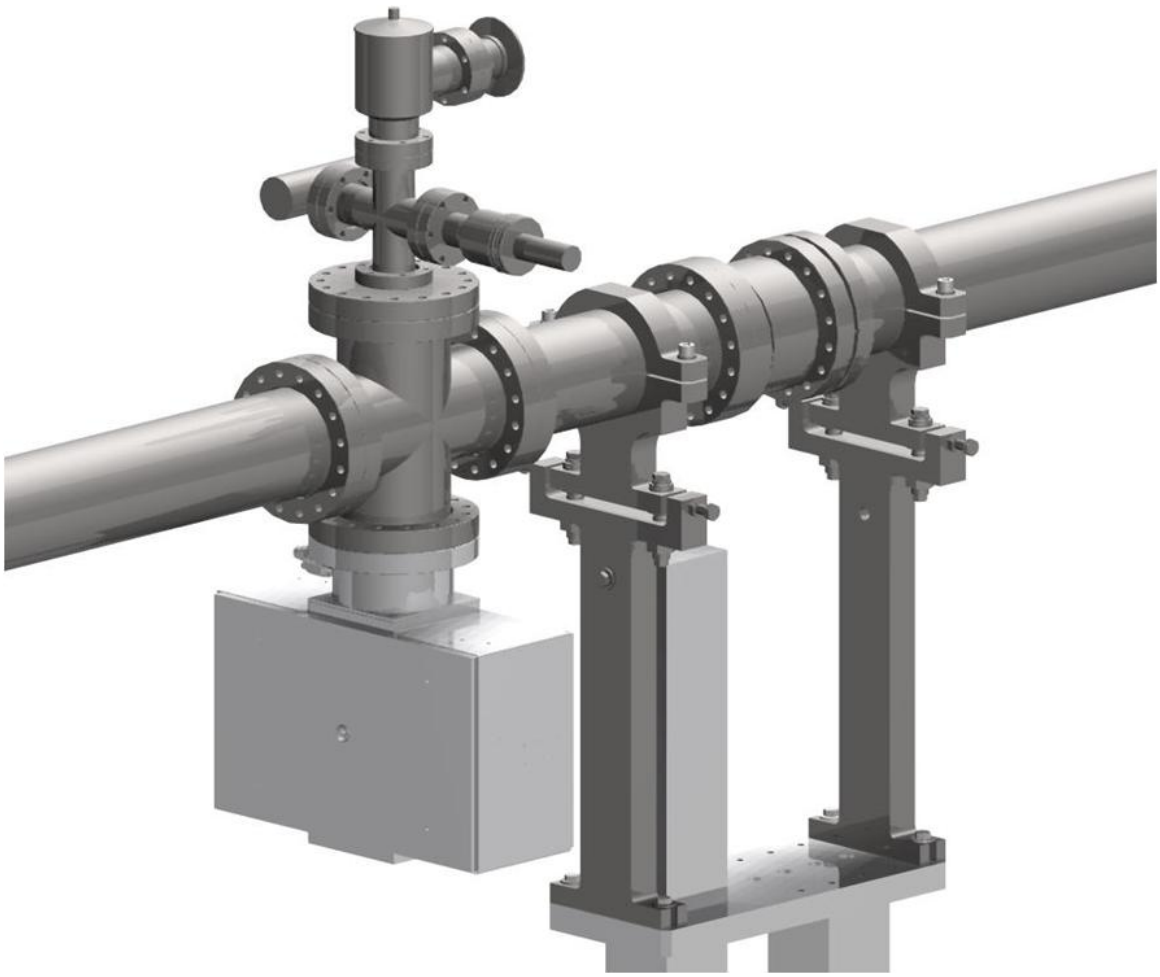

Figure 8.8. CAD model image of the standard LCLS-II pump section.

Furthermore, it has become evident from LCLS-I operation that the mirror systems may be particularly prone to carbon depositions on the optic surface. The specifice vacuum requirements at the mirrors are not yet defined, but are expected to be in the $<5x10^{-10}$ torr range and meet the LCLS requirements on partial presures of gasses with a mass of >44 AMU. In addition to lowering nominal base pressure, further efforts to improve operating conditions need to be implemented. Some of these steps are detailed in Section 8.4.10.5 mirror system optical-mechanical design. A concern is that low pressures the long mean path of molecules can result in deposition of contaminates on mirror surfaces which are then chemically activated by the high fluence FEL beam resulting in a hydrocarbon build up on the mirrors. For the offset mirror systems special differential ion pumps that provide line of sight pumping of the molecular beam will be installed between higher pressure and the optical systems [3]. This type of pump will be tested for its effectiveness at pumping Xe and Kr, which may be used in the gas attenuator, see Section 8.4.6.

8.4.2 Controls

Local controls of the diagnostic equipment are discussed within each component section of this chapter. Remote controls are discussed in the controls section, Chapter 11.

8.4.3 Multipurpose Diagnostic Chamber

A means for rapid implementation of simple diagnostics was found to be extremely useful at LCLS. The LCLS-II systems will have chambers specifically designed for rapid installation of diagnostics. During commissioning and early operations of the LCLS a number of diagnostics and test were performed in the ST-0 chamber, a Coherent Optical Transition Radiation (COTR) blocking foil was installed after it was found that there was a substantial amount of COTR being produced along with the FEL beam, a YAG imager was installed days before it was used to detect the first FEL beam, a set of K-edge filters was installed and used to calibrate SHAB second harmonic production, a double slit system was installed for some of the first x-ray FEL coherence measurements, and numerous material damage test have been made as the energy per pulse and photon energy range has increased beyond the design parameters. With LCLS-II there may be equivalent, but different unforeseen needs.

There are two multipurpose diagnostics chambers in each of the main x-ray lines: one upstream, of the first adjustable aperture, for diagnostics that can measure the full beam power and large divergence angle spontaneous radiation; and the second, downstream of calorimeter and attenuator system, for devices that require an attenuated or apertured beam. The chambers have multiple ports perpendicular to the beam line for installation of diagnostic tools, which will generally be on linear actuators so they can be inserted and withdrawn. Each chamber is isolated from the rest of the beam line by valves for rapid venting and pump down as diagnostics tools are added and changed.

8.4.4 Adjustable Apertures

Adjustable apertures in the form of movables slits are included to be able to block the majority of the spontaneous Synchrotron Radiation (SR) that accompanies the FEL beam. The apertures need to be adjustable because the FEL beam size varies approximately inversely with photon energy. Such radiation has a very broad and hard spectrum with a critical photon energy around 150 keV at the maximum electron beam energy. In some cases such radiation could affect measurements of the FEL beam. The adjustable slits can also be used to define a spatially narrow source for the purpose of calibrating detectors and spectrometers, aid in the alignment of other apertures, provide an independent means of measuring beam sizes, and can provide a known source small size source for beam divergence measurements.

The concept for the LCLS-II Adjustable Aperture is based on those used in LCLS-I and is illustrated in Figure 8.9. The assembly contains four independently movable Boron Carbide/Tungsten Heavy Alloy (WHA) blocks. It is located upstream of the primary wide-field-of-view systems and diagnostics. The Boron Carbide protects the WHA from FEL damage. The first two blocks are horizontally opposed and offset in the beam-line direction. The second two blocks are vertically opposed and also offset in the beam-line direction. The beam-line direction offset prevents any possibility of the slit blocks colliding with each other. Each slit block can completely block the beam centerline. This transverse overlap also allows for relaxed manufacturing and alignment tolerances.

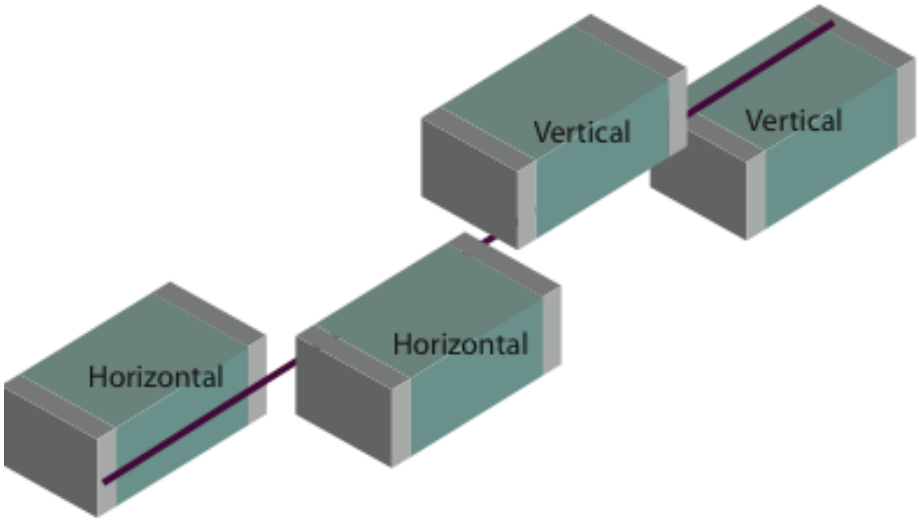

Figure 8.9. Adjustable aperture concept of four independently movable blocks.

There will be a second set of adjustable apertures just upstream of the first optical system on each beam line. They are for aperturing the optics and will not have the Tungsten Heavy Alloy to stop the very hard radiation. They will be similar to the slits used in the LUCI instruments.

8.4.5 Energy Monitor

The pulse energy will be monitored at two points in the beam transport lines. The first just upstream of the attenuator systems and then again downstream of them. The un-attenuated pulse energy is generally used by accelerator operations and the attenuated by the experimenters. The two systems are also used to calibrate the attenuators. For relative pulse energy measurements LCLS has already commissioned and used a gas detector that measures the fluorescence of N_2 induced by the FEL beam. [4] It has been used over the energy range of 540eV to 9keV and shows good performance. As is shown in Figure 8.10, this gas detector measures the N_2 fluorescence produced by the FEL beam entering a 30 cm long and 8 cm diameter gas chamber which is pressurized between 0.02-1.2 Torr. The aluminum chamber walls are grooved to suppress any stray light entering the two perpendicularly-installed photomultiplier tubes. Magnetic coils around the chamber confine the photoelectrons and maximize the fluorescence signal. The nitrogen ionization leads to the emission of photo - and Auger electrons, which deposit their energy in the nitrogen gas until they thermalize or collide with the chamber walls. The exited N_2 molecules relax by fluorescence in the near UV, between 300-400 nm. The fluorescence yield in nitrogen has been studied in detail for the detection of highly-energetic cosmic rays [5] and it was found that the fluorescence yield per deposited energy is well correlated and a good measure of the incident FEL radiation.

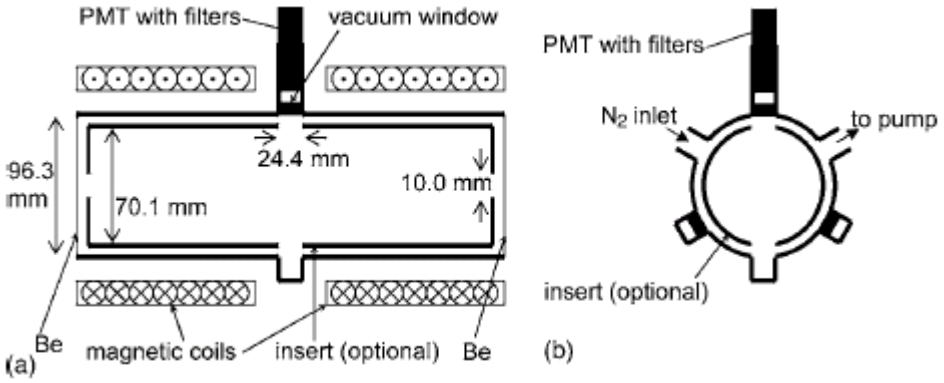

Figure 8.10. Schematic of the gas detector used for LCLS-I (a). Cross section through the center of the chamber.

Extending the energy range over the operating range from LCLS-I to LCLS-II of 250-13keV will require further studies. The issues to be addressed is at high energies the gas pressures required for adequate signal have density fluctuation that results in small angles scattering. A mixture of higher Z gasses with the nitrogen will be investigated. The addition of higher Z noble gasses would increase the absorption of photons at low pressures. The emitted electrons trapped in the magnetic field would transfer energy to the nitrogen until they have thermalized. The fluorescence from the nitrogen would then be detected by the photomultiplier tubes. The sensitivity and linearity of gas mixtures for high energy operations will be assessed on LCLS-I.

In the soft x-ray range the nitrogen K-edge at 410 eV needs to be avoided. This will be done using an alternate type of gas monitor based on a PTB/DESY design [6]. The PTB/DESY design measures the atomic ionization of rare gas at low pressure 10^{-3} Pa (see Figure 8.11). It operates down into the UV range at FLASH and has been tested at the LCLS up to 2keV. The electron and ion charge is measured by Faraday cups. Pulse by pulse measurements are deduced from the ion and electron signals with an accuracy of about 10%. This detector has been demonstrated to perform well at lower energies and is calibrated absolutely at the PTB laboratory at the storage ring BESSY II. This detector could be modified to extend to higher photon energies where photoionization cross section decreases [7]. This type of gas monitor resolves issue with operating at the Nitrogen K-Edge by using different noble gasses. Though its effectiveness has not been tested at high energies, it may also resolve the issue of high gas pressures at high energies.

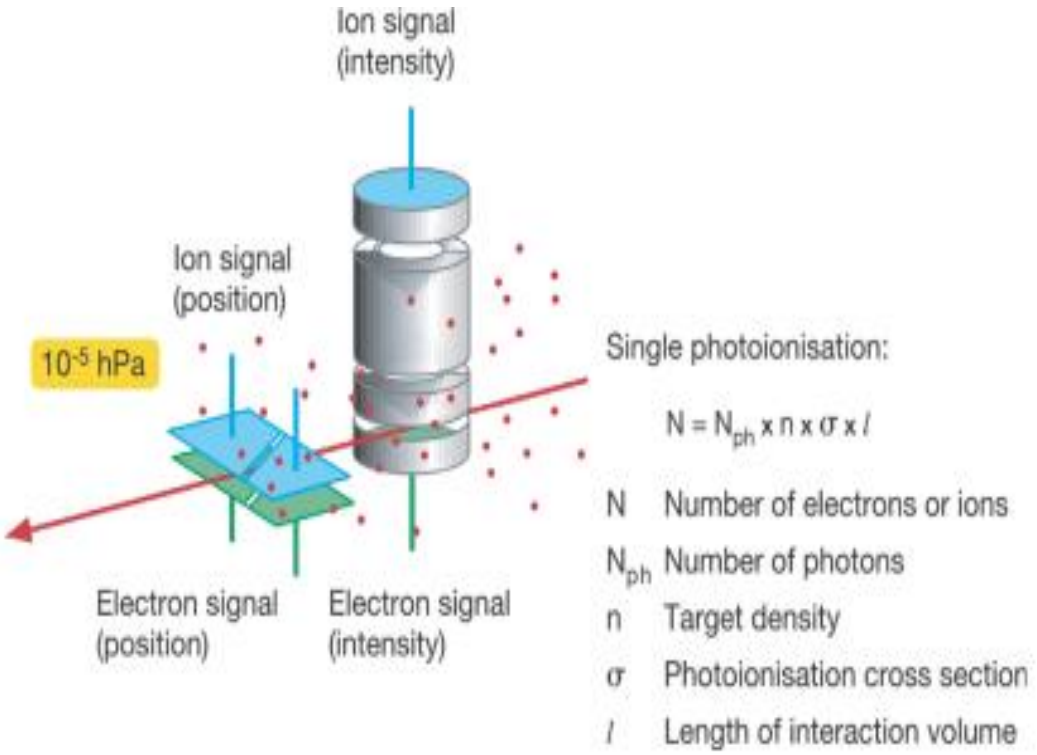

Figure 8.11. Schematics of the Gas Monitor Detector (GMD) operated at UV FEL at FLASH. Included is the option of a combined beam position measurement.

An alternate method used for the hard x-ray range are solid foils of the type used on the LUCI instruments, these are not ideal at 2 keV where the thinnest practical diamond crystals will attenuate the beam by a factor of 2. The HXR line could be operated with gas energy monitor at long wavelengths and LUCI type solid energy monitor at short. The effort invested in optimizing a gas energy monitor system should be limited to finding a cost effective pulse energy monitor by comparison to the cost and complexity of building two systems with overlapping ranges.

8.4.6 Gas Attenuator

A gas cell attenuator will be used to control the power of the SXR beam to the experimenters. If we assume an active length of 3 meters, and a maximum attenuation of 10^6 the required pressure for several gasses is given in Figure 8.12. The x-ray beam size varies with photon energy. In Figure 8.13 we plot the required clear aperture for a 6 sigma clearance with an additional 1mm diameter to account for misalignments.

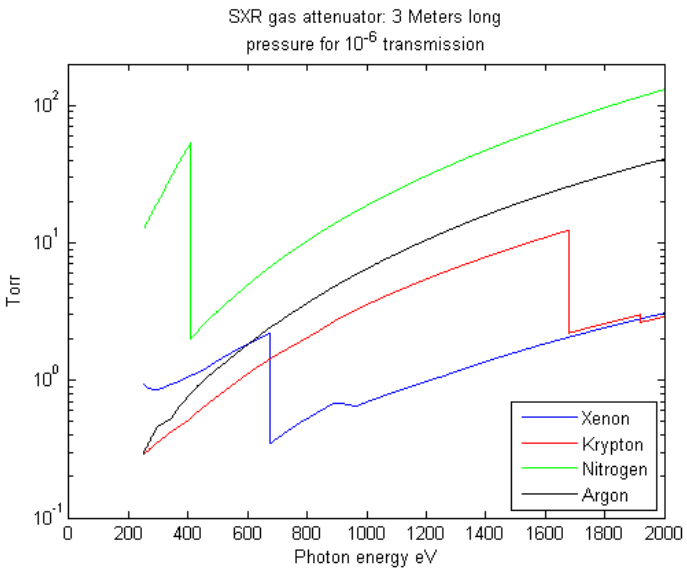

Figure 8.12. Gas cell attenuator/required pressure for various gasses with photon energy.

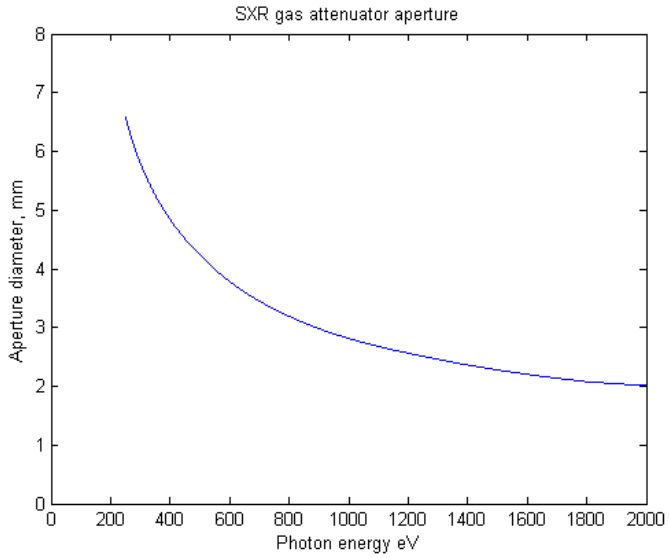

Figure 8.13. Required clear aperture for soft x-ray gas attenuator with photon energy.

It is not practical to isolate the gas volume with a foil so differential pumping must be used. The required pressure rises with increasing photon energy, but the required aperture size decreases. If the pumping aperture size is allowed to vary with wavelength the mass throughput is shown in Figure 8.14. This figure assumes molecular flow, the real flow is in the difficult to model transition between molecular and turbulent flow, but error in the estimate is less than a factor of 2. For reference, a large commercially available turbo-molecular pump has a throughput of about 10 Torr-Liters / second.

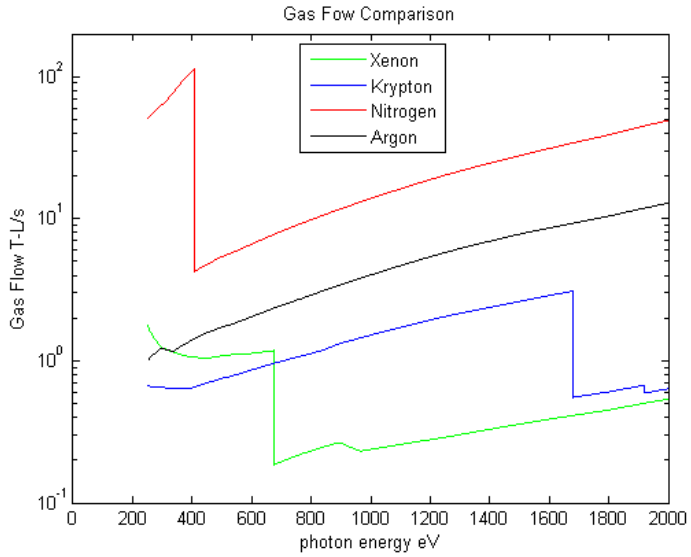

Figure 8.14. Gas flow comparison for a variable aperture differential pumping system.

If we allow a choice of Kr or Xe depending on wavelength, the maximum throughput is 1 T-L/sec as shown in Figure 8.15. A modest sized vacuum pump with a nominal 2000L/S speed and an input pressure of 10^{-3} Torr will have approximately a 2 T-L/sec throughput. For operation at photon energies near absorption edges in Xe or Ne, the alternate gas can be used.

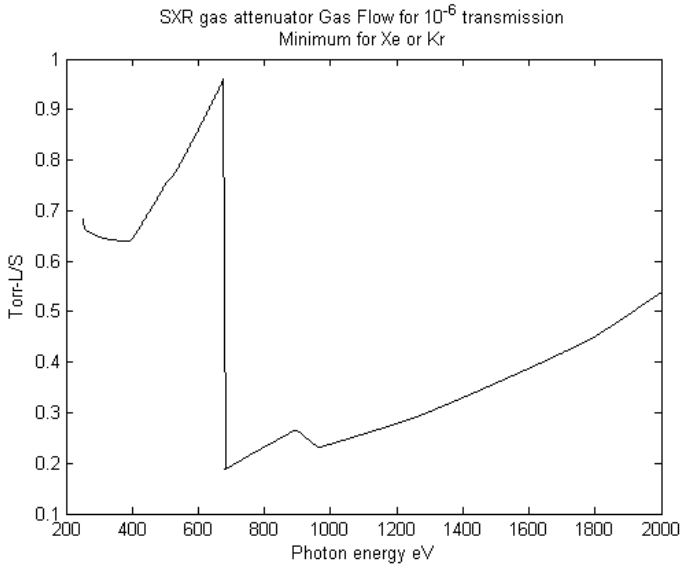

Figure 8.15. Gas attenuator gas flow.

The price of Xenon gas is approximately $15/standard Liter. This corresponds to ~$100/hour for gas use. This makes it desirable to have a gas recirculation system; however perfect recovery is not required. Gas can be vented as necessary for pressure changes or to switch between Kr and Xe.

If we assume variable pumping apertures for the main gas volume, and fixed 7mm apertures for the differential pumping stages the result is a system shown schematically in Figure 8.16. The apertures in the gas attenuator and particularly the variable apertures will have to be made of a low Z refractory material such as B_4C. There is still the potential for damaging the apertures at low photon energies. The

apertures will have to be interlocked to be opened as the photon energy decreases. At low energies when there is potential to damage any of the apertures the pulse energy will be interlocked to shut down the beam if miss-steering is detected. Several technologies to detect beam strikes on apertures are available including x-ray scattering, acoustic detection and fluorescence. This only needs to be implemented on the first or limited number of apertures.

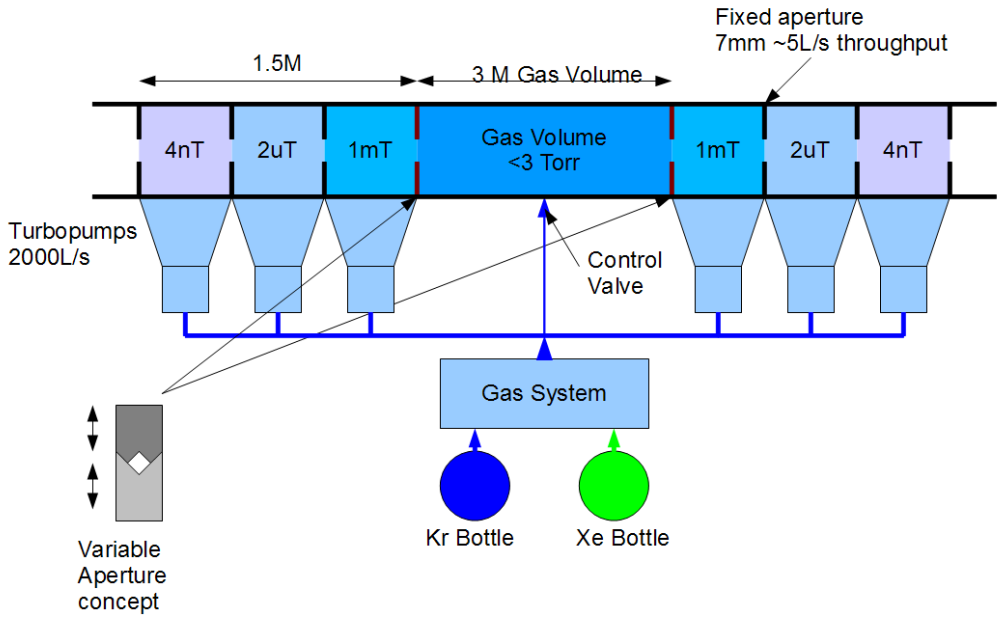

Figure 8.16. Configuration of a variable aperture differential pumps and gas attenuator system.

The total system length is 6 Meters. The neighboring elements of the vacuum system are exposed to a gas load of 20 nano-torr Liters/second. This could be reduced if necessary by an additional ion-pumped differential pumping cell.

The differential pumping system cannot stop direct molecular streaming from the pressure cell through the apertures. The LCLS-I system uses a special type of ion pump where the discharge surrounds the vacuum chamber to stop the streaming gas molecules. A similar system will be used for LCLS-II. See section 8.4.1 for details.

8.4.7 Solid Attenuator Systems

For x-ray photon energies above several keV, the gas attenuator designed for soft x-rays becomes ineffective without using very high gas pressure and high-Z gases. Moreover, at high pressures the small angle scattering arising from the density fluctuations will become significant, thus rendering it less desirable especially for user experiments aimed at utilizing the excellent coherence properties of the FEL beam. As such, solid attenuators consisting of beryllium foils of varying thicknesses were conceived and used for LCLS-I. However, it has been found that although the type of polycrystalline beryllium used was of the best optical grade, the residual density non-uniformity has led to speckle patterns that were completely unacceptable to many user experiments. A similar design for the LUSI instruments using single crystal silicon proved to perform much better in minimizing wavefront degradation as well as

small angle scatterings. Therefore, the LCLS-II solid attenuator systems will be based on single crystal planar samples such as silicon and diamond.

The conceptual design of the solid attenuator system is shown in Figure 8.17, where stacks of diamond and silicon single crystal wafers of varying thicknesses are arranged in sequences. The diamond sub-stack will be up-stream of the silicon sub-stack for damage protection of the Silicon attenuators. Due to the higher total FEL beam energy for the LCLS-II, the fluence at the designated attenuator location, diamond will be the only material that can sustain the full LCLS-II beam even down to 2 keV, as shown on the left panel in Figure 8.18. This is however not the case for silicon as indicated on the right panel in Figure 8.18, and thus it is necessary to use the diamond filters upstream as pre-filters to reduce the fluence by the required attenuation factor whenever the silicon filters are being used.

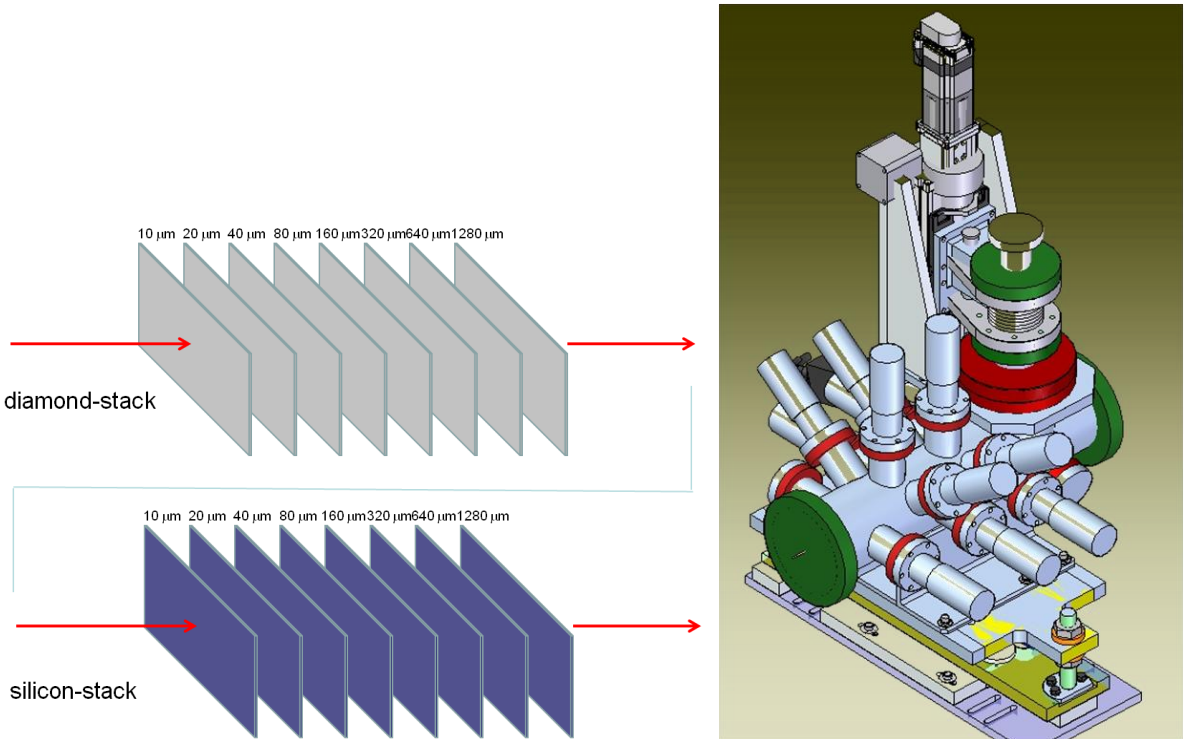

Figure 8.17. Conceptual design of the Solid Attenuator Systems. (Left) Arrangement of the diamond and Silicon single-crystal wafers with diamond in upstream positions. (Right) Mechanical design.

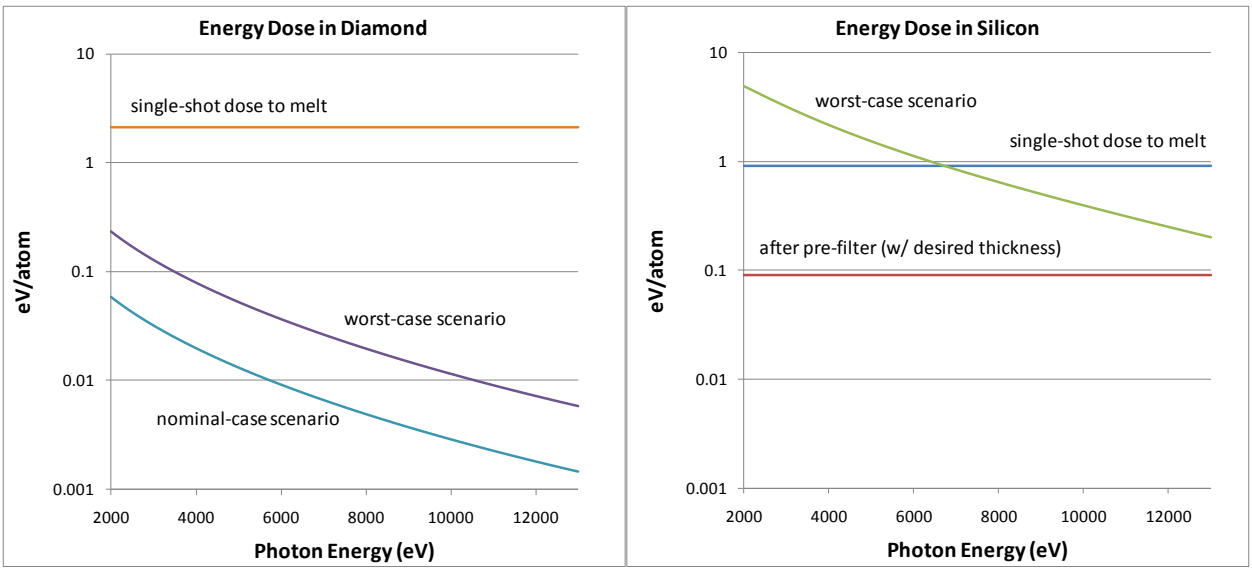

Figure 8.18. Energy dose in diamond and silicon by the LCLS-II full beam at normal incidence. (Left) Diamond, damage safe for all energies; (Right) Silicon, diamond pre-filter is used to avoid damage for x-ray energies below 6 keV.

Both the diamond and silicon attenuator systems will use a binary scheme where the sequence of the thickness increases by a factor of 2 for the subsequent thicker filter. This system has the advantage of providing all combinations of thickness in secession in exactly an equal amount equal to the thinnest filter. Since at a given energy the attenuation depends exponentially on the total thickness of the filter, an equal amount in succession of thicknesses gives a constant factor in attenuation, albeit this constant factor will change as energy varies. An attenuator system of 8 attenuators is equivalent to a binary counting system of 8 bits, capable of providing up to 2^8-1 discrete levels of total thickness.

There will be two solid attenuator sub-systems, one for operating at lower-end of hard x-ray energies from 2000 eV to 6000 eV using diamond single crystals, and the other from 6000 to 13000 eV using silicon single crystals in conjunction with diamond pre-attenuation. The diamond attenuator system uses 8 filters of 10, 20, 40, 80, 160, 320, 640, 1280 μm thick wafers, providing 255 combinations of evenly increasing thicknesses starting at 10 μm and up to 2550 μm. The attenuations achieved are shown in Figure 8.19, where it displays the attenuation as a function of incident x-ray photon energy for a given combined thickness. The achieved attenuation is bound between the top curve in the top figure for 10 μm filter and the bottom curve for the sum of all 8 filters, and virtually any desired attenuation can be obtained in-between the boundary curves with granularity reaching its maximum value at 2000 eV and decreasing with energy.

Similarly the silicon 8-step attenuator system uses a thinnest of 10 μm thick wafer and thickest of 1280μm. To protect the silicon filter from the FEL full beam, diamond filters will always be used in conjunction and upstream of the Silicon filters. The attenuations for the silicon with the diamond pre-attenuation are shown in Figure 8.33 as a function of the x-ray photon energy.

The maximum power absorbed at 2 keV in the first diamond attenuator is 5mJ per pulse or 0.6W at 120 Hz. Conductive cooling through the holders should be adequate to handle this power. On LCLS 20 μm thick silicon attenuators have been in operation at roughly half this power without negligible effect on the wavefront. The thermal performance of the filter at LCLS-II power levels will be modeled.

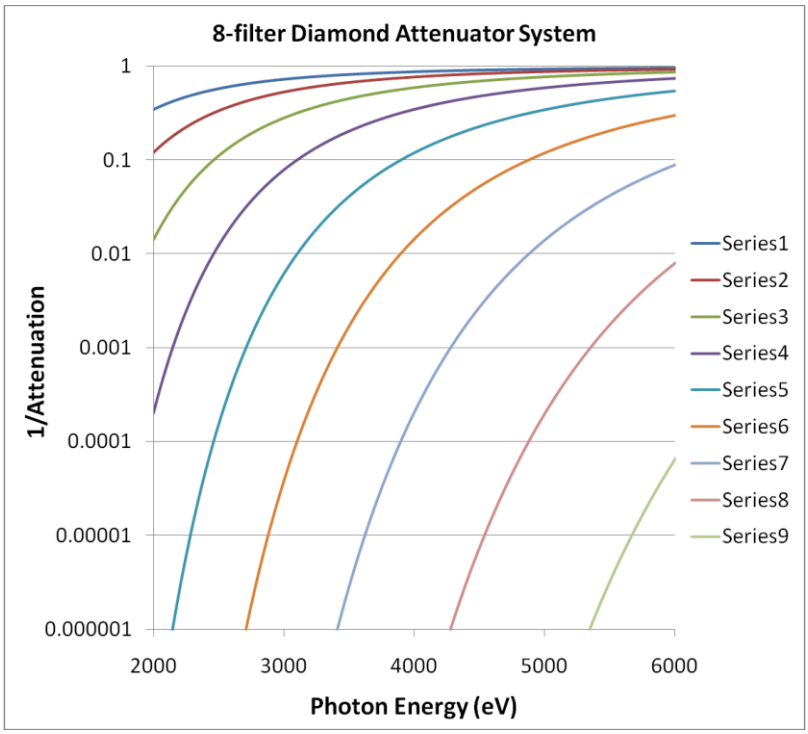

Figure 8.19. The 8-filter Diamond Attenuator System operating from 2000 to 6000 eV. Attenuation as a function of x-ray photon energy for various thicknesses.

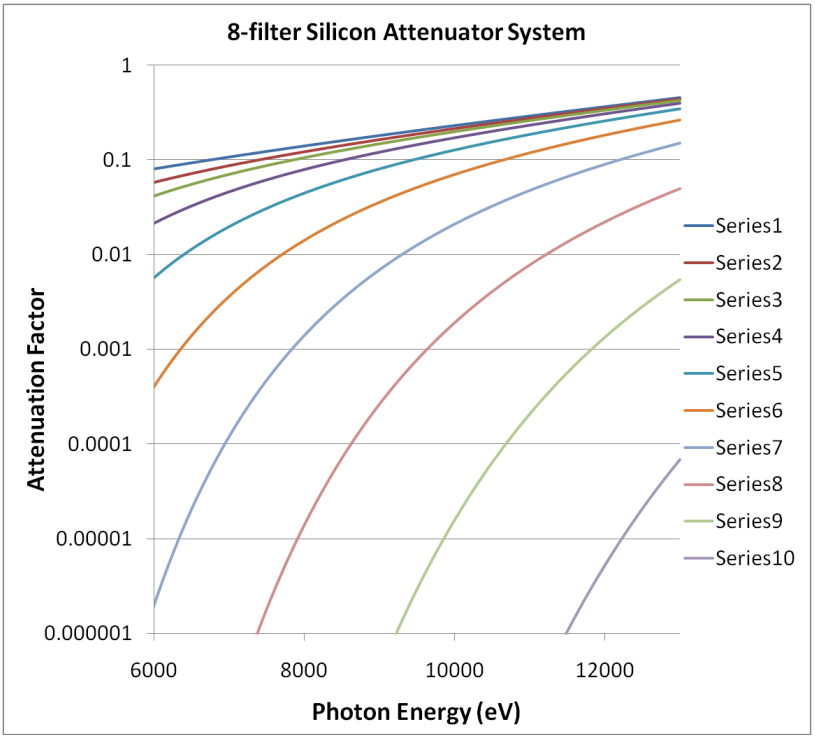

Figure 8.20. The 8-filter Silicon Attenuator System operating from 6000 to 13000 eV. Attenuation as a function of x-ray photon energy for various thicknesses of Silicon filters.

8.4.8 Calorimeter

The measurement of the pulse energy of the FEL beam is an important parameter which is required for tuning the machine during commissioning and for efficiently changing operating modes. Additionally during operation, basically all user experiments depend on the measurement of the pulse energy, especially for such investigating non-linear effects.

Due to the SASE process each pulse varies and its pulse energy can significantly differ. Therefore it is necessary to have pulse resolved energy diagnostic which is non-beam-intercepting, allowing experiments to operate in parallel. Similar to LCLS-I we are planning to employ two types of energy monitors; one beam intercepting device for absolute energy measurement and a second one for pulse-by-pulse operation, which is non-beam-intercepting and can be calibrated by the absolute device.

For measuring the absolute pulse energy we are planning to use a calorimeter. Cryogenic radiometers are used as a primary standard for measuring absolute intensity of photon beams at some National Metrology Institutes (PTB, NIST, NMIJ) [8]. Cryogenic radiometers are usually used for continuous, intense light sources such CW lasers and have been demonstrated to be reliable at lower intensity, lower pulse width and high repetition rate light sources such as synchrotrons light sources. Recent studies have demonstrated that cryogenic radiometers provide reliable measurements for high intense and strongly pulsed FEL radiation. [7]

These cryogenic radiometers also called electrical- substitution radiometers, and work on the basis of the equivalence of electrical and radiant heating. As shown in Figure 8.21 a cavity absorber of known absorbance collects the incident radiation and converts it to heat. The absorber is equipped with a thermometer to measure the temperature and a heater element to supply electrical power to the absorber. The absorber is coupled to a heat sink which is held at a constant temperature and collects all excess heat from the absorber. Accuracy, response time and sensitivity are a function of the absorber temperature. Cryogenic radiometers using liquid helium have been used to measure the power of monochromatized soft x-rays with an uncertainty of 0.2% or less.[9] An example of such a radiometer is shown in Figure 8.21.

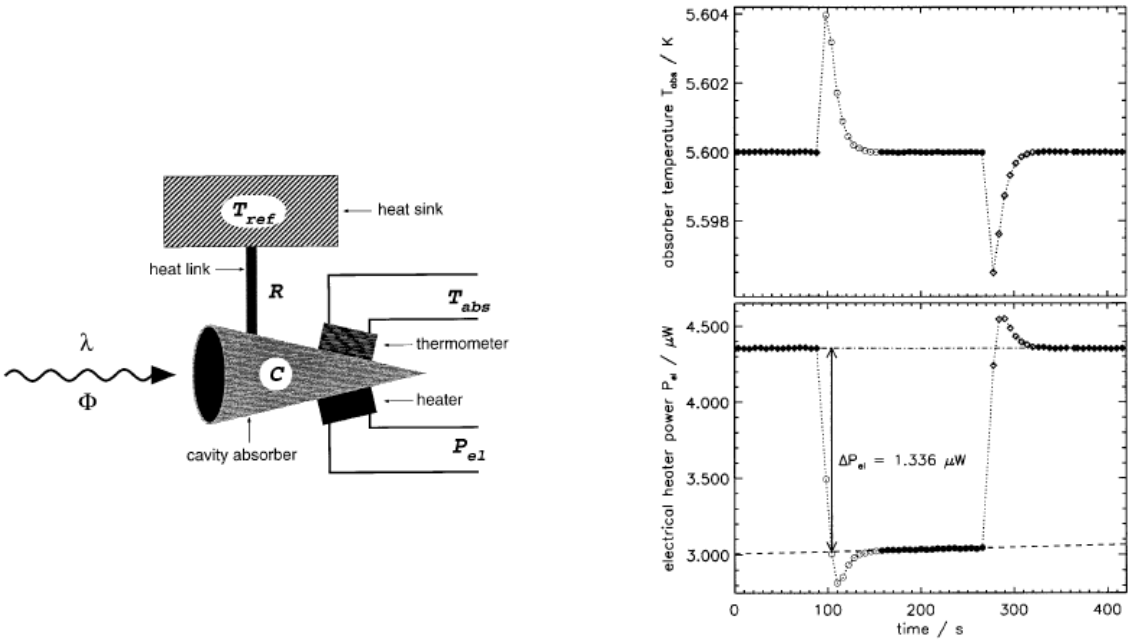

Figure 8.21. Schematic of a cryogenic radiometer (a), and an example of a radiant–power measurement exposed to a synchrotron beam.

Absorber temperature (top) and electrical heater power (bottom) as a function of time. At about t=90 sec. the shutter is opened and the feedback loop reduces the electrical heater power to the initial temperature after a settling time of about 60 sec. [10]

The suitability of cryogenic radiometers for hard x-rays needs further evaluation. Some of the issues include: the material to absorb the x-rays and the integrated power at which they will operate. This will be part of the development of the calorimeter system.

8.4.9 Imagers

Imaging of the FEL radiation was proven to be extremely valuable in helping diagnose and optimize the LCLS-I lasing process as well as in alignment of various optical elements in the front-end enclosure. The LCLS-I direct imagers were based on optical imaging of an x-ray scintillation material impinged on by the FEL beam. For LCLS-II, the same design principle will be used but with improvements in higher resolution, variable Field-Of-View (FOV), adjustable working distance, and simultaneous operation of multiple devices at hard x-ray energies.

The conceptual design of the LCLS-II Direct Imager is shown schematically in Figure 8.22. The optical assembly consists of an x-ray scintillation screen, an optical reflecting but x-ray partial transmissive mirror, a zoom lens, an optical Charge Coupled Device (CCD) camera capable of per-pulse operation, and associated read-out electronics. Both the scintillation screen and the mirror are retractable to permit normal FEL delivery. The model on the right is that of the LCLS Ultrafast Scientific Instruments (LUSI) profile monitor deployed for all LCLS hard x-ray instruments.

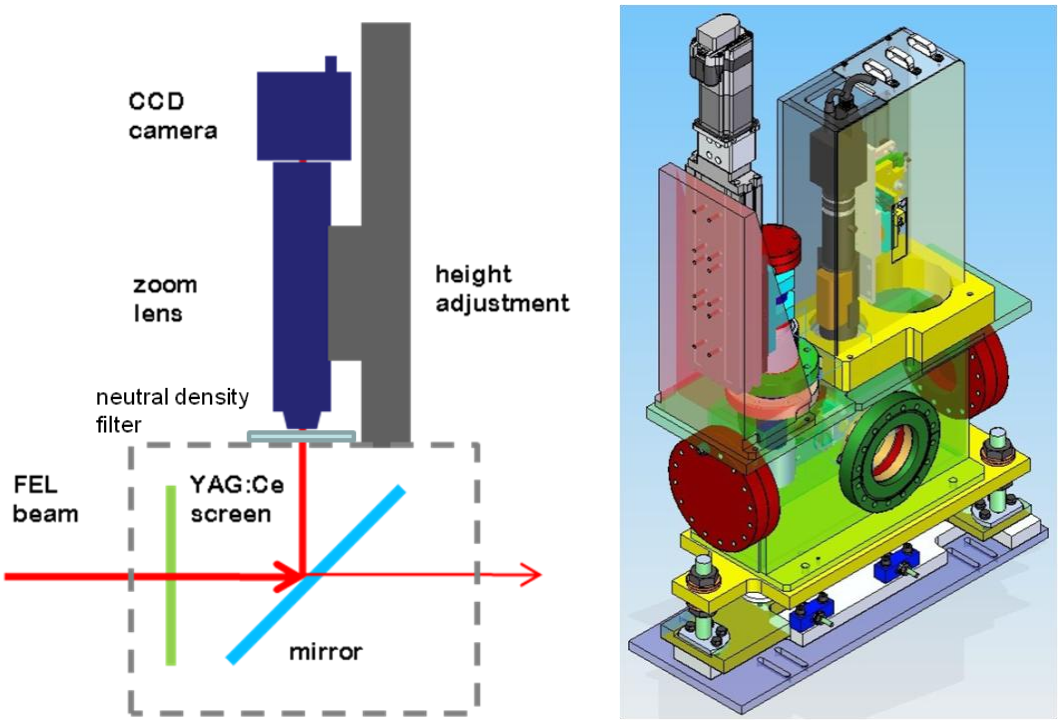

Figure 8.22. Schematics of the Direct Imager. (Left) Optical imaging system; (Right) Mechanical model.

A Cerium-doped Yttrium Aluminum Garnet (YAG:Ce) single crystal sample is used as the x-ray scintillating material which has been shown to exhibit characteristics suitable for imaging x-ray sources like the FEL. At the high fluences the LCLS can deliver it is in a non -linear saturation regime. Attenuating the beam can reduce the problems with saturation. At high attenuation the higher harmonics can contaminate the image. Alternate fluorescent materials that do not saturate are being investigated. YAG t has a very high melting temperature, high thermal conductivity, and is capable of sustaining unfocused FEL beam at normal incidence with only moderate attenuation even at low x-ray photon energies. It is a fast scintillator with its maximum luminescence yield at 550 nm that matches well with the quantum efficiency curve of a typical optical CCD. Its scintillation image is not as diffuse as using phosphor materials, thus very high spatial resolution can be achieved and is only limited by the numerical aperture of the lens and/or the pixilation of the CCD camera. A similar imaging system used on the LCLS X-Ray Pump/Probe (XPP) instrument was demonstrated to have achieved 2 μm resolutions in user experiments with YAG:Ce screen is positioned with it surface normal parallel to the FEL beam for obtaining high resolution. For short wavelength photons a thickness of about 20 μm is optimal for high resolution with sufficient florescence yield. The mirror is oriented at 45°, and is made of an aluminized thin Si_3N_4 membrane which is partially transmissive to hard x-rays to permit simultaneous operation with multiple imaging systems or other beam diagnostics.

The damage calculation for the YAG:Ce screen is shown in Figure 8.23, where the energy deposited per atom is calculated based on the LCLS-II FEL beam divergence, total energy, and assumed location of the Direct Imager in the front-end-enclosure from the source. Certain attenuation is needed to reduce the energy deposition to below 100 meV/atom to protect the screen from damage by prolonged FEL exposure. This attenuation will be provided by the solid attenuators for hard x-rays above 2 keV and the gas attenuator for soft x-rays below 2 keV.

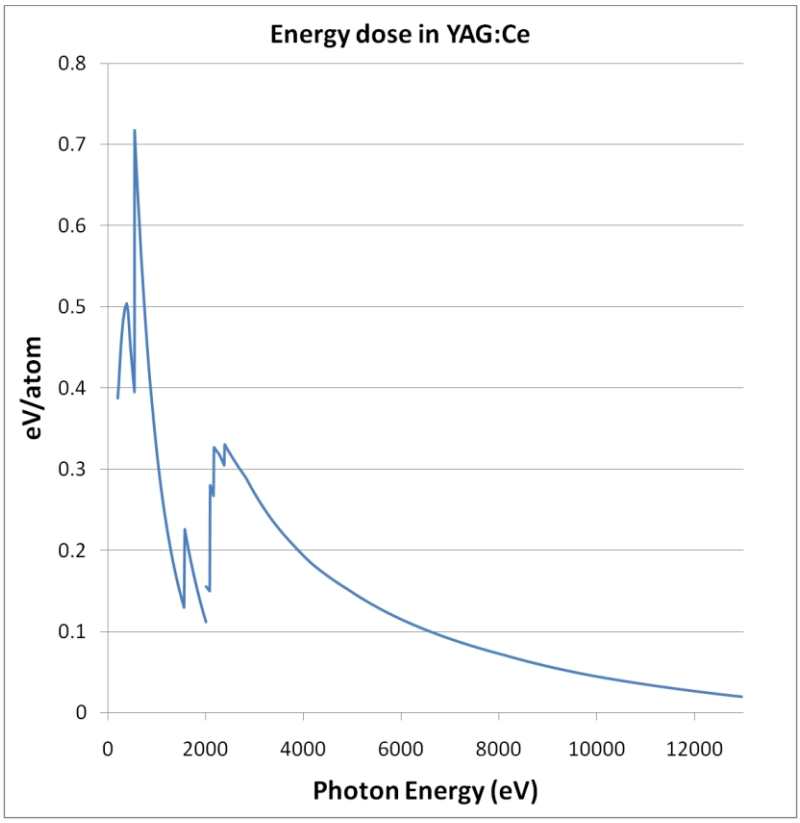

Figure 8.23. Energy deposited in YAG:Ce screen at its designed location by the full LCLS-II beam.

An optical pixelated camera having > 1 megapixels, more than 10 bit grey-levels, and capable of high frame rate (up to 120 Hz) will be used along with a zoom lens (> 10x magnification) which is mounted on a height adjustable fixture. This optical design allows the Direct Imager to operate in two working distances with continually variable FOVs ranging from 50 mm to 0.5 mm, and resolutions from 100 μm to 2.2 μm. Note that the single-line pair resolution is about a factor of two smaller the resolution number stated above.

8.4.10 Mirror Systems

The principal function of the mirror systems is to transport the FEL radiation to the experimental end-stations with a minimum loss of flux and distortion of the wave front. The mirrors also deflect the FEL beam out of the cone of bremsstrahlung radiation and cut off the high energy harmonics of the FEL and spontaneous radiation. The two principle challenges for the x-ray optical systems are delivering extremely high peak power and minimizing the wave front distortions.

8.4.10.1 Optical Damage

The time averaged power in the FEL beam is modest, but the energy in a single pulse can be quite large and the absorbed energy from a single pulse can take many materials over their melting temperatures. At an absorbed power above that to take a material to its melting point ablation can occur. Low Z, refractory materials have been used in the LCLS for both normal incident absorber and optical coatings to minimize the absorbed power and for a large energy to take the materials to their melt temperatures. A similar approach will be used with LCLS-II.

The mirrors must be operated below their damage threshold. For total external reflection below the critical angle the 1/e penetration depth of the evanescent wave is given 11

$$\boldsymbol{d_{1/e} = \frac{\lambda\zeta}{4\pi\beta}} \tag{1}$$

with

$$\boldsymbol{\zeta = \sqrt{0.5(sin^2\theta - 2\delta + \sqrt{(sin^2\theta - 2\delta)^2 + 4\beta^2}\,)}} \tag{2}$$

and δ and β are the real and imaginary parts of the index of refraction, n

$$\boldsymbol{n = 1 - \delta - i\beta} \tag{3}$$

The absorbed dose per atom at the mirror surface is given by

$$\boldsymbol{D_{atom} = \frac{(1-R)P_d\, sin\theta}{d_{1/e}\rho_{atom}}} \tag{4}$$

With P_d peak normal incidence power density, ρ_{atom} number of atoms per unit volume and θ the grazing angle of incidence. The evanescent wave has a depth of ~3.5nm for the cases of interest with LCLS-II and some of the energy is transported out of the absorbing volume on a very short time scale by fast photoelectrons [12] but this decrease in the deposited power is not considered in the analysis below.

The maximum dose at the surface of a mirror is at the critical energy for a given energy (see Figure 8.24). The dose monotonically decreases from the maxima as the grazing angle gets smaller or quickly approaches that at normal incidence as angle gets larger.

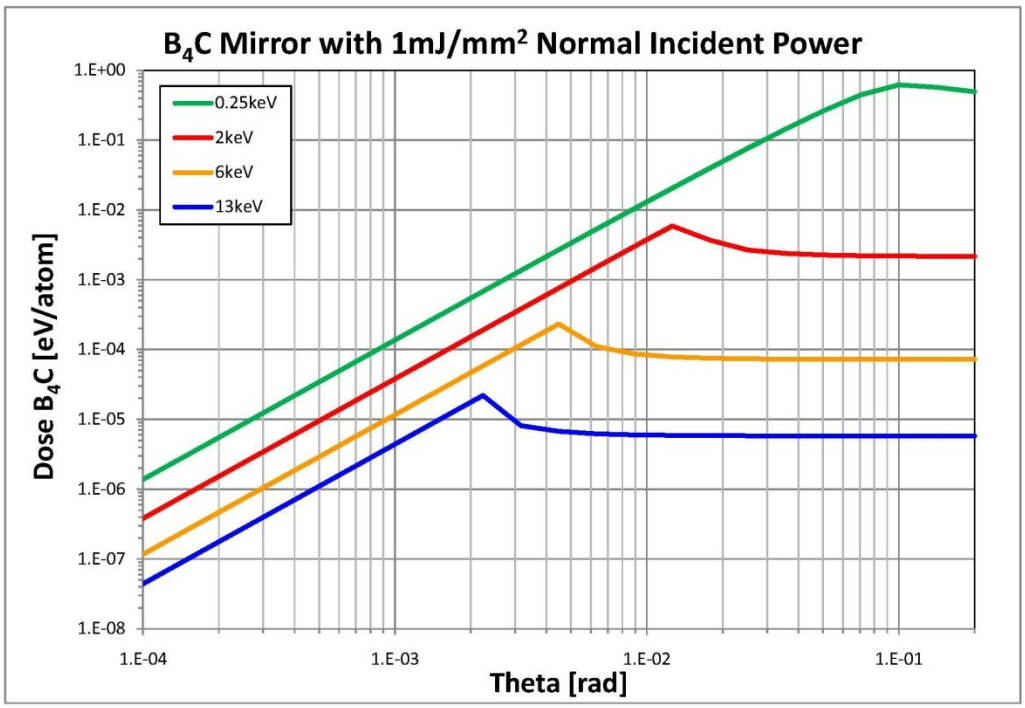

Figure 8.24. Dose at surface of a B_4C mirror for 1mJ/mm2 normal incident power as a function grazing incidence.

The acceptance of mirrors in their tangential dimension is important for optical system throughput, intensity stability given positional jitter, and diffraction effects of a finite aperture. (It is assumed the sagittal acceptance of the mirror is large relative to the beam size.) The effective aperture mirror is the length, *l*, times the sin of the grazing angle, θ, as the grazing angle is small it is ~*l* θ. The (1-R) term in equation 4 is essentially linear with θ below the critical angle, so the dose below the critical angle goes as the square of the normal incidence power density (note the example in Figure 8.24). The normal incidence power density goes as $1/r^2$. If the acceptance of a mirror in the tangential direction is held constant as the distance from the source changed the dose on the surface is essentially constant up to the critical angle. The advantages of the moving the first mirror as far upstream as possible are: 1) higher reflectivities at the lower angles of incidence, 2) less wave-front distortion for a given figure error (see Section 8.4.10.2). The limit at the high angle end is the reflectivity cutoff at the critical angle. There are limits for operating mirrors at low angles: 1) the capability of the mirror to cut off higher harmonics and spontaneous radiation, 2) deflecting the beam a sufficient angle to achieve adequate separation of experimental stations. Once the grazing angle limit is defined the distance from the source can be set to ensure the survivability of the optical coating.

8.4.10.2 Figure error requirements for x-ray beam transport mirrors

The transport Optics Mirror System (OMS) strives to minimally degrade the intrinsic characteristics of the LCLS FEL beam. It should preserve the LCLS Wavefront (WF) quality and minimize decoherence effects. The quality of the optics is often characterized by RMS WF distortions σ_{rms} expressed in terms of wavelength's fraction e.g. 1/5, 1/10. Specular reflectivity or focusability – the Strehl Ratio (SR)13]are related in a simply way to rms WF distortion σ_{rms}:

$$SR \approx e^{-(2\pi\sigma_{rms})^2} \quad (5)$$

The Strehl Ratio is defined as a ratio of the intensity in the focus, with and without wavefront distortions.

For a "well-corrected" optical system, the SR should exceed 0.8. This requirement is called the Maréchal Criterion. [14] Corresponding rms wavefront distortion may not exceed λ/14 rms. In turn, the distortion can be related to path length errors caused by surface height differences in a grazing-incidence geometry: $\sigma_{rms}=2\alpha h_{rms}/\lambda$ here h_{rms} is the rms surface height error, λ is the wavelength of the incident FEL light and α is the grazing-incidence angle. Finally, since the transport optics system may consist of multiple optical elements, the total height error requirement must be apportioned among the different elements. The result is:

$$h_{rms} < \frac{\lambda}{14 \cdot \sqrt{N} \cdot 2\alpha} \tag{6}$$

where N is the number of optical elements in the OMS. The rms height errors can be seen as the most important parameter characterizing OMS quality. For the incident angle which is a fraction (e.g. 1/3) of the critical angle it follows from the equation (2) that the h_{rms} error should be in order of or smaller than a nanometer.

8.4.10.3 Soft X-ray Mirrors

To minimize wave-front distortions and maximize throughput, the number of mirrors should be minimized in the optical layout. Two mirrors are required before the shielding separating the accelerator from the experimental hall, the first to deflect the beam out of the collimated cone bremsstrahlung and spontaneous radiation and the second to direct the beam out of the scattered bremsstrahlung and secondary radiation from pair production in the first mirror or other primary absorbers. In addition these mirrors will horizontally separate the two soft x-ray end stations. A Kirkpatrick-Baez (K-B) pair of mirrors to focus the FEL beam on a sample and optics to monochromatize the beam are part of the AMO and SXR instruments, but these are not part of LCLS-II scope. It is not possible to achieve the required figure errors currently with aspherical mirrors, so it is assumed that mirrors will be flats, flats bent to cylinders that focus in only one dimension. The present state of art is for mirrors with the substrate length limited to 800 mm. The clear aperture having figure error specification < 1nm rms is in the central 300 mm and having an error of 1-2 nm rms out to a 750 mm aperture. The XFEL community is working with vendors to achieve figure error < 1nm rms over larger clear apertures and on longer substrates. The combined effect of beam cutting and wave front distortion on specular reflectivity of system of consisting of three mirrors is illustrated in Figure 8.25. The specular reflectivity in the left part of Figure 8.25 is calculated for four different rms figure errors: 0.5 nm, 1 nm, 2 nm and 3 nm. In this case the figure error has the same value over the full length of the 800 mm long mirror. The right part of Figure 8.25 illustrates the influence of the beam divergence on the SR for mirrors at the present state of the art. In this case the mirrors have 1 nm rms figure error in the central 300 mm part and an error of 2 nm out to 800 mm aperture.

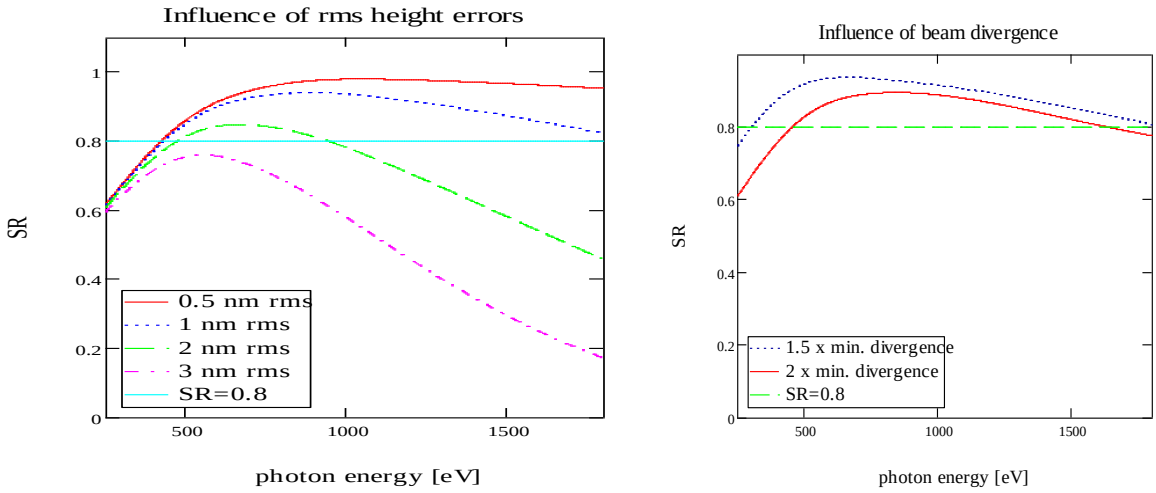

Figure 8.25. The combined effect of beam cutting and wave front distortion on specular reflectivity. Left figure as function of height errors. Right figure with beam divergence.

In LCLS, both B_4C, for Soft X-ray Offset Mirror System (SOMS) and SiC for the Hard X-ray Offset Mirror System (HOMS) mirrors were used as optical coatings. SiC potentially can be used again with the hard x-ray beam optics, but the soft x-ray range now goes from 250eV to 2000eV and includes the Carbon k-edge at 285eV, so B_4C cannot solely be used at this energy. There are two primary options to pursue: 1) Use mirrors with two optical coatings, one stripe of B_4C and a second of Si; or 2) Use a single optical coating of B. The reflectivities of these three materials are compared in Figure 8.26. The reflectivity of Si is for thick optical coating, that is a solid Si mirror. The reflectivities for B_4C and B are for a 50 nm optical coating on a Si substrate. All reflectivities assume o.4 nm rms roughness and do not including a native oxide layer.

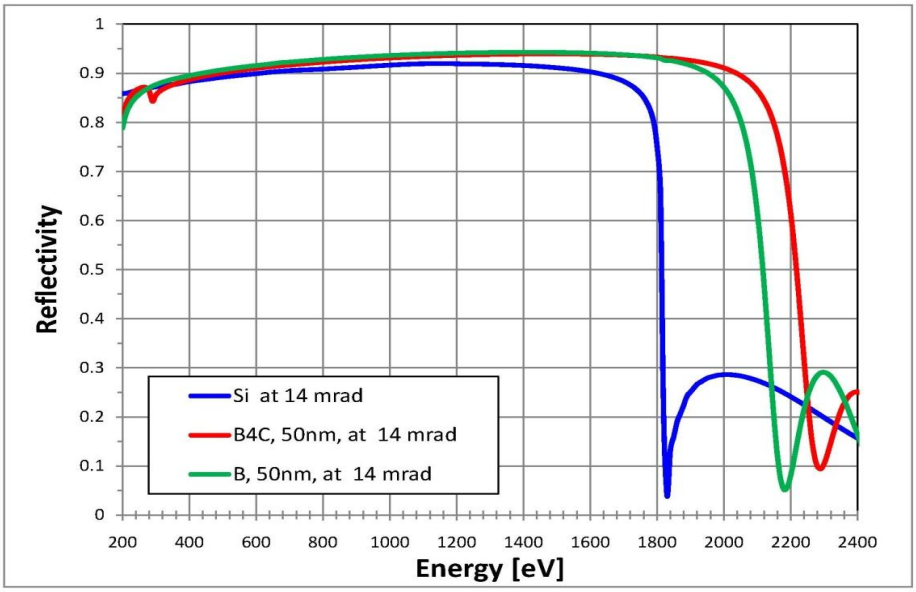

Figure 8.26. Reflectivities of Si, B_4C and B at 14mrad grazing incidence.

The advantages of Si optics are: It is one of the preferred materials for fabrication super smooth mirrors and requires no optical coating after figuring, which always degrades the figure to some extent. It has no structure at the Carbon k-edge. Though silicon has a native oxide layer, it is very stable. Silicon's

disadvantages are: It has the lowest reflectivity above 400eV and cuts off strongly by 1800 eV, the Si k-edge is at 1840eV. Si, being a heavier element and with lower reflectivity, has higher dose at a given critical angle and energy. Silicon also has a low energy to melting temperature, 0.34eV/atom. At a grazing angle of 14 mrad the dose in Si at the maximum energy per pulse is 0.03 eV/atom at 250 eV. It increased to 0.1 eV/atom at 500 eV. Si will have to be tested to see if it will survive as a long wave length optical surface at the highest fluences form LCLS-II. It is likely to damage at shorter wavelengths, see Figure 8. 27.

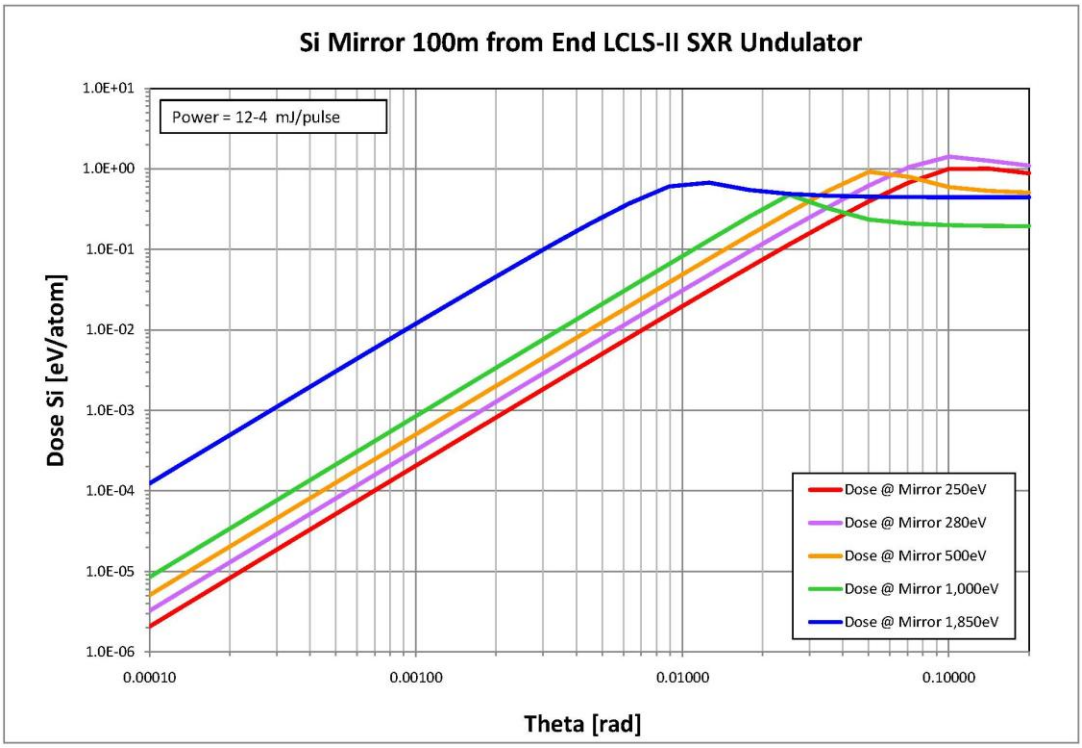

Figure 8. 27. Dose for Si mirror at 100m from the soft x-ray undulator as a function of incidence angle.

B_4C has been well characterized on LCLS-I. It can be deposited on Si substrates, though the optical figure has to be corrected for the stress from the B_4C coating. B_4C forms a minimal oxide layer and can be used of the oxygen K-edge. Above the C k-edge it has good reflectivity to the desired cutoff energy at 14mrad. It has a high energy to melting temperature, 0.63eV/atom. The example of a B_4C mirror at 100m from the undulator is shown in Figure 8.28. Power per pulse and FEL divergence were calculated for the parameters listed. The divergence used for calculating dose is that at saturation. Its principal drawback of B_4C is that it cannot be used at the carbon edge.

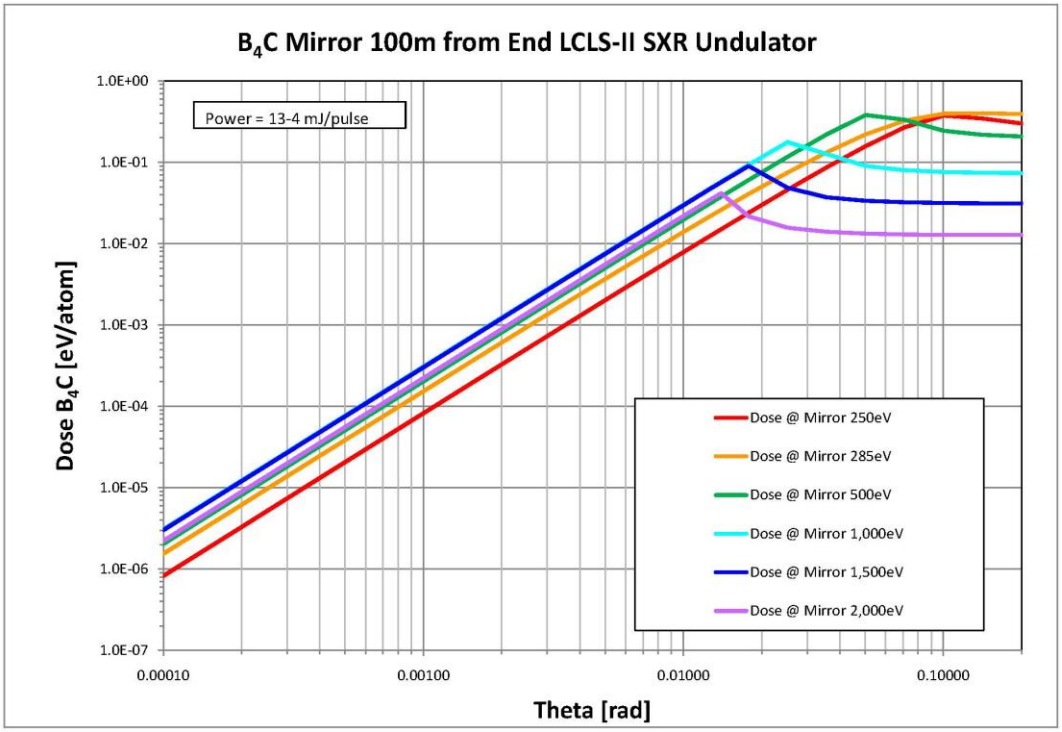

Figure 8.28. Dose for B_4C mirror at 100m from the soft x-ray undulator as a function of incidence angle.

Boron is a potential coating material that covers the entire energy range. It has good reflectivity up to 1800eV then cuts off at a slightly lower energy than B_4C. It is refractory, with an energy to melting temperature of 0.54eV/atom. It forms an oxide layer that is not as stable as the one that forms on silicon. B is not used often in optical coatings and more characterization would be required.

The final focusing mirrors will be at 120 to 130m from the end of the undulator. If these mirrors, which are part of the AMO and SXR systems, are moved as proposed they will be aperture limiting. Replacing or upgrading these mirrors, and the SXR monochromator, for effective operation down to 250 eV is not part of the LCLS-II scope.

8.4.10.4 Hard X-ray Mirrors

The Hard X-ray Offset Mirror System (HOMS) is designed to spatially separate the useful FEL radiation from high-energy spontaneous radiation and bremsstrahlung γ-rays and direct the radiation to an experimental station. The requirement for the LCLS hard x-ray line to cover a range up to 24keV resulted in the choice of SiC at a grazing angle of 1.3mrad for the HOMS mirrors. The LCLS-II hard x-ray mirrors should cut off at 13 keV. To achieve a lower cut off the mirror have to operated at and higher angle. A B_4C optical coating at 2.3mrad has very good reflectivity and a sharp cut off, see Figure 8.29. The LCLS experience shows that silicon mirrors coated with B_4C layer work well for such systems. We show below that, with present technology in hand, B_4C coated mirrors should serve well also for the LCLS-II.

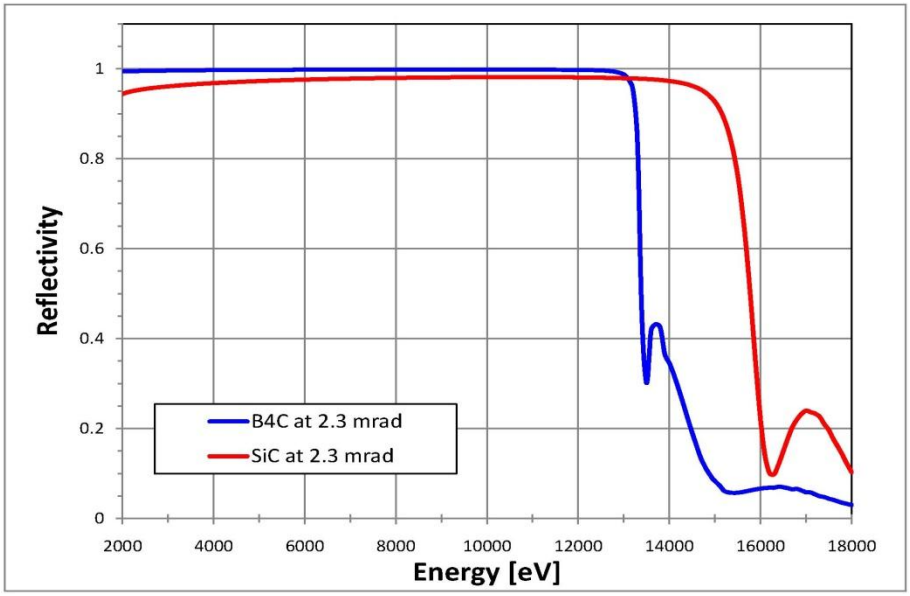

Figure 8.29. Reflectivities of SiC and B_4C 2.3mrad grazing incidence.

Minimizing WF distortions and decoherence effects calls for small grazing incidence angles. On other hand, for a given beam size, shallow incidence angles can cause clipping of the beam by the mirror's edges. In order to minimize this effect one should place the HOMS as close as possible to the end of the undulator.

The combined effect of beam cutting and WF distortion on specular reflectivity is illustrated in Figure 8.30. The SR was calculated for two 800 mm long, Si mirrors, coated with 50nm B_4C layer having 2.27 g/cm^3 density. We assumed the maximum divergence (2 x nominal value) for a given photon energy. The mirrors are located 50 m from the end of hard x-ray undulator. In this case the figure error has the same value over the full length of the 800 mm long mirror.

One can see from this figure that the maximum angle of incidence at 13 keV is about 2.3 mrad. Figure 8.30 also shows that: 1) The optics meets the Maréchal Criterion in the 2000eV 13000 eV energy range if the h_{rms} error is smaller than 1 nm rms; and 2) The degradation of the SR is caused by the cutting the LCLS beam by mirror's edges at the lower energy end by the figure errors at the high energy end.

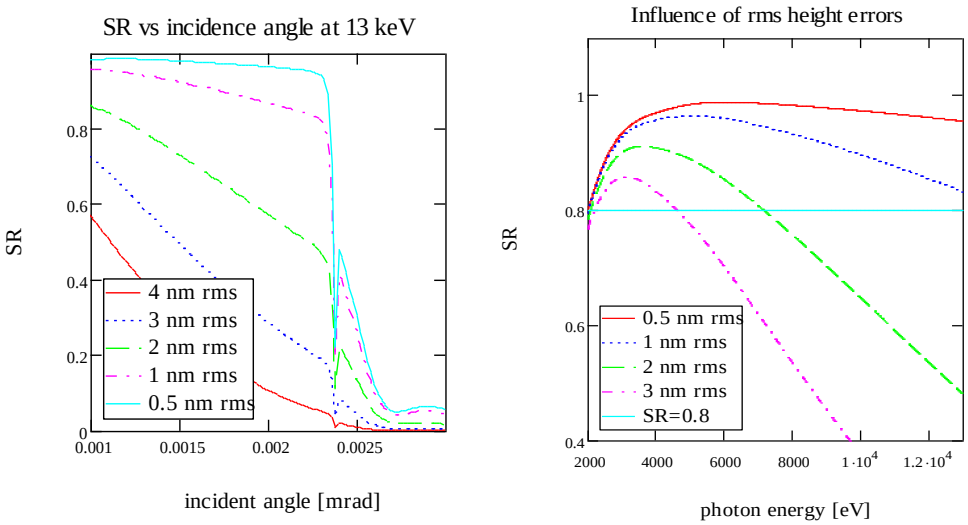

Figure 8.30. The combined effect of WF distortion and beam cutting on the Specular Reflectivity (SR). Left figure shows the dependence of the SR on the incidence angle at 13 keV photon energy. The right figure shows the dependence of the SR on photon energy at the 2.3 mrad incidence angle.

The dependence of the SR on the beam divergence is shown in the left part of Figure 8.31. The mirror that has the figure error of 1 nm rms in the central 300 mm aperture and the 2 nm rms error out to 800 mm aperture. The deviation from the nominal divergence has significant effect mainly in the photon energy range 2 keV – 4 keV.

The right part of Figure 8.31 illustrates the fact that the HOMS performance depends mostly on the surface quality in the central part of the mirror. The plot a) in this figure shows the SR dependence vs. photon energy for the mirror that has the figure error of 1 nm rms in the central 300 mm aperture and the of 2 nm rms error out to 800 mm aperture. Plot b) and c) shows the same dependence for the 800 mm long mirror that has the 1 nm rms and 2 nm rms figure error over the entire length respectively. Clearly, one does not need to impose the 1 nm rms quality over the entire mirror's length.

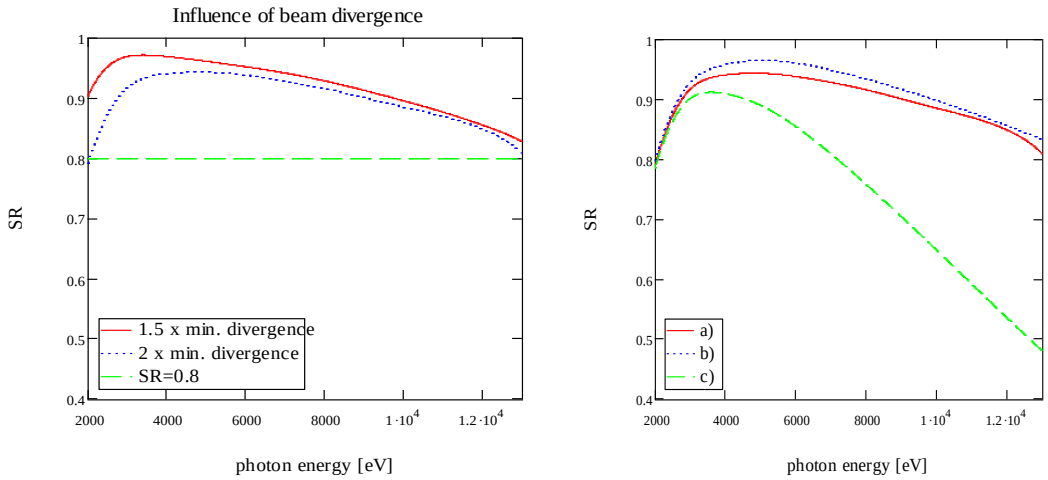

Figure 8.31. Left: the dependence of the Specular Reflectivity (SR), on the beam divergence. Right: dependence of SR on mirror figure error size and tolerances: a) the SR dependence vs. photon energy for the mirror that has the figure error of 1 nm rms in the central 300 mm aperture and the 2 nm rms error out to 800 mm aperture. b) and c) the same dependence for the 800 mm long mirror that has the 1 nm rms and 2 nm rms figure error over the entire length respectively.

In summary the present state of the art of the x-ray mirror technology allows meeting the Maréchal Criterion for well corrected optics in the 2000eV 13000 eV energy range. The maximum energy density deposited in the surface layer of the mirror by the LCLS photon beam occurs at 2 keV photon energy. The instantaneous dose calculated for the nominal divergence, at 2.3 mrad grazing incidence angle, and for the position of the mirror equal to 50 m measured from the undulator end do not exceed 0.001 eV per atom. Such a dose should not create any damage to the mirrors' surface quality.

8.4.10.5 Optical-Mechanical Design

The HOMS opto-mechanical system design approach will have the functionality of the present HOMS system that consists of the five assemblies illustrated in Figure 8.32. The assemblies include the:

- support pedestal and floor anchors
- installation alignment adjustments
- pointing and centering devices
- mirror and mount assembly
- vacuum chamber

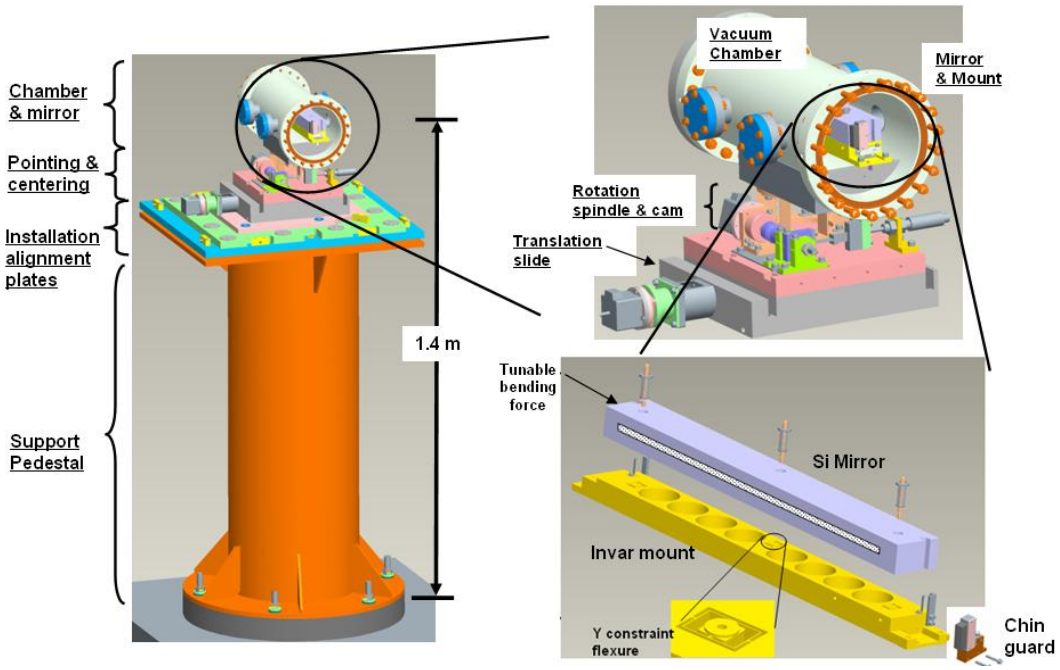

Figure 8.32. Assemblies that constitute each HOMS and SOMS mirror system.

The basic functional requirements for the optical mechanical systems for LCLS-II are very similar to the existing LCLS-I systems: support the polished substrates with minimal figure distortion and provide dynamic controls for both steering the FEL beam and correcting components of the residual figure errors. At the time, the demanding performance requirements of the LCLS-I systems pushed the existing substrate manufacturing and mirror component systems beyond their previous limits. The LCLS-II performance requirements necessitate further extending these limits, both in terms of tighter fabrication and assembly tolerances as well applying these requirements to significantly larger optics. It is expected that these capabilities in conjunction with the appropriate metrology will continue to evolve in response to the growing community need.

A CAD model representation of the LCLS-I system is shown in Figure 8.32. The LCLS-II mechanical design will be and evolutionary combination of the merits of the existing design, elements of the LCLS-I KB mirror bending system, and new developments in figure compensation technology (e.g. piezo actuators). Additionally, it is apparent from LCLS-I operation that these mirror figure correction schemes must be well characterized and implemented with some form of beam based measurement and compensation paradigm.

8.4.11 Spectrometers

Spectrometer instruments are used to characterize the distribution of photon intensity as a function of photon energy. Such measurements are valuable with respect to both the FEL beam and the spontaneous undulator radiation. Separate instruments will operate on the hard x-ray and soft x-ray beam lines. Two categories of spectrometer measurements are anticipated: FEL spectra and spontaneous undulator radiation spectra used for undulator alignment.

FEL spectra are intended to resolve the natural emission band of an FEL pulse. Ideally, the spectrometer should be tunable, and cover the entire photon energy tuning range available for the emitted FEL fundamental. Over at least part of that range, the instrument should be capable of single-shot measurements. FEL spectrometer measurements tend to be "invasive", but this is deemed acceptable.

To achieve SASE lasing the magnetic deflections parameter, K, must be set so the fundamental energy of each undulator segment has a distribution that is less than the energy spread, ρ, induced in the electron beam by lasing. On LCLS a K Mono was developed for characterizing the undulators. This instrument operated at a fixed energy requiring the electron energy to be scanned to get the spectra from either spontaneous or FEL radiation. On LCLS-II the spectrometers will be used which can record the spectra from single electron pulses. The spectra are taken at the high-photon-energy edge of the undulator fundamental, or at the higher odd harmonics. Interpretation of the spectra permits precise vertical centering of the segment magnetic arrays around the electron beam, as well as characterization of the magnetic field strength, for use in "matching" to the other undulator segments. These measurements are also invasive.

8.4.11.1 Soft X-Ray Spectrometer

The SXR instrument will serve as the soft x-ray spectrometer for LCLS-II. This instrument is currently employed at NEH Hutch 2, but will move eventually to LCLS-II. It can be used as both a monochromator and as a spectrometer. In spectrometer mode, the SXR optical system is schematically illustrated in Figure 8.33.

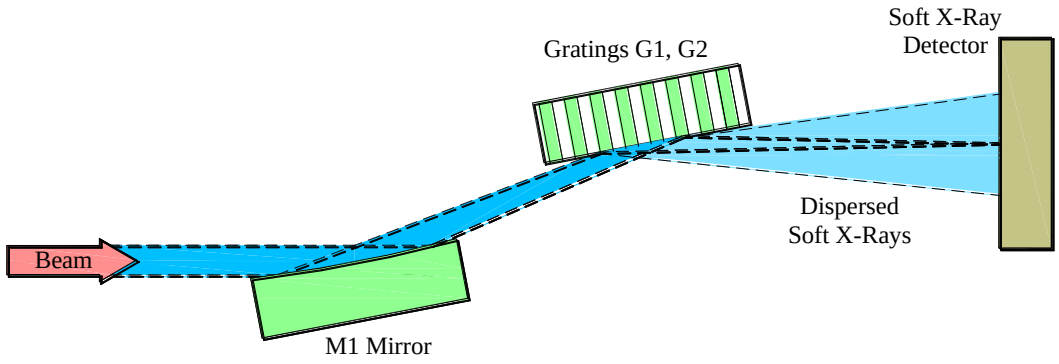

Figure 8.33. Schematic illustration of the SXR instrument optical system in spectrometer mode.

Incoming FEL or spontaneous radiation is first incident on the spherical M1 mirror, which produces a converging beam in the vertical. The gratings diffract that beam onto the exit slit location, where the exit slit is replaced by a two-dimensional, position-sensitive detector.

Single-shot spectrometer measurements for the current LCLS FEL are routinely obtained with the SXR instrument, with a resolution of ~3000 (photon energy E/ΔE). However, for use at LCLS-II, some extensions to the existing instrument may be necessary. A more sensitive detector will be developed capable of recording single shot spontaneous radiation spectra from single undulator segments. In addition, modifications may be needed to extend the operating photon energy range of the instrument to the entire soft x-ray range at LCLS-II.

8.4.11.2 Hard X-Ray Spectrometer

The hard x-ray spectrometer is based upon the scheme successfully demonstrated by Yabashi and Hastings [15] and illustrated in Figure 8.34. The incoming beam is initially incident on an elliptical cylinder focusing mirror, which produces a more strongly converging, and then diverging, beam of x-rays. The diverging beam is then dispersed by Bragg diffraction from a flat, perfect single crystal. This dispersed beam finally falls on a position-sensitive x-ray detector.

For the setup demonstrated at SPring-8, a monochromatic incident photon beam of divergence 0.3 μrad, at a photon energy of E = 10 keV, was utilized. The analyzer crystal received an incident beam of divergence 2.3 mrad from the focusing mirror, and utilized a symmetric Si(555) reflection, at a Bragg angle of 81.3°. The demonstrated spectrometer photon energy resolution was ΔE = 13.1 meV, with a single-shot total photon energy range of ΔE_w = 3.5 eV.

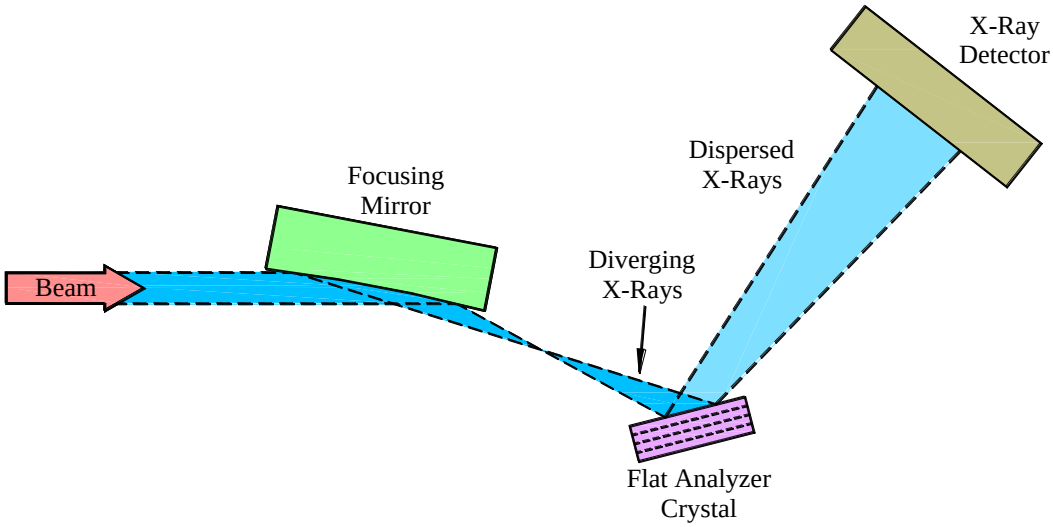

Figure 8.34. Schematic optical layout of a single-shot x-ray spectrometer, similar to that demonstrated by [15]

For FEL spectrometer measurements at LCLS-II, it may be desirable to increase the single-shot total photon energy range, ΔE_w, ~10 times over that demonstrated in the SPring-8 set up, to record the entire SASE FEL spectrum in a single shot. $\Delta E_w/E$ depends upon the divergence produced by the focusing mirror and the Bragg angle utilized. If a focusing mirror similar to that used at SPring-8 is assumed, a Bragg angle of ~30° is required at E = 10 keV to produce ΔE_w = 35 eV. Such geometry is illustrated in Figure 8.34, and would probably occupy ~2 m along the beam direction.

This geometry may also be useful at a number of different photon energies, even without moving the optical elements or detector. A flat Si(111) crystal was utilized at SPring-8, but operated at a higher harmonic reflection, the Si(555), for incident photons at 10 keV. However, by utilizing other silicon reflections, Si(111), Si(333), and Si(444), photon energies of 2 keV, 6 keV, and 8 keV can be analyzed. For these other photon energies, both ΔE_w and the spectrometer energy resolution, ΔE, change with the different Bragg reflections.

For general coverage of the LCLS-II hard x-ray photon energy range, tracking rotation of the analyzer crystal and detector will be employed, together with interchangeable analyzer crystals. Such variability also permits greater control of the single-shot total photon energy range, ΔE_w, and the spectrometer energy resolution, ΔE.

For the second category of spectrometer measurements, of spontaneous radiation from a single undulator segment, a modified spectrometer set up is required, due to the angle/photon-energy correlation of the spontaneous radiation at the high-photon-energy edge of the fundamental. The focusing mirror in the original set up could be withdrawn from the beam path, and the incident photon beam received directly by the flat analyzer crystal. Alternatively, if a bent mirror were used to form the

diverging beam, returning the mirror to a flat figure in situ would convert the spectrometer for single-undulator-segment measurements.

For a given photon energy of interest, an appropriate setting of the analyzer crystal Bragg angle and x-ray detector position is made and fixed. Multi-shot data acquisition is used to generate the spectrum, following a procedure similar to that used with the current *K-Mono* at LCLS.

8.4.12 Collimator System

A system of collimators around the optical paths defined by mirrors and undulators, confines the FEL beam and insures that no significant amounts of bremsstrahlung or hard spontaneous radiation can reach the interior of the experimental hall.

To block the FEL beam, the collimator design uses the same concept as the stoppers. Below about 600 eV (see Figure 8.1), the FEL beam may be sufficiently intense that the dose to B_4C would exceed the maximum safe working dose of 0.1 eV/atom. To remove the possibility of a burning through, each collimator includes an air gap behind a B_4C surface. The air gap is connected to ambient air and insures that even in the unexpected case that the beam burns through the B_4C, the air in the gap will block the beam. The range of 600 eV photons in ambient air is less than 1 mm.

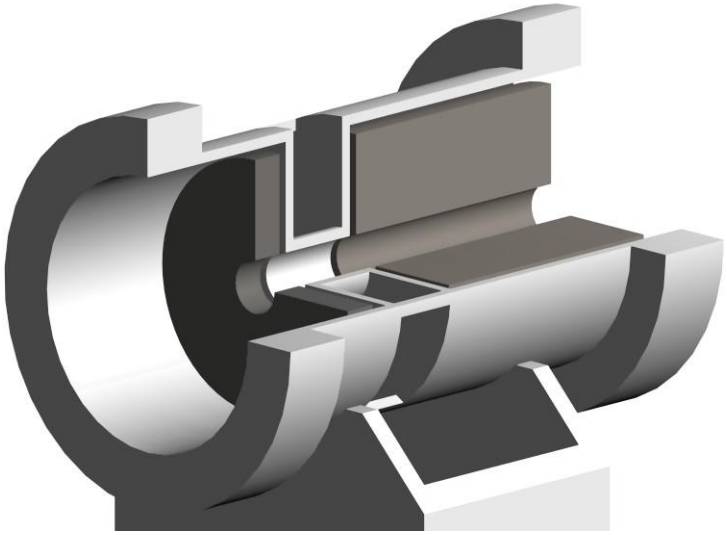

Figure 8.35. Collimator with air gap.

8.4.13 Stoppers

There will be photon beam stoppers and shutters to block the FEL beam at critical points along the beam path. Personnel Protection System (PPS) stoppers will be designed to indefinitely absorb the maximum credible beam the LCLS-II system. The PPS stoppers, in conjunction with collimators, are to insure that no significant bremsstrahlung, and hard spontaneous radiation, scattering off mirrors or other components, can reach the floor of the Experimental Hall. To block the beam, the stoppers uses the concept developed for LCLS-I collimators on the SXR instrument. An air gap, with a path open to ambient air, located behind a primary B_4C absorber insures that even in the unexpected case that the beam burns through the B_4C, the air gap will attenuate the FEL beam to a safe fluence. A tungsten block after the air gap absorbs the hard spontaneous and bremsstrahlung radiation. PPS stoppers are configured as redundant pairs. Where required PPS stoppers will be preceded by an MPS shutter designed to take the maximum operational beam, see Figure 8.36.

Machine Protection System (MPS) and experimental shutters must be capable of absorbing the maximum operating FEL beam for finite time. The potential for the FEL beam to damage the primary absorbing material of a stopper or shutter is the greatest at low photon energy due to the short absorption lengths. The requirement for a MPS component is less stringent than for a PPS one and maintenance procedures are less involved. The absorbing material in these shutters may be periodically replenished or replaced. See Section 8.2.2 for the discussion of damage.

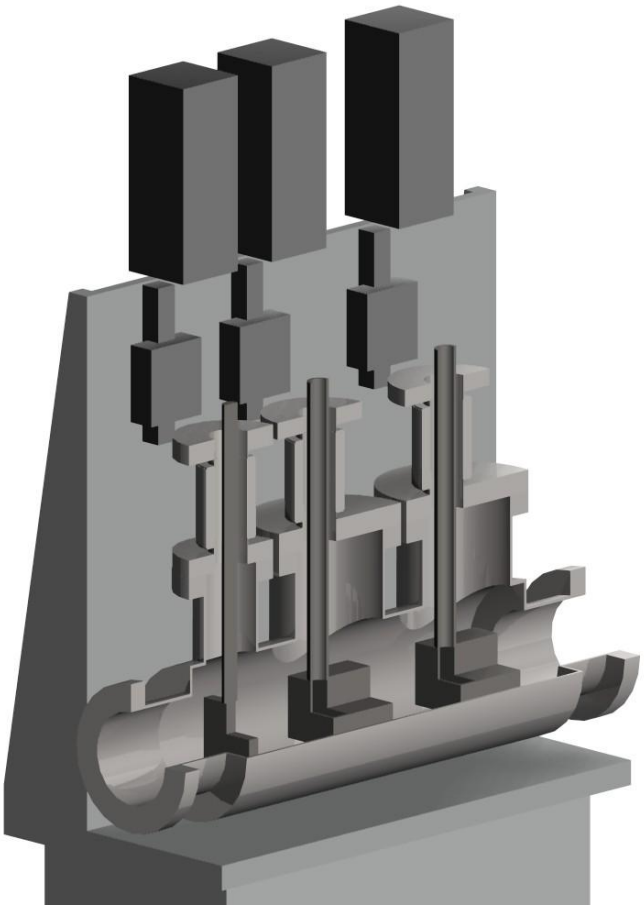

Figure 8.36. MPS shutter followed by dual B4C-air-tungsten PPS stoppers. The FEL beam goes from left to right.

8.5 Summary

The X-ray Transport, Optics and Diagnostics systems for LCLS-II are well defined in this chapter. LCLS-II will build on the knowledge and proven designs of the LCLS. The experience from the LCLS has greatly improved the confidence in the systems that work and also with what should be done to systems that need improvements. The expanded spectral range and particularly the increase in pulse energy at long wavelengths will require development of larger optics with new coatings and a number of changes in diagnostic systems.

The areas where LCLS-II requirements result in significant changes in optics and diagnostic systems are:

- The optics for LCLS-II will be longer than those presently in use at LCLS. They are required to collect full beam at the low energy end of the spectral range. Significant development work is required. This will include both working with venders to deliver long mirrors with the high figure

quality that is required and developing the methods for mounting and maintaining the mirror figure in the operational environment.

- The range of the gas energy monitor will be extended to 13keV, the upper limit of the hard x-ray beamline. The effort will be limited as there is an alternate solution, the solid foil energy monitors used on LUSI, which work well at short wavelengths.
- The multi-pulse damage threshold of B_4C will be more accurately defined and measurements extended down to 250eV. These measurements will be made at both LCLS and FLASH.
- A hard x-ray spectrometer will be developed based on an existing design.
- On LCLS-II there will also be work demonstrating that cryogenic radiometers work throughout the x-ray region for absolute energy calibration.

Though there are changes there are no major advances required to successfully implement the XTOD systems for LCLS-II.

8.6 References

1. Hau-Riege, S P; London, R A; Graf, A; Baker, S L; Soufli, R; Sobierajski, R; Burian, T; Chalupsky, J; Juha, L; Gaudin, J; Krzywinski, J; Moeller, S; Messerschmidt, M; Bozek, J; Bostedt, C. *Interaction of short x-ray pulses with low-Z x-ray optics materials at the LCLS free-electron laser* Optics Express, Vol. 18 Issue 23, pp.23933-23938 (2010).
2. Z, Huang, K-J. Kim, Physical Review Special Topics – Accelerators and Beams **10**, 034801 (2007).
3 Warburton W., Pianetta P., Nucl. Instr. and Meth. A, 291 350 (1990)
4 S. Hau-Riege et al. J Appl. Phys. **103**, 053306 (2008)
5. M. Nagano et al., Astropart. Phys. **22**, 235, (2004)
6. Tiedtke et al., J. Appl. Phys. **103**, 094511 (2008)
7. Tiedtke et al., J. Appl. Phys. **103**, 094511 (2008)
8. Kato et al AIP Conf. Proc. **879**, 1129 (2007)
9 Saito et al, Metrologia 47 21-23 (2010)
10. Rabus et al., Applied Optics Vol. 36, No. 22 (1997)
11 B. L. Henke, P. Lee, T. J. Tanaka, R. L. Shimabukuro, B. K. Fujikawa, *Low-Energy X-ray Interaction Coefficients: Photoabsorption, Scattering, and Reflection*, Atomic Data and Nuclear Tables, **27**, 1-144 (1982).
12 J. Chalupsky et al., APL **95**, 031111(2009)
13 James C. Wyant and Katherine Creath in Applied Optics and Optical Engineering, Volume XI, edited by Robert R. Shannon and James C. Wyant (Academic Press, San Diego, 1992) and Max Born and Emil Wolf, Principles of Optics, 7th ed. (Cambridge University Press, Cambridge, 1999).
14 A.Maréchal, Revue d'Optique, Theorique et Instrumentale **26**, 257 (1947).
15 Makina Yabashi, Jerome B. Hastings, Max S. Zolotorev, Hidekazu Mimura, Hirokatsu Yumoto, Satoshi Matsuyama, Kazuto Yamauchi, and Tetsuya Ishikawa, *Single-Shot Spectrometry for X-Ray Free-Electron Lasers*, Physical Review Letters **97**, 084802 (2006)

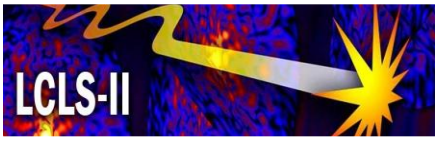

9 Experimental Facilities

Technical Synopsis

The X-ray Experimental Systems, XES, will be housed in the LCLS-II Experimental Hall (EH2) a two-level cavern, which will provide space for four x-ray instruments in addition to a setup area, laboratory space and control rooms. Two soft x-ray and two hard x-ray beam paths enter the hall from the x-ray front end. The four x-ray instruments are arranged sequentially. The Atomic, Molecular and Optical Science (AMO) and Soft X-ray (SXR) instruments will be transferred from the LCLS Near Experimental Hall (NEH) to the LCLS-II Experimental Hall (EH2). Two hard x-ray stations will be added in the future. The laser systems providing optical beams to the x-ray instruments will reside in a laser hall on the second floor and a timing system will provide relative electron beam arrival time at the dump.

9.1 Introduction

The LCLS-II Experimental Hall (EH2) is in a cavern type chamber designed to support four experimental stations, supplied with Free Electron Laser (FEL) x-rays from two undulator sources. It is located just to the southeast of the existing LCLS NEH. Though the buildings are separate, it will be very easy to travel between these halls. The EH2 hall will have two levels: on the lower level is the experimental floor, setup space and control areas; on the mezzanine are laser labs, sample prep lab, electronics racks and additional setup space. The control areas and ancillary services will be in alcoves off the main cavern. The existing AMO and SXR instruments will be moved into this new hall. While the new hard x-ray experimental stations themselves lie outside the scope of the LCLS-II Project, some assumptions about their basic layout and space requirements were used to define the requirements of the hall. These assumptions are based largely on the existing LCLS experimental stations, and experience with them to date.

The two undulator sources are separated in the undulator tunnel by 2.5m and since the grazing-incidence optics used for LCLS-II x-ray beams create only small angular deflections of the beams, the stations must be arranged sequentially in the experimental hall, rather than side by side. A long cavern type hall allows for a large space for each experimental station. The hall is 80m long by 14m wide with the control rooms in alcoves. This leaves area 20 m long by roughly 11 m wide on average for each of the four EH2 experimental stations. This area is larger than the LCLS stations in the NEH, similar to some of the stations in the FEH. The width of the cavern is the same as the existing Far Experimental Hall (FEH). The mezzanine will be supported from the walls so there will be no physical barriers at the experimental level. The space can be allocated as instruments are developed.

9.2 Layout drawing

The experimental stations are located on lower level. The mezzanine contains laser rooms, electronics racks and setup space. There will be elevator service between the levels. Both the experimental floor and the mezzanine can be accessed by ramps from the outside, for moving large or heavy items .

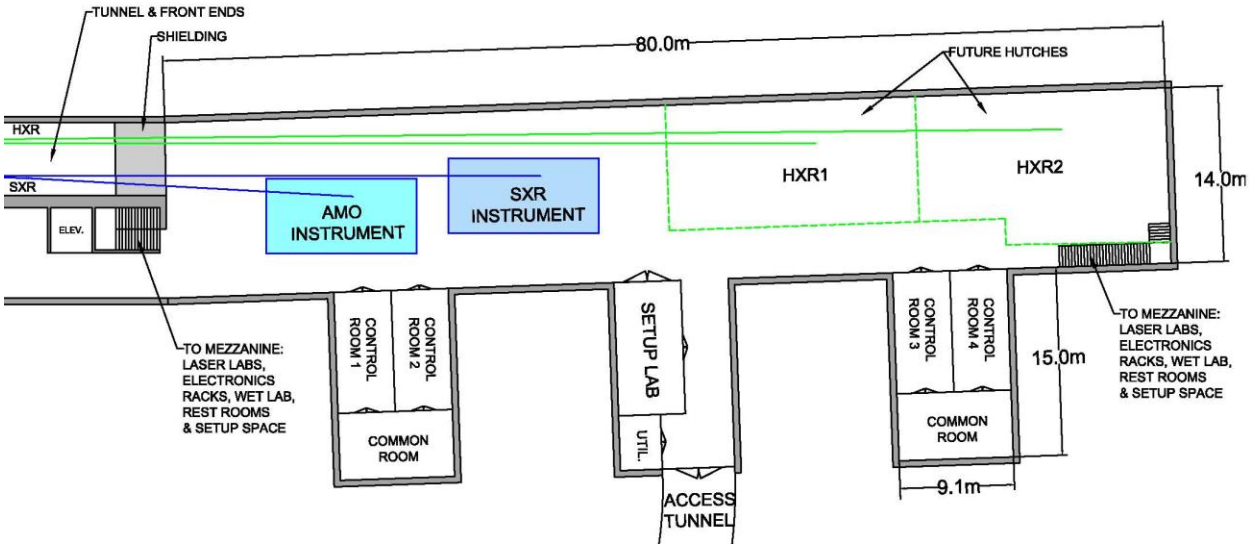

Figure 9.1. Layout for the LCLS-II cavern type Experimental Hall, Level 1, Experimental Areas.

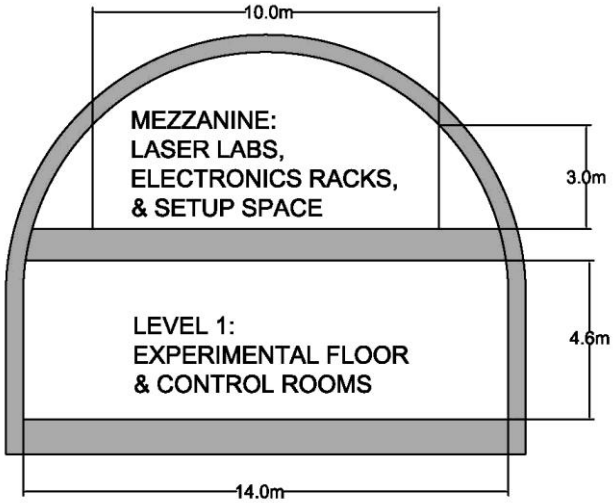

Figure 9.2. Cross section of LCLS-II cavern type Experimental Hall.

9.3 Description of the building layout

Figure 9.1 shows the EH2 experimental floor of the hall. Beam paths are shown entering the hall from the FEE at the upper left. The uppermost path (along the north side of the Hall) is the hard x-ray beam path, leading to two hard x-ray experimental hutches in the upper right part of the figure. The hard x-ray beamline will be split using mirrors. However, the hutches and stations are only conceptual space holders; they are not included in the LCLS-II project.

Two soft x-ray beam paths are shown leading to two soft x-ray experimental stations in the upper left area of the figure. Since the photon energy range of these beam lines will be limited to <2 keV, it is anticipated that no radiation-shielding hutches will be required.

Experience with LCLS has shown that that users will bring a great variety of experimental chambers and sample environments to be installed at LCLS-II. For best efficiency this instrumentation needs to be set up and tested carefully, immediately before use at the beamlines. There is a large setup space at the experimental level and additional space on the mezzanine with elevator access to main level (and access by ramps via the outside). On the mezzanine there will also be a sample preparation lab and rest rooms. Crane coverage over the left (west) half of the EH2 will expedite installation of the large chambers typical of soft x-ray instruments.

LCLS experience has also shown the wisdom of having dedicated space for optical lasers for each x-ray experimental station, close to the station but isolated from it. This allows the optical lasers to be adjusted and tested safely while simultaneously allowing access to the x-ray stations. There will be two laser labs on the mezzanine, one to service the two soft x-ray instruments and the other to service the future hard x-ray instruments. The mezzanine floor will meet the stability requirements for the laser labs. Laser beams will be brought down to optical tables near each experimental station. These tables will support laser elements that must be near the stations, such as compressors and diagnostics. Some form of laser shielding will certainly be needed around these stations, but it will be easily reconfigurable.

The control cabins for the experimental stations will be located in alcoves off of the main cavern. The final configuration of the control areas should build on the experience of initial LCLS experiments, which involved large experimental teams, significant preparations time, and short experiments. Shown are four control cabins with two shared common rooms for meetings or a quiet area to analyze data. The

walls to these control cabins should not be structural elements, to allow for changes as dictated by changes in the style of LCLS experiments.

Figure 9.2 shows a cross section of the main cavern. The mezzanine will span the width of the cavern. Most of the instrument racks associated with the stations are also located on this level, along with server racks for a limited amount of local data storage. Some experimental equipment such as large vacuum pumps will also be located on this floor to free up valuable space and isolate noise. This floor also contains specialized setup lab space, including a small chemistry lab for sample preparation and rest rooms.

There is ramp access to from outside to both levels of the EH2, by which equipment can rolled to the experiment stations or labs. Access between the experimental floor and the mezzanine can also be achieved by way of two staircases and an elevator. The EH2 experimental floor will have a temperature stability of $\leq \pm 1^\circ$ C and humidity of 50% ± 20%. Local temperature stability is more critical than uniformity over the hall.

9.4 X-ray beam delivery

The LCLS-II Experimental Hall (EH2) provides space and infrastructure for four x-ray instruments. Two of these instruments operate using hard x-rays from the Hard X-ray (HXR) undulator, and two use soft x-rays from the SXR undulator.

In the LCLS-II front end, there are mirrors which deflect the x-ray beams at small horizontal angles before entering the experimental hall. These mirrors are described in detail in Chapter 8. The layout of the x-ray beams is shown in Figure 9.1. Hard and soft x-ray beams enter from the top left and both use an equivalent set of three mirrors. One of the mirrors is insertable so the FEL beam can be directed into one or the other of two branch lines. Thus two soft x-ray and eventually two hard x-ray stations can be serviced. There is 2.5m horizontal displacement from the adjacent hard x-ray beam path to the nearest soft x-ray instrument (the SXR instrument transplanted from NEH). The upstream soft x-ray instrument (the AMO instrument moved from NEH) has about 1.6 m horizontal separation from the SXR x-ray beam path. The two future HXR stations will have a horizontal separation of ~0.9m.

9.5 Move of AMO and SXR instruments

The AMO instrument and the SXR instrument will be moved from the LCLS NEH to the LCLS-II experimental hall. The AMO instrument was the first at the LCLS and has been operating since the fall of 2009. The AMO instrument consists of Kirkpatrick-Baez focusing optics, a high field physics end station and a diagnostics chamber. The instrument has been used to study atomic and molecular samples. In one example, multiphoton absorption processes were observed in neon [1]. The SXR instrument has been in operation since the summer of 2010. The SXR instrument includes a varied-line-spacing grating monochromator and Kirkpatrick-Baez focusing optics, and several experimental chambers which are optimized for different experiments. Chambers are typically installed for a set of experiments and then removed from the instrument. Experiments at SXR have mainly examined different aspects of materials research including surfaces, correlated materials, liquids and magnetism.

All the required experimental infrastructure, including electrical power, cooling water and networking, will be built for the AMO and SXR instruments as well as for the two future hard x-ray instruments. The controls systems for the AMO and SXR instruments will be moved, reconnected and tested.

Since the AMO and SXR instruments use soft x-rays, hutchless operation will be possible because of the short x-ray attenuation lengths at low photon energies. The photon energy range of the LCLS-II soft x-ray

undulator extends to 250 eV, below the current minimum energy of LCLS (480 eV), which will allow the study of elemental absorption edges down to the carbon edge. Personnel protection systems for these stations are included in the LCLS-II Project.

The existing x-ray optics of the AMO and SXR instruments are not optimized for the lowest LCLS-II photon energies. At LCLS-II, these optics will form limiting apertures cutting off the tails of the FEL distribution at the lower energies. In additional, a new low energy grating would be needed for the SXR monochromator to accommodate the extended energy range with the desired resolution and efficiency. The modifications of the AMO and SXR instruments that will be needed to accept the extended energy range of LCLS-II are not included in the LCLS-II scope.

9.6 Laser systems

The laser systems providing optical pump or probe beams to the x-ray hutches will reside in a 10m x 25m laser hall on the second floor – see Figure 9.2 above. This room will house the optical lasers as well as the fiber-optic RF distribution and locking system that synchronizes these laser systems with the FEL. These Ti:sapphire laser systems will generate energetic femtosecond pulses for use in pump probe experiments. For each experimental station, the stretched and amplified pulses will be relay-imaged into a laser safety enclosure on the lower floor near the station, where it will then be recompressed to <50 fs. The pulses can then be used as is or converted in wavelength with either a harmonics package or an Optical Parametric Amplifier (OPA). The desired optical pulses will then be transported from the safety enclosure to the experiment.

The EH2 laser labs will be environmentally controlled, with no windows, and with access control to limit access to the lasers. A temperature stability of ± 1° C and humidity of 50% ± 10% are required. The entrance door will be locked with a magnetic lock that is controlled by a Laser Safety System (LSS). This LSS will be similar to the system used in the NEH laser hall and hutches and will monitor and control laser state and access to the facility.

9.7 Timing

9.7.1 Electron Beam Timing Monitor

The LCLS-II will have the capability for optical pump / x-ray probe experiments with femtosecond resolution. The design of the LCLS-II injector and linac is similar to the LCLS-I and is expected to have similar timing performance, with an electron beam arrival time jitter of 60 femtoseconds RMS relative to a perfect clock. Experiments can be performed at higher resolution by measuring the shot to shot timing of the electron beam and correcting the data offline.

The LCLS-II electron beam time measurement will be similar to that used in the LCLS-I: The phase of the ringing signal in a Radio Frequency (RF) cavity excited by the beam fields will be measured relative to a reference clock. That reference will be transmitted by an interferometrically stabilized fiber system to the experiment optical pump laser.

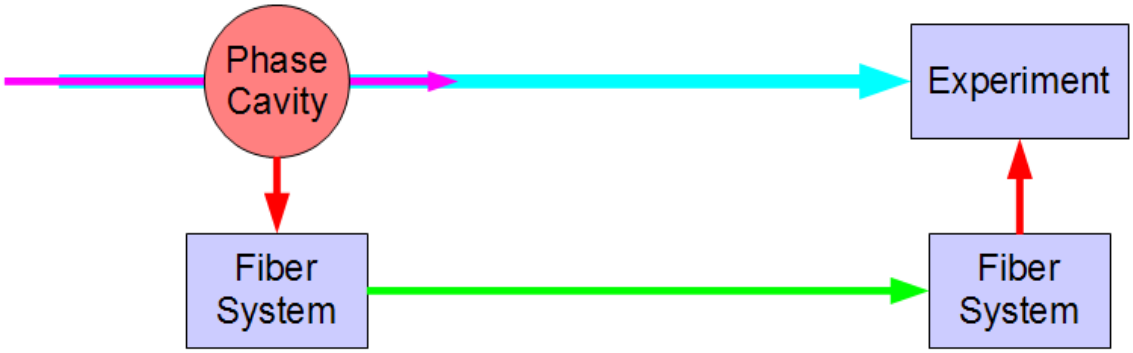

Figure 9.3. LCLS-II electron beam time measurement.

The current LCLS timing system uses two duplicate phase cavity systems to measure timing noise of approximately 10 femtoseconds Root Mean Square (RMS) at 250pC and 20 femtoseconds RMS at 20pC. Electronics upgrades are expected to improve this for LCLS-II to <10 femtoseconds at charges above 10pC.

The existing LCLS fiber system has demonstrated <20 femtosecond stability in the lab, and the associated laser locking system provides 30-50 femtosecond RMS jitter. The total timing jitter (after offline correction) between the experiment pump laser and the x-ray beam is estimated at 50 femtoseconds RMS. Improvements to 25 femtoseconds RMS are expected for LCLS-II. This is probably near the limit of performance for an electronic system. LCLS-II does not propose to develop these improvements, but will incorporate the current state of the art when the timing system is built.

The LCLS-II will be capable of producing sub 10 femtosecond x-ray pulses. In order to take full advantage of these short pulses, direct x-ray vs. laser cross-correlation will need to be performed in the experimental chambers as described in the next section.

9.7.2 X-ray Pulse Arrival and Length Monitoring

X-ray pulse duration diagnostics in the sub-picosecond range are currently very poorly developed. This is an area of active development by both LCLS and user groups. Both arrival time and pulse length can be modified by X-ray Transport, Optics and Diagnostics (XTOD) and instrument optics. These parameters need to be monitored at or near the sample.

The following methods are actively being investigated, either at the LCLS or by user groups and at other FELs:

- Measurements based on analysis of the pulse spectrum.
- Interferometry.
- Autocorrelation techniques based on nonlinear effects such as analysis of a spectrum of x-ray photoelectrons or Auger electrons dressed by optical laser fields.
- Streaking of electron replicas of x-ray pulses by laser fields
- Analysis of high field phenomena.

In the initial phase of LCLS-II operation we are planning to use the spectrometers described in chapter 8 to estimate pulse duration form measured pulse spectra. [2]

There is no Research & Development (R&D) funding in the project for arrival time and pulse length measurement. The techniques that are being developed by LCLS and users and are the most promising at the time the instruments are moved will be brought with those instruments.

9.8 Summary

The new experimental hall which will house the x-ray experimental systems will be in a cavern just downstream of the FEE. It will eventually accommodate a minimum of 4 experimental stations, 2 soft x-ray and 2 hard x-ray. The hall will include the basic support facilities for the experiments: setup space, laser labs, a sample prep lab and control rooms. Access will primarily be by ramps on which large equipment can be brought into the hall or labs. The AMO and SXR instruments with their control and laser systems will be moved from the NEH to the new hall. Upgrades to these two instruments are not part of LCLS-II. New personnel protection and laser safety systems will be installed in the new hall. An electron beam timing monitor system based on the existing system in LCLS-I will be installed. There is no R&D in the XES component of LCLS-II.

9.9 References

1. L. Young et al., Nature 466, 56 (2010)
2. Makina Yabashi, Jerome B. Hastings, Max S. Zolotorev, Hidekazu Mimura, Hirokatsu Yumoto, Satoshi Matsuyama, Kazuto Yamauchi, and Tetsuya Ishikawa, *Single-Shot Spectrometry for X-Ray Free-Electron Lasers*, Physical Review Letters **97**, 084802 (2006)

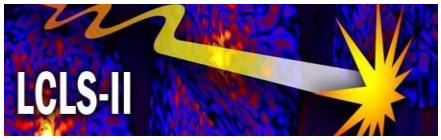

10 Conventional Facilities

Technical Synopsis

The LCLS-II conventional facilities design and construction takes advantage of the existing infrastructure and recent construction at SLAC. The project uses the last two-thirds of the existing 3 km linac including an existing enclosure and utilities. A new injector will be installed at Sector-10 in the Off-Axis Injector Tunnel. This branch tunnel was constructed as part of the original construction at SLAC in the 1960s for just such an injector. The drive laser at Sector 10 will be housed in a new injector support building to be constructed on the surface directly above the injector tunnel. The design will be similar to the injector support building constructed at Sector 20 for LCLS-I. The existing linac equipment including the klystrons and modulators will be used. The injector tunnel will require some modifications to bring it to current safety standards and to accommodate the specific requirements of the LCLS-II injector.

The beam transport segment, downstream of the Injector will be a combination of existing and new. Construction of the beam transport will require some modifications to the existing facilities to accept the new injector beam and constructing an extension of the recently completed Beam Transport Hall headhouse to traverse the Research Yard area. The modified beam transport hall will have a target finished floor elevation of 76.012 meters (249.38 feet) (SLAC datum), which is 0.6479 meters (2.125 feet) higher than the existing LCLS-I floor elevation.

The LCLS-II Undulator X-ray Tunnel, which will house the undulator magnets, electron beam dump and many front end x-ray diagnostics and optics, is a new tunnel that traverses approximately 305 meters under an existing hill and terminates at a new Experimental Hall 2. The undulator magnet hall and the electron beam dump segments closely resemble the existing LCLS-I segments. The undulator magnet devices are very low power and cooling requirement devices.

The undulator magnet devices have tight alignment requirements, which place stringent requirements on the foundations and on the temperature stability of the air and water in the tunnel. The existing Undulator Hall includes a dedicated heating and air conditioning plant to ensure temperature variations meet the stringent requirements. A similar system is proposed for the new LCLS-II Undulator Hall. Floor stability is addressed by increasing the thickness of the concrete floor and locating the hall underground where favorable geologic conditions and temperature environment exist.

The electron beam dump (EBD2) and front end enclosure (FEE2) will be constructed between the end of the undulator magnet devices and the new experimental hall. A model similar to the LCLS-I beam dump will be used, however the FEE2 will be expanded based on prior experience and to gain sufficient separation of the proposed beams, the FEE2 will include a secure access way to the new experimental hall.

One new experimental hall (EH2) will be built. The hall will extend for approximately 80 meters in the direction of the beam(s). EH2 will be a cavern similar to the existing Far Experimental Hall; approximately 14 meters wide and 10 meters high. The experimental (lowest) floor of the hall will provide sufficient space for up to 4 experiments and the associated control cabins with limited set up space for instruments. Laser rooms and electrical / mechanical rooms and additional set up space will be provided on a mezzanine floor above the experimental floor.

Conventional facilities scope also includes LCLS-II project-specific and minor modifications to existing lab-wide infrastructure systems, construction of dedicated support buildings and an Auxiliary Utility Plant to augment the existing LCLS-I Central Utility Plant.

SLAC, as a Federal facility, is required to comply with Executive Order 13423 "Strengthening Federal Environmental, Energy, and Transportation Management", dated January 24, 2007. The order sets goals in the areas of energy efficiency, acquisition, renewable energy, toxics reductions, recycling, renewable energy, sustainable buildings, electronics stewardships, fleets, and water conservation. The proposed LCLS-II project will comply with EO 13423 and will conduct a sustainability workshop early on in the design process to identify candidate elements for complying with the requirements of EO 13423 to the extent practicable.

10.1 Introduction and Overview

The conventional facilities scope includes the construction of an extension to the at grade Beam Transport Hall (BTH), a new tunnel to house the Undulator X-ray Tunnel (UXT) and a new Experimental Hall (EH2). The new conventional facilities will align with and contain the electron beam along the (-)2.4-degree angle that defines the beam path. (see Figure 10.1 and Figure 10.2). The BTH will cross the Research Yard (RSY) and connect to the undulator hall (UH2). The hall will extend beyond the ridge between the Research Yard and the existing LCLS-I experimental and office facilities. The electron beam dump (EBD2) pit and the Front End Enclosure (FEE2) will complete the UXT. The EH2 will be east and south of the existing LCLS-I Near Experimental Hall. The UXT will be constructed in a tunnel.and EH2 will be constructed in a cavern similar in shape to the existing Far Experimental Hall and will include alcoves for the control rooms and an access tunnel for access in and out of the cavern. Support buildings for the various sections of the new construction will be constructed as required with support from existing support buildings used to the maximum extent. The new experimental facilities will require an auxiliary utility plant to augment the existing central utility plant. The following sections provide more detailed requirements for each of the Conventional Facilities components.

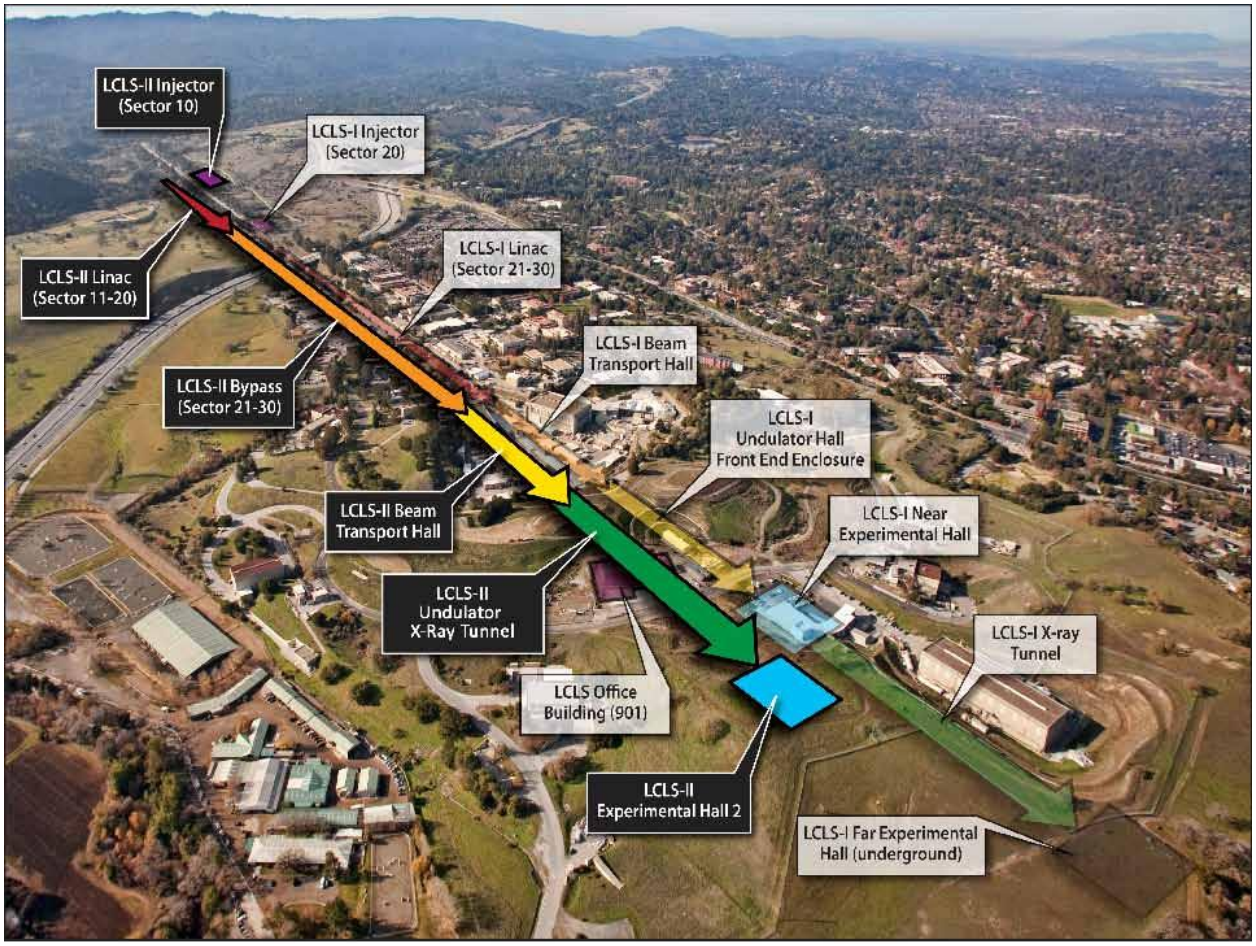

Figure 10.1. Project Overlay.

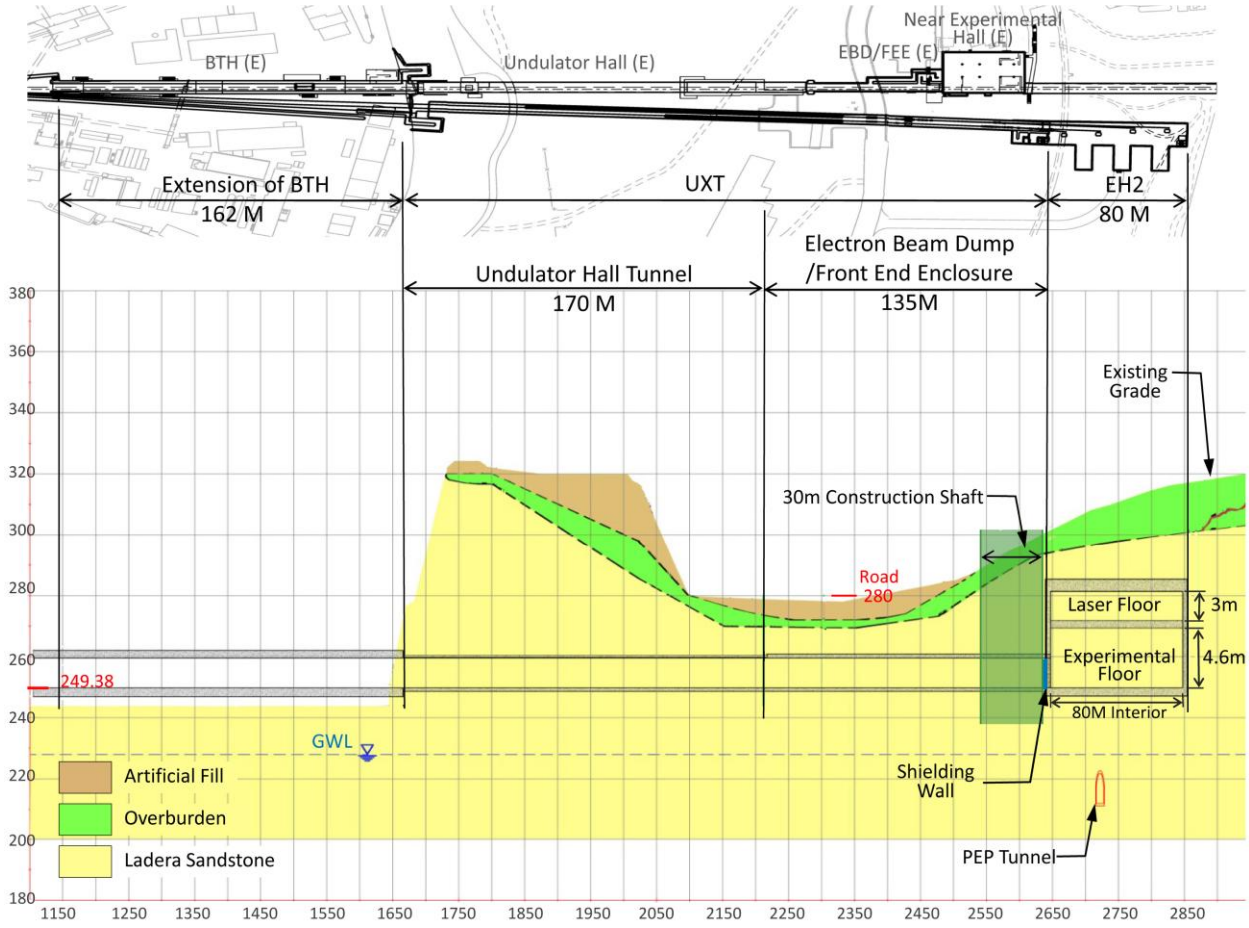

Figure 10.2. Plan and Profile.

10.1.1 Sector 10 Injector

When the SLAC linac was originally constructed in 1962, two short tunnels were built on the north side of the main linac tunnel. One is at the 1/3-point (Sector-10) and another at the 2/3-point (Sector-20). These tunnels were included to house future injectors that would allow efficient use of segments of the linac. The tunnel at Sector-10 is strategically located for the LCLS-II injector. The construction includes a surface building and utilities to support the injector (see Figure 10.3).

Modifications to the existing facility include reconfiguration of the shielding between the off-axis tunnel and the main tunnel to accommodate the beam pipe, the waveguides, an alignment pipe and other utilities. There are two spare penetrations between the surface building and the injector tunnel to accommodate the laser beam transfer pipe, control signals, and power connections. Additional penetrations will be required to suit the injector design and configuration.

The support building will be designed to provide an enclosure for the injector laser. Personnel exclusion walls will be built with a pair of doors on the west side for personnel access to the tunnel. The interlock for these doors will be integrated into the existing linac Personnel Protection System (PPS).

The injector will be powered by existing klystrons in the klystron gallery. No new linac resources will be required. As described in Chapter 6, klystron output power will be redirected to the off-axis tunnel with a new waveguide system described in the injector section.

Utilities will be provided for the magnet power supplies, controls, lasers, vacuum, and diagnostics. Cooling water will come from the main linac tunnel to cool the accelerator components. Cooling water will come from the klystron gallery for the laser and the equipment in the support building. In both cases, there is adequate capacity but new plumbing and wiring are required.

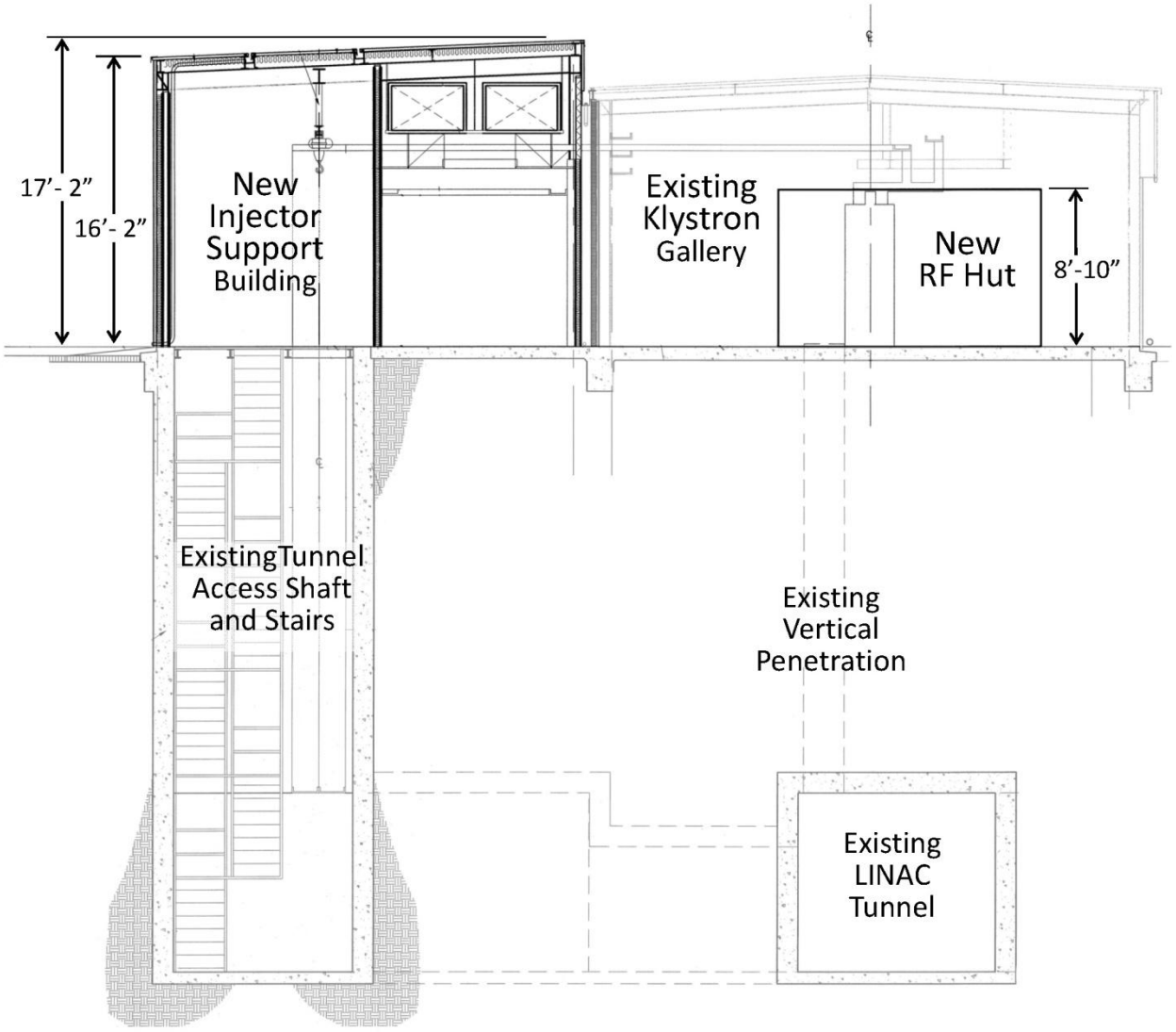

Figure 10.3. S10 Injector Support Building.

10.1.1.1 Architectural

The project includes the demolition of the existing Sector 10 Alcove located on the north side of the Klystron Gallery, and the construction of a new Injector Support Building (ISB), a new RF Hut within Sector 10 of the Gallery and injector supporting utilities.

The demolition scope requires the removal of the existing Sector 10 Alcove exterior metal roof & wall panels, structural steel lean-to framing, all interior metal & wood stud walls, doors and windows. The demolition will also remove all mechanical, electrical, plumbing, fire protection, fire alarm and telecom/data systems and supporting equipment. The demolition will also include asbestos and lead paint abatement.

The new Injector Support Building (ISB) will be designed and constructed utilizing a metal building system, including primary & secondary structural steel framing, with standing seam metal roof and wall panels. All exterior metal will be galvanized steel with urethane enamel coating system. Exposed fasteners will be of the same metal as being fastened with the same finish system.

The standing seam roofing system will have a minimum 20-year warranty. Roof assembly will have a minimum slope of ½" per foot. In compliance with the DOE memo from the Secretary of Energy, dated June 1, 2010, the roof assembly will be designed and installed to have a thermal resistance of at least R-30 and meet the requirements of Cool Roof Rating Council program.

The ISB will be designed and constructed to provide space for the injector laser, an optical work area, material loading and work areas and a 2-ton monorail crane. Modifications to the existing Klystron Gallery will also include the construction of a new RF Hut within Sector 10 to support the electronics racks.

In the interior work and service areas the floor slabs will have sealed concrete finish. Perimeter walls will be protected from impact damage to a minimum of 8'-0" A.F.F. Generally all work spaces will be finished with a heavy latex enamel (water borne, low VOC) paint finish. Specific areas such as the injector laser work room will be finished with a water-borne epoxy. Interior doors will be painted hollow metal, with painted hollow metal frames. Doors in high-use areas will receive protective stainless steel panels to lever height.

Typical interior partition walls will consist of 3-5/8" steel studs with 5/8" gypsum wallboard on both sides. Fire barrier walls will comply with Underwriters Laboratories (UL) designs for one-hour separations where required. Sound batt insulation will be installed to provide acoustic insulation to adjacent spaces.

The existing tunnel access shaft and stair enclosure will be of 1-hr rated construction, including a 1-hr rated cable shaft and fire rated exit doors. The shaft access/exit doors will include an interlock that is integrated into the existing Linac Personnel Protection System (PPS).

Exit signs will be edge-lit with concealed lamp and integral lettering on a clear lens. Where low-level exit signs are required, they will be backlit and set flush with the adjacent wall.

Fire extinguishers will be provided in accordance with NFPA 10, throughout the building. The maximum travel distance to an extinguisher from any point in the building will be 50 feet. Fire extinguishers will be placed in surface mounted steel cabinets with baked enamel paint finish, with upper edge at +4'-6". Frameless doors will have a solar gray glass lite and silk-screened letters. All cabinets will be sized to house the code required size extinguisher.

Noise criteria for HVAC system-related background sound in work rooms will be in accordance with data indicated in the ASHRAE HVAC Applications Handbook 2007, Sound and Vibration Control, and/or specific SLAC EH2&S recommendations for each space type. Acoustical and vibration control treatments will be provided, as required, to all HVAC system components, to maintain specified space noise criteria.

The conceptual acoustical design basis is as follows:

Injector Laser Work Area: NC 55 to 60 maximum allowable HVAC noise levels, as measured from the center of the room. Resultant noise levels when selecting mechanical equipment and designing distribution systems will not exceed criteria indicated above. These noise criteria levels are based upon an unoccupied space with only mechanical systems operating, and do not take into account any noise generated by users, or scientific equipment within the space.

10.1.1.2 Structural

Structural work includes demolition of existing concrete slab, grade beams, and structural framing system of Sector 10 Alcove and the construction of new Injector Support Building (ISB). This new building will be a metal frame building capable of supporting MEP loads as well as 2 ton monorail crane. Besides the new building, a concrete equipment pad will be built at the west end of ISB.

Structural Design Criteria

The metal building will be designed to conform to CBC 2010 requirements as well as SLAC Building & Site-Wide Design guidelines (DS-018-000-01-R0).

Design Dead and Live Loads (will not be less than ASCE 7 minimum requirements)

- Dead loads of structure as calculated
- Collateral dead load for sprinkler, ducts, piping, electrical conduits and lighting - 5 to10 psf or as calculated, whichever is higher
- Live floor load - 150 psf or equipment weight whichever is higher
- Laser rooms live load – 350 psf or equipment weight whichever is higher
- Platforms, stairs, and corridor live loads - 100 psf
- 5 ton monorail crane

Wind Load Parameters

ASCE 7 - Basic “three-second gust” wind speed: 85 mph; Exposure C

Seismic Design

The structures will be designed and constructed to resist seismic loads and to limit the deflections generated by strong ground motion during a seismic event. The seismic design will comply with the following:

Geologic Hazard Evaluation and site specific response spectral data in the report provided by SLAC. Base shears will be based on using the site-specific spectral acceleration curves. Base shears calculated using dynamic analysis will be compared with CBC requirements and the most conservative loading will govern. ISB will be located approximately 1.5 miles west from San Andreas Fault.

CBC 2010 design requirements:

- Occupancy Category II (Importance Factor I= 1.0, Ip =1.0).
- Seismic Design Category E
- Soil Class will be determined by Geotechnical consultant for project site.
- Seismic coefficients will be determined based on the location latitudes and longitudes.
- Following are seismic coefficients at Injector Support Building, based on the assumption of Class D soil:

Latitude:		37.41374 deg.
Longitude:		-122.22788 deg.
Ss	=	2.493 g
S1	=	1.169 g > 0.75g therefore SDC = “E” (ASCE 7.05, article11.6)
SMS	=	2.493 g
SM1	=	1.754 g
SDS	=	1.662 g
SD1	=	1.169 g
Fa	=	1.0
Fv	=	1.5

10.1.1.3 Mechanical Systems

General

ISB and RF HUT will require general space conditioning, in addition to process cooling water for various technical components. Technical components are housed in three distinct areas and as such, will require independent air conditioning zones to handle each specific space temperature set points. The east end of the ISB will be zoned differently from the west end, and the RF HUT zone stands alone. A mechanical equipment plant will provide the infrastructure space cooling water and hot water needs.

Adjacent to the space conditioning mechanical equipment plant, there will be a process cooling chiller plant to support various water-cooled technical components in all areas of Sector 10.

Chilled Water System

The space cooling plant will consist of a 45-ton packaged, water-cooled chiller with associated circulating chilled water pumps to support the air handling system of Sector 10. The circulating chilled water pump system will be a set of two pumps, each sized to operate independently with the other serving as a standby at all time.

The process cooling plant will consist of two 5-ton packaged chillers with associated circulating chilled water pumps to support the process cooling water (PCW) of Sector 10. The chilled water system will serve to reject heat generated from the water-cooled injector technical components via a heat exchanger. A single 5-ton chiller will provide+ the PCW needs of the all water-cooled technical components of Sector 10. The second of the two 5-ton chillers will serve as a standby in the event of an operating chiller failure.

Both space and process chiller systems will be furnished with all necessary supporting mechanical devices and appurtenances.

Heating Hot Water System

The heating hot water system will consist of an electric, 55kW boiler with associated recirculating pumps and heating hot water distribution piping.

The heating hot water system serves the purpose of maintaining room temperature set points in all rooms of the Injector Support Building via reheat coils.

The hot water systems will be furnished with all necessary supporting mechanical devices and appurtenances.

Air Handling System

Approximately half the floor space of the ISB, the east end, houses the Laser Room. Unlike the west end, which houses the Optical, Lock Load and Loading Areas, the Laser Room requires constant volume air distribution to support a laser room environment. The air handler for the east end will deliver a constant 12,000 cubic feet per minute (CFM) of conditioned air to the Laser Room. The air handler will be a packaged Fanwall typed, furnished with 30% prefilter, 95% high efficiency filter, chilled water coils, hot water reheat coils, humidifier, HEPA filters and associated variable frequency drive (VFD). The Fanwall typed air handler, with its multiple fans, will provide superior fan redundancy in the event of a supply fan failure.

A second air handler will deliver an equivalent 7,000 CFM of supply air to the west end of the ISB. The air handler unit will be similar to the abovementioned air handler with the exception of a humidifier and a HEPA filter section. The final filter section in the subject air handler will be 85% high efficiency.

A third air handling unit will be a 3000 CFM, indoor, floor-mounted, chilled water air handling unit. The unit will be of a high quality, specialty-typed air handling unit used for critical data room applications.

The unit will be furnished with humidifier control, reheat coils, condensate pump and leak detection system. The unit's microprocessor control panel will locally maintain room temperature and humidity set points.

Duct mounted smoke detectors will be provided to the air handling units as required, per California Mechanical Code (CMC).

Ductwork & Air Distribution

The air flow delivery system for the east end of the ISB consists of lined, rectangular, galvanized supply and return ductwork will extend from the air handler, which is located at nearby mechanical equipment plant and terminate inside the Laser Room. Supply air will terminate at T-bar ceiling with Lami-Vent or equivalent supply air diffusers placed equal-distance throughout the Laser Room T-bar ceiling.

The air flow delivery system for the west end of the ISB will extend from the second air handler and terminate inside the west end of the Injector Support Building. The west end will maintain room temperature with variable air volume boxes (VAV) with reheat coils. The three areas in the west end share a single air handler, but will have independent room temperature set points.

EMS & Controls

Direct Digital Controls (DDC) will be provided to monitor and control mechanical equipment, and it will be integrated to the existing site-wide Automatic Logic Control (ALC), WebCTRL Monitoring System.

Process Cooling Water System

Process cooling water system at Sector 10 will comprise of a low conductivity water system (LCW) and a laser process cooling water system (PCW). Both water cooling systems provide cooling to technical components. The LCW system will consist of modification to the existing LCW piping in the Linac.

Table 10.1. Low Conductivity Water System Parameters (Laser Room & RF Hut).

Supply Temperature	78.5 °F (25.8 °C)
Temperature Stability	± 0.5 °F (± 0.28 °C)
Average Temperature Rise	10 °F (5.6 °C)
System Pressure	125 PSIG (862 kPa)
System Flow	60 GPM (227 liters/min)
Total System Heat Capacity	300,000 Btu/hr (87.9 kW)

A 3 inch low conductivity water line coupled with a heat exchanger will extend to both the Injector Support and RF Hut Buildings to support LCW utilities requirement of the Sector 10. A set of two pumps, one operating and the other as a backup will provide 300,000 Btuh of heat exchange capacity to the water-cooled technical components in both the Laser Room and the RF Hut. The returning heat from the LCW system will be rejected via the heat exchanger to the existing cooling tower system.

Table 10.2 Low Conductivity Water System Parameters (Injector Vault).

Supply Temperature	113 °F (45 °C)
Temperature Stability	± 0.3 °F (± 0.17 °C)
System Flow	32 GPM (121 liters/min)

In addition to the LCW plant at grade level, a line will be provided to the Injector Vault located below ground. Provisions will be made to connect a 32 GPM, 2 inch LCW line from the existing Accelerator Cooling Water main to the Injector Vault of Sector-10.

The LCW system will be controlled and monitored by the existing SLAC Distributed Controlled System (DCS) Network.

Table 10.3. Process Cooling Water System Parameters.

Supply Temperature	56 °F (13.3 °C)
Temperature Stability	± 0.5 °F (± 0.28 °C)
Average Temperature Rise	10 °F (5.6 °C)
System Pressure	60 PSIG (414 kPa)
System Flow	40 GPM (151 liters/min)
Total System Heat Capacity	176,000 Btu/hr (51.6 kW)

A 2-1/2 inch process cooling water line will extend from the process chiller plant to support PCW utilities requirement of the area sector. A set of two pumps, one primary and the other a backup will provide 176,000 Btuh of heat exchange capacity to the water-cooled technical components in both the Laser Room and the RF Hut.

Fire Protection

The Fire Protection piping system will be a wet type fire sprinkler system designed per NFPA 13, for Ordinary Hazard (Group 1). The sprinkler system will be connected to the nearby existing riser sprinkler main. Sprinkler system is designed per NFPA 13 at 0.10 GPM/FT2 with 155°F heads. Each head is designed to cover a maximum of 130 square feet. A single zone with zone control valve with supervisory and flow switches where the system enters into the building. A Fire Department connection shall be provided for at the sprinkler system riser.

10.1.1.4 Electrical Systems

Injector Support Building

The electrical distribution service to Injector Support Building will be fed from a new 2000A, 3 phase, 3 wire Motor Control Center (MCC) located at sector 10 Klystron Gallery. The power source of this new

MCC is fed from a new outdoor 12.47KV, 1500KVA substation located at the north side of Klystron Gallery Sector 10 area.

The 2000A, 480V MCC will be provided with 100% rated solid state type main circuit breaker with LSIG trip unit, branch breakers, starters, monitoring, metering, instruments, signal/control devices. The detail arc flash, short circuit, load flow, balancing and all other applicable design requirements will be implemented in the detailed design. The new MCC will support the following:

- Power to step down feeders of Sector 10 injector laser rooms.
- Power to mechanical equipment to support sector 10 injector laser such as air handling units, welding plug in the injector area, electrical boiler, air and water cooled chillers, pumps, humidifier, fan coil units and LCW system etc.
- Power to specialized equipment such as cranes, arc welder in the injector area.
- Power to equipment in injector vault at tunnel level.

Distribution panelboards

480V or 120V/208V distribution panelboards will be provided to Injector Laser power requirement. Distribution panelboards shall be dead-front, dead-rear, solid state type main circuit breaker, branch circuit breakers are group mounted, front accessible bolt-on thermal magnetic molded case type with adjustable magnetic trip settings. Full length buss for both voltage and 200% neutral bussing on 208V distribution panels.

Dry type transformer

Transformer will be NEMA TP-1 compliant, Energy Star labeled transformers to step down to 120V/208V, 3 phase, 4 wire, K13 rated, 200% neutral.

Individual neutral wire for each phase wire.

Arc Flash rating

For 480V system, use solid state type breakers for coordination selectivity to reduce fault clearing time, for 208V system, preferable limit step down transformer to 112.5 KVA.

Lighting System

Industrial fluorescent and recessed fluorescent fixtures will be provided for Injector Support Building and the vault at the tunnel level. High Intensity Discharge (HID) fixtures will be provided as outdoor lighting. Lighting level shall be designed in accordance with Illuminating Engineering Society (IES) recommendations and suitable for the injector laser application. Fixtures shall be fluorescent type with energy saving T8 lamps, 3500 Kelvin color temperature with high efficiency electronic ballasts 95% power factor, total harmonic distortion (THD) of less than 10%. Lighting control will be designed to meet or exceed the requirement of Title 24 and injector laser requirement. Exit and emergency lights will be provided per code. Exterior lighting will be provided at the entrances, landings, equipment pads.

Grounding and Bonding System

Service grounding will be design per CEC and NEC requirement. All ground buss will be connected back to building grounding bus in Linac Section 10 Klystron Gallery. All systems and equipments will be bonded as per NEC and NFPA requirements. The detail grounding and bonding system will be designed in preliminary and final design phases.

Fire Alarm and Detection System

The fire alarm system will be met utilizing Siemens products to integrate with the existing campus network. The fire alarm system will be designed to comply with NFPA 72 and all associated codes and regulations. The new fire alarm system will consist of, but not limited to, a fire alarm control unit, alarm initiating devices, occupant notification appliances, and associated ancillary equipment for interfacing the new fire alarm system with the existing SLAC alarm receiving equipment. The fire alarm system will also communicate with other life safety systems, building system equipment as applicable. The final design of the fire alarm system will be detailed in preliminary and final design phases.

The fire detection system will be integrated with the existing campus network. The fire detection system will be design to comply with NFPA 72 and all associated codes and regulations. The fire detection system will be VESDA Air Sampling and Early Warning Smoke Detection. The VESDA system will consist of, but not limited to, the sampling pipe network, highly sensitive LASER-based smoke detectors, aspirators, filters, detector assemble network, digital communication ports. The fire detection system will be also communication with other life safety systems, building system equipment as applicable. The final design of the fire detection system will detailed in preliminary and final design phases.

Telecommunication System

The telecommunication system will be provided to support the physical transmission facility for voice, data and low voltage networks. The system consists of, but not limited to, the following:

- Telecommunication backbone pathways includes dedicated point-to-point (BDF to IDF) pathway system. These pathways may be comprised of cable tray, raceways, boxes, inner duct in cable tray, cable suspension products, and seismic bracing.
- Telephone and data structure cabling system will be designed to comply with the requirement of EIA/TIA 569 Commercial Building Standard for telecommunications pathways and spaces. The cabling system will be designed to comply with pertinent codes, rules, regulations and laws of the Authorities having jurisdiction. The cabling system includes building pathways, backbone cabling, horizontal cabling and an administration system to manage the pathways and cabling.

RF Hut

Electrical System

The electrical distribution service to RF Hut will be fed from a new 2000A, 3 phase, 3 wire Motor Control Center (MCC) located at sector 10 Klystron Gallery. The power to RF Hut is distributed via step down transformer and power panelboard.

Distribution panelboards

120V/208V distribution panelboard will be provided per RF Hut power requirement. Power panelboard shall be dead-front, dead-rear, mold-on main circuit breaker, branch circuit breakers are group mounted, front accessible bolt-on thermal magnetic molded case type with adjustable magnetic trip settings. Full length buss for both voltage and 200% neutral bussing on 208V distribution panels.

Dry type transformer

Transformer will be NEMA TP-1 compliant, Energy Star labeled transformer to step down to 120V/208V, 3 phase, 4 wire, K13 rated, 200% neutral.

Individual neutral wire for each phase wire.

Arc Flash rating

For 480V system, use solid state type breakers for coordination selectivity to reduce fault clearing time, for 208V system, preferable limit step down transformer to 112.5 KVA.

Lighting System

Industrial fluorescent and/or recessed fluorescent fixtures will be provided for RF Hut. Lighting level shall be designed in accordance with Illuminating Engineering Society (IES) recommendations and suitable for RF Hut application. Fixtures shall be fluorescent type with energy saving T8 lamps, 3500 Kelvin color temperature with high efficiency electronic ballasts 95% power factor, total harmonic distortion (THD) of less than 10%. Lighting control will be designed to meet or exceed the requirement of Title 24 and RF Hut requirement. Exit and emergency lights will be provided per code.

Grounding and Bonding System

Service grounding will be design per CEC and NEC requirement. All ground buss will be connected back to building grounding bus in Linac Section 10 Klystron Gallery. All systems and equipments will be bonded as per NEC, NFPA requirements. The detail grounding and bonded system will be designed in preliminary and final design phases.

Fire Alarm and Detection System

The fire alarm system will be met utilizing Siemens product to integrate with the existing campus network. The fire alarm system will be designed to comply with NFPA 72 and all associated code and regulations. The new fire alarm system will consist of, but not limited to, a fire alarm control unit, alarm initiating devices, occupant notification appliances, and associated ancillary equipment for interfacing the new fire alarm system with the existing SLAC alarm receiving equipment. The fire alarm system will also communicate with other life safety systems, building system equipment as applicable. The final design of the fire alarm system will be detailed in preliminary and final design phases.

The fire detection system will be integrated with the existing campus network. The fire detection system will be design to comply with NFPA 72 and all associated codes and regulations. The fire detection system will be VESDA Air Sampling and Early Warning Smoke Detection. The VESDA system will consist of, but not limited to, the sampling pipe network, highly sensitive LASER-based smoke detectors,

aspirators, filters, detector assemble network, digital communication ports. The fire detection system will be also communication with other life safety systems, building system equipment as applicable. The final design of the fire detection system will detailed in preliminary and final design phases.

Telecommunication System

The telecommunication system will be provided to support the physical transmission facility for voice, data and low voltage neworks. The system consists of, but not limited to, the following:

- Telecommunication backbone pathways includes dedicated point-to-point (BDF to IDF) pathway system. These pathways may be comprised of cable tray, raceways, boxes, inner duct in cable tray, cable suspension products, and seismic bracing.
- Telephone and data structure cabling system will be designed to comply with the requirement of EIA/TIA 569 Commercial Building Standard for telecommunications pathways and spaces. The cabling system will be designed to comply with pertinent codes, rules, regulations and laws of the Authorities having jurisdiction. The cabling system includes building pathways, backbone cabling, horizontal cabling and an administration system to manage the pathways and cabling.

Sector 10 Linac Upgrade

Installation of a new 12KV, 1500KVA Electrical Substation to support Sector 10 Injector Support Building

One (1) 15KV Outdoor Medium Voltage SF6 Switchgear

A new outdoor medium voltage pad mounted SF6 Switchgear will be provided to isolate the new substation for Sector 10 Injector Facility loads and the existing substation K5 for Sector 10 Linac and Klystron Gallery existing loads. The new SF6 switchgear will be arc-resistant rated, 15kV, 25kA symmetrical SC rating, split-bus with two (2) 600A fault interrupted switch ways, bus tie switch, and two (2)600A load taps vacuum interrupted switch ways with CT's and microprocessor based electronic relays, equipped with micro-At source transfer with manual/auto switch, self-powered controls, 12.47KV VT with fusing per NEC, remote control operator package and terminal connection of remote supervisory control and monitoring, Ethernet, web-enabled communications capability. The SF6 switchgear will be installed with 15KV separable connector feed-thru bushing termination on the incoming (2) fault interrupted ways in the extended enclosure. Provide new concrete pad, utility handhole and underground concrete encased duct bank to existing manhole. The SF6 Switchgear will be located on the south side of Sector 10 Klystron Gallery area.

One (1) 12KV, 1500KVA Substation

A new outdoor medium voltage pad mounted substation will be provided for support Injector Support Building and RF Hut equipment, mechanical, HVAC, utility loads. The power source to this new 12KV substation will be fed from existing 12.47KV feed C2 through the new SF6 Switchgear to new substation. The conceptual design of this new substation feeder from SF6 Switchgear will be routed underground across the south side road into Sector 10 Klystron Gallery and surface mount the 12KV feeder inside

Sector 10 Klystron Gallery to the north side. New concrete pad for new substation will be provided. The final routing will be determined during detailed design.

The new outdoor 12KV substation will consist of, but not limited to, the following:

- An outdoor 12KV medium voltage metal clad switchgear vacuum circuit breaker rated 15KV, 1500KVA, 1200A, 3 phase, insulated copper bus, with (1) vacuum circuit breaker including CPT, VT, CT's, microprocessor based protective relays, power monitoring devices.
- An outdoor liquid-filled, substation type transformer rated 1500KVA, 3 phase, 12.47KV primary delta, with 5 primary no-load tap changer of two 2-1/2% above and two 2-1/2% below nominal, 480V/277V wye grounded secondary, 3-phase, 4-wire, 60 Hertz, %Z=5.75, Class OA/OA/FFA, 55/65 degree C, aluminum, FR3 less-flammable vegetable-based seed oil insulation per NEC, equipped with self containment.
- An outdoor 480V/277V low voltage metal clad enclosure section rated 2000A, 480Y/277V, 3-phase, 4-wire, insulated copper bus & tin plated ground bus, 65KAIC symmetrical, main circuit breaker compartment of (1) 2000AF main breaker. The main breaker will be equipped with LSIG electronic trip units, completed with protective relays, transformer differential, undervoltage & overcurrent relays.

New 12KV power feed to existing K5 Substation

A new 12KV power feed will be provided from new SF6 Switchgear to existing K5 Substation.

10.1.2 Linac Facility Upgrade

The LCLS-II uses the last 2 km of the existing linac, from Sector-10 through Sector-30. The existing utilities will be adequate for the new operation. In two sectors, Sector-10 and Sector-15, sections of the linac will be removed and replaced with magnets and vacuum chambers for electron beam pulse compression. Rearrangement of some low conductivity water and electrical power distribution will be required at these locations but the total capacity is adequate for the new requirements. The costs for these changes to the utilities are included with the linac costs.

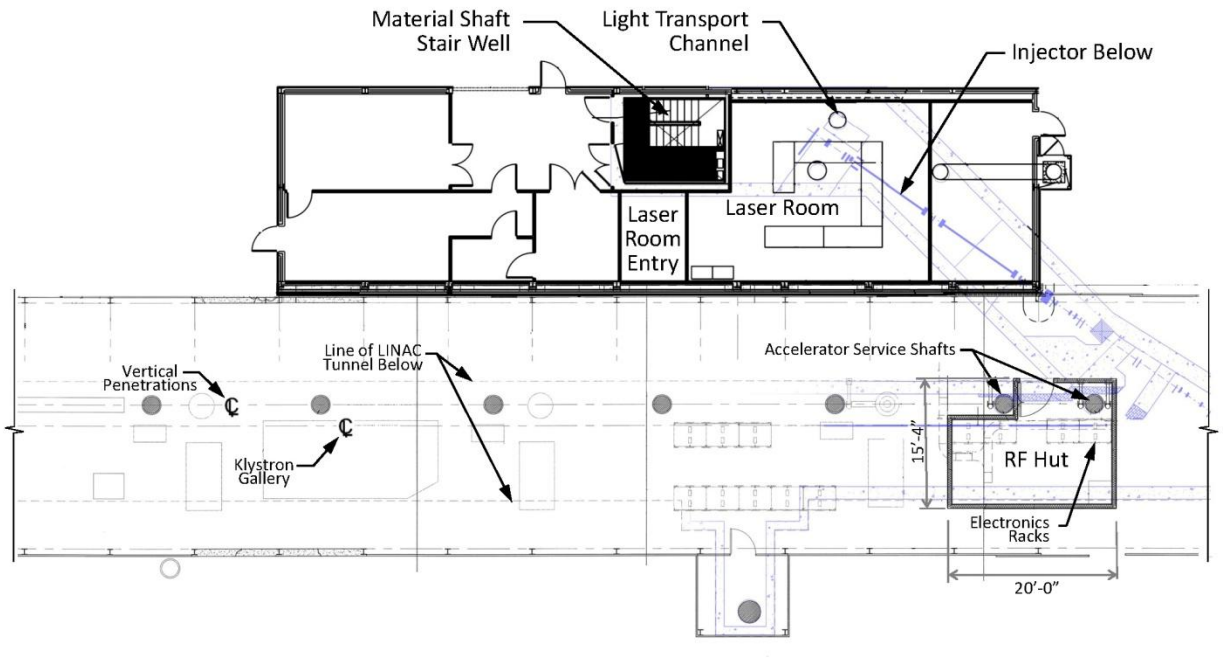

Figure 10.4. Layout of the Injector Support Building and RF Hut.

10.1.3 Beam Transport Hall Expansion (BTH)

The new BTH expansion will be approximately 160 meters long and similar in construction to the existing BTH. The existing hall is constructed of formed concrete (seeFigure 10.5). The inside dimensions of the new facility will be similar in the typical sections, but nominally increases in width as it crosses the Research Yard to accommodate the diverging beam line. It is proposed to integrate the existing and new structures by making use of a common wall between the existing and new facility. This will reduce the total volume of concrete that is required for shielding purposes. The new hall will be located and sufficiently sized to house two beam lines.

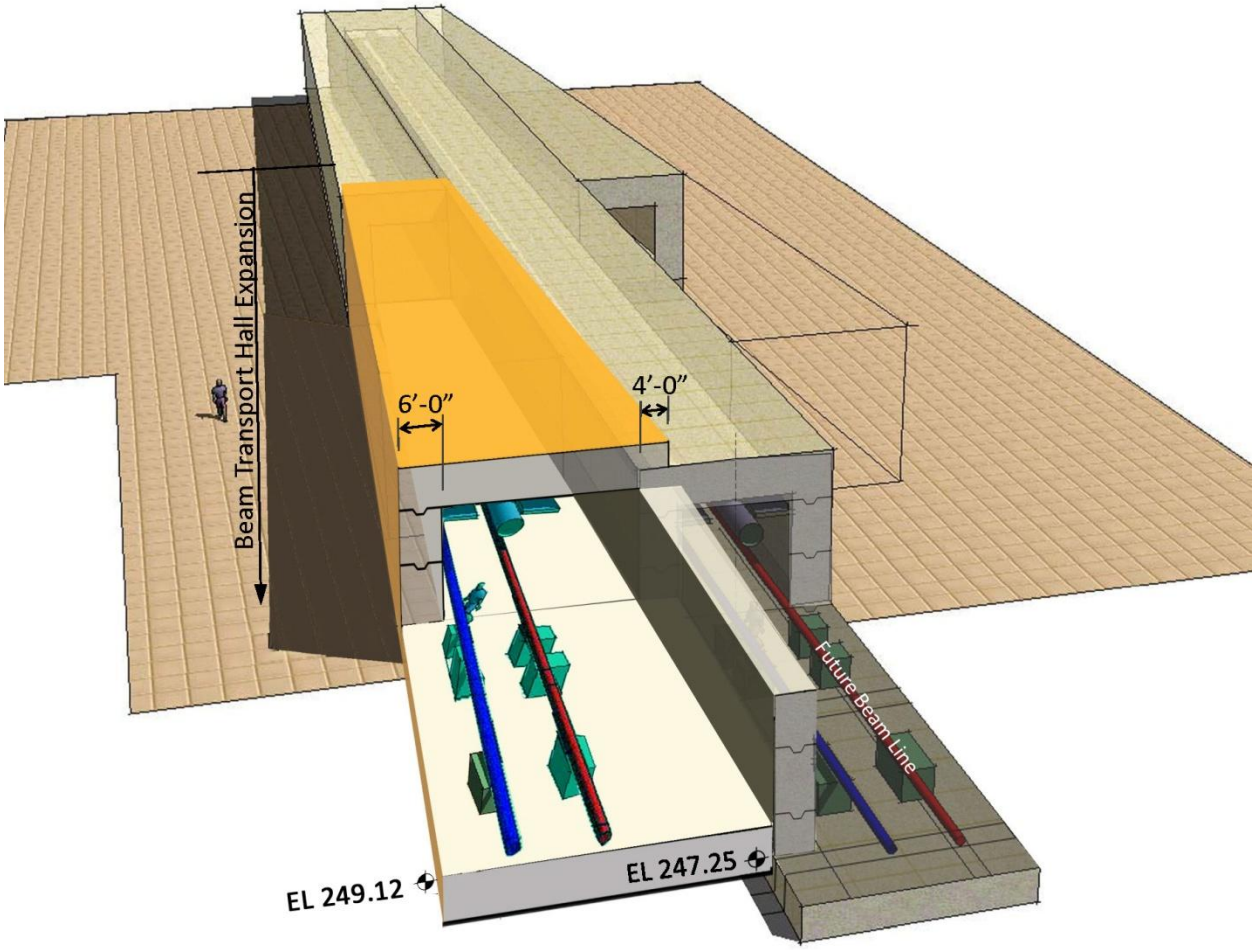

Figure 10.5. Beam Transport Hall Perspective

10.1.3.1 Architectural

The existing BTH bisects the research yard and extends from the beam switch yard to the beginning of the existing LCLS-I Undulator Hall. The LCLS-II project will expand the BTH to the south to house two new beam-lines, and support equipment. The total length of the expanded BTH is 160 meters (~525'). Its purpose is to carry the high-energy beam into the Undulator X-ray Tunnel (UXT).

The expanded BTH will be trapezoidal in shape with an interior width of 14'-10" at the west end and an interior width of approximately 33'-4" at the east end. The expanded BTH is physically defined as the space between the end wall of the existing BTH Head House to the west and to the start of the fire & life safety rated horizontal exit at the UXT to the east.

The interior of the BTH will house the split beam lines at - 2.4 degrees, and appurtenant equipment. The interior finish on the walls and ceiling will be a smooth finish – typically all work spaces will be finished with a heavy latex enamel (water borne, low VOC) paint finish, floor slabs will have sealed concrete finish. Low profile fluorescent lighting will be provided in the entire length of the BTH. A minimum of 8'-

0” clear height is required for operations and maintenance. The floor level is to remain constant throughout the entire length of the LCLS-II at 249.38 feet. The radiological requirements at SLAC dictate the necessity for 72" thick concrete walls, and 48" thick concrete roof for the BTH in the yard. An additional 24" of slab thickness is required for the roof, where personnel may access or cross over the BTH. Roof will have a minimum slope of ½” per foot. The exposed roof portions will be coated with fluid applied roof coating and the exposed exterior deck coated with fluid applied traffic coating.

This is a radiologicaly controlled area, so compliance with SLAC Radiological Criteria is required. This also implies that special attention needs to be given to the floor thickness of the service building situated above the BTH. The vibration tolerances for the BTH floor are critical to the success of LCLS-II (refer to the Floor Vibration Specifications, LCLS-II document SLAC-I-060-102-001-00-00-R000); therefore isolation of floor from Research Yard is required. A fire life safety rated horizontal exit barrier is also required to isolate the interior of BTH from Undulator X-ray Tunnel downstream. The expanded BTH will require two new fire life safety egress labyrinths at each end of the hall (east & west).

The expansion of the BTH requires the removal of the existing building B211. The demolition will also remove all mechanical, electrical, plumbing, fire protection, fire alarm and telecom/data systems and supporting equipment. The site demolition includes adjacent AC Paving, and concrete equipment pads.

The BTH will also include one service building. This will be located above the middle section of the expanded BTH. The service building will house data racks, electrical panels and transformers. The roof penetrations for data cabling from the service building will be comprised of a grouping of 6 - 4 inch diameter embedded steel pipe. The service building will have an adjacent exterior deck which will support the necessary HVAC support equipment. Two access stairs are required for the exterior deck and provide access to the service building and cross-over points within the RSY. Guardrails are required along the entire perimeter of the exterior deck and swinging guardrail gates are required for equipment access from the north Research Yard.

The Service Building will be designed and constructed utilizing a metal building system, including primary & secondary structural steel framing, with standing seam metal roof and wall panels (see Figure 10.6). All exterior metal will be galvanized steel with urethane enamel coating system. Exposed fasteners will be of the same metal as being fastened with the same finish system.

The standing seam roofing system will have a minimum 20-year warranty. Roof assembly will have a minimum slope of ½” per foot. In compliance with the DOE memo from the Secretary of Energy, dated June 1, 2010, the roof assembly will be designed and installed to have a thermal resistance of at least R-30 and meet the requirements of Cool Roof Rating Council program.

The interior work and service areas floor slabs will have sealed concrete finish. Perimeter walls will be protected from impact damage to a minimum of 8’-0” A.F.F. All exposed construction will have a painted finish. Interior doors will be painted hollow metal, with painted hollow metal frames. Doors in high-use areas will receive protective stainless steel panels to lever height.

Typical interior partition walls will consist of 3-5/8” steel studs with 5/8” gypsum wallboard on both sides. Fire barrier walls will comply with Underwriters Laboratories (UL) designs for one-hour

separations where required. Sound batt insulation will be installed to provide acoustic insulation to adjacent spaces. Generally all work spaces will be finished with a heavy latex enamel (water borne, low VOC) paint finish.

Exit signs will be edge-lit with concealed lamp and integral lettering on a clear lens. Where low-level exit signs are required, they will be backlit and set flush with the adjacent wall.

Fire extinguishers will be provided in accordance with NFPA 10, throughout the building. The maximum travel distance to an extinguisher from any point in the building will be 50 feet. Fire extinguishers will be placed in surface mounted steel cabinets with baked enamel paint finish, with upper edge at +4'-6". Frameless doors will have a solar gray glass lite and silk-screened letters. All cabinets will be sized to house the code required size extinguisher.

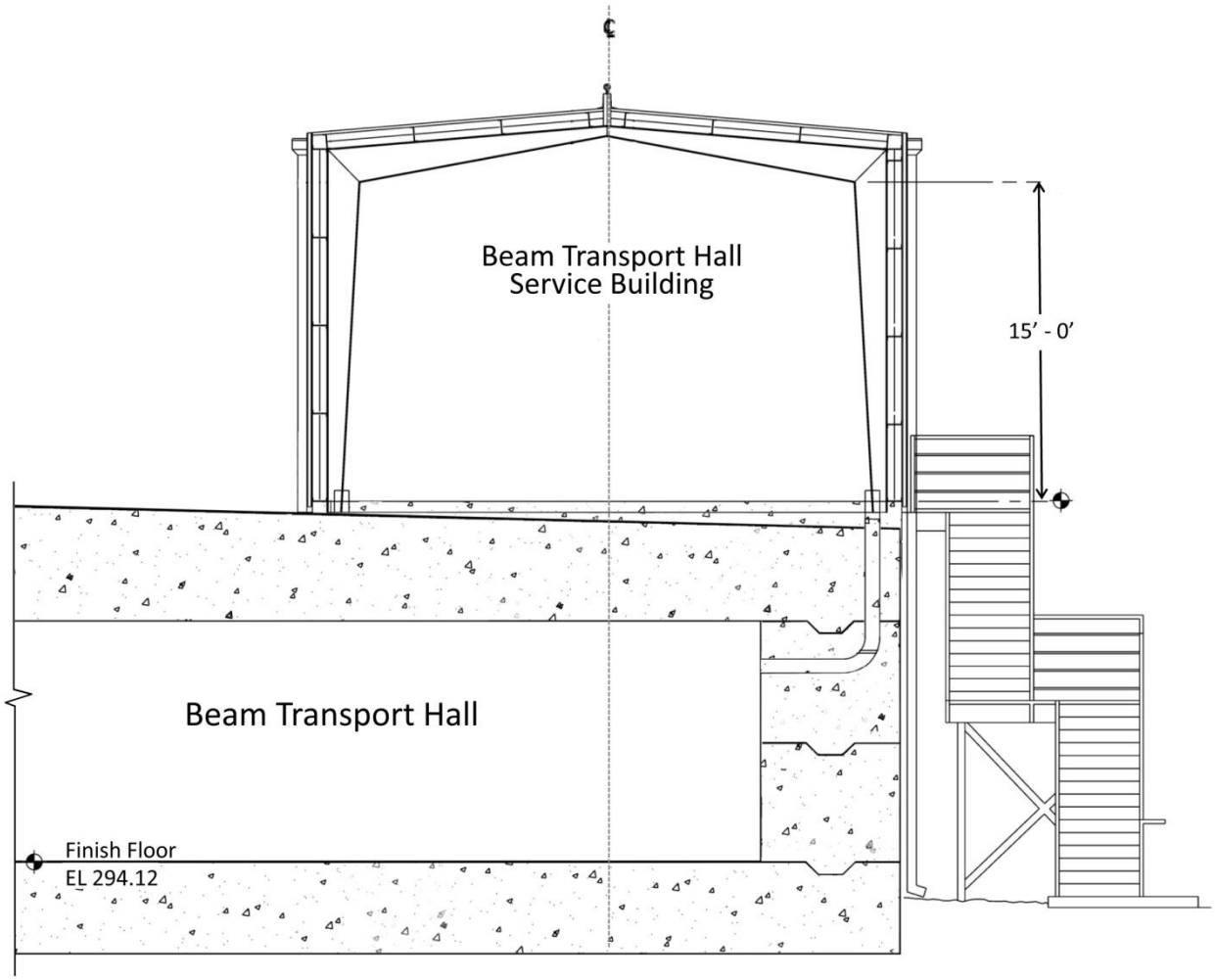

Figure 10.6. BTH Section at Service Building.

10.1.3.2 Structural

The Beam Transport Hall (BTH2) is the first segment of the LCLS II project and will be located in the Research Service Yard (RSY). It is constructed adjacent to existing BTH1 tunnel. The 6 ft thick south wall of existing BTH 1 tunnel will be shared by BTH1 and BTH2.

The walls of BTH2 will be typically 6 ft thick concrete walls for radiation protection. The thickness of the BTH2 concrete roof will typically be 4 ft thick except at the service buildings and HVAC deck where the the floor thickness will be increased to 6ft for radiation protection. This is a radiologically-controlled area, so compliance with SLAC Radiological Criteria is required. Floor will be flat and leveled and designed to minimize vibration as well as short and long term distortion. Floor will be isolated from the SLAC Research Yard to minimize thermal expansion effects. The finish floor will have zero percent slope in the direction of beam adjusted for earth curvature. All joints in contact with earth will have water stops and protected with waterproofing systems. The BTH2 will be supported by a new metal service building which will be placed on the 6 ft thick BTH2 concrete roof. The service building which will contain data racks, electrical panels and transformers will be designed to carry all equipment and utilities dead loads.

Existing metal stairs and utilities located on the south wall of existing BTH will be relocated to allow BTH2 construction.

Structural Design Criteria

The metal building will be designed to conform to CBC 2010 requirements as well as SLAC Building & Site-Wide Design guidelines (DS-018-000-01-R0).

Design Dead and Live Loads (will not be less than ASCE 7 minimum requirements)

- Dead loads of structure as calculated
- Collateral dead load allowable for sprinklers, ducts, piping, electrical conduits and lighting - 5 to 10 psf or as calculated whichever is higher
- Service building/HVAC deck floor live load - equipment weight or 350 psf, whichever is greater
- Floor Live Load = 100 psf
- Platforms, stairs, and corridor live loads = 100 psf

Wind Load Parameters

ASCE 7 - Basic “three-second gust” wind speed: 85 mph; Exposure C

Seismic Design

The structures will be designed and constructed to resist seismic loads and to limit the deflections generated by strong ground motion during a seismic event. The seismic design will comply with the following:

Geologic Hazard Evaluation and site specific response spectral data in the report provided by SLAC. Base shears will be based on using the site-specific spectral acceleration curves. Base shears calculated using dynamic analysis will be compared with CBC requirements and the most conservative loading will govern.

CBC 2010 requirements:

- Service Buildings & BTH2 tunnel Occupancy Category II (Importance Factor I = 1.0, Ip =1.0).
- Seismic Design Category E
- Soil Class will be determined by Geotechnical Consultant for project site.
- Seismic coefficients will be determined based on the location latitudes and longitudes
- Following are seismic coefficients at BTH area, based on the assumption of Class D soil:

  Latitude: 37.416928 deg.

  Longitude: -122.200955 deg.

  Ss = 2.414 g

  S1 = 0.997 g > 0.75g therefore SDC = “E” (ASCE 7.05, article11.6)

  SMS = 2.414 g

  SM1 = 1.495 g

  SDS = 1.609 g

  SD1 = 0.997 g

  Fa = 1.0

  Fv = 1.5

- Design structure to resist lateral earth pressures and surcharge loads and seismic increment, on basement walls as defined in the CBC or geotechnical report whichever is more stringent.
- A continuous load path with adequate strength and stiffness will be designed and detailed to transfer all seismic forces from the point of application to the final point of resistance.

10.1.3.3 Mechanical Systems

BTH will have a ventilation system that will be activated when the beam is “OFF”. Ventilation will provide more than 2 air changes per hour (ACH). A roof mounted exhaust fan with ductwork will provide the necessary ventilation. The fan will be monitored and controlled by SLAC’s Energy Management System.

Low Conductivity Water (LCW) system

Supply and return piping with pressure gauges, isolation valves will be mounted on the wall of the BTH. LCWS and LCWR connections for magnets and other equipment will be spaced along the BTH tunnel.

New LCW piping system will be connected to existing 1801 LCW piping.

LCW supply temperature is 87°F, with a total demand of approximately 320 GPM for two beam lines.

The LCW system will be controlled and monitored by the existing SLAC Distributed Controlled System (DCS) Network.

Compressed air system

Clean, dry compressed air at 100 psig will be provided along the length of the BTH. Compressed air piping will be mounted along the south wall with shut-off valves and pressure gauges. The compressed air piping system will be connected to SLAC site-wide compressed air piping. The estimated demand for two beam lines is 20 SCFM.

Drainage

Sump pumps along the tunnel will collect any accumulated water, and drainage piping will route the water to a storage tank outside the BTH. The storage tank will drain into the sanitary waste piping once the water has been tested. A high level indicator will monitor the level and it will be connected to SLAC Distributed Control System (DCS) network.

Service Building

An Air Handling Unit (AHU) with cooling coil, economizer, air filters, and chilled water piping will provide conditioned air to the service building. The AHU will remove the heat generated by the electronic racks. Chilled water piping will be connected to the Auxiliary Utility Plant (AUP).

The AHU will be installed on the roof of the BTH, next to the service building. Air distribution ductwork (supply and return) will be provided inside the building. The operation of the AHU will be controlled and monitored by SLAC Energy Management System (EMS).

Duct mounted smoke detectors will be provided per California Mechanical Code (CMC).

Fire Protection system

The fire protection piping system for the service building will be designed to meet NFPA 13 and Life Safety Code 101. The service building will be an Ordinary Hazard (Group I) facility. The BTH service building will have a wet fire sprinkler system. Zone control valve with supervisory and flow switches will be provided where the piping system enters the building. The fire protection piping will be connected to existing SLAC underground water distribution piping system.

10.1.3.4 Electrical System

BTH Tunnel

The electrical distribution service to the Beam Transport Hall and Service Building will be fed from a new 277V/480V, 1600A, BTH-M Switchgear. The power source to this new BTH-M switchgear will be fed from existing 277V/480V, 4000A RA-2 Substation. The conceptual design of a new 277V/480V, 1600A feeder from existing RA-2 substation to new switchgear BTH-M will be routed through the existing underground utility tunnel, stub out from existing utility vault "B" and run conduits to new switchgear location. The final routing of this new feeder and size of the switchgear will be determined during detailed design.

The new 1600A, 277V/480V, 3 phase, 4 wire BTH-M switchgear shall be outdoor type, NEMA 3R rated, free standing, dead-front, tamper resistant insulated copper bus & tin plated ground bus, 65kAIC symmetrical, minimum short circuit rating. The main circuit breaker shall be 100% rated drawout type equipped with LSIG electronic trip units and complete with protective relays, power monitoring and metering devices. The detail arc flash, short circuit, load flow, balancing and all other applicable design requirements will be implemented in the detailed design.

The new 1600A BTH-M switchgear will provide power to the Beam Transport Hall, service building and a portion of the Undulator Hall.

Power Distribution

The BTH Hall will be provided with 120V convenience outlets and 480V welding receptacles.

Lighting System

Industrial fluorescent fixtures will be provided to achieve adequate lighting level. Lighting level will be designed in accordance with Illuminating Engineering Society (IES) recommendations. The facility access lighting will be switched from the lighting panels with provisions included to interface with the Personal Protection System (PPS). Exit and emergency lights will be provided per code. Tunnel lights will be provided with magnetic ballasts and emergency lights will be provided with remote mounted batteries. Exterior lighting will be provided at entrances, and at selected points along the exterior of the BTH Hall.

Grounding and Bonded System

A new ground grid system will be installed along the length of the new beam line. A new perimeter grounding ring with ground rods and test wells will be installed for the BTH Hall and will be tied into the ground grids. All systems and equipment will be bonded per NEC and NFPA requirements. The new ground grid will be tied into the existing ground system at selected locations. Grounding and bonding system will be designed per CEC and NEC requirement. The detail grounding system will be designed in preliminary and final design phases.

Fire Alarm and Detection System

The fire alarm system will be met utilizing Siemens products to integrate with the existing campus network. The fire alarm system will be designed to comply with NFPA 72 and all associated codes and regulations. The new fire alarm system will consist of, but not limited to, a fire alarm control unit, alarm

initiating devices, occupant notification appliances, and associated ancillary equipment for interfacing the new fire alarm system with the existing SLAC alarm receiving equipment. The fire alarm system will also communicate with other life safety systems, building system equipment as applicable. The final design of the fire alarm system will be detailed in preliminary and final design phases.

The fire detection system will be integrated with the existing campus network. The fire detection system will be design to comply with NFPA 72 and all associated codes and regulations. The fire detection system will be VESDA Air Sampling and Early Warning Smoke Detection. The VESDA system will consist of, but not limited to, the sampling pipe network, highly sensitive LASER-based smoke detectors, aspirators, filters, detector assemble network, digital communication ports. The fire detection system will be also communication with other life safety systems, building system equipment as applicable. The final design of the fire detection system will detailed in preliminary and final design phases.

The Audible Alarm Notification and Manual Voice Paging System will be designed and integrated with existing campus network. The audible alarm notification system will be by voice evacuation and tone signals on loudspeakers in areas. The manual voice paging system will be configured to allow voice paging. Upon activation of any speaker manual control switch, the alarm tone will be sounded over all speakers in that group. The final design of systems will be determined in detailed design.

Telecommunication System

The telecommunication system will be provided to support the physical transmission facility for voice, data and low voltage networks. The system consists of, but not limited to, the following:

- Telecommunication backbone pathways includes dedicated point-to-point (BDF to IDF) pathway system. These pathways may be comprised of cable tray, raceways, boxes, inner duct in cable tray, cable suspension products, and seismic bracing.
- Telephone and data structure cabling system will be designed to comply with the requirement of EIA/TIA 569 Commercial Building Standard for telecommunications pathways and spaces. The cabling system will be designed to comply with pertinent codes, rules, regulations and laws of the Authorities having jurisdiction. The cabling system includes building pathways, backbone cabling, horizontal cabling and an administration system to manage the pathways and cabling.

Relocation of Existing Electrical Raceway

Due to making use of existing BTH wall as a common wal between the existing and new BTH facility, the existing electrical raceway attached to the exterior wall of existing BTH will be re-routed. The relocated routing of the electrical raceway will be detailed out during preliminary and final designs.

BTH Service Building

Service Building houses BTH process rack lineups along with a portion of UH2 process racks.

Main switchboard

An 800A, 277V/480V, 3 Phase, 4 Wire Main Switchboard will be provided inside Service Building for power distribution. Main switchboard will be front accessible only and will have power monitor meter.

Main feeder circuit breakers in the switchboard will be 100% rated solid state type with LSIG trip unit. This main switchboard will provide power to mechanical/HVAC loads associated with ventilation of the BTH, power to HVAC systems associated with the service building, power to the step down feeders of beam line clean/dirty and utility process panels for BTH2 and portion of UH2.

Distribution panelboards

277V/480V or 120V/208V, 3 phase, 4 wire distribution panelboards shall be dead-front, dead-rear, solid state type main circuit breaker, branch circuit breakers are group mounted, front accessible bolt-on thermal magnetic molded case type with adjustable magnetic trip settings. Full length buss for both voltage and 200% neutral bussing on 208V distribution panels.

Dry type transformer

Transformer will be NEMA TP-1 compliant, Energy Star labeled transformers to step down to 120V/208V, 3 phase, 4 wire, K13 rated, 200% neutral.

Individual neutral wire for each phase wire.

Arc Flash rating

For 480V system, use solid state type breakers for coordination selectivity to reduce fault clearing time, for 208V system, limit step down transformer to 112.5 KVA.

Lighting System

Industrial fluorescent fixtures will be provided inside Service Building. High Intensity Discharge (HID) fixtures will be provided as outdoor lighting for the service building. Lighting level shall be designed in accordance with Illuminating Engineering Society (IES) recommendations. Fixtures shall be fluorescent type with energy saving T8 lamps, 3500 Kelvin color temperature with high efficiency electronic ballasts 95% power factor, total harmonic distortion (THD) of less than 10%. Lighting control will be designed to meet or exceed the requirement of Title 24 and Service Building requirement. Exit and emergency lights will be provided per code. Exterior lighting will be provided at the entrances, landings, equipment pads and access stairs.

Grounding and Bonding System

Grounding and bonding system will be designed per CEC and NEC requirement. Building ground bus shall be located in main electrical equipment area. All ground buss in the Service building will be connected back to the building main ground buss. All systems and equipments will be bonded per NEC and NFPA requirements. The grounding system in the service building shall tied to new grounding grid. The detail grounding and bonding system will be designed in preliminary and final design phases.

Fire Alarm and Detection System

The fire alarm system will be met utilizing Siemens product to integrate with the existing campus network. The fire alarm system will be designed to comply with NFPA 72 and all associated codes and regulations. The new fire alarm system will consist of, but not limited to, a fire alarm control unit, alarm initiating devices, occupant notification appliances, and associated ancillary equipment for interfacing

the new fire alarm system with the existing SLAC alarm receiving equipment. The fire alarm system will also communicate with other life safety systems, building system equipment as applicable. The final design of the fire alarm system will be detailed in preliminary and final design phases.

Telecommunication System

The telecommunication system will be provided to support the physical transmission facility for voice, data and low voltage networks. The system consists of, but not limited to, the following:

- Telecommunication backbone pathways includes dedicated point-to-point (BDF to IDF) pathway system. These pathways may be comprised of cable tray, raceways, boxes, inner duct in cable tray, cable suspension products, and seismic bracing.
- Telephone and data structure cabling system will be designed to comply with the requirement of EIA/TIA 569 Commercial Building Standard for telecommunications pathways and spaces. The cabling system will be designed to comply with pertinent codes, rules, regulations and laws of the Authorities having jurisdiction. The cabling system includes building pathways, backbone cabling, horizontal cabling and an administration system to manage the pathways and cabling.

10.1.4 Undulator X-ray Transport (UXT)

The UXT which consist of 3 segments Undulator Hall (UH2), Electron Beam Dump (EBD2), and Front End Enclosure (FEE2) will be 19'-0" diameter mined tunnel having a barrel vault shape with vertical side walls. The underside of the arch is 19'-6" from the top of finished floor.

Undulator Hall 2

The new undulator hall will be approximately 170m long and house the electron beam dogleg and the undulator. The tunnel is in line with the Beam Transport Hall (BTH). The downstream part is constructed in the vicinity of the existing Building 901 (see Figure 10.7).

The LCLS-II undulator requires stringent space temperature control. New stable supports will be installed in the tunnel for the undulator. The heat load in the tunnel will be somewhat higher than in the existing tunnel due to the presence of two undulator systems with motors for gap control.

The utilities required in the tunnel for the LCLS-II are those required to support the technical systems for photons beam and electron beams. New utility resources are required including new plumbing, wiring, cable trays, heating, ventilation, air conditioning and power. The costs for these elements are included in the undulator sections.

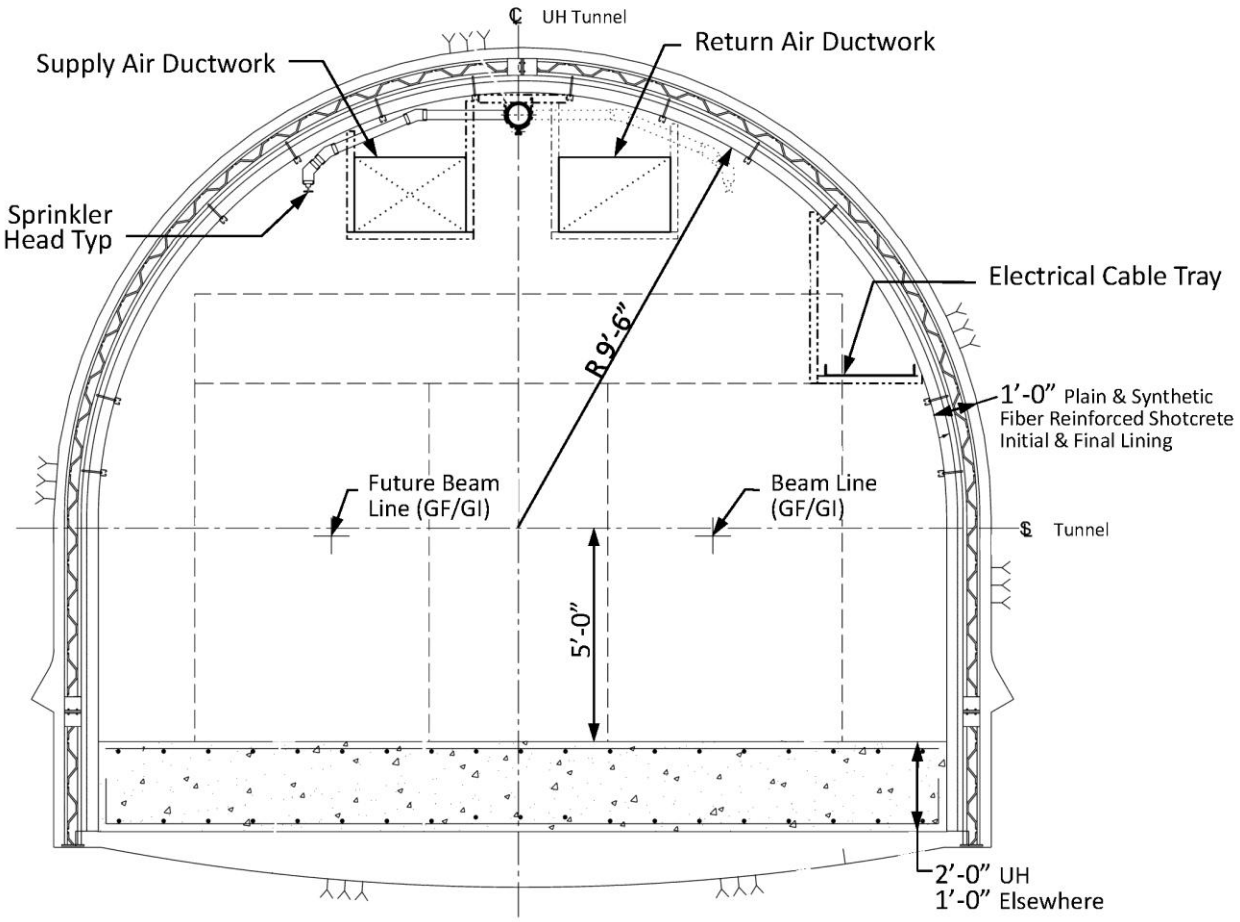

Figure 10.7. Undulator Hall (Typical Cross-Section).

10.1.4.1 Architectural Undulator and Service Building

The Undulator Hall (UH2) contains the undulator magnets and ancillary scientific equipments. These undulators magnets are set on metal stands and girders located on the floor of the tunnel. The high-energy beam passes to the expanded BTH and enters the undulator magnets before it travels through the Electron Beam Dump (EBD2) and into the beam dump pit. The UH2 measures a total of 170 meters (~558') from the end of the expanded BTH to the beginning of the Electron Beam Dump 2.

The UH2 is physically defined by the space contained between the two thermal barriers, which are located at the end of the expanded BTH to the west, and before the start of the Electron Beam Dump (EBD2) to the east. It is structurally defined as a semi-circular tunnel with an internal cross-sectional dimensions of 14'-6" x 14'-10" (H x W). The technical and functional requirement for the UH2 is amongst the most challenging in the LCLS-II facility. Service access into the UH-2 will need to be wide enough to allow for variable gap magnets. This access point may be from either the expanded BTH to the west or from the Experimental Hall (EH2) to the east. Furthermore, a 4'-0" wide maintenance and service walkway will be required between the beam-lines along the length of the tunnel. This is also a radiologically-controlled area (RCA), so compliance with SLAC Radiological Criteria is critical. The reinforced concrete and shotcrete tunnel together with the earth cover provides adequate shielding.

Low profile and low heat generating light fixtures are required in the UH2. The interior finish on the walls and ceiling will be a rough finish – typically a heavy latex enamel (water borne, low VOC) paint finish, the concrete floor requires an epoxy based flooring system to sustain heavy loads; and all mechanical, electrical and control cabling will be supported by cable trays running lengthwise along the UH2 walls and ceiling. The clear height required for operation and maintenance of the undulator equipment is a minimum of 9'-0".

At 249.38 feet the floor elevation of the tunnel is same as the other LCLS-II segments. However, a monolithic floor is needed for the UH2 since it is extremely sensitive to seismic conditions, vibrations and differential settlement of soil. This monolithic floor could be made of separate 'keyed-in' slabs that eventually act as a single, monolithic structure.

The tolerances for physical and ambient environment inside the UH2 are very tight. Two thermal barriers comprised of 3-5/8" steel studs with multiple layers of 5/8" gypsum wallboard on both sides plus R-19 thermal insulation, at either end help control the temperature, humidity, and airflow for the entire volume of the tunnel. These thermal barriers are 3-hr fire & life safety rated walls with a 4'-0" wide 2- hr. fire rated door for access.

Exit signs will be edge-lit with concealed lamp and integral lettering on a clear lens. Where low-level exit signs are required, they will be backlit and set flush with the adjacent wall.

Fire extinguishers will be provided in accordance with NFPA 10, throughout the building. The maximum travel distance to an extinguisher from any point in the building will be 50 feet. Fire extinguishers will be placed in surface mounted steel cabinets with baked enamel paint finish, with upper edge at +4'-6". Frameless doors will have a solar gray glass lite and silk-screened letters. All cabinets will be sized to house the code required size extinguisher.

The UH2 will also support a 2,000 gsf service building for the LCLS-II facility. This will be located above the UH2 at grade. The service building will house data racks, electrical panels and transformers. Provide a maximum of 17 electrical/data/fire alarm penetrations to UH2 below. Penetrations will be constructed of a 6" dia. embedded steel pipe sleeve, secured and grouted in place, with threaded steel pipe cap and fire stopping per specifications.

The Service Building will be designed and constructed utilizing an 18' high bay metal building system, including primary & secondary structural steel framing, with standing seam metal roof and wall panels. All exterior metal will be galvanized steel with urethane enamel coating system. Exposed fasteners will be of the same metal as being fastened with the same finish system.

The standing seam roofing system will have a minimum 20-year warranty. Roof assembly will have a minimum slope of ½" per foot. In compliance with the DOE memo from the Secretary of Energy, dated June 1, 2010, the roof assembly will be designed and installed to have a thermal resistance of at least R-30 and meet the requirements of Cool Roof Rating Council program.

The interior work and service areas floor slabs will have sealed concrete finish. Perimeter walls will be protected from impact damage to a minimum of 8'-0" A.F.F. Typically all exposed construction will be finished with a heavy latex enamel (water borne, low VOC) paint finish. Interior doors will be painted

hollow metal, with painted hollow metal frames. Doors in high-use areas will receive protective stainless steel panels to lever height.

Exit signs will be edge-lit with concealed lamp and integral lettering on a clear lens. Where low-level exit signs are required, they will be backlit and set flush with the adjacent wall.

Fire extinguishers will be provided in accordance with NFPA 10, throughout the building. The maximum travel distance to an extinguisher from any point in the building will be 50 feet. Fire extinguishers will be placed in surface mounted steel cabinets with baked enamel paint finish, with upper edge at +4'-6". Frameless doors will have a solar gray glass lite and silk-screened letters. All cabinets will be sized to house the code required size extinguisher.

10.1.4.2 Structural

Undulator X-Ray Transport (UXT), Service Building & Construction Shaft

The UXT which consist of 3 segments Undulator Hall (UH2), Electron Beam Dump (EBD2), and Front End Enclosure (FEE2) will be 19'-0" diameter mined tunnel having a barrel vault shape with vertical side walls. The underside of the arch is 19'-6" from the top of finished floor. The tunnel surfaces in contact with soil will be lined with water proofing material to prevent water leaks in the tunnel. Water stops will be provided at concrete joints. Pipe/duct penetrations through concrete will be provided with water stops and will be water tight. Drainage strips could be provided on the inside of tunnel surface in critical areas.

Floor slab for UXT will be designed to minimize the effects due to differential settlement and shrinkage. The floor will be doweled with the floor of BTH2 and the floor of FEE2 to minimize differential settlement. Floor surface will be flat and leveled and designed to minimize vibration as well as short and long term distortion. The finish floor for UXT will have zero percent slope in the direction of beam adjusted for earth curvature. All joints in contact with earth will have water stops and protected with waterproofing systems.

The mechanical service for UXT will be provided by exterior mechanical equipment (MEP) yard located near/above the tunnel. A utility shaft will be provided to connect utilities from the MEP yard to the tunnel. Concrete utility shaft will be water tight and will not allow any water to reach the tunnel. MEP yard will be fenced and the surface (grade) covered with concrete slab. The areas around the yard will be well drained to prevent water percolating to the tunnel surface.

Structural Design Criteria

The metal building will be designed to conform to CBC 2010 requirements as well as SLAC Building & Site-Wide Design guidelines (DS-018-000-01-R0).

Design Dead and Live Loads (will not be less than ASCE 7 minimum requirements)

- Dead loads from structure as calculated
- Collateral dead load allowable for sprinklers, piping, ducts, electrical conduits and lighting – 5 to10 psf or as calculated whichever is higher

- Laser rooms floor live load - Equipment weight or 350 psf, whichever is greater
- Live load (other areas) - 100 psf
- Platforms, stairs, and corridor live loads - 100 psf
- Two 3-ton cranes at EBD2
- Floors to be designed for vibration levels provided by vibration consultant based on equipment specifications.
- 1 kip/ft at beam line, 25 kips at any joint
- Lateral earth pressures and surcharge loads provided in Geotechnical report

Cut & Cover Roof where used:

- Dead loads from backfill at 130 pcf as calculated, along with a down drag overburden factor of 1.25 (to be confirmed with geotechnical report). Possible surcharge from trees to be planted along the alignment of this structure.
- Live load: Design for traffic surcharge at parking and Pep Ring Road crossing using HS20-44 truck loading - two 32 kip axle loads and one 8 kip axle load; LT-40 lift truck – 98,500 lb each front wheel and 9000 lb rear wheel

Seismic Design

The structures will be designed and constructed to resist seismic loads and to limit the deflections generated by strong ground motion during a seismic event. The seismic design will comply with the following:

Geologic Hazard Evaluation and site specific response spectral data in the report provided by SLAC. Base shears will be based on using the site-specific spectral acceleration curves. Base shears calculated using dynamic analysis will be compared with CBC requirements and the most conservative loading will govern.

CBC 2010 requirements:

- Occupancy Category II (Importance Factor I= 1.0, Ip =1.0). An Occupancy Category III with an importance factor of I = 1.25 could be considered for the design of concrete tunnels to prevent cracking due to ground motions, and thus reducing potential water leaks.
- Design structure to resist lateral earth pressures and surcharge loads and seismic increment, on tunnel walls and roof as defined in the CBC or geotechnical report whichever is more stringent
- A continuous load path with adequate strength and stiffness will be designed and detailed to transfer all seismic forces from the point of application to the final point of resistance.

Floor Vibrations Specifications for X-Ray Mirrors

Specifies vibration levels to design to for floors on which x-ray mirrors which have critical pointing stability for the FEL x-ray beam are to be located. This specification is intended to be used as a generic specification for the most vibration-sensitive areas in LCLS-II conventional facilities. In particular, the specification is applicable for areas where there are x-ray mirrors for which pointing stability is critical. The specification applies to vibration measured at the floor in the absence of vibration generating beamline equipment, such as large scroll pumps, but with normal conventional utilities in operation, such as HVAC equipment and process cooling water. Given the assumptions 2-6, a mirror supported from the floor should have pointing stability within the stated range in assumption 1, insofar as floor vibrations are the cause of mirror motion.

Assumptions

The nominal rms angular stability of a mirror is 0.2 micro-radians or less. Note that 0.2 micro-radians is 1/10 of the rms angular spread in the 0.15 nm LCLS FEL beam.

The vibration levels will be less than the specified limit 99% of the time (4σ). It is therefore permissible for transient vibrations levels to exceed the specified level.

The amplification factor for mirror angular motion to floor angular motion is 32 (30 dB). The effective shear wave velocity of the floor is 1800 feet per second. This velocity is used to convert slope change with transverse motion.

Ambient background vibration levels, measured before construction, are substantially below the level specified here.

Below 6 Hz, feedback can control the pointing stability of the mirror. Alternately, it is assumed that below 6 Hz floor motions are highly correlated over long distances so that the net angular velocity between mirror and source, or mirror and target, is within the specified tolerance.

Definitions

$\sigma_v(f_i)$ is the time-average rms of the vertical or horizontal velocity of a point on the floor, integrated over a 1/3 octave frequency band centered on f_i, under normal ambient conditions.

$s\phi(f_i)$ is the time-average rms angular position, either horizontal or vertical, of the mirror or similar object.

Specification

$\sqrt{\sum_i s^2_v(f_i)}$ < 9 microns/s summed over f_i > 6 Hz.

Notes

$s_v(f)_i = v_s s_y$ is the formula relating angular velocity to translational displacement.

The limit on the sum of $S_v(f_i)$ is calculated from $S_v(f_i) = \frac{v_s s_y ¢}{4G}$, where G is the amplification factor. A factor of 1/4 is included to account for the 99% availability assumption. See reference: *Vibration Measurement Results*, LCLS Undulator Hall - Borehole B3, WIA report, Sept. 2004. W. Pritchard**.**

Tunneling

Design Rock Properties

The Ladera Sandstone rock properties are based on the project preliminary report prepared for LCLS-1. The results of these investigations are summarized in a series of reports and memoranda dated from August 2003 to May 2005 by Rutherford & Chekene. The intact rock properties are based on laboratory tests of intact rock core samples obtained during the subsurface investigations. The rock mass properties are obtained by calibrating or reducing the intact rock properties using the widely accepted rock mass classification indices (i.e. Q, RMR and GSI) based on the rock cores observation and other geologic considerations including previous tunneling experience in the area. The latest version of the Hoek-Brown and the equivalent Mohr-Coulomb failure criteria are used to represent both the intact rock and rock mass strengths during the design analyses. The rock modulus of deformation is based on laboratory measurements of intact rock samples, field pressure meter test results, and empirical correlations with other rock mass properties. No specific in-situ stress measurement was done for the project. Therefore, the in-situ stress is estimated based on the regional geologic condition and the laboratory Poisson's Ratio measurement.

In general, due to the additional subsurface investigation and testing, the design rock mass modulus for LCLS-II is higher than LCLS-I designs. However, the overall rock mass condition and behavior during tunneling are not expected to change significantly. Furthermore from the limited test's data, the rock appears to have minimum shrink/swell potential or creep susceptibility. Therefore, no special considerations are given in the analyses due to these aspects. The laboratory analyses of soil/rock and groundwater samples seem to indicate an elevated corrosive ground environment. The concrete/shotcrete mixes and steel rebar requirements are specified accordingly to deal with this environment.

Undulator Hall, X-Ray and Access Tunnels Excavation and Initial Support

Due to the weak nature of the on-site rock, the design will assume the tunnel excavations will be performed by mechanical means such as using road header, with relatively minor disturbance to the rock surrounding the tunnel. The UXT tunnels are all expected to be excavated in a single large top heading, followed by invert bench excavation. The main purposes of the bench are to provide temporary face support, and also to protect the final invert from disturbance due to construction activities. The design should rely as much as possible on the ability of the surrounding rock to mostly support itself during tunneling, and employs relatively flexible, passive support systems, that will allow controlled ground deformations and prevent the tunnel failure or collapse at the same time. Therefore, the sequence of excavation and the timing of support installation are of paramount importance and to be specified. In areas with minimum or shallow covers such as near the tunnel portals and the eastern end of the Undulator Hall interfacing with the Beam Dump Tunnel, the amount of rock cover alone may not be adequate to maintain stability, and therefore pre-support systems using grouted pipe canopy and forepoling or spiling may be considered. In addition to the basic initial support design, a set of contingency measures should be incorporated into the support design requirements to account for the varying ground conditions such as localized poorer (than typical) areas of rock. The application of these contingencies will be based on the actual ground behavior observed during construction.

In general, the typical or average tunneling ground condition is anticipated to be firm to slowly raveling, with pockets of weakly cemented or uncemented sandstone which could lead to local instability in the tunnel perimeter or heading. For tunnel excavations in this typical ground condition, initial tunnel support system consisting of Fiber Reinforced Shotcrete (FRS), reinforced with regularly spaced steel lattice girders should be employed. Due to the high susceptibility of the rock to slaking when subjected to a wetting and drying cycle, immediate application of an initial shotcrete layer at or close to the tunnel heading to protect the rock surface against deterioration should be considered. To protect the final tunnel invert against construction traffic, a temporary invert bench should be specified, with the application of a working slab or other invert protection immediately upon the bench excavation. Based on the available subsurface information, it is expected the stand-up time in the typical tunnel heading or opening to range between several hours to several days, depending on the size of openings and ground condition. Therefore, the maximum length of excavation round and timing of support installation are specified as part of the support requirements. For the existing tunnel dimensions and method of excavation anticipated, the average advance rate of the tunneling is anticipated to be in the order of about 4 to 8 LF of tunnel length per working shift/day.

In areas with rock covers generally less than one tunnel diameter or heading width, pre-support measures with forepoling using grouted pipe arches or canopies are specified. Contingencies for the worse than typical ground conditions, localized unstable rock wedges, and the anticipated zones or pockets of unstable or "running" sands include grouted pipe spiling, shotcrete at the tunnel face or temporary side walls, fiberglass rods at the temporary tunnel headings, and spot rock bolting as necessary. The extents of all the special measures and contingencies (non-standard support system) described above will be defined in the contract documents for bidding purposes. The tunnel ground behavior that warrants the application of these special measures will be qualitatively defined.

Instrumentation of the ground above and around the tunnel are specified to monitor the impact of tunneling. The use of in-tunnel instrumentation will be limited to convergence points and monitoring, that is expected to cause no or only minimum impact to the tunnel excavation progress.

Because of the very weak or soft nature of the sandstone rock, the failure mode in the tunnel will be mostly governed by the plastic failure or yielding of the rock mass surrounding the tunnel opening, instead of controlled by rock discontinuities. Therefore, a continuum mechanics finite element method will be mostly used to analyze the support requirements. In some areas, such as the tunnel portals and intersections, where the rock is relatively good and its discontinuities are well defined, there will also be potential for localized blocks or wedges or rock to fall out during excavation. Although formal wedge stability analyses in this case are not performed due to lack of joints information, extra bolts are specified as necessary at certain locations to cope with this type of failure mode.

Floor Stability

The UXT floor slab has stringent performance requirements due to the very sensitive equipment that will be operating in the finished tunnel. In order to limit beam line maintenance, a year after construction, the root mean square differential movement between supports 10 meters apart should be in the order of magnitude of only 2-3 microns/week. The original design criterion for the floor slab is to provide a design that is at or beyond the "state of the art". In order to try and meet the design criteria, several concepts will be explored during Title I and Title II design.

Design approach will be to provide a tunnel with equal or greater stiffness than existing SLAC tunnels. Consider that differential movements along the UH2 should be similar to the performance of existing tunnels, which was mined in the Ladera sandstone at a similar but slightly deeper location than the UH. Differential movement data from 1985 to 1987 provided by SLAC, is considered to be typical for the PEP tunnel in this area.

Data analysis indicated that the root mean square average differential settlement in this area is less than 0.5 microns/day, which approaches the SLAC operating requirements of 2-3 microns per week. Therefore, by providing a stiffer tunnel with greater construction control, the performance criteria for the tunnel may be achieved using the "traditional" approach.

The construction specifications for existing UH required that the Contractor provide greater protection of the tunnel invert than in earlier tunnel contracts, which help provide better performance. The specifications required that a minimum 3 foot thick invert bench of sandstone be maintained through the entire UH tunnel during excavation and initial support of the remainder of the tunnel. This will help prevent disturbance to the invert during the majority of the earthmoving operations. Limits were also placed on excavation equipment to be used for the bench, and the amount of bench excavation that can be performed before pouring a working slab to protect the sandstone subgrade. Lastly, the concrete mix for the invert floor slab was specified as a low-shrink mix to assure that, together with the grouted dowels, the invert slab will be in full contact with the shotcrete walls and thus provide the full shear transfer across that vertical joint. These features allowed the entire cross section to act together to resist ground movements longitudinally along the tunnel alignment.

Final Lining and Seismic Design for tunnels

The final lining for the tunnels will consists of additional layers of plain or unreinforced shotcrete for serviceability purpose, final graded to the required surface tolerance or smoothness. Additional reinforcement with Welded Wire Fabric (WWF) is used to satisfy the long-term structural, seismic, and code requirements of the tunnel final lining. The design criteria for the final lining are based on the static (i.e. gravity) load of rock above the tunnels and the seismic structural requirements governed by the project. The long-term gravity rock load is based on the anticipated ground behavior during excavation (as predicted by the analytical models), and widely accepted empirical formulas using the rock mass characteristics, but in no case will be greater than one tunnel width or diameter of rock load above the tunnel crown (form prior experience in similar tunneling ground conditions).

The seismic performance criteria for the tunnel and cavern structures are based on the widely accepted methods of seismic design and analysis of underground structures, as well as all applicable codes and SLAC project specific seismic criteria as described in the following references:

Seismic Design and Analysis of Underground Structures by Youssef M.A. Hashash et.al., Tunneling and Underground Space Technology 16 (2001);

Seismic Considerations for Design of SLC Tunnels, Appendix C of SLAC Architecture/Engineering Design Guidelines by Earth Sciences Associates (October 2003);

CALTRANS Seismic Design Criteria, Version 1.3 (February 2004);

Other structures and building codes as listed in the SLAC Site-Wide Design Guidelines.

The analyses utilize the seismic soil/rock parameters described in the geotechnical report by Rutherford & Chekene (January 2005), the resulting incremental strains over the static loading described above are then checked against the lining capacities to determine reinforcement requirements. The most restrictive reinforcements obtained from the seismic analyses, static analyses, and any minimum combinations as required by the codes will then be used for the final lining design in the tunnels and caverns.

Water Proofing

Water proofing of exterior tunnel surfaces will be considered to avoid leaks in the tunnel. The effect of ground water table if noted in the geotechnical report (depending on the location and depth of tunnel) will also be considered, including hydrostatic loads on the tunnel structure. For serviceability purpose to maintain relatively dry tunnels and cavern, the use of low-permeability shotcrete will be specified. A drainage sump system embedded within the final invert slabs will be provided to collect any surface run-off or remaining seepage through the tunnel liners, which is to be pumped to the designated locations out of the facilities. The final invert slab for the tunnels and cavern will be reinforced cast-in-place concrete placed after the tunnel is completed. These slabs are designed to be structurally integrated with the surrounding tunnel liners and structures. For the Undulator Hall (UH2), where specific long-term ground movement criterion requires it to achieve similar or better performance than the existing UH1 tunnel, the final slab thickness and connection will be determined to achieve at least a similar or better overall tunnel stiffness to

that of the existing tunnels. For the other tunnels , the invert slabs are designed to support the loading requirements within these facilities, in addition to the tunnel support requirements as described previously.

10.1.4.3 Mechanical Systems

Undulator Hall (UH2)

HVAC System

The Undulator Hall (UH2) tunnel will have a dedicated HVAC system to maintain space temperature inside the tunnel at 68°F, at all times. Two air handler units (AHUs) will re-circulate the conditioned air and will provide outside air. AHUs will be installed at the surface level at the east end of the UH tunnel.

AHUs equipment will be fully redundant to allow service and maintenance. The air handling units will have pre-heat coil, temperature control valves, return fans, heating and cooling coils and economizer. Chilled (CHW) and hot water (HW) piping will be connected to the each AHU. BTH will have a ventilation system that will be activated when the beam is “OFF”. Ventilation will provide more than 2 air changes per hour (ACH). The operation of the AHUs will be monitored and controlled by SLAC’s Energy Management System. Duct mounted smoke detectors will be provided per California Mechanical Code (CMC).

Process Cooling Water (PCW) System

Insulated supply and return PCW piping with pressure gauges, isolation valves, circuit setters will be mounted on the wall of the UH2. PCWS and PCWR connections for experimental equipment will be spaced along the wall of the tunnel. A PCW piping system will be installed outside the service building at ground level. The PCW system will consist of re-circulating pumps, plate heat exchanger, control valves, temperature and pressure sensors, valves and piping. Chilled water (CHW) piping from the Auxiliary Utility Plan will be connected to the heat exchanger to remove the heat from the PCW system.

PCW supply temperature is 68°F, with a total estimated demand of approximately 100 GPM for two beam lines.

The operation of the PCW system and equipment will be controlled and monitored by SLAC’s Energy Management System (EMS).

Compressed Air System

Clean, dry compressed air at 100 psig will be provided along the length of the Undulator Hall tunnel. Compressed air piping will be mounted along the south wall with shut-off valves and pressure gauges. The compressed air piping system will be connected to SLAC site wide compressed air piping. The estimated demand for two beam lines is approximately 30 SCFM.

Fire Protection system

The fire protection piping system will be designed to meet NFPA 13 and Life Safety Code 101. The Undulator Hall 2 will be an Ordinary Hazard (Group I) facility. The UH2 facility will have a wet fire sprinkler system. Zone control valve with supervisory and flow switches will be provided where the piping system enters the UH 2. A fire department connection (FDC) will be provided at the sprinkler

system riser. The fire protection piping will be connected to existing SLAC underground water distribution piping system.

Drainage

Sump pumps along the tunnel will collect any accumulated water and drainage piping will route the water to an outdoor storage tank that will be located on the south side of the BTH. The storage tank will drain into the sanitary waste piping once the water has been tested. A high level indicator will monitor the level and it will be connected to SLAC Distributed Control System (DCS) network.

Service Building

An Air Handling Unit (AHU) with cooling coils, economizer and chilled water piping and air filters will provide conditioned air to the service building. The AHU will remove the heat generated by the electronic racks.

The AHU will be installed next to the service building. Air distribution ductwork (supply and return) will be provided inside the building. The operation of the AHU will be controlled and monitored by SLAC Energy Management System (EMS). Duct mounted smoke detectors will be provided per California Mechanical Code (CMC).

Fire Protection system

The fire protection piping system for the UH service building will be designed to meet NFPA 13 and Life Safety Code 101. The service building will be an Ordinary Hazard (Group I) facility. The service building will have a wet fire sprinkler system. Zone control valve with supervisory and flow switches will be provided where the piping system enters the building. The fire protection piping will be connected to existing SLAC underground water distribution piping system.

10.1.4.4 Electrical System

Undulator Hall

The electrical distribution service to Undulator Hall (UH2), UH2 Service Building, Electron Beam Dump (EBD2), Front End Enclosure (FEE2), Experimental Hall (EH2) Level 1, Mezzanine Level and Access Tunnel will be fed from the new 12KV/480V Unit substation installed close by or inside new Auxiliary Utility Plant (AUP). The final location of this new unit substation will be determined in detailed design.

A new 800A, 277V/480V, 3Phase, 4 wire feed from this unit substation will be provided to service the Undulator Hall.

Power Distribution

The Undulator Hall will be provided with 120V convenience outlets and 480V welding receptacles.

Lighting System

Industrial fluorescent fixtures will be provided to achieve adequate lighting levels. Lighting level will be designed in accordance with Illuminating Engineering Society (IES) recommendations and in accordance to Undulator Hall operation requirement. The tunnel access lighting will be switched from the lighting

panels with provisions included to interface with the Personal Protection System (PPS) and beam operation . Exit and emergency lights will be provided per code. Tunnel lights will be provided with magnetic ballasts and emergency lights will be provided with remote mounted batteries. Exterior lighting will be provided at entrances, and at selected points along the exterior of the Undulator Hall.

Grounding and Bonding System

A new perimeter grounding rings with ground rods and test well as required will be installed for Undulator Hall and will be tied into the ground grids. All systems and equipment will be bonded per NEC and NFPA requirements. The new ground grids will be tied into the existing ground system at selected locations. Grounding system shall be designed per CEC and NEC requirement. The detail grounding system will be designed in preliminary and final design phases.

Fire Alarm and Detection System

The fire alarm system will be met utilizing Siemens products to integrate with the existing campus network. The fire alarm system will be designed to comply with NFPA 72 and all associated codes and regulations. The new fire alarm system will consist of, but not limited to, a fire alarm control unit, alarm initiating devices, occupant notification appliances, and associated ancillary equipment for interfacing the new fire alarm system with the existing SLAC alarm receiving equipment. The fire alarm system will also communicate with other life safety systems, building system equipment as applicable. The final design of the fire alarm system will be detailed in preliminary and final design phases.

The fire detection system will be integrated with the existing campus network. The fire detection system will be design to comply with NFPA 72 and all associated codes and regulations. The fire detection system will be VESDA Air Sampling and Early Warning Smoke Detection. The VESDA system will consist of, but not limited to, the sampling pipe network, highly sensitive LASER-based smoke detectors, aspirators, filters, detector assemble network, digital communication ports. The fire detection system will be also communication with other life safety systems, building system equipment as applicable. The final design of the fire detection system will detailed in preliminary and final design phases.

The Audible Alarm Notification and Manual Voice Paging System will be designed and integrated with existing campus network. The audible alarm notification system will be by voice evacuation and tone signals on loudspeakers in areas. The manual voice paging system will be configured to allow voice paging. Upon activation of any speaker manual control switch, the alarm tone will be sounded over all speakers in that group. The final design of systems will be determined in detailed design.

Telecommunication System

The telecommunication system will be provided to support the physical transmission facility for voice, data and low voltage networks. The system consists of, but not limited to, the following:

- Telecommunication backbone pathways includes dedicated point-to-point (BDF to IDF) pathway system. These pathways may be comprised of cable tray, raceways, boxes, inner duct in cable tray, cable suspension products, and seismic bracing.

- Telephone and data structure cabling system will be designed to comply with the requirement of EIA/TIA 569 Commercial Building Standard for telecommunications pathways and spaces. The cabling system will be designed to comply with pertinent codes, rules, regulations and laws of the Authorities having jurisdiction. The cabling system includes building pathways, backbone cabling, horizontal cabling and an administration system to manage the pathways and cabling.

Undulator Hall Service Building

Service Building houses UH2 process rack lineups along with a portion of the Beam Dump (EBD2) process racks.

Main switchboard

A 800A, 277V/480V, 3 Phase, 4 Wire Main Switchboard shall be provided inside Service Building for power distribution. Main switchboard shall be front accessible only, and shall have power monitor meter. Main feeder circuit breakers in the switchboard shall be 100% rated solid state type with LSIG trip unit. The detail arc flash, short circuit, load flow, balancing and all other applicable design requirements will be implemented in detailed design. This main switchboard will provide power to the step down feeders of the beam line clean/dirty, utility process panels and one 480V, 3 phase, 3 wire, 400A Motor Control Center (MCC). This MCC is to serve the mechanical/HVAC loads associated with space conditioning of UH2 along with HVAC systems associated with the service building.

The Motor Control Center (MCC)

The MCC will be provided with main circuit breaker, branch breakers, starters, power monitoring, metering, instrument, signal/control devices.

Distribution panelboards

277V/480V or 120V/208V, 3 phase, 4 wire distribution panelboards will be dead-front, dead-rear, solid state type main circuit breaker, branch circuit breakers are group mounted, front accessible bolt-on thermal magnetic molded case type with adjustable magnetic trip settings. Full length buss for both voltage and 200% neutral bussing on 208V distribution panels.

Dry type transformer

Transformer will be NEMA TP-1 compliant, Energy Star labeled transformers to step down to 120V/208V, 3 phase, 4 wire, K13 rated, 200% neutral.

Individual neutral wire for each phase wire.

Arc Flash rating

For 480V system, use solid state type breakers for coordination selectivity to reduce fault clearing time, for 208V system, preferable limit step down transformer to 112.5 KVA.

Lighting System

Industrial fluorescent fixtures will be provided inside Service Building. High Intensity Discharge (HID) fixtures will be provided as outdoor lighting for the service building. Lighting level shall be designed in

accordance with Illuminating Engineering Society (IES) recommendations. Fixtures shall be fluorescent type with energy saving T8 lamps, 3500 Kelvin color temperature with high efficiency electronic ballasts 95% power factor, total harmonic distortion (THD) of less than 10%. Lighting control will be designed to meet or exceed the requirement of Title 24 and Service Building requirement. Exit and emergency lights will be provided per code. Exterior lighting will be provided at the entrances, landings, equipment pads and access stairs.

Grounding and Bonding System

Grounding and bonding system will be designed per CEC and NEC requirement. Building ground bus shall be located in main electrical equipment area. All ground buss in the Service building shall be connected back to the building main ground buss. All systems and equipments will be bonded per NEC and NFPA requirements. The grounding and bonding system in service building will be tied to new grounding grids. The detail grounding system will be designed in preliminary and final design phases.

Fire Alarm and Detection System

The fire alarm system will be met utilizing Siemens products to integrate with the existing campus network. The fire alarm system will be designed to comply with NFPA 72 and all associated codes and regulations. The new fire alarm system will consist of, but not limited to, a fire alarm control unit, alarm initiating devices, occupant notification appliances, and associated ancillary equipment for interfacing the new fire alarm system with the existing SLAC alarm receiving equipment. The fire alarm system will also communicate with other life safety systems, building system equipment as applicable. The final design of the fire alarm system will be detailed in preliminary and final design phases.

Telecommunication System

The telecommunication system will be provided to support the physical transmission facility for voice, data and low voltage networks. The system consists of, but not limited to, the following:

- Telecommunication backbone pathways includes dedicated point-to-point (BDF to IDF) pathway system. These pathways may be comprised of cable tray, raceways, boxes, inner duct in cable tray, cable suspension products, and seismic bracing.

Telephone and data structure cabling system will be designed to comply with the requirement of EIA/TIA 569 Commercial Building Standard for telecommunications pathways and spaces. The cabling system will be designed to comply with pertinent codes, rules, regulations and laws of the Authorities having jurisdiction. The cabling system includes building pathways, backbone cabling, horizontal cabling and an administration system to manage the pathways and cabling.

10.1.5 Electron Beam Dump

The electron beam dump area will be modeled after the successful LCLS-I beam dump with one significant change: there will be no shielding wall separating the beam dump area from the first elements of the x-ray optics. The shielding wall will be installed at the EH2. The beam dump will consist of a permanent magnet to deflect the electron beam and a beam dump device installed in a properly

shielded dump area (see Figure 10.8). The total length of the beam dump and front end enclosure is approximately 135 meters.

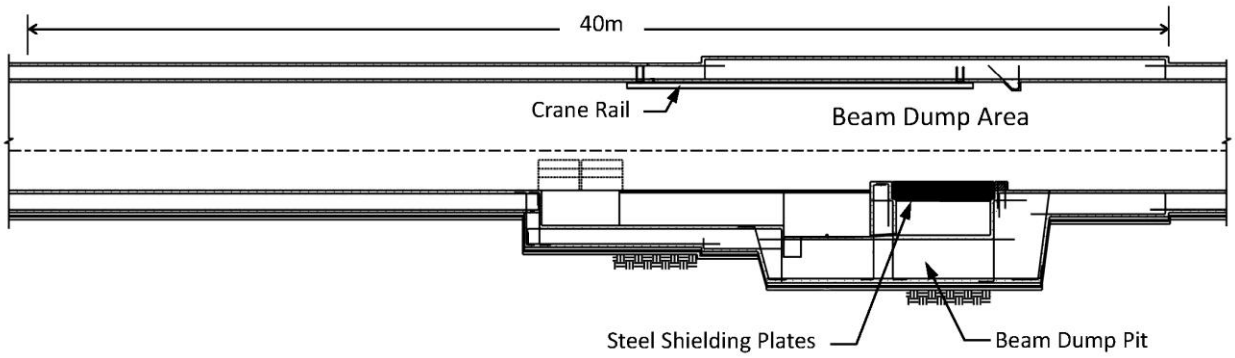

Figure 10.8. Electron Beam Dump longitudinal section.

Figure 10.9. Electro-Magnets at Beam Dump.

10.1.5.1 Architectural

The function of the Electron Beam Dump (EBD2) is to act as a terminal point for the high-energy electron beam. The electron beam separated from the x-ray bends downwards from within the Electron Beam Dump and terminates into the core of the Dump. The dump is located directly below the Electron Beam Dump and can be occasionally accessed for maintenance or during an emergency.

The radiated core of the Beam Dump needs to be cooled. This is made possible by having cooling water circulate around the core. The radiated aluminum core does not need regular servicing, however a provision for hoisting the core out of the Dump will be required. A service staircase or gangway needs to be provided from within the Dump to access the core level below. The Dump walls around the core are highly shielded to protect from both primary and secondary radiation beams.

The Electron Beam Dump is physically defined as the space between the end of the Thermal Barrier and the separation wall downstream. The interior finish on the walls and ceiling will be shotcrete – typically with white paint, the concrete floor will be sealed. The Beam Dump floor begins to dive down from the tunnel floor level of 249.38 feet, and ends up at approximately 241'-0". The diving floor is characterized by two narrow grooves (each approximately 20" wide) with a level walkway in the center of the -2.4+/- 0 degree beam-lines. This walkway remains at the 249.38 foot level. Each beam-line splits right above the start of the 'diving groove' in the floor, where the electron beam part is segregated from the x-ray beam. The grooves will be covered with metal plates while allowing the electron beam to penetrate through. The end of the walkway in the center is marked by a ladder that climbs down into the pit 8' below. This pit is at the same level as the Dump immediately downstream. The ceiling of the Dump at 249.38 feet is made of massive concrete blocks that cover the dump below. The Dump itself is located in the enclosure below the concrete blocks next the 8' deep pit.

A departure from LCLS-I, the 3' thick metal/steel block at the end of the EBD, which acts as a radiation shield will be moved and combined with the second metal shield (4' feet wide) located in the FEE2. These blocks will be designed and constructed to stop radiation from entering the Experimental Hall (EH2) facility downstream.

Exit signs will be edge-lit with concealed lamp and integral lettering on a clear lens. Where low-level exit signs are required, they will be backlit and set flush with the adjacent wall.

Fire extinguishers will be provided in accordance with NFPA 10, throughout the building. The maximum travel distance to an extinguisher from any point in the building will be 50 feet. Fire extinguishers will be placed in surface mounted steel cabinets with baked enamel paint finish, with upper edge at +4'-6". Frameless doors will have a solar gray glass lite and silk-screened letters. All cabinets will be sized to house the code required size extinguisher.

10.1.5.2 Structure

The Beam Dump (BD2) will be downstream of the Undulator Hall. The Beam Dump acts as the terminal point of the high-energy electron beam. The electrons are removed from the light beam and are bent downward and terminate at the core of the Dump. This core is comprised of a copper block and will be located below the stacked steel plate lid. The walls of the pit will be lined with steel plating and concrete.

Two monorail cranes of 3 ton each will be provided on the north and south walls adjacent to the core of the EBD2. Structural Design criteria for EBD2 will be same as for UXT.

The Beam Dump will be a mined tunnel construction and interfaces with UH2 with a specially designed separation wall. Access to the Beam Dump will be from the Experimental Hall (EH2) via a radiation shielding maze.

10.1.5.3 Mechanical System

HVAC System

The Electron Beam Dump (EBD2) tunnel will have an HVAC system to provide ventilation when the tunnel is occupied. Double dampers in the supply and return ductwork will isolate the EBD2 area when the beam is in operation. An exhaust fan will remove any excess heat when the beam is off. Operation of the exhaust fan and AHU will be interlocked. Both equipment will be controlled and monitored by SLAC's Energy Management System. The air handling unit will have cooling coils and economizer. Chilled (CHW) piping will be connected to the AHU. The ventilation system will be activated only when the beam is "OFF". Ventilation will provide more than 2 air changes per hour (ACH). Duct mounted smoke detectors will be provided per California Mechanical Code (CMC).

The chilled piping will be routed inside the tunnel from the Auxiliary Utility Plant (AUP).

Low Conductivity Water (LCW) System

Supply and return piping with pressure gauges, isolation valves will be mounted on the wall of the Electron Beam Dump tunnel. LCWS and LCWR connections for magnets, beam dump and other equipment will be spaced along the wall of the tunnel.

The LCW piping system will be connected to existing 1801 LCW piping at the Research Yard (RSY).

LCW supply temperature is 87°F, with a total demand of approximately 150 GPM for two beam lines.

Compressed Air System

Clean, dry compressed air at 100 psig will be provided along the length of the EBD2 tunnel. Compressed air piping will be mounted along the south wall with shut-off valves and pressure gauges. The compressed air piping system will be connected to SLAC site wide compressed air piping. The estimated demand for two beam lines is approximately 40 SCFM.

Drainage

Sump pumps along the tunnel will collect any accumulated water and drainage piping will route the water to an outdoor storage tank that will be located on the south side of the BTH. Drainage piping will be pressurized and it will be mounted at ceiling level of the tunnel. The storage tank will drain into the sanitary waste piping once the water has been tested. A high level indicator will monitor the level and it will be connected to SLAC Distributed Control System (DCS) network.

Fire Protection system

The fire protection piping system for the Electron Beam Dump will be designed to meet NFPA 13 and Life Safety Code 101. The EBD2 will be an Ordinary Hazard (Group I) facility. The service building will have a wet fire sprinkler system. Zone control valve with supervisory and flow switches will be provided where the piping system enters the EBD tunnel. The fire protection piping will be connected to existing SLAC underground water distribution piping system.

10.1.5.4 Electrical System

The electrical distribution service to Undulator Hall (UH2), UH2 Service Building, Electron Beam Dump (EBD2), Front End Enclosure (FEE2), Experimental Hall (EH2) Level 1, Mezzanine Level and Access Tunnel will be fed from the new 12KV/480V Unit substation installed close by or inside new Auxiliary Utility Plant (AUP). The final location of this new unit substation will be determined in detailed design.

A new 800A, 277V/480V, 3 Phase, 4 wire feed from this unit substation will be provided to service EBD2 and FEE2 process and facilities loads. The majority of the EBD2 process racks and associated transformers and distribution panels will be located in UH2 service building with selected equipment located in the Front End Enclosure (FEE2). There is no separate service building provided for the EBD2 area.

Power Distribution

The Electronic Beam Dump Tunnel will be provided with 120V convenience outlets and 480V welding receptacles.

Lighting System

Industrial fluorescent fixtures will be provided to achieve adequate lighting levels. Lighting level will be designed in accordance with Illuminating Engineering Society (IES) recommendations and in accordance to EBD2 operation requirement. The tunnel access lighting will be switched from the lighting panels with provisions included to interface with the Personal Protection System (PPS) . Exit and emergency lights will be provided per code. Tunnel lights will be provided with magnetic ballasts and emergency lights will be provided with remote mounted batteries. Exterior lighting will be provided at entrances, and at selected points along the exterior of the EBD2 Tunnel.

Grounding and Bonding System

A new perimeter grounding ring with ground rods and test wells as required will be installed for EBD2 tunnel and will be tied into the ground grids. All systems and equipments will be bonded per NEC and NFPA requirement. The new ground grids will be tied into the existing ground system at selected locations. Grounding and bonding system will be designed per CEC and NEC requirement. The detail grounding system will be designed in preliminary and final design phases.

Fire Alarm and Detection System

The fire alarm system will be met utilizing Siemens products to integrate with the existing campus network. The fire alarm system will be designed to comply with NFPA 72 and all associated codes and regulations. The new fire alarm system will consist of, but not limited to, a fire alarm control unit , alarm initiating devices, occupant notification appliances, and associated ancillary equipment for interfacing the new fire alarm system with the existing SLAC alarm receiving equipment. The fire alarm system will also communicate with other life safety systems, building system equipment as applicable. The final design of the fire alarm system will be detailed in preliminary and final design phases.

The fire detection system will be integrated with the existing campus network. The fire detection system will be design to comply with NFPA 72 and all associated codes and regulations. The fire detection system will be VESDA Air Sampling and Early Warning Smoke Detection. The VESDA system will consist of, but not limited to, the sampling pipe network, highly sensitive LASER-based smoke detectors, aspirators, filters, detector assemble network, digital communication ports. The fire detection system will be also communication with other life safety systems, building system equipment as applicable. The final design of the fire detection system will detailed in preliminary and final design phases.

The Audible Alarm Notification and Manual Voice Paging System will be designed and integrated with existing campus network. The audible alarm notification system will be by voice evacuation and tone signals on loudspeakers in areas. The manual voice paging system will be configured to allow voice paging. Upon activation of any speaker manual control switch, the alarm tone will be sounded over all speakers in that group. The final design of systems will be determined in detailed design.

Telecommunication System

The telecommunication system will be provided to support the physical transmission facility for voice, data and low voltage networks. The system consists of, but not limited to, the following:

- Telecommunication backbone pathways includes dedicated point-to-point (BDF to IDF) pathway system. These pathways may be comprised of cable tray, raceways, boxes, inner duct in cable tray, cable suspension products, and seismic bracing.
- Telephone and data structure cabling system will be designed to comply with the requirement of EIA/TIA 569 Commercial Building Standard for telecommunications pathways and spaces. The cabling system will be designed to comply with pertinent codes, rules, regulations and laws of the Authorities having jurisdiction. The cabling system includes building pathways, backbone cabling, horizontal cabling and an administration system to manage the pathways and cabling.

10.1.6 Front End Enclosure

The Front End Enclosure (FEE) will also be constructed within the 135-meter-long space that houses both the electron beam dump and the front ends enclosure (see Figure 10.10). Access to the Electron Beam Dump (EBD) and FEE will be through the EH2 and appropriately controlled using the Personnel Protection System (PPS) interlocks. A shielding wall will be constructed at the junction between the FEE and the EH2.

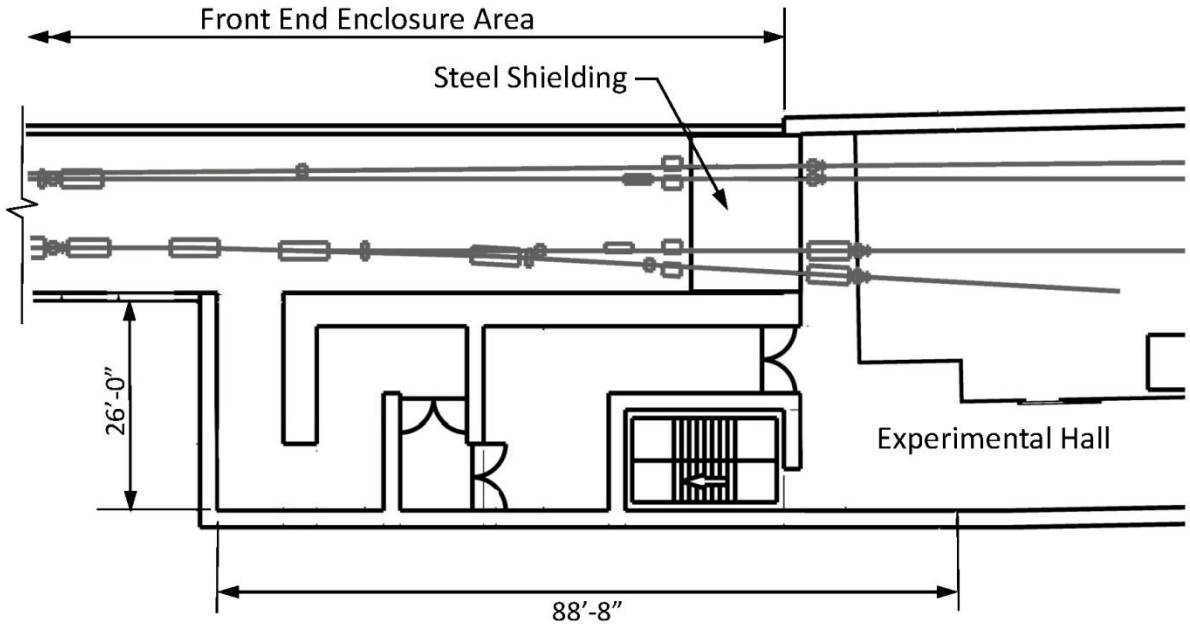

Figure 10.10. Front Ends Enclosure plan view.

10.1.6.1 Architecture

The FEE2 floor is lined with several pieces of LCLS-II equipment with varying power requirements. The FEE2 will be partly in tunnel and partly in a construction shaft. Within the construction shaft, a cast-in-place concrete facility will be built using formed concrete construction technique. The cross-section will be rectangular in shape. On the interior, the entire length of the FEE will have numerous cable trays and other equipment lining the ceiling and floors.

The FEE2 is physically defined by the space between the end of the beam dump and the start of the Experimental Hall (EH2) wall (or end of the steel shield). Within the construction shaft the FEE2 will be a cast-in-place concrete structure with a rectangular cross-section measuring 14'-6" x 19'-0" (H x W). The floor of the FEE2 is lined with numerous diagnostic, experimental and support equipment. All of the technical components, associated controls, and mechanical/electrical cables are connected/powered through cable trays running at the ceiling level. HVAC ducts and sprinkler heads line the top of the ceiling and run lengthwise. Access into the FEE2 can be made through the egress labyrinth attached to the EH2. The labyrinth requires special radiation protection from the FEE2 and the EBD2. The interior finish on the walls and ceiling will be a smooth finish – typically all work spaces will be finished with a heavy latex enamel (water borne, low VOC) paint finish, the concrete floor will be sealed. Fluorescent lighting and light switches located within the labyrinth are also required as a part of the FEE2 program.

Exit signs will be edge-lit with concealed lamp and integral lettering on a clear lens. Where low-level exit signs are required, they will be backlit and set flush with the adjacent wall.

Fire extinguishers will be provided in accordance with NFPA 10, throughout the building. The maximum travel distance to an extinguisher from any point in the building will be 50 feet. Fire extinguishers will be

placed in surface mounted steel cabinets with baked enamel paint finish, with upper edge at +4'-6". Frameless doors will have a solar gray glass lite and silk-screened letters. All cabinets will be sized to house the code required size extinguisher.

10.1.6.2 Structural

Front Ends Enclosure (FEE2)

Further downstream from the Beam Dump the light beam (sans electrons) continues through the Muon Shield (a 3 foot thick concrete and 7 foot thick steel shield) into the Front Ends Enclosure (FEE2). The underside of the rectangular concrete ceiling lid is 12'-6" above the main tunnel floor level.

Throughout the length of the FEE2, SLAC will provide numerous floor mounted LCLS process, scientific and support equipment such as X-Ray mirrors. This area is vibration sensitive and the floors will be designed to conform to vibration level requirements provided by SLAC. Foundations for X-Ray mirrors will be isolated. Structural design criteria for dead and live loads and seismic design will be the same as for UXT.

Access to FEE2 will be from the Experimental Hall (EH2) via a radiation shielding maze. Both the FEE and BD are separated from the EH2 by a fire-rated horizontal exit.

Construction Shaft

Construction shaft approximately 45 ft wide x 100 ft long x 50 ft deep will be provided at the east end of FEE2. Construction shaft will be made of drilled solid piles, wailers, and horizontal struts. The top of FEE2 roof slab within the perimeter of construction shaft will be covered with water proofing material. The roof slab will be designed for soil weights and other surcharges.

10.1.6.3 Mechanical System

HVAC System

The Front End Enclosure (FEE2) tunnel will have a dedicated HVAC system to provide ventilation and conditioned air.

An outdoor exhaust fan (EF) with ductwork and dampers inside the tunnel. The exhaust fan will remove the heat from technical components. Operation of the exhaust fan and AHU will be interlocked and both equipment will be controlled and monitored by SLAC's Energy Management System. The air handling unit will have cooling coils, temperature control valves, control dampers, air filters and an economizer. Chilled (CHW) piping will be connected to the AHU. Ventilation will provide more than 4 air changes per hour (ACH). Duct mounted smoke detectors will be provided per California Mechanical Code (CMC).

The chilled water piping will be routed inside the tunnel from the existing and Auxiliary Central Utility Plant (AUP).

Process Cooling Water (PCW) System

Supply and return PCW piping with pressure gauges, isolation valves will be mounted on the wall of the FEE2 tunnel. PCWS and PCWR connections for experimental equipment will be spaced along the wall of

the tunnel. A PCW piping system will be installed in the Auxiliary Utility Plant (AUP), and the PCW system will consist of re-circulating pumps, plate heat exchanger, control valves, temperature and pressure sensors, valves and piping. Chilled water (CHW) piping from the Auxiliary Utility Plan will be connected to the heat exchanger to remove the heat from the PCW systems.

PCW supply temperature is 68°F, with a total demand of approximately 30 GPM for two beam lines.

The operation of the PCW system and equipment will be controlled and monitored by SLAC's Energy Management System.

Compressed Air System

Clean, dry compressed air at 100 psig will be provided along the length of the FEE2 tunnel. Compressed air piping will be mounted along the south wall with shut-off valves and pressure gauges. The compressed air piping system will be connected to SLAC site wide compressed air piping. The estimated demand for two beam lines is approximately 30 SCFM.

Drainage

Sump pumps along the tunnel will collect any accumulated water and drainage piping will route the water to an outdoor storage tank that will be located on the south side of the BTH. The storage tank will drain into the sanitary waste piping once the water has been tested. A high level indicator will monitor the level and it will be connected to SLAC Distributed Control System (DCS) network.

Fire Protection System

The fire protection piping system for the Front End Enclosure (FEE2) will be designed to meet NFPA 13 and Life Safety Code 101. The FEE2 will be an Ordinary Hazard (Group I) facility. The facility will have a wet fire sprinkler system. Zone control valve with supervisory and flow switches will be provided where the piping system enters the FEE2 tunnel. The fire protection piping will be connected to existing SLAC underground water distribution piping system.

10.1.6.4 Electrical System

The electrical distribution service to Undulator Hall (UH2), UH2 Service Building, Electron Beam Dump (EBD2), Front End Enclosure (FEE2), Experimental Hall (EH2) Level 1, Mezzanine Level and Access Tunnel will be fed from the new 12KV/480V Unit substation installed close by or inside new Auxiliary Utility Plant (AUP). The final location of this new unit substation will be determined in detailed design.

A new 800A, 277V/480V, 3Phase, 4 wire feed from this unit substation will be provided to service EBD2 and FEE2 process and facilities loads. The majority of the FEE2 process racks and associated transformers and distribution panels will be located in the FEE2 enclosure. There is no separate service building provided for the FEE2 area.

Power Distribution

The Front End Enclosure (FEE2) will be provided with 120V convenience outlets and 480V welding receptacles.

Lighting System

Industrial fluorescent fixtures will be provided to achieve adequate lighting levels. Lighting level will be designed in accordance with Illuminating Engineering Society (IES) recommendations and in accordance to FEE2 operation requirement. The tunnel access lighting will be switched from the lighting panels with provisions included to interface with the Personal Protection System (PPS) . Exit and emergency lights will be provided per code. Tunnel lights will be provided with magnetic ballasts and emergency lights will be provided with remote mounted batteries. Exterior lighting will be provided at entrances, and at selected points along the exterior of the FEE2 Tunnel.

Grounding and Bonding System

A new perimeter grounding rings with ground rods and test well as required will be installed for FEE2 and will be tied into the ground grids. All systems and equipments will be bonded per NEC and NFPA requirements. The new ground grids will be tied into the existing ground system at selected locations. Grounding and bonding system shall be designed per CEC and NEC requirement. The detail grounding system will be designed in preliminary and final design phases.

Fire Alarm and Detection System

The fire alarm system will be met utilizing Siemens product to integrate with the existing campus network. The fire alarm system will be designed to comply with NFPA 72 and all associated code and regulations. The new fire alarm system will consist of, but not limited to, a fire alarm control unit , alarm initiating devices, occupant notification appliances, and associated ancillary equipment for interfacing the new fire alarm system with the existing SLAC alarm receiving equipment. The fire alarm system will also communicate with other life safety systems, building system equipment as applicable. The final design of the fire alarm system will be detailed in preliminary and final design phases.

The fire detection system will be integrated with the existing campus network. The fire detection system will be design to comply with NFPA 72 and all associated codes and regulations. The fire detection system will be VESDA Air Sampling and Early Warning Smoke Detection. The VESDA system will consist of, but not limited to, the sampling pipe network, highly sensitive LASER-based smoke detectors, aspirators, filters, detector assemble network, digital communication ports. The fire detection system will be also communication with other life safety systems, building system equipment as applicable. The final design of the fire detection system will detailed in preliminary and final design phases.

The Audible Alarm Notification and Manual Voice Paging System will be designed and integrated with existing campus network. The audible alarm notification system will be by voice evacuation and tone signals on loudspeakers in areas. The manual voice paging system will be configured to allow voice paging. Upon activation of any speaker manual control switch, the alarm tone will be sounded over all speakers in that group. The final design of systems will be determined in detailed design.

Telecommunication System

The telecommunication system will be provided to support the physical transmission facility for voice, data and low voltage networks. The system consists of, but not limited to, the following:

- Telecommunication backbone pathways includes dedicated point-to-point (BDF to IDF) pathway system. These pathways may be comprised of cable tray, raceways, boxes, inner duct in cable tray, cable suspension products, and seismic bracing.
- Telephone and data structure cabling system will be designed to comply with the requirement of EIA/TIA 569 Commercial Building Standard for telecommunications pathways and spaces. The cabling system will be designed to comply with pertinent codes, rules, regulations and laws of the Authorities having jurisdiction. The cabling system includes building pathways, backbone cabling, horizontal cabling and an administration system to manage the pathways and cabling.

10.1.7 Experimental Hall

The LCLS-II requires one experimental hall; the hall is located 305 meters downstream of the start of the undulator and x-ray transport tunnel. The experimental hall will be constructed immediately downstream of the FEE2. This hall will be approximately 14 meters wide by 80 meters long in the direction of the beam (see Figure 10.11).

The LCLS-II Experimental Hall (EH2) is a single level with mezzanine facility designed to support four experimental stations, supplied with FEL x-rays from two undulator sources. The experimental stations themselves lie outside the scope of the LCLS-II Project, but some assumptions about their basic layout and space requirements were used to define the requirements of the hall. These assumptions are based largely on the existing LCLS experimental stations, and experience with them to date. The preferred layout of the experimental hall will maximize the use of open floor plans, clear spans and high ceilings to create the most flexibility for layout of experiments, experimental hutches, set-up and assembly space, control rooms and collaboration. Laser and server rooms will be constructed on the mezzanine level of the facility.

The conventional facilities provide basic infrastructure (power, HVAC, water cooling, fire alarm, fire protection, network, etc) for developing two hard x-ray experimental stations and two soft x-ray experimental stations all located on the first level experimental floor.

In addition to space for the experimental stations, the EH2 includes control cabins and limited setup space in close proximity to the stations. On the mezzanine level of the Hall there are laser laboratories for housing equipment for generating optical laser pulses precisely synchronized to the FEL pulses. Additional experimental equipment such as instrument racks and vacuum pumps are also located upstairs, above the experimental stations. The mezzanine floor also houses a data server room and specialized lab space for preparing samples. The entrance to the hall is on the lower level, with access to the experimental floor by way of stairways and a large elevator or hoist way.

The LCLS-II Experimental Hall is located just to the south of the existing LCLS NEH2.

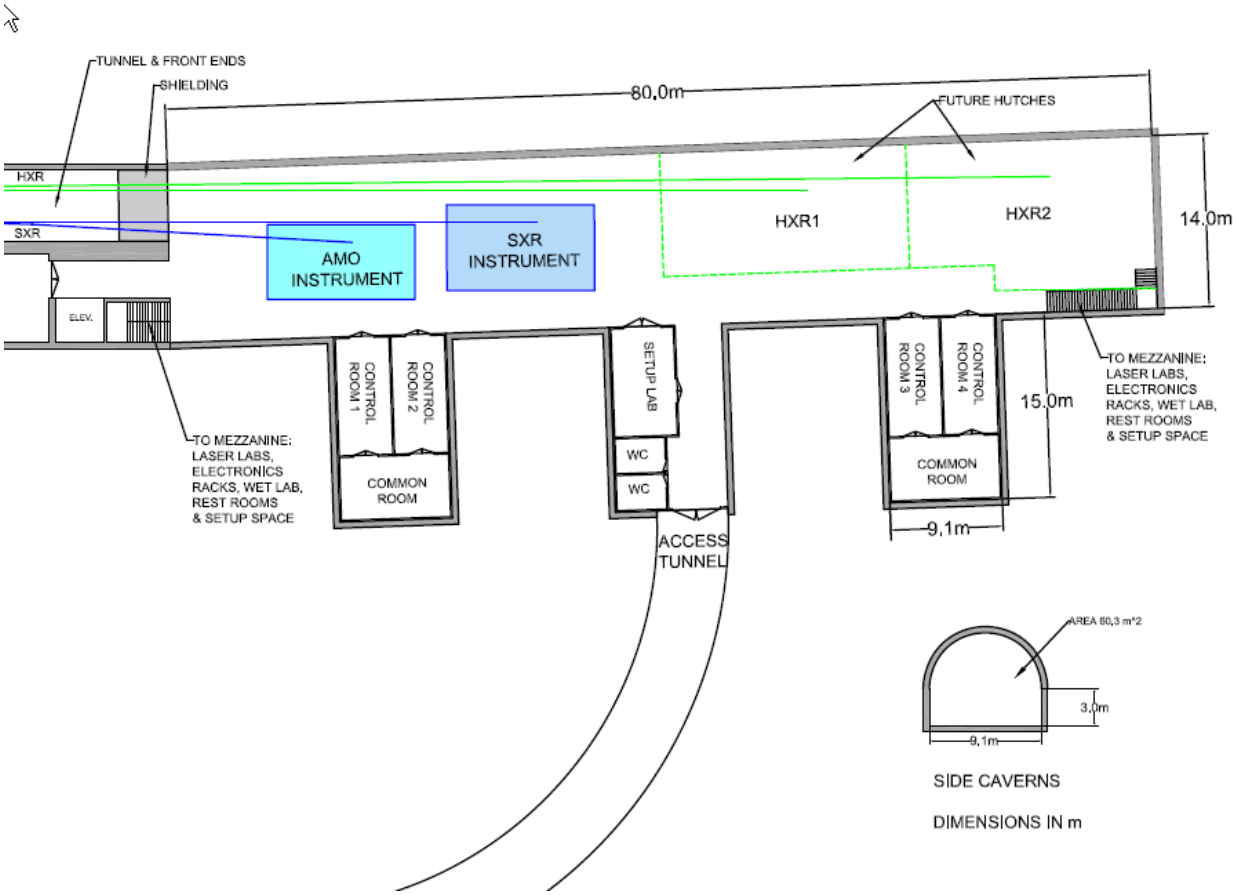

Figure 10.11. LCLS-II Experimental Hall first level plan.

10.1.7.1 Architectural

The function of the Experimental Hall (EH2) is to provide experimentation stations, control areas, preparation area for hard and soft x-ray related experiments, laser laboratories and server rooms. The EH2 is located 305 meters (~1,000') downstream of the UXT. The EH2 will be constructed immediately downstream of the FEE2. This hall will be a cavern approximately 14 meters (~ 46') wide by 80 meters (~262') long, by 10.6 meters (~35') high housing a mezzanine steel structure. The hall also includes 3 perpendicular tunnels to house the control rooms, utility support space and an access tunnel to the exterior parking area east of the PEP Ring Road.

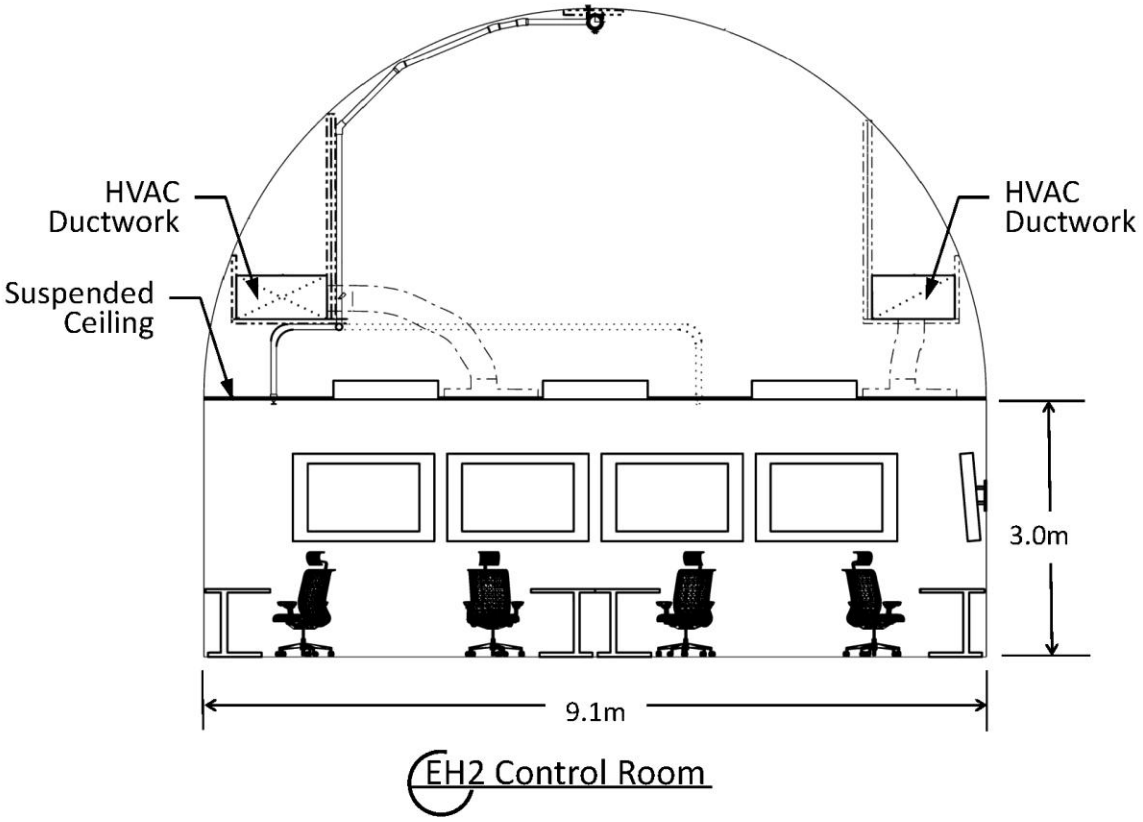

Figure 10.12. Section: EH2 Control Room.

The ~12,052 gsf first level will have a floor to floor height of 5.5 meters (~18') with exposed structure and support utility systems (HVAC ducts, cable trays, electrical conduit, etc.). Partition walls will be furred out with metal studs and gypsum board with a level 4 finish and typical heavy latex enamel (water borne, low VOC) paint finish, sealed concrete floors; and all mechanical, electrical and control cabling will be supported by cable trays running lengthwise.

The ~8,646 gsf mezzanine area which includes the laser rooms will have a 9'-6" clear ceiling height with a utility and equipment support grid suspended below the cavern vaulted structure. Typical interior perimeter and partition walls will consist of 3-5/8” steel studs with 5/8” gypsum wallboard on both sides. Fire barrier walls will comply with Underwriters Laboratories (UL) designs for one-hour separations where required. Sound batt insulation will be installed to provide acoustic insulation to adjacent spaces. Generally all rooms will be finished with a heavy latex enamel (water borne, low VOC) paint finish.

Laser room doors will be hollow metal, all laser room doors will have card readers and electrically activated hardware (i.e. electric strike, magnetic lock, etc) to be determined during detailed design. All door hardware will allow for exit passage without the use of any tool or special knowledge, such as passage lever hardware.

Doors at laser rooms housing Class 3b or 4 lasers will be flush, hollow metal only with no window openings. These doors will also include interlock sensors for use with laser safety systems. Doors without lasers in use will have vision glass panels for safety. Vision glass will be 6” x 16” minimum size.

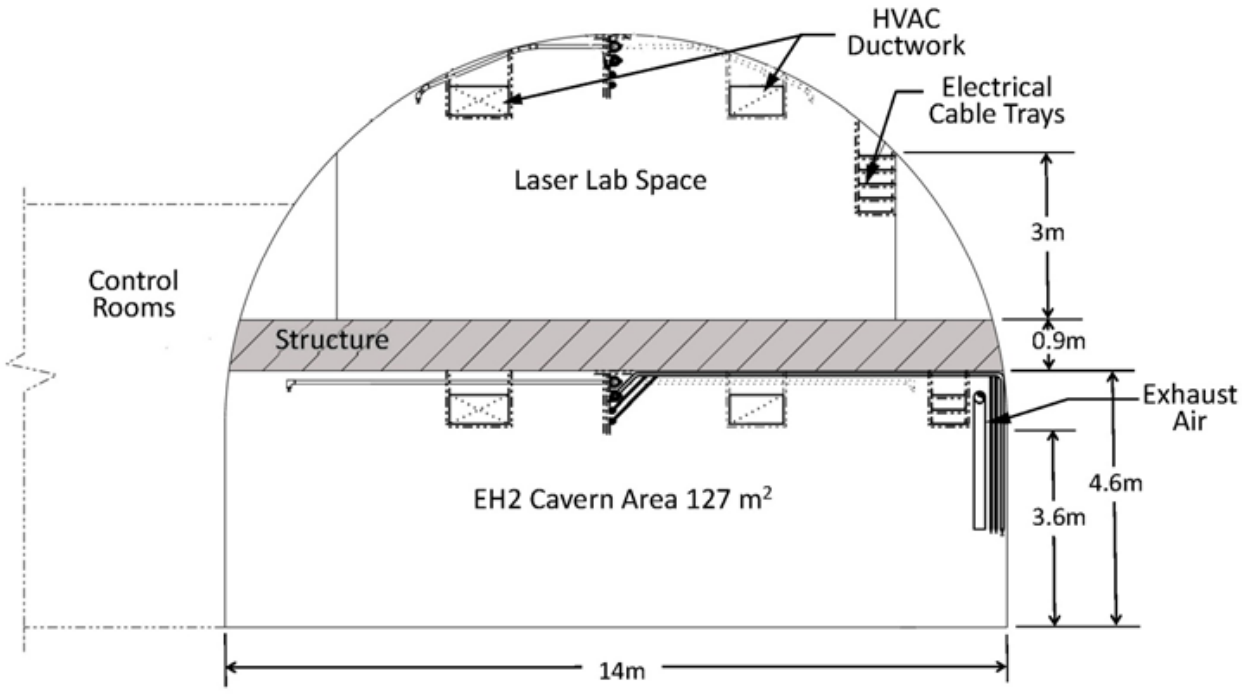

Figure 10.13. EH2 Main Cavern Section.

Laser Safety System

Emergency shutdown buttons will be provided at exit to labs and at the main entrance.

The system will include restricted access control using electric door hardware and RFDI sensors at each entry door. If equipment entry doors are provided, they should only be operable from inside the laser room and will be connected to a safety shutdown interlock or safety shutter system.

An illuminated sign board with up to 6 programmed messages will be used to indicate the laser system status. The illuminated sign board will be located at the exterior of the room near the entry door.

The design will include as a minimum junction boxes and conduit for installation of access control components, door releases, sign boards, etc, accommodating required power and control cables. Some cabling may need to be installed as part of the design. SLAC will provide details for conduit size and routing.

The laser safety system will include a safety shutdown interlock or safety shutter system that will be installed by SLAC during equipment installation.

Laser room floors will be sealed concrete. All floors will be provided with rubber base at wall and casework perimeters.

The three perpendicular tunnels which house the control rooms and utility support spaces will have a 9'-6" clear ceiling height. Typical perimeter and interior partitions will be floor to suspended ceiling, 3-5/8" 20 gauge metal studs at 16" O.C. braced to the structure above. Stud sizes will increase in width as needed for utilities. Ceilings in control room areas will be lay-in acoustical suspended ceilings at approximately 9'-6". Ceilings in restrooms will be gypsum board ceilings at 8'-0". Typical interior finishes will include sealed concrete floors, rubber base and painted walls in control rooms and support spaces, with ceramic tile flooring, base and wainscot and painted walls in restrooms. Typical doors are 3'-0" x 7'-0" flush painted hollow metal doors and frames and lever hardware. Millwork in control room space is plastic laminate upper and lower cabinets; AWS Custom-grade frameless flush overlay style; white melamine interiors.

Rest Rooms

Access will be designed to prevent inappropriate sightlines into the toilet room from the corridor. Men's and women's rooms will be in close proximity to each other.

Toilet partitions will be ceiling hung, stainless steel or solid phenolic composition.

Provide tile walls below the lavatory counter and full height tile walls at the toilets and urinals. The ceiling and all remaining walls should be painted gypsum board. Recycled content is advised.

Floor finish will be sealed unglazed ceramic tile or better with a cove base. Provide a central drain immediately under the toilet partition. Recycled content is advised. Floor tile or similar impervious material should be extended at least 5" up on walls.

Ceiling finish will be painted gypsum board. Provide fluorescent light above the lavatory mirrors and stalls.

Mirrors (full width above lavatories and full length adjacent to exit) will be vision quality glass.

Counters and backsplashes will be of high quality, durable material (e.g. solid surface or natural stone) and be contained by end walls. Plastic laminate and cast plastic are not appropriate.

Under set, porcelain lavatories or integral will be fitted with spread-set accessibility-compliant motion activated faucets and soap dispensers. A stainless steel or millwork apron to match countertop will provide protection from exposed plumbing; foam or plastic plumbing chase covers are not appropriate. Stainless steel should be treated with protectant.

Toilets and urinals will utilize motion-activated flush valves.

Coordinate toilet room accessories with SLAC material supply requirements.

Toilet accessories will have a brushed stainless surface. Accessories will include toilet paper dispensers, seat cover dispensers, automatic towel dispensers, waste receptacles; grab bars, coat hooks, sanitary napkin dispensers and soap dispensers mounted at the sinks. Primary waste receptacles will be sized according to manufacturer's recommendation for a lab building that is serviced once a day. The shower area accessories will include a recessed soap dish, shower seat, towel bar, mirror, shower curtain and rod. All accessories will be provided by a single manufacturer for aesthetic continuity.

Exit signs will be edge-lit with concealed lamp and integral lettering on a clear lens. Where low-level exit signs are required, they will be backlit and set flush with the adjacent wall.

Fire sprinklers in lay-in ceilings will have white on white, powder coated semi-recessed heads and will be placed in center of tile. All sprinklers will be equipped with concealed heads at gypsum board ceilings.

Fire extinguishers will be placed in surface mounted steel cabinets with baked enamel painted finish. Frameless door will have a solar gray glass lite and silk-screened letters.

Exit Stairways

Exit stairs will be used for intra-departmental circulation between floors and will be designed accordingly. Treads and landings will be a concrete-filled, pre-manufactured metal pan assembly. Stair stringers will be under slung or comprised of steel channels for reasons of aesthetics and performance. All steel surfaces will be painted. Landings will receive rubber flooring with top-set rubber base.

Walls and underside of landings will be painted gypsum board.

Whenever stairwells are designed to incorporate internal circulation, fire sprinkler risers, standpipes and other conduits and plumbing risers will be contained within a furred gypsum board and metal stud enclosure, with access panels as required.

Handrails will be offset from a standard 42” guardrail.

Stairways will be fitted with a false tread at the upstairs portion of each landing, so as to maintain an even handrail height.

The mezzanine level will be accessible via two exit stairs and a Machine-Room-Less (MRL) traction elevator, with a contract speed of not less than 350 fpm and a capacity of 4,500 lbs. The elevator cab will have a minimum clear height of 9'-0" and 4'-0" wide by 8'-0" high two-speed side opening doors.

10.1.7.2 Structural

Experimental Hall (EH2)

The Experimental Hall (EH2) is comprised of the Level 1 (tunnel main floor) and a Mezzanine level. Level 1 will contain hutches and set-up areas. Mezzanine level will contain laser labs, set-up areas, and mechanical rooms. High energy X-Ray beam experiments will be conducted in the hutches, as such these areas will be designed to conform with vibration level requirements. EH2 hutches will be designed to support future 2-Ton monorail cranes. Unistrut members will be anchored to the underside of the hutch concrete structural slab in each hutch.

Floor slab must be designed to minimize the effects due to differential settlement and shrinkage. The floor will be monolithic with the floor of FEE2 to minimize differential settlement. Floor surface will be flat and leveled and designed to minimize vibration as well as short and long term distortion. The finish floor will have zero percent slope in the direction of beam adjusted for earth curvature. All joints in contact with earth will have water stops and protected with waterproofing systems.

EH2 access tunnel slopes down from the parking area and AUP building to the EH2. EH2 will also have a concrete elevator shaft and utility shaft. Construction of retaining walls will be necessary.

Structural Design Criteria

The structure will be designed to conform to CBC 2010 requirements as well as SLAC Building & Site-Wide Design guidelines (DS-018-000-01-R0).

Design Floor Loads Dead and Live Loads (will not be less than ASCE 7 minimum requirements)

- Dead loads from the structure as calculated
- Collateral dead load allowable for sprinkler, piping, ducts, electrical conduits and lighting = 5 -10 psf or as calculated whichever is higher
- Laser rooms - Equipment weight or 350 psf, whichever is greater
- Main floor – 150 psf or equipment load whichever is higher
- Mezzanine floor – 150 psf or equipment load whichever is higher
- Platforms, stairs, and corridor live loads = 100 psf
- Design for future 2 ton monorail crane at each hutch
- Floors to be designed for vibration levels provided by geotechnical consultant based on equipment specifications.
- 1 kip/ft at beam line, 25 kips at any joint
- Lateral earth pressures and surcharge loads provided in Geotechnical report

Seismic Design

The structures will be designed and constructed to resist seismic loads and to limit the deflections generated by strong ground motion during a seismic event. The seismic design will comply with the following:

Geologic Hazard Evaluation and site specific response spectral data in the report provided by SLAC. Base shears will be based on using the site-specific spectral acceleration curves. Base shears calculated using dynamic analysis will be compared with CBC requirements and the most conservative loading will govern.

CBC 2010 requirements:

- Occupancy Category II (Importance Factor I= 1.0, Ip =1.0). An occupancy Category III with an importance factor of I = 1.25 could be considered for the design of tunnels to prevent cracking that causes water leaks.
- Design structure to resist lateral earth pressures and surcharge loads and seismic increment, on tunnel walls and roof as defined in the CBC or geotechnical report whichever is more stringent.

- A continuous load path with adequate strength and stiffness will be designed and detailed to transfer all seismic forces from the point of application to the final point of resistance.

Floor Vibrations Specifications for EH2

Vibration specifications for floor design will be provided by vibration consultant, based on SLAC engineering specifications document.

Tunneling

Experimental Hall Excavation and Initial Support

The design approach for the EH2 cavern excavation and support is similar to the one for the tunnels described above. However, due to its relatively large size, the EH2 will need to be excavated in multiple headings and benches, the size and sequence of which will be specified (as a minimum) to maintain the excavated openings stability, and also to facilitate construction and the initial support installation. Based on the current analyses, the EH2 excavation is anticipated to start with a top center heading followed by two side drifts. A single level of benches, i.e. a center and two side benches, will be needed to finish the cavern excavation. The initial support for the cavern will consist of fiber reinforced shotcrete and lattice girders with fully cement-grouted galvanized rock dowels to be used also as part of the final lining.

Final Lining and Seismic Design for tunnels

The final lining for the tunnels and cavern will consists of additional layers of plain or unreinforced shotcrete for serviceability purpose, final graded to the required surface tolerance or smoothness. Additional reinforcement with Welded Wire Fabric (WWF) is used to satisfy the long-term structural, seismic, and code requirements of the tunnel final lining. The design criteria for the final lining are based on the static (i.e. gravity) load of rock above the tunnels and the seismic structural requirements governed by the project. The long-term gravity rock load is based on the anticipated ground behavior during excavation (as predicted by the analytical models), and widely accepted empirical formulas using the rock mass characteristics, but in no case will be greater than one tunnel width or diameter of rock load above the tunnel crown (form prior experience in similar tunneling ground conditions).

The seismic performance criteria for the tunnel and cavern structures are based on the widely accepted methods of seismic design and analysis of underground structures, as well as all applicable codes and SLAC project specific seismic criteria as described in the following references:

Seismic Design and Analysis of Underground Structures by Youssef M.A. Hashash et.al., Tunneling and Underground Space Technology 16 (2001);

Seismic Considerations for Design of SLC Tunnels, Appendix C of SLAC Architecture/Engineering Design Guidelines by Earth Sciences Associates (October 2003);

CALTRANS Seismic Design Criteria, Version 1.3 (February 2004);

Other structures and building codes as listed in the SLAC Site-Wide Design Guidelines.

The analyses utilize the seismic soil/rock parameters described in the geotechnical report by Rutherford & Chekene (January 2005), the resulting incremental strains over the static loading described above are then checked against the lining capacities to determine reinforcement requirements. The most restrictive reinforcements obtained from the seismic analyses, static analyses, and any minimum combinations as required by the codes will then be used for the final lining design in the tunnels and caverns.

Water Proofing

Water proofing of exterior tunnel surfaces will be considered to avoid leaks in the tunnel. The effect of ground water table if noted in the geotechnical report (depending on the location and depth of tunnel) will also be considered, including hydrostatic loads on the tunnel structure. For serviceability purpose to maintain relatively dry tunnels and cavern, the use of low-permeability shotcrete will be specified. A drainage sump system embedded within the final invert slabs will be provided to collect any surface run-off or remaining seepage through the tunnel liners, which is to be pumped to the designated locations out of the facilities. The final invert slab for the tunnels and cavern will be reinforced cast-in-place concrete placed after the tunnel is completed. These slabs are designed to be structurally integrated with the surrounding tunnel liners and structures.

10.1.7.3 Mechanical Systems

General

All areas of the Experimental Hall (EH2) will have conditioned air. Air Handling Units (AHUs) and exhaust fans will provide the necessary outside air, ventilation and re-circulating air to all experimental and support areas. All air delivering systems will be strategically located in a mechanical room on each level to minimize large duct runs and loss of clearance space for technical component installation.

Duct mounted smoke detectors will be provided for the air handling systems per California Mechanical Code (CMC).

Chilled Water System

Chilled water system for the Experimental Hall will comprise of a 6 inch water main supplied from the Auxiliary Utility Plant (AUP). Chilled water supply temperature is 44°F. The 6 inch chilled water main will traverse the two levels via a mechanical shaft and terminate at the associated air handlers on each of the two levels.

Heating Hot Water System

Heating hot water supply to the air handlers and re-heat coils will be provided from the existing boilers located at the existing CUP, B950A. Hot water supply temperature will be 180°F. The heating hot water peak demand of the Experimental Hall is estimated at 2,400 MBH.

A 4 inch heating hot water pipe main will extend from to the existing 4 inch heating hot water point of connection near the south end of the NEH to inside the EH to distribute hot water to all re-heat coils.

The existing hot water pumps at the CUP will be modified to provide the necessary pressure head to accommodate the new Experimental Hall hot water demand. The existing main hot water piping at the CUP has adequate capacity to meet the heating hot water demand of the Experimental Hall.

Air Handling System

Air handling system at the EH2 will comprise of four independent air handling units. Three will be Fanwall typed air handlers for the laboratories and ancillary areas and one will be a unitary-typed data room fan coil.

Two air handlers will be located in the mechanical room of the lower floor. One will be dedicated to serve the experimental areas on the lower floor and the other will serve ancillary spaces located in both the lower and upper floors of the facility. A third air handler will be located in the upper floor mechanical room, sharing floor space with a make-up air unit. The air handler will serve all four laser rooms located on the upper floor. The air handlers will be furnished with 35% prefilter, 95% high efficiency, HEPA filters, chilled and hot water coils, and associated variable frequency drive (VFD). The VFDs will operate in concert with the Fanwall to deliver of the supply air to maintain experimental environment. The Fanwall type air handler, with its multiple fans, will provide superior fan redundancy in the event of supply fan failure.

The fan coil unit will be of a high quality, specialty-typed unit used for data room applications. The fan coil unit will be furnished with humidifier control, reheat coils, condensate pump and leak detection system. The unit's microprocessor control panel will locally maintain room temperature and humidity set points of the server room.

A single make-up air unit, located in the mechanical room of the upper floor will supply conditioned code required minimum outside air and space air pressure balance to the new EH2. The make-up air unit will also be a packaged Fanwall typed, furnished with 35% prefilter, 95% high efficiency, humidifier, chilled and hot water coils, and associated variable frequency drive (VFD).

Duct mounted smoke detectors will be provided per California Mechanical Code (CMC).

Exhaust System

All experimental areas will be provided with exhaust ductwork and associated fans. Exhausted air will be ducted to the outside of the EH.

Per Code dedicated exhaust system will be provided to specific experimental areas. A single exhaust fan will serve general exhaust needs all toilets and utilities rooms.

Ductwork Distribution

Conditioned air will be delivered throughout via galvanized ductwork (lined for rectangular and wrapped for round duct work). Main rectangular ductwork will extend from a dedicated air handler in the mechanical room on each floor and terminate at the reheat coil at each intended space. Ancillary areas will have variable volume boxes with reheat coils while experimental will be supplied with constant volume air with reheat coils.

Air intake ductwork associated with the make-up air unit will travel along a provided a shaft up to grade level.

Ductwork associated with the exhaust system will traverse across the floors from below, travel along a provided shaft and connect to exhaust fans above at the exhaust fan mechanical yard.

EMS & Controls

Direct Digital Controls (DDC) will be provided to monitor and control mechanical equipment and it will be integrated to existing site wide Automatic Logic Control (ALC), WebCTRL Monitoring System.

Process Cooling Water System

Insulated supply and return PCW piping with pressure gauges, isolation valves, circuit setters will be mounted on the walls of the Experimental Hall. PCWS and PCWR connections for experimental equipment will be spaced along the walls. A PCW piping system will be installed at the Auxiliary Utility Plant. The PCW system will consist of re-circulating pumps, plate heat exchanger, control valves, temperature and pressure sensors, valves and piping. Chilled water (CHW) piping from the Auxiliary Utility Plan will be connected to the heat exchanger to remove the heat from the PCW system.

PCW supply temperature is 68°F, with a total estimated demand of approximately 270 GPM.

A 6 inch process cooling water supply and return main will extend from the AUP, along the access tunnel to inside the EH2. In the EH2 the PCW piping will traverse across the two floors and terminate at experimental areas on the lower and upper floors of the EH2.

The operation of the PCW system and equipment will be controlled and monitored by SLAC's Energy Management System (EMS).

Compressed Air System

Clean, dry compressed air at 100 psig will be provided in all experimental areas of the EH. Compressed air piping will be mounted along the walls with shut-off valves and pressure gauges. The compressed air piping system will be connected to SLAC site wide compressed air piping. The estimated demand for the EH is 120 SCFM.

Fire Protection

The Experimental Hall will be provided with a wet fire sprinkler system designed per NFPA 13, for Ordinary Hazard (Group 1). The system will be connected to the riser located outside the access tunnel. The sprinkler system will be designed per NFPA 13 at 0.10 GPM/FT2 over the most remote 4000 square feet. Each head will be designed to cover a maximum of 130 square feet. The Experimental Hall is a single zone with zone control valve with supervisory and flow switches where the system enters into the hall. A Fire Department Connection (FDC) will be provided for at the sprinkler system riser. Wet sprinkler system will be monitored by SLAC's site wide fire detection system.

Plumbing and Drainage

Toilet and utilities rooms will be provided with domestic hot and cold water, vent and sanitary waste piping. The sanitary waste from the toilet rooms and utilities rooms will discharge to a sewage ejector located at the lower floor. The sewage ejector will pump the waste flow up to the point of connection to the sanitary main waste line located outside the Experimental Hall.

10.1.7.4 Electrical System

Experimental Hall (EH2) Level 1

The electrical distribution service to Undulator Hall (UH2), UH2 Service Building, Electron Beam Dump (EBD2), Front End Enclosure (FEE2), Experimental Hall (EH2) Level 1, Mezzanine Level and Access Tunnel will be fed from the new 12KV/480V Unit substation to be installed closed by new Auxiliary Utility Plant (AUP). The final location of this new unit substation will be determined in detailed design.

A new 800A, 277V/480V, 3Phase, 4 wire feed from this unit substation will be provided to service EH2 Level 1 process, x-ray experiment station loads and facilities loads.

Power Distribution

A new 800A, 277V/480V, 3 phase, 4 wire Main Switchboard will be provided in EH2 Level 1 Electrical room for power distribution. Main switchboard will be front accessible only, and have power monitor meter. Main feeder circuit breaker in the switchboard will be 100% rated solid state type with LSIG trip unit. The detail arc flash, short circuit, load flow, balancing and all other applicable design requirements will be implemented in preliminary and final design phases. This main switchboard will provide power to x-ray experimental stations, control cabins, step down feeders to beam line clean/dirty and utility process panels and the 480V welding receptacles.

Distribution panelboard

277V/480V or 120V/208V, 3 phase, 4wire distribution panelboards will be dead-front, dead-rear, solid state type main circuit breaker, branch circuit breakers are group mounted, front accessible bolt-on thermal magnetic molded case type with adjustable magnetic trip settings. Full length buss for both voltage and 200% neutral bussing on 208V distribution panels.

Dry type transformer

Transformer will be NEMA TP-1 compliant, Energy Star labeled transformers to step down to 120V/208V, 3 phase, 4 wire, K13 rated, 200% neutral.

Individual neutral wire for each phase wire.

Arc Flash rating

For 480V system, use solid state type breakers for coordination selectivity to reduce fault clearing time, for 208V system, preferable limit step down transformer to 112.5KVA.

Lighting System

Surface mounted industrial fluorescent and/or recessed fluorescent fixtures will be provided as it is suitable to the area to achieve adequate lighting levels. Lighting level shall be designed in accordance with illuminating Engineering Society (IES) recommendations. Fixtures shall be fluorescent type with energy saving T8 lamps, 3500 Kelvin color temperature with high efficiency electronic ballast 95% power factor, total harmonic distortion (THD) of less than 10%. Lighting control system will be designed to meet and exceed the requirement of Title 24 and to meet the intended use of the area. Exit and emergency lights will be provided per code.

Grounding and Bonding System

A new perimeter grounding rings with ground rods and test well as required will be installed for EH2 Level 1 and will be tied into the ground grids. All systems and equipments will be bonded per NEC and NFPA requirements. The new ground grids will be tied into the existing ground system at selected locations. Grounding system shall be designed per CEC and NEC requirement. The detail grounding system will be designed in preliminary and final design phases.

Fire Alarm and Detection System

The fire alarm system will be met utilizing Siemens products to integrate with the existing campus network. The fire alarm system will be designed to comply with NFPA 72 and all associated codes and regulations. The new fire alarm system will consist of, but not limited to, a fire alarm control unit , alarm initiating devices, occupant notification appliances, and associated ancillary equipment for interfacing the new fire alarm system with the existing SLAC alarm receiving equipment. The fire alarm system will also communicate with other life safety systems, building system equipment as applicable. The final design of the fire alarm system will be detailed in preliminary and final design phases.

The fire detection system will be integrated with the existing campus network. The fire detection system will be design to comply with NFPA 72 and all associated codes and regulations. The fire detection system will be VESDA Air Sampling and Early Warning Smoke Detection. The VESDA system will consist of, but not limited to, the sampling pipe network, highly sensitive LASER-based smoke detectors, aspirators, filters, detector assemble network, digital communication ports. The fire detection system will be also communication with other life safety systems, building system equipment as applicable. The final design of the fire detection system will detailed in preliminary and final design phases.

The Audible Alarm Notification and Manual Voice Paging System will be designed and integrated with existing campus network. The audible alarm notification system will be by voice evacuation and tone signals on loudspeakers in areas. The manual voice paging system will be configured to allow voice paging. Upon activation of any speaker manual control switch, the alarm tone will be sounded over all speakers in that group. The final design of systems will be determined in detailed design.

Telecommunication System

The telecommunication system will be provided to support the physical transmission facility for voice, data and low voltage networks. The system consists of, but not limited to, the following:

- Telecommunication backbone pathways includes dedicated point-to-point (BDF to IDF) pathway system. These pathways may be comprised of cable tray, raceways, boxes, inner duct in cable tray, cable suspension products, and seismic bracing.
- Telephone and data structure cabling system will be designed to comply with the requirement of EIA/TIA 569 Commercial Building Standard for telecommunications pathways and spaces. The cabling system will be designed to comply with pertinent codes, rules, regulations and laws of the Authorities having jurisdiction. The cabling system includes building pathways, backbone cabling, horizontal cabling and an administration system to manage the pathways and cabling.

Experimental Hall (EH2) Mezzanine

Power Distribution

A new 800A, 277V/480V, 3 phase, 4 wire Main Switchboard will be provided in EH2 Mezzanine Electrical room for power distribution. Main switchboard shall be front accessible only, and shall have power monitor meter. Main feeder circuit breaker in the switchboard shall be 100% rated solid state type with LSIG trip unit. This main switchboard will provide power to instrument racks loads, data server loads, vacuum pumps loads elevator loads, step down feeders to laser bay clean/dirty and utility process panels, the 480V welding receptacles as required.

Distribution panelboard

277V/480V or 120V/208V, 3 phase, 4wire distribution panelboards will be dead-front, dead-rear, solid state type main circuit breaker, branch circuit breakers are group mounted, front accessible bolt-on thermal magnetic molded case type with adjustable magnetic trip settings. Full length buss for both voltage and 200% neutral bussing on 208V distribution panels.

Dry type transformer

Transformer will be NEMA TP-1 compliant, Energy Star labeled transformers to step down to 120V/208V, 3 phase, 4 wire, K13 rated, and 200% neutral.

Individual neutral wire for each phase wire.

Arc Flash rating

For 480V system, use solid state type breakers for coordination selectivity to reduce fault clearing time, for 208V system, preferable limit step down transformer to 112.5KVA.

Lighting System

Surface mounted industrial fluorescent and/or recessed fluorescent fixtures will be provided as it is suitable to the area to achieve adequate lighting levels. Lighting level shall be designed in accordance with illuminating Engineering Society (IES) recommendations. Fixtures shall be fluorescent type with energy saving T8 lamps, 3500 Kelvin color temperature with high efficiency electronic ballast 95% power factor, total harmonic distortion (THD) of less than 10%. Lighting control system will be designed to meet and exceed the requirement of Title 24 and to meet the intended use of the area. Exit and

emergency lights will be provided per code. Exterior lighting will be provided at the entrances, landings, equipment pads and access stairs.

Grounding and Bonding System

A new perimeter grounding ring with ground rods and test well as required will be installed for EH2 Mezzanine Level and will be tied into the ground grid. All systems and equipments will be bonded per NEC and NFPA requirements. The new ground grid will be tied into the existing ground system at selected locations. Grounding system shall be designed per CEC and NEC requirement. The detail grounding and bonding system will be designed in preliminary and final design phases.

Fire Alarm and Detection System

The fire alarm system will be met utilizing Siemens products to integrate with the existing campus network. The fire alarm system will be designed to comply with NFPA 72 and all associated codes and regulations. The new fire alarm system will consist of, but not limited to, a fire alarm control unit , alarm initiating devices, occupant notification appliances, and associated ancillary equipment for interfacing the new fire alarm system with the existing SLAC alarm receiving equipment. The fire alarm system will also communicate with other life safety systems, building system equipment as applicable. The final design of the fire alarm system will be detailed in preliminary and final design phases.

The fire detection system will be integrated with the existing campus network. The fire detection system will be design to comply with NFPA 72 and all associated codes and regulations. The fire detection system will be VESDA Air Sampling and Early Warning Smoke Detection. The VESDA system will consist of, but not limited to, the sampling pipe network, highly sensitive LASER-based smoke detectors, aspirators, filters, detector assemble network, digital communication ports. The fire detection system will be also communication with other life safety systems, building system equipment as applicable. The final design of the fire detection system will detailed in preliminary and final design phases.

The Audible Alarm Notification and Manual Voice Paging System will be designed and integrated with existing campus network. The audible alarm notification system will be by voice evacuation and tone signals on loudspeakers in areas. The manual voice paging system will be configured to allow voice paging. Upon activation of any speaker manual control switch, the alarm tone will be sounded over all speakers in that group. The final design of systems will be determined in detailed design.

Telecommunication System

The telecommunication system will be provided to support the physical transmission facility for voice, data and low voltage networks. The system consists of, but not limited to, the following:

- Telecommunication backbone pathways includes dedicated point-to-point (BDF to IDF) pathway system. These pathways may be comprised of cable tray, raceways, boxes, inner duct in cable tray, cable suspension products, and seismic bracing.
- Telephone and data structure cabling system will be designed to comply with the requirement of EIA/TIA 569 Commercial Building Standard for telecommunications pathways and spaces. The cabling system will be designed to comply with pertinent codes, rules, regulations and laws of

the Authorities having jurisdiction. The cabling system includes building pathways, backbone cabling, horizontal cabling and an administration system to manage the pathways and cabling.

Experimental Hall (EH2) Access Tunnel

Power Distribution

The Access Tunnel will be provided with 120V convenience outlets and the associated dedicated specialized receptacles as needed.

Lighting System

Surface mounted industrial fluorescent fixtures will be provided to achieve adequate lighting levels. Lighting level shall be designed in accordance with illuminating Engineering Society (IES) recommendations. Fixtures shall be fluorescent type with energy saving T8 lamps, 3500 Kelvin color temperature with high efficiency electronic ballast 95% power factor, total harmonic distortion (THD) of less than 10%. Lighting control system will be designed to meet and exceed the requirement of Title 24 and to meet the intended use of the area. Exit and emergency lights will be provided per code. Exterior lighting will be provided at the entrances, landings, equipment pads and access stairs as required.

Grounding and Bonding System

The new perimeter grounding ring installed for EH2 Mezzanine level will be extended to access tunnel area. All systems and equipments will be bonding per NEC and NFPA requirements.

Fire Alarm and Detection System

The fire alarm system will be met utilizing Siemens products to integrate with the existing campus network. The fire alarm system will be designed to comply with NFPA 72 and all associated codes and regulations. The new fire alarm system will consist of, but not limited to, a fire alarm control unit , alarm initiating devices, occupant notification appliances, and associated ancillary equipment for interfacing the new fire alarm system with the existing SLAC alarm receiving equipment. The fire alarm system will also communicate with other life safety systems, building system equipment as applicable. The final design of the fire alarm system will be detailed in preliminary and final design phases.

The fire detection system will be integrated with the existing campus network. The fire detection system will be design to comply with NFPA 72 and all associated codes and regulations. The fire detection system will be VESDA Air Sampling and Early Warning Smoke Detection. The VESDA system will consist of, but not limited to, the sampling pipe network, highly sensitive LASER-based smoke detectors, aspirators, filters, detector assemble network, digital communication ports. The fire detection system will be also communication with other life safety systems, building system equipment as applicable. The final design of the fire detection system will detailed in preliminary and final design phases.

The Audible Alarm Notification and Manual Voice Paging System will be designed and integrated with existing campus network. The audible alarm notification system will be by voice evacuation and tone signals on loudspeakers in areas. The manual voice paging system will be configured to allow voice

paging. Upon activation of any speaker manual control switch, the alarm tone will be sounded over all speakers in that group. The final design of systems will be determined in detailed design.

10.2 Site Civil Utilities Design

General

Site civil utilities improvements includes site sanitary sewer service, potable water service, fire protection water service and storm drainage systems and will conform with all current codes and CBC 2010 requirements. Design guidleines set in SLAC Building & Site-Wide Design guidelines(DS-018-000-01-R0) will be considered. All existing underground utilities mains have adequate capacity to handle the additional loads imposed by the LCLS-II Project.

General Approach

All existing underground utilities in the vicinity of the beam line alignment will be identified and located from as-built SLAC survey drawings and underground utility location surveys which will need to be performed during the design phase.

Existing utility tunnels with all utilities will not be disturbed unless approved by SLAC.

All utility lines that are to remain in operation will be protected and supported as necessary.

Gravity lines (storm drains and sanitary sewers) will be maintained.

Non-gravity utility lines will yield to gravity lines in case of conflicts.

Corrosion / Cathodic protection for the pipelines will be considered.

All existing utilities that are to be abandoned will comply with the following:

If within the building footprint, utilities will be removed completely. If outside the building footprint and shallower than 6 feet in depth, utilities will be removed completely. If more than 6 feet deep, utilities will be filled with grout and abandoned in place.

Sanitary Sewer

Sewer service for the new service buildings/tunnels will be designed to provide capacity for the calculated sewer flows. Minimum slope for the pipe will be determined based on a minimum design velocity of 2.0 feet per second at peak flow and a minimum of 4 inches in diameter. New sanitary sewers lines from EH2 and AUP will be be connected to existing 8” sanitary sewer system at manhole MH SSMH-9B (Drawing # ID 383-900-84-CO) near NEH2 Building 950.

The relocation of the existing sanitary sewer mains if needed, will be designed based on existing conditions of the existing main (size, slope, and flow capacity). The capacity of the relocated main will be equal or exceed the capacity of the existing main and any additional estimated flows based on the new building loads.

Size

Pipes less than or equal to 10 inches in diameter will be sized to handle peak flows at 75% of full pipe capacity.

No gravity sewer mains will be less than 8 inches in diameter and no sewer laterals less than 4 inches in diameter.

As a rule, when a smaller sewer joins a large one, the top of both pipes (crowns) should be at the same elevation.

Slope

All sewers will be designed and constructed to have mean velocities when flowing full, of not less than 2.0 feet per second. The minimum slopes for 8" pipe will be 0.34 per 100 ft.

Depth

In general, the sewer lines will have a minimum of 36 inches of cover to finished grade.

Crown (top inside surface of the pipe) of any inlet pipe will not be lower than the elevation of the outlet main crown in the manhole.

Alignment

During construction the horizontal and vertical alignment of sewers will be maintained by the use of laser survey equipment. All sewers will be constructed straight and at uniform grade between manholes.

Manholes

Manholes will be installed at the following conditions: at the end of each lines; at all grade changes, size or alignment changes; at all intersections; and at distances not greater than 400 feet. Greater spacing may be permitted in large sewers greater than 30 inches in diameter if approved by SLAC.

Storm Drainage

Design flows will be based on calculations using the rational method and typically using a 20 yr storm event for onsite drainage. County of San Mateo rainfall intensity duration frequency graph will be considered with a minimum duration (Tc) of 10 minutes. New storm drainage system at EH2 Access Ramp, Parking lot, and Auxiliary Utility Plant will be connected to existing 24" storm drain at SDMH-9D or SDMH-9F (Drawing # ID-383-900-84-CO) near NEH2 Building 950.

Catch basins in vehicular areas will be specified in the following descending order of preference, based upon ease of maintenance and minimization of obstruction to pedestrian traffic. All catch basins will be traffic rated for the maximum probable loading anticipated.

- Precast grated curb inlet/ catch basins
- Precast or poured in place trench drains
- Traffic rated pre-cast catch basins

Drainage design in pedestrian areas will consider the comfort of the pedestrian by directing concentration of water for pickup to areas away from paths of travel, such as in planting areas and the requirement for minimum spacing of the inlet openings.

Catch basin grates will be designed to comply with accessible regulations for grates and slopes.

Catch basins in paved pedestrian areas will be specified in the following descending order of preference:

- Precast or poured- in- place curb inlet/catch basins
- Precast or poured-in-place, grated catch basins
- Precast area drains

Size

Pipes less than or equal to 10 inches in diameter will be sized to handle peak flows at 75% of full pipe capacity. Pipes greater than 10 inches in diameter will be sized to handle peak flows at 90% of full pipe capacity.

No gravity storm drain mains will be less than 12 inches in diameter and collector laterals not less than 4 inches in diameter.

As a rule, when a smaller storm line joins a large one, the top of both pipes (crowns) should be at the same elevation.

Slope

All storm drain mains will be designed and constructed to have mean velocities when flowing full of not less than 2.0 feet per second.

Depth

In general, the storm lines will have a minimum of 36 inches of cover to finished grade.

Crown (top inside surface of the pipe) of any inlet pipe will not be lower than the elevation of the outlet main crown in the manhole.

Alignment

During construction the horizontal and vertical alignment of storm drains will be maintained by the use of laser survey equipment. All sewers will be constructed straight and at uniform grade between manholes.

Manholes

Manholes will be installed at the following conditions: at the end of each lines; at all changes in grade, size or alignment; at all intersections; and at distances not greater than 300 feet.

All site finish grading will be designed such that overflow protection is provided to prohibit runoff from entering buildings should site storm drains become inoperable. Maintain a minimum of 1’ free-board from lowest finish floor elevation to overland release path grades.

Domestic Water

The domestic and fire water service connections will be designed based on all applicable codes and on the sizing requirements for the building. Metering for the domestic service, backflow prevention and valve control for the services will be included. Approval for fire services will be under the direction of the SLAC fire Marshal. All water connections, domestic, fire and irrigation is supplied from one master source on the SLAC campus. Point of connection will be to a 8" water main located in front of NEH2 building 950.

Meters for the domestic service will be installed so as to not impair pedestrian movements. Meter boxes will not be located in driveways or the traveled portion of the roadway; however, if such location is unavoidable, boxes and covers will be capable of supporting traffic loads. Meter boxes will be clear of sidewalks; however, if such location is unavoidable, boxes and covers will be installed to provide a smooth and safe walk area. No metal lids will be allowed in the sidewalk area.

Design Criteria

Pipe will have a minimum cover of 3 feet. Cover less than 3 feet may be considered, but only if some other protection is provided and the proposed installation is approved by SLAC.

Valves

Valves located within the roadway will be protected by suitable valve boxes and installed so that the designed roadway surface adjacent to the valve box is not distorted. Valve boxes will be set in concrete. Valves for the fire service will be monitored by the Fire Alarm system.

Fire Hydrant

Fire hydrant location will not create a sidewalk obstruction and will be as specified and approved by the SLAC fire marshal. Hydrants will generally be located 20 inches behind the face of curb to centerline of hydrant.

Hydrants will be provided at the appropriate spacing per the NFPA and the California Fire code to provide fire protection for all adjacent building structures.

Hydrant number and spacing will comply with California Fire Code Appendices.

Hydrants will be designed and installed per SLAC Fire Marshal requirements.

Fire Department Connection (FDC):

- Fire Department connections will be visible from the adjacent roadway and will be located within a minimum distance from a site hydrant based on SLAC requirements. Fire Department connections will be located at least 40 feet from the building being protected and at least 6 feet from the PIV.
- Fire Department connections will not be installed where there is the possibility of injury by falling objects. Fire Department Connections will not be permitted below and within 10 feet of signage, cornices, soffits, balconies or other cantilevered objects.

- Fire Department connections will be installed so that the centerlines of the inlets are located at a minimum height of 18 inches and a maximum height of 36 inches above the adjacent finish grade.
- Fire Department connections will be located a maximum of 50 feet from a fire hydrant.
- Fire Department connections will be installed on the system side of the indicating valves.

10.3 Civil Site Improvements Design

Parking Lot, Roadways, and Sidewalks

Parking lot at new access tunnel/ramp to Experimental Hall (EH2) will have a minimum 60 parking stalls including minimum 8 parking stalls with charging stations for government electric vehicles. Parking lots will be provided with minimum lighting of 1 foot candle. Parking lot at UXT service building will have parking capacity for minimum 10 vehicles. New parking lots will be connected to existing PEP Ring Road with new roadways and sidewalks. Sidewalks will also be constructed from parking lots to service buildings and access tunnel/ramp. Existing parking lot at existing BTH will be modified to accommodate new BTH addition and restriped to accommodate new parking stalls, charging stations and lighting. Parking lots will have curbs and gutters, and drainage system will be connected to existing drains.

General Requirements

Design will conform to all current codes and CBC 2010 requirements. Design guidelines provided in SLAC Building & Site-Wide Design guidelines (DS-018-000-01-R0) will be considered.

Design of the parking lot pavement and roadway structural section will be based on recommendation provided in the project geotechnical report. Consideration will be given in the design of the structural section to reusing the existing pavement asphalt and base as recycled sub base material to reduce the required import of base material.

The consultant will perform a civil site survey to validate existing conditions and for the use in the design and construction of this project.

AC pavement for parking lots and roadways will be designed to sustain 75,000 pound load per the fire code requirements, H20-44 loads, and FL-40 forklift loads(98,500 lb each front wheel, 9500 lb rear wheels).

Consideration will be given for the use of a permeable pavement material (asphalt, concrete or permeable paver) to reduce the amount of impermeable area on the overall site and reduce the increase in storm water runoff.

Signage and striping will be in compliance current codes and SLAC requirements.

All parking stalls and associated curb ramps designated for ADA accessibility will be designed per current ADA regulations.

Cross slope of asphalt pavement for parking lots will be a minimum of 2%. Minimum slope along flow lines or gutter flow for asphalt will be 2%. If less than 2%, concrete gutters will be required.

A written evaluation and assessment of the existing pavement that is to remain on the site will be prepared by the design consultant and submitted to SLAC for review. Assessment will include at a minimum a visual inspection of the pavement to identify areas of failure, excessive cracking and overall pavement distress. Recommendations for pavement rehabilitation will be included in the report for SLAC review.

At a minimum, the existing pavement will be sealed with a crack sealer and with a recommended pavement slurry seal coat and any existing striping redone.

Roadway Design criteria

Roadway width:	26’ minimum
Maximum roadway slope:	10%
Roadway section:	crowned section/cross slopes – 2%
Minimum outside turning radius	48’
Maximum hump for a 50’ trailer:	2.3”
Surfacing:	AC pavement over Class 2 Aggregate base
Drainage:	100 yr storm runoff/San Mateo County rainfall

Roadways will be designed for H20-44 truck loading, fire truck loading, and FL-40 forklift loading(98,500 lb each front wheel, 9,500 lb rear wheels). Roadways willl have curb and gutters and catch basins where needed. Catch basins will be connected to existing drainage system.

Site Earthwork Design

General requirements:

- Earthwork will be designed in accordance with the recommendations provided in the project geotechnical report.
- Consideration will be given to the use of recycled roadway base and asphalt pavement as part of the site earthwork fill requirements for the site.
- Site grading design will be done to minimize the need for imported fill material.
- Existing asphalt, concrete, soil to be excavated will be characterized by SLAC for possible contamination to determine disposal/reuse prior to start of work.

10.4 Auxiliary Utilities Plant (AUP)

10.4.1 Architectural

The LCLS-II will also require a 5,500 gsf Auxiliary Utilities Plant (AUP) support building. This will be located above the EH2 at grade. The AUP building will house the mechanical room.

The AUP building will be designed and constructed utilizing a 24' high bay metal building system, including primary & secondary structural steel framing, with standing seam metal roof and wall panels. All exterior metal will be galvanized steel with urethane enamel coating system. Exposed fasteners will be of the same metal as being fastened with the same finish system.

The standing seam roofing system will have a minimum 20-year warranty. Roof assembly will have a minimum slope of ½" per foot.

The interior work and service areas floor slabs will have sealed concrete finish. Perimeter walls will be protected from impact damage to a minimum of 8'-0" A.F.F. Typically all exposed construction will be finished with a heavy latex enamel (water borne, low VOC) paint finish. Interior doors will be painted hollow metal, with painted hollow metal frames. Doors in high-use areas will receive protective stainless steel panels to lever height.

Typical interior partition walls will consist of 3-5/8" steel studs with 5/8" gypsum wallboard on both sides. Full height fire barrier walls will consist of 6" steel studs and will comply with Underwriters Laboratories (UL) designs for one-hour separations as required. Sound and thermal batt insulation will be installed to provide acoustic and thermal insulation to adjacent spaces.

Exit signs will be edge-lit with concealed lamp and integral lettering on a clear lens. Where low-level exit signs are required, they will be backlit and set flush with the adjacent wall.

Fire extinguishers will be provided in accordance with NFPA 10, throughout the building. The maximum travel distance to an extinguisher from any point in the building will be 50 feet. Fire extinguishers will be placed in surface mounted steel cabinets with baked enamel paint finish, with upper edge at +4'-6". Frameless doors will have a solar gray glass lite and silk-screened letters. All cabinets will be sized to house the code required size extinguisher.

10.4.2 Structural

Structural

Auxiliary Utility Plant (AUP) will be a metal building on concrete slab foundation and located above grade near or above the EH2 tunnel. It will contain a large mechanical room accommodating make-up air unit and exhaust systems, a Boiler Room, a Chiller Room and an Electrical Room containing switch gear. Exterior substations will be located adjacent to the Electrical Room.

Structural Design Criteria

The metal building will be designed to conform to CBC 2010 requirements as well as SLAC Building & Site-Wide Design guidelines (DS-018-000-01-R0).

Design Floor Loads Dead and Live Loads (will not be less than ASCE 7 minimum requirements)

- Dead loads from the structure as calculated
- Collateral dead load allowable for sprinkler, piping, ducts, electrical conduits and lighting = 5 -10 psf or as calculated whichever is higher

- Live load – 150 psf or weight of equipment whichever is higher.

Seismic Design

The structures will be designed and constructed to resist seismic loads and to limit the deflections generated by strong ground motion during a seismic event. The seismic design will comply CBC 2010 requirements:

- Occupancy Category II (Importance Factor I= 1.0, Ip =1.0)

10.4.3 Mechanical Systems

General

The AUP will comprise of a chiller and mechanical rooms. Provisions will be made to locate the AUP near to the Experimental Hall (EH2).

Chilled Water System

The chilled water system at the AUP will make up of two 300-ton centrifugal, water-cooled chillers. One will serve as a primary chiller with the other operating as a back-up. The plant will support HVAC loads and heat exchangers of PCW systems for LCLS-II. Each chiller will provide a nominal water flow of 450 GPM at 16F delta water temperature. Insulated 6” inch chilled water supply and return main piping will run from the chiller room to the serve the EH2, FEE2, EBD2, UH2 and BTH service buildings. The chilled water system will be furnished with a primary and redundant water pumps, VFDs, temperature and pressure sensors and all necessary appurtenances.

The chiller room will have a refrigerant monitoring system per CMC Code requirements. Heat from the chillers will be rejected to existing cooling tower piping system.

Heating Hot Water System

Existing boilers at the CUP, B950-A have adequate capacity to meet the heating hot water demand of the LCLS-II Facility.

Air Handling System

A 5-ton air handler unit, with cooling coil, filters, temperature control valves,etc., will be provided to maintain room temperature set point in the electrical room. A set of 1-1/2 inch chilled water supply and return lines, complete with all necessary piping appurtenances, will extend from the chiller room. The unit will be connected to the existing ALC Controls System for remote room temperature monitoring.

Duct mounted smoke detectors will be provided per California Mechanical Code (CMC).

Exhaust System

The AUP chiller plant shall be furnished with adequate ventilation, as per the California Mechanical Code (CMC). Approximately 6,000 exhaust CFM will be required to provide adequate air change per hour in the space. The chiller room exhaust system will comprise of a high efficiency wall-mount exhaust fan,

coupled with sidewall louvers. The exhaust system will operate continuously and interlocked with site DDC monitoring system.

The AUP mechanical room ventilation system will consist of an analogous wall-mount exhaust system similar to that of the chiller room exhaust system. Approximately 4000 exhaust CFM will be required to provide adequate general ventilation for the space. Design of the mechanical room ventilation system will comply with appropriate provisions of the California Mechanical and Building Codes.

EMS & Controls

Direct Digital Controls (DDC) will be provided to monitor and control mechanical equipment via existing Automatic Logic Control WebCTRL Monitoring System.

Process Cooling Water System

A 300 GPM process cooling water system will be provided to meet the heat rejection demand of the water-cooled technical components. The PCW system will comprise of a plate heat exchanger, a dual pump set, VFDs, chemical feeder, air separator, expansion tank and all associated piping appurtenances. A new 4 inch PCW supply and return main will run along the LCSL Facility, branch out to the specific areas of the facility and terminate with isolation valves.

All supporting mechanical equipment of the process cooling system will be housed in the mechanical room, adjacent to the chiller room at the AUP.

Insulated supply and return PCW piping with pressure gauges, isolation valves, circuit setters will be mounted on the walls of the Experimental Hall. PCWS and PCWR connections for the technical components will be spaced along the walls. Chilled water (CHW) piping from the Auxiliary Utility Plan will be connected to the heat exchangers for heat removal from the PCW system.

PCW supply temperature is 68°F, with a total estimated demand of approximately 300 GPM.

A 4 inch process cooling water supply and return main will extend from the AUP, along the access tunnel to inside the EH. In the EH2 the PCW piping will traverse across the two floors and terminate at experimental areas on the lower and upper floors of the EH2.

The operation of the PCW system and equipment will be controlled and monitored by SLAC's Energy Management System (EMS).

Plumbing

Make up water piping will be provided to chilled water and PCW systems.

Fire Protection

A wet fire sprinkler system designed per NFPA 13, for Ordinary Hazard (Group 1). The AUP system will be connected to the riser main in the space. The sprinkler system will be designed per NFPA 13 at 0.10 GPM/FT2 over the most remote 4000 square feet, with 155°F heads. Each head will be designed to cover a maximum of 130 square feet. The AUP is a single zone with zone control valve with supervisory and

flow switches where the system enters into the hall. A Fire Department connection will be provided for at the sprinkler system riser.

10.4.4 Electrical System

Installation of a new 12KV, 2500KVA Electrical Substation for UH2, EBD2, FEE2, EH2

A new 12KV, 2500KVA substation at the new Auxiliary Utility Plant (AUP) will be installed to support power to feed the UH2, EBD2, FEE2, EH2 and Service Buildings. The power source to this new 12KV substation will be fed from existing 12KV IR4 Substation, Breaker (#328) rated at 1200AF. The conceptual design of the new 12KV, 2500KVA substation feeder from existing IR4 Substation will be routed underground through existing medium voltage manholes 47, 48 to the new substation location. Extensive field verification of the availability/capacity of underground ductbank is needed. A new medium voltage duckbank along with all associated medium voltage manholes will be required to install if the capacity of existing duckbank is exhausted. The final routing of this new feeder and final location and footprint of the new substation will be determined during detailed design.

This new 12KV substation will consist of, but not be limited to, the following:

- An outdoor 12KV medium voltage metal clad switchgear vacuum circuit breaker rated 15KV, 1200A, 2500KVA, 3 phase.
- An outdoor liquid-filled, substation type transformer rated 2500KVA, 3 phase, 12.47KV primary delta, 480V/277V wye grounded secondary, 3 phase, 4 wire, 60 Hz, %Z=5.75, Class OA/OA/FFA, 55/65 degree C, aluminum, FR3 less-flammable vegetable-based seed oil insulation per NEC, equipped with self containment.
- An indoor lineup of low voltage metal enclosed Main Distribution Switchgear rated 4000A, 480V/277V, 3phse, 4wire, insulated copper bus & tin plated ground bus, 65KAIC symmetrical, minimum short circuit rating.
- New separate free standing enclosed sections for breaker remote control panel with hinged door and separate hinged swing type panel for mimic bus graphic display unit with PLC controls and communication capability.
- The interface devices and associated accessories for system integration of new power monitoring and controls to connect to SLAC existing DCS system.
- An indoor new battery bank, 125V dc, lead acid type, new battery charger, safety & monitoring devices, DC distribution panel, ducted ventilation system from battery system exhaust fan to CUP2 building exterior.
- Power to the following areas will be provided by four (4)800A feeds from this new substation:
- One (1)800A feeder from this new substation will feed the Undulator Hall/Tunnel and Service Building.

- One (1)800A feeder from this new substation will feed the Electron Beam Dump (EBD2), Front End Enclosure (FEE2).
- One (1)800A feeder from this new substation will feed the Experimental Hall Level 1.
- One (1)800A feeder from this new substation will feed the Experimental Hall Mezzanine Level.

Utilized existing 12KV, 2500KVA Substation "12SUB03-950" for Mechanical loads in AUP

The electrical service

Service to new equipment loads in the new Auxiliary Utility Plant (AUP) will be provided from existing 4000A, 480V, 3phase, 3 wire switchgear "4SSG03-950" located at the existing CUP electrical room. The estimated equipment loads of 1300KVA in AUP are based on existing equipment loads in existing CUP. The available capacity of the existing switchgear "4SSG03-950" is adequate to support the new equipment loads in AUP. Power to support equipment in AUP will be provided by four (4)800A feeds from switchgear "4SSG03-950". Extensive field verification is needed to determine the exact power feed routing from switchgear "4SSG03-950" to AUP location during the detailed design.

Power distribution

Power to equipment loads in AUP will be provided via Motor Control Center (MCC). Space for starters and number of circuit breakers will be determined during detailed design.

AUP Chiller Room

Two (2)800A MCC will be provided in AUP Chiller room to support two new chillers, chilled water pumps. Refer to Mechanical section for size of the chillers and chilled pumps. VFD and integral disconnect switch for chilled pumps will be provided as required.

AUP Mechanical Room

One (1)800A MCC will be provided in AUP Mechanical room to support EH2, FEE2, EBD2 HVAC equipment.

AUP Electrical Room

One (1) 800A MCC will be provided in AUP Electrical room to support EH2 primary system chilled water pumps and associated mechanical equipment, air handling unit, etc.

10.5 Sustainability Approach

10.5.1 Sustainability Background

SLAC, as a Federal facility, is required to comply with Executive Order 13423 "Strengthening Federal Environmental, Energy, and Transportation Management", dated January 24, 2007. The order sets goals in the areas of energy efficiency, acquisition, renewable energy, toxics reductions, recycling, renewable energy, sustainable buildings, electronics stewardships, fleets, and water conservation. In EO 13423, Section 2(f), Federal agencies are required to ensure that new construction and major renovation of agency buildings comply with the Guiding Principles for Federal Leadership in High Performance and Sustainable Buildings set forth in the Federal Leadership in High Performance and Sustainable Buildings Memorandum of Understanding (2006).

The approach to be taken by the project toward this initiative includes:

- Meet High Performance and Sustainable Buildings practices for new construction and renovations in the Conventional Facilities scope for LCLS-II.
- Meet Leadership in Energy and Environmental Design (LEED) Gold certification practices for new construction, as applicable.

See http://www.fedcenter.gov/programs/greenbuildings/ for additional information.

LCLS-II will undertake a formal process to determine candidate elements of the project that may qualify for LEED Gold. The process involves a Sustainable Workshop facilitated by a LEED Accredited Professional (LEED AP) to produce a strategy as outlined by the LEED scorecard that identifies the LEED credits for each candidate CF element, if any. Since LEED does not have specific requirements defined for accelerator facilities, the workshop is particularly important for defining the sustainable plan for the Project.

The focus of this sustainable workshop is to have the design team, in tandem with the client team, identify if LEED certification (Gold or otherwise) is possible by reviewing the LEED Minimum Project Requirements (MPRs). Whether established that LEED certification is possible or not, the team will identify all credits that are potentially achievable using the LEED rating system to ascertain the realistic level of certification given the scope of the project. Following determination of achievable credits, the team will establish a firm plan of action for achieving them during the course of the project.

The team will consider not only pertinent credits from the different LEED Rating Systems, but also those in the California Green Building Code, and learned sustainable design principles to insure the LCLS-II project addresses all realistic measures in meeting viable Department of Energy environmental guidelines.

This preliminary assessment would allow the SLAC LCLS-II team to report back to the DOE on the sustainable strategies being utilized to meet the DOE environmental guidelines.

10.5.2 Sustainability Coordination

A Sustainability Coordinator familiar with LEED requirements and other sustainable best practices will be a key team member to formally evaluate sustainability strategies attainable by the LCLS-II project. The coordinator will be in charge of managing the sustainability documentation process while assisting each discipline's endeavors to meet the project's targeted goals. At the beginning of this process, the Sustainability Workshop will be conducted and will include SLAC, the Architect, General Contractor, MEP consultants, and all other key team members. Through the Sustainability Workshop, the team will fine-tune plausible elements of the project that may be achievable and further develop the strategic plan for the entire project. If LEED certification is deemed achievable, the project will be registered through LEED online. Each discipline will have assigned responsibilities that will be tracked on a sustainability action list and reviewed monthly at project meetings to track the team's completion of assigned responsibilities.

10.5.3 Sustainability Plan

The sustainability effort runs through the following phases: Advanced Conceptual Design, Title I, Title II, and Title III, all as outlined below.

Advanced Conceptual Design

- Establish key sustainable goals and vision for the project
- Meet with the project team to coordinate schedule and identify process
- Assist SLAC in developing the Owner's Project Requirements (OPR) documenting the project's sustainable design elements and objectives
- Confirm green building requirements from the Department of Energy for permit application

Title I

- Further develop Sustainability Plan and LEED scorecard identifying additional strategies and potential credits
- Host Sustainability Workshop with the project team to prioritize sustainable goals for the project including alternative energy systems and energy efficient technologies
- Establish LEED eligible elements of the entire project identifying LEED required data and support materials
- Conduct a project team meeting to review findings and direct team
- Establish a LEED submission deadline with General Contractor and SLAC, if applicable

Title II

- Register project with the Green Building Certification Institute, if applicable

- Generate an action list assigning credit responsibility and communicate the goals and priorities to the project team
- Identify issues requiring credit/tactic research and interpretation
- Host monthly team meetings to review issues and status updates
- Incorporate Sustainability Plan and LEED requirements into project specifications
- Assemble pertinent drawings, submittals, calculations and exhibits for attaching to the Sustainability Plan and LEED Credit Forms
- Research opportunities for innovation in design
- Review 100% DD drawings and specifications for sustainability and LEED compliance
- Complete Credit Forms on LEED Online, if applicable
- Review 50% and 90% CD drawings and specifications for sustainability and LEED compliance
- Coordinate and review draft of Sustainability Plan and LEED design submittals
- Submit LEED Design Submittal to GBCI for review, if applicable

Title III

- Provide sustainable and LEED language for bidding documents and performance requirements
- Review General Contractor and Sub-Contractors sustainability and LEED experience
- Host meeting with the project team to update Sustainability Plan and LEED construction strategies for the project if needed
- Review LEED Design Submittal report from GBCI and distribute assignments to team members for the response to GBCI regarding the final submittal, if applicable
- Review contractor submittals as they relate to the Sustainability Plan and LEED credits
- Visit site and write report related to the Sustainability Plan and LEED issues
- Coordinate with General Contractor for the submission of all construction related credit data for the LEED Construction Submittal, if applicable
- Review, finalize and submit LEED Construction Submittals and any outstanding design submittals on LEED online, if applicable
- Update Sustainability Plan as needed
- Submit final Sustainability Plan for record and LEED Construction Submittal to the GBCI for project certification, if applicable

10.5.4 Conceptual Sustainability Strategies

As stated in the preface, the Sustainability Plan will be pulled together using multiple resources to assist the LCLS-II in exceeding basic sustainability goals. Similar to the LEED Rating Systems, the goals of this Sustainability Plan will be addressed in 6 categories: sustainable site, water efficiency, energy and atmosphere, materials and resources, indoor environmental quality and innovation in design.

Sustainable Sites

- Have a construction activity pollution plan in place to control soil erosion, sedimentation, and airborne dust generation
- Encourage reduction of pollution and land development impacts from automobile use by providing alternative means of transportation such as access to public transportation, providing bicycle storage, and by extending the use of alternative fuel vehicles between site facilities
- Conserve existing natural areas by limiting all site disturbance during construction
- Implement a stormwater management plan that reduces impervious cover and increases on-site infiltration with the installation of bioswales and permeable pavers. The plan should also limit disruption and pollution of natural water flows through best management practices like infiltration basins
- Reduce heat islands with the selection of hardscape and roofing materials with high solar reflective values such as white concrete
- Minimize the amount of light trespass from the building and site by shielding all exterior luminaires or specifying cutoff luminaires. Install automatic controls to turn off or lower light levels during inactive periods

Water Efficiency

- Increase water efficiency by 40% within the facility by installing ultra low flow fixtures and fittings at restrooms and possible shower locations. The Environmental Protection Agency WaterSense products will aide in meeting this threshold
- Though there may be minimal potable water use, installation of indoor and outdoor water meters will provide SLAC and the DOE accurate water usage data
- If landscape is added to the scope, specifying drought tolerant plants and an efficient irrigation system will limit the use of potable water by 50% for landscaping. Though it is often costly, installing a cistern for rainwater capture can eliminate the demand for potable water altogether
- In addition to installing efficient irrigation such as the drip system, implementation of weather based or soil moisture based irrigation controls will ensure minimal waste of outdoor potable water if cisterns are not an option

Energy and Atmosphere

- Implement enhanced commissioning by beginning the commissioning process early in the design process and executing additional activities after systems performance verification is completed
- Design building and systems with a minimum 30% improvement in energy efficiency against set standards. Being an accelerator facility, meeting this threshold can be extremely difficult.

  Lighting Power

  - Reduce lighting power densities by specifying high-efficacy sources and high internal reflectances such as LEDs, ceramic metal halides, and T5-HO

  Lighting Controls

  - Because this facility will be accessed sporadically, it would be beneficial to install occupancy sensors for the entire connected lighting load to avoid cost accumulation in inactive areas where lights could unknowingly be on for long periods of time

  HVAC

  - Maintaining a constant temperature throughout the entire facility will have the largest influence on total energy usage. Spending the upfront cost on a highly efficient HVAC system combined with the use of enthalpy wheels for energy recovery and fuel cells to reduce grid dependence can contribute to an even more efficient and cost effective system.

  Equipment and Appliances

  - Falling under the research facility category, the types of equipment to be installed in this project may not be Energy Star qualified. If these types of equipment or appliances are available however, it should be standard practice to have Energy Star products specified
- Reduce stratospheric ozone depletion by specifying vapor-compression HVAC&R equipment or HVAC&R systems that use natural, low ozone-depletion and/or low global-warming potential refrigerants.
- Invest in at least 7.5% on-site renewable energy (photovoltaic systems, wind energy systems, and fuel cells) to offset building energy costs
- Engage in at least a 2-year renewable energy contract to provide at least 35% of the building's electricity from renewable sources
- Develop and implement a measurement and verification plan to provide for ongoing accountability of building's energy consumption over time. Though it can be costly, specifying a Building Management System will provide even more detailed information in determining energy problems and usage

- Though the benefits of benchmarking are not evident until at least a year of tracking, the Energy Star Portfolio Manager will provide comparative data with each year of operation

Materials and Resources

- SLAC has a campus-wide recycling program in place that addresses the collection of paper, cardboard, glass, plastic, and metals. The program should extend to meet this facility's needs
- During construction, require the General Contractor to implement a construction waste management plan that diverts a minimum of 75% of construction and demolition debris from disposal in landfills
- Further touching on the diversion of construction waste from landfills, the California Building Code also requires 100% recycling of excavated soil and land clearing debris. This may be a huge challenge given the amount of excavation needed for this project, but local markets for salvage can be further researched for viability
- Given the boom in the green industry, the need to make products with high amounts of recycled content is wide-spread. Attaining a minimum 20% threshold for recycled content will be easily attainable by addressing key components such as concrete and steel in the specifications
- With concrete and steel being the main materials for this project, the LCLS-II will reduce environmental impacts resulting from extraction and processing of virgin materials by specifying at least 20% of total materials to be regionally extracted and manufactured
- If wood-based materials are to be used, specify FSC certified products to encourage environmentally responsible forest management
- When applicable, bio-based materials and environmentally preferable products should be specified, encouraging a reduction in environmental impact and effects on occupant well-being

Indoor Environmental Quality

As stated before, during the Sustainability Workshop the LCLS-II team will evaluate if certain elements of the project are eligible for LEED certification. One of the minimum project requirements to qualify for LEED is that the project must serve 1 or more Full Time Equivalent occupants. If less than 1, the optional credits under the Indoor Environmental Quality category cannot be earned. Under the current description, the designed facility is only to be accessed for maintenance purposes. If the scope were to expand or if it is established during the Workshop that there are 1 or more Full Time Equivalents, the LCLS-II will endeavor to meet the following Indoor Environmental Quality strategies:

- Establish minimum indoor air quality requirements against baseline standards through proper ventilation of the facility
- Minimize exposure to environmental tobacco smoke as established with the SLAC Smoke Free Policy

- Install carbon dioxide monitors to ensure that ventilation systems maintain design minimum requirements
- Provide additional outdoor air ventilation above minimum required rates to promote occupant comfort and productivity. Aside from lowering peak energy demand, enthalpy wheels aide in increasing ventilation and fresh air needs
- Implement a construction indoor air quality management plan during construction and perform a flush-out prior to occupancy to reduce air quality problems resulting from construction
- Reduce the quantity of indoor air contaminants with the specification of low-emitting materials
- Design to minimize and control the entry of pollutants into buildings and later cross-contamination with entryway systems
- Design the HVAC system and building envelope to meet set thermal standards
- Provide a monitoring system that ensures the building performance is meeting the desired comfort criteria and conduct a thermal comfort survey of the building occupants
- With a majority of the LCLS-II facility being under ground, proper details demonstrating moisture control is necessary to minimize mold contamination
- Filters with a Minimum Efficiency Reporting Value (MERV) 8 or higher installed at return air grilles is an additional step that can improve indoor air quality

Innovation in Design

- A critical element that is often overlooked when designing structures is the need for an integrated team with sustainability advocates supporting the project from start to finish. Adding sustainable elements as an afterthought is ineffective and can make inexpensive environmental strategies cost-prohibitive further down the line
- For further support and encouragement in meeting the sustainability goals of this project, having LEED Accredited Professionals on-board is key

Following is a sustainability checklist highlighting these targeted strategies of the LCLS-II project.

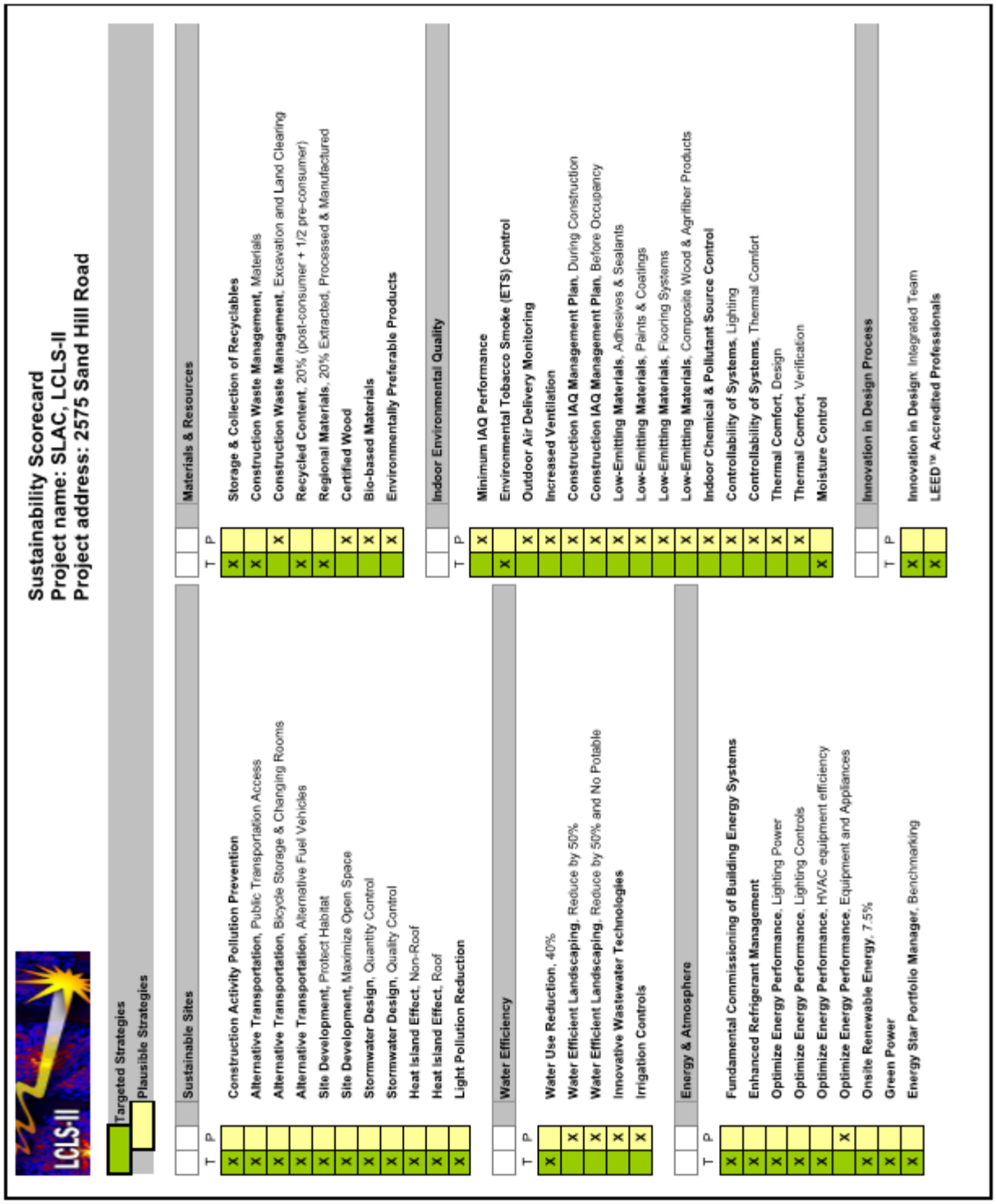

Figure 10.14. LCLS-II Sustainability Checklist.

10.5.5 Code Analysis

The SLAC LCLS-II facility, being a federally funded project through the Department of Energy (DOE), will be designed to meet, as a minimum, the requirements of the codes and regulatory references cited below, along with the SLAC Building & Site-Wide Design Guidelines (DS-018-000-01-R0). In addition, the SLAC Environmental, Safety & Health Division, in conjunction with the DOE, will act as the "Authority Having Jurisdiction" (AHJ).

The design and construction of the SLAC LCLS-II facility will be in accordance with the following Codes and Regulatory References:

10CFR851
OSHA 29CFR1910
OSHA 29CFR1926.800
DOE Order 420.1B/C
2010 California Building Code
    Primary code in conjunction with NFPA codes (except beamline area exiting/egress requirements, see below). Code conflicts to be analyzed by A/E and forwarded to BIO/SLAC Fire Marshal for assessment.
2010 California Plumbing Code
2010 California Mechanical Code
2010 California Fire Code
2010 California Energy Code
2009 NFPA 101 Life Safety Code, particularly Chapter 40 (Industrial Occupancies)
    Primary code for accelerator and x-ray laser beam line occupancy/exiting characteristics and related topics explicitly addressed in NFPA 101 Chap. 40 . Classification is as a Special Industrial Occupancy. In lieu use of NFPA 101 for CBC egress-related requirements specifically adressed in federal guidance document for 10CFR851.
2011 NFPA 70, National Electric Code
2009 NFPA 13, Sprinklers
2010 NFPA 24, Underground Piping
2008 NFPA 30, Combustible and Flammable Liquids
2011 NFPA 45, Chemical Laboratories
2010 NFPA 72, National Fire Alarm Code
2010 NFPA 80, Fire Doors
2009 NFPA 90A, HVAC Systems
2008 SLAC Seismic Design Specification for Buildings, Structures, Equipment, and Systems
1999 DOE Standard 1066
FM Global Datasheets for appicable highly protected risk guidance.
1984 Uniform Federal Accessibility Standards (UFAS), Americans with Disabilities Act and Architectural Barriers Act Accessibility Guidelines, and section 504 of the Rehabilitation Act of 1973, used in conjunction with the CBC Chapter 11.

2005 Fed Building Performance Stds. Sec. 109,
2005 Energy Conservation & Production Act, Sec. 305(a)

Code Analysis / Building	Automatic Fire Protection Syst	Occupancy Type	Construction Type	Allowable Height & Area		Fire Resistant Rating (hrs.) for Building Elements									Maximum Travel Distance (ft.)
				Height (stories)	Area (Gross Sq. Ft.)	Structure	Bearing walls	Non-Bearing walls	Floor Construction	Roof Construction	Area Separation	Corridors	Shaft Walls	Max. Occupant Load	
Injector Support Bldg. (ISB) 1-story, 2,250 gsf	✓	F-1	II-NR	2	15,500	0	0	0	0	0	0	0	1	23	300
Beam Transport Hall (BTH)* 1-story, 12,900 gsf	✓	Unoccupied area, accessed for maintenance & repair only.													400
BTH Service Building 1- Story, 2,200 gsf	✓	F-1	II-NR	2	15,500	0	0	0	0	0	0	0	1	22	300
Undulator X-ray Tunnel (UXT)* 1-story, 11,160 gsf	✓	Unoccupied area, accessed for maintenance & repair only.													400
Electron Beam Dump* 1-story, 6,890 gsf	✓	Unoccupied area, accessed for maintenance & repair only.													300
Front End Enclosure* 1-story, 1,970 gsf	✓	Unoccupied area, accessed for maintenance & repair only.													300
UXT Service Building 1-story, 2,000 gsf	✓	F-1	II-NR	2	15,500	0	0	0	0	0	0	0	1	20	300
Experimental Hall (EH)* 1-level + mezzanine, 20,700 gsf	✓	F-1	I-1hr	2	31,000	0	0	0	0	0	0	0	1	104	300
Auxiliary CUP (ACUP) 1-story, 5,500 gsf	✓	F-1	II-NR	2	15,500	0	0	0	0	0	0	0	1	28	300

*Three-hour fire rated area separation wall required between BTH & UXT, UXT & EBD, EBD & FEE, and FEE & EH.

Figure 10.15. Code Analysis.

Experimental Hall (EH2) Egress Design

The attached SLAC ES&H Preliminary Code Analysis identified the following three (3) Egress Design Alternatives for the Experimental Hall:

1. Provide an exit path through the beam line tunnel
2. Extend west stairway to grade via exit passageway (tunnel)
3. Provide enclosed exit passageway within EH2 access tunnel.

Due to the potential additional costs to widen the beam line tunnel and the EH2 access tunnel, the project will pursue alternative 2, which will require the extention of the west stairway (within

construction shaft) up to a maximum distance of 29 feet above the first level of the Experimental Hall, into a horizontal exit to the west, daylighting at the parking lot at a maximum elevation of 279.0 feet.

Accessibility Requirements

The LCLS II project will meet the accessibility requirements of the 2010 California Building Code as well as the 2010 Americans with Disabilities Act and the Architectural Barriers Act. The most stringent requirements of all three standards govern. Furthermore, the more stringent requirements of these standards compared to any other specification must be used.

Based on the requirements of the above standards, the following spaces are not required to be accessible. These elements, however, shall be on an accessible route:

Equipment areas, such as:

- Beam line tunnel
- Mechanical and electrical equipment rooms.
- Experimental equipment areas within the beam tunnel and in the Experimental Hall (EH) such as beam target hutches that are intended to be accessed only by trained technical personnel for the purpose of installing, adjusting and operating specialized beam target equipment. This equipment has essential geometric considerations that make full accessibility into hutches infeasible.
- Other equipment areas accessed only by service or maintenance personnel.
- Catwalks, platforms and other elevated work surfaces.

As a general guideline going forward, the following elements and spaces for the proposed work are required to be accessible to persons with disabilities:

- Accessible parking spaces adjacent to building
- An accessible path of travel from parking, adjacent buildings and/or the common pedestrian route to the new space.
- All ground floor entrances and exits of the building.
- An accessible route within the space including accessible vertical access to all levels.
- Stairs, elevators and ramps.
- Conference and meeting rooms.
- Offices.
- Control rooms.
- Common use spaces such as copy rooms, break rooms, etc.
- All restrooms, including showers.

- Employee lockers, storage spaces, changing rooms, etc. shall have a portion of them accessible.
- Signage.
- Alarm systems.
- Eyewash stations and emergency showers.

Revision Record

Revision	Date Revised	Description of Change
R001	April 14, 2011	Figure 10.2 replaced; Figure 10.14 labeled..
R000	April 8, 2011	Original release.

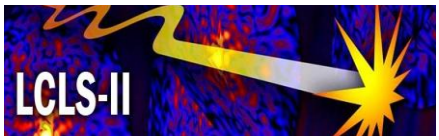

11 Controls

Technical Synopsis

The recent experience implementing the LCLS-I will greatly benefit the control system effort for the LCLS-II. The components and layout of LCLS-II largely mimic those of the LCLS-I, with some new requirements for controlling the variable gap undulators. Some new challenges for the timing and protection systems will exist in interleaving the operation of the two machines and in providing the correct data acquisition tools to assess any interference between them. The control system architecture will be based exclusively on the Experimental Physics and Industrial Control System *(EPICS) toolkit, as is the case for the LCLS-I. As explained in previous chapters, the electron beam requirements are the same as those for the LCLS-I, with respect to timing, beam rate, emittance, and bunch intensity. Hence, the foreseen doubling of scientific capacity provided by the LCLS-II is reflected in an approximate doubling of the current LCLS-I controls implementation. The duplication and extension of the LCLS-I control system will be largely straightforward and built upon a modernized front-end controls platform.*

The strict availability constraints of LCLS-I operations – 95% uptime during user runs, with a much smaller downtime "budget" for Controls, has largely been met. Front-end controls hardware upgrades preceeding and during LCLS-II construction will be aimed at enhancing controls system reliability to further improve our ability to provide the required availability.

The control system will also be designed and implemented so as ***not*** *to limit anticipated enhancements to meet future physics and operational needs of the LCLS-I and LCLS-II, such as multi-bunch operation, higher beam rates, full energy beam (LCLS-I and LCLS-II as one accelerator), and "cross-over" operations between LCLS-I and LCLS-II undulator halls.*

11.1 Introduction and Overview

A high-level overview of the control system architecture is presented in Figure 11.1. Beam-line devices are interfaced directly to EPICS Input/ Output Controller (IOC) front-ends or indirectly to EPICS via Programmable Logic Controllers (PLCs). EPICS Channel Access over Ethernet provides the communication between front-end computers and to mid- and upper-level control system elements. Many EPICS “soft IOCs” -- processes running in servers -- perform important control functions which require no direct hardware I/O. The distributed controls architecture has a backbone network connection supporting EPICS Channel Access protocol, plus several dedicated networks for timing, feedback and MPS.

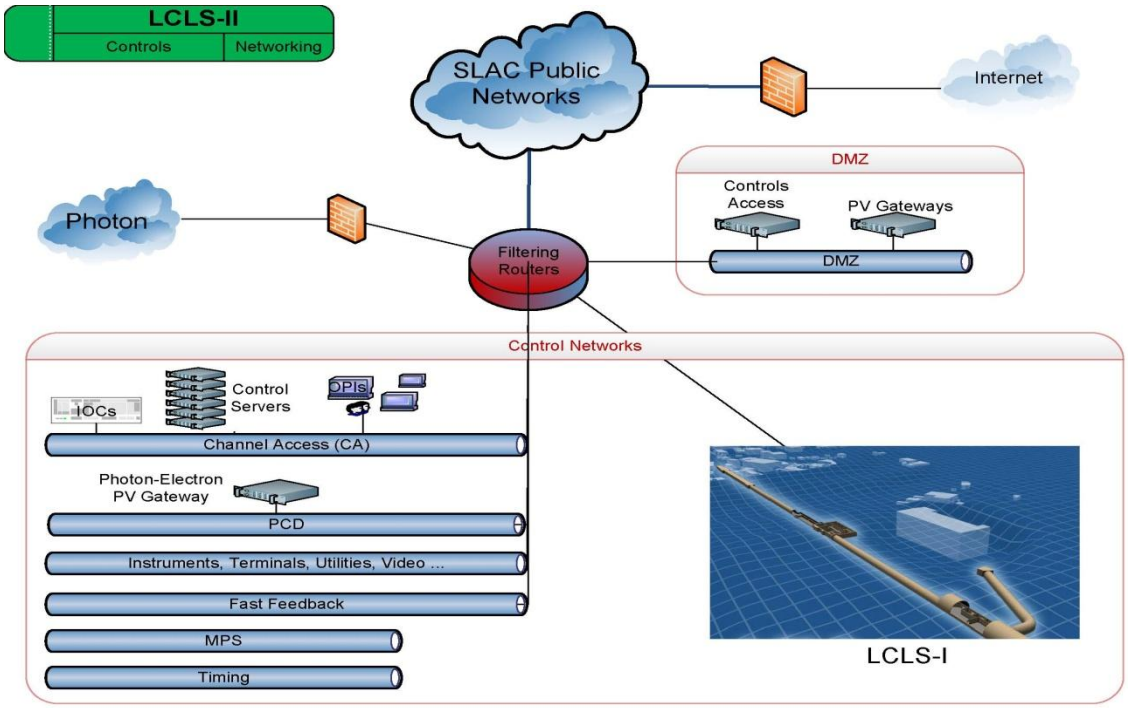

Figure 11.1. High-level network overview.

Some computing hardware and software services will be shared between the two LCLS machines, and other services will be dedicated to either LCLS-I or LCLS-II; the software section of this chapter has details.

The Data Acquisition (DAQ) system is the set of hardware and software responsible for correctly and coherently transporting data from experiment-specific x-ray detectors to offline storage. Each experiment has a unique set of digitizers, cameras, and devices that are required in order to accomplish the experiment's objectives. The data acquisition system is used to configure, calibrate, and control these devices and coordinate their readout with the arrival of the beam. The DAQ system in each hutch is isolated from the DAQ systems in other hutches by exclusive private subnets. Only the DAQ components which are shared among the LCLS-II instruments are part of the LCLS-II scope.

In the following sections we present:

- Global systems, defined as those which span the whole LCLS-II accelerator (injector through undulator) and whose individual elements work in concert with each other
- General instrumentation and control sub-systems
- Software
- Photon area controls and data systems

11.2 Global Systems

Figure 11.2 shows a network-based overview of the global system support. All networks cover the whole of LCLS-II, from the injector to the experimental areas.

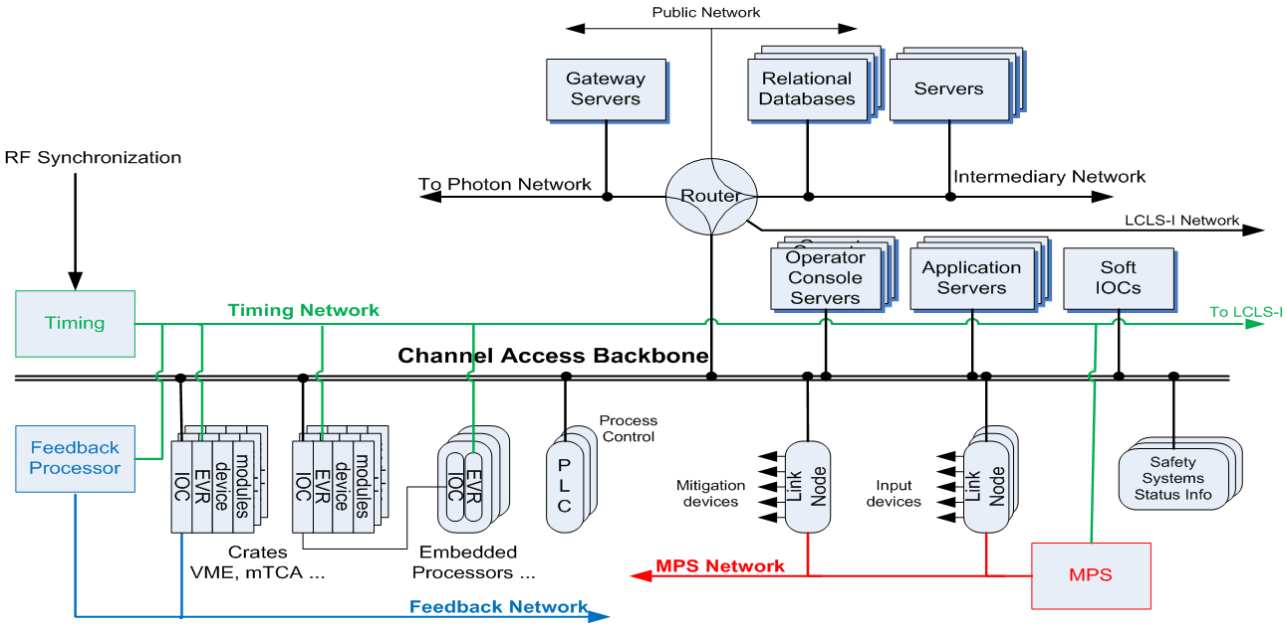

Figure 11.2. Electron control systems overview.

11.2.1 Timing System

The role of the timing system is to provide pulse to pulse coordination (timing patterns) for beam control and data acquisition and to remain synchronized with the Low Level RF 119 MHz phase reference distribution and 360 Hz AC power line phase. In order to operate side by side, the LCLS-II timing system must be slaved to the same RF source as LCLS-I and share the same timing patterns. The timing system will be required to drive LCLS-II on separate, interleaved 120 Hz timeslots to minimize interference between the two machines, or be configured to drive the two machines synchronously for possible future two-beam coincidence experiments. At the same time, the timing systems for the two machines must be sufficiently decoupled to operate independently when one system is down for maintenance or restarted as part of LCLS-II commissioning activities. The expected normal operational mode is for each machine to operate independently at 120Hz, each machine using two of the six available 360Hz time slots.

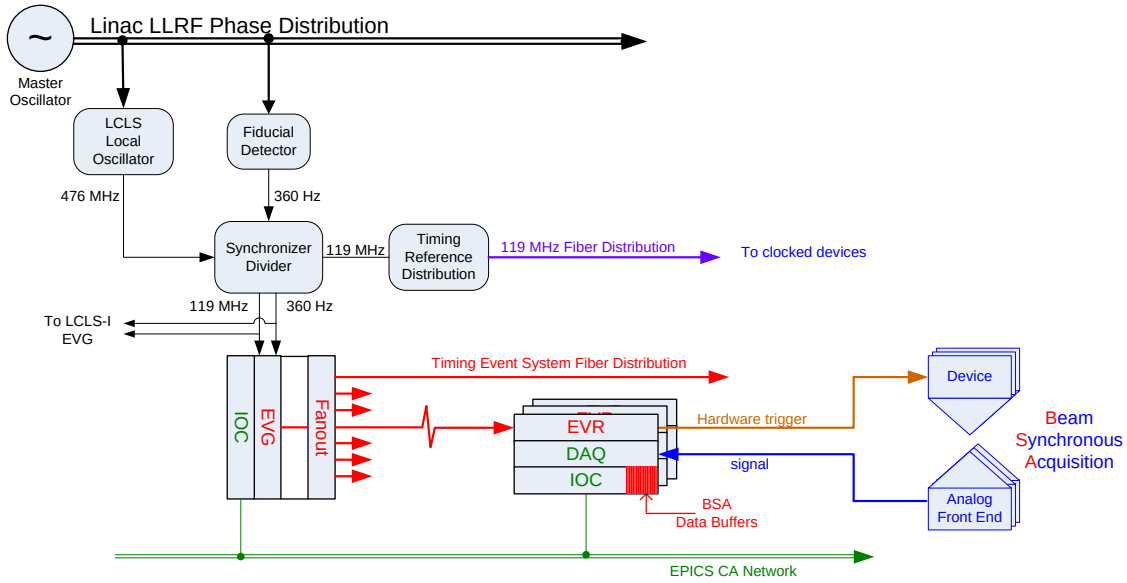

Figure 11.3. Timing event system.

11.2.1.1 Timing Hardware

EVG (Event Generator)

A second Event Generator (EVG) will broadcast timing events over a second timing fiber network to LCLS-II devices and systems, sharing the same master oscillator for clocking and containing duplicate event codes. The current EVG software will be enhanced to allow more than the single event code now used by LCLS-I.

The present LCLS-I timing system is being decoupled from the legacy control system by replacing the legacy Master Pattern Generator (MPG) and Pattern Network Module (PNET) receiver with new functionality in the LCLS-I EPICS EVG module. The current Commercial-Off-The-Shelf (COTS) EVG module fulfills LCLS-I and -II requirements – producing programmable beam rate triggers up to 120 Hz on each machine (interleaved) and with a long term jitter of less than 10 ps -- for broadcasting patterns at 360 Hz over a 2.5 Gb/s optical serial link to the Event Receivers (EVRs).

EVR (Event Receiver)

The 8 bit timing patterns broadcast over the fiber link are received by EVRs that translate them into hardware timing signals and software event codes with a delay resolution of 8.4 ns (1/119 MHz). Finer resolution at the picoseconds level is possible but has not been a requirement for LCLS-I. The EVR also allows for software interrupts in the IOC and time-stamping of events. COTS EVR modules are available as both a 1-slot VME module and as a PMC module that resides on a carrier board. Future versions may also be embedded into other Field Programmable Gate Array (FPGA) modules used for diagnostic and controls purposes.

11.2.1.2 Timing Software--Beam Synchronous Acquisition

In order to characterize the pulse to pulse stability (jitter) of the machine it is necessary to record the data from every pulsed device (beam position monitors, low-level RF, etc.) in the machine on the same event pulse. The data from synchronized pulses is written to buffers with up to 2800 consecutive pulses at 120 Hz. The EVRs write to a software application on the IOC to initiate and capture the Beam

Synchronous Acquisition (BSA) data which is used by higher level applications for analysis and beam tuning.

The BSA package will be extended to capture data from both LCLS-I and LCLS-II on the same set of pulses to analyze jitter between the two machines.

11.2.2 Networks

The LCLS-II Controls Network will be essentially a clone of the LCLS-I controls network. The controls network will consist of distribution switches located near the control system devices in each accelerator area. The distribution switches will be connected to redundant large core switches in Main Control Center (MCC) by fiber optic cables. A sufficient number of fiber optic cables will be pulled to each accelerator area so that multiple fiber optic cables can be used for increased bandwidth or to isolate traffic when needed. Redundant fiber links between the distribution switches and the core switches will allow immediate recovery from the failure of a single fiber link.

As shown earlier in Figure 11.2, the LCLS-II Controls Network will consist of many separate networks, including channel access, instruments, terminals, utilities, Machine Protection System (MPS), timing, video and Fast Feedback. The MPS network will use a separate core switch in the MCC and separate fiber links to MPS link nodes in the accelerator areas. The timing system network will use separate fiber links and connect directly to timing system devices. An intermediate controls network (commonly known as the “Demilitarized Zone” {DMZ}), shared between LCLS-I and LCLS-II, will allow limited and controlled access between the controls network and SLAC public networks through dedicated controls access servers on this DMZ network. Authorized users are authenticated by a Control Access server and given “control room” access to the control system; other SLAC users have read-only access via EPICS Gateway processes. The switch’s architecture allows all of these networks to be isolated from each other but still share the same switches and fiber uplinks. Additional networks can be added when needed. The Fast Feedback network will use fiber links separate from the other controls networks. Central redundant core routers will allow controlled connections between the any of the LCLS-I and LCLS-II controls networks when needed.

As is the case for LCLS-I, the LCLS-II controls network will be isolated from the rest of the SLAC public network. No accelerator control points will be visible to SLAC campus or internet networks. This avoids denial of service and other types of hacker attacks from networks outside of the controls network. Read-only data access will be provided by EPICS Channel Access Gateways on the DMZ network for authorized users on SLAC public networks.

11.2.3 Machine Protection System

The role of the Machine Protection System (MPS) is to turn off the electron beam, or limit the average power by lowering the repetition rate of the beam, when a fault is detected. This is not a life safety system [see Beam Containment System (BCS) and Personnel Protection System (PPS) descriptions], but is designed to prevent excessive losses of the electron beam which would otherwise cause damage to sensitive machine components. The LCLS-II MPS system will largely be a carbon copy of the LCLS-I MPS system. Like LCLS-I, the MPS design for LCLS-II is particularly critical because of the sensitivity of the undulator permanent magnet material to radiation damage. This single aspect drives a key parameter for the design, namely that the beam turn off within one beam pulse of a fault being detected that could damage the undulator. With a machine repletion rate of 120 Hz this means that the MPS must detect, diagnose and shutoff the beam within 8.3 ms before the next pulse arrives.

The MPS takes input from many different devices such as the vacuum system, beam charge monitors, beam loss monitors, protection ion chambers, etc. These inputs are fed into the MPS system via the link nodes (hardware) as inputs with the output of the MPS system used to either rate limit the beam or completely shut off the beam. The mitigation devices include the gun laser pockels cell, the gun laser mechanical shutter and the downstream single bunch beam dumper. The choice of mitigation device used depends upon the location of the fault and the type of mitigation desired (rate limiting vs. beam shut off). An overview of the system as implemented in LCLS-I is shown in Figure 11.4.

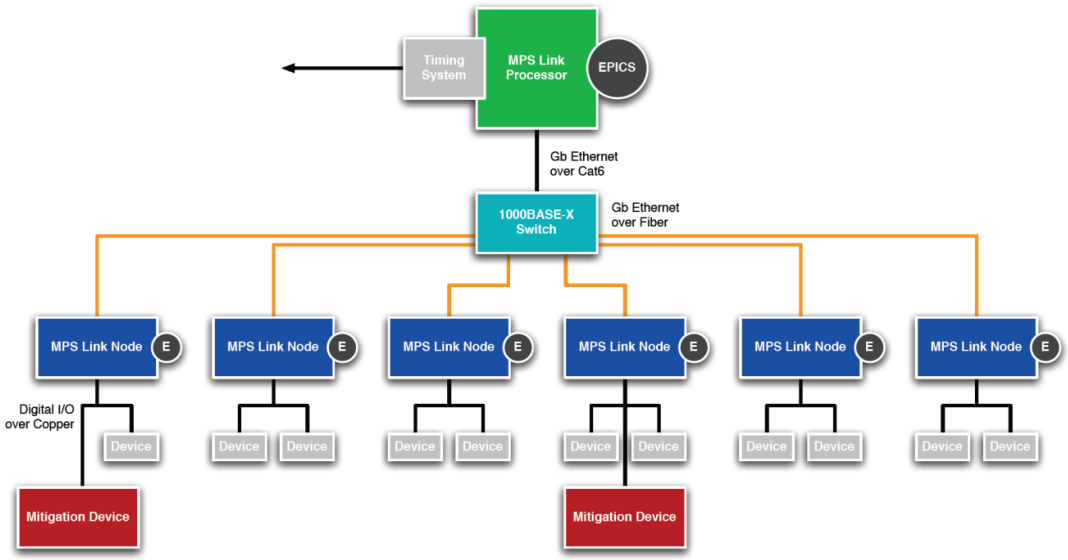

Figure 11.4. MPS Link Node System overview as implemented in LCLS-I.

11.2.3.1 Link node system specifications

The main specifications of the MPS Link nodes are that they be configurable to receive inputs from various devices with differing signal types, pass fault information, and respond to the link processor within one beam pulse to ensure that the beam can be mitigated should potentially damaging conditions exist.

11.2.3.2 Degree of independence between LCLS-I and LCLS-II

LCLS-II adds several new complexities in that there will be multiple beam sources and beam destinations. The MPS will operate independently if a separate network of link nodes and link processors is used on each machine. However, the beamlines in some areas share the same housing so that a beam loss from one machine would trip both machines.

If the pulses from the two machines are interleaved, as described in the timing section, it is possible to discriminate in time between losses from one machine and the other.

11.2.4 Feedback Systems

The beam-based feedback is a networked system that corrects disturbances in the charge, energy, bunch length and trajectory of the beam. The feedback system uses a number of instrumentation systems, such as Beam Position Monitors (BPM) and bunch length monitors, to measure the beam parameters on a pulse-by-pulse basis at various points along the accelerator and beamlines. An algorithm processor computes corrections that are then sent to devices controlling the power, phase,

amplitude and steering and are applied before the next bunch arrives. The 8.3 ms bunch separation at 120 Hz operation requires that a dedicated fast communication network is used to transmit the measurement and correction information between the controller and the devices distributed along the accelerator. At repetition rates above 60 Hz the SLAC accelerator is subject to what is termed “time-slot noise” that originates in the deviations between the six different 60 Hz line phases of the AC site power. The feedback works in conjunction with the global timing system to apply timing-pattern specific corrections to beam pulses that line up with each of these 60 Hz time slots. Such a system has been developed for LCLS-I to ensure beam stability at 120 Hz operation. The beam-based feedback for LCLS-II must use the same control architecture so that LCLS-I and II are aware of each other via the global timing system. The pulsed power load of the klystrons on one machine will create power line noise with a particular time pattern that will influence the other machine, and which can only be compensated by timing-pattern-aware correction actuators on the two machines.

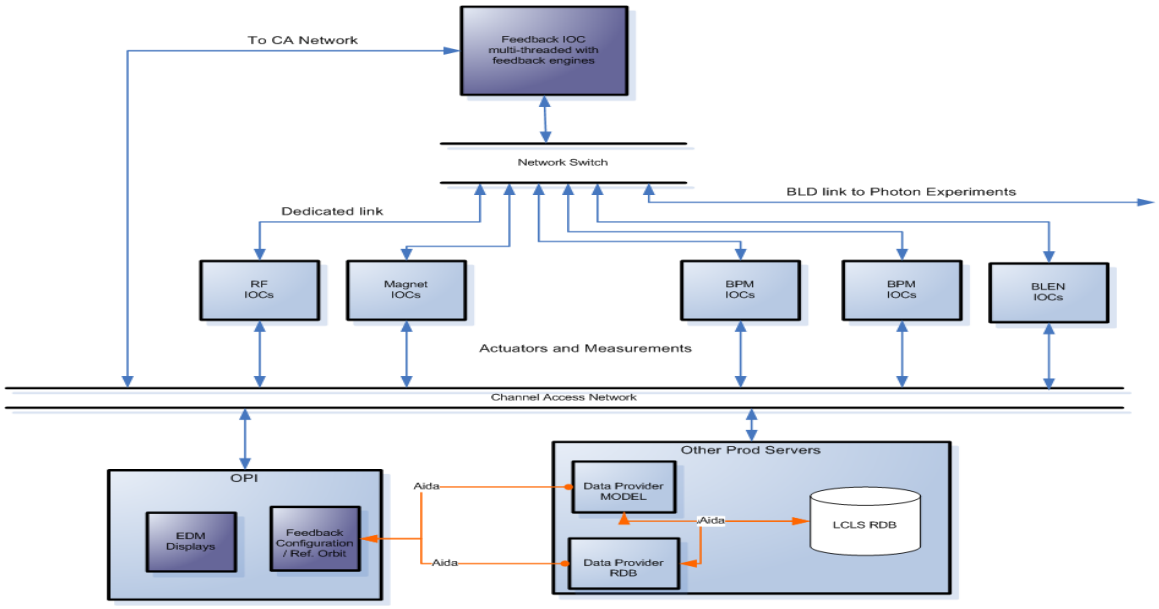

Figure 11.5. Fast feedback data paths.

The timing-pattern-aware actuators have an impact on the design of other systems such as the low level RF controls, in particular the phase and amplitude controllers (PACs) which must be combined with a Timing Event Receiver module to apply timing-pattern-specific changes to the Radio Frequency (RF). This must be made compatible with the internal hardware feedback loops inside each PAC as well. The magnet control system for the steering correctors used in the fast (120 Hz) undulator launch trajectory feedback is also designed to be timing-patter-aware.

11.2.5 Safety Systems

The Personnel Protection System (PPS) and Beam Containment System (BCS) span the entire LCLS-II, from injector to x-ray hutches. Both systems are currently part of the LCLS-I, and the LCLS-II implementation will be very similar.

11.2.5.1 PPS

Two types of Access Control Systems (ACS) with somewhat differing requirements are utilized for the LCLS-I: (1) Personnel Protection Systems (PPS) are used for electron beam enclosures (injector vault,

dump enclosure) and controlled remotely by qualified Operators at the Main Control Center (MCC); (2) Hutch Protection Systems (HPS) are used for x-ray beamlines and controlled locally by qualified users.

The ACS is to provide a number of entry gates and fail-safe and redundant interlock systems to provide safe access to each of the zones described. In addition, the operating modes and access conditions are defined by the location of beam stoppers, or beam dumps, and by the shielding for containing the beam within a nominal hazard zone. The specification for the type of interlock system will be given in the Engineering Specification Documents for the PPS. LCLS-II PPS Zones will be implemented with three standard access states: No Access, Controlled Access, and Permitted Access.

All PPS entry modules will have a door and a gate as well as a standard SLAC keybank for use in controlled entry. Locked doors will have a crash bar for emergency egress. Intercom systems and video cameras will be included at all controlled access entry points. Emergency off buttons, audio-visual warnings, access state annunciators, and yellow/magenta lights shall also be provided per current SLAC engineering practices. The “engineered safe” installation of all new electrical hardware removes their PPS-interlocking requirement and simplifies administrative and training requirements for tunnel access, as well as lock, tag, and verify procedures.

The logic of the LCLS-I and LCLS-II PPS systems is interconnected. Entry into common accelerator segments is precluded by either machine running. On the other hand, entry into LCLS-II sectors 10-20 will be permitted with LCLS-I running. Should the LCLS-II injector be used as a test facility, linac beam will not interfere with injector tunnel access, but injector running will preclude entry into the linac.

Each HPS entry module has a single door for entry and uses only two effective access states: Search Set (or No Access), and Permitted Access. The HPS will be equipped with biometrics controls in order to facilitate identification of users’ access privileges and, in some cases, to grant access to the hutch. Where necessary, in addition to biometric interlocks, a single key will be used for controlling entry.

The presets are located strategically within the Hutch and are completed with either a simple button push or an administratively-controlled key. Complex beam-through operations will be managed through a hybrid system of hardwired panels and touch panels with synoptic diagrams.

11.2.5.2 BCS

The Beam Containment System (BCS) is designed to protect the integrity of beam protection collimators and PPS stoppers, to prevent beam losses inside the accelerator enclosure that can cause unacceptable radiation levels outside the enclosure, and to ensure beam operations remain within the operational safety envelope. Ideally, the BCS should minimize the mutual interference across the LCLS-I and LCLS-II programs by providing targeted shutoffs. Alternatively, a BCS fault anywhere could shut off all beams.

BCS Shutoff Mechanisms:

Beam shut-off mechanisms comprise a key component in the BCS. There shall be three independent shut-off mechanisms for the LCLS-II, which mirrors the requirements of LCLS-I as recommended in the *SLAC Radiation Safety Systems Technical Basis Document*:

A dedicated BCS Laser Safety System (LSS) will stop laser light from striking the RF Gun cathode, stopping the production of beam. This shutter will be situated as close to the production point of laser light as practicable.

Assuming an RF Gun, the BCS will move the gun from an accelerate time to a standby time. This will permit the gun to operate in order to maintain a constant duty factor and temperature.

The solid state sub-boosters accelerate triggers will be moved to 'staggered standby' times, whereby RF timing signals are rendered non-synchronous so that no beam or dark current can be accelerated.

Four independent shutoff paths variously drive these shutoff mechanisms.

BCS Sensors:

Seven different types of sensors are used to monitor the accelerator for the BCS:

1. Protection Ion Chamber (PIC): Typically situated on or near the mechanical device that is to be protected.
2. Long Ion Chamber (LION): Typically installed along the inside walls of the accelerator housings where shielding is inadequate.
3. Flow switch: Installed in cooling water systems for dumps, collimators, and slits.
4. Pressure switch: Installed in PIC and LION gas systems.
5. Microswitch: Used to confirm the correct position of mechanical beam line components, such as stoppers.
6. Current Transducer: Used to monitor current in magnet power supply.
7. Toroid: Current transformers that produce an output proportional to beam current.

11.3 Instrumentation

LCLS-II requirements for instrumentation and control are largely the same as for LCLS-I, so implementation can in many cases be a copy of existing systems. In some cases improvements in design or technology will be implemented based on (1) satisfying the functionality requirements, (2) improving reliability, (3) increasing the level of standardization and maintainability of the systems (e.g. aligning the systems with any new industry standards), (4) reducing costs either in the development or implementation phases, and (5) taking advantage of COTS hardware.

All subsystems will use EPICS, but different individual subsystems will use variously new hardware solutions, Versa Module Eurocard (VME) crate-based IOCs, and PLC/soft IOC combinations.

11.3.1 Diagnostic Systems

Digital data acquisition for diagnostic systems is well integrated into the LCLS-I EPICS controls and Beam Synchronous Acquisition. BPM and RF diagnostic waveforms are digitized with current state-of-the-art 16 bit 125 MHz ADCs. Future implementations will continue to use the direct digitization scheme developed at LCLS-I together with enhancements in performance and packaging as technology becomes commercially available.

The Beam Position Monitoring (BPM) system uses signals from stripline pickups throughout the accelerator and transfer lines while resonant x-band cavity pickups are used in the undulator region. The stripline BPM system uses a direct digitization scheme where the long-haul cable from each of the four striplines connects into an analogue front end consisting of a passive bandpass filter and programmable attenuators. Between the 120 Hz beam pulses the control system is able to send test pulses down the cables to each stripline to continuously maintain calibration of all elements in the signal path. For a given beam charge and stripline geometry the resolution of the system is set by the bandwidth of the bandpass filter. A resolution of a few microns is achieved with the present 10 MHz bandwidth of the

filter at 1 nC beam charge. It should be noted that the bandwidth limitation causes the stripline signal to ring for the order of a microsecond so that sufficient data points are captured by the 125 MHz digitizer, and that this precludes any temporal resolution of multibunches with submicrosecond spacing. The undulator BPMs use a resonant cavity to achieve the same affect as the bandwidth filter for the stripline pickups, and the very high Q of the cavities gives a much larger signal to be digitized and a longer ring time. The cavities are tuned to X-band so the signal is actively mixed down before digitization but the overall high signal-to-noise ratio of the system results in submicron single-bunch position resolution for the BPM system. Both the stripline and cavity systems use the same ADC for digitization. For the cavity system they are packaged in a VME form factor with several BPM modules per crate, while the stripline processors are housed in individual chassis. Future designs will refine the layout to take advantage of standardization of the control system components throughout the machine.

Beam size measurements using single shot image capture rely on fast digitization at the highest possible resolution, which is usually a compromise between number of pixels, bit-depth resolution and frame rate. Commercially available cameras are selected depending on the application, where high repetition rates for laser steering feedback at 120 Hz have lower pixel counts, and high resolution profile monitor screens with greater bit size are limited to 10 Hz. The control system interface for LCLS-I has been via camera-link protocol over fiber links, but this may be extended to include Ethernet as more advanced cameras become available with this interface.

Wire scanners have become more widespread in use than originally anticipated for LCLS-I because of the coherent radiation problem encountered with profile monitor screens showing optical transition radiation. Performance of the wirescanners is now more critical since they are used more frequently during machine tuning. Improvements for LCLS-II wire scanners could include using different layout and motor technology to allow the scanners to complete both x- and y-scans in a much shorter time. Photo multiplier detectors for the wire scanners are incorporated in the existing beam synchronous acquisition scheme of LCLS-I.

Bunch length measurements rely on digitization of Terahertz signals from detectors used in conjunction with insertable filters and attenuators. The design has gone through several iterations with LCLS-I and will be optimized for cost and standardization with LCLS-II. Absolute calibration of the bunch length monitors is based on the measurements with the transverse deflecting cavity which uses LLRF controls and the image acquisition system.

Requirements for beam charge measurement with toroids are covered by existing digitizer designs that also incorporate comparators to measure signals from two toroids and trip BCS interlocks if they differ by more than a preset amount.

11.3.2 Standard Controls from LCLS-I

Control and readback of the vacuum system, the interface to conventional facilities such as Heating, Ventilation and Air Conditioning (HVAC), and basic motion control will be implemented as on LCLS-I.

Control of DC power for magnets will also be implemented as on LCLS-I given that the power supply technology remains unchanged. Pulsed power for klystron modulators will have been upgraded from the legacy controls as part of a linac-wide upgrade plan.

Laser controls for the injector will be adapted according to the type of laser that will eventually be installed, since laser design is also evolving with the technology. On LCLS-I, proprietary laser controls were shipped with the laser and only status readback was implemented into the LCLS-I control system.

11.3.3 Subsystem Implementations extended from LCLS-I

The variable gap undulators will require an expansion and modification of the current undulator control. The details of motor control for adjusting the undulators will be different from that used in LCLS-I, but the scope of work is equivalent.

The use of multiple undulators and beam destinations on LCLS-II has implications on the timing system, as discussed earlier, and will also require control of pulsed devices to switch the beam between beamlines on a pulse by pulse basis.

Experience on LCLS-I has shown that greater flexibility in Low Level Radio Frequency (LLRF) control is desirable for monitoring and correcting pulse-to-pulse stability. Operation of multiple undulators is likely to increase the need for pulsed control of the LLRF to accommodate different beam tuning requirements on each pulse. Future designs of LLRF controllers implemented in the linac-wide upgrade will allow for integration of beam synchronous acquisition of all relevant RF signals and give flexible control over phase and amplitude of individual klystrons.

11.4 Software

11.4.1 Software Infrastructure

11.4.1.1 Controls Computing

LCLS-I controls computing infrastructure, which provides services to LCLS-I controls applications from front-end IOCs, to mid-level software, to upper-level Operator Interfaces (OPIs), is highly distributed, secure, and robust. The LCLS-II computing infrastructure will be basically cloned from LCLS-I, with most critical services hosted on a private controls network similar to LCLS-I. Some general services will be shared between LCLS-I and LCLS-II on the DMZ (controls intermediate) network. Table 11.1 below lists all services essential to operations.

Table 11.1. Controls services essential to operations.[1]

System	Description	Shared
NFS Server	File server and data storage for controls applications, boot server for IOCs and filesystem for all other servers. Will be upgraded to be a highly reliable and scalable system.	✓
TCP/IP Services	NTP, DNS, DHCP, and etc. for all controls networked devices and nodes.	✓
Controls Access	Providing limited and controlled access between controls networks and SLAC public.	✓
Public Gateway	Providing SLAC public Read-only PVs access for monitoring and analysis.	✓
HELP System	Providing information support for operations. Centralized and context-sensitive.	✓
E-log Systems	Electronic logbooks for operations and for physicists.	✓
Oracle server	Database for controls.	✓
Data Server	Providing EPICS Channel Archiver data to operations and SLAC public.	✓
Photon Gateway Server	A pair of PV gateways with access rules which permit Read/Write access to selected PVs between Electron and Photon controls.	✓
Daemon Servers	Hosting soft IOCs, CMLOG (distributed message logging system), IRMIS (integrated relational model of installed system), data provider services, services for high level applications and OPIs, etc.	
Interactive Servers	Hosting MATLAB applications, high level applications, and EPICS CA client applications, etc.	
Archiver Engine System	Channel Archiver sampling system. A new reliable and scalable Archiver system will be developed for LCLS-II.	
Build system	Providing a platform for application build and deployment.	
CUDs and OPIs	Providing operators status displays and operation consoles.	

11.4.2 Operational Software

11.4.2.1 EPICS Software

LCLS-I takes advantage of EPICS to control approximately 500 Input/Output Controllers (IOCs) networked together to allow communication between them and to provide control and readback for the various parts of machine devices. Most “hard”, VME-based, IOCs execute various I/O and local control tasks, and publish this information, in the form of process variables (PVs) to clients using the Channel Access (CA) network protocol. The “soft” IOCs- which do not perform device I/O- are hosted on Linux server machines. LCLS-I now has approximately 1.5 million PVs, 150,000 of which are being archived.

Embedded Low Level

The EPICS-based low-level software currently used for LCLS-I consists of:

- Open source Real-Time Executive for Multiprocessor Systems (RTEMS) Real-Time Operating System (RTOS)
- EPICS base, board support packages, drivers, device and record support

[1] See Appendix A, Glossary, for definitions of acronyms in all tables which are not otherwise defined in chapter text.

Embedded Application Level

The EPICS application layer which communicates to the lower level consists of:

- EPICS thread model, custom Open Systems Interconnection (OSI) threading, EPICS database support, state machines
- Common IOC libraries for admin (IOCAdmin), management (IOCManager),

11.4.2.2 EPICS Clients

There are many open source EPICS clients used in Operations, including applications which encapsulate the following functionality:

- Bumpless reboot - channel watcher and autosave
- Display manager – EDM, which serves up hundreds of status, diagnostic and control screens
- Archiving [2]
- Alarm handler
- Electronic logbooks
- EPICS Channel Access gateways ¬– provide access security and name translation
- Message logging
- IRMIS –EPICS process variable crawler; output stored in Relational Database (RDB)
- Strip tool
- PV diagnostic tools

11.4.2.3 Relational Database (RDB)

Oracle hosts several databases in support of operations and engineering teams, including snapshots of operational setpoints/readbacks, machine model design lattice and model-run data, the Operations electronic logbook, crawled PV data, device parameters, and machine fault history. Management of EPICS generated PVs and the numerous EPICS client application configurations which need to incorporate them is very engineering resource intensive for large distributed systems. PV management automation will be added to support the growing demands.

11.4.2.4 High Level Applications

Table 11.2 introduces the various frameworks, applications, and Graphical User Interfaces developed by the Controls department. These applications are associated with and supported by large, robust control and/or relational database frameworks.

[2] With LCLS-II, the total PV population is expected to climb to over three million total PVs. In order to accommodate LCLS-I's growing data archiving demand and the PV growth projected with LCLS-II, higher performance and scaleable archiving architectures are currently being explored.

Table 11.2. Controls support systems.

Category	Name
Machine State Analysis	SCORE snapshot facility
	Archive Viewer
	Message Log Viewer
	Alarm top, Alarm Handler
	Orbit Display
	MPS History
Model Based Applications	Model Manager
	Linac Energy Manager
	Steering
Fast Feedback Framework	Transverse and 120Hz Longitudinal Feedback Loops
MATLAB Applications[3] and Toolkit[4]	Support for Physics Group applications

11.4.2.5 Common Operational Considerations

Since both LCLS-I and LCLS-II will be run from the same control room, and most controls software will be identical for both machines, we plan to have a common code and user-interface base able to operate each machine independently. All user interfaces will be clearly designated so that no confusion arises as to which machine is being controlled.

In order to ease the burden of operating two machines by the same staff from a single control room, in collaboration with accelerator operations and machine physicists, we are exploring the possibility of automating routine and frequent tasks such as machine tuning and beam parameter changes.

11.5 Electron-system/Photon-system Controls Interface

The interface between electron and photon controls will be as it is for the current LCLS-I: “Electron controls” includes all aspects from the electron laser and injector through the undulator up to the electron dump; “Photon controls” starts just past the electron beam dumps, and includes all aspects of x-ray transport and experimental support.

EPICS Channel Access gateways have provided the name translation and access security between the electron and photon controls support areas in LCLS-I; this implementation will be duplicated for the LCLS-II.

11.6 Photon Controls and Data Systems

The Photon Controls and Data Systems (PCDS) provide all the computing capabilities needed to operate the Front End Enclosure (FEE) and the LCLS instruments and acquire and analyze the science data

[3] The Physics Group has developed approximately 100 MATLAB applications for analyzing and computing physics data as well as for control and diagnostics. The bulk of these applications will also use the same code base as LCLS-I. Controls provides software versioning and basic support for these MATLAB application environments.

[4] The MATLAB Toolkit contains Application Programming Interfaces (APIs) for machine control functionality, including setpoint/readback control for PVs, beam synchronous acquisition data, and PV allocation for computed physics data.

generated by these instruments. These three activities correspond to the three core PCDS subsystems: controls, data acquisition (DAQ), and offline analysis.

This section describes the FEE controls subsystem and the DAQ components which live in the server room in the new LCLS-II experimental facility. Note that the controls and DAQ components which live in the hutches and the offline analysis subsystem are not in the scope of LCLS-II and will not be described in this document.

The core computing services for the LCLS-II photon data systems will be provided by LCLS-I. These include:

- Network file system servers for the user home directories, for the instrument operator accounts, for the user groups, for the disk-less nodes.
- Disk and tape backups.
- Timing services, naming services, host configuration services, authentication services, web authentication, directory database.
- Experiment database, web server, electronic logbook, system monitoring, logging services.

A simplified diagram of the photon systems networking is shown in Figure 11.6. Each instrument has its own controls network and its own DAQ network. Network traffic among the different networks, and with the accelerator, is managed by the LCLS-I router in the NEH server room.

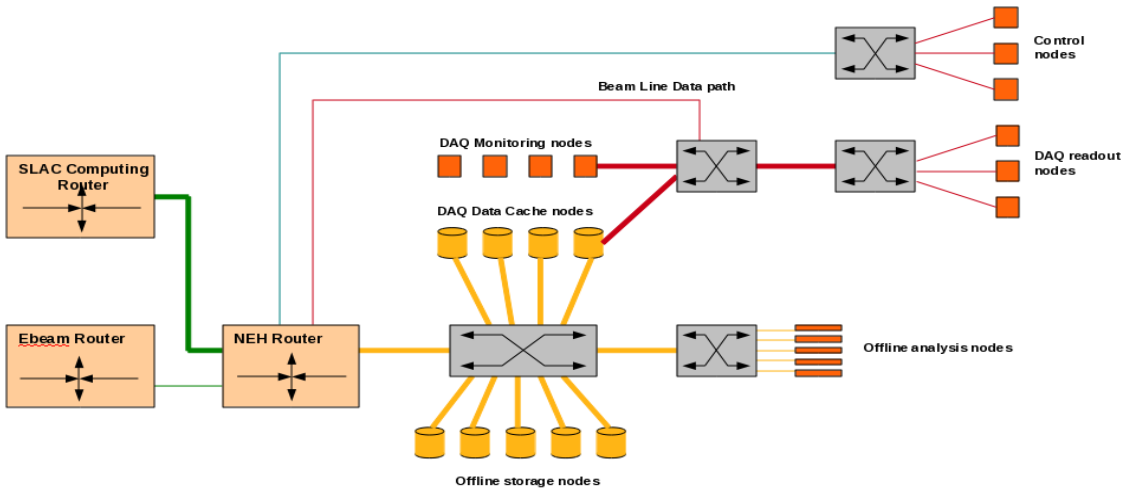

Figure 11.6. PCDS networking: Simplified diagram of the photon systems networking.

Only one instrument is shown. The bold lines represent 10Gbps ethernet connections. The thin lines represent 1Gbps connections. The grey boxes are Layer-2 (L2) ethernet switches.

11.6.1 Front End Enclosure

11.6.1.1 Guidelines

Instruments: FEE-II will reproduce FEE-I instruments where they match the requirements. At present these include the gas detectors, gas attenuator direct imager, solid attenuators, spectrometer, and pop-in cameras. There will be some technical improvements based on FEE-I experience, but this incremental approach will significantly reduce engineering and cost risks. FEE-II will use instruments is use in the

LCLS-I hutches: 4-jaw slit assemblies; and an instrument now being developed in the LCLS-I dump area, total energy monitor, which is expected to be fully mature.

Machine Protection System (MPS): The will generally have independent paths, either direct from hardware [like Solenoid Chassis (SNC), Profile Monitor Chassis (PMC)], via relays, or via PLC. However, energy-dependence will require some new inputs for fail-safe operation.

Areas: About 30-40% of components will be in the Dump area; these components form the shared line which contains the upstream mirror assemblies to split and direct the photon beam and the timing hardware. Following the shared line will be two soft lines (250eV-2keV) and one hard line (2-13keV), where the balance of the instruments will be deployed. Quite a few will be duplicated, thus adding no engineering and cost risks.

11.6.1.2 Instruments

The controls for the soft x-ray line and the hard x-ray line instruments are described in the following two tables. Generous space will be provided for equipment racks throughout, spanning most of the south wall, keeping cable runs short. Thermocouples and pressure/temperature/flow transducers for N2, H2O, and compressed air will be provided.

Table 11.3. Soft X-Ray line instruments.

Instrument	Components	Comments
4jaw slits	Motion, temperature	
Gas detector	HV; LV; pressure; gas handling; digitizer; pumping	PLC-based 2x
Gas attenuator	Pressure; gas handling; digitizer; pumping	PLC-based
Total energy monitor	Bias V; digitizer	Thermal-acoustic
Direct imager	Motion; camera; illuminator	With zoom plus iris (PMC-based, same as pop-in)
Mirrors	Motion; temperature control	X/dX motion and new mechanicals 2x
Popins	Solenoid; camera; illuminator	With zoom plus iris (PMC-based, same as direct imager) 2x Needs MPS
Vacuum	Pumps/gauges/valves	Ion pumps + pirani/cold-cathode gauging

Table 11.4. Hard X-Ray line instruments.

Instrument	Components	Comments
4jaw slits	Motion; temperature	
Gas detector	HV; LV; pressure; gas handling; digitizer; pumping	PLC-based 2x
Solid attenuator	Solid attenuator: solenoids	Needs MPS
Spectrometer	Motion; digitizer; signals	With k-monochromator
Total energy monitor	Bias V; digitizer	Thermal-acoustic
Direct imager	Direct imager: motion; camera; illuminator	With zoom plus iris (PMC-based, same as pop-in)
Mirrors	Mirror: motion; temperature control	X/dX motion and new mechanicals
Popin	Solenoid; camera; illuminator	With zoom plus iris (PMC-based, same as direct imager) Needs MPS
Vacuum	Pumps/gauges/valves	Ion pumps plus pirani/cold-cathode gauging

11.6.1.3 Components

The FEE-II controls system will build on top of the components described in the Table 11.5.

Table 11.5. FEE-II controls components.

Component	Interface	Comment
Motion	Serial	Smart motors and absolute rotary and linear encoders
Cameras	PCIe	Camera Link protocol
Digitizers	cPCI chassis	High speed, high resolution
High Voltage	Ethernet Modbus SNMP	
High current	Ethernet	
Miscellaneous temperatures, analog/digital	Ethernet Modbus	
Vacuum	Ethernet Ether/IP	PLC
IOC		Rack mount 1U or 2U servers running Linux with real-time patches and PCIe EVR
Racks		40U, water cooled, 14x
Timing		FEE-II will receive one timing fiber from server room level-2 fan-out; additional level-3 and level-4 fan outs in FEE-II area will provide links for all IOCs
Software		EPICS at then current community release; standard high-level applications

11.6.2 Data Acquisition

11.6.2.1 Guidelines

Architecture: The Data Acquisition (DAQ) system will adopt the same architecture as the LCLS-I DAQ system. A diagram of this architecture is shown in Figure 11.7. Each instrument will have a dedicated DAQ system with a dedicated network. Each of these systems will be built around one high performance L2 Ethernet edge switch in the instrument hutch, one 10Gb Ethernet switch in the server room, one or more console nodes in the control room, a set of readout nodes in the instrument hutch and a set of data cache and monitoring nodes in the server room. DAQ for the two soft X-Ray instruments, AMO and SXR, moving from the NEH to the new Experimental Hall are included.

Data rate: The data acquisition system will be able to record a maximum of 2 GB/s at a trigger rate of 120 Hz.

Infrastructure: A fiber trunk will connect the Near Experimental Hall (NEH) server room and the server room in the new facility. The server room, which will be shared among the different instruments, will be connected to each instrument with a dedicated fiber trunk for networking and timing. The expansion from LCLS-I to LCLS-II is similar to the installation of experiments in the Far Experimental Hall (FEH). The core services in NEH are already able to scale to adjust for the new facility.

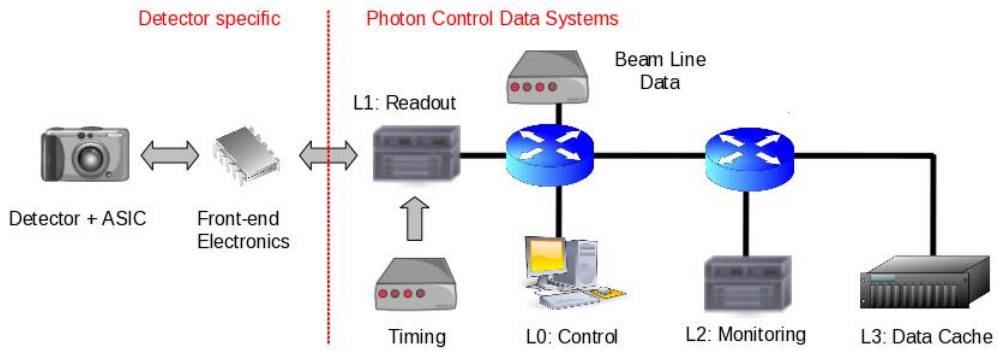

Figure 11.7. DAQ diagram: Architecture of the data acquisition system.

11.6.2.2 Data cache

The data cache nodes assemble the components from the different readout nodes which correspond to the same pulse and store the full event to the local file system. These file systems form the online data cache which isolates the DAQ system from users operations and allows the experiments to take data even during outages of the offline system.

The data files will be copied over 10Gbps links from the online cache to the offline storage where they are made available to the users for offline analysis and for off-site transfer.

11.6.2.3 Monitoring

The online monitoring is implemented by snooping on the multicast traffic between the readout nodes and the data cache nodes. Users will be able to augment the existing monitoring features by dynamically plugging in their code to the core monitoring framework.

11.6.2.4 Controls System Interface

The DAQ system will be able to interface to the controls system in order to store some user selected EPICS process variables together with the science data and to control any device that can be used to perform a scan or a calibration run.

11.6.2.5 Timing System Interface

The expansion of the timing system from LCLS to LCLS-II simply requires an additional fiber from MCC, an additional compensation oven and a second fan-out board to distribute timing information to the hutches in the new experimental hall.

11.6.2.6 Beam Line Data Interface

Beam Line Data (BLD) must be transmitted on every LCLS shot and archived together with the rest of the science data. The sources of the beam line data are the FEE gas detector, the phase cavity, and the accelerator fast feedback system. The BLD contributions of the latter system are the charge, energy, and position of the electron beam. These data are used by the scientists to refine the energy and the precision of the beam arrival time on a pulse by pulse basis.

Time stamped beam information contained in User Datagram Protocol (UDP) packets is sent via multi-cast to the experiments interested in it. For LCLS-II there will be a new source of beam line data from FEE to describe the beam parameters for the new electron bypass line. The same technique will be used to collect and package the beam line data from this new region.

11.6.3 Move of AMO and SXR Instrument and Laser Controls

11.6.3.1 Move of Instrument Controls

The controls hardware currently in hutch 1 and hutch 2 of the NEH for the AMO and SXR instruments will be moved to the new experimental hall. Since the physical layout in the new hall will be different, a new set of rack-to-instrument cables will be provided.

11.6.3.2 Move of Laser Controls

The controls hardware for one laser currently in NEH laser room will be moved to the new experimental hall laser room. A Laser Safety System for the new hall will be installed.

11.6.3.3 RF Cavity Timing

In order to provide timing to the instruments, a copy of the RF Cavity system currently in operation in the LCLS-I undulator hall will be provided for the LCLS-II undulator hall.

12 Alignment

Technical Synopsis

This section describes the procedures and methods used to position the LCLS-II components with their required accuracy. Most of the alignment requirements for the injector, linac and electron beam transport are well within the range of proven traditional accelerator alignment techniques. The alignment requirements of the FEL undulator section are the most demanding part of the project. State-of-the-art equipment and procedures will be needed to meet the positioning requirements.

The alignment coordinate system will be the existing Cartesian right-handed system, which was implemented for the SLC project and was also used for the LCLS-I project. The alignment network will consist of tunnel networks in the different areas building on the existing network for LCLS-I and a surface network to integrate the different sections into the overall coordinate system. The network geometry is driven by the tunnel and machine layout and should permit observation of each target point from at least three stations. The design philosophy is based on a 3D monument design providing the best possible positional accuracy. Floor and two wall monuments on opposing walls are placed in regular intervals every 10 m.

The alignment instrumentation will be a laser tracker / digital level used in combination. In conjunction with least-squares solutions, the laser tracker will provide excellent 3D positional accuracy. In addition, the digital level will improve the rotational stability of the narrow linear network. To meet the global straightness and local relative alignment needed for beam-based alignment to converge quickly, the optical measurements will be supported by stretched-wire based straightness measurements.

12.1 Procedural Overview

The alignment for the injector, linac, BSY and transport line is based on the following procedure. During installation, conventional alignment methods will be used to position components to their individual tolerances. Position adjustments will be applied mechanically.

Initial alignment of x-ray components follows the same procedure as above, after which additional steps might have to be used depending on the component (e.g. setting the roll of mirrors with auto-collimation techniques).

The alignment of the undulator system will be carried out in four distinct steps:

During installation, conventional alignment methods will be used to position the undulator segments, quadrupoles, correctors, Beam Position Monitors (BPMs), vacuum chamber and other components to about ±150 µm. Position adjustments will be applied mechanically, i.e., remote movers will not be used for this task.

To refine the installation alignment, the effective centerline of undulator segments, vacuum chamber, quadrupoles and BPM modules will be aligned to 100 µm, with respect to a global straight line. This global straight line may deviate significantly from the nominal axis (which is an extension of the axis of the linac) in position and orientation. A portable stretched wire system [1] with a sensor capable of absolute measurements will be used in the horizontal plane to achieve the x-axis tolerances in combination with laser tracker measurements. The y-axis tolerance can be achieved with digital leveling. Position adjustments will be done remotely for the undulator segments and the magnet quadrupoles, and locally for the BPM modules.

The relative position difference between undulator segments and adjacent quadrupoles will be mapped and recorded. A measurement tolerance of better than 50 µm is expected.

After the conventional alignment and thereafter at periodic intervals of a few weeks, or as needed, the Beam-Based-Alignment (BBA) procedure as described in Chapter 7, Section 11 will be applied. The BBA procedure moves the quadrupoles to correct the electron beam trajectory; subsequently, the undulator segments are moved accordingly to maintain relative alignment to the quadrupoles. At the first time, the undulator vacuum chamber alignment may need to be corrected. This procedure will create a straight beam trajectory and align the undulators to the axis within the tolerances defined in Chapter 7, Section 11. Once this is achieved, the BPM readings will be recorded as the reference zero positions. Successive alignment procedures are expected to be much quicker than the initial procedure. Feedback systems will be employed to keep the trajectory straight to the BPM modules by using the movable quadrupoles as correctors.

If it turns out that the x-ray beam, as produced by the undulator initially, points too far away from the desired target points in the experimental halls, iterations of the above step sequence can be used to re-point the undulator. This might require a realignment of the undulator vacuum chamber.

12.2 LCLS-II Surveying Reference Frame

Horizontal position differences between the projection of points on the geoid[1] , or a best fitting local ellipsoid, and those on a local tangential plane are not significant for a project of the size of the LCLS-II. Hence, it is not necessary to project original observations like angles and distances into the local planar system to arrive at planar rectangular coordinates [2].

However, in the vertical plane, the curvature of the earth needs to be considered. Because leveling is done with respect to gravity, the reference surface is the geoid. Due to the relatively small area of the LCLS-II project, one can substitute the nonparametric geoid with a locally best-fitting sphere. Notice that for distances as short as 20 m the deviation between plane and sphere is already 0.03 mm.

12.2.1 Alignment Coordinate System

The alignment coordinate system is a cartesian right-handed system. The origin is at Linac Station 100 (analogous to the SLC coordinate system). There is no monument at the origin, it is purely a virtual point. The y-axis assumes the direction of the gravity vector at the origin but with opposite sign. The z-axis is in the direction of the linac, and the x-axis is perpendicular to both the y and z-axes. The signs are defined by the right-handed rule (see Figure 12.1).

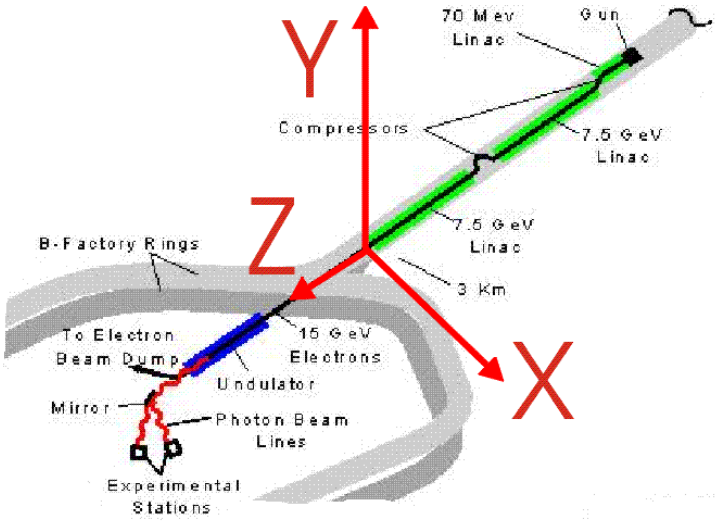

Figure 12.1. Coordinate system definition.

12.2.1.1 SLAC Linear Accelerator Coordinate System

The SLAC linear accelerator coordinate system is used for the LCLS injector and accelerator structures and systems installed in the accelerator enclosure. The origin is at the beginning of the linac and the z axis follows the (straight) beam line. The station number datums are located on this z axis. The beam axis of the linac is not level with respect to gravity and has approximately a 0.5 % slope as explained

[1] The geoid is the reference surface described by gravity; it is the equipotential surface at mean sea level that is everywhere normal to the gravity vector. Although it is a more regular figure than the earth's surface, it is still irregular due to local mass anomalies that cause departures of up to 150 m from the reference ellipsoid. As a result, the geoid is nonsymmetric and its mathematical description nonparametric, rendering it unsuitable as a reference surface for calculations. It is, however, the surface on which most survey measurements are made as the majority of survey instruments are set up with respect to gravity

below. The linac coordinate system will be used from the injector through the linac and in the Beam Switch Yard (BSY).

12.2.1.2 LCLS Undulator Coordinate System[3]

The SLAC accelerator is designed with a downward slope heading eastward, with respect to the local gravity vector, of ϕ_{50} = 5.000000 mrad at station-50 (in the middle of the linac). This downward slope, due to the Earth's curvature, becomes ϕ_{100} = 4.760000 mrad at station-100[2] at the end of the linac. Starting in the 1980's, all alignment computations were based on the Gaussian sphere associated to the Clarke's ellipsoid of 1866 for a latitude of 37˚ 25' which set R = 6372508.025 m. Note that the station-100 accelerator level is located at a height h = 77.643680 m[3] above mean sea level, and 1.857543 m down beam of the center of the 50Q1 quadrupole magnet, and 14.325082 m up beam[4] of the center of the 50Q2 quadrupole magnet.

The layout is depicted in Figure 12.2, where the (x, y, z) coordinates (in blue) are established along the existing linac axis (with z = 3048 m at station-100[5]), while the (x', y', z') coordinates (in red) are vertically normal to the Earth's surface under the LCLS-I undulator's (rounded to the nearest meter) center. The undulator coordinate system as defined in Figure 12.2 will be used for LCLS-II downstream of the BSY. Local coordinate systems for the convenience of the designers might be derived from the undulator system by adding offsets and by rotating the system around the z-axis.

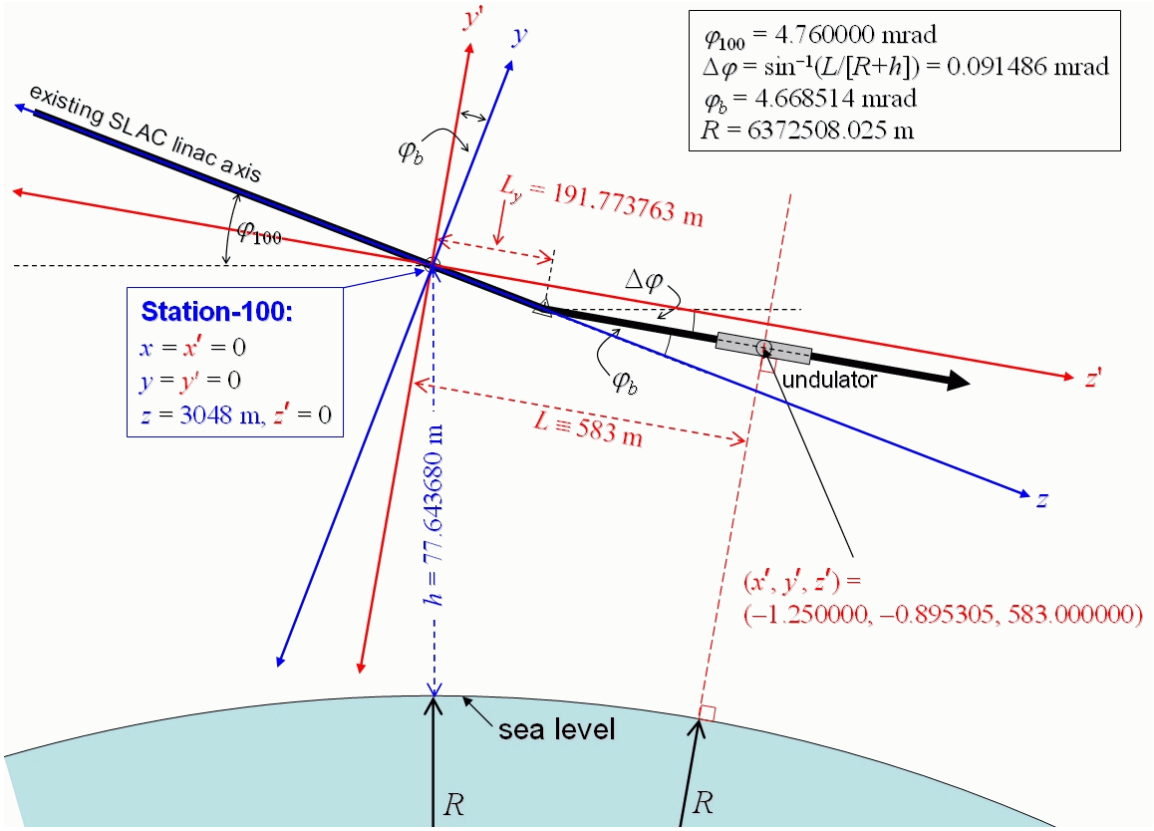

Figure 12.2. SLAC linac coordinate system (x,y,z), and LCLS undulator system (x', y', z').

[2] Unpublished note from Geodesy Division, Coast and Geodetic Survey, Appendix J, February 26, 1963.
[3] Value adopted during SLC installation and used ever since for projects originated in the BSY.
[4] This distance is measured along the local beam line.
[5] The value of 3048 m is exact and is based on 100 feet of linac length per station number.

12.2.2 Network Design Philosophy

The different machine sections will have different functions and tolerances. In general the new alignment network will build up on existing network installations around Sectors 20-23 and the Beam Transport Hall (BTH) west. For some areas, new tunnel networks need to be installed. The relatively weak links between machine sections make it necessary to support the tunnel networks with a surface network, particularly around the new tunnel constructions

The reference point monuments are based on a 3D design, which was already used for the LCLS-I. This approach is centered around a 1.5 inch sphere. Different targets can be incorporated into the sphere in such a way that the position of the target is invariant to any rotation of the sphere. Receptacles for the spheres, which are usually referred to as “nests” or “cups,” have been designed to accommodate different functions. Designs are available at SLAC for cups grouted into the floor, tack-welded onto magnets, mounted on wall brackets, and for a “centered” removable mounting, placed into tooling ball bushings (see Figure 12.3 and Figure 12.4). This reference system performed very well in the alignment of LCLS-I components.

Figure 12.3. Sphere mounted glass and air reflectors.

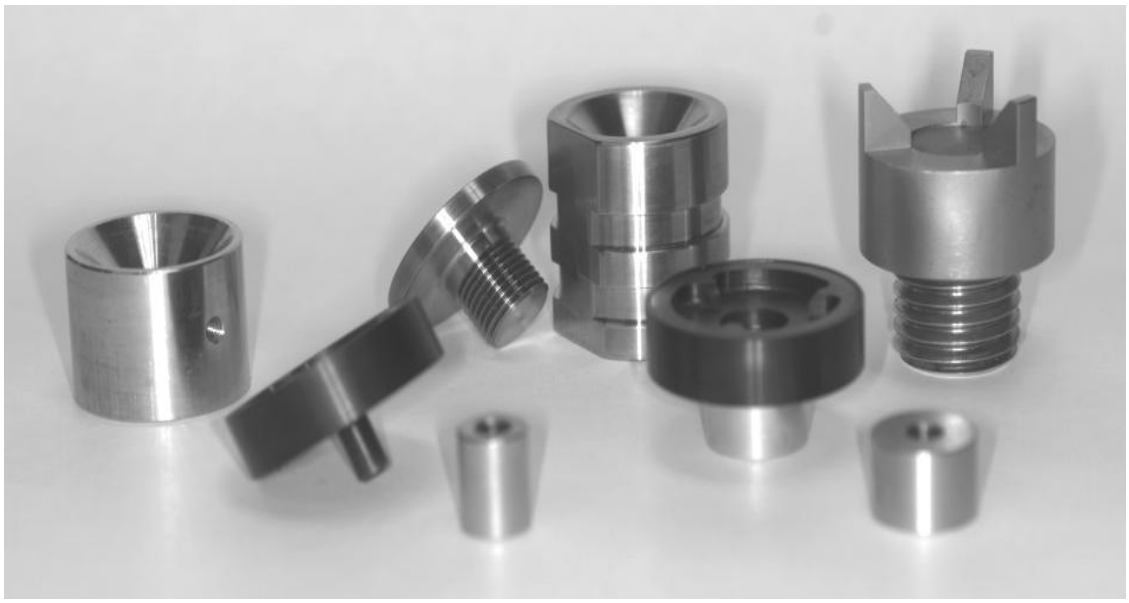

Figure 12.4. Sphere receptacles: floor, component, and wall bracket fixed-mount version, removable centered version.

12.2.3 Network Layout

The alignment network has to be established in all parts of the machine.

12.2.3.1 Injector Network

The injector network will support the survey and alignment of the injector components. Standard networking design and measurement techniques can be used since the injector components have fairly conventional positioning tolerance requirements. A horizontal sight pipe through the shielding wall allows a connection of the reference systems in the injector and linac tunnels.

12.2.3.2 Linac Network

Local networks need to be implemented to support linac modifications and to align the bypass line quadrupoles. Existing networks at sector 19-23 will be incorporated.

12.2.3.3 BSY Network

A new reference network has to be implemented throughout the BSY. Existing LCLS components will be used as tie-in points.

12.2.3.4 Undulator Hall Network

The undulator hall network's overall geometry is dictated by the tunnel geometry, machine layout, and the fact that the free-stationing method requires a greater number of reference points. The geometry should also permit observing each target point from at least three different stations.

Figure 12.5 shows a typical section of the layout. Two wall monuments are placed across from each other, prefereably at the location of a quadrupole to allow better visibility. The variable gap undulator might obstruct the line of sight due to its height. The floor monuments are staggered in respect to the wall monument to allow line of sight in cases when the laser tracker is set up at a quadrupole.

12.2.3.5 Transport Line/Experimental Area Network

The transport line networks (undulator to FEE to experimental area) will support the survey and alignment of the FEE and transport line components. Network designs and measurement techniques similar to the undulator hall can be used to achieve the tolerance requirements of the transport line components.

The directional accuracy of the transport line networks is not sufficient to support the component installation and position requirements in the experimental area. A small surface network is necessary to accurately connect this area to the undulator.

12.2.4 Tunnel Network Survey

The most efficient instrumentation for the network observations will be the combination of a laser tracker with a digital level. Laser trackers will contribute mainly to horizontal positional accuracy and digital levels to vertical positional and rotational accuracy.

A laser tracker will be placed close to the middle between two opposing wall points (see Figure 12.5). From there, sixteen points will be measured. The measurement procedure will include two sets of distance and direction measurements to the same sixteen points in both front and reverse instrument orientations. After that the laser tracker will be advanced by one wall monument; the goal is a triple coverage of all monuments. All reference points will also be observed with a standard high precision double-run level procedure. A digital level in combination with 2 m invar rods will be used.

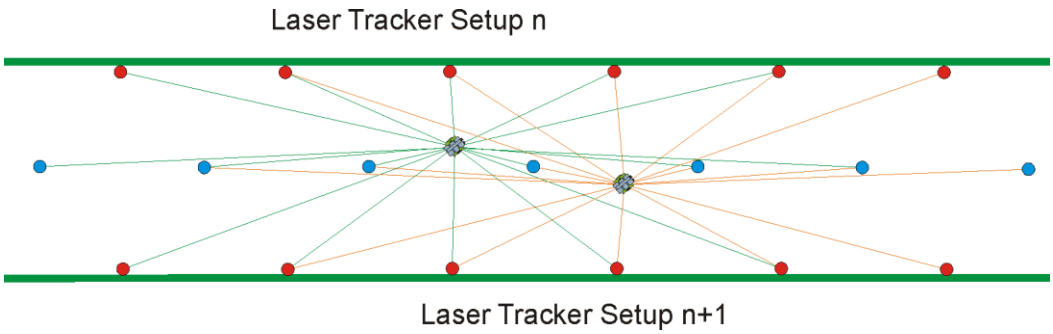

Figure 12.5. Observation plan.

12.2.5 Surface Network

Standard Global Positioning System (GPS) technology will provide the required accuracy. To connect GPS measurements to the undulator axis, the axis needs to be referenced to monuments on the surface. Monuments above and below the shafts will be referenced by optical plummet (Leica NL) measurements. The monuments below the shafts will be integrated into the regular tunnel network. The BSY shaft points will be linked to the undulator hall network by a temporary network. The monuments above the shafts will be connected to adjacent network monuments by GPS or optical triangulation measurements.

12.2.6 Data Analysis and Data Flow

To reduce the data from the measurements as described above, specialized software has been developed. This type of analysis software is based on the photogrammetric bundle approach. Because a photogrammetric sensor is arbitrarily oriented in space, not only its translational parameters but also its

rotational orientation parameters must be treated as unknowns and become part of the solution. With traditional trilateration/triangulation-based analysis software, however, pitch and roll are supposed to be oriented to gravity, and yaw is expressed as a function of translations. Additionally, traditional software assumes that the instrument is centered on a point to which sufficient measurements have been taken. This analysis approach does not work well with free-stationing, and does not work at all with present generation laser trackers, since they cannot be oriented accurately enough to gravity.

To reduce errors stemming from transcription of data, the data-flow will be automated. The instruments will support direct connection to field computers. The fully automated data-flow will extend from field computers through data analysis to data storage.

Measurements with any type of instrument will be guided by software based on rigid procedures running on field data logging computers. The data-logging software will also pre-analyze the measurements in an attempt to determine and flag possible outliers before the measurement setup is broken down. This method combined with an automated data-flow will greatly reduce errors and improve measurement consistency and reliability.

12.3 Layout Description Reference Frame

12.3.1 Lattice Coordinate System

The LCLS-II lattice is designed in a right-handed beam-following (s-axis) coordinate system, where the positive y-axis is perpendicular to the design plane, the z-axis is pointing in the beam direction and perpendicular to the y-axis, and the x-axis is perpendicular to both the y and z-axes.

12.3.2 Tolerance Lists

The alignment system is designed based on the tolerances listed in Table 12.1.

Table 12.1. LCLS-II positioning tolerances.

	σ_x [μm]	σ_y [μm]	σ_{roll} [mrad]
Injector components	150	150	0.2
Linac components	150	150	0.2
Undulator Quadrupole initial alignment	150	150	1
Relative alignment between undulator magnets and neighboring quadrupoles	100	50	1
Experimental area components	300	300	0.2

n/a = not applicable

12.4 Fiducializing LCLS-II Magnets

The correct fiducialization of magnets is as important as their correct alignment since an error in either task will affect the particles' trajectory and cannot be distinguished from each other. Fiducialization can be accomplished either through opto-mechanical and opto-electrical measurements or by using fixtures, which refer to a magnet's reference features.

Since the undulator sections will be aligned relative to their adjacent quadrupoles, both the undulator segments and the quadrupoles need to be fiducialized to better than 30 µm in order to leave a reasonable error budget for the alignment process.

The quadrupoles will be fiducialized using the same method as was used for LCLS-I [4].

If the LCLS-II undulators are significantly larger than the LCLS-I undulators, the final step of measuring undulator reference point positions with respect to the magnetic axis will not be possible with a CMM. Other measuring instruments are only accurate to approximately 30 μm. A detailed analysis at the error budget will be made. A Research & Development (R&D) program has been started to determine how to implement these measurements. Since the undulators have variable gaps it is necessary to fiducialize them with a predefined gap setting which will then be reproduced in the tunnel while setting the undulator.

Components for the injector, linac, and dump line will be fiducialized using standard techniques.

12.5 Positioning of Components

Common to all parts of the machine, free-stationed laser trackers, oriented to at least four neighboring points, are used for the absolute positioning measurements. The tracking capabilities of these instruments will significantly aid in facilitating the control of any alignment operation, e.g. moving components into position.

12.5.1 Undulator Positioning

The positioning is carried out in several steps. At first, the anchor hole positions for the component supports are marked on the floor. Next, after the supports and the magnet movers are installed, they will be aligned to within 0.3 mm of their nominal positions in order to retain as much mover range as possible. At this stage, the components can be installed. Since the components mechanically register to the support/magnet mover geometry, the installation will already place them to within 0.5 mm. Finally, the position of the components will be surveyed and adjusted using a laser tracker in reference to adjacent network points. Position accuracy relative to the network points of about 100 μm can be achieved.

The undulator sections will be aligned relative to their neighboring quadrupoles to 100 μm horizontally and 50 μm verticaly . The initial quadrupole position is a result of an optical/mechanical alignment process, which subsequently is refined by a beam-based alignment procedure.[6.] For the beam-based alignment algorithm to converge efficiently, an 150 μm initial placement is desired and can be achieved by the steps described above.

12.5.2 Injector, Linac, Transport Line and Experimental Area Positioning

The absolute positioning of these components will follow the same procedure as described above. No relative alignment step is required to achieve the final position tolerances in these areas.

[6] The electron trajectory within the undulator needs to be straight to a high degree of accuracy so that the undulator radiation overlaps the electron beam sufficiently within each gain length of the undulator. This level of trajectory straightness, ~2 μm rms over 10 m, cannot reliably be achieved with optical alignment methods. Therefore, a beam-based alignment technique has been developed that determines quadrupole position corrections from BPM readings as a function of large, deliberate variations in the electron energy. Remotely controlled movers are used to apply the corrections.

12.5.3 Quality Control

Once the above steps are completed, the components will be mapped as a quality control measure. If any positional residuals exceed the tolerance, a second iteration needs to be carried out. A quality control survey will always follow the completion of the alignment process.

12.6 References

1. G. Gassner and C. LeCocq, *Portable Wire Measurement System*, IWAA 2008, February 2008.
2. R. Ruland, *Magnet Support and Alignment*, in H. Winick, Editor, Synchrotron Radiation Sources–A
3. E. Bong, P. Emma, C. LeCocq, T. Montagne and J. Welch, *LCLS Undulator Coordinate System*, LCLS-TN-03-8, April, 2004.
4. Z. Wolf, M. Levashov, E. Lundahl, E. Reese, C. LeCocq, R. Ruland, *LCLS Undulator Quadrupole Fiducialization Plan*. (August 2007).

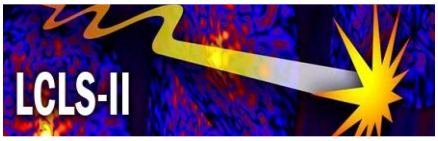

13 Environment, Safety, Health, and Quality Assurance

Technical Synopsis

SLAC is committed to the success of the mission objectives of the LCLS-II Project and to the safety of its users, staff, and the public. It is our vision to provide a "Best in Class" safety program. We view such a program as essential to the safety of the workers as well as the successful completion of the project. We will seek to provide an injury free work environment and will measure our performance by comparison with only those who have achieved recognition as "Best in Class." LCLS-II management will design and build the LCLS-II with the assistance of a fully involved Quality Assurance (QA) Program. The primary objective of the QA program is to implement quality assurance criteria in a way that achieves adequate protection of the workers, the public, and the environment, taking into account the work to be performed and the associated hazards.

13.1 Introduction and Overview

It is SLAC's policy to integrate safety and environmental protection into its management and work practices at all levels in order to achieve its mission while protecting the worker, the public, and the environment. To achieve this objective SLAC has developed and implemented an Integrated Safety and Environmental Management System plan[1] (ISEMS)[1], compliant with DOE P450.4, *Safety Management System Policy*. SLAC encourages and supports the use of the necessary and sufficient approach, as described by DOE Order 450.3, through the application of standards that are either required by law/regulation (necessary) or contribute significantly to the protection of workers, the public, and the environment (sufficient).

Existing and mature programs at SLAC will be followed to ensure that all aspects of the design, installation, testing, operational, decommissioning phases of the project are reviewed and consistent with good practices. For example, experimental activities follow SLAC's Experimental Project Review Process to ensure the Environment, Safety, and Health (ESH) aspects of the experiment are adequately identified and addressed before authorization and release of project activities. This review process includes the involvement of subject matter experts and institutional safety officers. (i.e. Radiation, Laser, Electrical etc.). Assurance of consistency of engineering conventional facilities designs with and Codes and Standards is established through independent peer review and internal SLAC evaluations conducted by the SLAC Building Inspection Office (BIO). The code checks are conducted by subject matter having relevant knowledge or skills [2] experts selected by the BIO.

Hazards and selected mitigation will be documented in the *LCLS-II Safety Assessment Document*.

SLAC has several decades' of experience operating electron accelerators and their accompanying accelerator based user facilities. Policies, procedures, engineered safety systems have been developed to control the hazards and risks associated with them. Table 13.1, summarizes the hazards and mitigating controls.

The LCLS-II project will not generate new hazards that have not already been contemplated and addressed during previous SLAC projects or routine operations. The potential hazards that have been initially identified can be mitigated through established SLAC ES&H policies and procedures. In some cases it is anticipated that new technologies will be developed to mitigate potential hazards.

[1] ISEMS contract clause from the DOE Acquisition Regulations [DEAR], specifically DEAR 970.5204.-2, "Integration of Environment Safety and Health into Planning and Execution".

Table 13.1. Hazard identification and mitigation.

Item	Hazard	Possible Causes	Mitigating Controls
1	Ionizing radiation exposure, outside accelerator housing or experimental area • prompt radiation	• Personnel error • Interlock failure • Inadequate Shielding (design or installation)	• Safety Procedures • Design, maintenance and inspection of shielding and other radiation safety systems • Training
2	Ionizing radiation exposure, inside accelerator housing or experimental area • prompt • residual • contamination	• Personnel error • Interlock failure	• Safety Procedures • Design, maintenance and inspection of radiation safety systems • Training
3	Fire; inside accelerator housing or experimental area • electrical • welding/cutting • smoking • hot work (soldering)	• Equipment failure • Personnel error	• Sprinklers and other fire suppression systems • Smoke Detectors • Fire Alarms • Exit Routes • Training • On site Fire Department
4	Fire; equipment and control areas • electrical • welding/cutting • smoking • hot work (soldering)	• Equipment failure • Personnel error	• Sprinklers • Smoke Detectors • Fire Alarms • Exit Routes • Training • On site Fire Department
5	Electric shock • high voltage • low voltage/high current • exposed 110V	• Personnel error • Equipment failure • Interlock failure	• NEC Compliance • Design, maintenance and inspection of electrical interlock systems. • Procedures (Lock Out/Tag Out) • Training • PPE

Item	Hazard	Possible Causes	Mitigating Controls
6	Non-Ionizing radiation exposure • RF • Laser	• Personnel error • Equipment failure • Interlock error	• Design, maintenance and inspection of interlock systems • Procedures • Training
7	Construction activities • heavy equipment • material handling/rigging • slips/trip/falls • excavation and tunneling	• Personnel error • Equipment failure • Improper Equipment	• Task Specific hazard analysis • Barriers • Procedures • Training • Inspections
8	Seismic hazards	• Earthquake	• Prework hazard analysis • Design, construction and upgrade of structures (buildings, accelerator housings) and equipment to building and structural codes • Field inspections
9	Exposure to hazardous materials, including: • cryogenics • solvents • oils • welding/cutting fumes	• Personnel error • Equipment failure	• Engineering analysis (ODH) and inspection of systems using hazardous materials • Procedures • PPE • Training (oxygen deficiency hazard ODH) • Ventilation
10	Adverse effects to the environment • Spills • Water discharges to sanitary and storm drains • Noise • Air emissions (dust, leaks) • Soil contamination	Construction and installation activities • Equipment failure • Personnel error	• Training • Procedures • Inspections

13.2 Ionizing Radiation

The design and operation of all radiation producing facilities at SLAC are governed by the As Low As Reasonably Achievable (ALARA) policy. SLAC has historically maintained radiation dose limits below regulatory limits.

13.2.1 Radiation Shielding

LCLS-II shielding will conform to the *SLAC Radiological Control Manual* [3]and and the *Radiation Safety Systems Technical Basis Document* [4] guidelines and requirements. Potential LCLS-II beam losses during the completed facility operation could produce high radiation doses. Local shielding, in some cases movable, will be used to mitigate this hazard to acceptable levels. The final configuration of the LCLS-II within the experimental halls and experiment hutches will dictate the type and amount of local shielding. Radiation loss monitors at the hutches will provide a diagnostic capability to determine where beam losses are taking place. These passive and active control mechanisms, in addition to the SLAC Beam Containment System (BCS) will further help maintain dose levels below allowable levels. Necessary shielding assessment documentation will be developed and reviewed defining radiation shielding requirements prior to an operational readiness review.

Shielding design criteria will be:

- 1 rem/yr at 30 cm from the shield surface, assuming a 2000 hr working year and an occupancy factor of 1.
- Non-radiological workers (Users) work area will be shielded to limit their annual effective dose below 0.1 rem/yr taking exposure duration and occupancy factors into account.
- The effective dose rate in the event of the Maximum Credible Incident (MCI) is limited to less than 25 rem/h, and the integrated effective dose to less than 3 rem [1]. The MCI is defined as the highest beam power that the accelerator can deliver to a point assuming that the BCS devices that limit beam power have failed.

13.2.2 Safety Systems

The Access Control System (ACS) consists of electrical interlocks and mechanical barriers whose primary function is to prevent exposure of personnel to prompt radiation; this is accomplished by controlling personnel access into a beam line enclosure and by turning off beam, Radio Frequency generators and electrical hazards when a security violation is detected.

Two types of Access Control Systems are utilized for the LCLS:

- Personnel Protection Systems (PPS) are used for electron beam enclosures (Injector vault, dump enclosure) and controlled remotely by qualified Operators at the Main Control Center;
- Hutch Protection Systems (HPS) are used for X-ray beam lines and controlled locally by qualified Floor Coordinators.

Other functions that the ACS must also accomplish are to:

- Provide failsafe and redundant interlocks to control access
- Allow for various access and beamthrough configurations
- Provide emergency shutoff capabilities

As installation of the LCLS-II will not require a significant change to the present shielding footprint, the PPS will undergo only necessary upgrades and enhancements to address the new facility and operating conditions. These upgrades include: additional status and control interfaces to accommodate new power supplies; access control modules for the injector and experimental areas; logic upgrades; interlocks with beam stoppers, Beam Shut Off Ion Chambers (BSOICs), and with burn-through monitors that are controlled through the PPS. The PPS will conceptually remain very close to other PPS installations used for LCLS in terms of design, functions and configuration.

Administrative requirements are mandated to ensure reliable operation. This requires that the PPS devices be certified, tested, and protected against unauthorized modification.

All additions and changes will conform to the *Radiation Safety Systems Technical Basis Document*, Chapter 2 Personnel Protection Systems [4].

13.2.3 Beam Containment System

Radiation safety at an accelerator requires that beams deposit their energy in or at devices capable of absorbing the planned maximum beam power. If the devices are incapable of absorbing the maximum beam power or if beams diverge from their proper channels, the resulting beam loss may create high radiation levels in unprotected areas. Certain components of the beam line, such as collimators, are designed to contain the beam if it should deviate from the designed beam path. Other components, such as beam dumps, are designed to terminate the beam in a well shielded area. These components are part of the Beam Containment System (BCS). The BCS also is made up of devices that detect when accelerated beams diverge from the desired channel, and when excessive beam intensity is detected, creating the risk that unacceptable radiation levels might be produced. When this happens, the beam delivery system is shut down.

The BCS is a combination of passive mechanical devices (e.g., collimators and beam dumps) and associated active electronic protection devices (e.g., toroids, current sensors, or ionization chambers) that assure that a beam is confined to an approved beam channel at an approved and allowed beam power to prevent excessive radiation levels in occupied areas. It should be noted that the BCS is also used to protect devices (e.g., stoppers and collimators) that have been designated as having a safety function.

Administrative requirements are mandated to ensure reliable operation. This requires that the BCS devices be certified, tested, and protected against unauthorized modification.

The BCS will conform to the guidelines in the *Radiation Safety Systems Technical Basis Document* Chapter 4 Beam Containment Systems [5].

13.2.4 Radiation Safety Training

In accordance with SLAC's site access and identification badges policies and procedures, all individuals at SLAC who enter the accelerator area or a Radiological Controlled Area (RCA) must be either properly trained or escorted by a properly trained individual. Levels of training are delineated in SLAC's policy on Minimum Training Requirement [6].

13.3 Electrical Safety

An accelerator facility by nature has subsystems that either produce or use high voltage or high current, either of which can present an electrical hazard to personnel if not managed properly. The LCLS-II will operate in a similar mode to other electron accelerators at SLAC; therefore, control and work procedures for electrical subsystems, as well as entry into the accelerator housing are well understood.

Primary mitigation of the hazard will be through deenergizing equipment, placement of barriers and the effective use of written system Lockout and Tagout (LOTO) procedures[7].

The design, upgrade, installation and operation of electrical equipment will be in compliance with the National Electrical Code, Title 29 Code of federal Regulations, Parts 1910 and 1926 (as applicable) and SLAC's policy on Electrical Safety, *SLAC ES&H Manual* Chapter 8[8]. Entry into the accelerator housing requires the mitigation of electrical hazards through either the lockout of power supplies or selective use of mechanical barriers, interlocked to further reduce the risk of exposure to electrical shock. Various levels of electrical safety training and LOTO training are provided by SLAC for those personnel who may work on or near potential electrical hazards.

Special procedures authorized through the SLAC Director will be developed to permit qualified personnel to occupy areas adjacent to energized magnets. These are called *Electrical Hazard Test Procedures* and allow local control of the electrical power supply feeding a single magnet, or unique string of magnets, that are to be tested.

13.4 Non-Ionizing Radiation, Lasers, and Magnetic Fields

The LCLS-II RF systems will produce radio frequency radiation in the 2856 MHz and 11424 MHz ranges, which when not controlled could have an adverse health effect on personnel working on or near the system. The LCLS-II will incorporate safety measures based on present operations. These include interlocked waveguides and vacuum chambers and strict adherence to procedures for installation, monitoring and testing of the RF system.

As the RF energy is fully contained within the envelope of these wave guides or vacuum chambers under ultrahigh vacuum, opening the system up will trigger the interlock through a pressurization of the system and effectively prevent the source from being energized. Running the RF in this mode precludes microwave leakage, as failure of the vacuum system will occur before exposure to non-ionizing RF radiation.

Procedures are also in place that ensure all flange bolts are torqued to a predetermined value as well as the completion of RF leak testing after all installations and maintenance activities, and periodically before start up of the system after scheduled shutdowns.

The LCLS-II operations and experimental programs utilizing Class 1, 2, 3a, 3b, and 4 lasers will be reviewed and controlled as required in national consensus standards and the SLAC Laser Safety Program. Locations for long-term use of Class 3b and Class 4 lasers will be identified during design and appropriate safety features (e.g. control of exposed beams) will be incorporated into the design of the facility. Lasers, particularly those in Class 3b and 4, will require written procedures for each device to control eye or skin exposure and associated electrical and industrial hygiene hazards e.g. exposure to solvents, dyes, and halogen gasses. As per LCLS-II laser safety procedures, Class 4 laser control areas are required to be interlocked with a failsafe system. The SLAC Laser Safety Program will define the required interlock systems, training and signage.

The LCLS-II will utilize equipment and devices that generate magnetic fields. The concern with all these devices is the strength and extent of the fringe fields and how they may affect persons and equipment in their vicinity. Fringe fields in excess of 5 gauss are of particular concern because they could affect medical electronic devices (pacemakers), while fields over 600 gauss could impact ferromagnetic implants (artificial joints) and other material (tools).

13.5 Emergency Preparedness

It has been estimated by the U. S. Geological Survey that the chance of one or more large earthquakes (magnitude 7 or greater) in the San Francisco Bay area in the coming 30 years is about 67 percent. This represents the emergency situation most likely to arise at SLAC. All SLAC personnel are trained in the immediate response to earthquakes and other emergencies via their supervisors and employee orientation.

13.5.1.1 Seismic Safety

SLAC structures are designed and constructed to limit the effects of a major earthquake to acceptable levels [9]. The majority of LCLS-II components will be installed in facilities where seismic stability is well documented and deemed acceptable. To further ensure and maintain a safe and healthful workplace, the design and construction of new experimental facilities buildings for the LCLS-II will also be reviewed for seismic safety by the ES&H Building Inspection Office (BIO).

13.5.1.2 Emergency Planning

The design, review, installation and operation of all experimental equipment at SLAC is done in a manner that minimizes the risk of accident or injury to personnel and property in the event of either a natural disaster or emergency situation. SLAC's formal emergency planning system as described in the *SLAC Emergency Preparedness* Plan [10] will help ensure a logical, organized, and efficient site wide response to any emergency. Facility specific procedures, which supplement the SLAC emergency plan, support a timely initial response, further decreasing the probability of personal injury and limiting potential loss or damage to both property and the environment.

13.6 Construction Safety

13.6.1 General

During construction operations, oversight of subcontractor activities and safety compliance remains a line organization responsibility through the Field Construction Manager (FCM) or project engineer, if a FCM is not assigned to the activity. Responsibilities of FCMs or project engineers include, but are not limited to:

- Apprising subcontractors of SLAC and DOE safety criteria prior to construction.
- Informing subcontractors of the hazards routinely found at SLAC.
- Conducting periodic inspections of subcontractor construction areas to evaluate the quality of the subcontractor's safety compliance program and quality of work.
- Providing information to the SLAC Chief Safety Officer as required or requested.
- Communicating and resolving safety or quality deficiencies identified by SLAC personnel with the subcontractor.
- Receiving subcontractor accident reports and compiling information for reporting to SLAC and the DOE.

Enforcement of subcontractor requirements is carried out by the SLAC Purchasing Department and may involve with holding payment(s) if applicable codes and standards are not met.

13.6.2 Tunneling and Excavation

The LCLS-II Project will construct one experimental hall with multiple hutches, connected to a tunnel housing that contains beam transport lines for electrons and x-rays. Early discussions and review of the tunnel portion of the project indicate the need for two separate engineered excavation techniques, both of which will be required during construction. The two techniques that will be used include: “cut and cover”, which in essence is akin to trenching but on a much larger scale; and mechanical excavation, such as the use of a Roadheader, for those portions of the beamline housing that cut and cover would be either technically or economically infeasible. Both of these methods have been used at SLAC for previous projects. Consequently, the hazards encountered are understood by the SLAC community as are the regulations governing this type of operation contained in both the *California Code of Regulations* and *Code of Federal Regulations*. Hazards relating to heavy equipment operation, rock support methods, spoil haulage, ventilation, and the open cut excavations process will be addressed as part of the hazard assessment process throughout the project.

The necessary excavation permits will be developed which includes a rigorous process of locating buried electrical, gas, water lines and structures.

13.7 Hazardous Materials

During the installation and operation phases of the LCLS-II it is anticipated that minimal quantities of hazardous materials will be used, examples would be paints, epoxies, solvents, oils and lead in the form of shielding, etc. There are no current or anticipated activities at the LCLS-II that would expose workers to levels of contaminants (dust, odors, and fumes) above permissible levels.

The SLAC Industrial Hygiene Program detailed in the *SLAC ES&H Manual* addresses potential hazards to workers from the use of hazardous materials. The program identifies how to evaluate workplace hazards at the earliest stages of the project and implement controls to eliminate or mitigate these hazards to an acceptable level. Industrial hygiene hazards will be evaluated, identified, and mitigated as part of the hazard assessment process.

Site and facility specific procedures are also in place for the safe handling, storing, transporting, inspecting and disposing of hazardous materials. These are contained in the *SLAC ES&H Manual* Chapter 17, “Hazardous Waste” [11] which describes minimum standards to maintain for compliance with Title 29, Code of Federal Regulations, Part 1910.

The FCM or project engineer has added responsibilities with respect to the management of hazardous materials. They ensure subcontractor personnel are aware of, and remain in compliance with *SLAC ES&H Manual* Chapter 40, “Hazardous Materials”[12], also keeping affected SLAC personnel informed of hazardous material usage and the associated hazards and risks.

The tunneling process means, methods and hazards will be identified separately in the LCLS-II Tunneling Plan. Specific hazards relating to the tunneling activities relating the LCLS-II Project will be addressed in this document.

13.8 Fire Safety

The probability of a fire in the LCLS-II is very low, similar to that for present operations, as accelerator and beamline components are primarily fabricated out of similar, nonflammable materials and combustible materials in general are kept to a minimum.

The Maximum Credible Fire Loss (MCFL) at SLAC, which assumes proper functioning of the smoke

detection and mitigation systems, and a normal response from the onsite fire department is limited to isolated components, such as magnets, vacuum chamber and associated cabling. The most hazardous "reasonably foreseeable" incident or event with any substantial consequences would be a fire in existing insulating material of the electrical cable plant caused by an overload condition. The hazard of greatest concern in this situation is the production of halogenated gases. The *ES&H Manual* Chapter 12, “Fire and Life Safety” [13] addresses all fire safety issues. A Fire and Life Safety Assessment of the LCLS Project will be completed by the SLAC Building Inspection Office (BIO) to verify that the facility meets all applicable NFPA and IBC regulatory requirements.

Installation of new cables for the LCLS-II will meet the current SLAC standards for cable insulation and comply with National Electric Code (NEC) standards concerning cable fire resistance. While this reduces the probability of a fire starting, an aspiration type smoke detection system (VESDA) in the accelerator housing, undulator tunnel and experimental hall; and fire breaks in the cable trays will limit fire travel. Support buildings for power supplies, electronic equipment or experimental areas are protected by automatic heat activated wet sprinkler systems and smoke detectors. Fire extinguishers are located in all buildings and accelerator housings for use by trained personnel. The combination of smoke detection systems, sprinklers and onsite fire department (response time <5 minutes) affords an early warning and timely response to fire or smoke related incidents. Burn injuries caused by a fire are not expected. Personnel access areas in both the Linac accelerator housing and support buildings are within 150 ft of an exit in both directions. Multiple entry/exit points will aid in keeping personnel emergency egress times and property damage to a minimum.

13.9 Environmental Protection

Installation of the LCLS-II requires the removal of some hardware (magnets and vacuum chambers) and the installation of new components suited to the proposed facility. Electrical distribution systems will be upgraded or installed as appropriate and minor installation and/or modifications to the Low Conductivity Water (LCW) system will be made to accommodate heat transfer needs. Removal of these materials and the subsequent installation activities will produce small quantities of hazardous, nonhazardous and radioactive waste that will be managed through defined processes. Past history indicates that normal operation of the accelerator does not typically produce waste. However, some hardware may have induced radioactivity associated with it from its proximity and time close to the beam. Other components may contain hazardous materials as part of their design, e.g., mineral oil in electrical components, or have radioactive contamination from the LCW system.

All material removed from within the accelerator housing will be surveyed for residual radioactivity or contamination, labeled, and held onsite for disposal evaluation, as defined in the SLAC Radiation Safety Program. Items that show residual radioactivity or contamination will be stored on site in the radioactive material storage yard for future reuse or ultimate disposal. Any hazardous waste will be disposed of in accordance with SLAC procedures and ultimately to a permitted treatment, storage and disposal facility, under regulations set forth in the Resource, Conservation and Recovery Act (RCRA).

Component manufacturing and system installation may also produce hazardous wastes, such as used solvent from degreasing baths or spent cutting fluids. These wastes are managed and controlled routinely during operations at SLAC in full compliance with SLAC's policies on the management of hazardous materials and waste minimization.

The proposed addition of an experimental hall and the required earth removal, tunneling and construction activities will be subject to an Environmental Assessment (EA) under the National Environmental Protection Act (NEPA). This document will look carefully at the consequences of siting a new facility at SLAC, taking into consideration environmental values and other technical and economic

consequences. NEPA also includes provisions to include coordination and integration of reviews of other environmental laws and executive orders. Examples are the Endangered Species Act, floodplain/wetlands regulations, Fish and Wildlife Coordination Act, “Greening the Government” initiatives, and the National Historic Preservation Act. The LCLS-II Tunneling Plan will also address EPA requirements which relate to tunneling and excavation construction activities including the SLAC National Pollutant Discharge Elimination System (NPDES) permitting process for total suspended solids released to surface water and storm water runoff requirements.

All activities will be managed to prevent adverse impact on ground water and storm water quality, air quality and to minimize any ground disturbing activities.

13.10 Quality Assurance

The *SLAC Assurance Program Description* [14] conforming with DOE Orders [15], was established at SLAC to provide laboratory management with guidance and requirements for achieving quality in pursuit of the laboratory mission. Overall responsibility for the implementation of this program lies with the SLAC Director, while accountability for managing the program at the directorate level rests with the respective Associate Laboratory Directors (ALDs). The LCLS-II Quality Assurance Manager has been given responsibility for staffing, documenting, generating Quality Implementing Procedures (QIPs) and implementing the LCLS-II QA program. At the project level this includes developing and maintaining required management systems, or using management systems that are already available.

The LCLS-II QA plan follows the SLAC's approach to implementing the ten criteria of DOE Order 414.1C:

Criterion 1 requires specific Quality Implementing Procedures for all SLAC projects where total project costs exceed $10,000,000.

Criterion 2 as appropriate defines specific requirements and assures adequate qualification and training for individuals connected with the project, including retention of training records.

Criterion 3 defines requirements for management's responsibility with respect to identification, analysis, resolution and follow up of ES&H, technical and compliance issues.

Criterion 4 provides policy for identification of documents (policy, procedures, drawings etc.), records and other specific elements that will have a significant impact on the project and need to be entered into a document control system.

Criterion 5 requires project leaders to define and maintain work processes for design, fabrication, assembly and installation efforts that have a significant programmatic impact.

Criterion 6 establishes a responsibility for line management to conduct design reviews and to promote the use of design standards.

Criterion 7 discusses a graded approach to the development of specifications for procurement of items and services based on cost and failure impact.

Criterion 8 established responsibility for the staffing, documenting, and performing of inspection and testing activities related to the project.

Criterion 9 requires participation in the *SLAC Institutional Self-Assessment Program*.

Criterion 10 provides the authority for the SLAC Office of Assurance and LCLS-II QA Manager to conduct independent assessments of all SLAC facilities and projects as warranted to verify the degree of conformance to QA and ES&H requirements.

Effective use of these criteria will enable the LCLS-II project to:

- Design in quality and reliability.
- Promote early detection of problems to minimize failure costs and impact on schedule.
- Develop appropriate documentation to support upgrade and operational requirements.
- Establish methods to identify critical systems and to release these systems based on demonstrated performance.
- Define the general requirements for design and readiness reviews for all aspects of the project.
- Assuring personnel are trained before performing critical activities, especially those that have ES&H consequences.

The LCLS-II QA Manager will develop an LCLS-II specific Quality Implementation Procedure that will detail how the quality assurance program for the LCLS-II project will be handled in keeping with the general requirements that are defined in the *SLAC Assurance Program Description*.

13.11 SLAC References

1. SLAC-I-720-0A00B-001-R005 (17 August 2005, Updated 7 December 2010)
2. SLAC-I-730-2A24Z-001-R002, *Project Review and Authorization Manual*
3. SLAC-I-720-0A05Z-001-R005, Radiological Control Manual
4. SLAC-I-720-0A05Z-002-R004, *Radiation Safety Systems,* Chapter 2 “Personnel Protection Systems”
5. SLAC-I-720-0A05Z-002-R004, *Radiation Safety Systems,* Chapter 4 “Beam Containment Systems”
6. SLAC-I-720-0A04S-001-R004 *SLAC ES&H Manual*, Chapter 24 “Training”
7. SLAC-I-720-0A29Z-001-R000 *SLAC ES&H Manual,* Chapter *51 “Control of Hazardous Energy”*
8. SLAC-I-720-0A29Z-001-R007 *SLAC ES&H Manual,* Chapter 8 “Electrical”
9. SLAC-I-720-0A05Z-002, *Specification for Seismic Design of Buildings, Structures, Equipment, and Systems at the Stanford Linear Accelerator Center*
10. SLAC-I-730-0A14A-001, *SLAC Emergency Preparedness Plan*
11. SLAC-I-720-0A29Z-001-R023, *SLAC ES&H Manual,* Chapter 17 “Hazardous Waste
12. SLAC-I-730-0A12Z-001-R000, *SLAC ES&H Manual,* Chapter 40 “Hazardous Materials”
13. SLAC-I-720-0A29Z-001-R007, SLAC *ES&H Manual,* Chapter 12 “Fire and Life Safety”
14. SLAC-I-0A-001-R002, *SLAC Assurance Program Description*
15. DOE Order 414.1C, “Quality Assurance”

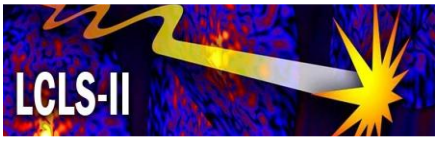

14 Radiological Considerations

Technical Synopsis

This chapter describes the radiation protection requirements and radiological considerations for LCLS-II. Experience with LCLS-I and dedicated Monte Carlo simulations for some of the new configurations have been instrumental to define preliminary specifications for the shielding, Beam Containment System (BCS) and *Personnel Protection System (PPS) of the new injector vault and laser room in Sector-10; the shielding for the tune-up dump kicker collimator and its optimal location in the Beam Switch Yard (BSY); the new shielding wall in the Beam Transport Hall (BTH), safety components and modes of access to the beam transport halls of LCLS-I and LCLS-II; the dimensions of the walls, roof and mazes of the new BTH and its BCS systems; the shielding of the undulator tune-up dumps and main electron dumps; the beam containment requirements and estimated Near Experimental Hall (NEH) wall thickness, and photon safety systems. X-Ray Free Electron Laser (X-FEL) burn through is not discussed in this introductory study.*

14.1 Overview

14.1.1 Introduction

Most of the radiation protection issues in the LCLS-II are similar to those encountered at LCLS-I. LCLS-II will be designed to ensure that radiation doses above background received by workers and the public are As Low As Reasonably Achievable (ALARA), as well as to prevent any person from receiving more radiation exposure than is permitted by SLAC radiation safety requirement.

Several technical, operations, and administrative systems exist to implement the radiation safety program for LCLS-II as described in the *SLAC Radiological Control Manual* [1] and the Radiation Safety Systems Technical Basis Document [2]. These systems are part of the SLAC Radiation Safety System (RSS), a combination of active and passive safety systems used to protect personnel from prompt radiation. The primary components of SLAC RSS include:

- Shielding, which attenuates radiation
- A personnel protection system (PPS), which comprises an access control system that prevents personnel from entering areas in which dangerous levels of radiation could be present .
- A beam containment system (BCS), which keeps dangerous levels of radiation outside of the shielding enclosure. BCS is comprised of a combination of electronic protection devices including current toroids, meter relays, protection ionization chambers(PIC) and mechanical devices (such as collimators and beam dumps) that: 1. monitor and limit the beam power in a beam line to the allowed value, 2. limit the losses along a beam line that is operating at its allowed power, 3. protect safety-related beam line components from damage, 4. shut off the beam if excessive radiation levels can be produced in occupied areas.

Other safety systems, such as burn-through monitors (BTMs) and beam shutoff ion chambers (BSOICs) are also integrated into the SLAC RSS. BTMs are pressure vessels located near shower maximum that are designed to rupture when the device being protected absorbs greater than its allowed beam power thus detecting the onset of damage to mechanical protection devices such as collimators, beam stoppers, and beam dumps. BSOICs are interlocked radiation detectors that are used to detect prompt radiation and terminate accelerator operation if excessive radiation is detected in potentially occupied areas. BSOICs trip limits limits are set to either 10 mrem/h or 100 mrem/h, depending on the location of the detector and the occupancy of the area. Figure 14.1 shows the RSS components that will be used for LCLS-II.

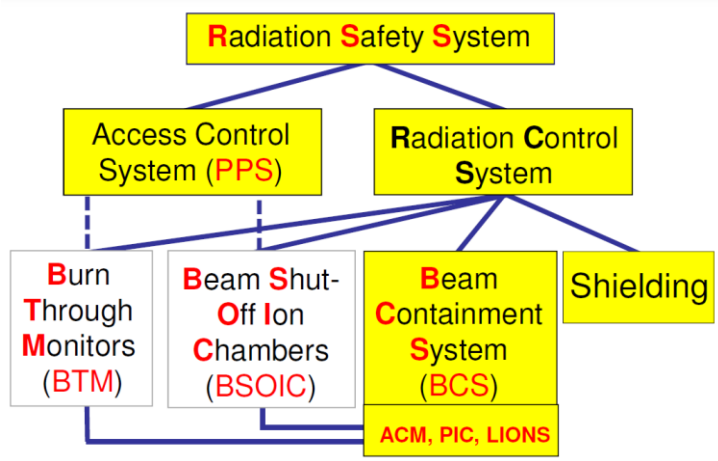

Figure 14.1. LCLS-II radiation safety system.

The SLAC Radiological Control Manual specifies an administrative control level of 500 mrem total effective dose (TED) per year and a dose-management "ALARA Level" of a maximum of 360 mrem TED per year above natural background levels for radiological workers. The actual dose that personnel at SLAC receive is much less than these limits. For example, the annual collective dose at SLAC has ranged from 10370 person-mrem in 2005 to 169 person-mrem in 2009. Majority of the SLAC population do not receive any doses; the average dose to SLAC population who have received doses from SLAC work is approximately 28 mrem per year in the same period.

The following radiation dose criteria are used for the design of the LCLS-II radiation safety systems:

1. The effective dose to personnel working inside and around the experimental halls should not exceed 100 mrem in a year for normal beam operation. The users of the LCLS-II who will be working in the experimental halls are not expected to be classified as radiological workers.
2. During normal operations the LCLS electron beam enclosures should be shielded to an average dose rate of less than 0.5 mrem/h.
3. The maximum effective dose rate in accessible areas at 30 cm from the shielding or barrier should not exceed 400 mrem/h for mis-steering conditions defined as conditions that are comprised of infrequent or short-duration situations in which the maximum allowable beam power, limited by Beam Containment System (BCS) devices is lost locally or in a limited area.
4. The effective dose-rate in the event of the Maximum Credible Incident (MCI) should not exceed 25 rem/h, and the integrated effective dose to less than 3 rem [1]. The MCI is defined as the highest beam power that the accelerator can deliver to a point assuming that the BCS devices that limit beam power have failed.
5. In addition to shielding (bulk and local), the LCLS-II radiation protection systems will have Beam Containment System (BCS) and Personnel Protection System (PPS) in the tunnel, and the Hutch Protection System (HPS) in the beam lines to achieve the designed goals.

Similar to LCLS-I, the sources of prompt ionizing radiation during LCLS-II beam operations are identified. These sources are due to beam interacting with machine components. The radiation sources for LCLS-II routine operations include but are not limited to: deposition of the entire beam

power in the main beam dump, partial or entire beam on the Tune-up Dump Kicker (TDKIK), a dump collimator preceded by a fast (120 Hz) kicker magnet; partial beam deposition in the Tune-up Dump up-beam of Undulators (TDUND); small fraction of the beam on the main Bending Dipole set in the Y/vertical axis (BYD) that deflect (by about 5 degrees) the electron beam towards the main beam dump. The amount of beam loss at various sources for routine operations and for abnormal situations are determined based on estimates provided by the project accelerator physicists, and reviewed by radiation protection department staff and peers. In addition to sources that are due to LCLS-II beam operations, radiation hazard due to other beam operations in the Linac are considered in design of shielding and radiation safety systems of LCLS-II. For example, FACET (Facilities AcCcelerator science and Experimental Test), a test beam facility that uses the first 20 sectors of the LINAC and delivers 2.3 kW, 23 GeV electrons at a target in sector 20. Therefore, hazards from FACET operations needed to be considered in the design of LCLS-II injector alcove, which is located in sector 10, to protect workers during the installation of LCLS-II injector.

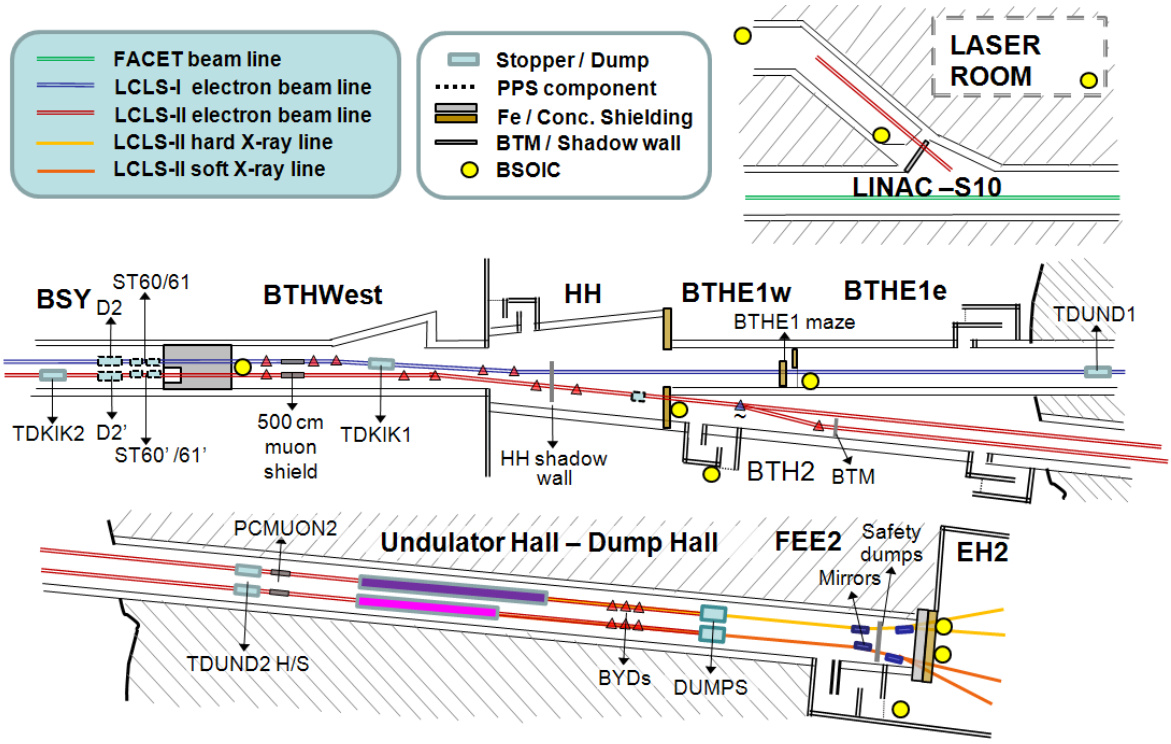

Figure 14.2. Overview schematic of LCLS-II radiation safety system.

The radiation safety design, radiation commissioning and routine operation for LCLS-I project has provided RP experience [3] [4] [5] [6] and lessons leaned for LCLS-II radiation safety design. Figure 14.2 shows the overview schematic of LCLS-II radiation safety systems at the injector, Beam Swith Yard (BSY), Beam Transport Halls (BTH) and the LCLS-II Undulator and Dump Halls. At the injector, bulk and local shielding are applied to protect personnel from beam loss during FACET operation. TDKIK of LCLS-II (TDKIK2) is moved to upstream of electron stoppers D2' and ST60'/61' to reduce the shielding requirements. Shielding for tune-up dump and main electron dump are similar to those in LCLS-I. The shadow wall in head house (HH) and the maze in LCLS-I BTHE (which splits that region into two zones which we identify as BTHE1w and BTHE1e) render access to BTHE1e during LCLS-II operation possible. BTMs are installed to protect personnel and components from mis-steered beam. The safety dumps / collimators and the wall that separates the Undulator Hall, Dump Hall and

Front End Enclosure (FEE2) region from the experimental hall (EH2) are designed for a safe radiation environment in EH2. BSOICs are placed at necessary locations and three mazes are set for construction to grant access to BTH2 and FEE2.

The major changes between LCLS-I and LCLS-II are listed as follows:

1. The LCLS-II injector and linac are nearly identical to the successful LCLS-I design, but moved one kilometer (1016 m) upstream to occupy Linac sectors 11-20. The LCLS-II injector will be built inside the Sector-10 vault. The shielding wall between LCLS-II injector vault and LINAC will protect the workers inside the vault during FACET operation. The shielding wall is thinner than that of Sector-20. The LCLS-II injector wall design is based on normal beam loss during FACET operation (0.5 mrem/h with 5 W beam loss) while the LCLS-I injector wall was based on high-power ESA operation (25 rem/h with 1200 kW maximum credible beam loss) [7].
2. An electron bypass line will transport the beam around LCLS-I using the existing, but modified PEP-II high-energy transport line presently suspended from the linac tunnel ceiling.
3. The existing muon shielding wall between BSY and BTHW was designed for 50-GeV and 2-kW electron beam operation. This shielding wall will be re-stacked for LCLS-II line. New requirements are based on 17-GeV and 5-kW electron beam operation; the preliminary calculations show that 40’ of iron may provide sufficient shielding.
4. LCLS-II Single-shot Beam Dump (SBD), TDKIK, will be moved upstream to BSY to reduce the radiation shielding requirements.
5. Access to LCLS-I BTH east will be allowed during LCLS-II operation.
6. The new undulator hall will have a pulsed magnet to distribute the pulses between two parallel undulators, (HXR to generate hard x-ray from 2 keV to 13 keV and SXR for soft x-ray from 250 eV to 2000 eV), followed by three mirrors in the hard x-ray line and three mirrors in the soft x-ray lines. Each undulator is preceded by a tune-up dump.
7. LCLS-I FEE is a separated PPS zone, coupled with full PPS interlock system. LCLS-II front end enclosure (FEE2) will be in the same PPS zone as BTH2, undulator and dump line hall.
8. A new experiment hall (EH2) is capable of accommodating four new experiment stations.

14.1.2 Summary

The radiation protection requirements envisaged for the LCLS-II design as of November 2010 are summarized in Table 14.1 and Table 14.2, and developed along this document.

Table 14.1. Summary of LCLS-II radiation safety systems for the electron beam lines.

		Shielding	PPS	BCS	BSOIC
1.	Access to LCLS-II injector vault and alcove (Ch. 14.2)	• One concrete wall plus local steel and lead shielding for FACET beam loss (Figure 14.3) • Iron shielding for alcove penetrations	• PPS door for injector vault • PPS barrier for the top opening of the stairway	*FACET BCS LIONs*	• One for injector vault interlock to FACET • Two upstairs of injector, one in the top of stairway and one in laser room, interlock to LCLS-II
2.	Access to BTHW for LCLS-II line (Ch. 14.3.1)	• 40’ muon shielding. TDKIK2 and PPS stoppers in the shielding. (Figure 14.6) • 0 degree muon shielding in BTHW: 500 cm long	Three PPS stoppers: D2, ST60 and ST61	• Three ACMs to limit beam power to 5 kW • Flow switches for D2 • PICs on PPS stoppers	One in BTHW near the muon wall, interlock to LCLS-I and LCLS-II
3.	Access to LCLS-I BTHE during LCLS-II operation (Ch. 14.3.2)	• 3’ local iron wall in the head-house • Concrete maze in BTHE (two walls: 3’ + 2’) (Figure 14.7)	PPS door and gate in the maze	BTMs and PICs on LCLS-II line	One downstream of the BTHE maze, interlocked to LCLS-II, by passed during LCLS-I operation
4.	Access to LCLS-II BTHE during LCLS-I operation (Ch. 14.3.3)		PPS stoppers upstream of south end plug	PICs on PPS stoppers	One downstream of the south end plug, interlock to LCLS-I, by passed during LCLS-II operation
5.	LCLS-II BTHE building (Ch. 14.4)	• 5’ concrete wall • Roof: 5’ concrete for service building and 3.5’ for non-occupied area • Two access mazes	PPS doors and gates in mazes	• BCS LIONs • BTMs and PICs	One outside LCLS-II BTH east maze
6.	Dump and dump line (Ch. 14.5.1 & 14.5.3)	• Dump shielding like LCLS-I (Figure 14.13) • Two 5-kW-Safety dumps, one for HXR and one for SXR	No new PPS	• One power supply for BYD magnets and dipole upstream of undulators • BTMs, collimators and PICs • Flow switches for dumps	None
7.	Undulator hall, dump hall and FEE2 tunnels / cut-cover (Ch. 14.5.4)	• Access maze (Figure 14.14) • FEE2-EH2 wall up to 13’ steel and concrete	PPS door and gate in maze	• BTMs and PICs • Collimators	• One outside the maze • Two after FEE2-EH2 wall, aligned with each safety dump

Table 14.2. Summary of LCLS-II radiation safety systems for the photon beam lines.

		Shielding	PPS	BCS	BSOIC
1.	Access to EH2 (Ch. 14.6)		Two shutters per photon branch line	• Photon BTMs • Collimators for photons	
2.	Experimental hutches, hard X-ray (Ch. 14.7)		Two hutch shutters per hutch	Collimators	One for each hutch

14.2 Radiation Shielding of the LCLS-II Injector Vault and Alcove

The radiation shielding for the injector vault at Sector-10 is designed for access to the LCLS-II injector vault during FACET operations. The associated beam losses, defined in [8] appear in Table 14.3 along with the shielding criteria and computed dose rates. Here the normal beam loss is the critical condition.

Table 14.3. Beam loss scenarios and radiation shielding criteria standard.

Scenario	Beam loss	Shielding criteria	Maximum expected dose
Normal	10 GeV, 5 W (limited by FACET BCS)	0.5 mrem/h	0.5 mrem/h
Maximum credible	14 GeV, 60 kW	25 rem/h	6 rem/h

Monte Carlo simulations with realistic 3-D models of the injector vault and Linac tunnel have been performed for the beam losses that appear in Table 14.3 (second column), and located at different positions along the FACET beamline. The minimum shielding that meets the criteria of Table 14.3 (third column) is sketched in Figure 14.3. The resulting dose rates are shown in Figure 14.4 and the numerical values appear on the fourth column of Table14.3. This shielding, which is considerably thinner than the Sector-20 injector shielding, includes the six components arranged in the following blocks:

- 6” thick, 8’ long steel plate inside the linac tunnel and adjacent the wall at the injector side (#1)
- 3 blocks perpendicular to the injector vault wall (while not to the injector vault wall):
    - 12” thick, ~ 4’ long lead block on the half of injector vault on the side with injector line (#2)
    - 12” thick, ~ 4’ long steel block on the other half of injector vault (#3)
    - 32” thick, ~ 8’ long concrete block (#4)
- 34” thick triangle concrete block (#5)
- A small triangle concrete block (#6)

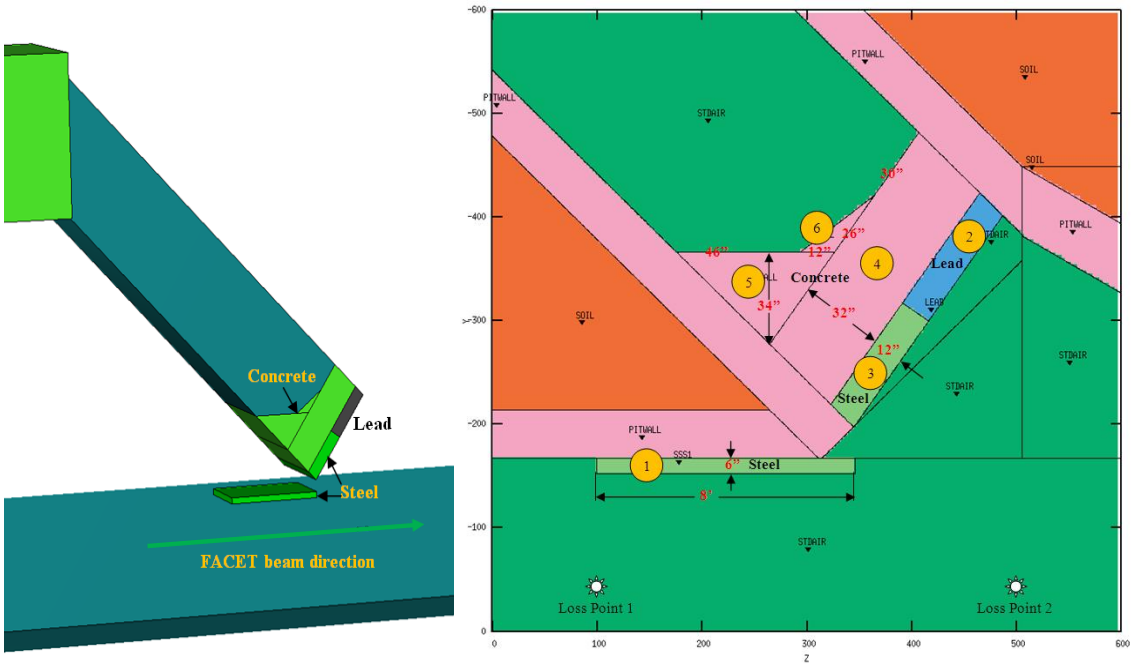

Figure 14.3. 3D scheme and plain view of the shielding design for the injector during FACET operation. Two test locations for losses are indicated as Loss Point 1 and 2.

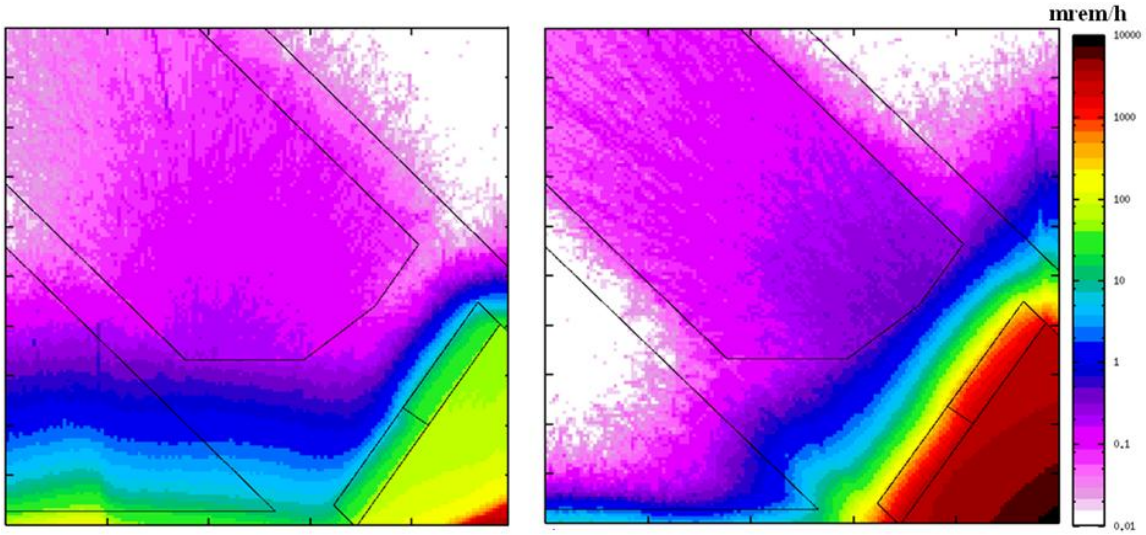

Figure 14.4. Top dose rate maps [mrem/h] at beam plane for Loss Point 1 (left) and 2 (right).

A BSOIC is required close to the concrete blocks where the radiation may be highest. The BSOIC should be set to trip at 10 mrem/h. Considering possible penetrations such as the injector beam line and RF waveguides, as well as construction constraints, the final shielding design may include modifications to this proposal.

Access to the LCLS-II injector vault will be through a PPS door.

The sector-10 Alcove will be rebuilt and used as the LCLS-II injector laser room. There are four penetrations from the Injector Vault to the ground surface of the alcove: 1) the stairway, 2) one laser penetration, 3) one unused penetration, and 4) one ventilation penetration.

The radiation entering the Sector-10 alcove has two sources:

1. Radiation streaming through the penetrations from the Injector Vault below,
2. Radiation from SLED cavities and klystrons in the adjacent klystron gallery.

Based on the radiation sources and nominal beam powers during operation of the LCLS-I defined in [9] and the estimated radiation levels in the alcove with the klystrons operating at 120 Hz, the following shielding items must be in place for LCLS-II injector operation:

- 7” iron for laser penetration.
- 18” iron for unused penetration.
- A PPS barrier to keep workers 1 foot away from the top opening of the stairway.

Note that the ventilation does not require any shielding.

Two BSOICs, set to trip at 10 mrem/hr, are required to limit the dose rate in the event of loss of the maximum credible beam during LCLS-II injector operation. One is located inside the laser room, and one is located at the top of the stairway.

14.3 BTHW, BTH Head-house and BTH Access Modes during LCLS-I and LCLS-II Operation

Figure 14.5 shows the schematic view of BTHW, BTH Head-house and BTH. Table 14.4 shows the PPS stopper requirements and beam losses in different access modes.

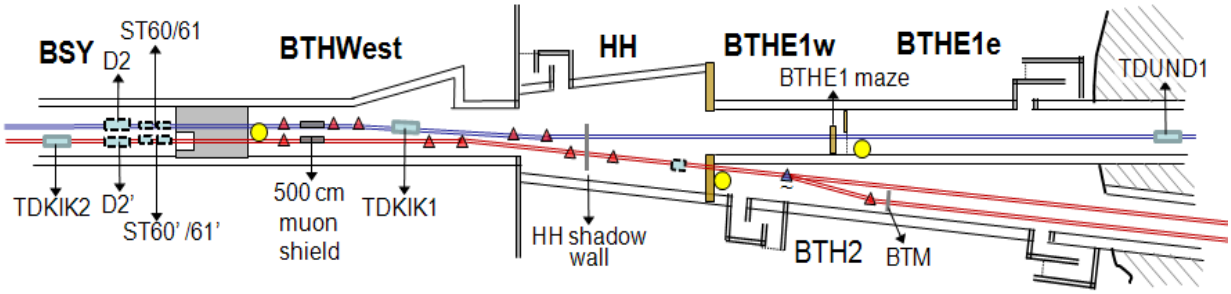

Figure 14.5. Schematic view of BTHW, BTH Head-house and BTH.

Note that, as advanced in 14.1, the major configuration change with respect to LCLS-I is the relocation of the TDKIK2 from its original planned location on top of TDKIK1 (at the end of BTHW) to BSY, just before the LCLS-II D2 triple PPS stopper set, and very likely in a 10’ deep cavity within the BSY-BTHW muon wall. This move will not affect LCLS-II beam energy diagnostics capabilities, because, unlike in LCLS-I [10] [11] [12] LCLS-II has bending magnets in Sector-19. The advantages of this configuration are multiple:

- Most of the massive lateral shielding that was needed for TDKIK can now be spared as it will be provided by the iron of the BSY-BTHW wall.

- The BSY-BTHW wall will not only shield the forward focused muons generated in D2, but now also from those of TDKIK. This means that a dedicated TDKIK2 muon collimator can be spared (in LCLS-I it was composed by four big lead blocks, each 1 m in length).
- More importantly, LCLS-I BTHE will require much less shielding to be accessible during LCLS-II operation, as the main normal operation loss source will now be upstream of the thick BSY-BTHW walls. More details in 14.3.2.
- Had TDKIK2 been placed on top of TDKIK1, the north muon plug might have required supplemental shielding if both LCLS-I and LCLS-II operated at 5 kW for a total of 10 kW (the plugs were designed for a total beam of 5 kW).

Table 14.4. PPS stopper requirements and beam losses in different access modes.

Access areas	Operation	PPS stoppers	Beam losses	Beam losses
BTHW Head house LCLS-I BTHE1W	LCLS-I	D2, ST60, ST61	5 kW on D2	
	LCLS-II	D2', ST60', ST61'	5 kW on D2'	
LCLS-I BTHE1E	LCLS-I	D2, ST60, ST61	5 kW on D2	
	LCLS-II	To LCLS-II dump	5 kW on LCLS-II SBD' New location	3.5 W continuous loss
LCLS-II BTH2	LCLS-I	To LCLS-I dump	5 kW on LCLS-I SBD	5 W continuous loss
	LCLS-II	D2', ST60', ST61' New PPS stopper close to south end-plug	5 kW on D2'	

14.3.1 Radiological Studies for Access to BTH West

Similar to LCLS-I, in order to access BTHW three PPS stoppers will be required upstream of the BSY-BTH muon wall. In the LCLS-I line, they are named as dump D2, stoppers ST60 and ST61. Dump D2, made of copper, is 30-r.l. long. This water-cooled dump with BCS flow switches is capable to absorb > 5 kW beam power. Stoppers ST60 and ST61, also made of copper, are 52 r.l. each, and are capable to absorb 500 W beam power. Dump D2 is protected by three protection ion chambers (PICs). Stoppers ST60 and ST61 are protected by one PIC each. TDKIK2 will be located upstream of the PPS stoppers. The LCLS-I PPS configuration will be copied to the LCLS-II line.

The beam power on the D2 dump should be limited to 5 kW by means of three BCS Average Current Monitors (ACMs). Moreover, D2 will incorporate flow switches.

The 4' long iron rods and 1' of borax installed in the alignment pipe should be kept in place to reduce the streaming of radiation from LCLS-I and LCLS-II D2 stoppers to BTHW through the light-pipe.

In LCLS-I, the D2 dump had lateral and top shielding (10" lead down beam and over D2, 3' lead followed + 2' concrete down beam) to reduce the photon and neutron radiation that goes over the thick muon shielding wall and is scattered down through the BTHW 1' concrete roof towards BTHW. In LCLS-II the tune-up dump kicker TDKIK2 along with the three PPS stoppers D2', ST60' and ST61' should be placed in BSY.

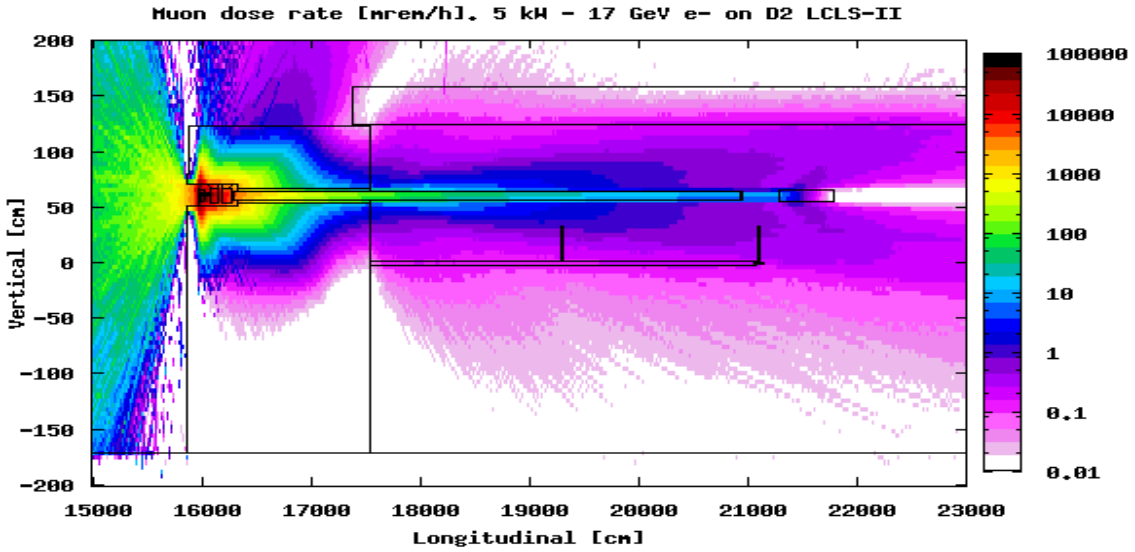

Figure 14.6. Muon dose rate [mrem/h] when 5 kW e- at 17 GeV are dumped on D2 for a 40' thick BSY-BTHW wall.

Currently the BSY-BTHW shielding wall is 55' and made of iron. This wall was designed to stop the highly penetrating muons generated by 2 kW electron beams at 50 GeV. Now it must be such that BTHW can be accessed when up to 5 kW e- at 17 GeV are stopped by TDKIK2 or by LCLS-II D2'. Simulations performed with 40 ft bulk iron BSY-BTHW shielding with stoppers D2', ST60' and ST61' inserted and a 3" pipe through the shielding encased in 5"x5" lead show (see Figure 14.6) that this configuration could be sufficient to keep the dose in BTHW below 0.5 mrem/h everywhere except for a 30-50 cm radius around the beam pipe close to the BSY wall.

A BSOIC (gamma probe only) set to trip at 10 mrem/h should be installed in BTHW near the muon wall to detect the radiation from LCLS-I D2 and LCLS-II D2' dumps.

The beam pipe that links BSY and BTHW is tilted down with a small angle. Two dipoles in BTHW straighten the electron beam trajectory. Due to their higher magnetic rigidity, the most energetic muons exit the beam pipe almost tangentially after the first vertical bend. As in LCLS-I, a muon shielding ought to be placed at that location. Measurements performed for LCLS-I and new simulations show (Figure 14.6) that, an assembly of lead, of 10 x 10 cm^2 cross section and 500 cm length is sufficient to shield a muon jet of 10 mrem/h/kW down to 0.05 mrem/h/5 kW. Detailed Monte Carlo simulations with the final geometry and magnetic fields can help optimize the vertical extents of the shield, so that lower energy muons (slightly bent by the dipole) are also caught by the shielding.

14.3.2 Shielding Requirements for Access to LCLS-I BTH East during LCLS-II Operation

A maze of two concrete walls (3' thick and 2' thick) should be installed in the LCLS-I BTHE (BTHE1) about 10 m downstream of the head house. This maze will divide BTHE into two areas, hereby called BTHE1w (upstream of the wall) and BTHE1e (downstream of the wall). Additionally a 2-3' thick, 6' wide, 3' tall iron muon scattering wall(s) should be installed in the Head House (HH) (named LCLS-I HH muon wall). The mission of the muon wall and of the maze is to stop the radiation (mainly muons) into BTHE1e originated by nominal 3.5 W-17 GeV beams losses and also eventual LCLS-II mis-steered beams (towards BTHE). Simulations have been performed for 17 GeV beams on the LCLS-I HH. The results, shown in Figure 14.7 indicate that the suggested wall and maze are appropriate to attenuate the dose rates below

0.05 mrem/h and 60 mrem/h, respectively, and, therefore, meeting the limits (0.05 mrem/h/3.5W and 400 mrem/k/5kW).

If TDKIK2 had been installed on top of TDKIK1, a much more restrictive solution would have been required to stop the muon flux from the 5 kW-17 GeV source starting at the BTHW. Figure 14.8 shows how a 6' thick LCLS-I HH muon wall and a four wall maze with two 5' thick iron walls and two 2' concrete walls would barely suffice to shield the muon stream from a TDKIK2 placed at BTHW. Moreover, a much larger area of BTHE would not have been accessible with the maze wall, placed about 50 m down-beam of the head house.

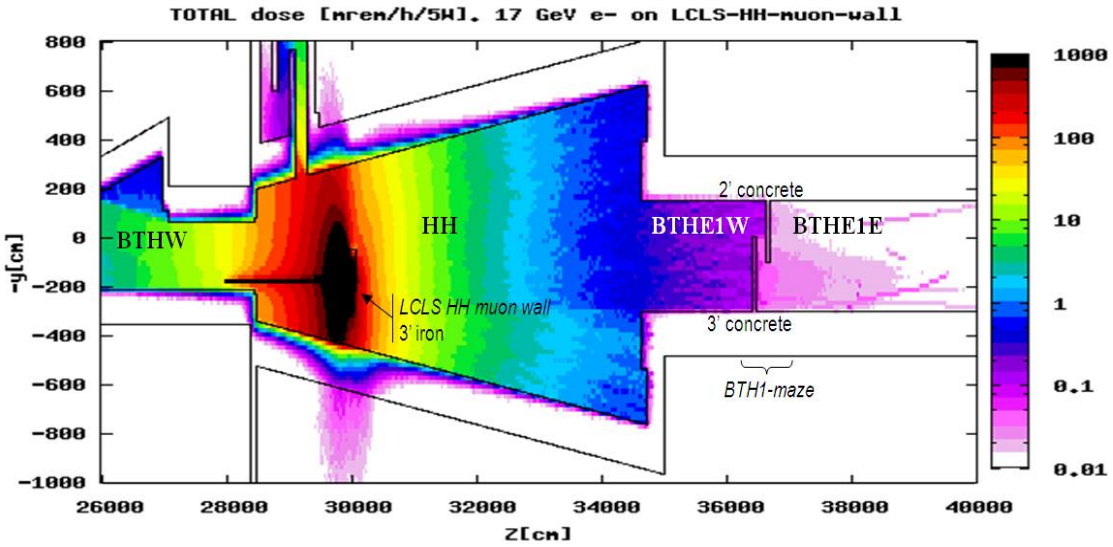

Figure 14.7. Total dose rate [mrem/h] top view map at LCLS-II beam plane collimator for a 5 W beam loss in LCLS-II. This can be rescaled by a factor of 1000 to obtain mis-steering losses intercepted by the LCLS-I HH muon wall.

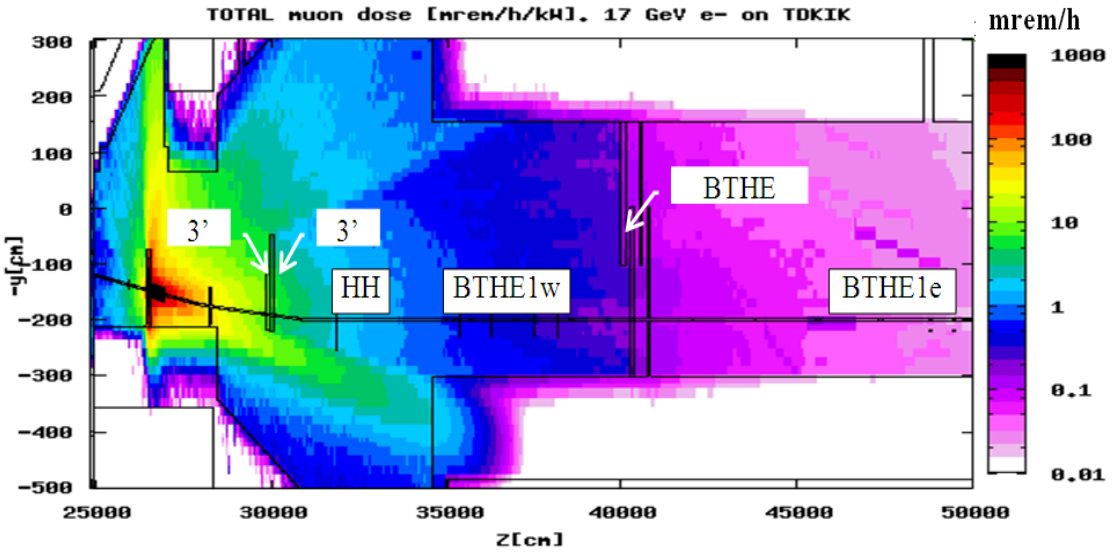

Figure 14.8. Muon dose rate [mrem/h] top view map at beam plane per each kW of e- at 17 GeV dumped on TDKIK2 if it had been placed at BTHW on top of TDKIK1.

This solution would have required a TDKIK 4-m lead PCMUON collimator, a 6' shadow wall and a 4-wall BTHE maze with two 5' thick iron walls and 2' concrete walls

14.3.3 Study of the Access to LCLS-II BTHE during LCLS-I Operation

The LCLS-II BTHE, hereby also named BTHE2 or simply BTH2, will be separated from the head house by the head-house south end concrete plug. This zone of LCLS-II, as well as all the downstream areas will be accessible to GERT during LCLS-I operation (and also if LCLS-II is on D2), including when a 5 kW-17 GeV LCLS-I beam is dumped on TDKIK1.

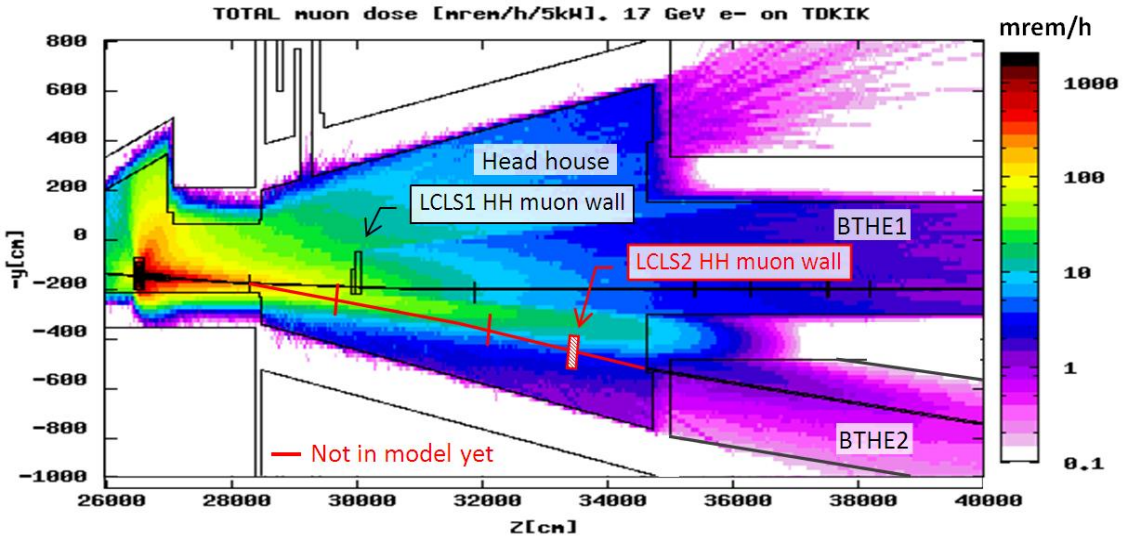

Figure 14.9. Muon dose rate [mrem/h] top view map at beam plane when 5 kW - 17 GeV e- are dumped on TDKIK1 and LCLS-II beamline components (BTMs, magnets, LCLS-II HH muon wall, collimators, stoppers, magnets) are not yet installed.

In order to achieve the previous scheme, recent Monte Carlo calculations that incorporate the new LCLS-I HH muon wall described in the previous section and a 3" diameter pipe through the south wall plug, indicate that a new LCLS-II HH muon wall collimator and stoppers upstream of the south end plug might be necessary to keep the dose in BTHE2 below 0.5 mrem/h. Figure 14.9 shows the expected muon dose when 5 kW are dumped on TDKIK1 and no BTMs, collimators or other LCLS-II beam line components are yet installed. Future simulations will incorporate all those components (including magnetic fields) to determine what the necessary dimensions of LCLS-II HH muon wall are.

The south end plug BSOIC should be moved to the highest expected dose position, between the LCLS-II beam and the BTHE1 south wall. The trip setting should be 10 mrem/h. This BSOIC will be by-passed during LCLS-II operation.

14.4 Radiation Protection Requirements for the Head House and the LCLS-II BTH

14.4.1 Side Walls, Roof and Mazes of New LCLS-II BTH (BTH2)

The Head House (HH) walls are not new but they were designed for 5 W nominal losses, while the normal losses from the combined operation of LCLS-I and LCLS-II could reach 8.5 W. From the simulation

performed in 14.3 (Figure 14.7) this is not a problem since the expected dose rate outside the head house for a 8.5 W loss is below the 0.05 mrem/h limit.

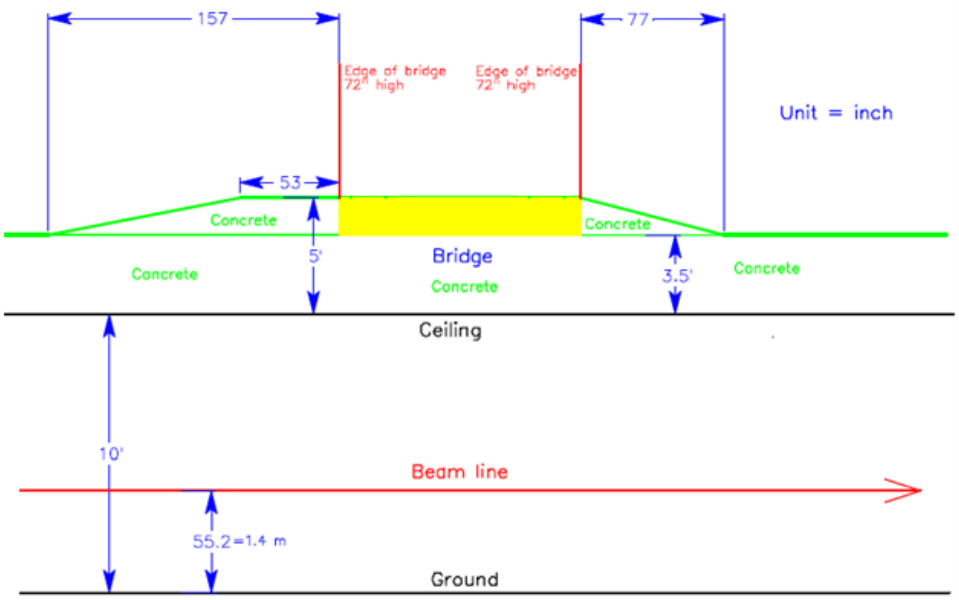

Figure 14.10. BTH2 roof shielding proposal (elevation view).

BTH2 could share a wall with LCLS-I (the LCLS-I south-side wall [13]) and then it would only need a new wall at the south side of the LCLS-II beamline. The new wall requires 5' thick concrete to ensure that the dose outside the building is below 0.5 mrem/h for 3.5 W beam loss in any point of the beam lines. The LCLS-II BCS LIONs will be set to trip accordingly. For any 3.5 W loss along the beamlines, the dose rates in the unoccupied areas and in occupied areas of the BTH roof shall stay below 3 mrem/h and 0.5 mrem/h respectively. The roof thickness is 3.5' and 5' for the unoccupied areas and occupied areas, respectively. The 5' platforms extend 5' upstream of the rails delimiting the occupied area and 2' downstream of those (see Figure 14.10). [14]

There will be two mazes (west and east) to access through PPS gates the BTH2 [14] [15]. The west maze is located at the connection between the HH and the new LCLS-II BTH. The maze is shown as Figure 14.11a (all sizes in the figure are in the unit of foot). The height of the maze is 10 feet. A PPS door and gate will be installed in the west maze.

The east maze is located at the downstream end of the new LCLS-II BTH. The maze is shown in Figure 14.11b (all sizes in the figure are in the unit of foot). The width of the walkway is 6 feet and the height of the maze is 10 feet. A PPS door and gate will be installed in each new maze, and one BSOIC should be placed outside of each new maze.

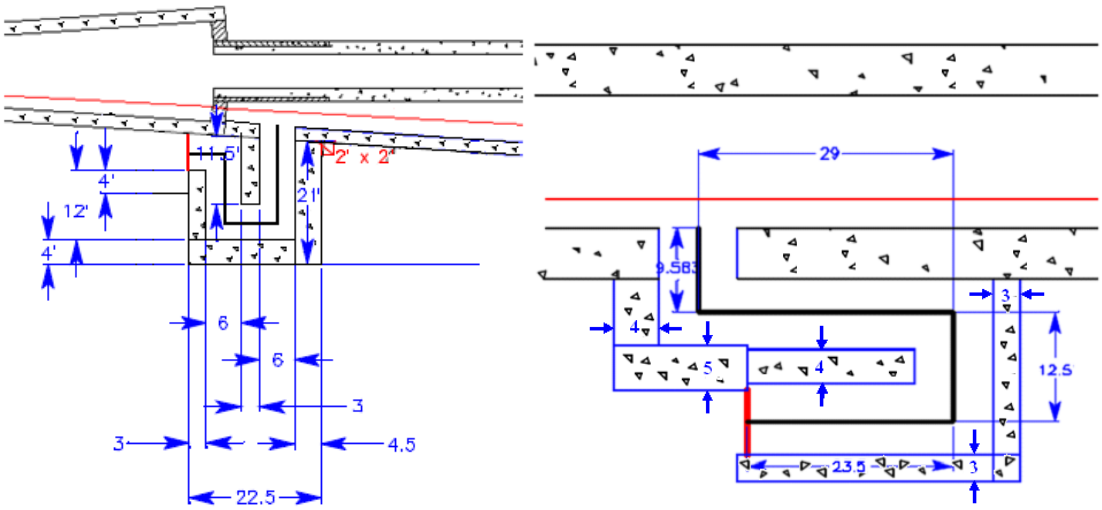

Figure 14.11. Proposed BTH2 mazes: West maze (a) and East maze (b).

14.4.2 LCLS-II Beam Containment System in the Head House and BTH2

In LCLS-I [16] [17] an analytic method was presented to estimate the angles in which the electron beam could be mis-steered as a result of its passage through up to three consecutive magnets incorrectly powered (with a potential ranging from V to –V, instead of V). Based on the resulting rays, one burn through monitor was installed in the head house and another four were placed 4, 16, 25 and 37 m into the BTHE. Those BTMs were designed to prevent mis-steered rays from reaching the lateral walls or roof within BTHE, or from escaping by the south plug in the head house, in the future occupied by the LCLS-II BTHE tunnel.

The BTM scheme in HH and BTH2 for LCLS-II may be evaluated once the beamline position and components, and wall tunnel are solidly established. The analytic technique introduced before might be supplemented by new simulation methods at RP, which may allow drawing the envelope of the mis-steered trajectories for a high number of permutations of magnet failures.

The BTHE2 will need as many LIONs as BTHE, as the length is very similar. The LIONs design trip setting will be 3.5 W and the actual setting will be determined after the radiation surveys. The ratio of the north and south LIONs trip level might be equal to one if the LCLS-II beamline is located at the center of its tunnel.

14.5 Radiological Studies for the LCLS-II Undulator – Dump Hall – FEE2

In LCLS-II, the dump hall and the front end enclosure (FEE2) are integrated into a single area and, unlike LCLS-I, they are not separated by a shielding wall (like LCLS-I ‘wall 1’). That zone is preceded by the undulator hall, also without any shielding wall in between (see Figure 14.12).

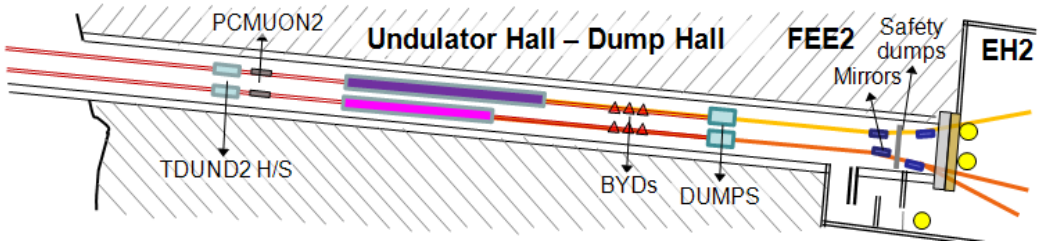

Figure 14.12. Scheme of the Undulator, Dump Hall and Front End Enclosure in LCLS-II.

The undulator hall will have a pulsed magnet to distribute the pulses between two parallel undulators, (HXR to generate hard x-ray and SXR for soft x-ray), followed by one mirror in the hard x-ray line (M1H) and followed by at least two mirrors in each x-ray line (M1S and M2S). Each undulator is preceded by a tune-up dump.

This section addresses radiation protection aspects related to the tune-up dumps, the radiation damage to the undulator, shielding of the main dump, burn through monitor and safety dump requirements. The wall between the undulator hall and the EH2 is described in Figure 14.12.

Note that the main dump hall will be accessible through a maze from EH2, equipped with a BSOIC and a PPS door and gate.

14.5.1 LCLS-II Undulator Tune–up Dumps (TDUND)

The LCLS-I TDUND shielding, described in [18] [19] [20] was designed with the following considerations:

- Prompt dose to accessible areas, i.e. backscattered radiation into research yard and muons and Bremsstrahlung directed towards the FEE/NEH.
- Activation of the tunnel near the dump and of downstream beam components.
- Residual dose from gamma-decay of the dump and its shielding.
- Environmental impact: activation of neighboring soil, air and cooling water.
- Demagnetization of the undulator permanent magnets.
- Damage/upset to electronic equipment located nearby.

For the same operating conditions as in LCLS-I (duty factor, access time), the lateral shielding of LCLS-II TDUNDs could be reduced (from TDUND1 reference) by:

- Selecting materials for the dump and the surrounding objects that minimize the neutron production, i.e. avoid tungsten and lead at or near the dump,
- Choosing dump alloys that get less activated, i.e. low trace cobalt content, vanadium alloys, etc.
- Using low sodium concrete for the pedestal and the tunnel walls near the dump.

Other recommendations for LCLS-II tune-up dump are the following:

- Install LCLS-II TDUNDs farther into the undulator tunnel (e.g. additional 5 m), so that no concrete patching of the BTH-II hill is required to reduce the expected backwards prompt dose, as it happened with LCLS-I.

- Augment the distance between LCLS-II TDUNDs and the undulators, and verify that in the PCMUON2 design the permanent magnets of the undulators of one line are not demagnetized by radiation from the tune-up dump of the other line.

14.5.2 Demagnetization Considerations for HXR and SXR

For the current design of LCLS-II the main candidate sources for demagnetization are LCLS-II TDUNDs, the pulsed magnet in front of the undulators and the mirrors if they are located near the end of the undulators.

LCLS-II TDUNDs should be placed as far from the undulators as possible, and LCLS-II PCMUONs should be designed so that both undulators are conveniently in the shade of the radiation from both dumps.

A higher degree of nominal and potential losses (halo and mis-steering) should be assumed at bends, i.e. in the pulsed magnet and the dipoles placed before HXR and SXR. The burn through monitors required between the kicker-switch and the undulators should be designed not only to avoid mis-steered beams from hitting the FEE2-EH2 wall, but also to protect the undulator magnets from showers of normal and mis-steered losses.

Local shielding and/or distance should be present between the first x-ray mirrors (M1S and M1H) and the preceding undulators to avoid demagnetization from showers induced in those mirrors by halo electrons, Bremsstrahlung and muons.

Beam loss monitors should be installed and calibrated to monitor the losses.

14.5.3 Shielding of the Main Electron Dumps

The shielding around the main dumps must be such that:

- The combined prompt dose reaching general public areas is below 0.05 mrem/h.
- The radioisotope concentration in the groundwater is below detection limits.
- The dose to public from release of radioactive air stays below limits.
- Interventions can be brief so that the collected dose is small.

The LCLS-I dump was designed [21] [22] [23] [24] to meet all of the above for a 5 kW beam at 17 GeV. We assume that the full LCLS-II 5 kW beam power could be sent to any of the two dumps or shared between them. Therefore, the LCLS-I dump shielding is adequate for LCLS-II. The main shielding dimensions for LCLS-I are sketched below, as well as the expected prompt doses (see Figure 14.13).

Depending on the soil density, the top soil coverage may be reduced from 16 to 12 ft. This coverage will ensure with a safety factor of two that the dose rate in the ground stays below 0.05 mrem/h even if the soil is not compacted to the nominal density of 2.1 g/cm3, but just to 1.75 g/cm3.

The main dumps should be equipped with flow switches and a burn-through monitor.

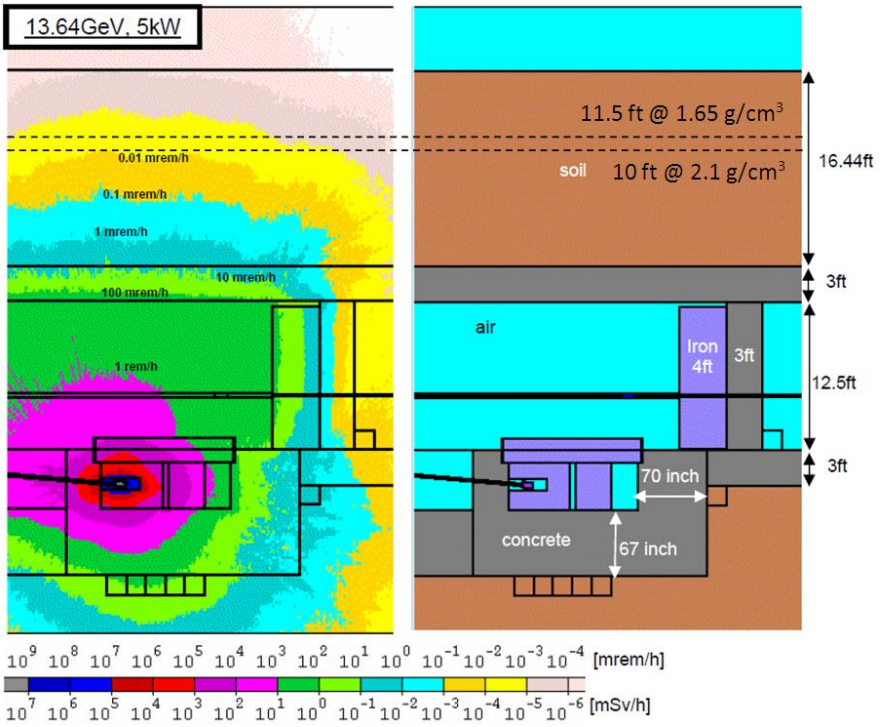

Figure 14.13. Sketch of the shielding around the LCLS-I dump and MARS15 computed prompt dose rates for a 13.64 GeV-5 kW electron beam.

14.5.4 Shielding BCS and PPS Requirements in the Undulator / Dump Hall / FEE2

For LCLS-II two undulators are envisaged, HXR and SXR. As in LCLS-I, ray-tracing should be carried out for both lines to determine the location and dimensions of burn through monitors (BTM) and protection collimators.

Behind each BTMs, a pair of ion chambers shall be installed.

Two safety dumps / collimators [25] [26] are foreseen at the zero-degree angle downbeam of the BYDs (one downstream of M1H and another downstream of M1S) to attenuate and scatter un-bent beams that would otherwise hit the FEE2-EH2 wall. A pair of ion chambers will be installed next to each safety dump to detect such events. Moreover, BSOICS will be installed behind the FEE2-EH2 wall.

An additional safety layer, which protects against BYD power supply failure, consists in having the dipoles that bend the electrons down towards the beam dumps (BYD) and the energy chicane dipoles at the BTH share a common power supply.

An advantage of LCLS-II is that the mirrors are installed before the wall so that Bremsstrahlung radiation from insertion devices, spontaneous radiation and muons generated by beam-halo interactions do not make it directly through the wall. However, these radiation sources may generate showers in the mirrors and other components and a fraction of them may point at the beam pipe apertures through the wall. Therefore, a tight collimation system will be required. A set of collimators similar to those in the LCLS-I FEE will be needed.

We estimate that several collimators per beamline will be needed in this enclosure. For each beamline, one of these collimators should be located on the upstream face of the wall separating the FEE2 from the EH2, where the beamline crosses the wall.

Moreover, a pair of shutters should be installed for each of the beam-line branches.

14.5.5 Bremsstrahlung leakage to the EH2. Study of mirrors and collimators

The insertion of devices (e.g. thin beam diagnostics) in the electron path and beam scraping in collimators and bends (mainly in BYD) generates Bresstrahlung radiation that points towards the EH2. From LCLS-I studies and operational experience it is believed that the Bremsstrahlung power is in the order of 200 mW or less. These forward-focused photons, together with the spontaneous photons generated along the undulator, the synchrotron radiation from the BYD and the muons created in beam-accelerator interactions will hit the mirrors in the HXR and SXR lines. Some secondary photons in the subsequent showers will join the fraction of high energy photons that is scattered with the right angle to penetrate the EH2 hall through the FEL beampipe. All that intruding, highly energetic radiation can ultimately strike apertures (flanges, collimators, valves) or the beampipe at the EH2 therby creating radiation levels above those allowed for general public.

In order to investigate these effects and to help determine which systems could be needed to remedy such situations, RP performed FLUKA simulations with an initial configuration provided by LCLS where there was 1 mirror per beamline. Results for that arrangement showed too high doses in SXR and even higher values near HXR. Moreover, the incoming photons would be fairly energetic (a few tens of MeV in average), meaning that substantially large and thick hutches would be required to keep the public away from such potential dose levels. It was therefore concluded that each beamline would require two mirrors and collimators in between them and at both ends of the wall. The additional mirrors would reduce by several orders of magnitude the likelihood of photons been scattered (twice) with the FEL angle, and the collimators between them would avoid photons scattered from the first mirror to directly reach the hole in the wall.

Based on these results, a new scheme was tested, in which each the FEL reflects on two mirrors. Both the HXR and the SXR count with three mirrors each (M1H, M2H, M3H and M1S, M2S, M3S). The second mirror of each beam line (M2H and M2S) can be inserted or retracted, thereby creating two branches. Figure 14.14 shows the photon beam line configuration along with other components.

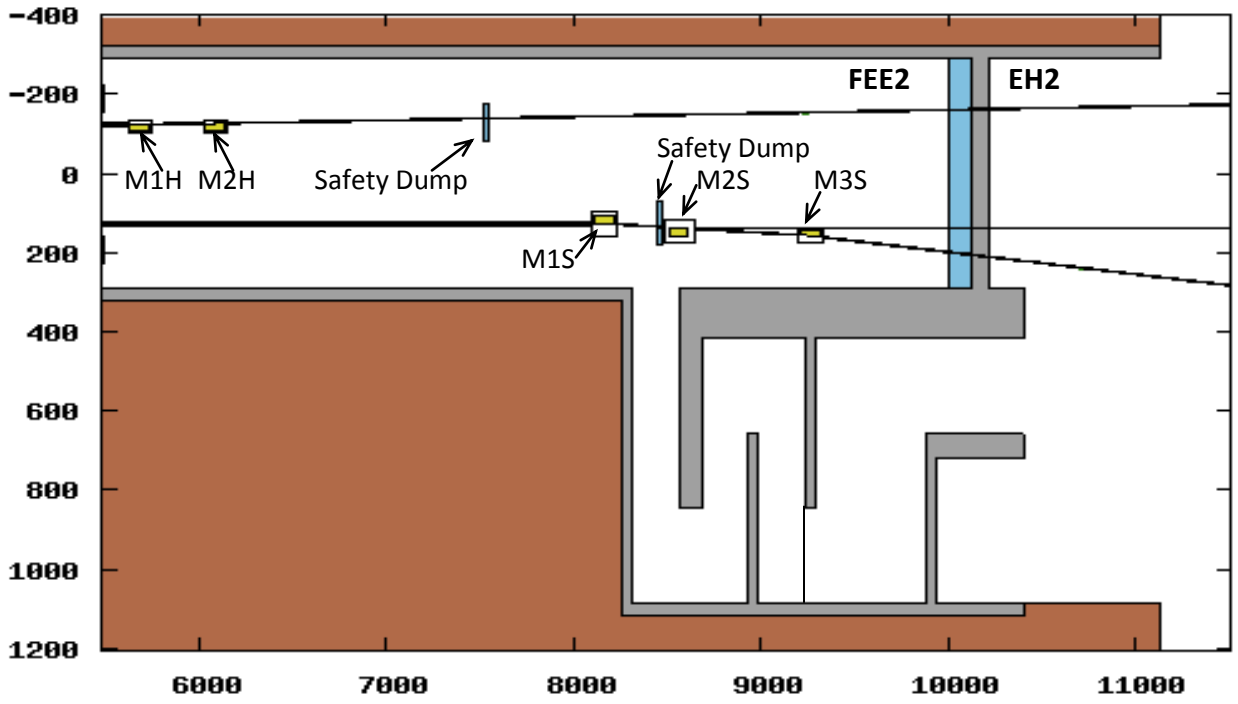

Figure 14.14. Top view of the FEE2-EH2 area as implemented in FLUKA (collimators are not shown). The second branch in the HXR has not yet been implemented in the model.

Figure 14.15 shows how in the 2-mirror-per-branch configuration the dose rates are strongly reduced leading to values below the allowed limits. In conclusion, the two-mirror solution seems necessary and adequate, although further studies are needed to define the exact collimation requirements taking into account possible misalignements.

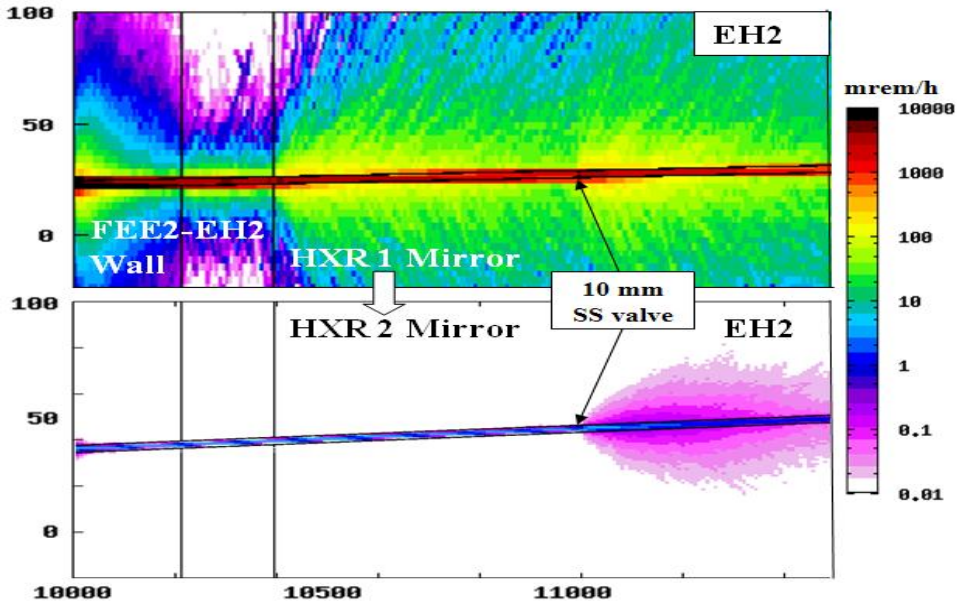

Figure 14.15. Top view dose rate maps [mrem/h] at EH2 per Watt of 15 GeV-Bremsstrahlung in HXR. Upper plot: HXR with 1 mirror; Lower plot: HXR with 2 mirrors.

14.6 Interface between the FEE2 and the EH2

The intense radiation fields of the FEE2 must be confined within that area so that general public can access and work in the adjacent EH2. In the previous section we described the sytems required to limit the radiation leaking through the FEL beamline into the EH2. In this section we describe the other two links between the FEE2 and the EH2: 1) The shield wall at the end of the UH-dump/FEE2 hall and 2) the access maze between FEE2 and EH2.

14.6.1 Shielding Wall between the Front End Enclosure and the EH2: FEE2-EH2

In LCLS-II the FEL is deflected in the mirrors of the FEE2 that are upstream of the EH2 shielding wall. This means that safety dumps/collimation walls can be installed behind the mirrors at the zero-degree angle to stop or spoil forward focused bremsstrahlung and muons generated by earlier electron beam interactions with apertures and insertion devices. If those safety dumps are built wide enough (similar to the extended 1 ft thick iron wall in the LCLS-I FEE [27] [28] [29] [30] [31] [32] [33]), they could also serve to spoil accidentally mis/unsteered electron beams that otherwise could hit the FEE2-EH2 wall.

The inclusion of the safety dumps reduces the thickness requirements of the FEE2-EH2 wall. This is more true the further appart the safety dumps and the wall are. Moreover, the more upstream the safety dump is located, the smaller its transverse dimensions need to be because it will cover a bigger solid angle of potential mis-steered beams. Figure 14.14 is a top view at photon beam-lines plane of the FEE2-EH2, area, including the soft x-ray lines (SXR), the HXR, the mirrors, the safety dump/collimators walls, the FEE2-UH2 wall and the access maze between the two areas.

The FEE2-EH2 wall should shield personnel in the EH2 from the following sources:

1) During normal operation Bremsstrahlung (typically up to 200 mW-15 GeV) and some muons hit the M1S and M1H mirrors. Neutrons, photons and muons are generated in the mirror and in the downstream components (including the safety dump/collimator wall).

2) Very low continuous neutron contribution from the main electron dumps (they are buried far upstream), and small muon fluxes from the undulator and tune-up dump.

3) Accidentally un/mis-steered beam goes straight (i.e. BYD magnets fail) and hits the safety dump or the mirrors. The maximum credible beam power is 100 kW [13], and the corresponding maximum allowable dose is 25 rem/h.

4) A mis-steered beam of up to 100 W – 15 GeV (limited by BCS) hits directly the wall. The dose rate in those circumstances cannot exceed 400 mrem/h.

Although a depth of up to 13’ has been reserved for the FEE2-EH2 wall, experience from the LCLS-I FEE-NEH wall (which shields for comparable radiation sources) indicates that, if 1’ thick iron safety dumps / collimators are placed far enough from the wall (i.e. 15 m upstream or more), then the wall thickness that we can expect may be in the order of 3 to 5 feet of iron followed by 3’ of concrete, or equivalent. The exact dimensions compatible with the above conditions are being optimized through detailed Monte Carlo calculations as locations of sources and components are being more accurately defined.

14.6.2 Access maze to the FEE2 from the EH2

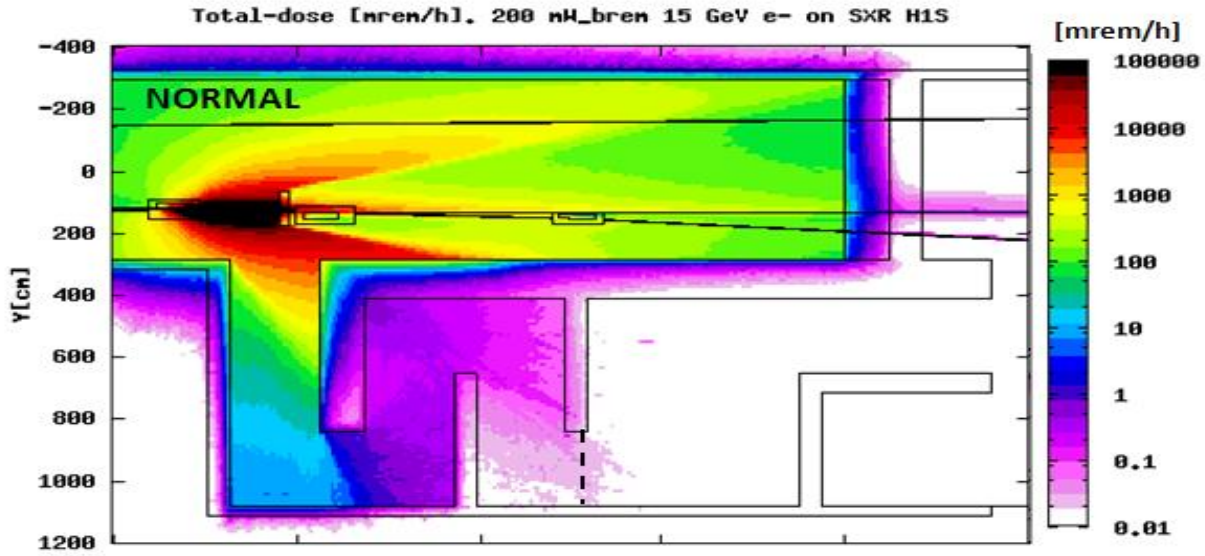

Figure 14.16. Top view dose rate map for 200 mW 15 GeV losses on M1S.

An access access maze to the FEE2 has been designed with a width of 96" (necessary to carry certain type of equipment between the FEE2 and EH2) and 10' high celing. In order to reduce the direct leakage of neutrons to the maze, the common wall between the maze and the FEE2 and the first perpendicular wall should be 4' thick. The other walls of the maze are 2' thick. Simulations were performed for normal losses (200 mW of 15 GeV Bremsstrahlung hits the first mirror) as well as for the accident case were 100 kW of 15 GeV electrons are first intercepted at the safety dump. Both cases were simulated at the SXR line because it is closer to the maze and therefore provides the worst possible results. Moreover, the current location of the M1S mirror and SXR Safety Dump, placed at the mouth of the maze also represent also the worst scenarios in terms of maze design.

Figure 14.16 displays the dose rate map at the beam-lines plane for normal losses. The dose rate at the PPS gate is in the order of 0.02 mrem/h for 200 mW Bremsstrahlung irradiation of the M1S mirror, simulations also show how for accidental 100 kW 15 GeV electron beam hitting the SXR safety dump, the dose rate at the PPS gate would just reach 2-3 rem/h. Both numbers are below their respective limits of 0.05 mrem/h and 25 rem/h. Therefore the FEE2-EH2 maze design seems adequate from the radiological perspective. A beam shut-off ion chamber will be installed at the PPS gate in the maze to detect abnormal dose rates at that location.

14.7 Experimental Halls

The instruments and the hutches downstream of the EH2 wall are not in the scope of LCLS-II CDR. The material referring to those systems is only given for informational purposes.

The hard X-ray hutch shielding requirements will be evaluated based on the reflectivity spectrum of the hard x-ray mirror and the reduction in spontaneous photon intensity provided by the FEE2 collimators. Calculation tools and experience gained in the design of beam lines, hutches and instruments for LCLS-I [34] [35] [36] [37] [38] [39] and LUSI will be used to design the shielding for LCLS-II photon beam lines and hutches.

The collimator and stopper requirements will need to be evaluated for the new FEE2 optic design. Collimators incorporating air gaps will be necessary for the soft x-ray beamlines, and should be strongly considered for the hard x-ray beamlines.

The PPS/BCS scope for the FEE2-EH2 section must include one safety beam dump with BTM for the HXR and another one for the SXR line, as well as two photon stoppers per branch line (similar to the current LCLS-I type stoppers). All stopper pairs should be equipped with an enable/disable keyswitch. The keyswitches for all stopper pairs except the pre-existing one on the SXR beamline should require two keys to enable.

The following assumes there will be two soft x-ray beamlines and two hard x-ray beamlines entering EH2: The 2 soft x-ray instruments, AMO and SXR, will be in an open hall, which will need *Hutch Protection Systems*. The systems should be independent for each of these instruments. They will have at a minimum vacuum interlocks (the VAT controllers and sensors will move over with the existing instruments) and On Line/ Off Line panels, lights, etc.

Each beamline in EH2 will need a vacuum interlock. Collimators (generally containing B4C and an air gap) and other passive BCS elements will be needed for each beamline. EH2 will require 4 BSOICs.

14.8 Radiological Environmental Considerations

The radiological environmental issues for LCLS-II are similar to those considered for LCLS-I.

14.8.1 Skyshine to Public

Various components along the LCLS-II could contribute radiation dose through skyshine to the public at site boundary. Analytical calculation for LCLS-I [40] shows that the dose to the MEI (Maximally Exposed Individual) from BC2 operation is about 2×10^{-5} mrem/y, assuming that 1 W of beam will park on CE21 for 365 days per year. On the other hand, beam loss at BTH PPS stopper D2, single beam dump TDKIK, undulator tune up dump TDUND and main dump during undulator complex operation could result in a maximum radiation dose of 0.4 mrem/year to the public at site boundary through skyshine [41].

14.8.2 Air Release to Environment

Radioactive gas, ^{15}O, ^{13}N, ^{11}C, and ^{41}Ar, will be generated from electron beamline operation. The gas could be released to environment during access and ventilation. SLAC has been using the EPA approved code CAP88-PC to calculate potential Effective Dose Equivalent (EDE) to individuals and to the population from the estimated airborne radioactivity released by SLAC electron beamline operation. Based on conservative estimates, the EDE to the Maximally Exposed Individual (MEI) of the off-site general public due to releases of airborne radioactivity at SLAC from CY09 operation was 8.3×10^{-4} mrem [42]. This mainly is from LCLS-I operation. The MEI from CY09 operation is well below the regulatory limit which requires releases to be limited so that no member of the public receives a dose in excess of 10 mrem/yr. The MEI location that corresponds to the highest calculated EDE for releases in CY09 is at the north end of SLAC, on Sand Hill road, about 350 meters from Sector 28. The maximum dose from a single release point is 5.4×10^{-4} mrem/yr (from the BSY release point) which is less than the 0.1 mrem/y limit for continuous monitoring requirement. LCLS-I and LCLS-II could be in operation at the same time, the EDE to the MEI of the off-site general public due to releases of airborne radioactivity at SLAC and the maximum dose from a single release point still are well below the limits if these estimated doses are increased by a factor of two.

14.8.3 Groundwater and Soil Activation

The 5 kW electron beam dump should be designed to meet the limits and to minimize the environmental impact. The radiation activation to soil and ground water around the LCLS-I electron beam dump has been analyzed through Monte Carlo simulations by MARS15 [21]. By adopting the dump design from LCLS-I, the activation levels of soil and ground water around the LCLS-II electron beam dump are:

- The maximum saturated activation of ^{3}H and ^{22}Na in soil around the electron beam dump is 0.03 and 0.07 Bq/g.
- The maximum saturated activation of water is 8300 pCi/L, which is less than the EPA drinking water limit of 20000 pCi/L.

14.9 References

1. ES&H Division, *Radiological Control Manual*, SLAC-I-720-0A05Z-001-R005, SLAC National Accelerator Laboratory, Menlo Park, CA, 2010.
2. ES&H Division, *Radiological Safety Systems*, SLAC-I-720-0A05Z-002-R003, SLAC National Accelerator Laboratory, Menlo Park, CA, 2010.
3. S.H. Rokni, A. Fassò, S. Mao, and H. Vincke, *Radiation Safety Aspects of the Linac Coherent Light Source Project at SLAC*, Radiation Measurement, Vol. **41**(S2): S247-S251, 2006.
4. X.S. Mao, A. Fassò, N. Nakao, S.H. Rokni, and H. Vincke, *The Linac Coherent Light Source at SLAC: Radiological Considerations and Shielding Calculations*, Nuclear Instrument Method A, Vol. **562**(2): 963-966, 2006
5. M. Santana-Leitner, A. Fassò, T. Sanami, S. Mao, J. Liu, and S. Rokni, *Radiological Studies for the LCLS BTH and Undulator*, Proceedings of 8th International Topical Meeting on Nuclear Applications and Utilization of Accelerators (AccAPP'07), Pocatello, Idaho, July 30 – August 2, 2007.
6. M. Santana-Leitner, J.M. Bauer, A. Fassò, J. Liu, X.S. Mao, A. Prinz, S.H. Rokni, T. Sanami and J. Vollaire, *Commissioning of the Electron Line of the Linac Coherent Light Source: Dose Rate Measurements and Simulations*, Proceedings of 9th International Topical Meeting on Nuclear Research Applications and Utilization of Accelerators (AccAPP'09), Vienna, IAEA, May 4-8, 2009.
7. X.S. Mao, N. Nakao and A.A. Prinz, *Radiation Protection Scheme for the LCLS Injector*, Proceedings of 8th International Topical Meeting on Nuclear Applications and Utilization of Accelerators (AccAPP'07), Pocatello, Idaho, July 30 – August 2, 2007.
8. X.S. Mao, N. Nakao, A.A. Prinz and D.H. Dowell, *Shielding Requirements for Phase One of LCLS Injector Operation*, RP-05-15, SLAC National Accelerator Laboratory, Menlo Park, CA, 2006.
9. P. Emma, D. Schultz, H. Nuhn, D. Marsh and J. Galayda, *Electron Beam Loss in the LCLS*, PRD 1.1-011, SLAC National Accelerator Laboratory, Menlo Park, CA, 2008.
10. M Santana-Leitner, X.S. Mao, S.H. Rokni, and J. Vollaire, *Radiological Studies for the LCLS Beam Abort System*, Presented in Health Physics Society Midyear Meeting 2008, Oakland, CA, January 27-30, 2008.
11. M. Santana-Leitner, *Radiation Protection Studies for the Single Beam Dumper of LCLS (I), Integrity of the Single Beam Dumper and Prompt Dose Studies*, RP-07-27, SLAC National Accelerator Laboratory, Menlo Park, CA, 2007.
12. M. Santana-Leitner, J. *Vollaire, Radiation Protection Studies for the Single Beam Dumper of LCLS (II), Residual dose rate and production of radioisotopes*, RP-07-28, SLAC National Accelerator Laboratory, Menlo Park, CA, 2007.
13. X.S. Mao, H. Vincke, A. Fassò, L. Keller, and S.H. Rokni, *Shielding Requirements for the LCLS Project (Title 1),* RP-04-14, SLAC National Accelerator Laboratory, Menlo Park, CA, 2004.

14. X.S. Mao, A. Fassò, S.H. Rokni, H. Vincke and N. Nakao, *Bulk Shielding for Beam Transport Hall and Undulator Hall (Title 2)*, RP-07-07, SLAC National Accelerator Laboratory, Menlo Park, CA, 2007.
15. A. Fassò, X.S. Mao and M. Santana-Leitner, *FLUKA Calculations for LCLS Mazes and Penetrations*, RP-06-09-R1, SLAC National Accelerator Laboratory, Menlo Park, CA, 2008.
16. M. Saleski, D. Schultz, P. Emma, D. Marsh and J. Galayda, *BTH Spot shielding Requirements and Ray Trace Methodology*, PRD 1.3-025, SLAC National Accelerator Laboratory, Menlo Park, CA, 2008.
17. M. Santana-Leitner, X.S. Mao and R.F. Boyce, *Shielding and beam containment system to protect people working in FEE from the Electron Beam Being Mis-steered by Quadrupole Magnets QU33, QUE1 and QUE2*, RP-09-07, SLAC National Accelerator Laboratory, Menlo Park, CA, 2009
18. M. Santana-Leitner, *Shielding Requirements for LCLS Tune-up Dump (TDUND),* RP-RPG-080324-MEM-02 , SLAC National Accelerator Laboratory, Menlo Park, CA, 2006.
19. M. Santana-Leitner, J. Vollaire and S. Roesler, *Radiation Protection Studies for the Undulator Tune Up Dump of LCLS: Residual Dose Rate and Radiation Damage to the Electronics*, RP-08-08-R2 , SLAC National Accelerator Laboratory, Menlo Park, CA, 2007.
20. M. Santana-Leitner, A. Fassò, X.S. Mao, H.D. Nuhn, S. Roesler, S.H. Rokni and J. Vollaire, *Radiation Protection Studies for LCLS Tune-up Dump*, Presented at 11th International Conference on Radiation Shielding (ICRS-11), Pine Mountain, GA, April 13-18, 2008.
21. T. Sanami and X.S. Mao, *Shielding Design for the LCLS 5 kW Electron Beam Dump*, RP-06-15, SLAC National Accelerator Laboratory, Menlo Park, CA, 2006.
22. T. Sanami and X.S. Mao, *Radiation Safety Evaluation for Engineering Implementation of the LCLS 5 kW Electron Dump and Shielding*, RP-07-17, SLAC National Accelerator Laboratory, Menlo Park, CA, 2007.
23. T. Sanami, M. Santana-Leitner, X.S. Mao and W.R. Nelson, *Calculation of Energy Deposition Distribution and Instantaneous Temperature Rise to Design LCLS Electron Beam Dump and Stoppers*, RP-07-18, SLAC National Accelerator Laboratory, Menlo Park, CA, 2007.
24. M. Santana-Leitner and X.S. Mao, *Total Dose for Interventions at the LCLS Main Electron Beam Dump*, RP-08-14, SLAC National Accelerator Laboratory, Menlo Park, CA, 2008.
25. T. Sanami and X. S. Mao, *Safety Analysis of Safety Dump Line of the LCLS Facility with Geometries of Engineering Specification Design for NEH phase 1 Operation*, RP-07-19, SLAC National Accelerator Laboratory, Menlo Park, CA, 2007.
26. M. Santana-Leitner and X.S. Mao, *Electron Safety-Dump Ray-Trace Study validation: FLUKA tracking of mis-steered rays through the safety dump line*, RP-09-02, SLAC National Accelerator Laboratory, Menlo Park, CA, 2009.
27. J. Vollaire, A. Fassò, J.C. Liu, X.S. Mao, A. Prinz, S.H. Rokni, and M. Santana-Leitner, *Radiation Protection Aspects of the Linac Coherent Light Source Front End Enclosure*, Proceedings of Free Electron Laser Conference (FEL2009), Liverpool, UK, August 23-28, 2009.
28. T. Sanami, X.S. Mao, *Prompt Dose in the FEE of the LCLS Facility for Beam Losses at BYD, ST1 and Safety Dump*, RP-07-01, SLAC National Accelerator Laboratory, Menlo Park, CA, 2007.
29. J. Vollaire, M. Santana-Leitner, J. Liu, A. Prinz, S. Mao, S.H. Rokni, *Overview of the Radiation Safety Systems for the operation of the LCLS Front End Enclosure (FEE),* RP-09-13, SLAC National Accelerator Laboratory, Menlo Park, CA, 2009.
30. M. Santana-Leitner and A. Fassò, *Studies of Bremsstrahlung Sources in the BTH and LCLS Undulator, Irradiation of the FEE by Bremsstrahlung Beams from these Sources*, RP-07-04, SLAC National Accelerator Laboratory, Menlo Park, CA, 2007.
31. M. Santana-Leitner, *Prompt Dose Study in the LCLS Undulator. Study of the Dose during Various Loss Scenarios in the LCLS Undulator*, RP-07-05, SLAC National Accelerator Laboratory, Menlo Park, CA, 2007.

32. T. Sanami, M. Santana-Leitner and X.S. Mao, *Evaluation of Beam Loss Model in BYD and Its Effect to the Downstream Regions for the LCLS Radiation Safety Design*, RP-07-16, SLAC National Accelerator Laboratory, Menlo Park, CA, 2007.
33. M. Santana-Leitner, *Radiation Levels in FEE and NEH from Insertion Devices Review of the Dose from the BFW33*, RP-07-26, SLAC National Accelerator Laboratory, Menlo Park, CA, 2007.
34. H. Vincke, X.S. Mao, and S.H. Rokni, *Radiation Safety Analysis for the Experimental Hutches at the Linac Coherent Light Source at SLAC*, Nuclear Instrument Method A, Vol. 562(2): 963-966, 2006.
35. A.A. Prinz, *Shielding for Soft X-ray Beamlines in the LCLS NEH*, RP-08-13, SLAC National Accelerator Laboratory, Menlo Park, CA 25, 2008.
36. A.A. Prinz, J.C. Liu, M. Santana-Leitner, J. Vollaire, *Radiation Safety Analysis of the AMO Experiment in the LCLS NEH*, RP-09-14, SLAC National Accelerator Laboratory, Menlo Park, CA, 2009.
37. A.A. Prinz, J.C. Liu and J. Vollaire, *Radiation Safety Analysis for the SXR Soft X-ray Beamline in the LCLS NEH*, RP-10-05, SLAC National Accelerator Laboratory, Menlo Park, CA, 2010.
38. J. Vollaire, *Shielding Calculations for the Hard X-Ray Beamline of the LCLS*, RP-09-15, SLAC National Accelerator Laboratory, Menlo Park, CA, 2009.
39. J. Vollaire, J.C. Liu and A.A. Prinz, *Radiation Safety Analysis for the Operation of the XPP instrument without Focusing Lenses in Hutch 3 of the NEH*, RP-10-08, SLAC National Accelerator Laboratory, Menlo Park, CA, 2010.
40. A.A. Prinz and X.S. Mao, *Radiation Safety Analysis for BC2 Chicane in Sector 24*, RP-07-24, SLAC National Accelerator Laboratory, Menlo Park, CA, 2007.
41. X.S. Mao and M. Santana, *Direct Radiation Dose to the Public at Site Boundary through Skyshine from the LCLS Undulator Complex Operation*, RP-RPG-081014-MEM-01, SLAC National Accelerator Laboratory, Menlo Park, CA, 2008.
42. SLAC 2009 NESHAP Report, SLAC National Accelerator Laboratory, Menlo Park, CA, 2009.

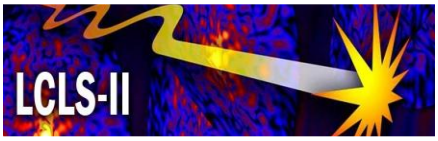

15 Work Breakdown Structure

Technical Synopsis

The Work Breakdown Structure (WBS) is used for defining work packages and developing and tracking the cost and schedule for the project. The WBS breakdown is product-oriented, to the extent possible. To the extent possible, WBS elements are defined to correspond to a well-defined deliverable objector subtask with a well-defined, relatively short time interval for performance. Finite-duration, finite scope WBS elements are, of course, easier to status without ambiguity.

WBS_#	WBS Name	Extended Definition
1	LCLS Project - PED and Construction	This summary WBS covers the Total Estimated Cost (TEC) Estimate for the LCLS II Project being constructed at SLAC. The LCLS II TEC is supported through Project Engineering and Design (PED) and Construction funds by the U.S. Department of Energy.
2	LCLS-II (Other Project Costs, OPC)	This summary WBS covers the Other Project Cost (OPC) Estimate for the LCLS II Project being constructed at SLAC. The LCLS OPC is supported through Research & Development (R&D), Spares and Commissioning funds by the U.S. Department of Energy.
1.01	LCLS Project Mgmt, Planning and Admin	This summary WBS covers the project management, planning and organization function of the PED and construction phases (TEC) of the LCLS II Project.
1.02	Injector System	This WBS defines the Total Estimated Cost (TEC) of the LCLS II electron injector system.
1.03	Linac System	This summary WBS defines the LINAC portion of the LCLS-II project. It includes all elements required to accelerate, transport and control the electron beam. It also includes elements required to dump the electron beam. It does not include any conventional facilities.
1.04	Undulator System	This summary WBS defines the Undulator systems portion of the LCLS-II project. It includes all elements to generate the FEL radiation, the undulators, and to transport, montor and control the electron beam through the undulator systems. It does not include the electron beam dump or any conventional facilities.
1.05	X-Ray Transport and Diagnostic Systems (XTOD)	This summary WBS defines all the project elements required to deliver and diagnose the x-ray beams from the end of the undulator to the experimental hall.
1.06	X-Ray Experimental Stations (XES)	This summary WBS defines all the project elements required to move the existing soft x-ray instruments from the NEH and support basic operation.

1.07	Global Interface Systems	This summary WBS defines all the project elements required for global technical support. This category includes global items whose functions are interconnected, distinguishing them from items used everywhere but which require no global interaction or correlation
1.09	Conventional Facilities	The Conventional Facilities for the Linac Coherent Light Source II (LCLS-II) will include all major systems and subsystems contained herein that will be required to support the LCLS-II programmatic requirements. The scope of the WBS will include 11 elements: Sector 10 Injector Facilities, Linac Upgrades, Research Yard Modifications, Beam Transport Hall 2, Front End Enclosure 2, Electron Beam Dump 2, Experimental Hall 2, Undulator Hall 2, BTH Service Building, UH Service Building, and Auxiliary Utility Plant.
2.01	Conceptual Design	This summary WBS covers the Other Project Cost (OPC) Estimate for the LCLS Project being constructed at SLAC. The LCLS OPC is supported through Research & Development (R&D) and Commissioning funds by the U.S. Department of Energy.
2.02	Validation and Verification	This WBS element covers commissioning costs for Injector Systems, Linac Systems, Undulator Systems, FEE, XTOD Systems and End Station Systems
1.01.01	Project Management	This summary WBS describes the project management function for the LCLS ii project at SLAC.
1.01.02	Environment Safety and Health - QA	This summary WBS describes the ES&H support for the LCLS II project at SLAC.
1.01.03	Technical Integration	This summary WBS describes the technical integration effort for the LCLS Project. These integration tasks are technical activities or tasks that support the global effort for the LCLS II.
1.02.01	Injector System Management & Integration	This WBS defines the TEC for management and integration engineering ot the LCLS II electron injector system.
1.02.02	Injector Technical Systems	This WBS defines the TEC for the engineering, fabrication, and installation of sub-systems for the LCLS II electron injector.

1.03.01	Linac System Management & Integration	This WBS section defines the level of effort system engineering and intergration of LCLS-II Linac (level of effort engineering and integration captures all activities required to complte and integrated function linac system but not directly statusable to specific subsystem tasks)
1.03.02	L1	This summary WBS defines all the project elements required for the initial acceleration of the electron beam after "injector" elements and before the first bunch compression region. It includes power conversion, controls, RF, magnet, diagnostic, vacuum subsystems and installation .
1.03.03	BC1	This summary WBS defines all the project elements required for the first bunch compression region for the electron beam. It includes power conversion, controls, RF, magnet, diagnostic, vacuum subsystems and installation .
1.03.04	L2	This summary WBS defines all the project elements required for the acceleration of the electron beam between the first and second bunch compression regions. It includes power conversion, controls, RF, magnet, diagnostic, vacuum subsystems and installation .
1.03.05	BC2	This summary WBS defines all the project elements required for the second bunch compression region for the electron beam. It includes power conversion, controls, RF, magnet, diagnostic, vacuum subsystems and installation .
1.03.06	L3	This summary WBS defines all the project elements required for the final acceleration of the electron beam, after the second bunch compression region. It includes power conversion, controls, RF, magnet, diagnostic, vacuum subsystems and installation .
1.03.07	Linac Bypass	This summary WBS defines all the project elements required for transport of the electron beam to the beam conditioning region, after the final acceleration. It includes power conversion, controls, RF, magnet, diagnostic, vacuum subsystems and installation .

1.03.08	Linac to Undulator (LTU)	This summary WBS defines all the project elements required for final conditioning of the electron beam prior to passing through the undulators, after the beam transport region. It includes power conversion, controls, RF, magnet, diagnostic, vacuum subsystems and installation .
1.03.09	Electron Dump (EBD)	This summary WBS defines all the project elements required to separate the electron beam from the FEL and safely dump it, after passing through the undulators. It includes power conversion, controls, RF, magnet, diagnostic, vacuum subsystems and installation .
1.04.01	Undulator System Management & Integration	This summary WBS defines undulator systems specific management and integration of the undulators systems at both SLAC and LBNL.
1.04.02	Undulator development and procurement at LBNL	This summary WBS defines undulator systems management and procurment at LBNL.
1.04.03	Hard X-ray Undulator System (HXU)	This summary WBS defines the costs for developing, producing and installing the vacuum systems, diagnostics, electron optics and the Hard X-ray Undulators (HXU) systems.
1.04.04	Soft X-ray Undulator System (SXU)	This summary WBS defines the costs for developing, producing and installing the vacuum systems, diagnostics, electron optics and the Soft X-ray Undulators (SXU) systems.
1.04.05	Development Common Undulator Systems	Summary WBS for engineering, protoyping and testing of common undulator system elements.
1.05.01	XTOD System Management & Integration	This summary WBS defines the project management and integration effort required for the design, fabrication, and installation of the XTOD technical systems.
1.05.02	XTOD Technical Systems	Summary WBS for the XTOD Technical Systems. The engineering, design, fabrication and installation of all components.
1.06.01	XES System Management & Integration	This summary WBS defines the project management and integration effort required for the design, fabrication, and installation of the XES technical systems.

1.06.02	XES Technical Systems	This summary WBS defines the technical systems required to move, install, and support the operation of the soft x-ray endstations that are transferred from the NEH.
1.07.01	Global Interface Systems Management and Integration	This element will provide the overall management and integration for Global Interface systems
1.07.02	Technical Systems	This summary WBS defines all the project elements required for global technical support. This includes the Personnel Protection System, the Beam Containment System backbone, the Machine Protection System backbone, the Timing System, the Network System, Centralized Computing Infrastructure, the Fast Feedback Infrastructure, General Software Support Infrastructure, and the management of the above. In addition, this WBS includes Cable Plant Installation, Design and Management.
1.09.01	CF System Management and Integration	This element will provide the overall project management to implement and integrate the design, construction, commissioning and close-out for all phases of the project related to conventional facilities.
1.09.03	Sector 10 Injector	This element will provide the requirements for Sector 10 Injector Facilities including the removal and rebuild/relocate Alcove Pump Room; RF Hut at approximately 2000 square feet; Alcove modifications to include a new Laser Room, Load Lock Room and Control Room.
1.09.05	Beam Transport Hall	The expanded Beam Transport Hall commences from the end of the existing BTH Headhouse and extends approximately 165 meters across the Research Yard. The expansion of the BTH will have roughly a trapezoidal footprint as the structure widens across the Research Yard to the Undulator hall tunnel.

1.09.06	BTH - Service Building	Service Buildings are included as pre-engineered buildings and are part of the Beam Transport Hall. The building components include the metal frame, exterior cladding, HVAC and electrical. There are two service buildings included in this element.
1.09.07	Linac Facility Upgrade	This element provides the LINAC upgrades required to support primarily the Sector 10 Injector Facility. The major elements are extending existing power to the Sector 10 Alcove building and modifications to the cooling water distribution for the technical systems
1.09.08	Undulator Hall	The Undulator Hall (UH) shall be a tunnel commencing from the downstream end of the Beam Transport Hall thermal barrier. It shall extend 170 meters in the direction of the beam to the downstream end of the UH where it shall be enclosed by another physical thermal barrier separating the UH from the Beam Dump/Frond End Enclosure. The UH will contain undulator magnets and associated equipment as it continues the electron beam to the Front End Enclosure and Beam Dump. The interior dimensions are 4.5 meters (width) by approximately 4.0 meters (height). Access into the UH will be through an entry provided from the Beam Transport Hall. The UH shall be provided with heating, cooling, and ventilation system. The floor elevation shall be maintained at 249.38’ and will remain constant throughout the entire LCLS facilities.
1.09.09	Undulator Hall Service Building	Service Building included as a pre-engineered building and is part of the Undulator Hall. The building components include the slab, metal frame, exterior cladding, HVAC and Electrical.

1.09.10	Research Yard Modifications	This element will provide the various activities required by SLAC and a general contractor (GC) within the existing SLAC Research Yard. Some of the buildings that may be affected as a result of the LCLS project are building 211, various storage containers and relocation of utilities, compressed gas tanks and metal stairs in preparation for major construction activities.
1.09.11	Electron Beam Dump	This facility is an underground concrete cast in-place facility used to absorb the electron beams. Two beam dumps wells will be constructed; one for each planned electron beam line. The beam dump device and shielding will be installed by SLAC and are not a part of this scope.
1.09.12	Front End Enclosure	The Front End Enclosure (FEE) shall contain various diagnostic beam line components to separate and distribute the x-ray beams. The FEE shall contain the appropriate shielding wall that will allow the x-ray beam(s) to continue into the Near (South) Experimental Hall and experiment components further downstream.
1.09.13	Experimental Hall 2	The Experimental Hall 2 (EH2) is a two-story structure (primarily below grade) that will begin downstream of the FEE and will extend approximately 60 meters in the direction of the beam. The primary function of the EH2 is to house four experimental areas, control rooms, laser labs and set-up space for experiments. The EH2 will be approximately 30 meters wide and 12 meters high, with a second floor above the experimental floor dedicated to the laser lab and set-up, conference and utility rooms.
1.09.14	Auxiliary Utility Plant (AUP)	The Auxiliary Utility Plant (AUP) includes a single level steel structure with metal panel cladding and metal standing seam roof assembly. Interiors include light gauge metal studs and painted drywall. The AUP will supplement the existing Central Utility Plant and provide electrical, boilers, HVAC, water and compressed air services.

2.01.01	Management & Mgmt Support	Project Management support of conceptual design phase
2.01.02	Management Support Subcontracts	This WBS covers the production of Conceptual Design Report (CDR) and technical activities supporting LCLS II conceptional design
2.01.03	Cost Review Preparation - Injector	This WBS covers conceptuall LCLS II Injector design and cost estimating
2.01.04	Cost Review Preparation - Linac	This WBS covers conceptuall LCLS II LINAC design and cost estimating
2.01.05	Cost Review Preparation - Undulator	This WBS covers conceptuall LCLS II Undulator design and cost estimating
2.01.06	CD1 cost review prep: XTOD	This WBS covers conceptuall LCLS II XTOD design and cost estimating
2.01.07	CD1 cost review prep: End Station Systems	This WBS covers conceptuall LCLS II End station systems design and cost estimating
2.01.08	CD1 cost review prep: Conventional Facilities	This WBS covers conceptuall LCLS II Coventional Facilities design and cost estimating
2.01.12	Measurement support of variable undulator	This WBS covers measurement of prototyping of variable gap undulator
2.01.14	FY10 Conceptual Design Actual Costs	These are actual cost accrued in fiscal 2010 for work done in preparation for CD1 (i.e. preliminary layout of new tunnel, cost estimating of systems, etc)
2.02.01	Validation and Verification	This WBS element covers commissioning costs for Injector Systems, Linac Systems, Undulator Systems, FEE, XTOD Systems and End Station Systems.

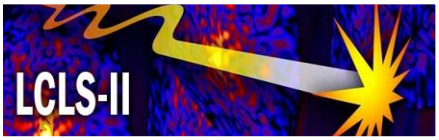

16 Parameter Tables

Technical Synopsis

This chapter provides a summary of the system parameters.

16.1 Major System Parameters

16.1.1 Major System Parameters - Overview

16.1.1.1 Major System Parameters - Overview - Electron Beam at Undulator Entrance

Parameter Name	Low e-Energy	All e-Energies	High e-Energy	Range	Unit
Electron energy	4.2		13.5	4.2 – 15	GeV
Electron bunch charge	250		250	10 – 1000	pC
Pulse repetition rate		120		1 – 120	Hz
Number of electron bunches per RF pulse		1		1 – 2	
Electron normalized rms *slice* emittance		0.6		0.1 – 1.2	µm
Electron normalized rms *projected* emittance		0.9		0.1 – 1.6	µm
Final peak current	3000		3000	500 – 5000	A
Electron normalized rms *slice* energy spread		1.4		0.1 – 1.5	MeV
Electron norm. rms *projected* energy spread		2		0.7 – 70	MeV
Max. avg. $e^{\square}$ power (15 GeV, 1000 pC/pulse)		1.8		0.04 – 1.8	kW
FWHM bunch length	83		83	50 –500	fs

16.1.1.2 Major System Parameters - Overview – Undulator System

Parameter Name	Low e-Energy	All e-Energies	High e-Energy	Range	Unit
Number of Undulators		2			

16.1.1.3 Major System Parameters - Overview - HXR Undulator Parameters

Parameter Name	Low e-Energy	All e-Energies	High e-Energy	Range	Unit
Undulator type		Planar Variable Gap PM Hybrid			
Magnet material		$Nd_2Fe_{14}B$			
Wiggle plane		horizontal			
Period length, λ_u		32			mm
Undulator gap (active)	12.9 – 20.4		7.2 – 10.3	0.0002 – 20.4	mm
Undulator gap (inactive)		100			mm
Number of periods		106			
Number of poles		212			
Segment length		3.400			m
Break length		1.00			m
Quadrupole spacing (center-to-center)		4.400			m
Undulator parameter, K (active)	0.80 – 1.8		2.5– 3.8	0.80 – 3.8	
Number of undulator segments		32			
Total magnetic undulator length		108.800			m
Total length		139.800			m

16.1.1.4 Major System Parameters - Overview - HXR FEL Output

Parameter Name	Low e- Energy	High e- Energy	Range	Unit
FEL parameter (1D)	7.1 – 17	4.0 – 5.9	4.0 – 17	10^{-4}
FEL parameter (3D)	2.5 – 6.8	2.6 – 4.0	2.5 – 6.8	10^{-4}
Power gain length (3D)	1.2 – 5.6	3.5 – 5.5	1.2 – 5.6	m
Saturation length incl. breaks	25 – 98	66 – 102	25 – 102	m
Peak saturation power	0.77 – 9.9	7.3 – 14	0.77 – 14	GW
Fundamental photon energy	0.821 – 4.11	8.10 – 12.5	0.6 – 13.1	keV
Peak photon flux	0.17 – 8.0	0.26 – 0.84	0.17 – 8.0	10^{10} Ph/fs
Peak brightness	0.11 – 0.20	5.0 – 6.2	0.11 – 6.2	10^{32} *
Projected rms photon band width	0.25 – 0.28	0.086 – 0.092	0.025 – 0.28	%
Waist size at saturation (FWHM)	37 – 46	25 – 27	25 – 46	μm
Far field divergence at sat (FWHM)	4.6- 15	1.7 – 2.5	1.7 – 15	μrad

* Ph./s/mm^2/mr^2/0.1%bw

16.1.1.5 Major System Parameters - Overview - SXR Undulator Parameters

Parameter Name	Low e- Energy	All e- Energies	High e- Energy	Unit
Undulator type		Planar Variable Gap PM Hybrid		
Magnet Material		$Nd_2Fe_{14}B$		
Wiggle plane		horizontal		
Period Length, λ_u		62		mm
Undulator gap (active)	16.4 – 35.5		7.2 – 13.6	mm
Undulator gap (inactive)		100		mm
Number of periods		61		
Number of poles		122		
Segment length		3.400		m
Break length		1.00		m
Quadrupole spacing		4.400		m
Undulator parameter, *K*	1.19 – 3.86		5.84 – 9.9	
Number of undulator segments		18		
Total magnetic undulator length		61.200		m
Total length		78.200		m

16.1.1.6 Major System Parameters - Overview - SXR FEL Output

Parameter Name	Low e- Energy	High e- Energy	Range	Unit
FEL parameter (1D)	15 – 31	12 – 17	1.6 – 31	10^{-4}
FEL parameter (3D)	8.4 – 21	9.1 – 13	8.4 – 21	10^{-4}
Power gain length (3D)	1.2 – 3.0	2.0 – 2.8	1.2 – 3.0	m
Saturation length incl. breaks	29 – 67	50 – 67	29 – 67	m
Peak saturation power	4.4 – 14	25 – 33	4.4 – 33	GW
Fundamental photon energy (provided)	0.25 – 1.2	0.63 – 1.7	0.25 – 2.0	keV
Peak photon flux	2.2 – 34	8.8 – 33	2.2 – 34	10^{10} ph/fs
Peak brightness	0.082 – 0.20	2.3 – 0.89	0.082 – 2.3	10^{32} *
Projected rms photon bandwidth at saturation[§]	0.32 – 0.37	0.12 – 0.15	0.12 – 0.37	%
Waist size at saturation (FWHM)	38 – 50	36 – 42	36 – 50	µm
Far field divergence at sat (FWHM)	9.1- 44	8.9 – 21	8.9 – 44	µrad

* Ph./s/mm^2/mr^2/0.1%bw, [§]for under-compressed electron bunch

16.2 Photo-Injector

16.2.1 Photo-Injector - Gun-Laser

16.2.1.1 Photo-Injector - Gun-Laser - Subsystem

Parameter Name	Low e$^-$ Energy	High e$^-$ Energy	All e$^-$ Energies	Unit
Oscillator			CW mode-locked	
Oscillator pump			Frequ.-doubled CW Nd:YAG laser	
Amplifier			Ti:sapphire	
Amplifier pump			Nd:YAG or YLF	
Output wavelength (IR)			758	nm
Freq, tripled wavelength (UV)			253	nm
Max. pulse repetition rate			120	Hz
No. of micropulses			1	
Maximum micropulse energy on cathode			250	µJ
Laser pulse diameter on cathode			1.2	mm
FWHM UV pulse length			5	ps
Longitudinal pulse form			Gaussian	
Longitudinal homogeneity on cathode (peak-to-peak)			<10	%
Transverse pulse form			uniform	
Transverse homogeneity on cathode			<15	%
RMS pulse-to-pulse energy jitter			<2	%
RMS pulse-to-pulse phase stability			<0.2	ps
Pointing stability (rms / spotsize rms)			< 3	%

16.2.2 Photo-Injector - Gun

16.2.2.1 Photo-Injector - Gun - Subsystem

Parameter Name	Low e- Energy	High e- Energy	All e- Energies	Unit
Cathode material			Cu	
Active useable diameter of cathode			12	mm
Cathode quantum efficiency at 253 nm			4	10^{-5}
Nominal extraction field			120	MV/m
Charge per bunch			0.25	nC
Longitudinal pulse form of electron bunch			Gaussian	
FWHM electron bunch duration			5	ps
RF frequency			2856	MHz
RF pulse duration			1.3	µs
Peak rf power			10	MW
Number of cells			1.6	
Electron beam energy at exit			6.0	MeV

16.2.2.2 Photo-Injector - Gun - Gun Solenoid

Parameter Name	Low e- Energy	High e- Energy	All e- Energies	Unit
Magnetic length			19.4	cm
On-axis field			0.237	T

16.2.3 Laser Heater

16.2.3.1 Laser Heater Electron Beam

Parameter Name	Low e- Energy	High e- Energy	All e- Energies	Unit
Electron energy			135	MeV
Rms bunch length			0.62	mm
Charge			0.25	nC
Peak current			35	A

16.2.4 L-0

16.2.4.1 L-0 Electron Beam

Parameter Name	Low e- Energy	High e- Energy	All e- Energies	Unit
Initial electron energy			6	MeV
Initial rms bunch length			0.62	mm
Initial charge			0.25	nC
Initial peak current			35	A
Final electron energy			135	MeV
Final normalized emittance (projected)			0.6	µm
Final rms bunch length			0.62	mm
Final charge			0.25	nC
Final peak current			35	A

16.2.4.2 L-0 Focusing

Parameter Name	Low e- Energy	High e- Energy	All e- Energies	Unit
Focusing structure			solenoids	

16.2.4.3 L-0 RF

Parameter Name	Low e⁻ Energy	High e⁻ Energy	All e⁻ Energies	Unit
Number of linac sections			2	
RF phase at exit			0	degrees
Mean rf phase jitter tolerance			0.1	degrees
Mean rf voltage jitter tolerance			0.1	%

16.2.5 DL-1

16.2.5.1 DL-1 Subsystem

Parameter Name	Low e- Energy	High e- Energy	All e- Energies	Unit
R56			+6.3	mm
Total bend angle			35	degrees
Total length			12	m

16.2.5.2 Electron Beam

Parameter Name	Low Energy	High Energy	All Energies	Unit
Initial electron energy			135	MeV
Initial normalized projected emittance			0.6	µm
Initital total energy spread			0.07	%
Initial slice energy spread			~0.013	%
Initial rms bunch length			0.62	mm
Initial peak current			35	A
Final electron energy			135	MeV
Final normalized projected emittance			0.6	µm
Final total energy spread			0.07	%
Final slice energy spread			~0.013	%
Final rms bunch length			0.62	mm
Final peak current			35	A

16.2.5.3 Dipole Magnets

Parameter Name	Low e- Energy	High e- Energy	All e- Energies	Unit
Number of dipoles			2	
Max. deflection angle			17.5	degrees
Magnetic length			0.2	m

16.3 LINAC

16.3.1 General

16.3.1.1 S-Band Accelerator Section

Parameter Name	Low e- Energy	High e- Energy	All e- Energies	Unit
S-band rf frequency			2856	MHz
S-band klystron type			5045	
S-band acceleration gradient			19	MV/m
S-band Q			13000-14000	
S-band shunt impedance			53-60	MOhm/m
S-band mean iris diameter			23	mm
Peak S-band rf power			60	MW

Mean S-band rf power			45	kW
Length of S-band rf section (s)			3	m

16.3.1.2 X-Band Accelerator Section

Parameter Name	Low e- Energy	High e- Energy	All e- Energies	Unit
X-band f frequency			11424	MHz
X-band mean iris diameter			9.4	mm
Length of X-band rf section (s)			0.6	m

16.3.2 L-1

16.3.2.1 Subsystem

Parameter Name	Low e^- Energy	High e^- Energy	All e^- Energies	Unit
Total length			9.7	m

16.3.2.2 Electron Beam

Parameter Name	Low e- Energy	High e- Energy	All e- Energies	Unit
Initial electron energy			135	MeV
Initial normalized projected emittance			0.6	µm
Initital total energy spread			0.07	%
Initial slice energy spread			0.013	%
Initial rms bunch length			0.62	mm
Initial peak current			35	A
Final electron energy			268	MeV
Final normalized projected emittance			0.6	µm
Final total energy spread			0.66	%
Final slice energy spread			0.0065	%
Final rms bunch length			0.62	mm
Final peak current			35	A

16.3.2.3 Focusing

Parameter Name	Low e- Energy	High e- Energy	All e- Energies	Unit
Phase advance per cell			75	degrees
Number of quadrupoles			3	
Quadrupole magnetic length			0.1	m

16.3.2.4 RF

Parameter Name	Low e- Energy	High e- Energy	All e- Energies	Unit
Number of linac sections			3	
RF-Compression phase			-20	degrees
Mean rf phase jitter tolerance			0.1	degrees
Mean rf voltage jitter tolerance			0.1	%

16.3.3 L-X

16.3.3.1 Subsystem

Parameter Name	Low e^- Energy	High e^- Energy	All e^- Energies	Unit
Total length			0.6	m

16.3.3.2 Electron Beam

Parameter Name	Low e- Energy	High e- Energy	All e- Energies	Unit
Initial electron energy			268	MeV
Initial normalized projected emittance			0.6	µm
Initial total energy spread			0.66	%
Initial slice energy spread			0.0065	%
Initial RMS bunch length			0.62	mm
Initial peak current			35	A
Final electron energy			250	MeV
Final normalized projected emittance			0.6	µm
Final total energy spread			1.07	%
Final slice energy spread			0.0070	%
Final RMS bunch length			0.62	mm
Final peak current			35	A

16.3.3.3 RF

Parameter Name	Low e- Energy	High e- Energy	All e- Energies	Unit
Number of RF sections			1	
RF phase			-160	degrees
RF phase tolerance			0.5	X-band degrees
RF voltage tolerance			0.25	%

16.3.4 BC-1

16.3.4.1 Subsystem

Parameter Name	Low e- Energy	High e- Energy	All e- Energies	Unit
Compressor type			chicane	
Total length			6.535	m
R56			-46.0	mm
Transverse offset of chicane			245	mm

16.3.4.2 Electron Beam

Parameter Name	Low e^- Energy	High e^- Energy	All e^- Energies	Unit
Initial electron energy			250	MeV
Initial normalized projected emittance			0.6	µm
Initital total energy spread			1.07	%
Initial slice energy spread			0.0070	%
Initial rms bunch length			0.62	mm
Initial peak current			35	A
Final electron energy			250	MeV
Final normalized projected emittance			0.63	µm
Final total energy spread			1.07	%
Final slice energy spread			0.033	%
Final rms bunch length			0.130	mm
Final peak current			190	A

16.3.4.3 Dipole Magnet

Parameter Name	Low e⁻ Energy	High e⁻ Energy	All e⁻ Energies	Unit
Total number of dipoles			4	
Bend angle of chicane dipoles			5.27	degrees
Magnetic length			0.2	m

16.3.5 L-2

16.3.5.1 Subsystem

Parameter Name	Low e⁻ Energy	High e⁻ Energy	All e⁻ Energies	Unit
Total length of active accelerator			326	m

16.3.5.2 Electron Beam

Parameter Name	Low e⁻ Energy	High e⁻ Energy	All e⁻ Energies	Unit
Initial electron energy			250	MeV
Initial normalized projected emittance			0.63	µm
Initital total energy spread			1.07	%
Initial slice energy spread			0.033	%
Initial rms bunch length			0.130	mm
Initial peak current			190	A
Final electron energy			4.20	GeV
Final normalized projected emittance			0.63	µm
Final total energy spread			0.43	%
Final slice energy spread			0.0020	%
Final RMS bunch length			0.130	mm
Final peak current			190	A

16.3.5.3 Focusing

Parameter Name	Low e⁻ Energy	High e⁻ Energy	All e⁻ Energies	Unit
Phase advance per cell			55	degrees
Number of quadrupoles			28	
Quadrupole magnetic length			0.1	m

16.3.5.4 RF

Parameter Name	Low e⁻ Energy	High e⁻ Energy	All e⁻ Energies	Unit
Number of linac sections			109	
RF-compression phase			-32	degrees
Mean rf phase jitter tolerance			0.07	degrees
Mean rf voltage tolerance			0.07	%

16.3.6 BC-2

16.3.6.1 Subsystem

Parameter Name	Low e⁻ Energy	High e⁻ Energy	All e⁻ Energies	Unit
Compressor Type			chicane	
Total length			23.0	m
R56			-29.0	mm
Transverse offset of chicane			0.392	m

16.3.6.2 Electron Beam

Parameter Name	Low e⁻ Energy	High e⁻ Energy	All e⁻ Energies	Unit
Initial electron energy			4.2	GeV
Initial normalized projected emittance			0.63	µm
Initital total energy spread			0.43	%
Initial slice energy spread			0.0020	%
Initial rms bunch length			0.130	mm
Initial peak current			190	A
Final electron energy			4.2	GeV
Final normalized projected emittance (x/y)			1.3/0.6	µm
Final total energy spread			0.43	%
Final slice energy spread			0.036	%
Final rms bunch length			0.0072	mm
Final peak current			3000	A

16.3.6.3 Dipole Magnet

Parameter Name	Low e⁻ Energy	High e⁻ Energy	All e⁻ Energies	Unit
Number of dipoles			4	
Bend angle of chicane dipoles			2.16	degrees
Magnetic length			0.54	m

16.3.7 L-3

16.3.7.1 Subsystem

Parameter Name	Low e⁻ Energy	High e⁻ Energy	All e⁻ Energies	Unit
Total length of active accelerator			582	m

16.3.7.2 Electron Beam

Parameter Name	Low e⁻ Energy	High e⁻ Energy	All e⁻ Energies	Unit
Initial electron energy			4.20	GeV
Initial normalized projected emittance (x/y)			1.32/0.60	µm
Initital total energy spread			0.43	%
Initial slice energy spread			0.036	%
Initial rms bunch length			0.0072	mm
Initial peak current			3000	A
Final electron energy	4.2	13. 5		GeV
Final norm proj emittance (x/y)	1.3/0.6	1.3/0.6		µm
Final total energy spread	0.09	0.03		%
Final slice energy spread	0.03	0.01		%
Final rms bunch length	0.0072	0.0072		mm
Final peak current	3000	3000		A

16.3.7.3 Focusing

Parameter Name	Low e⁻ Energy	High e⁻ Energy	All e⁻ Energies	Unit
Phase advance per cell			30	degrees
Number of quadrupoles			47	
Quadrupole magnetic length			0.1	m

16.3.7.4 RF

Parameter Name	Low e⁻ Energy	High e⁻ Energy	All e⁻ Energies	Unit
Number of linac sections			182	
RF phase	-	0		degrees
Mean rf phase jitter tolerance	-	0.07		degrees
Mean rf voltage jitter tolerance	-	0.05		%

16.3.8 LTU2

16.3.8.1 Subsystem

Parameter Name	Low e⁻ Energy	High e⁻ Energy	All e⁻ Energies	Unit
Section type			4-bend	
Total length			68	
Total R56			0	mm
Number of horizontal bends			4	
Bend angle of horizontal bends			0.60	degrees
Total horizontal angle			2.4	degrees
Magnetic length of horizontal bends			2.62	m
Number of vertical bends			2	
Bend angle of vertical bends			0.136	degrees
Vertical angle			0.273	degrees
Magnetic length of vertical bends			0.4	m

16.3.8.2 Electron Beam

Parameter Name	Low e⁻ Energy	High e⁻ Energy	All e⁻ Energies	Unit
Initial electron energy	4.2	13. 5		GeV
Initial norm proj emittance (x/y)	1.3/0.6	1.3/0.6		µm
Initital total energy spread	0.09	0.03		%
Initial slice energy spread	0.03	0.01		%
Initial rms bunch length	0.0072	0.0072		mm
Initial peak current	3000	3000		A
Final electron energy	4.2	13.5		GeV
Final norm proj emittance (x/y)	1.5/0.6	1.5/0.6		µm
Final total energy spread	0.09	0.03		%
Final slice energy spread	0.03	0.01		%
Final rms bunch length	0.0072	0.0072		mm
Final peak current	3000	3000		A

16.3.9 Beam-Dump

16.3.9.1 Subsystem

Parameter Name	Low e⁻ Energy	High e⁻ Energy	All e⁻ Energies	Unit
Total length		30		m

16.3.9.2 Electron Beam

Parameter Name	Low e^- Energy	High e^- Energy	All e^- Energies	Unit
Initial electron energy	4.2	13.5		GeV
Initial normalized projected emittance (x/y)	-	1.4/0.6		µm
Initial correlated energy spread	-	~0.10		%
Initial slice energy spread	-	~0.01		%
Initial rms bunch length	-	0.0072		mm
Initial peak current	-	3000		A

16.3.9.3 Dipole Magnets

Parameter Name	Low e^- Energy	High e^- Energy	All e^- Energies	Unit
Number of vertical dipoles			3	
Magnetic length of vertical dipoles			1.4	m
Total max vertical deflection angle			5.0	degrees

16.4 Undulators

16.4.1 Both Undulators

16.4.1.1 Electron Beam at Entrance

Parameter Name	Low e^- Energy	High e^- Energy	All e^- Energies	Unit
Initial electron energy	4.20	13.30		GeV
Initial normalized projected emittance (*x*/*y*)	1.2	1.2		µm
Initial normalized slice emittance	0.6	0.6		µm
Initital total energy spread	0.09	0.03		%
Initial slice energy spread	0.031	0.010		%
Initial rms bunch length	7	7		µm
Initial fwhm bunch duration	80	80		fs
Initial pulse charge	0.250	0.250		nC
Initial peak current	3000	3000		A

16.4.2 HXR Undulator

16.4.2.1 HXR Electron Beam Optics

Parameter Name	Low e^- Energy	High e^- Energy	All e^- Energies	Unit
Focusing method			separated function	
Focusing scheme			FODO	
Quadrupole length			10	cm
Quadrupole type			electromagnetic	
Integrated focusing quadrupole gradient			2.3	T
Integrated defocusing quadrupole gradient			-2.3	T
Total length of undulator focussing lattice			140.8	m
Total number of focussing cells			16	
Focusing cell length			8.800	m
Ave beta-function	11.9	36.1		m
Max beta-function	17.3	38.4		m
Min beta-function	8.2	30.8		m

Beta-function modulation	38	10		%
Horizontal Phase advance per cell	42	13		degrees

16.4.2.2 HXR Electron Trajectory Correction

Parameter Name	Low e^- Energy	High e^- Energy	All e^- Energies	Unit
Trajectory correction scheme			quadrupole displacement	
Center distance between steering quads			4.400	m
Number of steering quadrupoles			32	
Max. transverse quad displacement			500	µm
Max. kick angle from focusing quadrupole	178	56		µrad
Max. kick angle from defocusing quadrupole	178	56		µrad
Number of carbon wire stations			0	

16.4.2.3 HXR Beam-Based-Alignment

Parameter Name	Low e^- Energy	High e^- Energy	All e^- Energies	Unit
BPM rms resolution			1	µm
BPM offsets (uncorrelated)			50	µm
BPM offsets (correlated)			300	µm
BPM mean calibration errors			10	%
BPM rms calibration errors			3	%
Quadrupole offsets (uncorrelated)			50	µm
Quadrupole offsets (correlated)			300	µm
Mean beam energy error			2	%
RMS beam energy error			0.5	%
Quadrupole mean gradient error			0.3	%
Quadrupole rms gradient error			0.3	%
Undulator pole errors			0.04	%
Mover mean calibration errors			5	%
Mover rms calibration errors			3	%
Incoming trajectory bias			10	sigma
Incoming orbit jitter			0 - 0.1	sigma

16.4.2.4 HXR Electron Beam inside Undulator

Parameter Name	Low e^- Energy	High e^- Energy	All e^- Energies	Unit
Electron beam radius (rms)	29	29		µm
Electron beam divergence (rms)	2.5	0.8		µrad
Max undulation angle	458	142		µrad
Max. pk-pk undulation amplitude	4.7	1.4		µm
Max disp. function for ideal undulator	115	36		µm

16.4.2.5 HXR Spontaneous Radiation

Parameter Name	Low e^- Energy	High e^- Energy	All e^- Energies	Unit
Peak spontaneous power per pulse	6.0	62		GW
Average spontaneous power	0.06	0.60		W

Energy loss from spont. radiation	0.0019	0.020		GeV
Rel. energy loss from spont. radiation	0.046	0.15		%

16.4.2.6 HXR Vacuum System

Parameter Name	Low e^- Energy	High e^- Energy	All e^- Energies	Unit
Vacuum chamber height OD			6	mm
Vacuum chamber wall thickness			0.5	mm
Vacuum chamber material			aluminum	
Max inner surface roughness			15	mrad
Beam pipe straightness			200	µm / 10 m
Vacuum pressure			$< 10^{-6}$	mbar

16.4.2.7 HXR Radiation Damage

Parameter Name	Low e^- Energy	High e^- Energy	All e^- Energies	Unit
Expected neutron fluence per year			$<2\times10^{8}$	n/cm^2
Neutron fluence to damage mag. face Delta B/B_(r)=0.01 %		6.4×10^{10}	n/cm^2	

16.4.2.8 HXR Temperature Stability

Parameter Name	Low e^- Energy	High e^- Energy	All e^- Energies	Unit
Tunnel temperature stability			0.1	K
Und. water systems temp. stability			0.1	K

16.4.2.9 HXR Undulator Segment Alignment Tolerances

Parameter Name	Low e^- Energy	High e^- Energy	All e^- Energies	Unit
Horizontal segment location tolerance			250	µm
Vertical segment location tolerance			100	µm
Longitudinal segment location tolerance			500	µm
Segment roll tolerance			1000	µrad
Segment yaw tolerance			50	µrad
Segment pitch tolerance			250	µrad

16.4.2.10 HXR Quadrupole Alignment Tolerances

Parameter Name	Low e^- Energy	High e^- Energy	All e^- Energies	Unit
Horizontal quadrupole location tolerance			100	µm
Vertical quadrupole location tolerance			100	µm
Long. quadrupole location tolerance			-	µm
Quadrupole roll tolerance			10	mrad
Quadrupole yaw tolerance			-	mrad
Quadrupole pitch tolerance			-	mrad

16.4.2.11 HXR BPM Alignment Tolerances

Parameter Name	Low e^- Energy	High e^- Energy	All e^- Energies	Unit
Transverse BPM alignment tolerance			50	µm

16.4.3 SXR Undulator

16.4.3.1 SXR Electron Beam Optics

Parameter Name	Low e^- Energy	High e^- Energy	All e^- Energies	Unit
Focusing method			separated function	
Focusing scheme			FODO	
Quadrupole length			10	cm
Quadrupole type			electromagnetic	
Integrated focussing quadrupole gradient			4.5	T
Integrated defocussing quadrupole gradient			-4.5	T
Total length of undulator focussing lattice			79.2	m
Total number of focussing cells			9	
Focusing cell length			8.800	m
Ave beta-function	7.9	19.5		m
Max beta-function	15.3	25.6		m
Min beta-function	2.4	15.9		m
Beta-function modulation	82	25		%
Horizontal phase advance per cell	90	25		degrees

16.4.3.2 SXR Electron Trajectory Correction

Parameter Name	Low e^- Energy	High e^- Energy	All e^- Energies	Unit
Trajectory correction scheme			quadrupole displacement	
Center distance between steering quads			4.400	m
Number of steering quadrupoles			32	
Max. transverse quad displacement			500	µm
Max. kick angle from focussing quadrupole	178	56		µrad
Max. kick angle from defocussing	178	56		µrad
Number of carbon wire stations			0	

16.4.3.3 SXR Beam-Based-Alignment

Parameter Name	Low e^- Energy	High e^- Energy	All e^- Energies	Unit
BPM rms resolution			1	µm
BPM offsets (uncorrelated)			50	µm
BPM offsets (correlated)			300	µm
BPM mean calibration errors			10	%
BPM rms calibration errors			3	%
Quadrupole offsets (uncorrelated)			50	µm
Quadrupole offsets (correlated)			300	µm
Mean beam energy error			2	%
RMS beam energy error			0.5	%
Quadrupole mean gradient error			0.3	%
Quadrupole rms gradient error			0.3	%
Undulator pole errors			0.04	%

Mover mean calibration errors			5	%
Mover rms calibration errors			3	%
Incoming trajectory bias			10	sigma
Incoming orbit jitter			0 - 0.1	sigma

16.4.3.4 SXR Electron Beam inside Undulator

Parameter Name	**Low e^- Energy**	**High e^- Energy**	**All e^- Energies**	**Unit**
Electron beam radius (rms)	24	21		µm
Electron beam divergence (rms)	3.0	1.1		µrad
Max undulation angle	1205	375		µrad
Max. pk-pk undulation amplitude	21.1	6.6		µm
Max disp. function for ideal undulator	520	162		µm

16.4.3.5 SXR Spontaneous Radiation

Parameter Name	**Low e^- Energy**	**High e^- Energy**	**All e^- Energies**	**Unit**
Peak spontaneous power per pulse	8.0	82		GW
Average spontaneous power	0.08	0.79		W
Energy loss from spont. radiation	0.0025	0.026		GeV
Rel. energy loss from spont. radiation	0.0025	0.19		%

16.4.3.6 SXR Vacuum System

Parameter Name	**Low e^- Energy**	**High e^- Energy**	**All e^- Energies**	**Unit**
Vacuum chamber height OD			6	mm
Vacuum chamber wall thickness			0.5	mm
Vacuum chamber material			aluminum	
Max inner surface roughness			0.050	µm
Beam pipe straightness			200	µm / 10 m
Vacuum pressure			< 10-6	mbar

16.4.3.7 SXR Radiation Damage

Parameter Name	**Low e^- Energy**	**High e^- Energy**	**All e^- Energies**	**Unit**
Expected neutron fluence per year			$<2\times10^{8}$	n/cm^2
Neutron fluence to damage mag. face Delta B/B_(r)=0.01 %			6.4×10^{10}	n/cm^2

16.4.3.8 SXR Temperature Stability

Parameter Name	**Low e^- Energy**	**High e^- Energy**	**All e^- Energies**	**Unit**
Tunnel temperature stability			0.1	K
Und. water systems temperature. stability			0.1	K

16.4.3.9 SXR Undulator Segment Alignment Tolerances

Parameter Name	**Low e^- Energy**	**High e^- Energy**	**All e^- Energies**	**Unit**
Horizontal segment location tolerance			250	µm
Vertical segment location tolerance			100	µm
Longitudinal segment location tolerance			500	µm
Segment roll tolerance			1000	µrad
Segment yaw tolerance			50	µrad
Segment pitch tolerance			250	µrad

16.4.3.10 SXR Quadrupole Alignment Tolerances

Parameter Name	Low e^- Energy	High e^- Energy	All e^- Energies	Unit
Horizontal quadrupole location tolerance			100	µm
Vertical quadrupole location tolerance			100	µm
Long. quadrupole location tolerance			-	µm
Quadrupole roll tolerance			10	mrad
Quadrupole yaw tolerance			-	mrad
Quadrupole pitch tolerance			-	mrad

16.4.3.11 SXR BPM Alignment Tolerances

Parameter Name	Low e^- Energy	High e^- Energy	All e^- Energies	Unit
Transverse BPM alignment tolerance			50	µm

16.5 X-Ray-Optics

16.5.1 Radiation-Source

16.5.1.1 FEL Radiation SXR at high electron beam charge (low electron beam charge)

Parameter Name	Low X-ray Energy	High X-ray Energy	All X-ray Energies	Unit
Radiation photon energy	250	2000		eV
Macropulse rep rate			120	Hz
Number of micropulses per macropulse			1	
FEL source size FWHM	47	33		µm
FEL source divergence FWHM	47	7.1		µrad
FEL source position from end of undulator	-2	-9		m
FEL bandwidth (rms) at saturation	0.26	0.18		%
250 pC operation				
Pulse duration FWHM			83	fs
to saturation, only				
Energy/FEL pulse	2.5	1.1		mJ
Number of photons/FEL pulse	35	1.7		10^{12}
with optimum taper				
Energy/FEL pulse	10	2.2		mJ
Number of photons/FEL pulse	250	6		10^{12}
20 pC operation				
Pulse duration FWHM			7	fs
to saturation, only				
Energy/FEL pulse	0.2	0.09		mJ
Number of photons/FEL pulse	5	0.25		10^{12}
with optimum taper				
Energy/FEL pulse	0.7	0.2		mJ
Number of photons/FEL pulse	20	0.5		10^{12}

16.5.1.2 FEL Radiation HXR at high electron beam charge (low electron beam charge)

Parameter Name	Low X-ray Energy	High X-ray Energy	All X-ray Energies	Unit
Radiation photon energy	2000	13000		eV
Macropulse rep rate			120	Hz
Number of micropulses per macropulse			1	
FEL source size FWHM	36	28		μm
FEL source divergence FWHM	7.5	1.5		μrad
FEL source position from end of undulator	-10	-38		m
FEL bandwidth (rms) at saturation	0.18	0.08		%
250 pC operation				
Pulse duration FWHM			83	fs
to saturation, only				
Energy/FEL pulse	0.8	0.5		mJ
Number of photons/FEL pulse	2.5	0.22		10^{12}
with optimum taper				
Energy/FEL pulse	3.4	0.9		mJ
Number of photons/FEL pulse	10	0.44		10^{12}
20 pC operation				
Pulse duration FWHM			7	fs
to saturation, only				
Energy/FEL pulse	0.06	0.04		mJ
Number of photons/FEL pulse	0.2	0.02		10^{12}
with optimum taper				
Energy/FEL pulse	0.27	0.08		mJ
Number of photons/FEL pulse	0.84	0.04		10^{12}

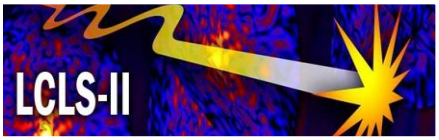

A Glossary

Technical Synopsis

This appendix is populated with acronyms/definitions used in the LCLS-II CDR.

ACM	Average Current Monitor
ACO	Anneaux Collisions Orsay, 500 MeV storage ring, LURE, Orsay, France
ACS	Access Control System
ADC	Analog to Digital Converter
ADONE	1.5 GeV storage ring, Frascati, Italy
ADS	Alignment Diagnostic System
ALARA	As Low As Reasonably Achievable
ALD	Associate Laboratory Director
ALS	Advanced Light Source (LBNL)
AMO	Atomic, Molecular and Optical Science
AMPERES 3D	Magnet Modeling Code
ANL	Argonne National Laboratory
ANSI	American National Standards Institute
API	Application Programming Interface
APS	Advanced Photon Source (ANL)
APS-U	Advanced Photon Source Upgrade
ASSET	Accelerator Structure Setup
ATF	Accelerator Test Facility (BNL)
B4C	Boron Carbide
BBA	Beam Based Alignment
BBO	BaB2O4 , Beta barium Borate
BC1	Bunch Compressor 1
BC2	Bunch Compressor 2
BC2-ED	Emittance Diagnostic Station following BC2
BCS	Beam Containment System
BER	Biological and Environmental Research
BES	Basic Energy Sciences
BESAC	Basic Energy Sciences Advisory Committee
BESSY	Berliner Elektronenspeicherring-Gesellschaft für Synchrotronstrahlung
BFW	Beam Finder Wire
BIO	SLAC Building Inspection Office
BLD	Beam Line Data
BLM	Beam Loss Monitor
BNL	Brookhaven National Laboratory
BPM	Beam Position Monitor
BSA	Beam Synchronous Acquisition
BSOIC	Beam Shut-Off Ion Chamber
BSY	Beam Switch Yard
BTH	Beam Transport Hall
BTH2	Beam Transport Hall, LCLS-II
BTHE	Beam Transport Hall East (separated from BTHW by head house)
BTHE1	LCLS-I Beam Transport Hall East
BTHE1E	East region of LCLS-I Beam Transport Hall East (separated from BTHE1W by a maze)
BTHE1W	West region of LCLS-I Beam Transport Hall East (separated from BTHE1E by a maze)
BTHE2	LCLS-II Beam Transport Hall East
BTHW	Beam Transport Hall West (separated from BTHE by head house)
BTM	Burn Through Monitor

BW	Band Width
BYD	Bend on Y-plane to Dump
CA	Channel Access
CAMAC	Computer Automated Measurement and Control
CAP88-PC	Clean Air Act Assessment Package-1988
CCD	Charge Coupled Device
CDR	Conceptual Design Report
CE21	Collimator in the middle of BC2
CEBAF	Continuous Electron Beam Accelerator Facility
CEH	Collider Experimental Hall (SLC)
CERN	Organisation Europeenne pour la Recherche Nucleaire
CESR	Cornell Electron Storage Ring
Ce:YAG	Cerium: Ytterium-Aluminum-Garnet
CLIC	CERN Linear Collider
CMLOG	Command and Message Logger
CMM	Coordinate Measuring Machine
CNC	Computerized Numerical Control
COTR	Coherent Optical Transition Radiation
COTS	Commercial-Off-The-Shelf
CPA	Chirped Pulse Amplification
CPU	Central Processing Unit
CSEM	Charge Sheet Equivalent Magnet
CSR	Coherent Synchrotron Radiation
CUD	Continuously Updating Display
CW	Continuous Wave
CXI	Coherent X-ray Imaging
D2	First PPS stopper for BTHW of LCLS-I line
D2'	First PPS stopper for BTHW of LCLS-II line
DAC	Diamond Anvil Cell
DAQ	Data Acquisition
DCI	Dispositive Collisions Igloo, LURE, Orsay, France
DDS	Direct Digital Synthesizer
DESY	Deutsches Elektronen-Synchrotron, Hamburg, Germany
DHCP	Dynamic Host Configuration Protocol
DL1	Dog Leg 1
DL2	Dog Leg 2
DMZ	“Demilitarized Zone”: a term used to refer to the intermediate controls network shared between LCLS-I and LCLS-II
DNS	Domain Name System
DOE	Department of Energy
DORIS	Synchrotron Radiation User Facility, DESY.
DPS	Differential Pumping Station
EA	Environmental Assessment
EBD	Electron Beam Dump
EDM	Extensible Display Manager (EPICS)
ED0	150 MeV Emittance Diagnostic Station following L0
ED1	Emittance Diagnostic Station following BC1

ED2	DL2 Emittance Diagnostic Station prior to the undulator
EDE	Effective Dose Equivalent
EEHG	Echo-Enabled Harmonic Generation
EGS	Electron Gamma Shower
EH2	Experimental Hall LCLS-II
ELETTRA	Synchrotron Radiation User Facility (Trieste, Italy)
ELF	Electron Laser Facility at the Livermore National Lab
EM	Electromagnetic
EPA	U.S. Environmental Protection Agency
EPICS	Experimental Physics and Industrial Control System
ESA	End Station A
ESH	Environment, Safety, Health
ESRF	European Synchrotron Radiation Facility
EVG	Event Generator
EVR	Event Receiver
EXAFS	Extended X-ray Absorption Fine Spectroscopy
FACET	Facility for Advanced aCcelerator Experimental Tests
FCM	Field Construction Manager
FEE	Front End Enclosure
FEEH	Front End Enclosure Hard X-ray
FEES	Front End Enclosure Soft X-ray
FEH	Far Experimental Hall
FEL	Free Electron Laser
FFTB	Final Focus Test Beam
FIFO	First In First Out
FLUKA	FLUctuating KAscades, a Monte Carlo radiation simulation code
FODO	Focussing-Drift-Defocusing-Drift
FONSI	Finding of No Significant Impact
FOV	Field-Of-View
FPGA	Field Programmable Gate Array
FRED-3D	An FEL Simulation Code
FW	Full Width
FWHM	Full Width at Half Maximum
FY	Fiscal Year
GENESIS 1.3	An FEL Simulation Code
GERT	General Employee Radiation Training
GINGER	An FEL Simulation Code
gpm	gallons per minute
GPS	Global Positioning System
GTL	Gun-To-Linac
HEPA	High Efficiency Particulate Air
HER	High Energy Ring
HGHG	High Gain Harmonic Generation
HH	Head House
HLS	Hydrostatic Leveling System
HOM	Higher Order Mode
HOMS	Hard X-ray Offset Mirror System

HPS	Hutch Protection System
HV	High Voltage
HVAC	Heating Ventilation And Air Conditioning
HWHM	Half Width at Half Maximum
HXR	Hard X-ray
I&Q	In-phase and Quadrature
I/O	Input/Output
ID	Inner Diameter
IE	Invariant Envelope
IEEE	Institute of Electrical and Electronic Engineers
IF	Intermediate Frequency
IG	Integrated Quadrupole Gradients
INFN	Istituto Nazionale di Fisica Nucleare
IOC	Input/Output Controller
IP	Internet Protocol
IR	Infra-Red
IRMIS	EPICS collaboration tool for tracking and reporting PV hosts and other usages
ISEMS	Integrated Safety and Environmental Management System
ISR	Incoherent Synchrotron Radiation
KB	Kirkpatrick-Baez
KEK	High Energy Accelerator Research Organization
Kr	Krypton
L0	Linac 0
L1	Linac 1
L2	Linac 2
L2	Layer-2 (as pertains to Ethernet switches)
L2-ED	Emittance Diagnostic Station at the end of L2
L3	Linac 3
L3-ED	Emittance Diagnostic Station in Sector 28 in L3
LANL	Los Alamos National Laboratory
LANSCE	Los Alamos Neutron Science Center
LBNL	Lawrence Berkeley National Laboratory
LCLS	Linac Coherent Light Source
LCLS-I	Linac Coherent Light Source I (original LCLS project)
LCLS-II	Linac Coherent Light Source II
LCW	Low Conductivity Water
LED	Light Emitting Diode
LEED	Leadership in Energy and Environmental Design
LEED AP	Leadership in Energy and Environmental Design Accredited Professional
LIAR	Linac Accelerator Research, particle tracking code.
LION	Long Ion Chamber
LITRACK	Linac Tracking, particle tracking code
LLNL	Lawrence Livermore National Laboratory
LLRF	Low Level Radio Frequency
LO	Local Oscillator
LOTO	Lockout Tagout
LSC	Longitudinal Space Charge
LSS	Laser Safety System

LUT	Linac-To-Undulator
LTU	Linac-To-Undulator
LTUH	Linac-To-Undulator Hard X-ray
LTUS	Linac-To-Undulator Soft X-ray
LURE	Laboratoire pour l'Utilisation du Rayonnement Electromagnetique, Orsay, France
LUSI	LCLS Ultrafast Scientific Instruments
LV	Low Voltage
LVDT	Linear Variable Differential Transformer
M&O	Managing and Operating
M1H	Mirror 1 of Hard X-ray Line
M1S	Mirror 1 of Soft X-ray Line
M2S	Mirror 2 of Soft X-ray Line
MAD	Multiple Anomalous Diffraction
MAD	Methodical Accelerator Design
MAFIA	MAxwell Equations with the Help of a Finite Integration Algorithm (A Family of Codes for Solving Maxwell's Equation)
MARS15	A Monte Carlo particle simulation code
MATLAB	A matrix manipulation software package available on VAX computers for computation and plotting.
MAX II	1.5 GeV Storage Ring Synchrotron Light Source, Lund, Sweden
MCC	Main Control Center, SLAC
MCFL	Maximum Credible Fire Loss
MCI	Maximum Credible Incident
MDL	Main Drive Line
MEC	Matter in Extreme Condition
MEI	Maximally Exposed Individual
Mg	Magnesium
MIT	Massachusetts Institute of Technology
MKS	Meter-Kilogram-Second (units)
MMF	Magnetic Measurement Facility
MNS	Mission Need Statement
LTUH	Linac-To-Undulator Hard X-ray
MPGR	Master Pattern Generator
MPR	Minimum Project Requirements
MPS	Machine Protection System
MUCARLO	Monte Carlo code for muon transport
MUON89	Muon transport code using analytic method
Nd:glass	Neodymium:glass
Nd:YAG	Neodymium:Ytterium-Aluminum-Garnet
Nd:YLF	Neodymium:Ytterium-Lithium-Fluoride
NdFeB	Neodymium-Iron-Boron, rare earth magnet material
Ne	Neon
NEC	National Electrical Code
NEH	Near Experimental Hall
NEPA	National Environmental Protection Act
NFS	Network File System
NIH	National Institutes of Health

NIST	National Institute of Standards and Technology
NLC	Next Linear Collider
NMIJ	National Metrology Institute of Japan
NMR	Nuclear Magnetic Resonance
NPDES	National Pollutant Discharge Elimination System
NSLS	National Synchrotron Light Source (BNL)
NTP	Network Transfer Protocol
OD	Outer Diameter
OEC	Oxygen-Evolving Complex
OFE	Oxygen Free Electrical copper
OMS	Optics Mirror System
OPA	Optical Parametric Amplifier
OPI	Operator Interface
OSHA	Occupational Safety and Health Administration
OSI	Open Systems Interconnection
OTR	Optical Transition Radiation
PAC	Phase and Amplitude Controller
PAD	Phase and Amplitude Detector
PARMELA	Phase and Radial Motion in Electron Linear Accelerators, computer tracking code.
PC	Protection Collimator
PCDS	Photon Controls and Data Systems
PCMUON	Protection Collimator for Muon
PCMUON2	Protection Collimator for Muon, LCLS-II
PEP	Positron Electron Project, SLAC
PEP-II	Positron Electron Project II (B-factory), SLAC
PETRA	Positron-Electron Tandem Ring Accelerator, DESY
PIC	Protection Ion Chamber
PIP	Project Implementation Plan
PLC	Programmable Logic Controller
PLL	Phase-Locked Loop
PLS	Pohang Light Source South Korea
PMC	Profile Monitor Chassis
PNET	Pattern Network Module
ppm	parts per million
PPS	Personnel Protection System
PRL	Phase Reference Line
PRR	Pulse Repetition Rate
PS II	Photosystem II
PSD	Photon Stimulated Desorption
PSD	Position Sensitive Detector
PSD	Power Spectral Density
PTB	Physikalisch-Technische Bundesanstalt, German National Institute of Standards and Technology
PV	Process Variable
QA	Quality Assurance
QD	Quadrupole Defocusing
QE	Quantum Efficiency

QF	Quadrupole Focusing
QIP	Quality Implementing Procedure
R&D	Research and Development
r.l.	radiation length
RCRA	Resource, Conservation, and Recovery Act
RDB	Relational Database
REC	Rare Earth-Cobalt
RF	Radio Frequency
RFBPM	Radio Frequency Beam Position Monitor
RMS	Root Mean Square
RP	Radiation Protection (Department at SLAC)
RSS	Radiation Safety System
RTEMS	Real-Time Executive for Multiprocessor Systems
RTOS	Real-Time Operating System
RW	Resistive Wall
RWG	Rectangular WaveGuide
S2E	Start-to-End
SASE	Self Amplified Spontaneous Emission
SBD	Single-shot Beam Dump
SBLC	S-Band Linear Collider (proposed, DESY)
SCORE	EPICS collaboration save & restore utility
SCSS	Spring-8 Compact SASE Source
SDL	Sub-Drive Line
Si	Silicon
SiC	Silicon Carbide
SLAC	SLAC National Accelerator Laboratory
SLC	SLAC Linear Collider
SLD	SLAC Large Detector
SLED	SLAC Energy Doubler
SMC	Stepper Motor Control
SNC	Solenoid Chassis
SOMS	Soft X-ray Offset Mirror System
SOP	Standard Operating Procedure
SOR	Synchrotron Orbital Radiation, Tokyo
SPEAR	Stanford Positron Electron Asymmetric Ring
Spring8	Super Photon Ring 8, Hyogo, Japan
SR	Synchrotron Radiation
SR	Spectral Reflectivity
SR	Strehl Ratio
SRRC	Synchrotron Radiation Research Center, Hsinchu, Taiwan
SRS	Synchrotron Radiation Source, Daresbury, England
SS	Stainless Steel
SSRL	Stanford Synchrotron Radiation Laboratory, SLAC
SSSB	Solid-State Sub-Booster
ST60	Second PPS stopper for BTHW of LCLS-I line
ST60'	Second PPS stopper for BTHW of LCLS-II line
ST61	Third PPS stopper for BTHW of LCLS-I line

ST61'	Third PPS stopper for BTHW of LCLS-II line
SUPERFISH	RF modeling code
SVD	Singular Value Decomposition
SXR	Soft X-ray
TCAV	Transverse CAVity
TCP	Transmission Control Protocol
TDA3D	3-D FEL simulation code
TDKIK	Tune-up Dump Kicker
TDKIK1	Tune-up Dump Kicker, LCLS-I
TDKIK2	Tune-up Dump Kicker, LCLS-II
TDUND	Tune-up Dump
TDUND1	Tune-up Dump, LCLS-I
TE	Transverse Electric
TED	Total Effective Dose
THz	Terahertz
Ti:Sapphire	Titanium Sapphire
TJNAF	Thomas Jefferson National Accelerator Facility
TLD	Thermo-Luminescent Dosimeter
TM	Transverse Magnetic
TPC	Total Project Cost
TROIKA	(ESRF beamline)
UCLA	University of California, Los Angeles
UDP	User Datagram Protocol
UH	Undulator Hall
UHV	Ultra High Vacuum
US	United States
UV	Ultra-Violet
VAC	Vacuum port
VACCALC	Vacuum Calculation, computer code to calculate pressures for outgassing
VAT	Vacuum seal company, Woburn, MA
VCC	Virtual Cathode Camera
VEPP-2M	Vstrechnye Electron – Positron Puchke 2M, Novosibirsk, Russia
VEPP-3	Vstrechnye Electron – Positron Puchke 3, Novosibirsk, Russia
VLS	Variable Line Spacing
VME	Versa Module Eurocard
VUV	Vacuum Ultra Violet
VXI	VMEbus eXtension for Instrumentation
Wall1	Wall between BTH and FEE of LCLS-I
Wall2	Wall between FEE and NEH of LCLS-I
WBS	Work Breakdown Structure
WCM	Wall Current Monitor
WPM	Wire Position Monitor
XAS	X-ray Absorption Scattering
XCS	X-ray Correlation Spectroscope
Xe	Xenon
XES	X-ray Emission Spectroscopy
XES	X-ray Experimental Systems

X-FEL	X-ray Free Electron Laser
XPCS	X-ray Photon Correlation Spectroscopy
XPP	X-ray Pump Probe
XPS	X-ray Photoelectron Spectroscopy
XRS	X-ray Raman Scattering
XTOD	X-ray Transport, Optics and Diagnostics
XUV	Extreme Ultraviolet
YAG	Ytterium-Aluminum-Garnet

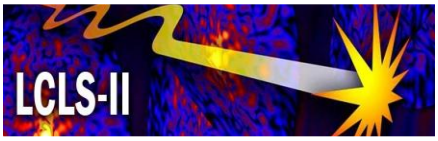

B Alternative Arrangement of Undulators

Technical Synopsis

An alternative Free Electron Laser (FEL) undulator configuration, which had been considered for LCLS-II, is a pair of linearly-polarized undulators directly in series, separated by a dog-leg transport element. In its simplest operational form, a single e- bunch produces coherent SASE radiation first in a long undulator tuned to Hard X-ray (HXR) energy (i.e., the range 2-12 keV) and then second in a following, somewhat shorter undulator tuned to a Soft X-ray (SXR) energy (i.e., the range 0.2-2 keV). The intervening dog leg changes the centerline angle between the two undulators, thus permitting the two radiation cones to be separated downstream and sent to different user stations. This appendix shows that that configuration provides very low efficiency and is not recommended. Instead, two independent undulators one HXR and one SXR are now planned for the LCLS-II project

Alternative Single Bunch drives two undulators

An alternative FEL undulator configuration, which had been considered for LCLS-II, is a pair of linearly-polarized undulators directly in series, separated by a dog-leg transport element. In its simplest operational form, a single e- bunch produces coherent SASE radiation first in a long undulator tuned to Hard X-ray (HXR) energy (*i.e.*, the range 2-12 keV) and then second in a following, somewhat shorter undulator tuned to a Soft X-ray (SXR) energy (*i.e.*, the range 0.2-2 keV). The intervening dogleg changes the centerline angle between the two undulators, thus permitting the two radiation cones to be separated downstream and sent to different user stations.

In order that this configuration work well, a number of conditions must be met: 1) The HXR undulator must be sufficiently long that "deep" saturation occurs over a reasonably broad energy range for a given electron energy. Here, "deep" saturation is defined as being ~1.5 standard gain lengths beyond saturation for nominal electron beam parameters. This ensures that the shot-to-shot fluctuations in radiation brightness at a given wavelength arising from electron beam jitter will be relatively small. 2) The induced instantaneous energy spread in the HXR undulator ($\Delta\gamma/\gamma_0 \sim \rho$ where ρ is the standard "FEL parameter") must remain sufficiently small that the SXR undulator will be long enough for deep saturation to occur over an interesting photon energy range. As is well known from simulations of multistage, FEL harmonic cascades, multi-undulator configurations become more and more sensitive to electron beam jitter as the number of stages is increased from one to two and higher.

To obtain a fuller understanding of the expected performance of the serial undulator configuration, a set of full time-dependent, particle-in-cell simulations was performed with the GINGER code [1] beginning from shot noise at the entrance to the HXR undulator ending at the exit from the downstream SXR undulator. To model the dispersion effects of the intervening dogleg, the output electron beam phase space departing the HXR undulator was sent through a strong chromatic dispersion section; such dispersion is expected in the dogleg and eliminates correlations between energy and longitudinal position. A new quiet start to the macroparticles was then applied and appropriate shot noise microbunching to the longitudinal position was added. This keeps the non-Gaussian energy distribution induced by the HXR FEL but, in principle, allows the SXR FEL to begin its SASE growth with the correct incoherent spontaneous emission (because the simulation macroparticle number is much smaller than the actual particle number. This artificial re-quieting and re-initialization of shot noise is necessary for correct random microbunching statistics).

As shown in Figure B.1, which plots output power versus photon energy, the GINGER results generally confirmed the simple Xie-model results for the upstream HXR FEL, especially at the higher energies which are not so deep into saturation. The agreement is also good for the output RMS energy spread where we have defined the predicted "MXie" output value as $\Delta\gamma = [\,(\rho_{3D}\,\gamma_0)^2 + (\Delta\gamma_0)^2\,]^{1/2}$. However, at lower photon energies, where the HXR undulator is long enough for deep SASE saturation to occur, the time-averaged output power and especially the output RMS energy spread are much larger (by 2 × or greater) than the predicted values. This phenomenon is not completely unexpected inasmuch as work by Bonifacio and collaborators [2] had predicted that following "first" SASE saturation, there is continued growth toward an asymptotic power level nearly 4× larger. Unfortunately, this continued growth has strong negative effects upon the performance of the downstream SXR undulator.

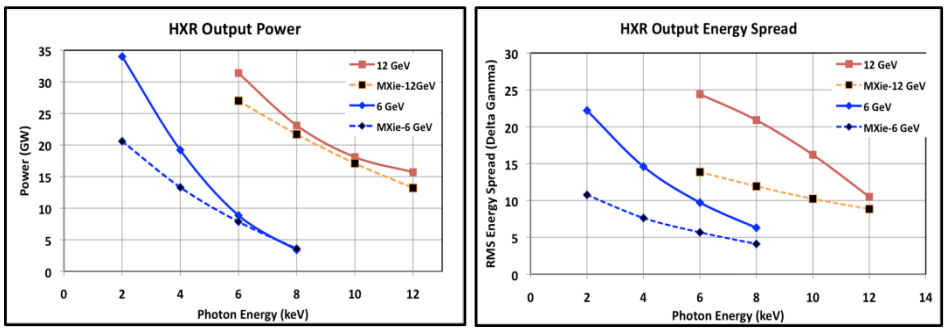

Figure B.1. Time-averaged HXR output power as a function of resonant photon energy for 6- and 12-GeV electron beam energies according to time-dependent GINGER simulations. The total undulator length was 103 m.

In Figure B.2 we plot the time-averaged, output SXR radiation power as a function of *z* for various photon energies for a 6-GeV electron beam that previously interacted in an HXR FEL operating at 2- or 6-keV photon energies. The right plot shows the same for a 12-GeV electron beam; here the HXR FEL resonant photon energy was set to 8-or 12-keV. The solid curves are from GINGER simulations while the dotted curves are produced with the Xie formalism with the input energy spread being set to the RMS value corresponding to exit at the HXR undulator. For photon energies where the SXR undulator is shorter than the predicted saturation length from the Xie formula, we have set $P_{XIE} = P_{NOISE} \times \exp(L_U / L_G)$ where P_{NOISE} = 1.5 kW, the value seen in the GINGER simulations and L_G is the 3D Xie-predicted gain length.

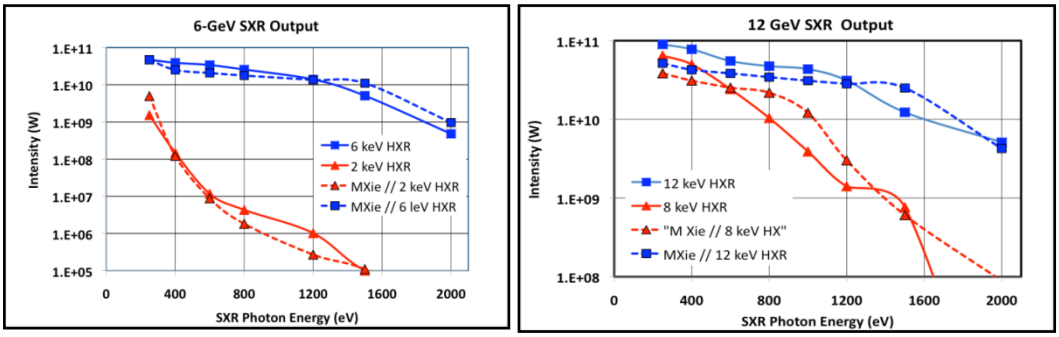

Figure B.2. Time-averaged SASE output power from the soft-x-ray undulator as a function of resonant photon energy for several HXR photon energies.

The solid curves refer to time-dependent GINGER simulations while the dotted curves are semi-analytical predictions using the Xie formalism. The figure on the left corresponds to a 6 GeV electron beam while that is for a 12-GeV beam.

One sees that for examples where the HXR undulator is operated into deep saturation (i.e., lower photon energies) with correspondingly large energy spread at exit, the SXR output (i.e., the red curves) is quite small except at the very lowest photon energies. When the HXR undulator is operated at relatively high output energies for which saturation barely occurs and where the output energy spread is approximately half as great as at the lower photon energies, the SXR FEL performs relatively well and can produce time-averaged output powers of 10 GW or larger.

Due to the strong coupling between the HXR and the SXR undulators, this option of the two undulators in series is not the baseline design.

References

1. W. Fawley, Report No. LBNL-49625, LBL, 2002.
2. R. Bonifacio *et al.,* Phys. Rev. Lett. **73**, 70 (1994).

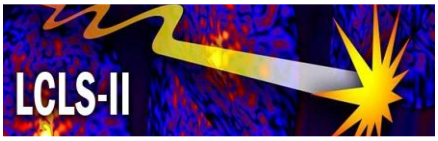

C LCLS Early Operations and Future Development

Technical Synopsis

The LCLS facility has met and exceeded project goals for brightness, tuning range, and pulse duration. Early experiments with LCLS have convincingly demonstrated the capabilities of this groundbreaking research tool. The need for a rapid expansion of LCLS has been demonstrated by both performance of the facility and overwhelming user demand for access. The existing LCLS experiment halls will be filled to capacity by 2012, with six experiment stations in operation. With a fixed-gap undulator it is of course necessary to change linac energy to obtain the desired photon energy. In addition there has been surprisingly strong user demand for frequent adjustment of the x-ray pulse duration. These combined demands for more capacity with independent control of both photon energy and pulse duration have shaped plans for the expansion of LCLS to include additional undulators, an additional independently controllable electron beam source, and space for more instruments.

LCLS-I Project, Transition to Operation and Scientific Productivity

LCLS is well on its way to realizing all the scientific capabilities envisioned in *LCLS – the First Experiments*, which described six broad areas of opportunity for research with an x-ray laser. The facility achieved its design goals in the first weeks of operation and develops new capabilities on an almost weekly basis. Essentially all the experiment techniques envisioned for LCLS-I are being tested and proven in early operation. The full suite of six experiment stations will be implemented by 2012, twenty years after the facility was conceived.

Start of the Experiment Program

The principal performance goals of LCLS-I were to produce

- X-ray pulses of 230 fs duration or shorter
- Photon energies ranging from 800 eV to 8,000 eV
- 1012 photons per pulse at 8 keV

These goals were achieved or exceeded promptly at the outset of Free Electron Laser (FEL) commissioning, in April- May 2009. This enabled a rapid and productive research program to commence with a 1,300 hour operation run, October-December 2009, during which 152 experimenters participated in 10 experiments. Productivity has continued to increase; In FY2010, 359 experimenters participated in LCLS experiments. Demand for access to LCLS continues to grow. However LCLS productivity is already limited by capacity; one in four proposals is approved.

LCLS Capabilities: Characteristics of the X-Ray Source

Rapid progress in accelerator research and accelerator commissioning has made it possible to expand LCLS capabilities well beyond LCLS-I goals. The energy produced in a single x-ray pulse has also exceeded project goals, reaching 4 mJ. The operating range of photon energies, originally specified at 800-8,000 eV, has been expanded to 500-10,000 eV, limited by the electron beam energy and the fixed period and magnetic field in the undulator; it is now known that the electron beam quality is high enough to achieve lasing at 16-20 keV.

Perhaps the most important measure by which LCLS-I has exceeded its design goals is in the duration of the x-ray pulse. The LCLS routinely operates with 80 femtosecond (fs) pulses, a duration at which it readily produces 2 mJ/pulse. Pulse duration can be readily adjusted from 4 fs to 500 fs in response to user needs. Such changes can be achieved in a matter of minutes in most cases. Generally, peak power remains constant or is increased somewhat as the pulse duration is reduced.

The ability to change pulse length has proven to be extremely important to LCLS experimenters. Control of pulse duration has made it possible to create and study double-core hole states in atoms, and to observe “bleaching” or increased transparency to x-rays resultant from depletion of inner-shell electrons. By varying pulse duration, it has been possible to confirm the feasibility of obtaining single-shot images of single virus particles even though these particles are immediately destroyed by LCLS x-rays. It has already been shown that it is possible to reconstruct, with 0.9 nm resolution, the structure of the photosystem-I protein from diffraction patterns of nanocrystals exposed to the LCLS beam. Data collection at several pulse durations is now a routine part of most LCLS experiments.

Table C.1. Typical present day LCLS operating parameters.

X-Ray Tuning Range	500 - 10,000	eV
Peak Power	up to 40	GW
Power Bandwidth, 8,000 eV	0.2 typical	% FWHM
Power Bandwidth, 800 eV	0.5 typical	% FWHM
X-Ray pulse duration	50-500	femtoseconds
Beam size at waist, 800 eV	20, typical	microns, RMS
Beam divergence, 800 eV	20, typical	microradian FWHM
Beam size at waist, 8,000 eV	15, typical	microns, RMS
Beam divergence, 8,000 eV	3, typical	microradian FWHM
Energy/Pulse	> 2 typical, 4.5 max	mJ
Pulse Energy Stability	5 typical	%
Pulse Repetition Rate	120	Hz

LCLS Operations – Capacity, Planned Growth and Operational Limitations

The LCLS-I project constructed three experiment stations in each of two experiment halls. One instrument, Atomic, Molecular and Optical Science (AMO), part of the LCLS project scope, is housed in the first station. A second instrument for soft x-ray research has been donated by a consortium, and has been operational since May 2010. Three more instruments are being constructed for research with hard x-rays as part of the LCLS Ultrafast Scientific Instruments (LUSI) equipment project. The first of the LUSI instruments began research in July 2010, and the remaining LUSI instruments will be commissioned in 2011-2012. A sixth instrument for the production and study of Matter in Extreme Conditions (MEC) will also begin its research program in 2012, at which time the LCLS experiment stations will be fully occupied.

Since LCLS-I constructed a single undulator source with fixed magnetic field, the energy of the linac must be changed to change the wavelength of the x-rays. An energy change can be accomplished in a fraction of an hour, at the request of the experimenter receiving the beam. The facility has settled into a routine in which x-rays steered to one instrument for 12 hours, and then re-tuned to support the program at another instrument for 12 hours. This has proven to be a very efficient routine for scheduling experiments. In the next few years of operations, the LCLS Facility will be operated at least 4,000 hours per year for experiments. Assuming that present practice continues and each approved experiment receives 60 hours of dedicated beam time, 67 experiments will be conducted per year. Since the size of a typical experiment team is 10-12 experimenters, the facility will host 600-700 researchers annually. This estimate assumes only one of the six instruments receives x-rays at any given time.

Lessons Learned in Early Operation

The LCLS has performed extremely well to date, and early experiments give strong evidence that the impact of LCLS science will be profound. However productivity and scientific impact will be limited by the limited access to the LCLS beam.

Not surprisingly, requests for changes in wavelength are common. In addition, however, LCLS operations experience has already shown a surprisingly high demand changes in x-ray pulse duration. It is common practice to change pulse durations once or twice a day. Changing pulse duration requires a straightforward readjustment of the electron source, which can be accomplished in 10-60 minutes.

Demand for access continues to build, and LCLS is working to develop optics that will split each x-ray pulse into two beams for true simultaneous operation of two or more instruments. It is reasonable to expect this will increase the productivity of the facility, perhaps by a factor of 2 or more, during hard x-ray operations. For soft x-ray operations however, scheduling experiments that are compatible for simultaneous running will be more difficult. Assuming a 50/50 split of operating hours between experiments that require dedicated operation of the FEL and experiments that can optically split or share the beam, it would be possible to complete 100 experiments per year; however it is too early in the hard x-ray research program to reliably predict throughput in split-beam operation; annual capacity could exceed this amount.

Priorities and Progress toward Expansion of Capability

The capabilities of LCLS-I continue to expand at a rapid pace. In the next few months and years, it will be possible to expand the photon energy range of LCLS to:

- *Extend the photon energy range to 16 keV*: Since the LCLS electron beam is considerably brighter than had been assumed in designing the undulator system, only 28 of the installed 33 undulators are required to reach maximum power for 8-9 keV x-rays. Therefore it has been possible to produce considerable x-ray power (~0.1 mJ/pulse) at 16-18 keV by means of a simple modification of the "extra" five undulators. This extended spectral range is already being tested in the x-ray pump/probe instrument.

- *Produce pulses with duration approaching 1 fs:* Two techniques for producing very short (~1fs) x-ray pulses were proposed during the design of LCLS [1,2], and both have yielded very good results during accelerator studies and in x-ray experiments. Operation with low (20 picocoulomb) charge, it has been possible to produce electron bunches shorter than 10 fs (this is presently the resolution limit of the bunch measurement diagnostics) with pulse energies of ~0.14 mJ. This configuration is used in routine operations at the request of x-ray experimenters. Using new techniques for measuring the electron bunch length, it may be possible to achieve 1 fs rms resolution. Direct measurement of the x-ray pulse length is perhaps even more important. Ongoing studies of the x-ray spectrum and development of accurate x-ray timing diagnostics will hopefully enable better understanding of the time structure of the x-ray pulse.

- P*roduce short, hard x-ray pulses with full temporal coherence;* A very attractive scheme for self-seeding short hard x-ray pulses [3] has been proposed, and will be tested in the LCLS. The scheme can be implemented without significant impact on other operating modes. Preparatory tests of compatibility with normal operations have begun, and first tests of seeding in LCLS will take place in 2012.

- *Provide polarization control:* This is an active area of theoretical and numerical FEL studies (see Appendix D). In addition, an APPLE undulator has been borrowed from SSRL for studies of magnetic field quality and reproducibility. The feasibility of using this magnet in LCLS is presently under study.

- *Provide a synchronized source of high-field pulsed THz radiation:* It is possible to pass the electron beam through a thin conducting foil, causing extremely high currents to flow the few femtoseconds during which the electrons pass. The acceleration of the electrons in the foil results in the emission of Optical Transition Radiation (OTR). With a bunch length of 10-100 fs, one can expect OTR in the frequency range 10-100 THz; however it is more useful to think of the OTR as an electromagnetic pulse with time structure similar to the derivative of the beam current. As explained in Chapter 3, there is an exciting opportunity to use OTR to produce

excitations in molecules adsorbed on catalysts, enabling study of the dynamics of catalyzed chemical reactions. SLAC researchers are presently investigating the feasibility of producing OTR pulse with electric fields in the range 0.1-1 volt per Ångstrom. If successful, these pulses can be transported to the Near Experiment Hall hutches for THz pump/x-ray probe investigations.

- *Provide two x-ray FEL pulses* (using two electron bunches), separated by a few nanoseconds, has been demonstrated. This is an enabling step toward novel techniques for pump/probe experiments with LCLS or simultaneous 120 Hz operation of multiple undulators using a single injector.

Expansion Options Anticipated in the LCLS-I Project

The LCLS-I project gave due consideration to future needs for facility expansion. Two options or stages for expansion were envisioned and integrated into the design:

- construction of an undulator system in the existing tunnel and
- construction of new tunnel and experiment hall facilities.

The LCLS-I was designed to accommodate a second undulator in its existing tunnel. The beam transport hall, undulator hall, beam dump area, and surface support buildings were sized to support the installation of a second undulator. Therefore the October 2009 proposals for LCLS-II could be carried out as a Major Item of Equipment project; no significant civil construction would be required.

To facilitate the addition of new tunnels for undulators, the upstream end of the electron Beam Transport Hall (BTH) was designed with a flare-out section to permit the addition of up to four more undulator tunnels and associated experiment halls. A concept for electron beam transport lines was developed, confirming that fan-out bends of +/- 2 degrees and +/- 4 degrees could deliver low-emittance electron beams to four or more undulator sources. The critical characteristics of the electron beam in the 2-degree lines should be virtually identical to those achieved in the LCLS today. Only minimal beam degradation is expected in the 4-degree bends. Experience with LCLS has confirmed the reliability of the computer models used to predict the characteristics of the electron beam at the output of these bends. Based on measured performance and tested predictive capability of the computer models of the FEL, it is safe to say that the LCLS facility could be expanded to house two undulator sources in each newly constructed tunnel.

References

1. P. Emma, K. Bane, M. Cornacchia, Z. Huang, H. Schlarb, G. Stupakov, and D. Walz, *Femtosecond and Subfemtosecond X-Ray Pulses from a Self-Amplified-Spontaneous-Emission-Based Free-Electron Laser*, Phys. Rev. Lett. **92**, 074801(4) (2004).
2. Y. Ding et. al. *Measurements and Simulations of Ultra-low Emittance and Ultra-short Electron Beams in the Linac Coherent Light Source*, Phys. Rev. Lett. **102**, 254801, (2009).
3. Gianluca Geloni, *Cost-effective way to enhance the capabilities of the LCLS baseline*, DESY 10-133, August 2010, http://arxiv.org/abs/1008.3036v1

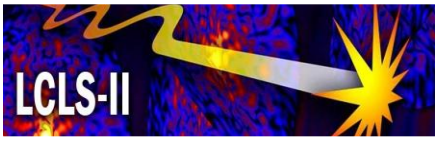

D Future Options and Upgrade Possibilities

Technical Synopsis

Several future options and upgrade possibilities to enhance the LCLS-II capabilities beyond the scope of the project are discussed. To reduce the SASE bandwidth and to control its temporal characteristics, self-seeding designs in both hard x-ray and soft x-ray wavelength ranges are considered. Four different but compatible polarization control options are described. Finally, an external echo-seeding scheme in the soft x-ray regime is presented. These options will not be implemented in the LCLS-II baseline but can be added on later with further development.

Introduction and Overview

The FEL theory related to the LCLS-II scope is described in Chapter 4. This Appendix describes future expansions and upgrades that have been considered of the LCLS-II beyond the scope of the project. The sections are organized to reflect the priorities of these options and upgrades.

Future Options and Upgrade Possibilities

Self-Seeding Schemes

As discussed in Section 1.3, radiation from a SASE FEL consists of many independent spikes in both the temporal and spectral regimes. The total number of such independent modes is estimated as $M = T/\tau_c$, where T is the electron bunch duration and τ_c is the SASE spike coherence time. Associated with each individual SASE spike is a (ω,t) phase space area that approximately satisfies the minimum value $\sigma_\omega\sigma_t \sim$ ½ corresponding to a transform-limited pulse, if one ignores the small frequency chirp within the spike developed in the FEL gain process. The SASE FEL pulse bandwidth may be taken as the coherent spike bandwidth; hence, the total phase space area of a SASE pulse is about $\sigma_\omega T \sim M\ \sigma_\omega\sigma_t \sim M/2$; *i.e.*, it is M times larger than that of a transform limited pulse. For the LCLS-II hard X-ray SASE FEL, M can be on the order of 100, *i.e.*, the SASE FEL phase space area can be 100 times larger than a transform limited pulse. For the soft X-ray, there are a few tens of spikes also. The self-seeding scheme [1] as a promising approach is to significantly narrow the SASE bandwidth and in principle to produce a nearly transform-limited pulse.

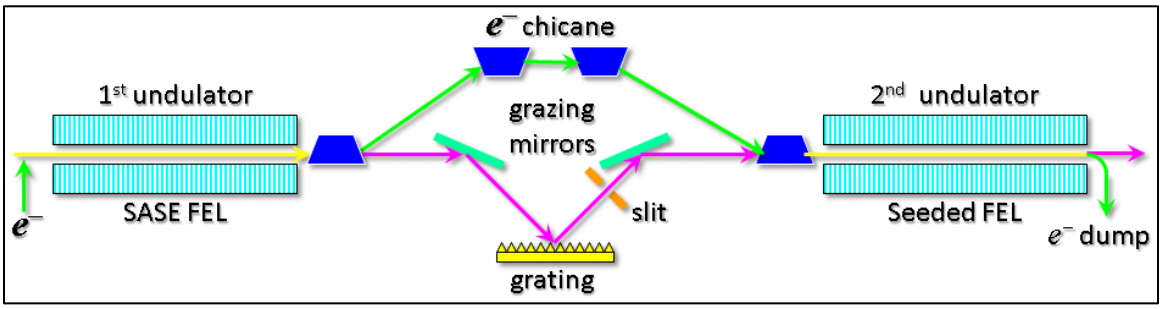

Figure D.1. Schematic plot of a self-seeding FEL, which consists of two undulator systems separated by photon monochromator and electron by-pass chicane

As shown in Figure D.1, the self-seeding scheme consists of two undulator systems separated by a photon monochromator and an electron bypass beam line, normally a 4-dipole chicane. The chicane has three functions. It provides a transverse offset for the electron beam to be separated from the photon monochromator system. The chicane also washes out the microbunching developed in the first undulator, so that no enhanced SASE will be generated from those michrobunching. The chicane is also a delay line for the electron bunch to recombine with the monochromatized photon beam. The two undulator systems are resonant to the same radiation wavelength. The first undulator has to work in the linear exponential growth regime, so that the electron bunch quality is till good enough to lase in the second undulator. The SASE radiation generated by the first undulator system passes through the narrow-band monochromator to create a transform-limited pulse for use as a coherent seed to the second undulator. Chromatic dispersion effects in the by-pass chicane will destroy the SASE-produced microbunching in the electron bunch. Following recombination with the monochromatized photon beam at the entrance of the second undulator system, the radiation is then amplified by the electron

bunch in the second undulator until FEL saturation. We discuss the implementation of self-seeding in both soft and hard x-ray lines, focusing on the highest photon energies in both beamlines.

Soft x-ray self-seeding

We use the same electron parameters as those measured for the LCLS-I 250-pC charge case. Based upon start-to-end simulation, when the electron bunch is under-compressed in BC2, we find that the electron current profile I_{pk} *(s)* exhibits double-horn structure along the longitudinal coordinate as shown in Figure D.2. Besides the peak current, there are also local structure and non-uniformity in all *6-D* phase space distribution. Detailed start-to-end simulation studies at both ends of the soft x-ray wavelength range can be found in [2]. Table D.1 summarizes the main parameters and the FEL performance.

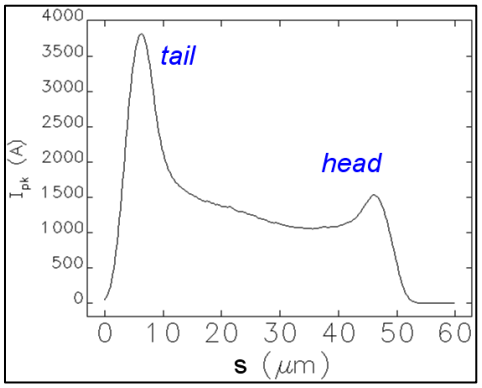

Figure D.2. A typical current profile at the undulator entrance when the electron bunch is under-compressed in BC2

Table D.1. Main pararameter for soft x-ray self-seeding at 2 keV (6 Å) and 250 eV (5 nm)

Parameter	**Symbol**	**Value**	**Units**
Electron beam energy	E	*4.3*	GeV
Normalized rms slice emittance	ε_n	*0.6*	μm
Peak current	I_{pk}	*3*	kA
FEL photon energy		*2 (0.25)*	keV
FEL Pulse temporal duration (*rms*)	σ_t	*12 (23)*	fs
FEL Pulse Bandwidth (*FWHM*)	$\Delta\omega_{FWHM}$	*5.2 (24)*	10^{-5}
Transform-Limited photon pulse bandwidth (*FWHM*)	$\Delta\omega_{FWHM}$	*4.4 (15)*	10^{-5}
Seed Power	P_{seed}	*0.1*	MW
Power into Monochromator	P_{mono}	*2000 (50)*	MW
Monochromator Efficiency	η_{mono}	*0.2 (10)*	%
Overall Efficiency	η	*5 (20)*	10^{-5}
Saturation Power	P_{sat}	*10 (5)*	GW
Saturation Length in the 2nd undulator	L_{sat}	*35 (30)*	m
Brightness Increment (compared to SASE)	R_B	*150 (50)*	

The proposed monochromator for the soft x-ray FEL is composed of rotational planar Variable-Line-Spacing (VLS) gratings [3]. A preliminary design of the gratings adopts a constant focal-point mode in order to have fixed slit location. The variation in optical delay is limited to 10% with a nominal value of 5 ps, when tuning the FEL energy. The electron by-pass chicane delays the electron bunch in order that the photon beam passing through the monochromator system recombines with the same electron bunch. The electron by-pass chicane provides a R_{56} of about 3 mm in order to match the optical delay and also smears out the SASE microbunching generated in the first undulator. The chicane is designed to not degrade the macroscopic bunch quality. The chicane including matching optics should occupy about 30 m distance. The chicane itself can be shorter than 20 m even for the highest energy and still preserve the electron bunch quality. For example, the emittance growth can be smaller than 5 %. Table D.1 shows both the monochromator efficiency (for a wide-band radiation) as well as the overall efficiency since the monochromator filters down the radiation bandwidth by 1 to 2 orders of magnitude.

The required seed power at the beginning of the second undulator (~0.1 MW) must dominate over the shot noise power within the gain bandpass, which is on the order of 1 kW. Given the overall efficiency of the monochromator $\eta = 5\times10^{-5}$ at 2 keV, in order to strongly dominate shot noise the required FEL power at the monochromator entrance has to be $P_{seed} = 2$ GW at the high-energy end of the soft x-ray spectral range. Figure D.3 shows a GENESIS [4] simulation of the power evolution in both undulators at 2 keV. Since the SASE FEL starts from random initial noise, the transmitted power after the narrow-band monochromator can have a relatively large shot-to-shot fluctuation because only one longitudinal mode is effectively passed. Hence, the second undulator must be sufficiently long to bring the FEL well into saturation in order to reduce the shot-to-shot FEL intensity fluctuation to 10 – 20 % level.

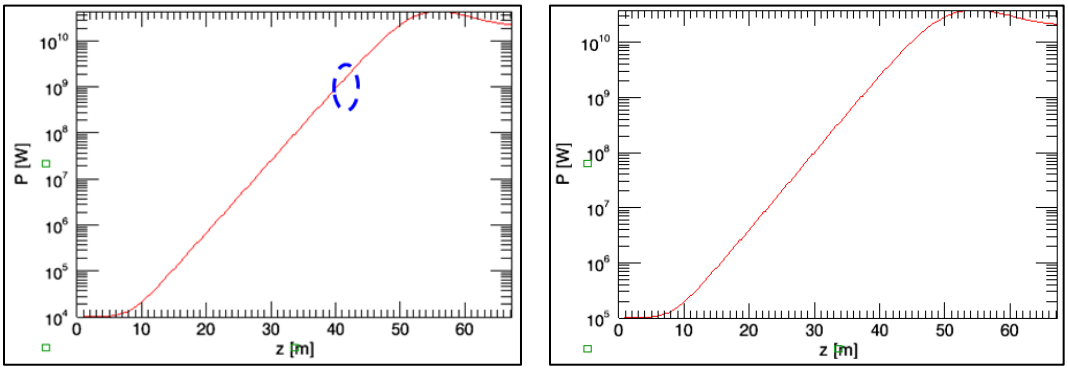

Figure D.3. (Left) SASE FEL power at 2 keV in the 1st undulator section: FEL power about 2 GW at 40 m magnetic length of the 1st undulator. (Right) The self-seeded power at 2 keV in the 2nd undulator: the FEL reaches saturation around 55 m of magnetic length

Figure D.4 shows the output FEL spectrum for both 2 keV and 250 eV photon energies starting with 0.1 MW input seed power. Such a narrow-bandwidth FEL produces nearly transform-limited x-ray pulses. A multi-layer grating could improve the overall efficiency of the monochromator by an order of magnitude, thus increasing the seed power to the second undulator by the same factor and reducing the required magnetic length.

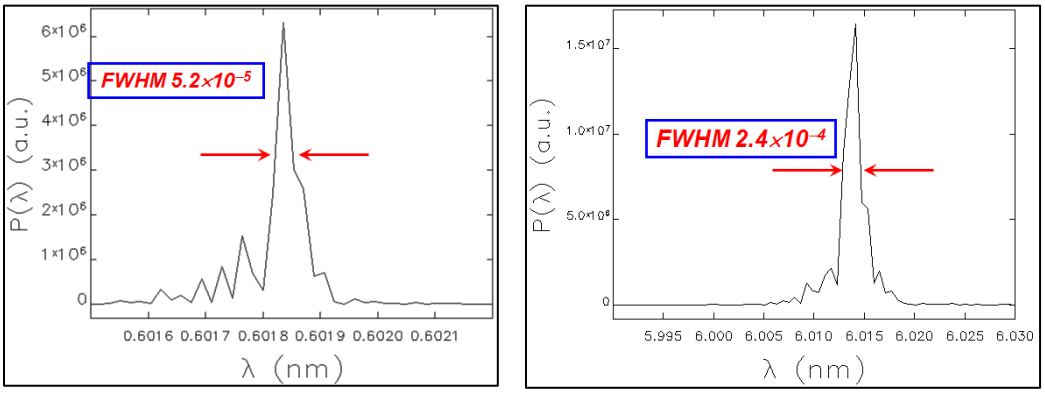

Figure D.4. (Left) The output FEL spectra at 0.6 nm (2 keV). (Right) The output FEL spectra at 6 nm (250 eV)

Hard x-ray self-seeding

For hard x-ray self-seeding, a monochromator is normally configured with crystals in the Bragg geometry. In a conventional 4-crystal monochromator, it is not easy to make the optical delay to be smaller than 2 to 3 mm; hence the high energy electron by-pass chicane must provide an R_{56} on order of 5 mm and leads to a large footprint. To avoid such a large chicane, a two-bunch self-seeding scheme has been proposed in Ref. [5] that uses the seed generated from the first electron bunch to interact with the next electron bunch that arrives at the second undulator entrance simultaneously with the optically delayed seed. Recently, a simpler and more straight-forward single bunch scheme has appeared [6] that uses the transmitted x-ray beam from a single crystal to seed the same bunch (see Figure D.5). We plan to test this new scheme in the LCLS-I and study its performance for the LCLS-II upgrade.

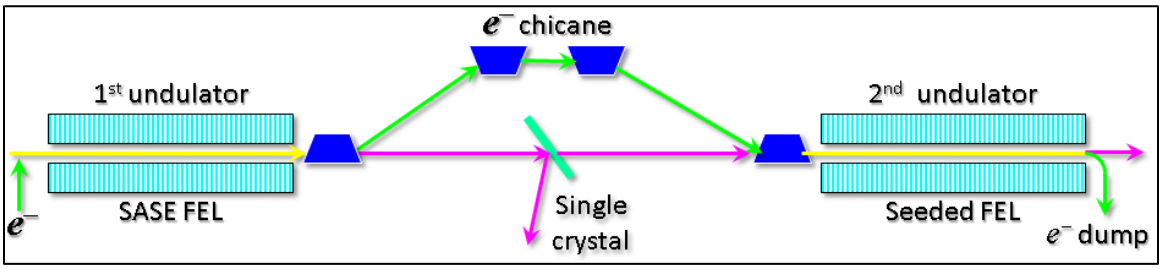

Figure D.5. Schematics of a single-crystal self-seeding scheme for hard x-ray. The single crystal is C(400) in Bragg geometry

For LCLS-II, we are examining the single-crystal self-seeding scheme in the context of the highest photon energy case (13 keV or 0.95 Å) for the HXR FEL. The electron bunch is assumed to work in the low charge mode, *i.e.*, Q = 20 pC, and a normalized emittance is ε_n = 0.4 μm instead of Q = 250 pC and ε_n = 0.6 μm as for the standard case. If the peak current is set at I_{pk} = 3 kA, then the electron bunch rms length is about σ_z~0.8 μm. For a Gaussian transform-limited FEL pulse with the same rms pulse length, the relative FWHM bandwidth for λ_{FEL}=0.95 Å, is about $\Delta\omega_{FWHM}/\omega$~$2.2\times10^{-5}$. Hence the required monochromator bandwidth should be smaller than 10^{-5}. Following Ref. [13], we use a thin (0.1-mm thickness) C(400) crystal that has a relative bandwidth ~1.0×10^{-5} as shown in Figure D.6. In that plot, the solid curve is the absolute value of the transmission function, and the dashed curve is the phase of the transmission function. The Bragg angle is set at 32 degrees for 13 keV photon energy. Due to the nearly 100% in-band reflectivity, the crystal works as a notch filter in the frequency domain for the transmitted

x-rays and generates a monochromatized wake in the time domain. The delay time of this monochromatized wake from the main FEL pulse is determined by the width of the notch filter, *i.e.*, the rocking curve of C(400).

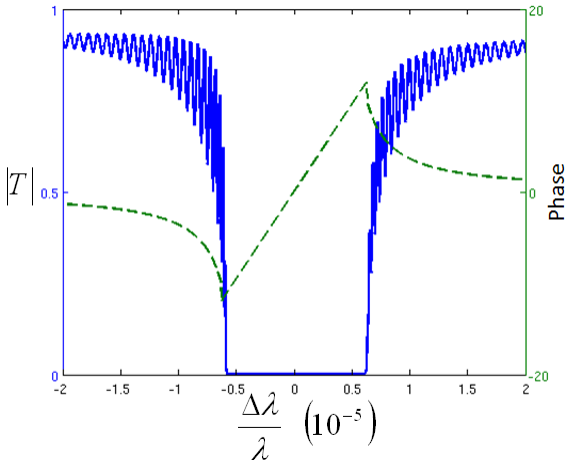

Figure D.6. The transmission function of C(400) for centroid wavelength at 0.95 Å. Solid curve is the absolute value of the transmission function, and the dashed curve is the phase.

In order for the seed to dominate the shot-noise generated in the second undulator section, the SASE FEL in the first undulator section has to provide sufficiently high FEL power to compensate for the power reduction associated with passage through the single-crystal monochromator. As shown in Figure D.7, we need about 60-m magnetic length of undulator to generate SASE FEL with peak power of 1.5 GW.

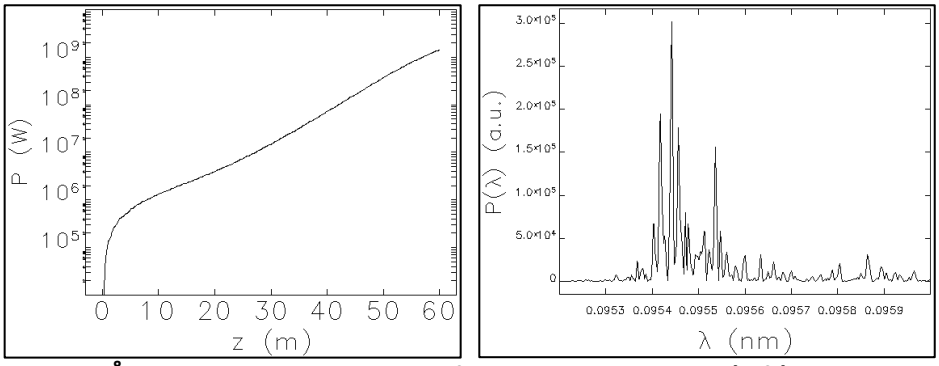

Figure D.7. The 0.95 Å SASE FEL power along the first undulator section (left) and the SASE spectrum at 60 m (right)

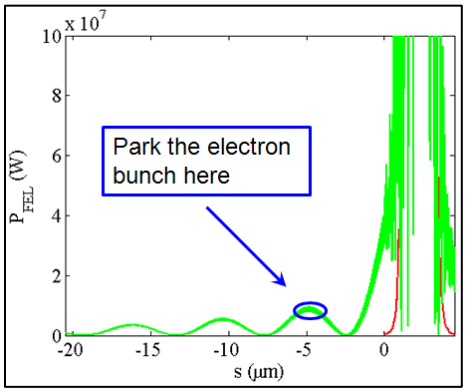

Figure D.8. The monochromatized trailing wake of the 0.95 Å SASE FEL passing through the C(400) single-crystal. The Red curve is the initial SASE FEL, and the Green is the light after passing through the C(400) crystal

As shown in Figure D.8, a monochromatized optical wake is generated after the SASE pulse passes through C(400). The peak of the wake is about 10 MW and is delayed from the main SASE pulse by 7-8 μm. A weak magnetic chicane (~4 m long) is sufficient to delay the electron bunch and to smear out the SASE microbunching. Since the electron rms bunch length is about σ_z~0.7 μm, this wake can cover the entire electron bunch after it passes through the chicane and thus act as the effective seed in the second undulator. About 45 m of magnetic length in the second undulator is required for the self-seeded FEL at 0.95 Å to reach saturation (see Figure D.9).

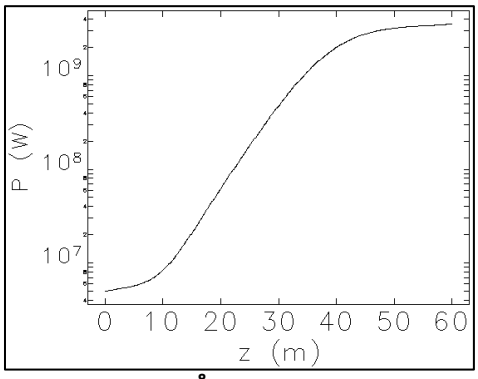

Figure D.9. Power from a seeded FEL at 0.95 Å in the second undulator section; saturation occurs around 45 m

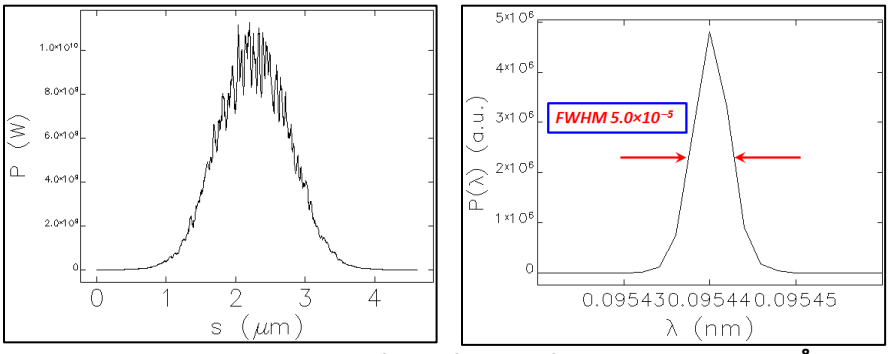

Figure D.10. The temporal and spectral profiles of the self-seeded FEL at 0.95 Å at 45 m magnetic length in the second undulator (at saturation)

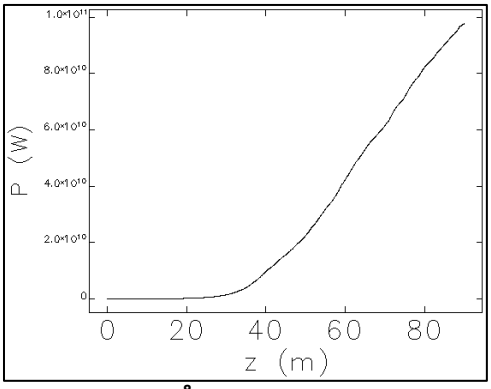

Figure D.11. Power from a seeded FEL at 0.95 Å in the second undulator section with tapering over the last 40 m; the power reaches ~80 GW at 85 m

Since the soft x-ray self-seeding scheme requires a much larger chicane and about 40 m longer tunnel length than the hard x-ray one, there is available length in the undulator hall to install an additional 40-m of tapered undulator to extract more HXR FEL power than present at saturation. As shown in Figure D.11, the FEL power at 0.95 Å reaches about 80 GW at 85-m magnetic length, or about one order of magnitude higher than the SASE saturation power.

X-Ray Polarization Control Options

Controlling the polarization state of the FEL radiation, both in the soft and hard x-ray radiation wavelength ranges, has broad applications for probing valence charge, spin, bonding dynamics, phonons and emergent phenomena on fundamental time and spatial scales. In the hard x-ray wavelength range, Bragg crystals may be used effectively to switch the polarization state of the x-rays. In the soft x-ray wavelength range, it is highly desirable to have direct polarization control of the x-ray source. In principle, an adjustable polarization undulator (such as APPLE-type [7]) can provide variable polarization by slow mechanical movement of undulator magnet blocks. An alternative approach for polarization control in x-ray FELs is the “crossed-planar undulator” scheme [8]. Since the LCLS-II soft x-ray undulators are planar type, we discuss several options that can be easily added onto the LCLS-II soft x-ray undulator line in order to control the output radiation polarization state.

We propose to install an APPLE undulator after the main planar undulator for flexible polarization control. The Apple undulator can operate in the helical mode to produce a circularly-polarized x-ray pulse, or it can operate in the vertically polarization mode as a crossed undulator for fast polarization

control. If both undulators operate at the same wavelength, the planar undulator should operate before saturation. Alternatively, if the APPLE undulator is resonant at the 2nd harmonic of the main undulator, the planar undulator can operate in saturation. The second harmonic radiation can be spectrally separated from the fundamental radiation wavelength.

In Figure D.12 we show two options that operate the downstream APPLE undulator at the same resonant wavelength as that of main undulator (U1). In Option A the length of U1 is chosen to be just a couple of gain lengths before saturation. The microbunched electron beam entering the helically-polarized APPLE undulator (U2) will generate circularly polarized x-rays; the U2 length is sufficient for FEL saturation. Since the circularly polarized radiation power quantitatively dominates over the horizontally-polarized radiation produced in U1, the total radiation should have a degree of circular polarization very close to 100%. The state of polarization can be changed by adjusting the polarization of the APPLE undulator via slow movements of undulator magnet blocks.

The Option B shown in Figure D.12 has the APPLE undulator U2 configured in vertically polarized mode to form a crossed undulator pair with the main planar undulator U1. When the length of APPLE undulator is chosen to be about 1.3 L_G [9], the time-averaged radiation power in the second undulator reaches about the same level as that of the first undulator. Together with a proper phase shifter that controls the relative phase between the two polarization directions, Option B can generate circularly polarized (or any arbitrarily elliptically-polarized) output x-ray pulses. If fast pulsed dipole magnets are employed in the phase shifter chicane, the relative phase between the two radiation components from the crossed undulators can vary at ~100 Hz, hence enabling fast polarization switching from shot to shot.

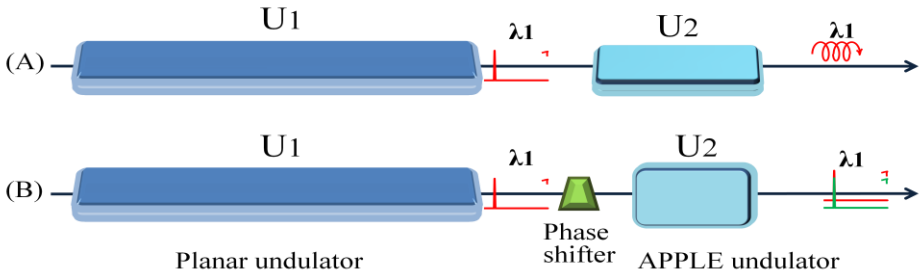

Figure D.12. Polarization control Options A and B

Both U1 and U2 operates at the fundamental wavelength. U1 is a planar undulator that produces horizontally polarized x-rays. U2 is an APPLE undulator that operates in the helical mode in Option A to produce circularly polarized x-rays, or it can operate in the vertically polarized mode in Option B as a crossed undulator.

The two options in Figure D.12 require sufficient length in the main planar undulator U1 to operate to nearly the end of the exponential regime. If the FEL were to reach actual saturation in U1 in Options A and B, the horizontally polarized x-ray power will be too large to allow for a high degree of circular polarization to be formed by U2. Here we discuss two additional schemes that would allow the FEL to reach saturation in U1 [10] *and* for U2 to provide variable polarization. The main idea is to operate U2 at the 2nd harmonic wavelength of U1, since the 2nd harmonic radiation in U1 should be negligibly small. As shown in Figure D.13 (Option C), the APPLE undulator U2 can be used in helical mode to produce circularly polarized x-rays at the 2nd harmonic, which can be easily separated from the fundamental radiation produced in U1. If fast pulse-to-pulse polarization control is desirable, we can use two different sections of the APPLE undulator to set up the crossed undulator configuration as shown in Figure D.13

Option D. In this case, U2 and U3 generate horizontally and vertically polarized components respectively.

Note that by using a variable-gap APPLE undulator for U2, all four options require a very similar hardware setup and thus U2 can be reconfigured to serve different user interests. As numerical examples to demonstrate some radiation characteristics of these options, we chose for both U1 and U2 an undulator period of 6 cm and undulator section lengths of 3.4 m separated by breaks of 0.7 m. The final radiation wavelength is 1 nm (1.2 keV photon energy), and the main electron beam parameters used in the simulations are listed in Table D.2.

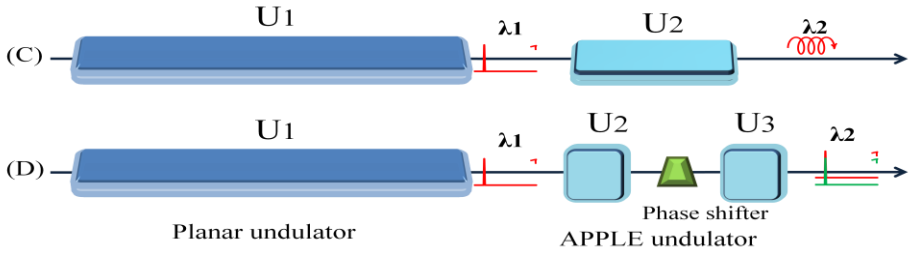

Figure D.13. Polarization control Option C and D

U1 is a planar undulator operates at saturation, while U2 and U3 are tuned to the 2nd harmonic of U1. U2 and U3 are APPLE undulators that can operate in the helical mode in Option C to produce 2nd harmonic circularly polarized x-rays, or they can form a pair of the crossed polarization undulators in Option D.

Table D.2. Main beam parameters used in the polarization control studies

Parameter	Symbol	Unit	Value
Electron beam energy	E	GeV	6
Peak current	I_{pk}	kA	3
Normalized rms slice emittance	$\gamma\varepsilon_{x,y}$	μm	0.6
RMS energy spread	σ_E	MeV	1.4

<u>Option A</u>: An APPLE undulator following the main planar undulator resonant at the same fundamental wavelength of 1 nm.

For this option, SASE growth in the main undulator stops a few gain lengths before power saturation. The microbunched electron beam is then injected into the APPLE undulator, which can be operated with horizontal linear polarization to continue producing linearly polarized radiation, or with the helical polarized to produce a circularly polarized output beam. With 6 GeV energy electrons to produce 1-nm FEL, the length of U1 is chosen 40.8 m (10 segments) in the simulations. The total radiation power from U1 is about 0.9 GW; half of it can serve as a seed for U2 operating with helical polarization. The circularly polarized radiation reaches saturation in U2 within 15 m, with an average power about 20 GW (Figure D.14). In this setup, the degree of circular polarization is 96%. Use of an undulator taper in the final part of U2 can increase the final power by up to a factor of 2.

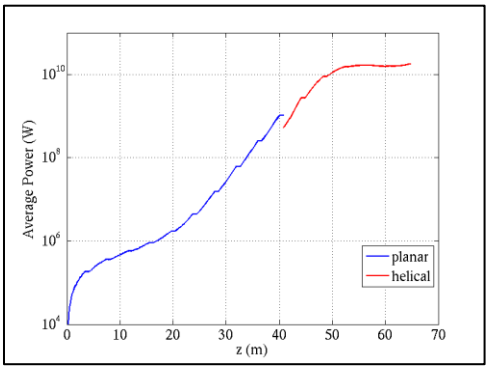

Figure D.14. Option A: Average power at the FEL wavelength 1 nm along the undulator distance from the planar U1 (blue curve) and the APPLE U2 (red curve)

<u>Option B:</u> Crossed-planar undulators at the fundamental wavelength 1 nm.

The APPLE undulator U2 can also be operated in the vertical polarization mode. The total radiation field after these undulators are $E_x + e^{i\varphi}E_y$, where φ can be adjusted by an electromagnetic phase shifter between U1 and U2. In the exponential gain regime, the required U2 length is 1.3 L_G to obtain the same radiation power as that from U1. For the 1-nm case, if we choose U1 to be 40.8 m (10 sections) and U2 to be about 2.6 m, both horizontally and vertically polarized components of the radiation power at the U1 exit are about 1 GW (Figure D.15). The degree of circular polarization is 89% at the optimal phase shift. In order to obtain more power, U1 can operate closer to saturation. For example, adding two more sections in U1 (to a total of 12 sections, 48.9 m) results in nearly 10 GW FEL power. Then a 6-m U2 can reach the same power level. The final degree of polarization is reduced to 70%. The depolarization effects mainly come from the relative slippage between E_x and E_y, and the lethargy effects during the initial radiation buildup process in U2 [3] . Compared to Option A, the advantage of the crossed undulator configuration is fast polarization switching capability via the phase shifter.

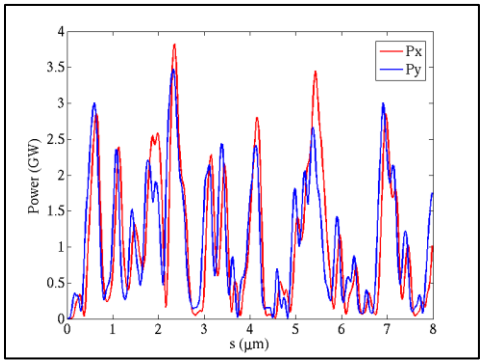

Figure D.15. Option B: An example of FEL power profiles at 1 nm for the crossed undulator (U1 and U2). Length of U1 = 40m (10 sections); Length of U2 = 2.6 m

<u>Option C:</u> Second harmonic radiation at 1 nm in the APPLE undulator.

It may be preferable to operate the main undulator U1 deep into power saturation for stability. For Options A and B where U1 and U2 operate at the same resonant FEL wavelength, it is difficult to achieve a high degree of circular polarization because the vertically-polarized power from U2 will be much smaller than the horizontally-polarized power from U1 in deep saturation. To circumvent this problem,

the second undulator can be tuned to operate at the second harmonic frequency of U1 since very little second harmonic radiation is generated in U1.

In Option C, the U1 undulator parameter is chosen to obtain FEL radiation at 2 nm wavelength. After power saturation (11 sections of U1), the electron beam is injected into the APPLE undulator U2 operating in helical mode and which is tuned to be resonant at 1 nm wavelength (the 2nd harmonic of U1). From U1, The electron beam is strongly bunched with rich harmonic content and will radiate coherently in U2 as shown in Figure D.16. The average power at 1-nm grows rapidly and then saturates (due to energy-spread caused debunching) beyond 8 m in U2 at the 3 GW level. Since the 1-nm (2nd harmonic) radiation from U1 is three orders of magnitude smaller, the degree of circular polarization is almost 100%.

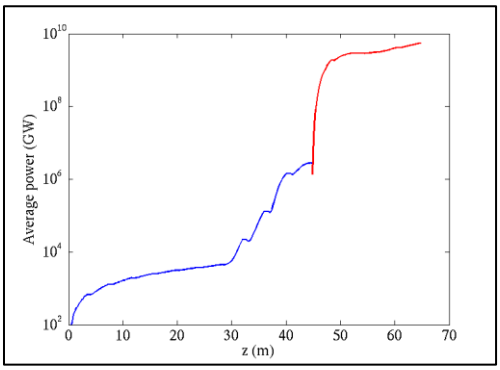

Figure D.16. Option C: The average FEL power at 1 nm along the planar U1 (blue curve) and the APPLE U2 (red curve). The fundamental wavelength of U1 is 2 nm, and that of U2 is 1nm. The length of U1 = 44.8m (11 sections)

<u>Option D:</u> Second harmonic radiation at 1 nm with crossed undulators.

Similar to the Option B, we can also set up the crossed undulator operating at the 2nd harmonic of U1. Since the 2nd harmonic radiation in U1 is negligibly small, we use the APPLE undulator to set up two short sections whose fundamental radiation wavelength is the 2nd harmonic of U1. The first section (U2) produces horizontally polarized x-rays while the second section (U3) produces a vertically polarized pulse. A phase shifter between U2 and U3 tunes the longitudinal phase difference between U2 and U3 and thus control the polarization state. Since U1 is already in the saturation regime, the lengths of U2 and U3 are typically short to avoid strong debunching. For example, following the previous example of 44.8 m U1 at 2 nm, we set the lengths of U2 and U3 to 2.1m each to obtain 1 nm radiation output power of about 0.8 GW in both transverse directions (Figure D.17). For optimal tuning of the phase shifter, the maximum degree of circular polarization can reach 85%.

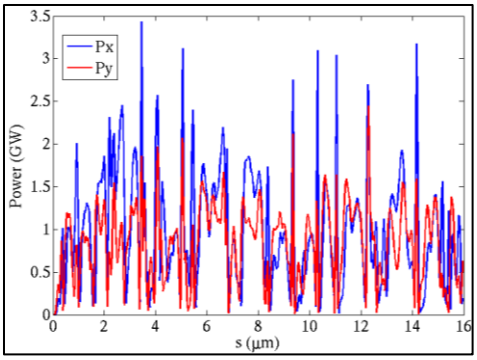

Figure D.17. Option D: An example of power profiles at 1 nm from the crossed undulator (U2 and U3). Length of U1 = 44.8m (11 sections); Length of U2 and U3 = 2.1 m

The four options are summarized in Table D.3.

Table D.3. Comparison of the four polarization control options

Option	A	B	C	D	units
Length of U1	40.8	40.8(48)	44.8	44.8	m
Length of U2	15	2.6 (6)	8	2.1	m
U2 (U3) operation mode	helical	cross	helical	cross	
Radiation wavelength in U1	1	1	2	2	nm
Radiation wavelength in U2	1	1	1	1	nm
Average FEL radiation power	20	1 (10)	3	0.8	GW
Degree of circular polarization	96	89 (70)	100	85	%
Polarization state switching	slow	fast	slow	fast	

External Seeding using Echo

Compared to self-seeding schemes, seeding with an external laser has the advantage that the FEL radiation is naturally synchronized with the seed laser, providing a “clock” highly useful for pump-probe user experiments. FEL laser-seeding techniques typically use a seed UV laser for generation of electron beam charge modulation at a harmonic of the laser frequency. This modulation can be further up-converted in frequency to generate fully coherent radiation at shorter wavelengths. The efficiency of the up-frequency conversion determines the highest harmonic number (the ratio of the seed laser wavelength to the output harmonic radiation wavelength) achievable and is critical to the overall performance of this approach.

Research on seeding an FEL with an external laser over the last two decades has focused on how to improve the up-frequency conversion efficiency to extend the harmonic number to the range of 20~50, so that the generation of fully coherent radiation at soft x-ray wavelengths can be achieved within a single stage using commercially available UV lasers. Various laser seeding techniques such as High-Gain Harmonic Generation (HGHG [11]), HGHG with a π-phase shifter [12], Echo-Enabled Harmonic

Generation (EEHG [13]), etc. have been envisioned to seed x-ray FELs, with the EEHG being the leading candidate because of its remarkable up-frequency conversion efficiency.

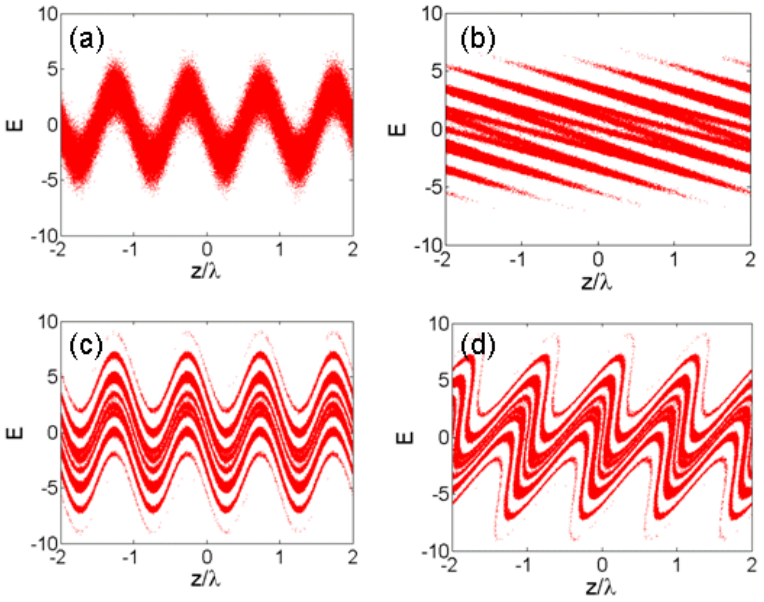

Figure D.18. Evolution of the longitudinal phase space in EEHG scheme

Evolution of the longitudinal phase space in EEHG scheme. (a) After the first modulator; (b) after the first chicane; (c) after the second modulator; (d) after the second chicane. The horizontal axis is the beam longitudinal position normalized to the laser wavelength and the vertical axis is particles energy deviation with respect to the reference particle normalized to the rms slice energy spread of the beam.

EEHG uses two modulators and two chicanes to generate high harmonic microbunching while producing relatively small energy modulation. The evolution of the longitudinal phase space in EEHG is shown in Figure D.182. A laser with wave number k_1 first interacts with the electron beam in the first modulator to generate coherent energy modulation (Figure D.18a). The beam is sent through the first chicane which has a large momentum compaction (R_{56}) that macroscopically washes out the energy modulation induced in the first modulator by shredding the phase space. At the same time, this smearing introduces a complicated fine structure into the phase space of the beam (Figure D.18b). A second laser with wave number k_2 (k_2 can be equal to k_1) is then used to energy modulate the electron beam in the second modulator (Figure D.18c). After passing through the second chicane, a coherent, high frequency density modulation with wavenumber nk_1+mk_2, where n and m are integers, will be generated as a recoherence effect, similar to an echo (Figure D.18d).

The key advantage of the EEHG scheme is that the amplitude of the achieved micobunching factor slowly decays with increasing harmonic number; consequently, generation of fully coherent soft x-ray emission based upon modulation from a UV seed laser within a single upshift stage becomes possible. The remarkable up-frequency conversion efficiency of EEHG has stimulated wide interest in using this technique to generate fully coherent soft x-rays in the last two years. The main challenge in implementing the EEHG scheme is the requirement for accurate control of the electron beam dynamics as the beam goes through the various undulators and chicanes, because the scheme involves a long-term memory of the beam phase space correlations. Recent success in the proof-of-principle EEHG experiment at SLAC [14] with a relatively large emittance beam has demonstrated the basic physics behind this technique.

Here we apply the EEHG technique to study the feasibility of using external seeding in LCLS-II to produce longitudinal coherence in the soft x-ray wavelength range. The baseline design for an echo-seeding LCLS-II upgrade is to generate fully coherent radiation at about 250 eV (~5 nm). While the electron beam energy for LCLS-II may be varied from 4.2 GeV to 14 GeV, we adopt a beam energy is 4.3 GeV in this study. The main parameters for the nominal ~5 nm case are listed in Table D.4.

Table D.4. Main parameters for the echo-seeding at 4.81 nm for the LCLS-II upgrade

Parameter	Symbol	Unit	Value
Electron energy	E	GeV	4.3
Electron peak current	I_{pk}	A	800
Electron rms horizontal or vertical normalized emittance	$\gamma\varepsilon_{x,y}$	μm	0.6
Electron rms slice energy spread	σ_E	MeV	0.7
Period length of the first and second modulators	λ_u	cm	35
Number of periods in the first and second modulators	N	-	8
Seed laser wavelength	λ_L	nm	202
Seed laser rms pulse length	σ_z	fs	100
Seed laser peak power	P	MW	300
Energy modulation amplitude in the first and second modulator	ΔE	MeV	1.4
Momentum compaction of the first chicane	$R_{56}^{(1)}$	mm	4.40
Momentum compaction of the second chicane	$R_{56}^{(2)}$	μm	109
FEL photon wavelength	λ	nm	4.81
FEL photon power	P_{FEL}	GW	8
FEL saturation length	L_{SAT}	m	18

The energy modulation amplitudes in the first (M1) and second modulator (M2) are both 1.4 MeV, a value two times larger than the incoherent energy spread. The modulators have a relatively long period of 35 cm in order to reduce the undulator K value, thus mitigating quantum diffusion effects. The modulator length is much shorter than the FEL gain length and therefore the interaction between the electron beam and the radiation generated from the modulated beam is negligible. The seed laser wavelength is assumed to be 202 nm corresponding to a frequency-quadrupled a Ti:Sapphire laser. This choice avoids the strong absorption effects in crystals for wavelengths below 200 nm.

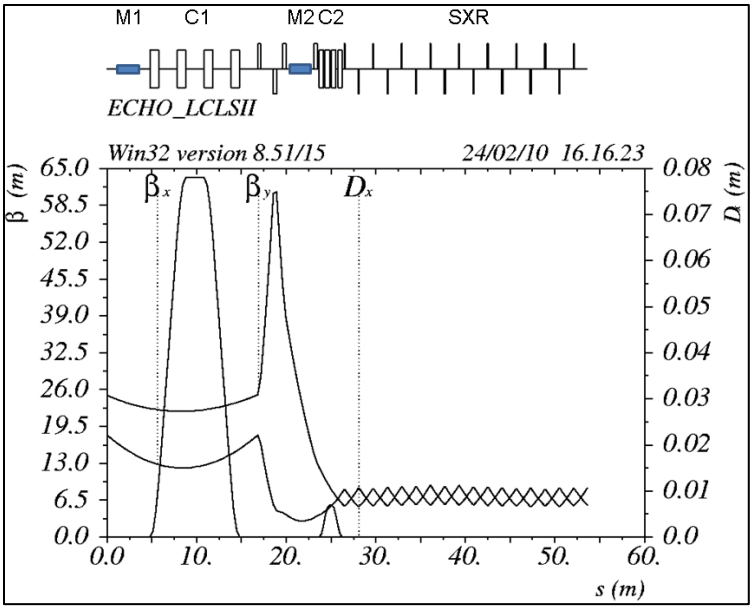

Figure D.19. Lattice of the echo-seeding beam line for the LCLS-II. M1 and M2 stand for the first and second modulator, C1 and C2 stand for the first and second chicane, SXR is the soft x-ray radiation beam line

The transport lattice for the echo-seeded beam line is shown in Figure D.19. One of the concerns in designing the lattice is where to put the matching quadrupoles that are necessary to match the beam to the small beta function lattice in the radiator undulator. Typically in the matching region, the beta function varies strongly with z and path length differences arising from second order transport effects can result in considerable smearing to the fine structures needed for the echo scheme. Considering the fact that the fine structures are on the order of the laser wavelength before the second modulator M2 and that they become on the order of the harmonic radiation wavelength after it, the matching quadrupoles are put upstream of M2. The average beta function in the modulators is about 15 m while that in the radiator SXR is 7 m. The seed laser waist sizes are 5 times larger than that of the electron beam in the modulators in order to provide uniform modulation in the transverse direction. Weak dipoles with lengths of 1 m and bending angles of 1.64 degrees are used in chicane C1 to mitigate the quantum diffusion from incoherent synchrotron radiation.

Full 3D simulations were performed to confirm the excellent performances of the echo-seeding scheme for LCLS-II upgrade. The GENESIS code FEL simulation was initialized with the macroparticles obtained from a start-to-end simulation by the ELEGANT code. Various characteristics of the electron beam phase space are shown in Figure D.20. The electron beam was optimized to have a flat-flat distribution (flat in both current and energy) in its central temporal part by properly choosing the RF phases in the linac. A laser heater increased the slice energy spread to about 25 keV in order to suppress the microbunching instability. Following the second bunch compressor, the current in the central part of the beam is about 800 A and the corresponding slice energy spread is about 700 keV.

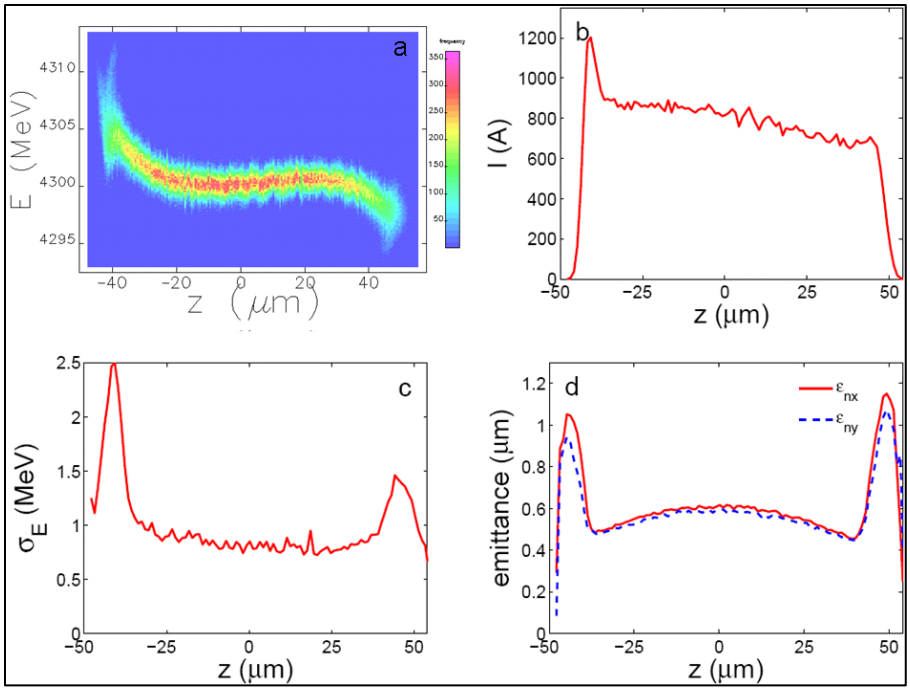

Figure D.20. Beam distribution at the entrance to M1 (bunch head to the right). (a) Longitudinal phase space; (b) Beam current distribution; (c) Beam slice energy spread; (d) Normalized beam slice emittance

Monochromatic (i.e., time-independent simulations)were first performed to find the suitable settings for the laser power and chicane strength that would yield a high bunching factor at the exit of C2. With the parameters shown in Table D.4, the bunching factor for the 42nd harmonic of the seed laser (λ_r=4.81 nm) is about 8% at the entrance to the SXR undulator. This large bunching factor allows a quick increase of the power of the coherent radiation to ~10 MW after one gain length; saturation occurs after about 10 gain lengths. The radiation power and spectrum at z=18 m in the SXR undulator from a full time-dependent simulation for the echo-seeded case adopting a 100-fs rms laser after 18 m are shown in Figure D.21. For convenience of comparison, the SASE radiation spectrum after 37 m in the SXR undulator is also shown in Figure D.21. *Note: SASE has a slow start-up and requires about twice the undulator length to reach saturation*. The FWHM bandwidth of the radiation spectrum with echo-seeding scheme is about 1.0×10^{-4}, ~50 times narrower than the SASE spectrum. The advantage of seeding the FEL with the EEHG technique is obvious: it requires only half of the undulators in order to reach saturation and provides fully coherent radiation with a well defined power profile and enhanced peak spectral brightness.

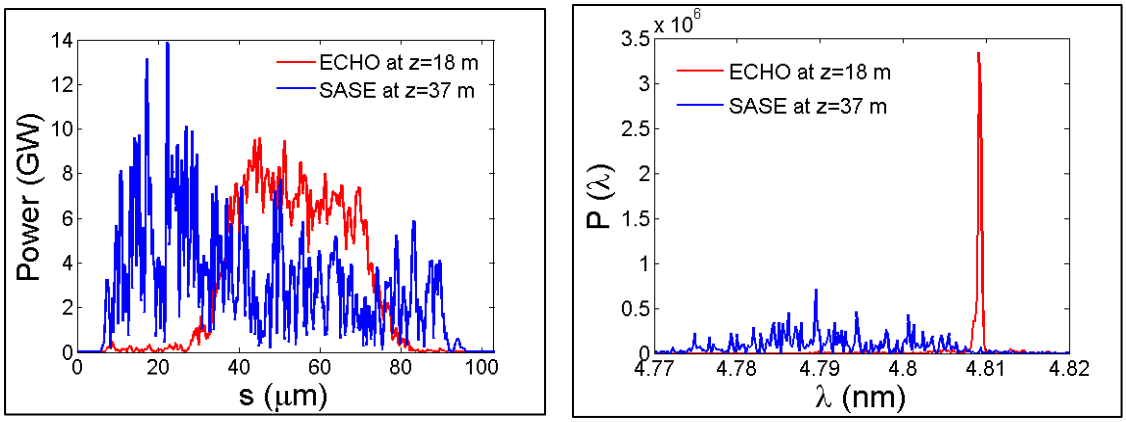

Figure D.21. Results of the echo-seeding scheme at 4.81 nm. (left) Radiation power profile; (right) Radiation spectrum

It is worth pointing out that the EEHG scheme also offers flexibility in radiation wavelength tuning. EEHG theory implies that given energy modulation amplitudes, the strength of the chicanes can be varied to maximize the bunching factor at a specific harmonic number. Furthermore, when the chicanes are optimized to provide a large bunching factor for the *n*-th harmonic, one also gets considerable bunching at the *2n*-th and *3n*-th harmonic. For instance, with the same set up for the lasers and the chicanes as listed in Table D.1, analysis shows that the bunching factor at the 84th harmonic (λ_f=2.40 nm) of the seed laser can be as high as 3%, large enough to dominate the shot noise microbunching. Therefore, one only needs to change the gap of the SXR undulator to generate fully coherent radiation at 2.40 nm.

In summary, external seeding employing echo scheme is a promising option for future LCLS-II upgrade. Echo-seeding enables the generation of nearly fully coherent soft x-ray radiation in LCLS-II upgrade with commercially available UV lasers. It also allows the radiation wavelength in the SXR beam line to be easily tuned in the range 2 to 5 nm.

References

1. J. Feldhaus *et al.*, *Possible application of x-ray optical elements for reducing the spectral bandwidth of an x-ray SASE FEL*, Optics Communications, **140**, 341 (1997).

2. J. Wu *et al.*, *Staged self-seeding scheme for narrow bandwidth, ultra-short x-ray harmonic generation free electron laser at LCLS*, Proceedings of 2010 FEL conference, Malmo, Sweden, 2010.

3. Y. Feng *et al.*, *Optics for self-seeding soft x-ray FEL undulators*, Proceedings of 2010 FEL conference, Malmo, Sweden, 2010.

4. S. Reiche, *GENESIS 1.3: a fully 3D time-dependent FEL simulation code*, Nucl. Instrum. Methods A **429**, 243 (1999).

5. Y. Ding, Z. Huang, and R. Ruth, *Two-bunch self-seeding for narrow-bandwidth hard x-ray free-electron lasersPhys*, Rev. ST Accel. Beam **13**, 060703 (2010);

   G. Geloni, V. Kocharyan, and E. Saldin, "*Scheme for generation of highly monochromatic X-rays from a baseline XFEL undulator*", DESY preprint 10-033, March 2010.

6. G. Geloni, V. Kocharyan, and E. Saldin, *A simple method for controlling the line width of SASE X-ray FELs*, DESY preprint 10-053, 2010.

7. S. Sasaki, *Analyses for a planar variably-polarizing undulator*, Nucl. Instr. And Meth. A **347**, 83 (1994).

8. K.-J. Kim, Circular polarization with crossed-planar undulators in high-gain FELs, Nucl. Instr. And Meth. A **445**, 329 (2000).

9. Y. Ding and Z. Huang, *Statistical analysis of crossed undulator for polarization control in a self-amplified spontaneous emission free electron laser*, Phys. Rev. ST Accel. Beams **11**, 030702 (2008).

10. H. Geng, Y. Ding, and Z. Huang, *Crossed undulator polarization control for x-ray FELs in the saturation regime*, Nucl. Instr. And Meth. A **622**, 276 (2010);

    E. Schneidmiller and M. Yurkov, *An option of frequency doubler at the european xfel for generation of circularly polarized radiation in the wavelength range 1–2.5 nm*, Proceedings of 2010 FEL conference, Malmo, Sweden, 2010.

11. L.H. Yu, *Generation of intense uv radiation by subharmonically seeded single-pass free-electron lasers*, Phys. Rev. A **44**, 5178 (1991).

12. B. McNeil, G. Robb and M. Poole, *Inducing strong density modulation with small energy dispersion in particle beams and the harmonic amplifier free electron laser*, Proceedings of PAC 2005, p1718, Knoxville, Tennessee, 2005;

    E. Allaria and G. De Ninno, *Soft-x-ray coherent radiation using a single-cascade free-electron laser*, Phys. Rev. Lett, **99**, 014801 (2007).

13. G Stupakov, *Using the beam-echo effect for generation of short-wavelength radiation*, Phys. Rev. Lett. **102**, 074801 (2009);

    D. Xiang and G. Stupakov, Echo-*enabled harmonic generation free electron laser*, Phys. Rev. ST Accel. Beams **12**, 030702 (2009).

14. D. Xiang et al., *Demonstration of the echo-enabled harmonic generation techniques for short-wavelength seeded free electron lasers*, Phys. Rev. Lett. **105**, 114801 (2010).